



**INTERPRAEVENT**

2021 – Norway

# 14<sup>th</sup> Congress **INTERPRAEVENT 2021**

May 31<sup>st</sup> to June 2<sup>nd</sup> 2021

Virtual Congress, Norway

Conference Proceedings

[www.interpraevent.at](http://www.interpraevent.at)

## **Natural hazards in a changing world**



Published by the International Research Society INTERPRAEVENT, Klagenfurt, Austria

**INTERPRAEVENT 2021 – Conference Proceedings © 2021 International Research Society INTERPRAEVENT**

The authors bear full responsibility for the contents of their contributions.

Edited by Niki Beyer Portner et. al

Layout: The organizing committee at the Norwegian Water Resources and Energy Directorate (NVE).

All rights reserved; no parts of this publication may be reproduced, stored or retrieved in any form or by any means without the prior written permission of the authors.

The International Research Society INTERPRAEVENT received the right for online and printed publishing.

ISBN 978-3-901164-28-6

[WWW.INTERPRAEVENT.AT](http://WWW.INTERPRAEVENT.AT)

# PREFACE

Interpraevent is considered to be “the expert network for the protection from natural hazards”. Within this frame we aim to attract experts from science, engineering and administration. Therefore, the call for papers for the 14<sup>th</sup> Interpraevent congress – entitled “Natural hazards in a changing world” – was spread out to this community of experts. We asked for written contributions to assess the state of the art and knowledge in natural hazards prevention.

To cover the entire risk circle the call comprised four main topics:

- Risk Governance and Policy
- Data Acquisition and Modelling
- Hazard and Risk Assessment
- Hazard and Risk Mitigation (land use planning, technical measures, nature based solutions, organizational measures)

For the first time we offered authors the chance to submit extended abstracts or papers in English language. After acceptance, it was possible to be invited for an oral presentation based on both types of submission. With this decision, we thought to be more attractive for authors working in practical fields. All other authors, not selected for an oral presentation, had the chance to present a poster.

Following the call, we received 185 extended abstracts and 55 papers submitted by authors from 21 different nations. The highest number of extended abstracts came from Austria (51), followed by Norway (45), Japan (25) and Switzerland (20). The highest number of papers came from Switzerland (15), followed by Norway and Austria (both 9), Italy and Japan (both 5). Nearly 40% of the contributions were submitted within the topic “Hazard and Risk Assessment”, covering all natural hazards processes. The predominant part of contributions can be connected to prevention. About half of the authors are scientists. Nevertheless, the amount of practitioners working in administration or as consultants is still that high, that Interpraevent reaches its own goal to bring research and praxis together.

Even Interpraevent was affected by the international COVID-19 crisis. The congress scheduled for May 2020 had to be cancelled and it was considered to shift the congress with physical attendance to 2021. Due to health safety reasons the decision was taken, to organize a virtual congress. With that, we wanted to assure that not all the work would be for nothing and that at least 43 papers and 115 extended abstracts could finally be published.

We are aware of the hard work of preparing and writing papers. However, after the submission, the editors’ job (selecting and convincing potential reviewers) and the reviewers’ job (critically reading submissions and giving feedback to authors) had to be done. Finally, the accepted submissions had to go through a layout process until authors gave their permission for the final publication.

Therefore, we are grateful to all authors, editors, reviewers and the Norwegian layout team for their valuable efforts to make Interpraevent to what it is: “the expert network for the protection from natural hazards”.

## **Niki Beyer Portner**

Chair of the Interpraevent Science & Technology Advisory Board (STAB)  
and Managing Editor of the IP2021 congress

## **Gernot Koboltschnig**

Business Manager of the International Research Society Interpraevent

# CONTENTS

## RISK GOVERNANCE AND POLICY (RGP)

<b>Roles in responsibility sharing for good governance in flood risk management</b> .....	<b>10</b>
Marie-Sophie Attems, Magdalena Rauter, Thomas Thaler, Sven Fuchs	

<b>Evaluation of the Extraordinary Avalanche Situation in January 2018 in Switzerland</b> .....	<b>17</b>
---	-----------

Michael Bründl, Elisabeth Hafner; Peter Bebi, Yves Bühler, Stefan Margreth, Christoph Marty, Mark Schaer, Lukas Stoffel, Frank Techel, Kurt Winkler, Benjamin Zweifel, Jürg Schweizer

<b>Local natural hazard advisors – a concept and its implementation</b> .....	<b>24</b>
---	-----------

Manuel Häberli, Roderick Kühne, Wanda Wicki, Gian Reto Bezzola

<b>Knowledge and perception of natural hazards: results from population surveys to innovate risk communication</b> .....	<b>33</b>
--	-----------

Lydia Pedoth, Agnieszka Elzbieta Stawinoga, Gernot Koboltschnig, Willigis Gallmetzer, Pierpaolo Macconi, Sönke Hartmann, Stefan Schneiderbauer, Doris Damyanovic

<b>Water sensitive planning and building – more acceptance by cooperation and highlighting co-benefits?</b> .....	<b>41</b>
---	-----------

Andreas Rimböck

## DATA ACQUISITION AND MODELLING (DAM)

<b>Vertical groundwater movement identification through Distributed Heat Tracing Tests. Case of Åknes, Norway</b> .....	<b>50</b>
---	-----------

José Acuna, Randi Kalskin Ramstad, Gustav Pless

<b>Physical modelling of debris flows to analyse the influence of a cascade on the flow behaviour and consequences on protection measures</b> .....	<b>62</b>
---	-----------

Catherine Berger, Andrea-Kristin Bachmann, J. Speerli, Florian Zimmermann, Walter Clausen

<b>Image processing techniques for grain size analysis of coarse soils</b> .....	<b>72</b>
--	-----------

Lorenzo Brezzi, Simonetta Cola, Paolo Zorzan

<b>Image-based flow monitoring in a remote alpine catchment</b> .....	<b>81</b>
---	-----------

Maxence Carrel, Salvador Peña-Haro, Beat Lüthi, Issa Hansen

<b>Regobs – an open geohazards-related data hub used in citizen science, warnings, preparedness and crisis management</b> .....	<b>90</b>
---	-----------

Rune Verpe Engeset, Ragnar Ekker, Priska Hiller, Tore Humstad

<b>Dynamics and geomorphological analysis of the Taan Fiord 2015 tsunamigenic landslide</b> .....	<b>99</b>
---	-----------

Andrea Franco, Andreas Huber, Jasper Moernaut, Barbara Schneider-Muntau, Markus Aufleger, Michael Strasser, Bernhard Gems

<b>Swiss surface runoff risk map</b> .....	<b>108</b>
Roberto Loat, Andy Kipfer, Natascia von Wattenwyl, Antoine Magnollay	
<b>The interaction between flood and morphology</b> .....	<b>120</b>
Lars Fredrik Lund, Gerard Dam	
<b>Active sediment control with a shutter and monitoring of sediment runoff in Jo-Gan-Ji River</b> .....	<b>126</b>
Koso Mikami, Tomoyuki Noro, Takahiko Nagayama, Tomohiko Furuya, Masaharu Fujita, Takahisa Mizuyama, Takahiro Itoh	
<b>River morphology and sediment transport processes numerical modeling applied to the fluvial environment of the Rhône River in Valais</b> .....	<b>138</b>
Francesc Molné, Giovanni de Cesare, Jose Luis García Rodríguez, Azin Amini, Jean-Noël Saugy	
<b>Image-based flow measurements in wide rivers using a multi-view approach</b> .....	<b>146</b>
Salvador Peña-Haro, Robert Lukes, Maxence Carrel, Beat Lüthi	
<b>Documentation of Natural Events and its Importance for the Integrated Risk Management. Review, current use and new developments in Switzerland</b> .....	<b>154</b>
Wolfgang Ruf, Mathias Zesiger	
<b>Third correction of the Rhône River in Switzerland: physical and numerical modelling of the “Martigny bend” priority measure</b> .....	<b>162</b>
Jean-Noël Saugy, Azin Amini, Giovanni De Cesare, Stéphanie André, Pierre Bourqui, Khalid Essyad, Irene Samora, Tony Arborino	
<b>Groundwater recharge and discharge in the Åknes rockslide – constraining uncertainties for the development of a numerical groundwater flow model</b> .....	<b>172</b>
Clara Sena, Alvar Braathen, José Acuna, Frida Bjørn-Hansen, Stig Runar Ringstad, Halvor Bruun, Gustav Pless, Mark Mulrooney	
<b>Examination of shape efficacy of steel pipe open sabo dam according to Impulsive Load of Debris Flow</b> .....	<b>181</b>
Osamu Shimakawa, Toshiyuki Horiguchi, Yoshiharu Komatsu, Satoshi Katsuki	
<b>HAZARD AND RISK ASSESSMENT (HRA)</b>	
<b>Comparing nets and forests for rockfall risk reduction along the Gotthard highway using cost-benefit-analysis and net present values</b> .....	<b>190</b>
Luuk Dorren, Christine Moos, Martin Nussbaumer, Steve Vogel, Philippe Arnold	

<b>Automated delineation of large-scale landslides based on high-resolution digital terrain models</b> .....	<b>198</b>
Bernhard Elsner	
<b>Driftwood and Hybrid Debris Barrier Interactions: Process of Trapping and Prevention of Releases during Overtopping</b> .....	<b>206</b>
Toshiyuki Horiguchi, Guillaume Piton, Muhammad Badar Munir, Vincent Mano	
<b>Evaluation of river Gail flood retention system after the flood 2018: experiences and limits</b> .....	<b>216</b>
Gernot Koboltschnig, Erwin Schumi, Christian Kopeinig	
<b>Meteorological and Hydrological Service in risk assessment and management of forest fire hazards in Croatia</b> .....	<b>224</b>
Tomislav Kozaric, Marija Mokoric, Tanja Renko	
<b>Slope collapses along the southern Åfjorden cliff (Hyllestad municipality-Sogn og Fjordane, Norway)</b> .....	<b>235</b>
Ivanna Penna, Vegard Nes, Reginald Hermanns, Marie Bredal, Lene Kristensen, Pierrick Nicolet	
<b>Mapping of the protective function of forests in Austria against shallow landslides</b> .....	<b>240</b>
Frank Perzl, Monika Rössel, Elisabeth Lauss, Michael Neuhauser	
<b>Impact of groundwater accumulation on slope failure initiation: A simulation of slope failure due to rainfall</b> .....	<b>249</b>
Xin Qin	
<b>Evaluation and adaption of existing protection measures to the Austrian Standards at the Poellinger Torrent</b> .....	<b>256</b>
Claudia Sauer Moser	
<b>The PermaRisk project - Emerging hazards due to mountain permafrost degradation in the French Alps</b> .....	<b>266</b>
Philippe Schoeneich, Xavier Bodin, Ludovic Ravanel, Pierre-Allain Duvillard, Marco Marcer, Thomas Echelard, Raphaële Charvet, André Revil, Diego Cusicanqui	
<b>WoodFlow project – large wood management in rivers</b> .....	<b>275</b>
Nicolas Steeb, Alexandre Badoux, Robert M. Boes, Eric Gasser, Dieter Rickenmann, Christian Rickli, Virginia Ruiz-Villanueva, Isabella Schalko, Lukas Schmocker, Massimiliano Schwarz, Markus Stoffel, Volker Weitbrech	
<b>Xgeo.no – A decision-support tool for assessing geohazards</b> .....	<b>284</b>
Heidi Bache Stranden, Graziella Devoli, Rune Engeset, Tuomo Saloranta, Jess Andersen, Søren Boje, Kjetil Melvold, Tore Humstad, Knut Inge Orset, Nils Kristian Orthe, Ragnar Ekker	

<b>A field study of a landslide dam outburst following progressive failure in the Ashiaraidani basin</b> .....	<b>294</b>
Shoki Takayama, Shusuke Miyata, Masamitsu Fujimoto, Yoshifumi Satofuka	
<b>Deciphering sediment Connectivity Index and erosion pattern in a debris flow catchment</b> .....	<b>303</b>
Loris Torresani, Vincenzo D'Agostino, Guillaume Piton	
<b>Comparison of techniques for estimating soil drainage for the assessment of empirical rainfall thresholds - a case study of ash-fall pyroclastic soil mantled slopes of southern Italy</b> .....	<b>312</b>
Rita Tufano, Pantaleone De Vita, Thomas Glade	
<b>HAZARD AND RISK MITIGATION (HRM)</b>	
<b>Building protection against surface runoff</b> .....	<b>322</b>
Markus Imhof, Benno Staub, Alain Marti, Gunthard Niederbäumer, Roberto Loat	
<b>A Virtual Reality Tool for Hazard and Risk Mitigation of Landslides through Serious Gamification</b> .....	<b>331</b>
Shafaq Irshad, Gebray H. Alene, Nitesh Godara, Oddbjørn Bruland, Vikas Thakur, Andrew Perkis	
<b>Avalanche- and Slush-Flow Dam Vallabøen, Ørsta Municipality, Western Norway</b> .....	<b>339</b>
Árni Jónsson, Peter Gauer, Marius S. Lianes, Marius Mathisen Søvik	
<b>Rapid revision of the hazard maps for debris flow and snowmelt-type mud flow caused by volcanic eruptions of unexpected magnitudes and from unexpected vents</b> .....	<b>349</b>
Norihisa Kumai, Takashi Kurogi, Shin-ichiro Shimomura, Keishi Saito, Yuya Aoyagi, Shun'ichi Niwa, Shusaku Shiiba, Shin-ichiro Hayashi, Marino Hiraoka, Yusuke Yamazaki, Yasuo Ishii, Yoko Tomita, Jun Minagawa	
<b>Forest stands from high elevation afforestation in the Austrian Alps – past, present and future at a glance</b> .....	<b>356</b>
Christian Norbert Scheidl, Micha Heiser, Veronika Lechner, Frank Perzl, Silvio Schueler, Georg Frank, Thomas Thaler, Gerhard Markart	
<b>Evaluation of an awareness raising campaign in Styria, Austria</b> .....	<b>365</b>
Sabrina Scheuer, Markus Eder, Helmut Habersack	
<b>Integrated operational avalanche risk management</b> .....	<b>375</b>
Walter Steinkogler, Stian Langeland, Sophia Demmel	
<b>“How-to” manage a torrential protection system in a holistic way: Integrated Torrent Development Concept (IWEK)</b> .....	<b>383</b>
Quirin Stimm, Franz Grüsser, Karl Mayer, Wolfgang Rieger, Andreas Rimböck	



# RISK GOVERNANCE AND POLICY (RGP)

---

# Roles in responsibility sharing for good governance in flood risk management

Marie-Sophie Attems<sup>1</sup>, Magdalena Rauter<sup>2</sup>, Thomas Thaler<sup>2</sup>, Sven Fuchs<sup>2</sup>

**Keywords:** Property level flood risk adaptation; governance; flood resilience; risk communication

## Abstract

Austrian municipalities face increasing risk from natural hazards due to a number of developments: the frequency and severity of extreme weather events are expected to rise due to a warmer climate; settlements are expanding in hazard-prone areas; and the monetary value of assets and property at risk is increasing. While the policy discourse in the last decades emphasised technical, structural measures, management approaches have recently expanded to include private flood preparedness. This paper evaluates the role, the willingness and the importance of private adaptive behaviour in natural hazards risk management. Here, we distinguish between private homeowners, public authorities and experts who give technical advice. Results show, that homeowners consider themselves to be responsible for their own protection, however only when responsibilities are shared with public authorities. Public authorities also consider shared responsibilities to be vital, however framework conditions to implement measures have to be made. Experts are seen to be mediators in this respect, and can only provide solutions for individual cases.

## Introduction

Due to increasing flood losses, discussions arise on encouraging private actors to take a more central role in flood risk management (UNISDR, 2015; Kron, et al., 2019). This development is linked to the emergence of new management approaches within integrated flood risk management, which consider land-use planning, risk communication, and participatory processes in addition to public flood protection. In particular, residual risks need to be considered in planning and decision-making processes, rather than aiming for complete flood protection (Bubeck, et al., 2013; Roth & Winnubst, 2014). Focusing on Austria, there are several administrative bodies at different federal levels which are concerned with flood risk management. These include the federal state, the nine provinces and a total of approx. 2100 municipalities. Additionally, several acts exist on federal and provincial level which do not align and thus lead to large differences concerning their implementation. The federal government sets standards for developments in flood prone

---

<sup>1</sup> Research Associate, Department für Bautechnik und Naturgefahren, Universität für Bodenkultur, Wien, Peter-Jordan-Straße 82, Vienna, Austria (marie.attems@boku.ac.at)

<sup>2</sup> University of Natural Resources and Life Sciences, Vienna

areas which also include the permission and/or restriction of building developments. Due to the legal and organisational fuzziness, adaptive responses towards floods need a new agreement between authorities and citizens in order to increase overall resilience in the communities. In medieval times flood risk management was an individual or a local collective task, as flood events were seen to be a result of individual actions or divine punishment. In the second half of the 19<sup>th</sup> century, basic pro-active protection measures were implemented. New regulations were established with the Service for Torrent and Avalanche control in the year 1884 due to extreme hazard events. This led to the creation of the Forestry Act in 1975, which included hazard zone planning. In the second half of the 20<sup>th</sup> century the debate about non-structural measures (e.g. involving land-use planning) emerged and led to a risk-based and integrative natural hazards management. This largely also included stakeholder engagement and bottom-up initiatives. As a result, responsibilities should be shared between public authorities and affected residents, which are largely homeowners, to respond more effectively and recover more efficiently in the case of future events. Key challenges are fostering the self-efficacy of homeowners in the shape of implementing property level flood risk adaptation (PLFRA) measures and keeping flood awareness at a high level. PLFRA measures are effective to diminish damage from flood events (Kreibich, et al., 2015). Such measures include wet flood-proofing (controlled water inlet and adapting interiors to increase water resistance), dry flood-proofing (sealing openings to keep flood waters out of buildings), avoidance of flood waters (elevation or amphibious buildings) and barrier systems (such as sandbags and stop logs) (Holub & Hübl, 2008; Attems, et al., 2020). In many cases, even small PLFRA measures can enhance already-constructed buildings to effectively protect against flood hazards. In the case of new buildings, designers and builders can integrate efficient measures during the construction process. Implementing PLFRA measures demands self-responsibility on the part of the residents affected, as these measures are largely voluntary (Rauter, et al., 2019). This approach incorporates the support of authorities to accept shared responsibilities in order to motivate the implementation of PLFRA measures among homeowners. This challenge can be met by enabling homeowners and authorities to interact through mutual knowledge transfer and participatory processes and thus to foster risk communication (Di Baldassarre, et al., 2019). The aim of this analysis is therefore to understand the specific perspectives of homeowners, public authorities and experts to clarify whether the implementation of PLFRA measures can be a step towards a more integrated flood risk management approach.

## Methods

This analysis uses a 3-step perspective: (1) homeowners living in flood prone areas and have experience with flood events; (2) public administration which is concerned with flood risk management and (3) experts giving technical advice on PLFRA measures. We applied a mixed-methods approach to gain further insights into the perspectives of public administration, homeowners and experts on the implementation of PLFRA measures. For the perspective of public authorities- and homeowners, we chose two case study areas in Austria in which both the interviewed representatives of public authorities and participating homeowners have experience with flood risk management or flooding. In addition to perspectives of public authorities and homeowners on PLFRA measures in Austria, we

included an expert focus group in Germany in order to get an overall picture on roles in responsibility sharing for good governance in flood risk management. Figure 1 illustrates the methods used for each of these groups.

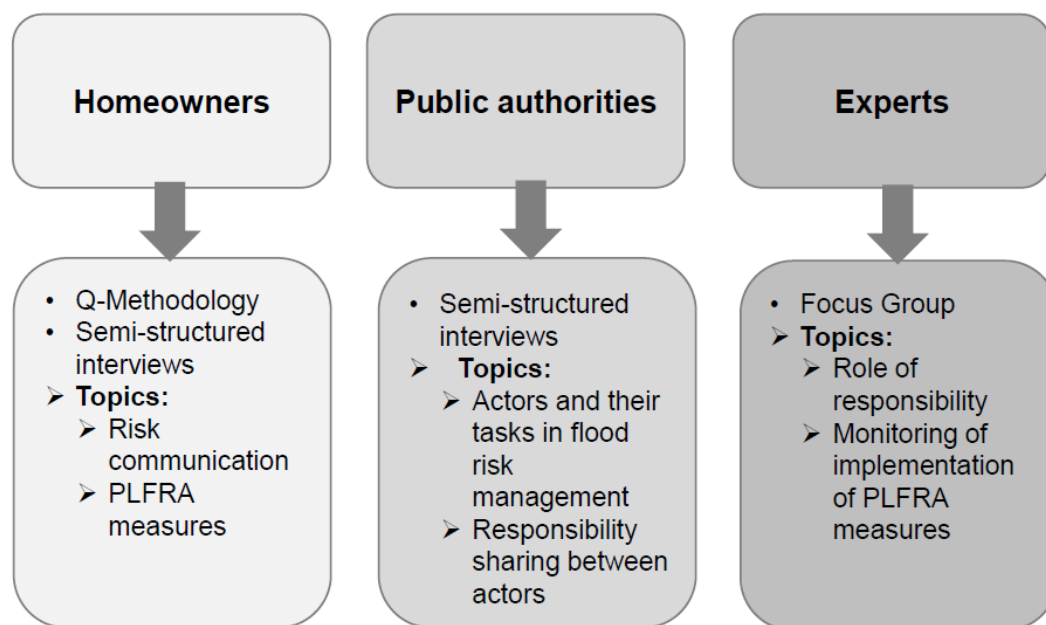


**Figure 1. The methods used to analyse the viewpoints of homeowners, public authorities and experts.**

Step 1: In order to analyse the homeowners' perspective, Q-methodology was applied in Graz, Austria, as this method is especially suitable for analysing subjectivities. In total, 20 affected residents who have experienced one or more floods in the past decade were included in the analysis. The properties at risk were largely single family homes, but also included apartment blocks. Several of the homeowners have been in contact with the city council, concerning the past implementation of retention basins in their neighbourhoods. Thus, the experience with floods was high. The goal was to identify the subjectivities among residents, concerning PLFRA measures, risk communication, trust in public protection measures and risk perception in general. Additionally, semi-structured interviews were conducted with these affected residents concerning the PLFRA measures taken and the mode of risk communication wished for, in order to get more detailed insights into the local situation.

Step 2: In Dornbirn, Austria, interview partners comprised a broad range of representatives with expertise in flood risk management in order to gain in-depth knowledge of the local situation. Overall, 22 qualitative semi-structured in-depth interviews were conducted with policymakers, representatives of public authorities and flood risk experts. Additionally, representatives of the regional and national level were interviewed, to broaden results and make them more applicable for other regions. Interviewees were actors of municipal spatial planning, emergency management, water engineering and flood risk management, geology, representatives of the provincial government, insurance parties and academia.

Step 3: The expert perspectives were analysed during a focus group in Dresden, Germany, with four relevant experts who have given technical advice on PLFRA measures to

homeowners inhabiting flood-prone areas. The experts had different educational backgrounds, although all within the range of hydraulic engineering. The topics covered during the focus group included (1) the role of the expert when giving technical advice to homeowners and (2) the process of monitoring the implementation of PLFRA measures. It has to be considered, that the experts had different origins as they were from Germany and Belgium. Although the legal system concerning flood risk management in these countries differ, the technical advice is seen as an overarching instrument to foster self-efficacy and adaptive behaviour and is thus not directly related to one country.

## Results and discussion

To create a comprehensive overview, we show the results from the perspectives of public authorities, homeowners and experts.

### *Perspective of homeowners*

The perspective of homeowners showed to be very homogenous. The majority of homeowners has implemented PLFRA measures, either through the experience of several flood events or through neighbourhood connections, friends and family. The PLFRA measures implemented by homeowners varied greatly in technical sophistication. However, self-efficacy was seen to be high among affected homeowners. There is a general distrust in public protection measures and these measures are not considered to provide full protection against floods. Thus, the understanding of residual risk is high. Although, homeowners believe that it is also their duty to take action, for instance by implementing PLFRA measures, they do not see it as their sole responsibility. A large part of affected residents highly trusts the fire brigade to help during flood events and also relies on the support of neighbours, friends and family. Generally, however, there is a wish to be incorporated in decision making processes and to be informed about PLFRA measures through independent experts. It can be concluded that face-to-face interaction with public authorities and experts is the type of communication which is needed to keep risk awareness high and thus motivate adaptive behaviour.

### *Perspective of public authorities*

From the perspective of public authorities, various stabilising factors are interconnected. Strong historical narratives, for example, strengthen adaptive expectations among homeowners who trust in existing flood measures. While affected residents need to be supported to take measures more efficiently, subsidies are seen as too much of a support, as such in turn increase the responsibility of the state. This would make responsibility sharing rather fuzzy. Yet, public authorities also rely on existing flood infrastructure and therefore minor efforts are taken to encourage risk adaptation. Partly, expertise is missing on how relevant information should be generated and it is unclear who is responsible to advocate change. Conflicts of interest might pose another challenge to responsibility sharing. Public authorities therefore have to better coordinate responsibilities. To do so, an allocation of financial resources is necessary, as currently no fixed budget is assigned to such tasks. The absence of change-inducing factors stabilises the current flood risk governance arrangement in which the emerging discourse on shifting responsibilities

between ‘public’ and ‘private’ is only slowly emerging. Additionally, expertise and rethinking processes about encouraging homeowners to implement PLFRA measures (especially where flood experience is missing) are slowly occurring among stakeholders, decision-makers and practitioners.

#### *Perspective of experts*

The experts involved in the focus group have all given technical advice on PLFRA measures in different parts of Germany and Belgium. Their viewpoints and experiences were, however, very homogenous. The results showed that experts see themselves responsible to motivate adaptive behaviour among homeowners. Homeowners, which actively contact experts, usually have already implemented PLFRA measures or have very clear vision of what they want. Thus, the expert has to build upon these visions and experiences of the residents. The process of giving technical advice therefore, not only relies on the knowledge and experience of the expert, but also heavily on mutual learning between expert and homeowner. The expert has to react differently regarding the individual case (e.g. building structure, extent of flood risk, type of flood risk, expectations of homeowner) to create individual solutions. Creating a “one-size-fits-all” solution concerning PLFRA measures is unrealistic. While the expert can give homeowners different recommendations on how to create more flood resilient homes, experts cannot make decisions for homeowners. Monitoring the implementation of PLFRA measures is seen as difficult, as homeowners will in some cases follow the given technical advice, whereas others might not as they do not see taking action as their responsibility.

## **Conclusions**

Flood events have caused high financial losses which could be reduced by the implementation of PLFRA measures. However, there is a need to distribute responsibilities more efficiently between all actors, in order to increase resilience among society. Currently, it seems that policy arrangements between national and local levels cannot tackle adaptation activities in a coordinated way and therefore might even hamper the implementation of PLFRA measures. We conclude that, in the past ten years, the shift towards a risk-based flood risk management approach and therefore towards risk governance predominantly occurred in the academic discourse. The following table (Table 1) summarises the viewpoints each actor expressed considering their role of responsibility towards minimising flood risks.

**Table 1. Summary of viewpoints concerning the roles of responsibility.**

<b>Homeowners</b>	<b>Public authorities</b>	<b>Experts</b>
They are responsible for their own protection, however not alone. Shared responsibility with the government is still seen as necessary by homeowners.	Sharing responsibility is necessary, however, the current system works well. Improvement is necessary regarding the implementation of PLFRA measures at the private level. Framework conditions to implement measures need to be made available by the public authorities.	They see their responsibility to motivate homeowners to adapt, however cannot force adaptive behaviour. They can provide solutions for individual cases, but cannot decide what homeowners should do.

It is obvious that to a certain extent all actors see their responsibilities in heightening the resilience towards flood risks. All actors emphasised the wish and need to share responsibilities. Among practitioners, discussions are gradually emerging. However, the shift in responsibilities has not been institutionalised yet or implemented in practice. While private actors need to increasingly take responsibility by implementing PLFRA measures, the public cannot shift off prevailing responsibilities. Importance is drawn, especially to local authorities, who need to become increasingly aware of their responsibilities when it comes to communicating risk more efficiently to foster knowledge. In this case, it is especially evident, that affected residents wish to be incorporated in decision-making processes. Thus, participatory processes would be necessary to keep risk awareness levels high and foster mutual knowledge transfer between homeowners and authorities. Thereby, social learning can be achieved and thus experiences between all groups exchanged. It is also vital to include experts in this process, to serve as motivating actors in this process. However, financial resources need to be provided, as well as social capacity and expertise, to reach a common optimum of responsibility sharing in current governance arrangements.

## **Additional note**

Marie-Sophie Attems and Magdalena Rauter should be considered as equally contributing authors.

## **References**

- Attems, M. S., Thaler, T., Genovese, E., & Fuchs, S. (2020). Implementation of property level flood risk adaptation (PLFRA) measures: choices and decisions. *Wiley Interdisciplinary Reviews: Water*, 7(1). doi: 10.1002/wat2.1404.
- Bubeck, P., Botzen, W. J. W., Kreibich, H., & Aerts, J. C. J. H. (2013). Detailed insights into the influence of flood-coping appraisals on mitigation behaviour. *Global Environmental Change*, 23(5), 1327-1338. doi: 10.1016/j.gloenvcha.2013.05.009.

- Di Baldassarre, G., Sivapalan, M., Rusca, M., Cudennec, C., Garcia, M., Kreibich, H., Konar, M., Mondino, E., Mård, J., Pande, S., Sanderson, M. R., Tian, F., Viglione, A., Wei, J., Wei, Y., Yu, D. J., Srinivasan, V., & Blöschl, G. (2019). Socio-hydrology: Scientific Challenges in Addressing a Societal Grand Challenge. *Water Resources Research*. doi: 10.1029/2018WR023901.
- Holub, M., & Hübl, J. (2008). Local protection against mountain hazards – state of the art and future needs. *Natural Hazards and Earth System Sciences*, 8, 81-99. doi: 10.5194/nhess-8-81-2008.
- Kreibich, H., Bubeck, P., Van Vliet, M., & De Moel, H. (2015). A review of damage-reducing measures to manage fluvial flood risks in a changing climate. *Mitigation and Adaptation Strategies for Global Change*, 20(6), 967-989. doi: 10.1007/s11027-014-9629-5.
- Kron, W., Löw, P., & Kundzewicz, Z. W. (2019). Changes in risk of extreme weather events in Europe. *Environmental Science & Policy*, 100, 74-83. doi: 10.1016/j.envsci.2019.06.007.
- Rauter, M., Schindelegger, A., Fuchs, S., & Thaler, T. (2019). Deconstructing the legal framework for flood protection in Austria: individual and state responsibilities from a planning perspective. *Water International*, 44(5), 571-587. doi: 10.1080/02508060.2019.1627641.
- Roth, D., & Winnubst, M. (2014). Moving out or living on a mound? Jointly planning a Dutch flood adaptation project. *Land Use Policy*, 41, 233-245. doi: 10.1016/j.landusepol.2014.06.001.
- UNISDR. (2015). Sendai framework for disaster risk reduction 2015–2030. Retrieved 12.08.2019, from United Nations Office for Disaster Risk Reduction [http://www.preventionweb.net/les/43291\\_sendaiframeworkfordrren.pdf](http://www.preventionweb.net/les/43291_sendaiframeworkfordrren.pdf).

---

# Evaluation of the Extraordinary Avalanche Situation in January 2018 in Switzerland

Michael Bründl<sup>1</sup>, Elisabeth Hafner<sup>2</sup>; Peter Bebi<sup>3</sup>, Yves Bühler<sup>4</sup>, Stefan Margreth<sup>5</sup>, Christoph Marty<sup>6</sup>, Mark Schaer<sup>7</sup>, Lukas Stoffel<sup>8</sup>, Frank Techel<sup>9</sup>, Kurt Winkler<sup>10</sup>, Benjamin Zweifel<sup>11</sup>, Jürg Schweizer<sup>12</sup>

**Keywords:** Avalanches; Prevention; Preparedness; Recovery; Science; Case Study or Practice Report

## Abstract

In January 2018, heavy snowfalls caused an extraordinary avalanche situation in Switzerland with an extent not observed since the avalanche winter of 1999. The amount of precipitation was far above the long-term average and in parts of the Swiss Alps even twice the average. For the first time since 1999, the highest danger level *5–Very High* was forecast for a 36-hour period and for most regions of the Swiss Alps. We present key findings of the analysis of this extraordinary event and show that the mitigation efforts taken after the catastrophic events in February 1999 were effective. Despite very high avalanche activity, there was no loss of life and damage to property was limited.

## Introduction

In January 2018, heavy snowfalls caused an extraordinary avalanche situation with an extent not observed since the avalanche winter of 1999. The amount of precipitation was far above the long-term average and in parts of the Alps (Valais and Grisons) even twice the average. For the first time since 1999, the highest danger level *5–Very High* was forecast for a 36-hour period and most regions of the Swiss Alps. Despite very high avalanche activity, there was no loss of life and damage to property was limited. The events allowed assessing whether the mitigation efforts taken after the catastrophic events in February 1999 were effective. In the following, we will present some key findings of this

---

<sup>1</sup> WSL-Institute for Snow and Avalanche Research SLF, Switzerland, (bruendl@slf.ch)

<sup>2</sup> WSL-Institute for Snow and Avalanche Research SLF, Switzerland

<sup>3</sup> WSL-Institute for Snow and Avalanche Research SLF, Switzerland

<sup>4</sup> WSL-Institute for Snow and Avalanche Research SLF, Switzerland

<sup>5</sup> WSL-Institute for Snow and Avalanche Research SLF, Switzerland

<sup>6</sup> WSL-Institute for Snow and Avalanche Research SLF, Switzerland

<sup>7</sup> WSL-Institute for Snow and Avalanche Research SLF, Switzerland

<sup>8</sup> WSL-Institute for Snow and Avalanche Research SLF, Switzerland

<sup>9</sup> WSL-Institute for Snow and Avalanche Research SLF, Switzerland

<sup>10</sup> WSL-Institute for Snow and Avalanche Research SLF, Switzerland

<sup>11</sup> WSL-Institute for Snow and Avalanche Research SLF, Switzerland

<sup>12</sup> WSL-Institute for Snow and Avalanche Research SLF, Switzerland

event analysis. More detailed information is provided in the full report (Bründl et al., 2019), which is available in German and French.

## Weather, snow and avalanche situation

The winter started early in 2017. In most areas of the Swiss Alps, snow depth was already above-average by the end of December 2017 and it further increased in the first days of 2018. The snowfall limit during the precipitation period varied and was partly as high as 2000 m a.s.l. In this period, some very large avalanches already occurred and safety measures had to be taken. The main precipitation period started in the evening of 20 January 2018. Until the morning of 23 January 2018, the sum of new snow above 2200 m a.s.l. was 100–150 cm in most regions of the Swiss Alps from the Valais to the lower Engadine.

By the end of the snowfall period snow depth were extraordinarily large. The return periods for the snow depth on 23 January were at many stations between 20 and 100 years compared to the snow depth maximum observed in January (Fig. 1). Most of the stations with a snow depth return period of more than 50 years were located in Valais. Since January 2018 was generally warmer than the long-term average, a strong increase of snow depth with elevation was observed. Snow depth at elevations between 1000 and 1600 m a.s.l. was locally below average in particular on the northern slopes of the Alps.

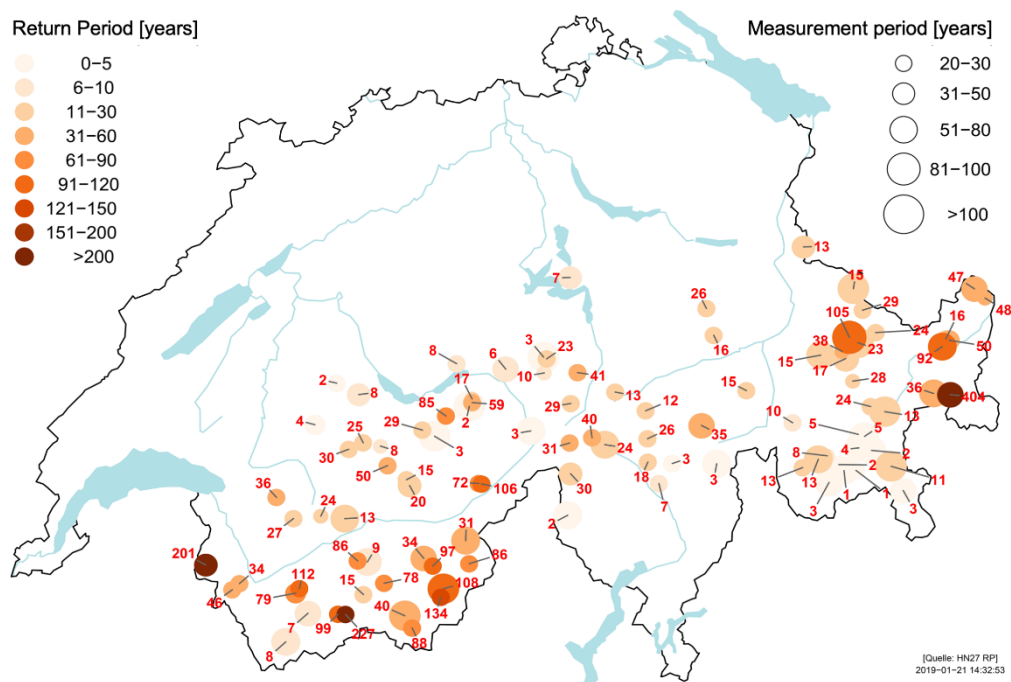


**Figure 1** Return period (numbers in red) of snow depth on 23 January 2018 compared to the maximum values in January at measurement stations above 1500 m a.s.l. The darker the circles the higher the return period. The larger the circles the longer the measurement period.

The 3-day avalanche period from 21 to 23 January 2019 was the most intense since 1999 as expressed with the avalanche activity index (AAI, Schweizer et al. 2003). The AAI is the sum of all observed avalanches weighted by size and type of triggering. On 22 and 23 January many large and very large natural avalanches were observed (size 4 and 5). The highest activity was observed in Valais and northern Grisons (Fig. 2).

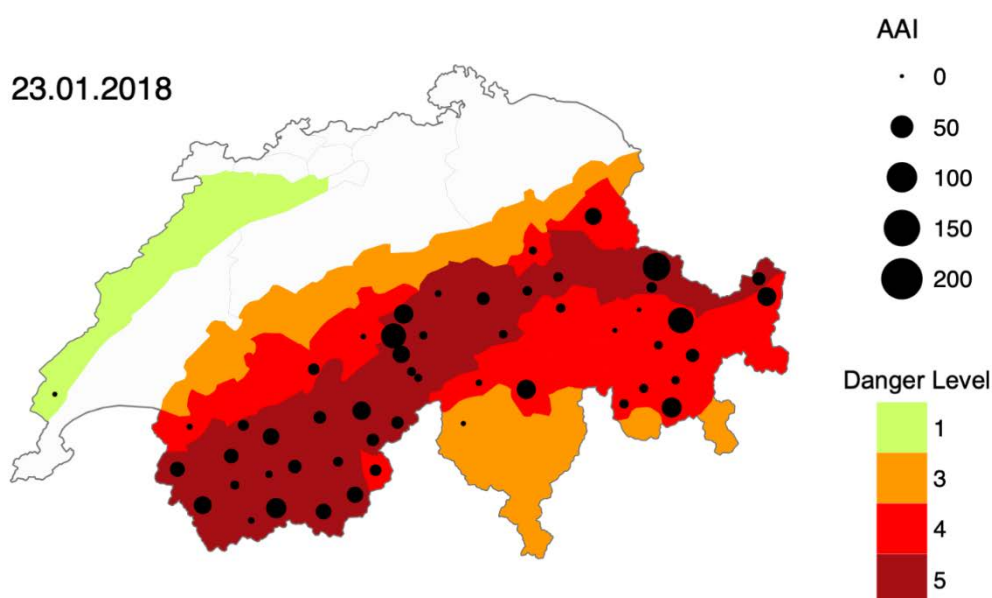


**Figure 2** Avalanche danger level forecast on 22 January, 17:00, for 23 January and avalanches reported by SLF observers expressed as regional avalanche activity index (AAI). Due to poor visibility and accessibility most likely not all avalanches were recorded. The regions with highest avalanche activity roughly coincide with the areas where danger level 5–Very High was forecast.

For the first time, SPOT6 satellite images were used to comprehensively map avalanche activity during an extraordinary avalanche situation (Bühler et al., 2019). On the pictures taken on 24 January 2018, the outlines of in total 18,737 avalanches were manually mapped. Comparing the mapped avalanches with the forecast avalanche danger level allowed verifying the avalanche forecast. Results indicate that the forecast was correct in most regions, with some over- and under-forecasting. For instance, in the region of Davos, the forecast danger level was 4–High and the avalanche activity was very high (AAI≈100) (Fig. 2) suggesting that the danger level 5–Very High would have been more appropriate.

## Damages and interrupted transportation lines

Although the avalanche situation was extraordinary, damages were comparably low and no people were killed in settlements or on roads. Nevertheless, a few avalanches hit inhabited houses, but no people were harmed. According to the SLF avalanche data base, 25 avalanches caused damage to buildings, 55 affected roads, railway and power lines, and 83

avalanches caused damage to forests. Only two permanently inhabited buildings suffered damage; most of property damage concerned agricultural buildings and mountain huts. Snow creep pressure caused damage amounting to 5.7 million Swiss Francs, mostly in Grisons.

Roads and railway lines had to be closed due to avalanche danger. The Gotthard highway had to be closed due to a debris flow and was kept closed due to avalanche danger for 22 hours. The Gotthard railway line had to be closed for 38 hours. Mountain railway lines were closed in total for about 30 days (Fig. 3). Further damages were recorded at power lines and mountain cable ways.

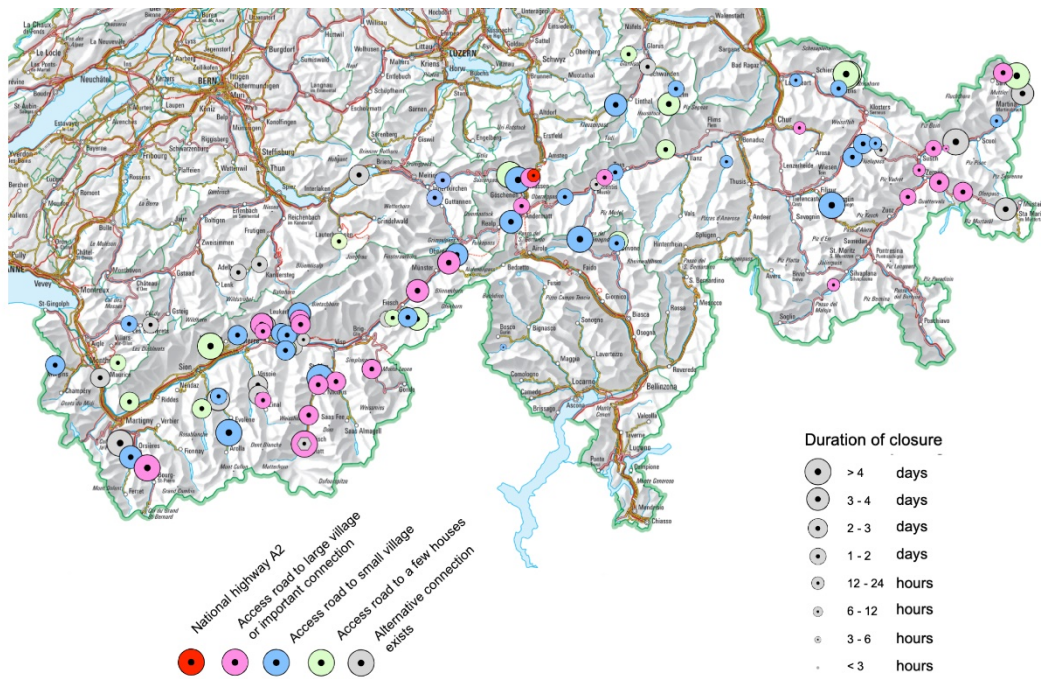


**Figure 3 Road closures between 21 and 25 January 2018. Different colours indicate the relevance of the access road and circle size refers to duration of closure. For instance, the national highway A2 (red circle) had to be closed after a debris flow; due to avalanche danger it was kept closed for 22 hours.**

Damage to forests amounted to 18,000 m<sup>3</sup> of timber. The overall damage was not high considering the extraordinary meteorological event. A few single events significantly contributed to this damage; for instance at Alp da Schlans (Trun, Grisons) an avalanche destroyed 200-year old trees (4,000 m<sup>3</sup> of timber).

## Effectiveness of integral avalanche protection

Integral avalanche protection denotes the combination of various mitigation measures such as structural measures, land use planning, biological measures and organizational measures including artificial avalanche release. Integral avalanche protection has been considerably improved in Switzerland in the last decades. The analysis of the avalanche winter 1999

showed that integral avalanche protection had stood the test. Some gaps were identified in all fields of integral avalanche protection but mainly concerning organizational measures. Most of the issues identified, such as the revision of hazard maps in areas where avalanches exceeded the limits of red or blue zones, or the construction of additional permanent avalanche protection were addressed in the last 20 years.

Snow depths were unusually high and many snow supporting structures were almost filled with snow by the end of the precipitation period in January. Since maximum snow depth is usually observed in April at the elevation of most starting zones, there were concerns that the structures could be fully covered with snow in the further course of the winter. As February and March were dryer than on average, only locally some supporting structures were fully buried. In most of the structures, the maximum snow depth was 1 – 2 m below the 100-year return period snow depth. Nevertheless, the large snow loads caused some damages at supporting structures such as bent supports or tilted or broken beams. Overall, the damage to structures was lower than in the avalanche winter 1999.

In 2018, 98% of the communities with avalanche exposed areas, had avalanche hazard maps implemented in communal land use planning. Very few avalanches did run beyond the limits of existing hazard zones. This positive outcome was related to rain at lower elevations. Between 1000 and 1600 m a.s.l., the snowpack was moist at the surface, which contributed to comparably short runout distances due to a change in flow regime from dry to wet. In areas with high avalanche activity such as the Saas and the Matter valley, many avalanches stopped within the red hazard zone and only some avalanches reached the blue hazard zone. Whereas no avalanches exceeded the hazard zones in the main flow direction, some avalanches laterally did run past the limits.

Evaluating the work of local avalanche safety services during the avalanches situation in February 1999 revealed a need for improving training, organization and communication between the services as well as between the national forecasting centre at SLF and local services. In response to these findings, the project “Intercantonal early warning and crisis information system IFKIS” was initialized in 2000. It included the development of an education and training programme for avalanche professionals, a checklist for the organization of avalanche safety services and the development and implementation of an information system (Bründl et al., 2004).

To assess the effectiveness of these measures taken after the avalanche winter 1999, we conducted interviews with 36 members of in total nine local avalanche safety services. The interviews revealed that safety services were much better organised and trained in January 2018 than in 1999. Most of the members of these services attended the basic and advanced courses “Snow and Avalanches” annually organised by the SLF. Since 2000, far more than 1000 people attended these courses, conducted alternatively in German, French and Italian. The analysis also showed that responsibilities should to be defined more clearly in some services, e.g. with regard to information and/or evacuation of remote buildings or the closure of road sections, where responsibilities of communities and road departments

overlap. Many services face difficulties in recruiting junior staff, as some of the experienced members in leading positions will retire in the next years.

The safety services stated that the available weather and snow related information has much improved since 1999. However, due to the change from the information system IFKIS introduced after the winter 1999 to the Common Information Platform GIN (Heil et al., 2014) after the floodings in 2005, they complained about the complexity and the decreasing user-friendliness of the information systems. They asked for a simple information system available on mobile devices, where the relevant information can easily be accessed and interpreted right in the field, where they have to make their decisions. Many avalanche safety services had to deal with glide-snow avalanches, which proved very difficult since their release can hardly be predicted. Moreover, many services were challenged by the varying snowfall limit. It was unclear how rain at mid and low elevations affected snow instability and avalanche runout.

In recent years, artificial avalanche release has become an indispensable part of integral avalanche protection. The number of remote avalanche control systems (RACS) such as gas exploders (Gazex) or avalanche towers (Inauen-Schätti or Wyssen) has much increased in the last years. In March 2018, 550 systems were in operational use in Switzerland, including about 250 for the protection of settlements, roads or railway lines; in comparison, in 1999, only 25 systems were in use. The RACS worked very reliably and only a few problems were recorded.

Alarm systems in avalanche tracks automatically close traffic routes when sensors register an avalanche release. The number of systems increased from four in 1999 to about 30 in 2018. The interviewed avalanche professionals reported that these systems worked very reliably. Doppler-radar systems observing avalanche tracks from the opposite slope detected many avalanches and infrasound systems for detecting avalanche releases provided useful information supporting safety services in their decisions. We conclude that thanks to better training and organization of avalanche safety services as well as technological advances, the effectiveness of organisational measures greatly improved since 1999.

## Conclusions

Although the new snow amounts and snow depths were extraordinary resulting in very high avalanche activity, the avalanche situation in January 2018 was less severe than in February 1999. Analysing the events showed that investments in improving integral avalanche protection taken since 1999 – especially with regard to organisational and temporary preventive measures – have paid off. Technological progress and modern information systems, well-educated and well-organised avalanche professionals working in communities and for infrastructure providers all contributed to improved avalanche safety. In settlements and on transportation routes, no people were killed during the days in January 2018 when the highest avalanche danger level was forecasted for most regions of the Swiss Alps. The analysis also showed that processes such as glide-snow avalanches are

still not sufficiently understood and that the effect of climate change on the formation and dynamics of snow avalanches requires further research.

## Acknowledgements

We thank the Federal Office for the Environment FOEN for financially supporting the event analysis and the commission for avalanche and rockfall protection under the lead of Reto Baumann (FOEN) for valuable comments on the analysis and its conclusions.

## References

Bründl, M., Etter, H.-J., Steiniger, M., Klingler, Ch., Rhyner, J., Ammann, W. J. (2004). "IFKIS – a basis for managing avalanche risk in settlements and on roads in Switzerland." *Natural Hazards and Earth System Sciences* 4: 257–262.

Bründl, M., Hafner, E., Bebi, P., Bühler, Y., Margreth, S., Marty, C., Schaer, M., Stoffel, L., Techel, F., Winkler, K., Zweifel, B., Schweizer, J. (2019). Ereignisanalyse Lawinensituation im Januar 2018. WSL Berichte, Heft 76, Davos und Birmensdorf, 162p.

Bühler, Y., Hafner, D., Zweifel, B., Zesiger, M., Heisig, H. (2019). "Where are the avalanches? Rapid mapping of a large snow avalanche period with optical satellites." *The Cryosphere Discuss.* 2019: 1-21.

Heil, B., et al. (2014). "The common information platform for natural hazards in Switzerland." *Natural Hazards* 70(3): 1673-1687.

Schweizer, J., Kronholm, K. and Wiesinger, T., 2003. Verification of regional snowpack stability and avalanche danger. *Cold Reg. Sci. Technol.*, 37(3): 277-288.

# Local natural hazard advisors – a concept and its implementation

Manuel Häberli<sup>1</sup>, Roderick Kühne<sup>2</sup>, Wanda Wicki<sup>3</sup>, Gian Reto Bezzola<sup>4</sup>

**Keywords:** natural hazard advisors; division of tasks between levels of government; emergency planning and intervention; civil staff unit; local knowledge

## Abstract

Analysis of major natural hazard events in Switzerland in the recent past has shown that local expertise is a crucial prerequisite for dealing successfully with such incidents. Civil staff units and emergency services are particularly reliant on local expert advice. With this in mind, the concept of local natural hazard advisors was developed in Switzerland in 2010. Their main purpose is to provide specialist advice for civil staff units and emergency services during planning of measures and during intervention, particularly at the local and regional level. The concept is embedded in a larger package of measures designed to optimise natural hazard warnings and alerts. The concept and its implementation is explained and exemplarily illustrated for the canton of Graubünden.

## Introduction

In Switzerland, the responsibility for dealing with natural hazard events lies with the communes (i.e. local authorities, also sometimes referred to as municipalities). In the case of major incidents, they may be supported by the relevant canton and the federal government, in accordance with the subsidiarity principle. Analyses of events such as the floods in 2005 and 2007 (Bezzola and Hegg 2008, Bezzola and Ruf 2009) have shown that appropriate local expertise to manage the intervention during such events was not sufficient. Local Civil staff units (the local bodies tasked with managing and coordinating responses to disasters and emergencies) and emergency services are particularly dependent on local expert knowledge in order to assess the situation, to interpret forecasts in the local context and thus to trigger and manage emergency measures (Buser et al. 2012). Therefore, a project was started 2010 in Switzerland with the aim to build up capacity for emergency management with local natural hazard advisors (LNHA) for civil staff units. Training local natural hazard advisors to ensure local expertise is an measure embedded within a larger action plan to optimize warning and alerts in the event of natural hazards, known as the OWARNA project (Wernli-Schärer et al. 2016).

---

<sup>1</sup> Scientific Officer, Federal Office for the Environment FOEN, Hazard Prevention Division, SWITZERLAND, [manuel.haeberli@bafu.admin.ch](mailto:manuel.haeberli@bafu.admin.ch)

<sup>2</sup> Office for Forestry and Natural Hazards, Canton of Graubünden

<sup>3</sup> MSc., Federal Office for the Environment (FOEN), Hazard Prevention Division

<sup>4</sup> Dr., Federal Office for the Environment (FOEN), Hazard Prevention Division

## Concept of local natural hazard advisors

The LNHA role was developed based on the findings of the 2005 and 2007 event analyses. The main tasks of LNHAs are to interpret warnings, measurement data and observations in the local context and thus to advise and support local and regional staff units and emergency services with their local expertise during events. They also assist local authorities with emergency planning and management of natural hazard events.

Each of Switzerland's three levels of government – Confederation, cantons and communes – has a specific role to play in relation to this training (Fig. 1). There is no legal obligation to establish the LNHA role within individual communes. LNHA training takes place on a voluntary basis.

However, the Confederation supports the cantons by providing the training documents in German and French and dispensing basic training to the cantonal trainers, covering both technical and teaching aspects. In addition, the cantons receive financial assistance to help them customise and carry out their training.

## Cantonal trainers trained by federal trainers

For the past ten years, the Federal Office for the Environment (FOEN) has been providing basic 'train the trainer' training to cantonal trainers, who then train the actual LNHAs in the communes and regions (Fig. 1).

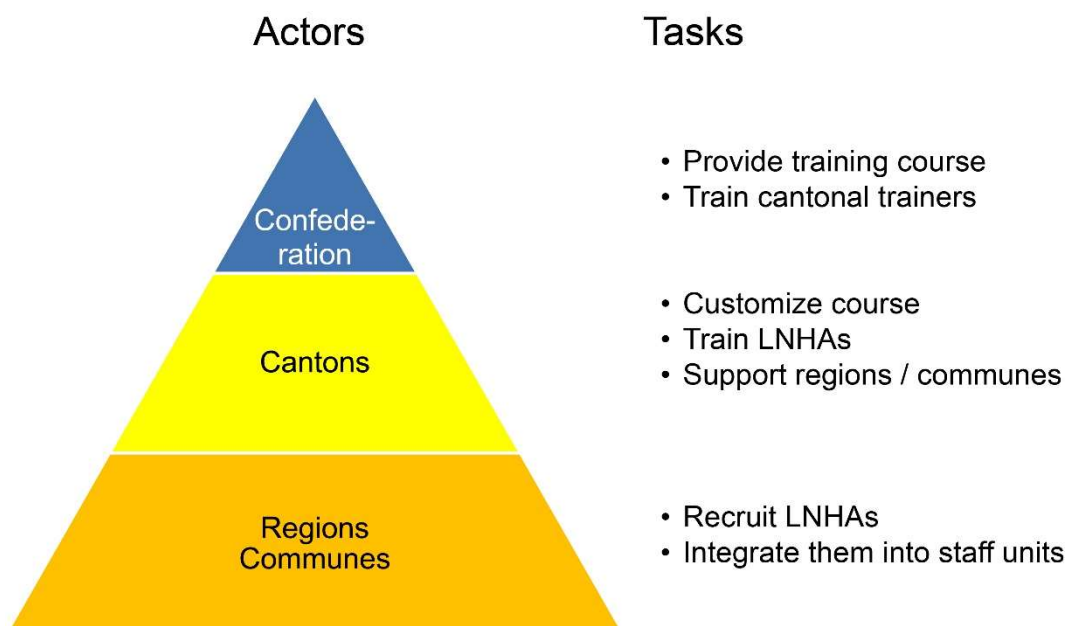


Figure 1: Tasks of the Confederation, cantons and regions/communes in training local natural hazard advisors for civil staff units.

The basic training is modular and tailored to the needs of the cantons. It covers topics such as meteorology, runoff and flood generation, geological mass movements, dealing with hazard data and documentation, occupational safety, information gathering, basic methodological and teaching techniques and staff work.

In addition to the basic training, the FOEN also offers continuing training courses and annual exchanges of experience covering recent events and the latest developments in forecasts and warnings. In the last ten years, a total of 108 individuals from 24 cantons have qualified as cantonal trainers.

## Differing implementation in cantons

The LNHA role is implemented differently in each canton, depending on topographical, geological and organisational factors and the canton's risk assessments (Fig. 2).

Ideally, there should be trained LNHAs for every commune. Local authorities are therefore recruiting suitable individuals with an interest in and understanding of natural hazards, and in particular with a high level of local knowledge.

However, cantons like e.g. Fribourg, communes group together and operate a regional staff unit, into which the LNHAs are integrated. Cantons like e.g. Lucerne and Uri make use of specialists at the cantonal level, thereby providing a pool of experts.

To date, a total of 390 LNHAs have been trained in 17 cantons across Switzerland.

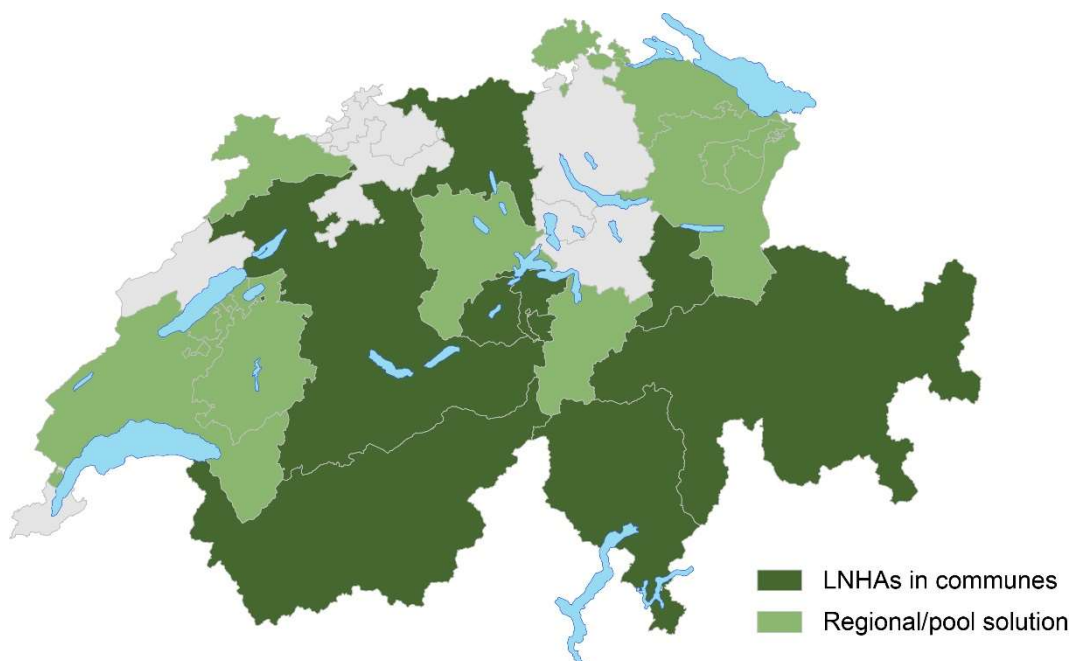


Figure 2: Different implementation models for LNHAs in the cantons.

The following section describes how the LNHA role is implemented, taking the canton of Graubünden as an example.

## **Need for local natural hazard advisors in Graubünden**

In several parts of the canton of Graubünden, structural protection measures have reached the limits of what is technically feasible and cost-effective. An integrated approach to managing natural risks is required, one in which organisational measures are deployed alongside, and on a par with, technical and spatial planning measures.

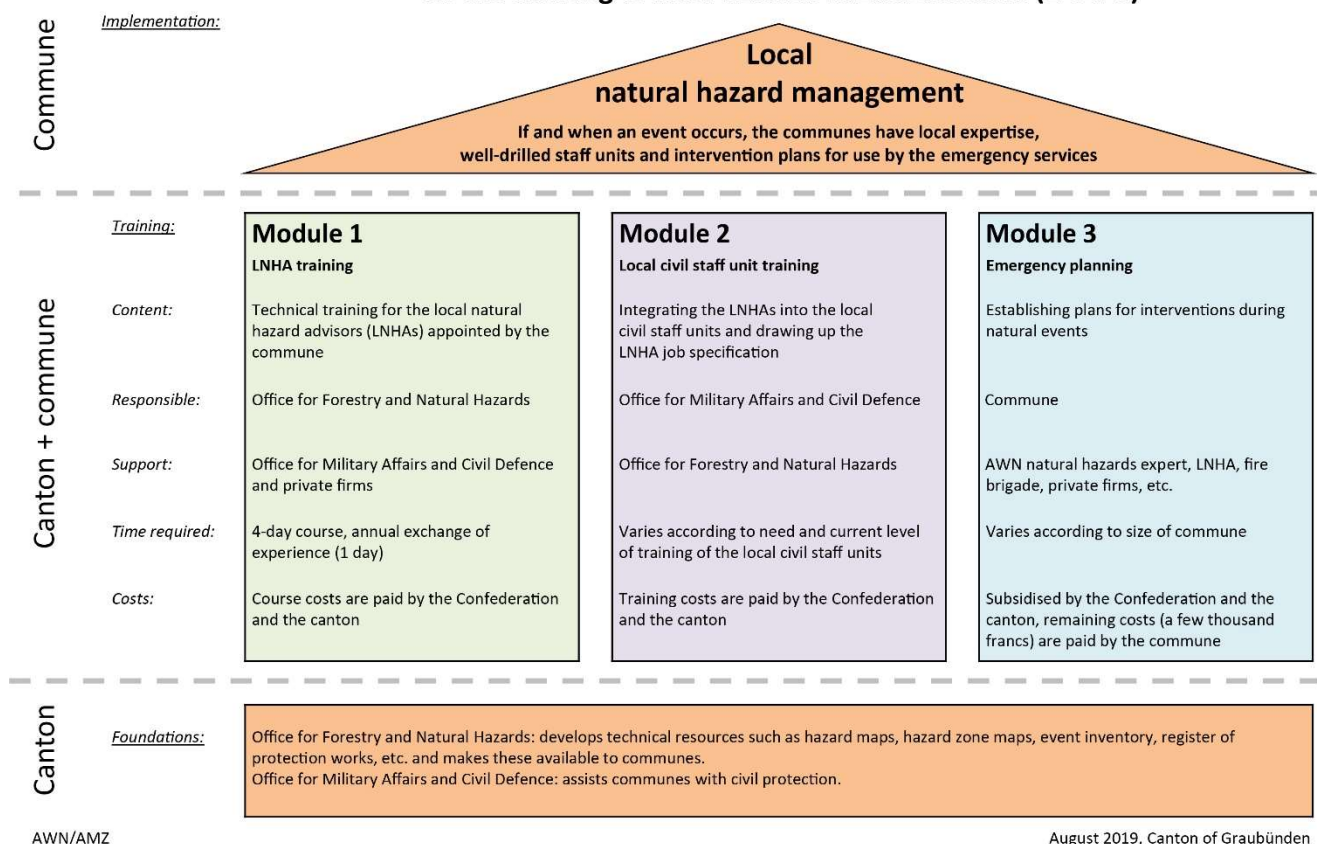
In a mountainous canton such as Graubünden, dealing with natural hazards and managing hazard events has always been a necessity. Many communes have organisational structures geared to this objective, often originating in avalanche warning services. Exceptional weather events such as that in Graubünden in 2002 (Wilhelm 2003) and the one that occurred throughout Switzerland in 2005 showed that in Graubünden, there was a need for improvement of emergency planning and management of natural hazard events. Particular needs identified included improving local expertise, forging networks among decision-makers and strengthening staff units. These findings at the cantonal level are in line with findings of the national analysis of the floods in 2005.

In 2011, the canton of Graubünden reviewed the role of LNHA's and conducted a needs assessment in its then 176 communes. This clearly identified a need for LNHA's in the communes as well as highlighting shortcomings in basic knowledge and management structures. These findings served as a basis for the three-tier concept described below.

## **Training of local natural hazard advisors in Graubünden**

The Graubünden Office for Forestry and Natural Hazards (Amt für Wald und Naturgefahren AWN) developed the three-tier 'Local natural hazard management' concept in 2012, with the aim of strengthening local competencies in dealing with such events (Fig. 3).

## Cooperation in the canton of Graubünden and its communes on the training of local natural hazard advisors (LNHAs)



AWN/AMZ

August 2019, Canton of Graubünden

**Figure 3: The three-tier concept for local natural hazard management in the canton of Graubünden.**

Given the canton's geography (size, limited accessibility in case of events, different weather regions), it was clear from the outset that a local solution, involving one LNHA per commune, should be implemented. This was also in line with federal specifications.

In their expert capacity, LNHAs have a seat on the Local Civil staff units, the body responsible for managing the response in the event of a disaster or emergency in the commune. LNHAs are often recruited from the ranks of local foresters, who know their regions very well.

Module 1 is a technical four-day basic training course for LNHAs. The content of the training follows federal specifications. Module 2 represents a special training comprising the working principles of civil staff units, whereas module 3 focusses on the elaboration of emergency plans.

Basic training for LNHAs takes place annually in the form of a four-day course with up to 14 participants. The course contents are taught by instructors from the cantonal authorities as well as by external specialists. The training prioritises practical relevance and the involvement of already trained LNHAs, who can pass on their personal experiences.

Additional follow-up training is also a key element of the process. A cantonal exchange of experience takes place every two years, at which LNHA's tasks and experiences are examined and shared using a case study. The aim of this continuing training is to consolidate and expand knowledge and allow LNHA's to share their practical experiences for the benefit of their colleagues (Fig. 4). Last but not least, the events also serve as a networking opportunity.

Communes' participation in the programme is voluntary. The LNHA's are often recruited amongst municipal employees. Working hours and remuneration are thus regulated by the communes. As a rule, the district forester carries out the LNGB activity because he has very good local knowledge, is networked with the community leaders and is usually familiar with the relevant hazard processes. Due to the obvious added value of an LNGB for the community, the recruitment is usually smooth after initial persuasion.

As an incentive, communes with a trained LNHA and a signed job specification document receive 5% higher subsidy rates for the construction of technical protection structures.



Figure 4: Local natural hazard advisors undergoing continuing training based on a case study.

## Tasks of local natural hazard advisors in Graubünden

The tasks of an LNHA are divided into precautionary planning, event management and event follow-up. When an event is likely to occur, LNHA's inform the authorities. They observe and assess the natural hazard situation and its development. They provide expert advice to the staff unit and emergency services about how the event might develop, areas at risk and measures that could be taken. After the event, they examine whether the hazard data and documentation and emergency plans need to be updated, and ensure that the event is logged in the StorMe event inventory (FOEN 2019).

## **Impact and evaluation of local natural hazard advisors in Graubünden**

LNHAs have proved their worth in dealing with various natural hazard events in communes. The presence of trained LNHA means that communes have an expert who can assist the authorities and, where appropriate, the emergency services in dealing with events.

Often, training an LNHA triggers a process within the commune that goes far beyond event management. Better use is made of emergency plans, organisational measures are consolidated and there is a growing awareness of integrated risk management. Local Civil staff unit structures and processes are further developed and risk dialogue with the population is enhanced.

For the cantonal authorities, LNHA act as 'sensors', flagging up the needs and challenges faced by communes and helping it to provide more effective support. Joint implementation of the three-tier 'Local natural hazard management' concept strengthens cooperation between the cantonal authorities and the communes, thereby consolidating the integrated system of civil protection.

The goal of including at least one trained LNHA in the staff unit of each commune has been almost completely achieved in the canton of Graubünden. Only a few communes (11) do not yet have this role in place. Further training courses will be held over the next few years to ensure that deputies are available and to avoid problems when LNHA leave their posts. LNHA training is a long-term task but one that can be considered a real success story for the canton.

The feedback from participants is extremely positive and the course is meeting a genuine need within the communes.

## **Challenges and outlook from the cantonal perspective**

Implementing the concept presents a number of challenges. First and foremost, it is simply impossible to teach all the complexities of natural hazard management on a four-day course. Specific further training is therefore key to advancing LNHA's technical expertise.

Equally, communes need to recognise the added value of the LNHA role and give it the priority it deserves. A number of recent events like the rockfall in Val Strem of March 2016 near Tujetsch, Fig. 4) and the flood and debris flow events on June 2019 in Splügen have opened their eyes in this respect.

Probably the biggest challenge is to maintain the level of awareness and knowledge as well as to ensure functioning event management structures. Consequently, another long-term task is ensuring that communes are as well prepared as possible to perform their tasks if and when an event occurs.

At the cantonal level, the assignment of tasks within the three modules has highlighted a need to clarify responsibilities. A need for legislation has also been identified to ensure that the newly launched activities are underpinned by a sound legal basis. With the ongoing revision of the cantonal forest law and the "Ordinance on Integral Risk Management", this requirement is now being met.

## **Conclusion from the cantonal and federal perspective**

With the three-tier concept, the canton of Graubünden has responded to the above-mentioned challenge as well as to the national OWARNA action plan and taken the necessary steps to address them.

Thus, the role of the LNHA embeds the issue of natural hazards within the commune and triggers various follow-up processes. By networking all stakeholders and developing a common risk culture, the three-pillar principle contributes significantly to strengthening the integrated system of natural hazard management. Training LNHA's in the canton of Graubünden has delivered real added value at comparatively little cost, in terms of both natural event management and also the general strengthening and enhancement of organisational measures in accordance with the initial objective.

As stated in the Swiss strategy on 'Management of Risks from Natural Hazards' (PLANAT 2018), the Swiss authorities believe that there is a need to raise and maintain awareness among all those who may be affected by natural events. This also requires a further expansion of the LNHA role.

Many communes rarely have the opportunity to gain experience in event management, so it is important for them to be able to learn and benefit from events in other communes. Given the ever more intensive use of space, increasing mobility and expected climatic changes (NCCS 2018), experts and institutions at the federal, cantonal and communal levels will need to adapt to new challenges.

## **References**

Bezzola G. R., Hegg C., Koschni A. (2008) Synthesis report on the event analysis: The floods of 2005 in Switzerland. Federal Department for the Environment, Transport, Energy and Communications DETEC. Bern.

<https://www.bafu.admin.ch/bafu/en/home/topics/natural-hazards/publications-studies/publications/the-floods-of-2005-in-switzerland.html>

Bezzola G. R., Ruf W. (ed.) (2009) Ereignisanalyse Hochwasser August 2007. Analyse der Mete- und Abflussvorhersagen; vertiefte Analyse der Hochwasserregulierung der Jurarandgewässer. Umwelt-Wissen No. 0927. Federal Office for the Environment, Bern.

<https://www.bafu.admin.ch/bafu/de/home/themen/wasser/publikationen-studien/publikationen-wasser/ereignisanalyse-hochwasser-august-2007.html>

Buser M., Bezzola G. R., Wicki W., Mani P. (2012) Local natural hazards advisors for civil staff units. *Interpraevent 2012*. Volume EA: 68–69.

FOEN (ed.) (2018) Optimierung der Warnung und Alarmierung OWARNA: zweiter Folgebericht. Steering Committee Intervention in Natural Hazards. Federal Department for the Environment, Transport, Energy and Communications DETEC. Bern.  
<https://www.news.admin.ch/news/message/attachments/52033.pdf>

FOEN (2019) Naturereigniskataster StorMe. Federal Department for the Environment, Transport, Energy and Communications DETEC. Bern.  
<https://www.bafu.admin.ch/bafu/de/home/themen/naturgefahren/fachinformationen/naturgefahrensituation-und-raumnutzung/gefahrengrundlagen/naturereigniskataster-storme.html>

NCCS (ed.) (2018) CH2018 Climate scenarios for Switzerland. National Centre for Climate Services. Zurich. <https://www.nccs.admin.ch/nccs/en/home/climate-change-and-impacts/swiss-climate-change-scenarios.html>

PLANAT (2018) Management of Risks from Natural Hazards. Strategy 2018. National Platform for Natural Hazards PLANAT. Bern. <http://www.planat.ch/en/strategy2018/>

Wernli-Schärer L., Bialek R., Buser M., Flury Ch., Gerber B., Haslinger F., Hegg Ch., Ottmer B., Overney O., Romang H., Schmutz Ch., Schweizer J. (2016) Strategies for the reduction of natural hazards damages by optimized warning, alarming and intervention in Switzerland. *Interpraevent 2016*. Volume 1: 1005–1013.

Wilhelm C. (2003) Unwetter 2002 – Ein Überblick. In: *Bündner Wald* No. 3/03, Volume 56: 5–9. Überblick. In: *Bündner Wald* No. 3/03, Volume 56: 5–9.

---

# Knowledge and perception of natural hazards: results from population surveys to innovate risk communication

Lydia Pedoth<sup>1</sup>, Agnieszka Elzbieta Stawinoga<sup>2</sup>, Gernot Koboltschnig<sup>3</sup>, Willigis Gallmetzer<sup>4</sup>, Pierpaolo Macconi<sup>5</sup>, Sönke Hartmann<sup>6</sup>, Stefan Schneiderbauer<sup>7</sup>, Doris Damyanovic<sup>8</sup>

**Keywords:** Risk governance; risk perception; risk communication; Alps

## Abstract

This paper shows results from a population survey carried out in South Tyrol (Italy) and in Carinthia (Austria) as part of the Interreg Italy-Austria Project “RiKoST-Risk communication strategies” that aims at improved, target-group-oriented risk communication. The aim of the survey is to assess people’s 1) state of knowledge about natural hazards, 2) risk perception 3) suggestions on how to improve risk communication. A better understanding and information about these aspects are crucial for risk communication activities. The data were collected in 13 municipalities in South Tyrol and Carinthia using questionnaires. Results show that there is a lack of knowledge about existing hazard maps and that respondents want to be better informed and more involved but that at the same time they delegate the responsibilities in risk management to institutions. Thanks to the close collaboration between researchers and practitioners the results of the survey will be implemented in practice for the development of new risk communication tools and the improvement of existing measures.

## Introduction

In the Alps the management of the risks linked to natural hazards has a long tradition. In the last decades academia and public authorities invested substantial efforts in generating and improving knowledge about hazardous processes and in collecting and mapping data (Permanent Secretariat of the Alpine Convention, 2019). The results are sound models and detailed hazard maps that are crucial for risk management but that are not elaborated as a tool for risk communication. Hazard maps are preliminary an expert tool, but the content of these maps is of relevance and should be known and have an impact on people’s actions. In order to change people’s behavior, these maps have to be integrated in a complementary

---

<sup>1</sup> Researcher, Eurac Research, ITALY, ([lydia.pedoth@eurac.edu](mailto:lydia.pedoth@eurac.edu))

<sup>2,6</sup> Eurac Research

<sup>3</sup> Regional Government of Carinthia

<sup>4,5</sup> Agency for Civil Protection, Autonomous Province of Bolzano- South Tyrol

<sup>7</sup> Eurac Research and United Nations University, Institute for Environment and Human Security

<sup>8</sup> University of Natural Resources and Life Sciences Vienna

risk communication strategy and the content has to be tailored to different target groups' needs (Wenk et al., 2018, Hagemeyer-Klose & Wagner, 2009). The existing knowledge must be adapted and transmitted whilst ensuring that it is useful, usable and used by practitioners, policy makers and potentially affected people (Boaz and Hayden, 2002). The latter can, if they are well informed and willing to actively engage and undertake private precautionary measures, support and contribute to risk management. This clearly shows why risk communication plays a crucial role but at the same time it also raises questions for public authorities such as: how should an effective risk communication strategy look like in order to reach people and have an impact on their behaviour? how should messages be designed and what channels (e.g. radio, television, sms, internet, newspapers) should be used? What do people know about natural hazards and how do they perceive risks? All this information is crucial for local authorities to be able to design and implement innovative risk communication tools, that can follow different goals such as information exchange but also awareness building or legitimisation of decision making (Renn, 1992; Höppner et al., 2012). Nowadays risk communication often occurs unidirectional without the interaction of institutions, stakeholders and the population. The lack of innovative and adaptive communication strategies means that technical knowledge is not communicated in a way that reaches and can be understood by a non-expert audience. Whether or not risk communication is successful is also strongly connected to people's risk perception. Risk perception is multifaceted and complex as several concepts show (Maidl & Buchecker 2015, Kellens et al. 2013) and is influenced by factors such knowledge, experience, values, attitudes, and emotions (Wachinger et al., 2013) as well as cultural determinants (Macgill, 1989). The use of questionnaires is a valid method to assess people's risk perception and the generated results can give important inputs for risk communication.

This contribution shows results from the Interreg Italy-Austria Project "RiKoST - Risk communication strategies". The project is a collaboration between partners from research and public authorities and aims at improved, target-group-oriented risk communication in South Tyrol (Italy) and Carinthia (Austria). One of the project's work packages carried out a population survey on knowledge about natural hazards and risk perception in selected municipalities in South Tyrol and in Carinthia. The reason behind is that knowing what people think about natural hazards, what structural and non-structural measures they know and how they perceive risks linked to natural hazards is considered an important starting point for the development of new and the improvement of existing risk communication tools and activities. The aim of the survey is to collect data about people's 1) state of knowledge about natural hazards, 2) risk perception 3) suggestions for the improvement of risk communication. Previous studies have shown that living in an area of risk does not automatically mean to be prepared (Pedoth et al., 2018). The collected data should give a better understanding about the relationship between knowledge, perception and preparedness and about the influencing factors of these three aspects. In South Tyrol, the Agency for civil protection uses the results of the survey as input for the development of a new online platform about natural hazards. In Carinthia, the results are used to adapt the communication within the process of hazard mapping and the elaboration of contingency plans.

## Methods

We selected 13 municipalities (8 in South Tyrol and 5 in Carinthia) for the population survey. In South Tyrol, the criteria for the selection of the pilot municipalities were 1) the size of the municipalities (small rural municipalities and urban municipality) 2) natural hazard events (municipalities that recently experienced a natural hazard event and municipalities that did not) and 3) the existence of natural hazard maps. This last criterion was selected because in South Tyrol natural hazard maps are a recently introduced legal binding planning instrument developed at municipality level. At this stage, about half of the municipalities have an approved hazard map. By selecting four municipalities that have an approved hazard map and four without we wanted to investigate if the introduction of such a plan has an impact on the knowledge, the risk perception, the feeling of safety and the actions and behavior of the population. In Carinthia, we selected municipalities with bilingual (Slovenian speaking) population that recently experienced flood events and where therefore exists a need and interest in improving existing risk communication activities and tools. We performed an extensive literature review about the state of the art of research in the field of risk communication and risk perception, about most important underlying theories and conceptual frameworks and about existing good practices. Based on the results of this review we developed a questionnaire to assess and better understand people's knowledge, perception and behavior linked to risks from natural hazards, including information about most used communication channels and perceived responsibilities in risk management. The questionnaire contains a total number of 42 questions of different types (e.g. multiple answers, Likert scale, open question) and is divided in four sections: 1) Knowledge about natural hazards, 2) Risk perception, 3) Responsibilities in risk management including the role of citizens and 4) suggestions on how to improve existing risk management activities with a focus on risk communication. For each respondent we collected also socio-demographic data such as age, gender, education, profession, length of residency, owner or tenant. The data were collected between June and August 2019. We used the same questionnaire in South Tyrol and in Carinthia, but the data collection method differed. In South Tyrol the data were collected through Computer Assisted Telephone Interviews (CATI) and Computer Assisted Personal Interviews (CAPI) of about 20 minutes in order to obtain a representative sample of full age residents. In Carinthia 8234 questionnaires were sent via post mail as an official communication from the regional government to all registered addresses in the municipalities. Due to the different data collection method, only data from South Tyrol can be considered representative. A total of 2292 answers to the questionnaire were collected, 1410 in South Tyrol and 882 in Carinthia (nearly 11% return rate). Subsequently, the data were analysed separately for the two regions using SPSS software (SPSS Inc., 2017). Descriptive statistics such as frequencies for categorical variables and mean values for Likert scale variables were calculated in order to explore the profile of the sample and the main emerging results related to knowledge about natural hazards and risk perception. As in South Tyrol only half of municipalities has a natural hazard map, we wanted to understand if the knowledge declared by the respondents (either "yes, my municipality has a natural hazard map;" or "no, my municipality do not have a natural hazard map;" or "I do not know") is in line with the real situation. By combining the knowledge about the natural hazard map with the municipality

of respondents, three groups were individuated for which frequencies distribution, an average risk perception and feeling of safety were calculated. Subsequently we identified the 5 most preferred information channels chosen by the three groups. The results are presented in the next section and in Figure 1.

## Results and discussion

In South Tyrol the respondents are 51,3% women and 48,7% men and show a well-balanced and veridic distribution for the different age classes (18-29; 30-39; 40-49; 50-59; 60-69; 70+) with respect to the current age and gender distribution in the municipalities. In terms of education the collected data cover different graduation grades (from elementary school degree to doctorate). Most of the respondents (74,3%) own their house or apartment they live in, 15,5% are tenants and 10,2% are non-commercial tenants. Previous studies showed that an important factor, which influences risk perception, is the perceived probability of being affected by a natural hazard event. Our data show that in South Tyrol the mean perceived probability that the municipality people live in will be affected by a natural hazard event in the upcoming 5 years is 37,8%. The probability that their house will be affected in the upcoming 5 years is perceived as much lower with a mean probability of 25,9%. In Carinthia the mean perceived probability for the municipality being affected in the upcoming 5 years is 62,7% whilst for the own house it is 46,7%. In both regions, respondents think that it is less probable that their house will be affected but in Carinthia both values are much higher than in South Tyrol. One reason for this difference is the fact that in Carinthia all municipalities recently experienced natural hazard events. In December 2017 and November 2018 foehn wind events with storm and flood damages hit the south eastern part of Carinthia and the degree of direct or at least indirect affection was very high.

Two other important aspects resulting from our study tackle the question if people think that the existing structural and non-structural measures are enough to protect the population from natural hazards and what people think about responsibilities in natural hazard management. In South Tyrol 80,4% of respondents stated that the existing measures are sufficient and mentioned the following reasons: 1) natural hazards are well-monitored; 2) there are enough structural protection measures in place in the municipality are and 3) the institutions and the civil protection organizations are well-coordinated and qualified. 8,3% of respondents stated that the existing measures are not sufficient. The main reasons are 1) more structural protection measures are necessary; 2) natural hazards should be better monitored and 3) the citizens are not sufficiently informed and involved. 11,3% stated that they do not know. We also asked respondents to indicate three actors responsible for risk management from a given list of different actors (including institutions, organisations and the themselves as citizens).

Our data show that in South Tyrol respondents think that the Province, the municipality and organisations (such as the voluntary fire brigade) are responsible for risk prevention. When looking at the response and recovery phase the responsible actors are the Province, the national state and the municipality. For prevention as well as for response and recovery, the most important actor is the Province. Respondents clearly think that risk management is the role of institutions (59,4%). One third of respondents (32,9%) states that citizens have

an important role and should be more actively involved. In Carinthia the percentage of respondents that think that the existing measures are sufficient is lower (37,7%) but the 3 main reasons are the same than in South Tyrol. Compared to South Tyrol more respondents said that the measures are not enough (23,6%) but the reasons mentioned are similar to South Tyrol with the difference that respondents in Carinthia mentioned the lack of money as one the three most important reasons. In Carinthia respondents think that the three main actors for the prevention of and the response to natural hazard events are the federal province of Carinthia, the national state and the municipality and that for both phases (prevention and response) the municipality has the most important role. Here we see a difference between the results from the two regions that reflects well the differences in the legal and organisational setting in the field of risk management (in South Tyrol the Province plays a key role for prevention and protection whilst in Carinthia the most important actor in this field is the municipality). In Carinthia, a higher percentage of persons (49,2%) think that citizens should be more involved and should have an active role in risk management and compared to South Tyrol, less respondents (38%) delegate this task to the institutions. Our interpretation is that people who experienced storm events do not expect that institutions could set preventive measures against storms. They feel that it is more helpful to receive information how to get prepared and what action they could undertake as individuals (e.g. buying an electric generator or laying in food storage).

In terms of knowledge about natural hazards as well as for the awareness and preparedness of the population, natural hazard maps are a key instrument and can, if adapted to a non-expert public, play an important role for risk communication (Wenk et al, 2018). Although in Carinthia there is a complete coverage with hazard maps, only 27 % of the respondents know that there are hazard maps available for their municipality. 60 % do not know about hazard maps. In South Tyrol 63,7% state that there is a hazard map for their municipality, 6,5% say there is no hazard map and 29,9% do not know. Considering that actually only half of the South Tyrolean municipality have a hazard map we performed some more detailed analysis combining the knowledge about the natural hazard map with the municipality of residency. Based on the data from South Tyrol we discovered three groups that we divided according to their knowledge about hazard maps (Figure 1). The first group, respondents that have “true” knowledge (47,1%), are persons who say that they know the hazard map and live in municipalities that have approved hazard maps or persons that say that there is no hazard map in municipalities which actually do not have an approved hazard map. The second group are persons that have “false” knowledge (18,6%) because they say that they know the hazard map of their municipality, but they live in municipalities that do not have an approved hazard map. The third group (34,2%) are persons that don’t know if their municipality has a hazard map or persons that say that there is no map in municipalities that have an approved hazard map.

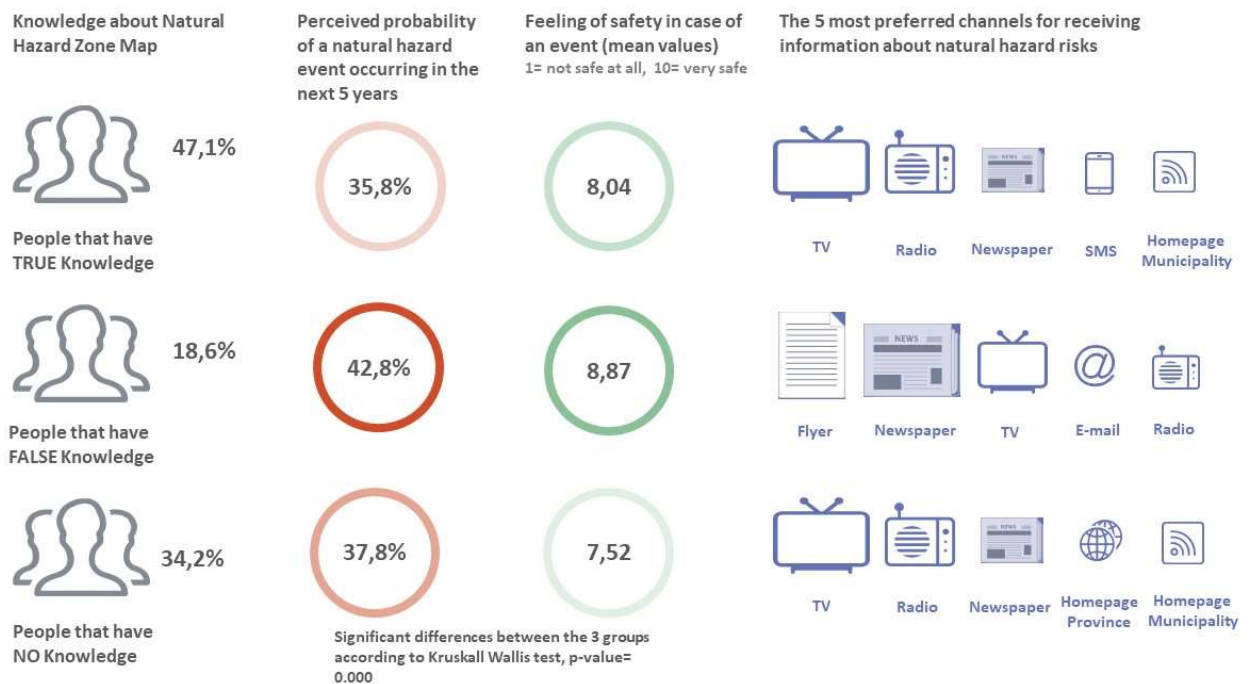


**Figure 1: The figure shows three population groups (individuated by combining respondents' knowledge about natural hazard maps and their municipality of residence) and the risk perception, the feeling of safety and the preferred information channels for each group. The figure is based on data collected in 8 municipalities in South Tyrol.**

Figure 1 shows that the second group, respondents that have false knowledge, perceive the probability of a natural hazard event happening higher compared to the other two groups. At the same time, they feel safer in case of an event happening. Also, in terms of the 5 most preferred information channels for risk communication this group has different preferences. The preferred channel for risk communication for that group is a flyer or information brochure whilst the other two groups choose the television as preferred information channel for risk communication. In terms of risk communication this raises the question why people belonging to this group think to know the hazard map even though it do not exist and how they could be reached and informed about the actual status of hazard mapping in their municipality. As next steps we will discuss these questions together with representatives from the municipalities in order to find possible reasons for this non accurate knowledge. One reason could be that people confound the hazard map with other instruments such as the civil protection plan. Results from the open question about what type of information people would like to receive show, that people ask for more and better information on how they could contribute to the prevention of natural hazard risks, what actions they could undertake and how to best behave before and during natural hazard events. The answers also show that people would like to receive information about natural hazards and related risks not only at the municipality level but also at the level of neighborhood or district.

## Conclusions

Results show that respondents would like to be better informed and receive clear information on what concrete measures they could undertake, in which way they could contribute and how they should behave in case of an event happening. At the same time, respondents tend to delegate the responsibility to institutions. Future work should address the question if more involvement of citizens should also result in more responsibility for example in terms of private precautionary actions.

The aim of the population survey was to generate results that could be used by public authorities to improve risk communication and support the development of new risk communication tools. For Carinthia, part of the replies was nearly as expected, for example that responses came mainly from people directly affected, but some were surprising. We did not expect for example that less than 30% of the respondents know about hazard maps in their municipality and that traditional communication channels such as TV, radio and newspaper are still so important. A surprising and positive result was that nearly 50% of the respondents would like to have a more active role within risk prevention and would like to be better informed about what actions they could undertake. These results show that future risk communication activities in Carinthia should focus on 1) a better information on hazard maps and which consequences they have, 2) individual prevention and protection measures and 3) communication activities that directly address affected people (in addition to communication activities for the whole community) . The regional government of Carinthia will use the results for working out natural hazard contingency plans. Within this process stakeholders as well as the affected population are invited to actively contribute and give input. In this way, the elaboration of such contingency plans can act as opportunity for bringing together different stakeholders and represent a platform for risk communication. In South Tyrol the agency for civil protection is working on the development of a new online platform for different type of information related to natural hazards and will use the results from the survey as input in order to create a tool for risk communication that is tailored to different user groups.

In terms of use and impact of results, this project has an added value because all activities have been developed and carried out together with partners from public authorities. This allows to integrate their knowledge and experiences, for example for the survey design and the development of questionnaires, and gives the opportunity to use the results of population surveys not only for advancing knowledge in terms of risk perception but also for implementing them in practice by supporting the development of new tools and the improvement of existing measures.

## References

Boaz A., Hayden, C. (2002). Pro-active evaluators: enabling research to be useful, usable and used. *Evaluation*. 8 (4), 440-453.

Hagemeier-Klose, M. & K. Wagner (2009). Evaluation of Flood Hazard Maps in Print and Web Mapping Services as Information Tools in Flood Risk Communication. *Natural*

Hazards and Earth System Science 9 (2): 563–74. <https://doi.org/10.5194/nhess-9-563-2009>. Höppner C., Whittle R., Bründl M., Buchecker M. (2012). Linking Social Capacities and Risk Communication in Europe: A Gap between Theory and Practice? *Natural Hazards* 64 (2): 1753–78. <https://doi.org/10.1007/s11069-012-0356-5>.

IBM Corp. Released 2017. IBM SPSS Statistics for Windows, Version 25.0. Armonk, NY: IBM Corp.

Kellens W., Terpstra T., De Maeyer P. (2013). Perception and Communication of Flood Risks: A Systematic Review of Empirical Research: Perception and Communication of Flood Risks. *Risk Analysis* 33 (1): 24–49. DOI: [10.1111/j.1539-6924.2012.01844.x](https://doi.org/10.1111/j.1539-6924.2012.01844.x)

Macgill S. (1989). Risk perception and the public. In: *Environmental Threats: Perception, Analysis and Management* (ed. J. Brown), 48–66. London: Belhaven Press

Maidl E. & Buchecker M. (2015). Raising Risk Preparedness by Flood Risk Communication. *Natural Hazards and Earth System Science* 15 (7): 1577–95. <https://doi.org/10.5194/nhess-15-1577-2015>.

Pedoth L., Taylor R., Kofler C., Stawinoga A., Forrester J., Matin N., and Schneiderbauer S. (2018). The role of risk perception and community networks in preparing for and responding to landslides: a Dolomite case study. In *Framing Community Disaster Resilience: resources, capacities, learning and action*. First Edition. Edited by Hugh Deeming, Maureen Fordham, Christian Kuhlicke, Lydia Pedoth, Stefan Schneiderbauer, and Cheney Shreve. Published 2018 by John Wiley & Sons Ltd. DOI: 10.1002/9781119166047.ch13

Permanent Secretariat of the Alpine Convention (2019). *Natural Hazard Risk Governance – Report on the State of the Alps*. Alpine Convention, Alpine Signals – Special Edition 7. ISBN: 9788897500490.

Renn, O. (1992). Risk Communication: Towards a Rational Discourse with the Public. *Journal of Hazardous Materials* 29 (3): 465–519. [https://doi.org/10.1016/0304-3894\(92\)85047-5](https://doi.org/10.1016/0304-3894(92)85047-5).

Wachinger, G., Renn O., Begg C., Kuhlicke C. (2013). The Risk Perception Paradox- Implications for Governance and Communication of Natural Hazards: The Risk Perception Paradox. *Risk Analysis* 33 (6): 1049–65. <https://doi.org/10.1111/j.1539-6924.2012.01942.x>.

Wenk, M., Neuhold C., Fuchs S. (2018). Zielgruppenspezifische Darstellung von Hochwassergefahren und -risiko. *Österreichische Wasser- und Abfallwirtschaft* 70 (5–6): 328–40. <https://doi.org/10.1007/s00506-018-0470-z>.

---

# Water sensitive planning and building – more acceptance by cooperation and highlighting co-benefits?

Andreas Rimböck<sup>1</sup>

**Keywords:** flood risk management, adapted planning and building, realisation, cooperation

## Abstract

Implementing several tasks of an integrated flood risk management into practice is still a demanding issue. Often other disciplines should react in an appropriate way and therefore, they need to be sensitised regarding the principles of flood risk management. In Bavaria we started some new approaches to reach this target especially in the field of water sensitive planning and building: cooperation between the most important professional associations and highlighting co-benefits coming along with water sensitive planning.

## Introduction

Effective flood risk management requires many different activities by several stakeholders. A very important field of action is to provide flood - adapted land use and to construct water-resistant or at least suitable buildings and infrastructure. We have to sensitize planners and building owners for this topic, otherwise we won't be successful in transforming these - up to now mainly theoretical - thoughts into practised standard action. To achieve this, some new activities were started in Bavaria: cooperation between relevant chambers and associations in the water, planning and building sector and highlighting the co-benefits of such multi-purpose planning principles.

## Situation

Water is the origin of different hazards for our settlement areas, infrastructure facilities and buildings: high discharge in creeks and rivers, high ground water levels, overloaded canalisations or even pluvial floods far away from watercourses after heavy local rainfall can cause big flood hazards. On the other hand, a lack of water can also cause severe troubles, such as droughts or problems with drinking water supply. All these hazards are supposed to increase by the climate change. In 2016 for example in Bavaria occurred severe floods, especially pluvial floods (comp. Rimböck et al 2018), and later in the same year the northern areas of Bavaria were exposed to very dry and hot weather. So modern water management issues have to regard all water balance aspects. Especially while planning our

---

<sup>1</sup> Dr., Wasserwirtschaftsamt Donauwörth, GERMANY, ([A\\_Rimboeck@web.de](mailto:A_Rimboeck@web.de))

villages and towns, both aspects of water management (drought and flood prevention) come close together and the link is climate change adaptation.



**Fig 1: many different aspects of water management within land-use and building planning – left: pluvial floods, right: droughts**

We only can find good, sustainable solutions reaching a wide consensus, if all partners consider these aspects in the planning process from the first beginning. Later amendments normally are technically difficult and expensive. So, the overall target is to sensitize all partners in the planning and design process and to enable them implementing water management issues into the chosen solutions. However, it is to say, that many disciplines have similar demands and so especially urban planners are faced with numerous and often contrary challenges or at least wishes. So, the right balance between sensitising and overloading the partners in the planning and design process has to be found.

In this context we started some new initiatives in Bavaria:

## Methods

### 1. Cooperation between professional associations

In Bavaria the most important chambers and professional associations in this field started a closer cooperation to reach the following goals:

- Sensitise professionals but also the wide public about the topic, to implement and spread water sensitive thoughts and to achieve effective, cheap and sustainable solutions, preferably within a wide consensus
- Make use of synergy effects around water sensitive planning, especially covering aspects like fluvial and pluvial floods, high groundwater and drought precaution as well as biodiversity and liveable cities
- Common attempts to influence politicians, mayors and other important decision makers and partners
- Regard all phases of planning, design and realisation of settlement and commercial areas, buildings and infrastructure (comp. fig. 3)

The collaborating partners in Bavaria and their role in the cooperation are:

- Initiator of the cooperation: The German Association for Water and Waste water and Waste (DWA) - regional Group Bavaria: provides technical experts concerning all water related hazards
- The Bavarian Chamber of Architects: represents the planners in the levels of land use / green planning and the design of buildings
- The Bavarian Chamber of (Civil) Engineer: represents planners within the phase of dimensioning and construction of buildings and infrastructure
- The Bavarian Chamber of Crafts: covers the phase of realisation of buildings and infrastructure with all engaged craftsmen and building firms

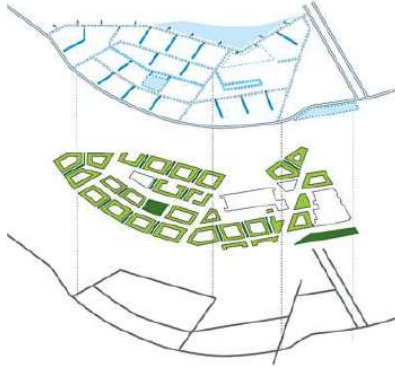


**Fig 2: presentation of the common declaration (22.05.2019) with President Peteranderl (Bavarian Chamber of Crafts), Vice-Chairman Dr. Rimböck and Chairman Prof. Dr. Günthert (regional group Bavaria of DWA), President Degenhart (Bavarian Chamber of Architects) and President Prof. Dr. Gebbeken (Bavarian Chamber of (Civil) Engineers) (from left to right)**

As a first step of the planned cooperation, the leaders signed a common declaration, which primarily addressed the own members and should underline the importance of the topic. By doing this within a press conference, additionally the public and the politicians were informed and a broader discussion should be started.

## Levels for water sensitive planning and building

- Land use planning



- planning of buildings / infrastructure



- construction work / renovation



Fig. 3: different planning levels for water sensitive cities (photos: left: DIFU (2018); Rimböck)

Future planned steps are for example:

- the exchange of technical information and experience (permanent),
- a common series of papers in the member publications (already started),
- common further trainings and
- contacting the universities to implement the topic in the lectures.

Furthermore, public or administrative bodies and the cooperation will coordinate their activities by regular exchange. By this, we try to avoid double work and to look for synergies. Main aim is to identify working fields in which the different actors can reach the targets most easily and so to work “hand in hand”. For example, the management plan of the flood directive includes measures concerning education or awareness rising for planners. In these measures, the cooperation can support the management plan, whereas the flood directive or discussions about climate adaption measures build a reliable foundation for the activities of the cooperation.

One already concrete planned activity by both sides (administration and cooperation) is to publish a booklet with interesting practical examples of suitable planning and building covering all planning levels together. By such a common publishing we hope to reach a much wider dissemination and higher acceptance. Another collaboration between administration and cooperation could be an already planned competition to develop a climate sensitive settlement. In this competition the administration could provide the framework and the cooperation could spread the call for contributions and support jury.

Within this project, the planners also should monetize the advantages of such planning principles.

Additional steps ongoing or planned of the cooperation up to now are:

- Letters to different stakeholders like politicians, mayors, universities ..... by the cooperation, highlighting the importance of the topic
- Consulting the organizer of the trade fair “Bau 2021”, how to implement the topic into the supporting programme
- Contact to other relevant associations or groups, like association of home- and landowners, association of teachers, to exchange knowledge, experience and to sensitize

## 2. Emphasize multi-purpose benefits of water sensitive planning and building

Regarding water hazards include so different hazard processes like fluvial flood, pluvial flood, high groundwater levels or backwater due to overloading of canalisation. Nevertheless, also drought or heat hazards are closely linked to water issues and water balance. Of course, water sensitive planning principles consider all of them.

What’s more, water sensitive planning can help to fulfil some other targets also. This could be a very strong argument in the public discussion. During the talks within the working group to start and implement the cooperation, we agreed on highlighting the multi-purpose use of water sensitive planning and building. Not to remain at the water topic but to emphasize also advantages in many other fields could be a very effective starting point and help to sensitize a wide public.

Modern urban planning is faced by numerous demands, like:

- make best and economic use of the rare land,
- provide an attractive living space,
- concern demographic change and inclusion
- and many more.

This shows that water sensitive planning is just one more aspect that is challenging. Highlighting the co-benefits, which come along with water sensitive planning, like providing water for attractive urban greenspaces, retention or cooling effects for climate change adaption, providing drought precaution and more, could help to emphasise the high need of water sensitive planning especially concerning future climate change. The “picture” of the sponge city is helpful to show those co-benefits and interrelations within the overall target to reach sustainable and liveable cities.

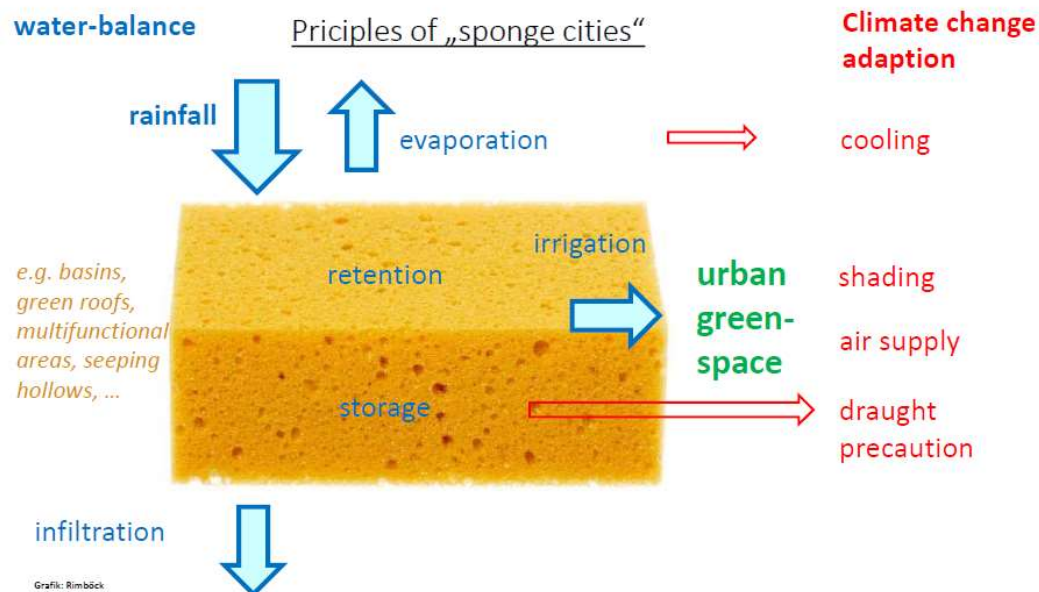


**Fig. 4: the multi-purpose approach “sponge cities” (Rimböck)**

Many synergies can be identified especially regarding the planning of the open spaces in the settlements as water is a key element regarding urban greenspace and climate change. Open spaces often can fulfil multiple purposes. At first, there are no buildings, which could suffer damages in case of natural hazards, so urban greenspace could lie within hazard areas. There they on the one hand can fulfil the function of a recreation or sports area for most of the time. This comes along with positive effects for (urban) climate aspects, providing shade, fresh air and living space for plants, animals and biodiversity. On the other hand, free space could serve as retention basin for some few hours or days. But not only greenspace can fulfil such multi-purpose benefits: for example, also less important streets or parking places can be used as retention areas in case of (pluvial) floods. Finally, such water - sensitive planning is not a contradiction to space – saving planning.



Fig. 5: multi-purpose use of open spaces: park, playground, plantation area during normal times; discharge, retention and infiltration area during heavy rainfall (Atelier Dreiseitl (2019))

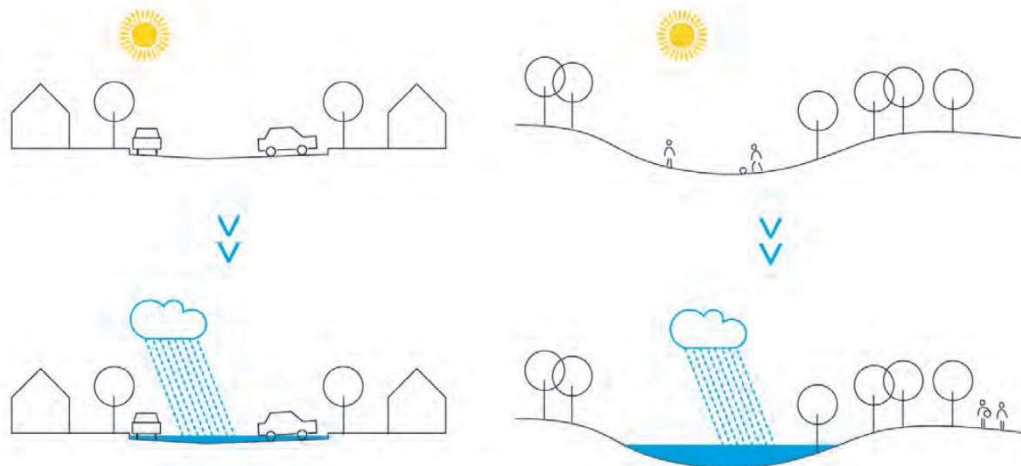


Fig. 6: multiple use of streets (left) or green space (right), (DBU (2019))

## Results and discussion

As many of the introduced activities are quite young, we have no long experience and no robust results up to now. Nevertheless, coming from theory to action within flood risk management is an urgent challenge for all involved parties, so all attempts in this direction are important and could help us for the future.

Our attempt of an intense cooperation between relevant associations should support education, sensitization and knowledge about water sensitive planning and building and should help to transfer these principles into practical action. The talks to prepare the cooperation helped us to gain a common understanding and to see the challenges of the other parties' point of view. Therefore, the preparation of the cooperation already lead to advantages for the future dialog. But of course the success of cooperation is highly dependent on the interests, willingness and commitment of the involved people.

Highlighting multi-purpose benefits of planning principles in our opinion could help to make our goals more understandable. In times with permanent increasing demands on urban planning and design of buildings and infrastructure from many different disciplines a kind of simplification seems to be most effective – at least if we discuss with a broad audience. The willingness for multi-purpose solutions combined with lots of co-benefits seems higher than for “one-dimensional” attempts. Helpful on this way is a very early and open discussion within all involved parties. Nevertheless, some basic common understanding for this early dialog is very helpful.

## References

Atelier Dreiseitl (2019): [http://www.landezine.com/index.php/2015/05/copenhagen-strategic-flood-masterplan-by-atelier-dreiseitl/copenhagen\\_cloudburst-masterplan-atelier-dreiseitl-10/](http://www.landezine.com/index.php/2015/05/copenhagen-strategic-flood-masterplan-by-atelier-dreiseitl/copenhagen_cloudburst-masterplan-atelier-dreiseitl-10/); download 16.08.2019

DIFU (2018): Kommunale Überflutungsvorsorge – Planer im Dialog; Deutsches Institut für Urbanistik (Hrsg.); <http://edoc.difu.de/edoc.php?id=C10ES5UZ>; download 16.08.2019

DBU [https://www.dbu.de/OPAC/ab/DBU-Extreme\\_Abschlussbericht-AZ-32223\\_01.pdf](https://www.dbu.de/OPAC/ab/DBU-Extreme_Abschlussbericht-AZ-32223_01.pdf); download 16.08.2019

Rimböck, A., Hübl, H. and Höhne, R. (2018): Extreme Torrential Flooding at Simbach on June 1st, 2016 - Key Finding of a Detailed Event Analysis -; Interpraevent 2018 in the Pacific Rim, Conference paper; p. 170 – 176

# DATA ACQUISITION AND MODELLING (DAM)

---

# Vertical groundwater movement identification through Distributed Heat Tracing Tests. Case of Åknes, Norway

José Acuna<sup>1</sup>, Randi Kalskin Ramstad<sup>2</sup>, Gustav Pless<sup>3</sup>

**Keywords:** Vertical groundwater movement; Distributed Heat Tracing Tests; Åknes

## Abstract

Heat tracing with Distributed Temperature Sensing has been used to help mapping groundwater movements in the cracked rock in Åknes. A brief insight into this work is shown in this paper. The final idea of this work is to provide information to a drainage program that intends to stabilize a mountain that threatens to fall into the fjord and cause a flood due to a growing crack in the 900-meter-high Åknesfjället in Norway. DTS technology, based on Raman optical time domain reflectometry, helps tracking heat waves with the help of back scattered signal along fiber optic cables over a period of time. This paper presents such measurements, carried out in Åknes during a measurement campaign in four boreholes (KH-01-17, KH-02-17, KH-01-18 and KH02-18). The application of heat in specific sections and the follow up of the heat front was used to get a qualitative and quantitative picture of the vertical component of the groundwater velocity along the boreholes (if any) and the location of re-charge and discharge zones.

## Introduction

Heat is relatively easy to manipulate and simple to detect, specially when using Distributed Temperature Sensing (DTS) equipment based on optical fiber deployed with one single cable instead of many local sensors. This principle has been used to help mapping the groundwater movements in the cracked rock (made of gneisses) in Åknes, western Norway. A brief insight into this work is shown in this paper.

The final idea of the above mentioned work is to provide information to a drainage program that intends to stabilize a mountain near the tourist resort of Geiranger that threatens to fall into the fjord and cause a flood due to a growing crack in the 900-meter-high Åknesfjället. The worst-case scenario is that about 54 million m<sup>3</sup> of rock would fall into the 320-meter-deep fjord, causing a tidal wave that may hit 10 municipalities and affect nearby communities such as Hellesylt, Geiranger, Stranda.

---

<sup>1</sup> Ph.D. NTNU, Norwegian University of Science and Technology, Norway

<sup>2</sup> Dr., NTNU, Norwegian University of Science and Technology, Norway

<sup>3</sup> NVE, The Norwegian Water Resources and Energy Directorate, Norway

Since 1993, the rock has been studied with the help of models and measurements. Several studies have been published during the last decade, e.g. (Ganerød et al, 2008), (Oppikofer et al, 2009), (Grøneng et al, 2010), among others. During 2018 and 2019, fiber-optic cable installations and so-called Distributed Heat Tracing Tests (DHTT) were carried out by the Norwegian Water Resources and Energy Directorate (NVE).

By sending a heat wave down into the groundwater in the boreholes and then using laser signals in the fiber cable to read how the heat front moves, DHTTs are used to map and quantify the vertical component of groundwater movement along boreholes and identify re-charge and discharge zones.

The working principle of DTS technology is based on Raman optical time domain reflectometry. It consists of the injection of laser light pulses through a length of optical fiber. The subsequent detection of a non-linear part of the reflected light (that is re-emitted with a different frequency than the input signal) that travels back through the fiber from the observed section. This frequency shifted light is called Raman scattering, and the temperature is determined by analysing it over a period of time.

Tracing heat in combination with DTS has been treated in (Anderson, 2005), (Leaf et al, 2012), (Read et al., 2015), (Sellwood et al. 2015a) and (Sellwood et al. 2015b), where fracture positions and estimates of the vertical heat flow were estimated and judged to have good precision.

This paper presents such measurements, carried out in Åknes during short measurement campaign in four boreholes (KH-01-17, KH-02-17, KH-01-18 and KH-02-18). The application of heat in specific sections (control volumes) and the follow up of the heat front was used to get a qualitative and quantitative picture of the vertical component of the groundwater velocity along the boreholes (if any) and the location of re-charge and discharge zones.

## Methods

The heat supply was carried out using a 25 cm long 2 kW electric heater at different sections of the boreholes, while the temperature was measured every 25 cm using a fiber cable and an instrument of type XT-DTSTM Silixa.

Figure 1 shows an illustration of the set up during the DHTTs. A more detailed illustration of the full test layout including lengths of cable, cable markings in and outside the borehole are shown in Figure 2 and Figure 3 for the different boreholes.

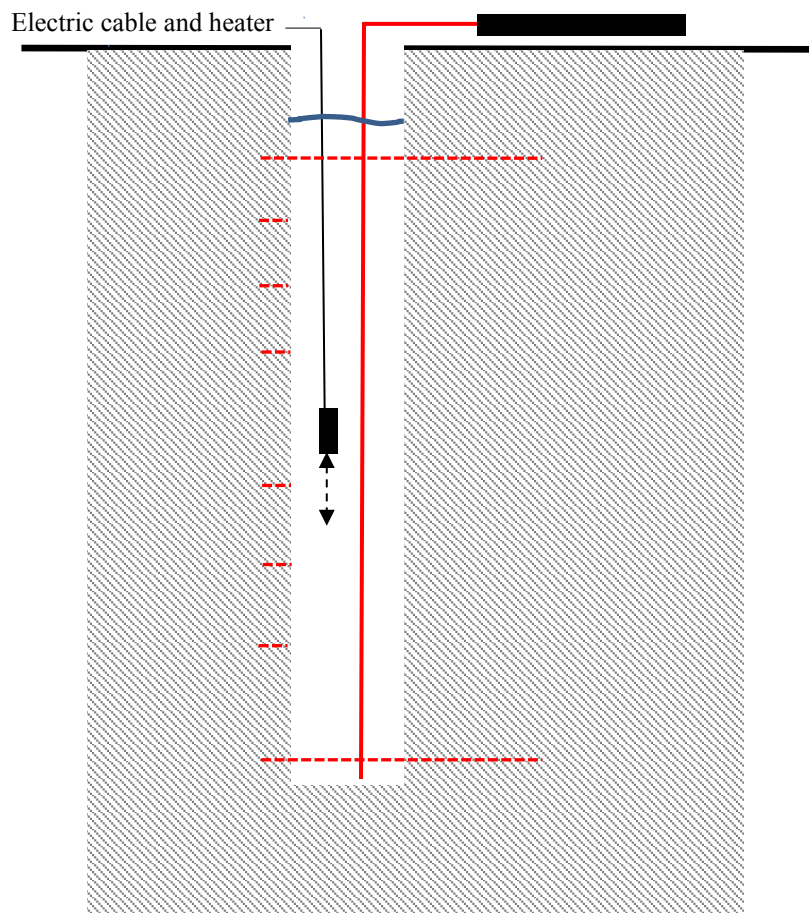


Figure 1 Illustration of the set up of a DHTT

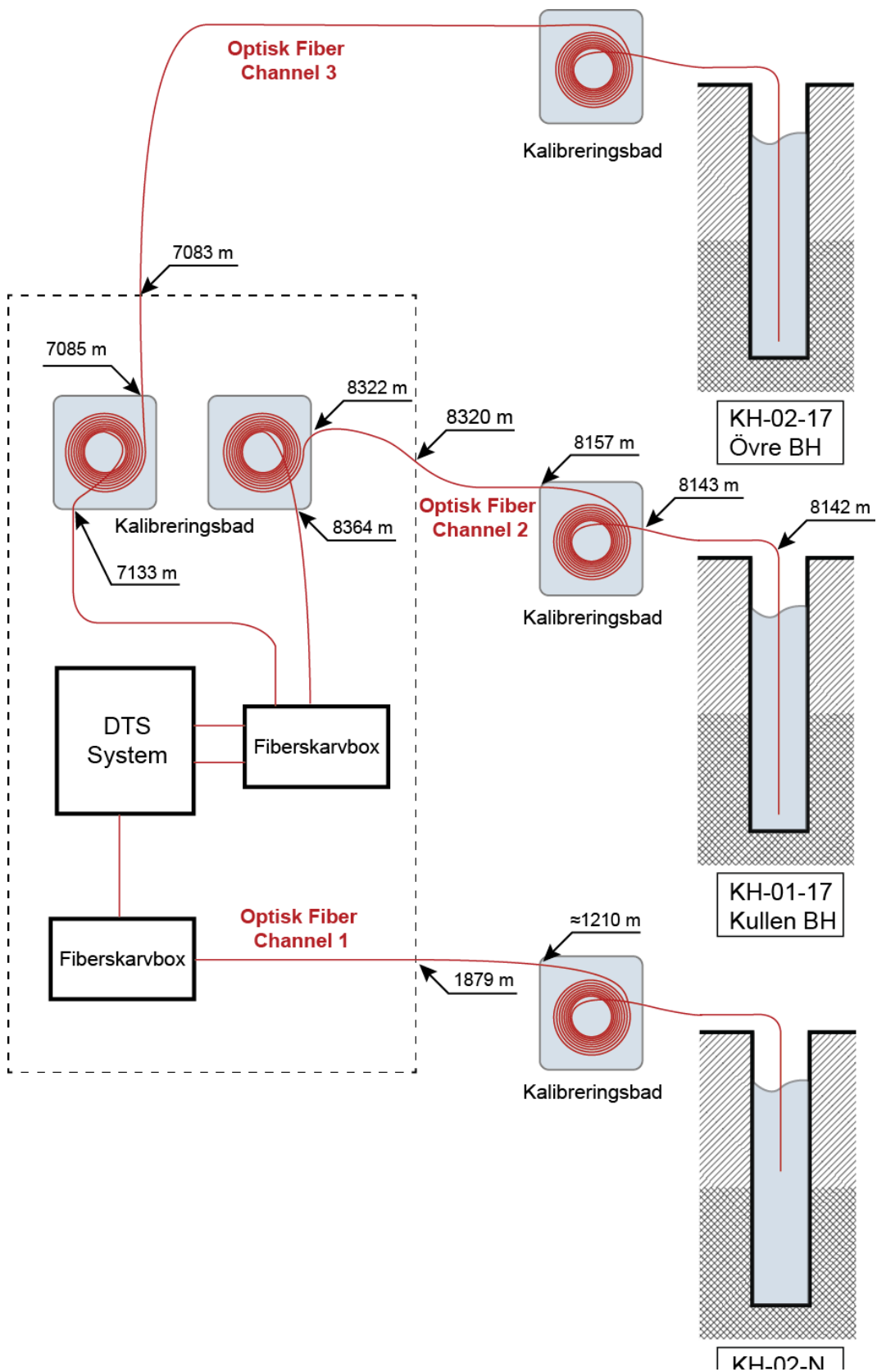


Figure 2 Measurement set up KH-01-17, KH-02-17 and KH-02-N



The fiber cables contain 4 multi-mode fibers, protected with steel and plastic sheath. The cable is of type MMF 50/125 LLK-BSTE 85°C 3.4 from BRUGG/SOLIFOS.

Table 1 shows other characteristics and info of the set up. Heating waves were injected continuously during a 30 minute period at each section and temperature profiles along the whole fiber cable length were integrated every 1 minute.

**Table 1. Borehole general characteristics**

	<b>KH-01-17</b>	<b>KH-02-17</b>	<b>KH-01-18</b>	<b>KH-02-18</b>
<b>Depth [m]</b>	300	300	220	200
<b>Groundwater level [m]*</b>	43	83	21,6	59,5
<b>Steel casing length [m]</b>	-	-	4,5	9
<b>Location of diver</b>	-	-	35	70
<b>Testets datum</b>	12-13 2018	june 2-3 july 2018	25-27 june 2019	

\*measured same day as the DHTTs

From a qualitative perspective, an indication of groundwater movements in the vertical direction can be (or not) visible as temperature profiles are measured and observed real time, specially after the heat is dissipated during the recovery (after the electrical heater is switched off) down into the borehole. Contour diagrams are used for visualizing the data during and/or after the tests.

A local temperature increase without vertical extension indicates no vertical movement of groundwater at the specific level.

The vertical component of the groundwater velocity is quantitatively estimated from a regression method, by calculating how quickly the temperature front moves in the borehole after the heat supply is turned off. The slope of the temperature front over time gives a value of the vertical velocity. A positive or negative value indicates the flow direction, depending on the adopted convention.

## Results and discussion

The results are summarized through contour diagrams with qualitative and quantitative information measured during the distributed heat tracing tests in all four boreholes.

Table 2 summarizes the flow direction and the location of re-charge and discharge zones for each borehole.

Table 2. Re-charge and discharge zones identified during the DHTTs

	KH-01-17	KH-02-17	KH-01-18	KH-02-18
ca re-charge zone	43-54 m	85m&130 m	210 m	130 m
ca discharge zone	100 m	120m&270-280 m	<45 m	<65 m
Flow direction	downwards	downwards	upwards	upwards

Figure 4 and Figure 5 show the results for the DHTTs in KH-01-17. Observe that these two figures have a different temperature scale (done on purpose in order to visualize the difference between the upper and lower part of the borehole). The groundwater temperature was about 32°C at the highest during the test, which can be compared to 5.3°C which is the undisturbed average temperature of the borehole.

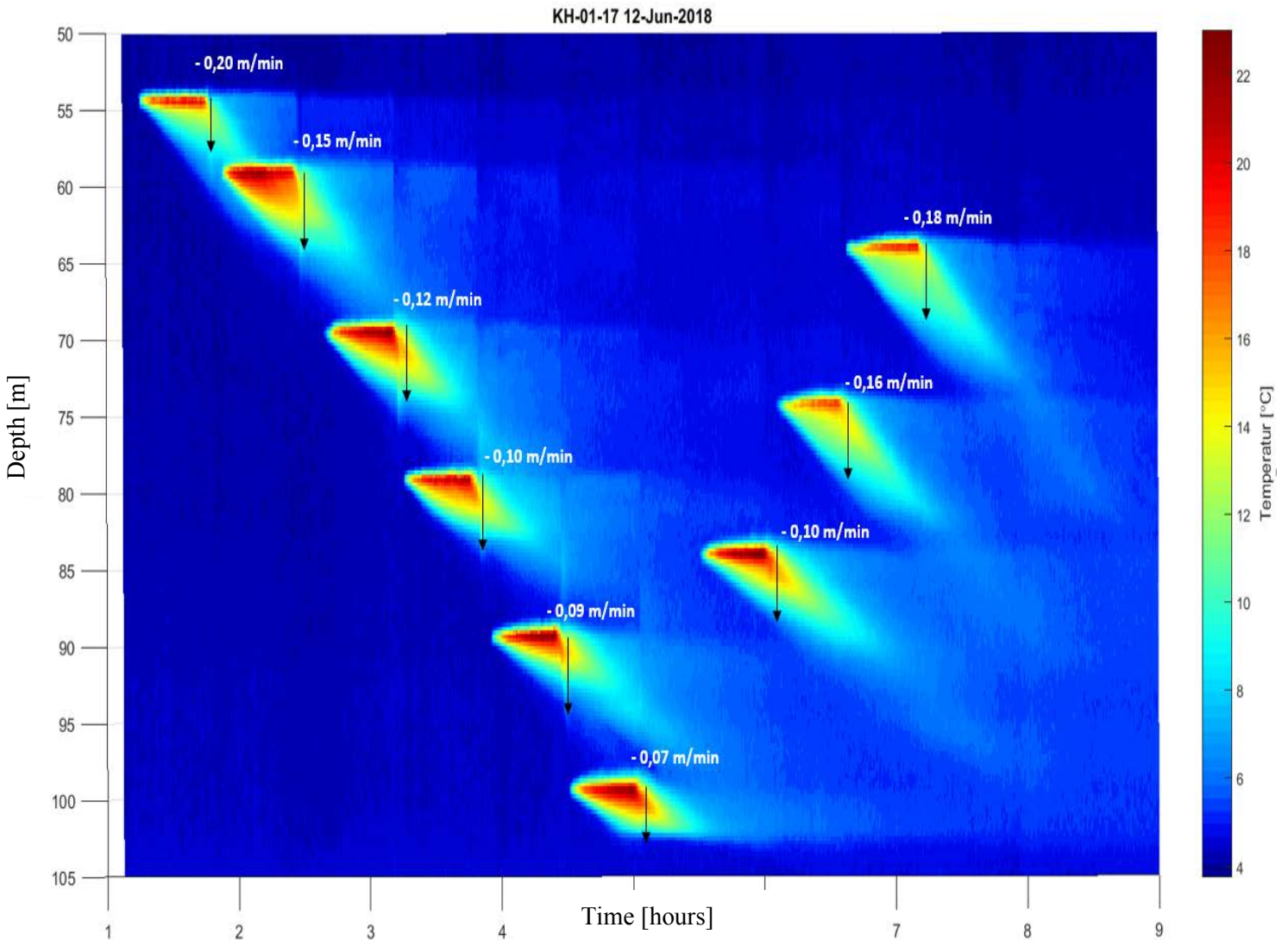


Figure 4 Temperatures and magnitude of vertical velocity component of groundwater flow for the upper part of KH-01-17

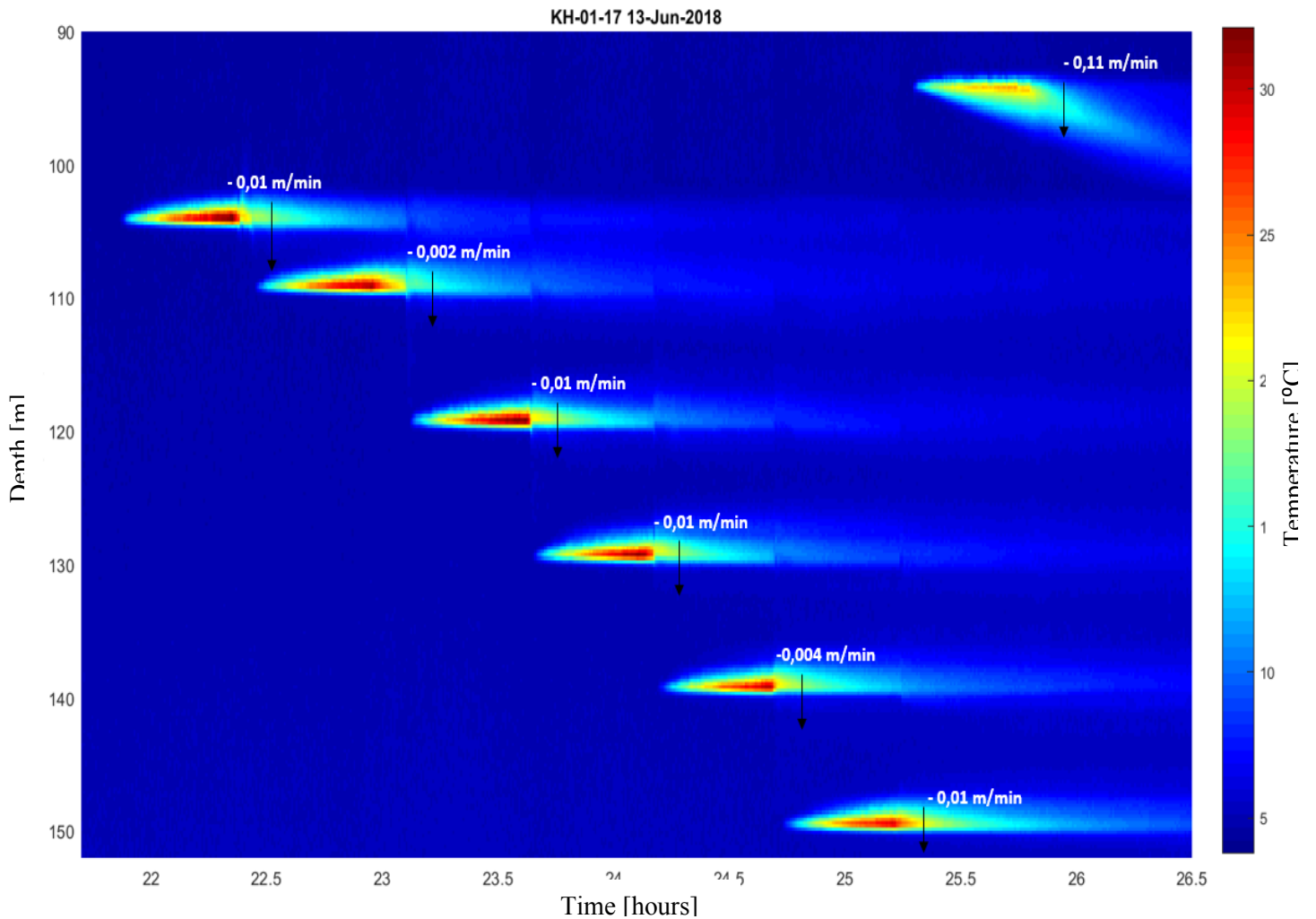


Figure 5 Temperatures and magnitude of vertical velocity component of groundwater flow for the lower part of KH-01-17

It can be observed that the velocity varies between about 0.2 and 0,07 meters per minute and that it has a tendency to decrease with the depth in the upper part of the borehole. At around 100 m depth and downwards, the velocity is close to zero and sometimes even in the upward direction, which can be created by natural convection. A clear discharge zone occurs at about 100 m depth.

Figure 6 shows the measurements in KH-02-17. The groundwater temperature was about 15°C at the highest during the test, which can be compared to 3.9°C which is the undisturbed average temperature of the borehole. The vertical component of the velocity was measured to be between 0.47 and 0.7 meters per minute in the downwards direction, with a re-charge zone at about 85 m and a discharge zone at about 270-280 m.

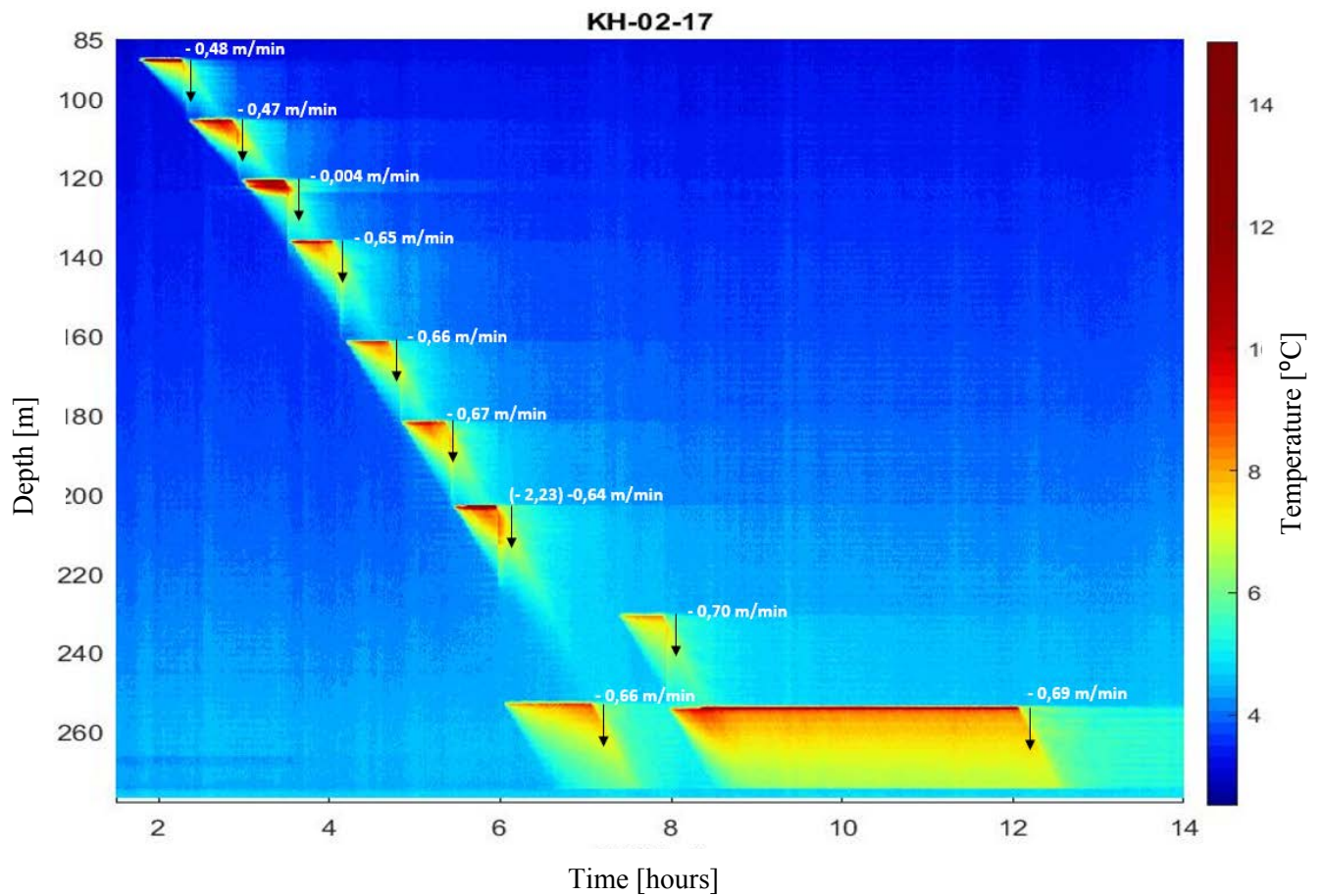


Figure 6 Temperatures and magnitude of vertical velocity component of groundwater flow in KH-02-17

The calculation of the velocities is at the moment ongoing for KH-01-18 and KH-02-18 but they are preliminarily around 0.20 m/min. However, qualitative observations have been done, as shown in Figure 7 and Figure 8, respectively. Both boreholes show a groundwater movement upwards. KH-01-18 has a re-charge zone at about 210 meter depth while water is discharged somewhere above 45 m depth. The recharge and discharge zones in KH-01-18 are located at about 130 m and above 65 m depth, respectively.

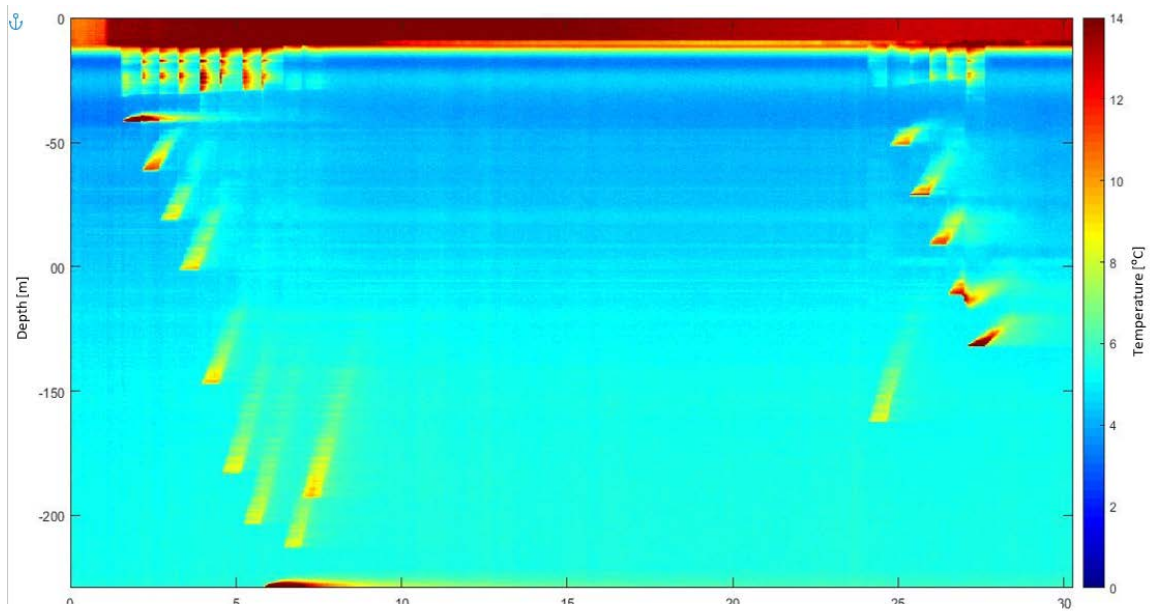


Figure 7 Preliminary data from the DHTT in DH-01-18

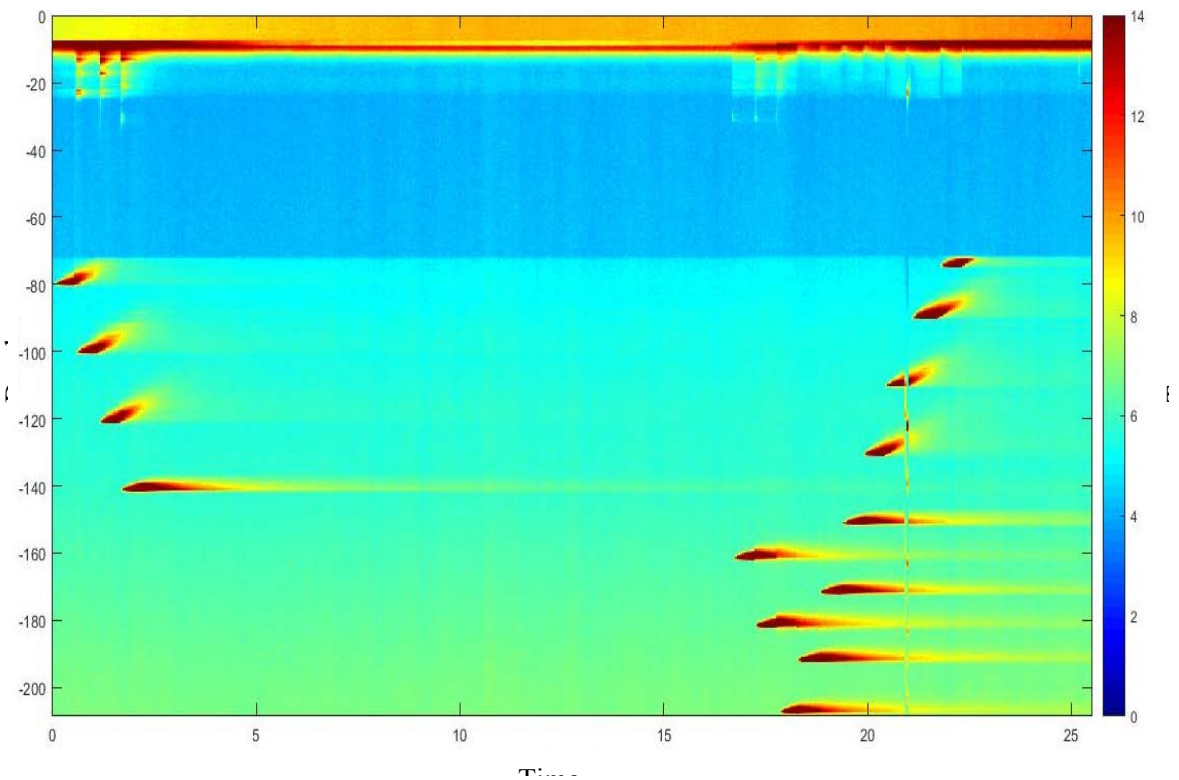


Figure 8 Preliminary data from the DHTT in DH-02-18

Figure 9 summarizes all observations. Future work consists of correlating these measurements with information from long time loggings, meteorological data, fracture and sliding zones among others.

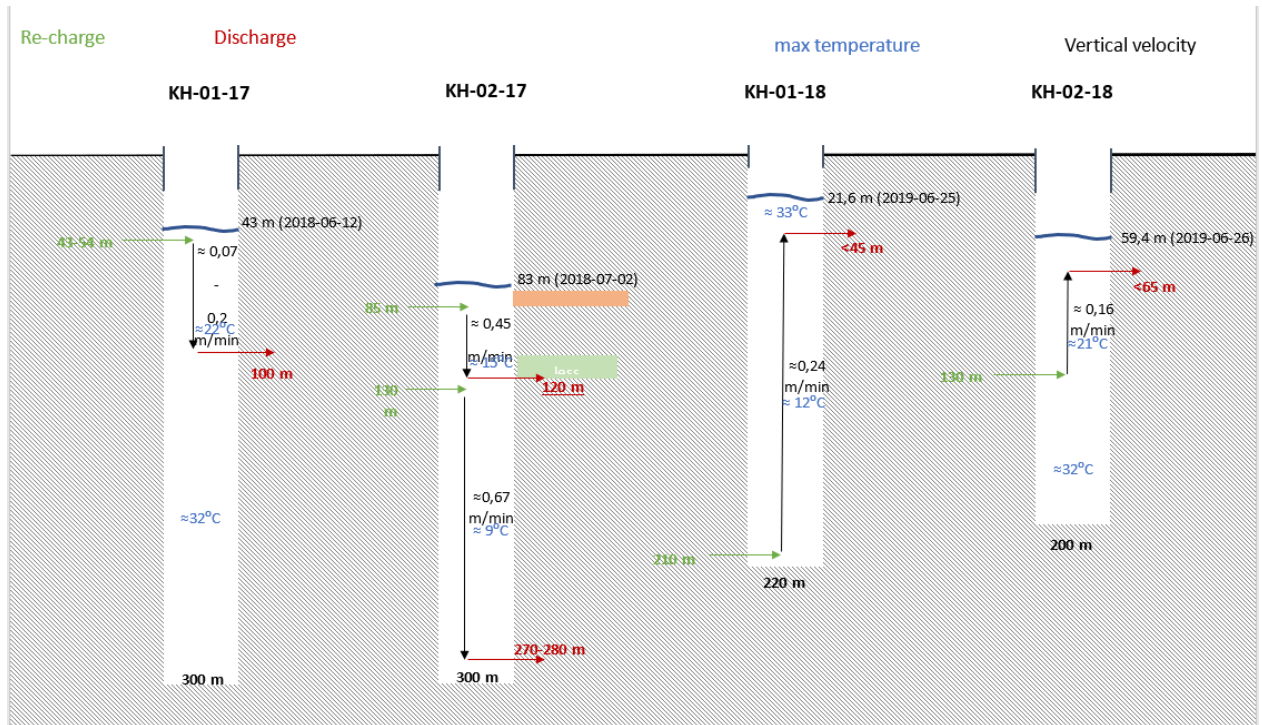


Figure 9 Collection of results

## References

Anderson, M. P. (2005). Heat as a Ground Water Tracer. *Groundwater*, 43(6), 951–968.

Ganerød G, Grøneng G, Rønning J, Dalsegg E, Elvebakk H, Tønnesen J, Kveldsvik V, Eiken T, Blikra L, Braathen A. (2008). Geological model of the Åknes rockslide, western Norway. *Engineering Geology* 102 1–18.

Grøneng G, Christiansen H, Nilsen B, Blikra L. (2011). Meteorological effects on seasonal displacements of the Åknes rockslide, western Norway. *Landslides* 8:1–15 © Springer-Verlag 2010.

Leaf A, Hart D, Bahr J. (2012). Active Thermal Tracer Tests for Improved Hydrostratigraphic Characterization. *Ground Water*, 50(5), 726–735.

Read T, Bense V, Hochreutener R, Bour O, Le Borgne T, Lavenant N, Selker J. (2015). Thermal-plume fibre optic tracking (T-POT) test for flow velocity measurement in groundwater boreholes. *Geoscientific Instrumentation, Methods and Data Systems*, 4(2), 197–202.

Sellwood S, Hart D, Bahr J. (2015a). An in-well heat-tracer-test method for evaluating borehole flow conditions. *Hydrogeology Journal*, 23(8), 1817–1830.

Sellwood S, Hart D, Bahr J. (2015b). Evaluating the Use of In-Well Heat Tracer Tests to Measure Borehole Flow Rates. *Groundwater Monitoring & Remediation*, 35(4), 85–94.

Oppikofer T, Jaboyedoff M, Blikra L, Derron M, Metzger R. (2009). Characterization and monitoring of the Aknes rockslide using terrestrial laserscanning. *Nat. Hazards Earth Syst. Sci.*, 9, 1003–1019.

---

# Physical modelling of debris flows to analyse the influence of a cascade on the flow behaviour and consequences on protection measures

Catherine Berger<sup>1</sup>, Andrea-Kristin Bachmann<sup>2</sup>, J. Speerli<sup>3</sup>, Florian Zimmermann<sup>4</sup>, Walter Clausen<sup>5</sup>

**Keywords:** debris flow, cascades, physical modelling, protection measures, flow behaviour;

## Abstract

The village Saas-Balen in southwestern Switzerland is endangered by large debris flows and protection measures have to be taken. A variety of different protection concepts was studied, but a natural cascade just above the fan apex leads to large uncertainties in process characteristics, flow behaviour and debris flow parameters which are critical for decision making and further design of protection measures. Therefore, a physical model test study is performed at the moment to learn in detail about the influence of the cascade on the behaviour of debris flows and consequences on protection measures. Model tests show that debris flow fronts are compacted and slowed down by the cascades slightly and the pool at the fan apex quasi resets the flow. The functionality of the protection concepts enlargement and diversion were optimized and verified.

## Keywords

debris flow; cascades; physical modelling; protection measures; flow behavior

## Introduction

Debris flows are counted among the most dangerous natural hazards in alpine regions and threaten people, settlements and infrastructure lines. Due to their high velocities, strong impacts and short intervention times, constructive and permanent protection measures are necessary (Jakob and Hungr, 2005). At the Fellbach torrent in Southwestern Switzerland, several debris flows occurred within the last two centuries. Triggering factors were at

---

<sup>1</sup> Ph.d, geo7 AG, Switzerland, (catherine.berger@geo7.ch)

<sup>2</sup> Ost Eastern Switzerland University of Applied Sciences, Rapperswil, Switzerland

<sup>3</sup> Ph.d., former Professor at HSR University of Applied Sciences, Rapperswil, Switzerland

<sup>4</sup> geo7 AG, Switzerland

<sup>5</sup> VWI Ingenieure AG. Switzerland

several times outbursts of proglacial lakes, enhanced by permafrost degradation processes and finally leading to debris flow events with volumes of up to 110,000 m<sup>3</sup>. Therefore, the consideration of process chains is essential. The village Saas-Balen is located on the debris fan of the Fellbach torrent. More than 30 residential houses and the cantonal road lie within the highly endangered area. Due to the high individual and collective risk, permanent protection measures have to be taken and a variety of different protection concepts was studied. However, a natural cascade just above the fan apex leads to large uncertainties in process characteristics, flow behaviour and debris flow parameters which are critical for decision making and further design of protection measures. Therefore, a physical model test study is performed to learn in detail about the influence of the cascade on the behaviour of debris flows and consequences on flow parameters. Based on the outcomes of the experiments and information on flow characteristics, protection measures are designed and functionality on debris flows is assessed.

## Fellbach field setting

The Fellbach torrent in Southwestern Switzerland comprises an alpine catchment of about 8.8 km<sup>2</sup> and extends from the highest point at 3,982 m ASL (Fletschhorn) to the fan apex at 1,540 m ASL (Figure 1). The upper catchment above 2,768 m ASL is characterized by the Gruben glacier (about 20 % of the total catchment area), steep rock faces, several proglacial lakes and vast zones of loose debris with permafrost processes including large rock glaciers.

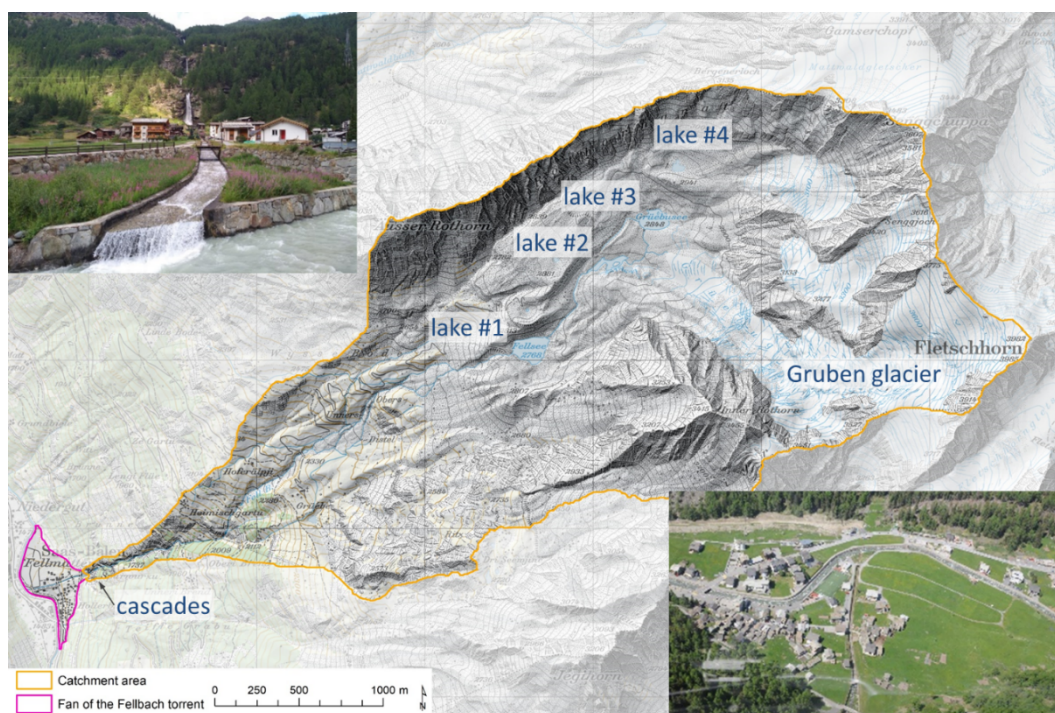


**Figure 1** : Fellbach catchment with Gruben glacier, lake #1 at 2,768 m ASL, downstream torrent section, cascades and fan with front view from the Fellbach outlet upstream towards the cascade (upper left) and overview of the fan (lower right). Data source: Swiss Map Raster 25 by Federal Office of Topography swiss topo.

Process rates are large and highly variable, mainly due to the retreat of the Gruben glacier, spatial and temporal variation of proglacial lakes and progradation of rock glaciers. The lowermost lake (called lake #1) is located on a large bastion moraine. The lower catchment downstream of lake #1 is characterized by typical torrent processes with sequences of erosional and depositional reaches. A series of three cascades with fall heights in downstream order of 55 m, 25 m and 70 m is located directly above the fan apex at 1,523 m ASL (Figure 3). The Fellbach torrent crosses the fan in a masoned channel and flows into the river Saaservispa at 1,475 m ASL (Figure 1). The village Saas-Balen is located directly on the fan and more than 30 residential houses and the cantonal road lie within the highly endangered area.

Several large debris flows are documented within the last 200 years. Major events occurred in summer 1968 and 1970, with debris volumes on the fan of about 110,000 and 100,000 m<sup>3</sup>, respectively, and led to considerable damage. During both events, proglacial lake outbursts led to increased discharge and subsequently triggered debris flows in the bastion moraine below lake #1. Downstream, sequences of erosion and deposition along the torrent were important factors for the bulking of the debris flows (Berger et al., 2011). Today, the outlet of lake #1 is stabilized artificially. However, debris flows are still expected to occur on the fan and process chains have to be considered. Scenarios used to delineate the hazard map and as a basis for the study of protection concepts are listed in Table 1. Triggering factors for more frequent scenarios include the damming-up of a proglacial lake by a snow cornice in combination with rainfall / snow melting. As a consequence of the break of the snow cornice, increased discharge entrains loose material and a transformation into a debris flow with downstream bulking of the flow is expected. For rare events, a collapse of lake #1 cannot be excluded.

**Table 1 : Event scenarios for the Fellbach torrent for different return periods, total debris flow volume, surge properties (volume and maximum discharge) and triggering factors.**

Return period	Total df volume [m <sup>3</sup> ]	Max. surge volume [m <sup>3</sup> ]	Max. discharge [m <sup>3</sup> /s]	Triggering factors
<b>30 years</b>	6,000 – 11,000	2,000	20	Small debris flow (df) triggered by hillslope processes
<b>100 years</b>	25,000- 28,000	10,000	150	df triggered by dam up of lake by snow cornice and in combination with rainfall / snow melt
<b>300 years</b>	33,000 – 41,000	20,000	300	
<b>&gt;&gt; 300 years</b>	120,000	70,000	300	lake outburst or glacier pocket with total collapse of lake #1

## Protection measures

Based on hazard and risk assessment as well as field observations, a preliminary design study for protection measures was performed. Permanent measures are needed mainly for the protection of the residential houses on the fan, with a focus on the village zone on the orographic left side. In combination with an enforcement of the outlet of lake #1 and optimization for overload, three main protection concepts crystallized during the pilot study. As a first option, the channel on the fan is enlarged and debris flows are directed straight into the receiving stream. However, transport capacity in the Saaservispa is very low and backwater effects would cause inundation in the valley bottom. In the second concept, the Fellbach torrent is bypassed at the fan apex to the right and a new streambed is created. In the third option, the present channel on the fan is still in use for normal discharge and smaller floods. However, when channel capacity is exceeded, debris flows are diverted at the fan apex to the deposit area on the right part of the fan. For all three concepts, the influence of the cascade on debris flows and their flow behaviour as well as resulting flow parameters such as velocity, flow depth, peak discharge and hydrograph are essential factors for the planning and dimensioning of the structures. With further knowledge on the expected flow parameters at the fan apex, structures can be designed, functionality during debris flows assessed and the geometry of the structures optimized. Finally, decision making for the selection of the best concept is supported.

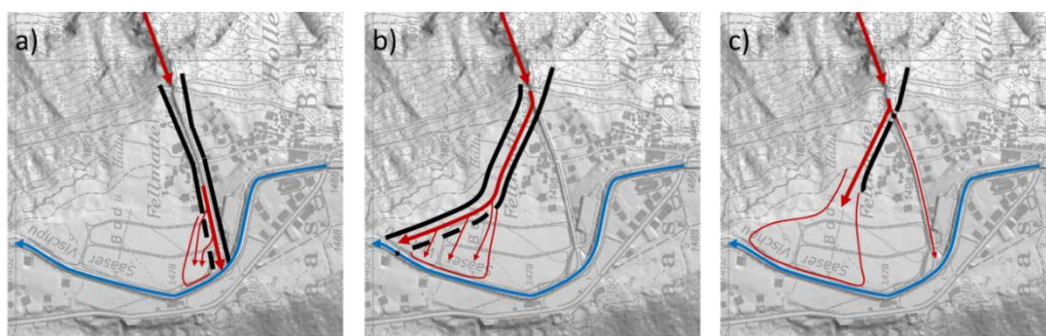


Figure 2 : Schematics of the three main protection concepts on the fan with a) enlargement and straight passing of the flow into the Saaservispa, b) bypass to the orographic right, c) diversion of major events to the deposit area. Data source: overview map, Cant on Valais.

## Physical model test study

A physical model test study is in progress at the hydraulic laboratory of the Eastern University of Applied Sciences, Rapperswil, Switzerland, in order to assess the debris flow parameters at the fan apex and to test the protection concepts on the fan. In order to generate a digital terrain model (DTM) of the Fellbach field setting, data acquisition was performed by drone and photos of the field area were taken. On the fan and along the cascades, reference points were marked and coordinates determined with a GPS measuring device. Using the photos and information on the reference points, an orthophoto (Figure 3) and DTM was generated using photogrammetry. Based on the DTM, cross sections were generated in order to build the physical model. The extent of the physical model covers a

length and width of 400 m and 150 m respectively, and spans an elevation difference of 200 m in nature.

It is not possible to model all debris flow phenomena in a physical model study, but for viscous debris flows, model similarity laws developed by Coussot (1994) and Coussot and Laigle (1994) were applied here. Similar to hydraulic model tests in fully rough turbulent flow conditions, velocity, peak discharge and volume of debris flows are modeled using Froude-number similarity.

Based on our experience with physical debris flow modelling (Speerli *et al.*, 2008; Speerli *et al.*, 2010, Berger *et al.* 2016) a model length scale of 1:50 was chosen. With this scale factor, the physical processes can be reproduced well. The composition of the debris flow material in the model was assessed by fixing peak discharge and volume of the debris flow at the upper part of the cascades in nature and adjusting model parameters stepwise. Five ultrasonic and five laser measuring devices along the Fellbach torrent laboratory model were used to determine the front and the depth of the debris flow. Knowing the distance from one measuring cross section (violet dots in Figure 3) to the following one and measuring the corresponding flow time the mean velocity of the debris flow front between two measuring cross sections was calculated. One additional ultrasonic device was used to determine the debris flow discharge into the model. More details about the measurement equipment and analysis of the data are given in Speerli *et al.*, 2010. The tests are performed in the following way: The debris flow mass is poured into a tank at the top of the model (yellow symbol in Figure 3). The debris flow mass is released from the tank via a ball valve (4'' diameter) into the model. At the bottom of the model, the debris-flow mass is collected in a container.

The following parameters can influence flow properties: Debris flow velocity at the start of the model perimeter: slow to fast; debris flow characteristic: fluid to viscous; debris flow grain distribution: fine to coarse. To get the range of debris flow properties at the beginning of the channel, a sensitivity analysis is performed and the above-mentioned parameters are varied systematically in the physical model test runs.

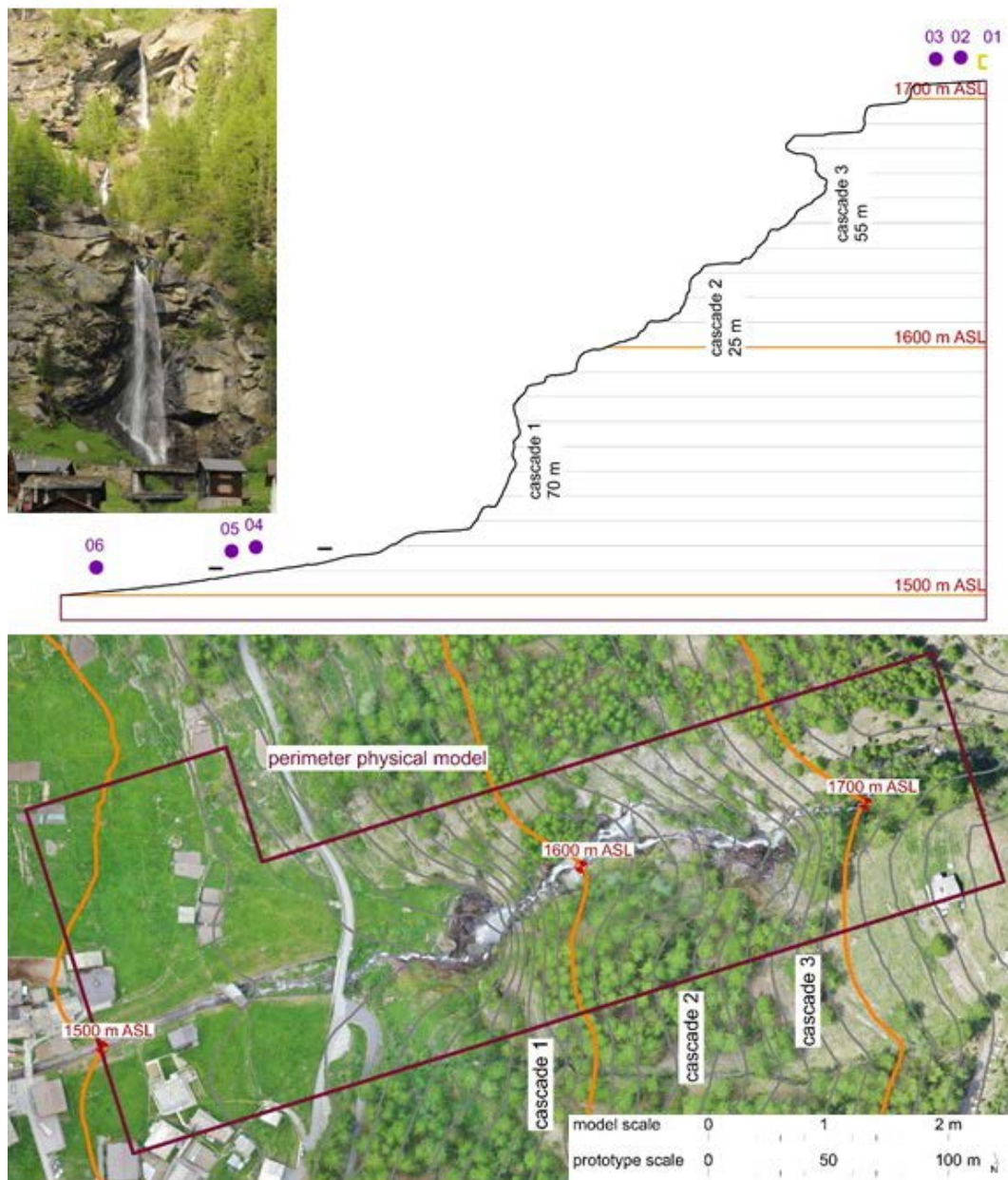


Figure 3 : Overview of the field case at Fellbach torrent with the three cascades. Below: orthophoto with contour lines and perimeter covered in the physical model (violet line). Upper left: front view of the Fellbach cascade in nature. Upper right: longitudinal profile of the torrent displayed in the physical model. For the equipment of the laboratory model, violet dots in the longitudinal profile indicate the locations of the measuring cross sections and the yellow symbol on top is marking the tank where the debris flow mass is entering the model. Orthophoto and digital terrain model generated in the field by drone.

The model investigation is carried out in three phases. In preliminary tests (phase 1), debris flow mixtures are tested in order to reproduce the target values of the 100 and 300 year surges. We start with the same debris flow model mixture as we used in similar laboratory investigations of the Glyssibach torrent (Speerli *et al*, 2008). Particle size distribution and

in particular water content are varied until target values are reached (see Table 1). In phase 2, the sensitivity and process behaviour of the debris flows are investigated. A main focus lies on the influence of the three cascades on the debris flow and how flow behaviour and parameters are affected by the overflow. In the context of a sensitivity analysis, the above-mentioned parameters are varied in order to demonstrate their influence on the flow behaviour. Thus, the range of flow properties (discharge, velocity, flow height) before and after the cascade can be determined and influence of the cascade analysed. In phase 3, the focus is set on understanding the processes as well as the performance of the protection measures and flow properties for the bypass and diversion structures.

## Results and discussion

The following variations were carried out (note that all numerical quantities below and as well in Figures refer to results scaled-up to the prototype scale):

- Water content of the debris flow mixture: 22% (thick liquid) – 30% (thin liquid). It has to be considered that small variations in water content change flow viscosity in the model much more than a similar alteration in nature.
- Largest grain size: 0.4 m – 1.6 m using four different grain size distributions. Distributions of the mixtures were A: 0 – 0.4 m; B: 0 – 0.8 m; C: 0 – 1.0 m and D: 0 – 1.6 m
- Surge Volume: 10,000 m<sup>3</sup> (100 year event) and 20,000 m<sup>3</sup> (300 year event)
- Protection concepts enlargement and diversion (see schematics in Figure 2)

Results on velocities of the debris flow front for different debris flow scenarios and grain size distributions are shown in Figure 4. The dots at chainage 0 m represent the debris flow velocity at the outlet of the tank. The following three sequences of line groups represent mean velocities at the beginning of the model, along the three cascades and in the enlarged masoned channel.

After entering the model debris flow velocity increases due to the model boundary condition. After a short flow distance, the debris flow falls like a broad waterfall over cascades 3 and 2. Before cascade 1, the discharge is concentrated in a narrow gorge before it falls again like a waterfall over cascade 1. A small natural stilling basin is located at the foot of cascade 1. At this place the debris flow is slowed down considerably and debris flow height has to increase first before it flows from the basin into the masoned torrent channel. Along the torrent channel on the fan, flow velocity increases again due to the longitudinal gradient of approx. 15%.

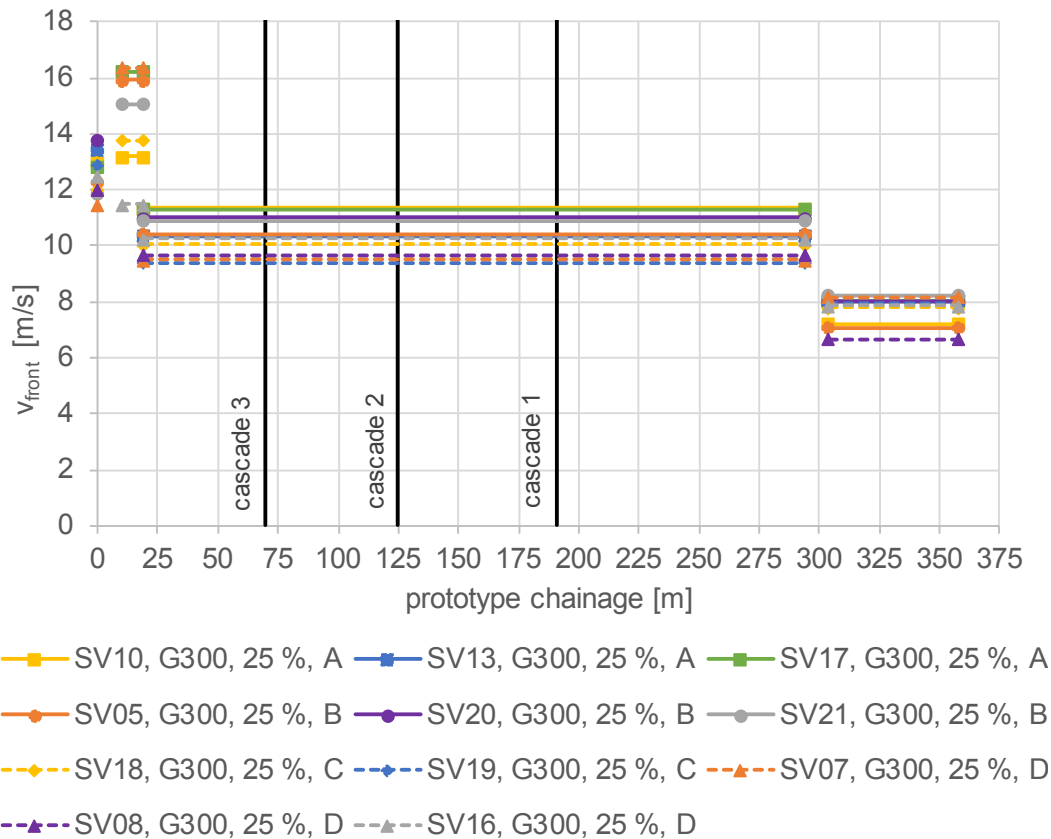


**Figure 4 : Velocities of the debris flow front for a 300 year event (G300), a water content of 25% and different grain size distributions (A-D). Grain size distribution A: 0 – 0.40 m; B: 0 – 0.8 m; C: 0 – 1.0 m and D: 0 – 1.6 m.**

The following conclusions can be drawn: The greater the surge volume, the greater the flow velocity. A larger water content leads tendentially to larger flow velocity. The behaviour of the flow velocity can be summarized as the following for 300 year events: The flow velocity at the outlet of the tank is between 11.5 and 14 m/s due to the model boundary conditions. The velocity at the start of the model (between outlet of the tank and just above cascade 3) varies between 11.5 and 16.5 m/s. The velocity over the three cascades until the beginning of the masoned torrent channel ranges between 9.5 to 11.5 m/s and along the masoned torrent channel from 6.5 to 8 m/s. The flow velocity in the masoned torrent channel is probably nearly independent of the flow conditions over the three cascades and the flow is quasi reset by the small pool at the foot of cascade 1.

Regarding the protection measures, model test showed that debris flows can be directed through the enlarged channel into the Saaservispa river, but bridges remain a critical factor for clogging. The diversion at the fan apex works well when consisting of an enlarged stilling basin and integration of the bridge and road passage into the concrete closing-off structure (Figure 5). A detailed analysis was performed on the dimensioning of the opening at the outlet (concept c in Figure 2) which is designed for the largest grain (0.4 m) of the smallest debris flow mixture (Serie A). Fluvial floods with bedload transport must be

directed through the opening into the masoned channel, debris flow events must block the opening and are diverted to the deposit area. The findings of the model tests can be summarized as the following. The maximum opening in the width should not exceed 1.5 times the largest grain size (here 0.4 m) of the debris flow mixture. If the height of the opening exceeds 3 m, debris flow material will flow out into the masoned channel. The larger blocks of the debris flow mixture are only clogging the opening in the lower part of the opening, the upper part remains open. Therefore, round bars (diameter 0.3 m) are set at a distance of 0.6 m and consequently form 4 openings with a total width of 3.3 m and height of 3 m (see Figure 5).



**Figure 5 :** 100-year debris flow (water content 25 %, grain size distribution A (0 – 0.4 m) passing the diversion structure at the fan apex. Opening (3.3 m width and 4 m height) with round bars (diameter 0.3 m) at a distance of 0.6 m. Truck in the right part of the image for scale reference.

## Conclusion

The tests show that the greater the surge volume, the greater the flow velocity. Debris flow velocity decreases slightly by the passage over the cascades and reaches values in the masoned torrent channel of around 6 to 8 m/s. However, discharges are not influenced by the cascades significantly. Consequently, debris flow fronts are compacted and slowed down by the cascades slightly and the pool at the fan apex quasi resets the flow. The functionality of the protection concepts enlargement and diversion could be optimized and verified.

## Acknowledgements

We thank the community of Saas-Balen and the Canton Valais for the support and constructive discussion in this project.

## References

- Berger, C., McArdell, B. W., Schlunegger, F. (2011). Sediment transfer patterns at the Illgraben catchment, Switzerland: Implications for the time scales of debris flow activities. *Geomorphology* 125: 421 – 432.
- Berger, C., Christen, M., Speerli, J., Lauber, G., Ulrich, M., McArdell, B. W. (2016). A comparison of physical and computer-based debris flow modelling of a deflection structure at Illgraben, Switzerland. *Proc. Int. Symp. Interpraevent*. Lucerne, 212-220.
- Coussot P. (1994). Lois d'écoulement des laves torrentielles boueuses. *La Houille Blanche* 49: 38-43.
- Coussot P. and Laigle D. (1994). Etude des laves torrentielles sur modèle réduit en similitude des phénomènes naturels. *La Houille Blanche* 49: 44-49.
- Jakob, M. and Hungr, O. (2005). *Debris-flow Hazards and Related Phenomena*. Springer Praxis Books. Springer, Berlin, Heidelberg.
- Speerli, J., Grob, M., Künzi, R., Wyss, P., Zimmermann, M., Pozzi, A. (2008). Glyssibach Brienz, Switzerland: Flood and debris flow event on August 22/23, 2005 – Protection measures against future floods and debris flows. *Proc. Int. Symp. Interpraevent*. Dornbirn, 384-385.
- Speerli, J., Hersperger, R., Wendeler, C., Roth, A. (2010). Physical modelling of debris flows over flexible ring net barriers. In: S. M. Springman, J. Laue, L.J. Seward (eds), *Proc. 7th International Conference on Physical Modelling in Geotechnics*, Institute for Geotechnical Engineering, ETH Zürich, 1285-1290.

---

# Image processing techniques for grain size analysis of coarse soils

Lorenzo Brezzi<sup>1</sup>, Simonetta Cola<sup>2</sup>, Paolo Zorzan<sup>3</sup>

**Keywords:** Image Processing; Granulometry; Photo analysis; Grain-size distribution; Coarse material

## Abstract

The granulometric curve is a key aspect to classify granular soils and obtain a first estimate of their mechanical properties. The traditional technique for determining the particle size distribution in laboratory is the method of sieving applied to a representative volume of the soil, which rapidly increases with the maximum grain size of the soil. New alternative methods based on image processing techniques (IPT) are now under development with the main aims to obtain the granulometric curve reducing the analysis time, to avoid the transport of material to the laboratory and to evaluate the material distribution on large areas. The paper shows some preliminary analyses carried out with a new procedure developed within this approach. The results obtained up to now seem to be very promising, even if some improvements have to be considered in the future, in order to better fitting the granulometric curve when the image processing is performed on a sample arranged in a natural way.

## Introduction

The knowledge of the dimensions of solid particles composing a coarse soil is a fundamental requirement for understanding the behaviour of the soil itself: soil features such as the permeability and shear resistance, as well as the capillarity phenomenon or other, often depend on the material granulometry. Traditionally, the grain size analysis of coarse soils, having particles greater than 75  $\mu\text{m}$ , is carried out in laboratory according with the method of sieving. This technique allows to subdivide the sample into different fractions, each of which contains grains of a given range of diameter; in this way, it is possible to obtain the distribution of mass percentage of the dry material of each fraction in relation to the mean diameter of its grains. From the percentage of passer-by at a certain sieve mesh, it is possible to define how much gravel, sand and finest fraction compose the soil. The fundamental requirement for obtaining a correct grain-size distribution curve is that the granulometric analysis has to be carried out on a volume of soil considered representative. The representative sample rapidly increases in weight with the maximum grain size of the soil, reaching a weight of several tens of kilos with very coarse-grained soils.

---

<sup>1</sup> Dr., ICEA department, Italy, University of Padova, (lorenzo.brezzi@dicea.unipd.it)

<sup>2</sup> Prof., ICEA department, Italy, University of Padova

<sup>3</sup> Dr., ICEA department, Italy, University of Padova

It is immediate to grasp some of the limitations of the method of sieving. First, the material has to be collected in the site and transported to the laboratory, but this may be difficult whereas the site of interest is a low accessible slope in mountainous areas or the soil under examination is very coarse-grained soil. This aspect has impact on the possibility to have representative samples and collect a large number of samples. On the other hand, the test does not consider the real shape of the single grain. The passage of the grain through the sieve mesh, in fact, occurs when two of the three main dimensions of the particle are less than the mesh size. The passage of one grain is therefore dependent on the intermediate size, and this aspect limits the effective and accurate recognition of the real grain size, especially when the grain has a very long or concave shape.

In recent years, the technological progress made it possible to apply innovative and radically different approaches to granulometric analysis of soils. The development of techniques based on the Image Processing (IPT) has in fact solved some of the problems of the traditional method but has also provoked some new ones. The strategy of IPT consists in collecting one or more photographs of the sample under exam and elaborating these images in order to recognize the shape and evaluate the sizes of all the contained grains. Up to now, researchers have followed many approaches to this purpose. Carbonneau et al. (2004) performed one of the first attempts of image-based granulometry, distinguishing two methods, namely Image Texture and Semi-variance. The approach aims to estimate grain size on the base of the spatial distribution of grey colour intensity measured in an image of a large land (i.e. the lateral sides and the bed of a river or a depositional place of a river). Dugdale et al. (2010) also used a statistical approach that considers the colour distribution in a pixel neighborhood, based on the Image Texture, in aerial photographs of the sample. Chung and Chang (2013) instead proposed a more structured methodology called R-AGS (Refined Automated Grain Sizing) which combines several algorithms, such as the DWT (Discrete Wavelet Transformation), the CFNN (Counter-propagation Fuzzy Neural Network) and the WST (Watershed Threshold). The authors paid particular care to the identification of more suitable threshold to the recognition of objects in the image, to convert the image thus obtained in black and white, and, finally to determine the grain characteristics. Black et al. (2014) resumed the Imaging Texture method of Carbonneau et al. (2004) and conducted two separate analyses for the fine and the coarse components of the site material. Detert and Weitbrecht (2012, 2013) propose a tool called BASEGRAIN that applies a series of morphological operations to detect objects on images previously converted in grayscale. Finally, Stähly et al. (2017) evaluated the various possible errors of the image-based analysis due to burial, foreshortening and overlapping of grains and suggested some strategies to correct them.

Of course, also these approaches have some limitations: firstly, the soil analysis is performed only on the visible part, and therefore it does not give information on part of material that is hidden by the upper layer of material. No information is in fact obtainable about the material variability in depth. It is also possible to characterize only grains that have recognizable dimensions, so the submillimetre particles cannot be sampled: for this, the common strategy is to characterize the granular content and to make assumptions on the fine material percentage. The image processing based on the analysis of a single image of the sample is a technique that considers only two dimensions of the grains. Comparison

with the classical granulometric curve is possible only by approximating the real shape of the grains with simplified forms, commonly ellipses, and assuming the length of the third axis. In any case the IPT seems very promising.

This paper presents a new method for determining the grain-size particle distribution developed within the IPT. The main novelty of the method consists in applying a series of morphological operations to all the different available channels of the same image, semi-automatically selecting the most reliable ones and thus obtaining a result with the least necessary external intervention. The method starts from the analysis of samples in which all the grains are undoubtedly recognizable because the particles are distributed on a base taking care, they are not in touch one with all the other. This limit situation is used to estimate which is the error introduced by IPT in the most favourable and easy to analyse situation. Then, the analysis moves to a naturally disposed sample and the loss of accuracy is again evaluated and discussed.

## **Analysis of soil sample with detached grains**

The methodology here following is based on the application of multiple image processing operations to some pictures of a granular soils, having a diameter ranging between 5 and 30 mm (Fig. 1a). The granulometric curve of the soil obtained with the traditional sieve analysis is shown in Figure 1b.

As previously introduced, the new procedure involves several steps. The final goal consists in the determination of the granulometry using just the soil pictures, without any hand-made operation on it. Anyway, to check the reliability of the results, a first validation phase is applied: the sample is initially divided in different fractions keeping some space between the grains; each fraction is then measured by photogrammetry, separately. In this way, the best possible identification of the grain's sizes is obtained. In a second phase, the algorithm is conversely applied to the mixed sample, with the aim of evaluating the stability of the results in presence of some almost unavoidable segmentation errors.

In the first phase, the sample is divided in different fractions using the ASTM sieves. Each fraction is placed on a blue base keeping the grains detached one from each other; a first photo (photo n.0) is captured taking the camera in a vertical position above the base. Then, other 40 photographs of the same fraction are taken from trip points distributed around the sample. All the images are processed using a photogrammetry software Metashape (formally known as PhotoScan, Agisoft) in order to obtain a very detailed 3D points clouds of the fraction (Fig. 2) and a raster containing the object distances from each shooting position.

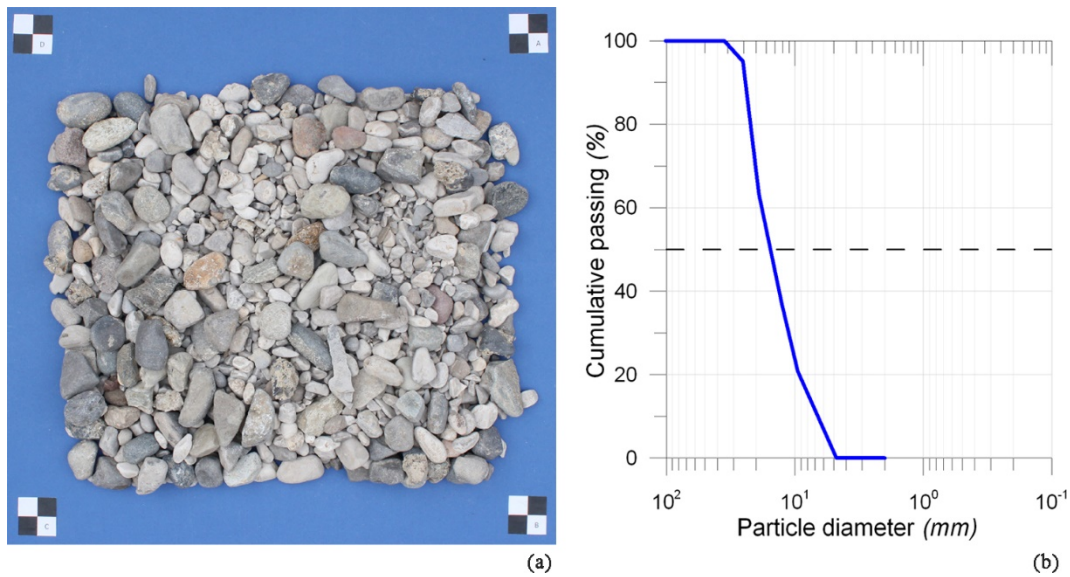


Figure 1: (a) Sample picture; (b) granulometric curve obtained with the method of sieving.

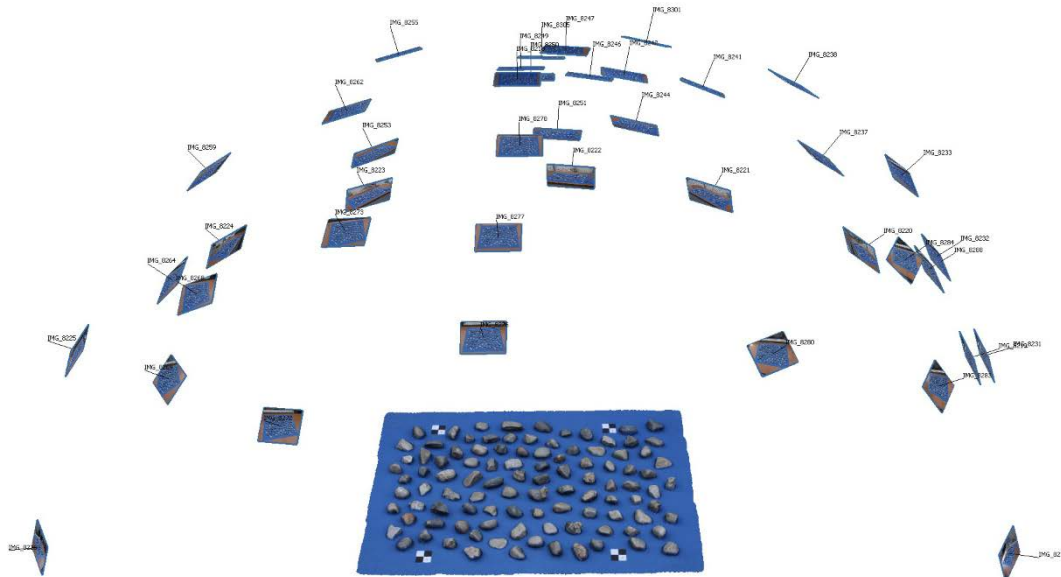


Figure 2: 3D points cloud of one fraction of the sample and view of the shooting positions.

If the “*photo n.0*” (Fig. 3a) is included in the group of processed pictures, it is possible to extract a grains depth map containing information concerning the particles heights (Fig. 3b). This grains depth map in fact consists in a matrix having the same size of the image defined as “*photo n.0*”, but it contains the measure of the distance between each recognized point of the specimen 3d cloud and the camera. Consequently, the position and the measure of the point belonging to each grain surface and having the relative maximum elevation above the base is easily obtainable, as marked with yellow circles in figure 3b.

The procedure continues applying to the photo of each fraction a filter based on a threshold of blue colour content which transforms the photo in B/W (binary image reported in Fig. 3c), in which the grains are white and the base black. The B/W photo is then analysed through a MATLAB script to recognize the region of every grain. Simplifying the shape of

grains in the photo with an ellipse, another passage allows automatically obtaining the two main axes of the ellipse (Fig. 3d). Finally, using the depth raster, it is possible to obtain for each grain the value of the third axis, normal to the shooting plane.

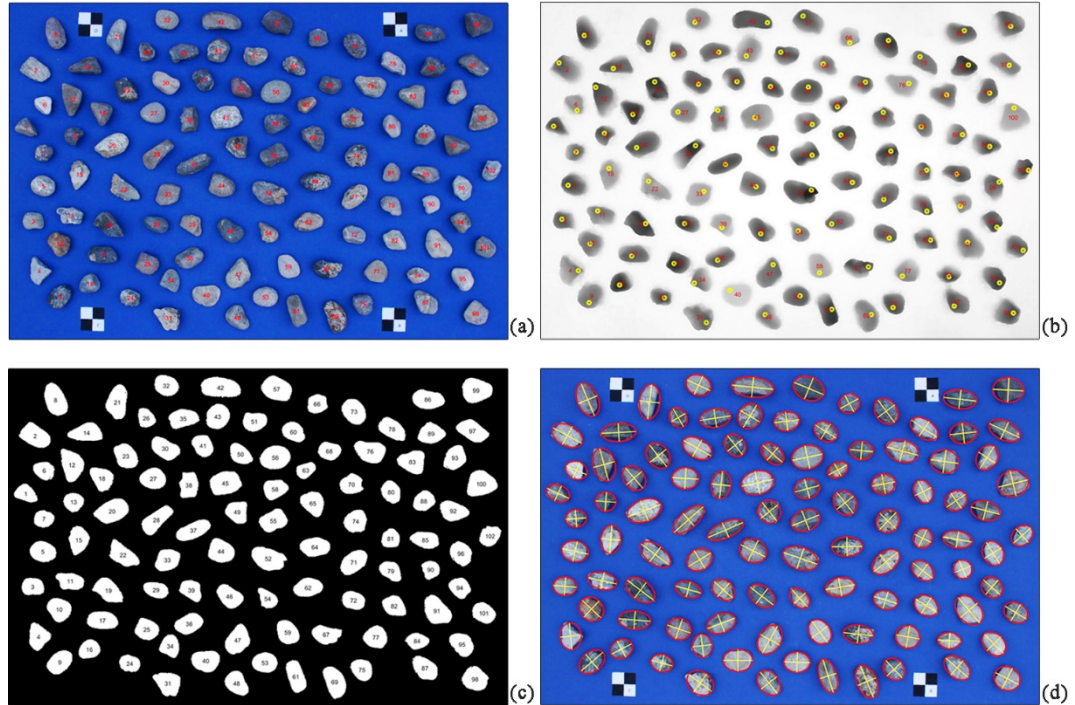


Figure 3: (a) Example of photo n.0 for one fraction; (b) Grain depth map with identification of the point of maximum elevation for each grain; (c) Binary image with identification and numbering of individual grains; (d) Identification of the ellipse approximating every white area of binary image and its major and minor axes.

By repeating the described operations for each fraction, a database containing information on all grains is obtained. It contains the values of the three main axes, two deriving from the photo n.0 and the third obtained from the photogrammetric model. To evaluate if the effectiveness of assuming an elliptical shape for the grains, it is evaluated two errors so defined:

$$E_A = \frac{1}{n} \sum_i \frac{A_{B,i} - A_{E,i}}{A_{B,i}} \cdot 100 \quad [\%] \quad (1)$$

- Error on 2D area in binary image:

$$E_V = \frac{V_D - \sum_i V_{E,i}}{V_D} \cdot 100 \quad [\%] \quad (2)$$

- Error on 3D volume:

In which:

- $A_{B,i}$  is the effective area of i-th grain measured in the binary image;
- $A_{E,i}$  is the area of ellipse approximating the i-th grain;
- $V_{E,i}$  is the volume of the ellipsoid approximating the i-th grain;
- $V_D$  is the real volume of the fraction obtained by dividing its weight by the solid grains density, resulting equal to  $27.6 \text{ kN/m}^3$ ;

- $i$  is the counter varying from 1 to the number of grains contained in each fraction.

**Table 1: Summary of the fraction weights, diameters and errors of areas and volumes due to the elliptical simplification.**

<b>Fraction</b>	<b>ASTM sieve #</b>	<b>Sieve size [mm]</b>	<b>Retained weight [g]</b>	$E_A$ [%]	$E_V$ [%]	<b>Mean x axis [mm]</b>	<b>Mean y axis [mm]</b>	<b>Mean z axis [mm]</b>
<b>A</b>	1	25.40	306.6	2.48	-15	32.07	41.72	22.58
<b>B</b>	3/4	19.10	1977.5	1.75	-14	25.77	36.35	16.28
<b>C</b>	1/2	12.70	1634.1	2.24	-8	17.27	24.55	11.57
<b>D</b>	3/8	9.52	1016.0	2.18	3	12.31	17.06	7.50
<b>E</b>	40	4.76	1299.2	2.88	18	6.96	9.84	4.21

## Analysis of soil sample with overlapped grains

It is obvious that a granulometric analysis based on already separated fractions of the sample has a limited application: it cannot be used in the site and this is contrast with the main aim of this research. It may be considered only a preliminary analysis with the aim of investigating the effectiveness of image processing procedure in a most simple case and, particularly, of the elliptical shape assumption in approximating the grains.

In order to have a more useful method it is essential to set up a procedure that considers a soil sample in which the grains are partially overlapped one to each other and disposed in a more natural way like in Fig. 1a, that can be named “mixed sample”. The procedure implemented to this aim consists in the application of a succession of morphological operations to the photo of the mixed sample, in order to pass from an RGB image to a well-segmented binary one. Also in this case, a user-made algorithm is created in Matlab language. The procedure consists first in the extraction of each color channel from the original RGB image. Not only the RGB channels are split in red, green and blue components, but also the HSV (Hue, saturation and brightness) and the YCbCr (luminance, chroma blue and chroma red) channels are considered: nine different grey scale images are in this way elaborated to reach a satisfactory level of binarization. The procedure applies on each channel the following operations:

1. Several morphological operations are applied: the pixels are subjected to opening, erosion, reconstruction and dilatation, in order to reduce the image noise that can lead to over-segmentation in the following steps. The result of this first point applied on Y-channel (Figure 4a) is visible in figure 4b;
2. The image is then saturated of the bottom 1% and the top 1% of all the pixel values, thus increasing the picture contrast; the image gradient is calculated and used to increase the grain boundary identification;
3. The greyscale image is now converted in black and white and a watershed segmenting operation is applied to separate the grains that are wrongly connected (Figure 4c);

- Once the segmentation is rightly calibrated and applied, each grain is disconnected from the others, so it can be easily recognized. The method still approximates each particle with an ellipse, storing the two axes in a database that allows to obtain the granulometric curve of the sample; the ellipses identification is visible in Figure 4d.

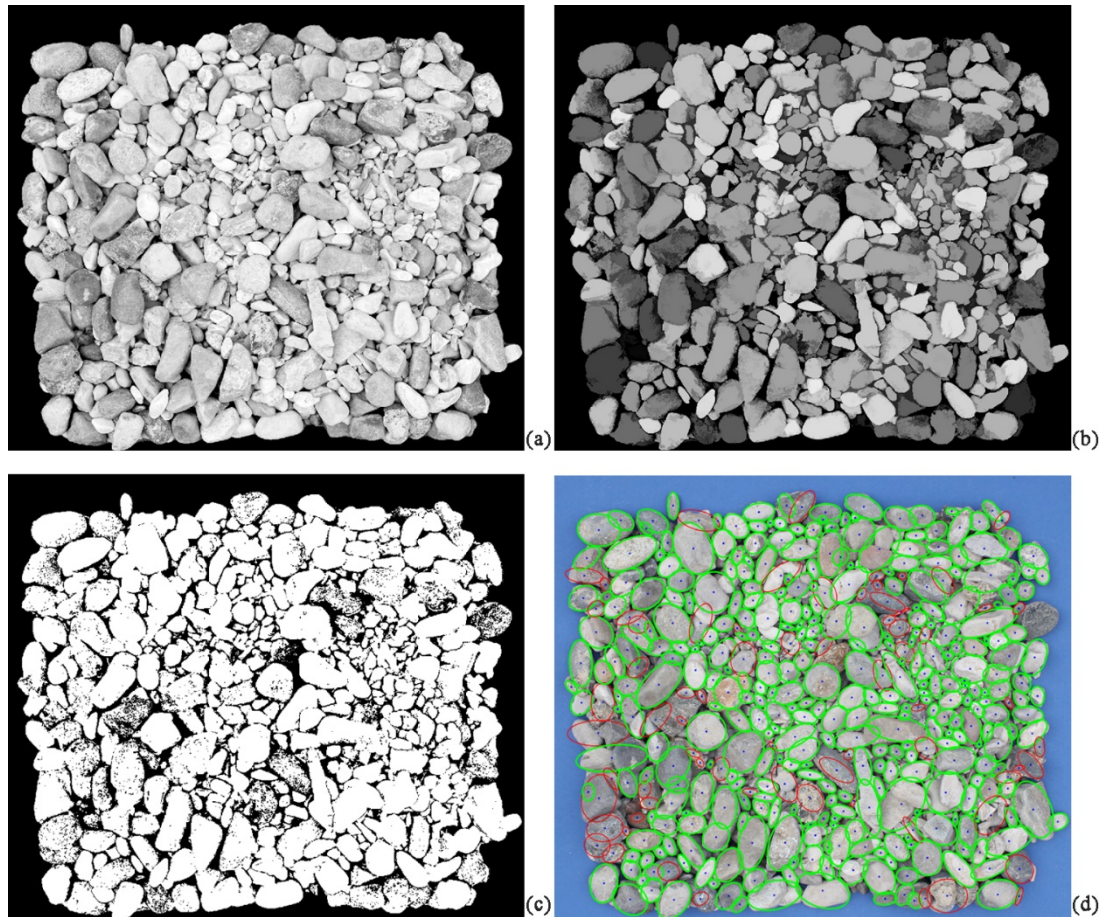


**Figure 4: (a) Y-channel of the picture; (b) Y-channel after the morphological operations; (c) Y-channel in black and white, after the segmentation; (d) ellipses recognition.**

Of course, the analysis of the single photo shown in Figure 4d allows the identification of two axes: it is therefore necessary to make an assumption about the length of the third axis in order to calculate the volume of each grain and then the volume of each fraction. To this aim, the results obtained with the previous analysis with separated grains can be used to estimate the relationship between the second and the third axes of each grain and to consistently assign here a hypothetical value to the third axis of each grain. With this procedure, it is possible to obtain the granulometric curve of the mixed sample on the base of a single image, the photo reported in Figure 1. The comparison between the three distributions thus obtained is visible in Figure 5: it is immediate to notice how the curve obtained from the analysis with separate grains is very close to that obtained with sieving, while the curve resulting from IPT applied to the mixed sample underestimates the smaller fractions, with a slight decrease in the average diameter. It should be noted how the

implemented algorithm is not yet optimized and sometimes shows a wrong image segmentation, with consequent inaccuracy in the collection of data useful to then construct the granulometric curve. Some grains are in fact not identified by the algorithm, and some others are wrongly segmented. However, a quite satisfactory percentage of the sample is rightly interpreted. Anyway, future improvement of the image segmentation with the overlapped grains will increase the reliability of the obtained results.

## Conclusion

Digital image processing of coarse soils is a very interesting strategy for determining the grain-size distribution curves characteristic of soils that are difficult to be sampled and transported in laboratory. In this paper, the results of a first attempt are presented. They show that the digital manipulation of the images allows a good identification of the soil granulometric curve when the grains are disposed on a base in detached way. On the contrary, the procedure implemented for analysing the image of a soil sample with naturally arranged grains, i.e. with grains partially overlapped one on the other, must be still improved because it overestimates the fraction of larger grains.

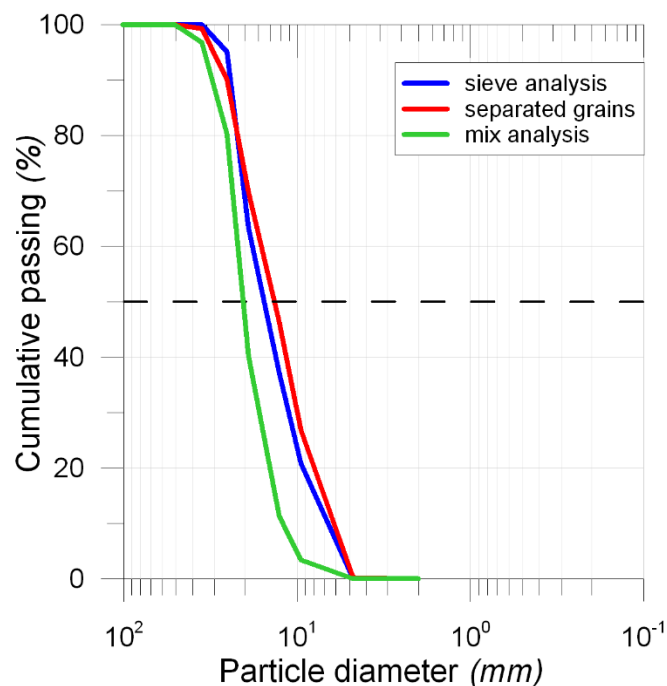


**Figure 5: Granulometric curves obtained with the mechanical sieving (blue), IPT on separate grains (red) and by image segmentation of the mixed sample (green).**

The future development may aim to improve on the one hand the image segmentation, in order to reduce errors in the grain identification. On the other hand, 3D approaches based on photogrammetry may help to characterize the sample, storing information on the shape factors and angularity of the soil and giving a more detailed definition of it.

## References

Black M., Carbonneau P., Church M., Warburton J. (2014). Mapping sub-pixel fluvial grain sizes with hyperspatial imagery. *Sedimentology* 61(3): 691-711.

Carbonneau P. E., Lane S. N., Bergeron N. E. (2004). Catchment-scale mapping of surface grain size in gravel bed rivers using airborne digital imagery. *Water resources research* 40(7).

Chung C. H. and Chang F. J. (2013). A refined automated grain sizing method for estimating river-bed grain size distribution of digital images. *Journal of hydrology* 486: 224-233.

Detert M. and Weitbrecht V. (2013). User guide to gravelometric image analysis by BASEGRAIN. *Advances in science and research*: 1789-1795.

Detert M. and Weitbrecht V. (2012). Automatic object detection to analyze the geometry of gravel grains—a free stand-alone tool. In *River flow*: 595-600. Taylor & Francis Group London.

Dugdale S. J., Carbonneau P. E., Campbell D. (2010). Aerial photosieving of exposed gravel bars for the rapid calibration of airborne grain size maps. *Earth Surf. Processes and Landforms: The Journal of the British Geomorphological Research Group* 35(6): 627-639.

Stähly S., Friedrich H., Detert M. (2017). Size ratio of fluvial grains' intermediate axes assessed by image processing and square-hole sieving. *Journal of Hydraulic Engineering*: 143(6), 06017005.

---

# Image-based flow monitoring in a remote alpine catchment

Maxence Carrel<sup>1</sup>, Salvador Peña-Haro<sup>2</sup>, Beat Lüthi<sup>2</sup>, Issa Hansen<sup>3</sup>

**Keywords:** Flow measurement; real-time monitoring; Flooding; image processing; alpine canyon

## Abstract

This paper presents an image-processing based method for measuring water level and volumetric flow rate for a stream located in an alpine catchment. The system is energetically self-sufficient and consists of an IP camera, a floodlight beamer, a processing and a transmission units. It can be accessed in real-time for monitoring the stream. The water level is detected automatically and several thresholds for water level or discharge warning can be implemented. The surface velocity field is measured by means of Surface Structure Image Velocimetry. Using the measured water level and velocity as an input, the flow rate can be computed using a physical model. A rating curve is continuously generated with the measured water level and discharge, thus allowing de-rating detection after extreme events.

## Introduction

Flow or discharge data of alpine catchments is key for a wide range of activities spanning from the planning and operation of dams and water intakes, the design of flood protection structures to hydrological modelling. In many cases, access to real-time data is very useful (e.g. dam operational purposes or early warning against floods). In the last decades, image-processing based technologies such as Particle Imaging Velocimetry (PIV) emerged as valuable alternatives for performing flow measurements for many different applications. The idea is to seed the fluid of interest with particles allowing to measure the surface velocity field using cross-correlation methods. Whereas these technologies first were applied to images acquired with high-speed cameras under laboratory conditions (Adrian R.J., 1991), their usage was progressively extended to field experiments (Fujita I. et al., 1999). In recent years, such measurements were also performed using images acquired by consumer-grade devices such as smartphones (Carrel et al., 2019) and drones (Bandini et al., 2019). However, the use of PIV techniques for continuous monitoring of flows under field conditions is hardly feasible as these techniques rely on the addition of tracer particles used to reveal the displacement of the fluid of interest (Muste et al., 2008). This

---

<sup>1</sup> Dr., Product Manager, Photrack Ltd, Ankerstrasse 16a, Zürich, Switzerland (carrel@photrack.ch)

<sup>2</sup> Photrack Ltd, Ankerstrasse 16a, Zürich, Switzerland

<sup>3</sup> SEBA Hydrometrie GmbH & Co. KG Gewerbestr. 61 A 87600 Kaufbeuren Germany

shortcoming was overcome by another Imaging Velocimetry technique introduced by Leitão et al. (2018) relying on naturally occurring Surface Structures (SSIV) to perform surface velocity measurements. This patented technology was shown to accurately allow the surface velocity measurement under night and day conditions, even for low resolution video recordings, which opens the door to applications in areas where data transmission may be limited by the bandwidth of the internet service as in remote mountainous regions for example. This study introduces an image-based flow measurement system installed in such a remote alpine catchment. Images are acquired with an IP camera and are processed on site using the SSIV technique, delivering water level and volumetric flow rate data, which are required to design the water intake of a hydropower facility under planning.

## Methods

The measurement system is installed at 2100 m.a.s.l. in a canyon (see Figure 1), around 500 m below the tongue of a glacier and is used from May to October to monitor water level and volumetric flow rate during the snow and glacier melt season. The system consists of a Vivotek Dom camera allowing precise and repeatable pan, tilt and zoom, a floodlight beamer, a solar panel, a fuel cell as well as processing and transmission units. This system performs water level and flow measurements at hourly intervals over night and day. The power supply of the system is covered by a battery that is recharged by the solar panel and the fuel cell. The floodlight beamer is installed and switched on synchronously with the camera during the night recordings. The camera records 5 seconds movies of a region of the stream that is used for water level detection and surface velocity measurements (8 bit images, 360 x 640 pixels resolution, 30 fps). The recordings are processed on site and the results pushed to a server. The system can be accessed in real-time for monitoring of the stream.



**Figure 1.** Canyon in which the measurement system is installed (top). Camera located below the bridge (right). Solar panel and box containing the fuel cell, processing and transmission units (bottom).

In order to calibrate the internal and external parameters of the camera, the position of ground control points (GCPs) distributed homogeneously within the field of view are measured with a distance meter (LEICA S910). Figure 2 A presents the position of the camera, the ground control points as well as the cross section of the stream. Figure 2 B shows the detected and computed position of the GCPs, testifying of the accurate calibration of the camera. The dry section of the bathymetry is reconstructed using photogrammetric methods based on images of the region of interest acquired under low-flow conditions. As a portion of the bathymetry remained immersed during the whole melting season, another approach was necessary in order to reconstruct its geometry. In order to obtain the wet section remaining, several possible cross-sections were generated and the discharge was computed using the Surface Structure Imaging Velocimetry approach described below. The results of the discharge measurements were compared with results of several tracer tests performed for different flow rates and the cross-section for which the discharge was best agreeing with the tracer tests was retained as the most plausible one (Figure 2 B). Therefore, the bathymetry considered for the discharge computation is not strictly speaking corresponding to the reality, it is rather an effective bathymetry yielding plausible discharge measurements.

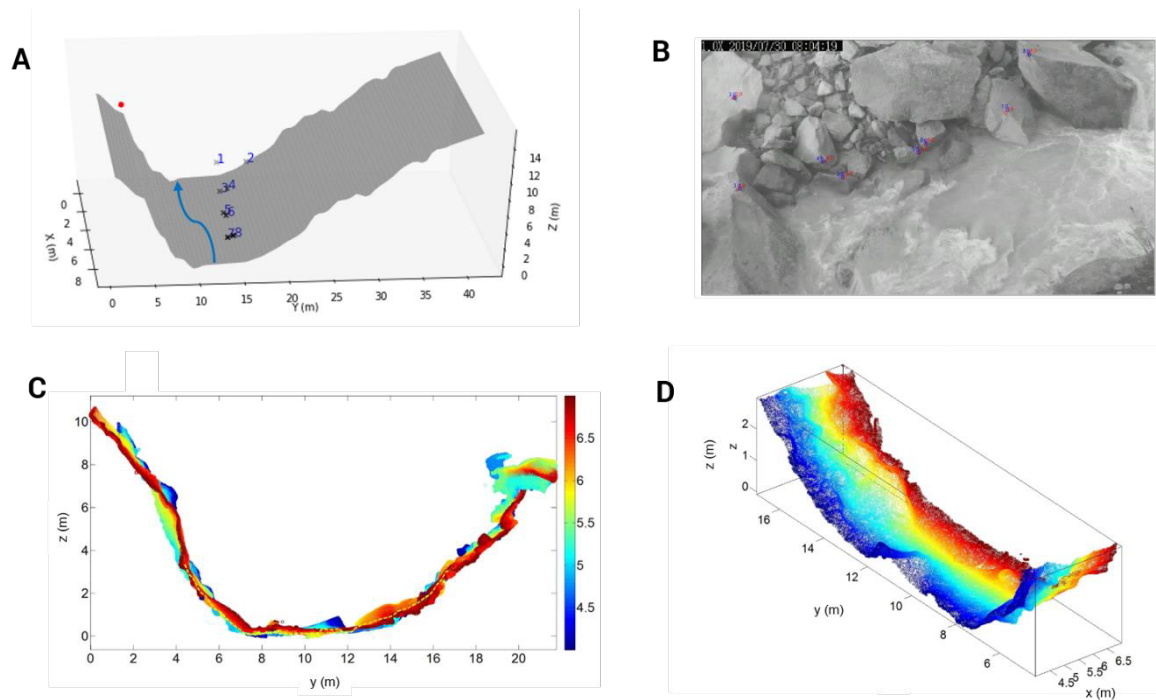


**Figure 2. (A) Camera (red) and ground control points (black crosses) with the bathymetry retained for the measurements and the direction of flow (blue arrow). (B) Detected position of the ground control points in image space (blue) and position obtained upon camera calibration (red). (C) 2D projection of the reconstructed canyon geometry (color-coded with the x - position), the yellow dashed-line represents the finally retained bathymetry. (D) Portion of the 3D reconstruction used for the bathymetry generation (color-coded with the x-position).**

The water level is automatically measured optically either using a direct segmentation of the 8 bit images or the texture of the flowing water depending on the light conditions. The surface velocity field was computed using the SSIV method for a region of interest of the field of view where the cross-section remained constant. Then, the streamwise surface velocity profile was obtained by applying a fit to the streamwise velocity components measured in the region of interest. Here, the vertical velocity profile was modelled automatically using a model based on Prandtl's mixing length hypothesis, as described by Absi (2006). However, depending on the measurement site, several other approaches for the discharge computation such as methods using alpha values (coefficient relating the depth-averaged velocities to the surface velocity) or the ISO standard 748:2007 (standard expressing the average velocity as a function of the depth, the surface velocity and a Manning roughness coefficient) can be implemented. Finally, the discharge was obtained by integrating the vertical velocity profiles over the width of the stream. The water level, surface velocity field as well as both the horizontal and vertical velocity profiles are presented in Figure 3.

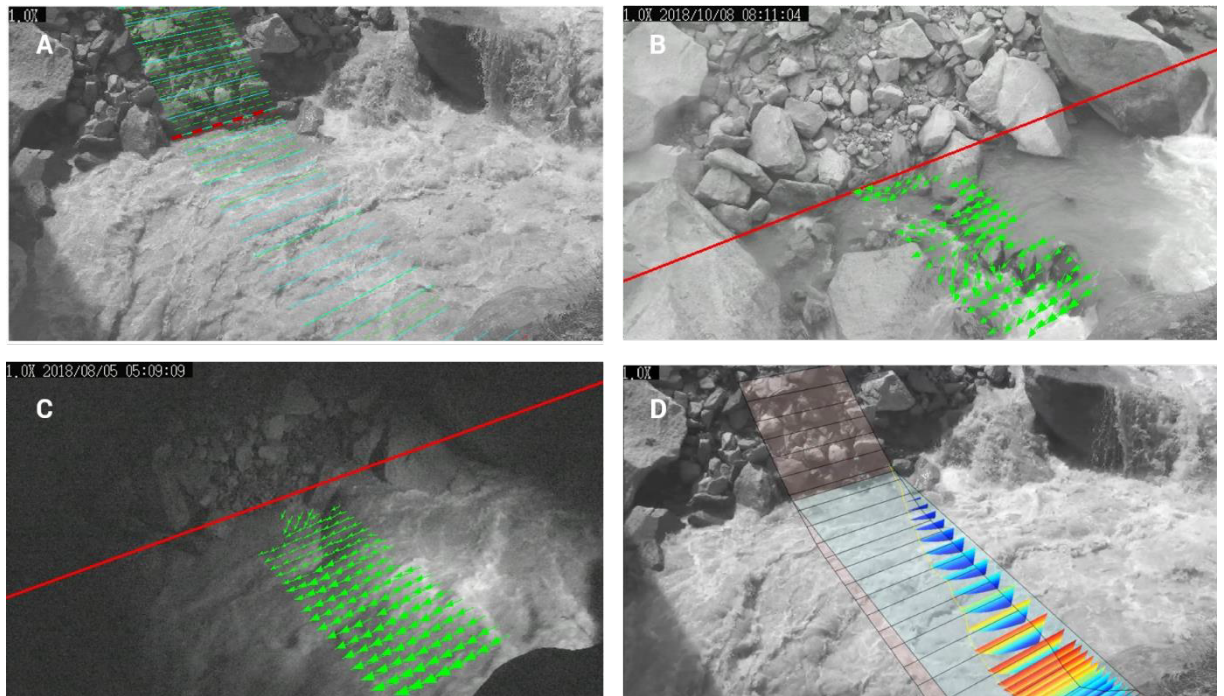


**Figure 3. (A) Bathymetry projected on an image of the canyon (green) and optically detected water level (red). (B) Measured water level and flow field under low flow conditions. (C) Water level and flow field obtained for a night measurement. (D) Horizontal and vertical profiles of the streamwise velocity component used for the discharge computation.**

## Results and discussion

The Figure 4 shows time series of the hourly and daily discharge measured for the melting seasons 2015 to 2018. The hourly data reveal the daily variation in discharge as the flow regime of the catchment considered heavily depends on snow and ice melt, so that the flow rates measured are generally lower at night. High flow rates are then either caused by high temperature and melt rates or subsequent to precipitation events. The night and day high frequency variations are smoothed out in the daily data, where the variations of lower frequencies correspond to temperature variations and responses of the catchment to precipitation events. These time series stretch over different time periods, as the installing and uninstalling dates of the system depended on the presence of snow or not at the measurement location.

In Figure 5, the measured flow rate data obtained for four melting seasons is plotted against the corresponding water level measurements. A possible rating curve or expression of the water level as a function of the discharge is obtained by fitting a power law to the measured data in a least-squares sense is suggested by the dashed line and corresponding 10 percent intervals by the dot-dashed lines. Most of the measured data lies within these intervals. Results of tracer tests are also shown in this Figure and are well corresponding with the possible rating curve.

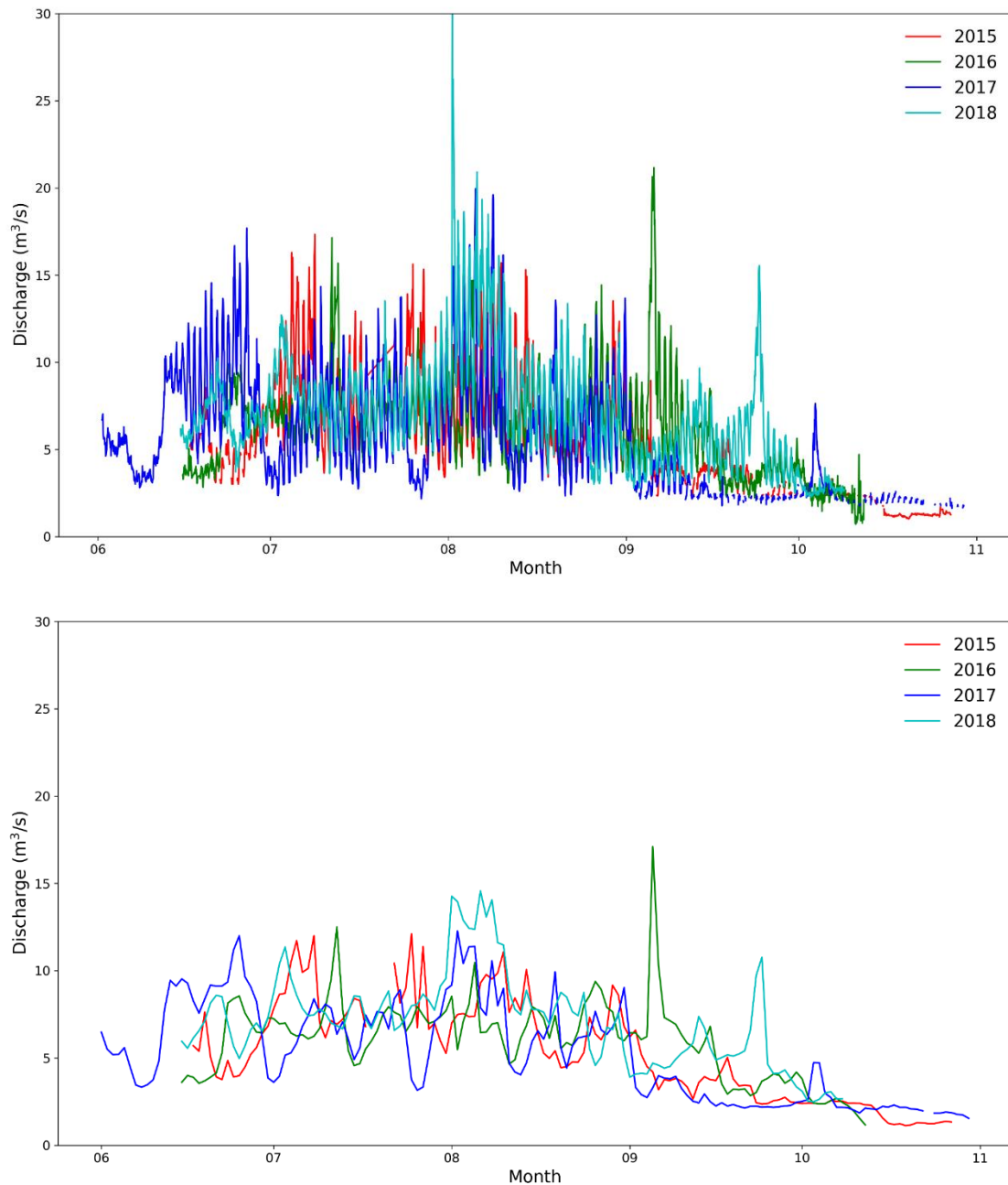


**Figure 4. Hourly (top) and daily (bottom) time series of flow data for the melting seasons of 2015 to 2018.**

As this measurement system provides simultaneous water level and flow measurements, it allows to detect events upon which the measured data deviates from the rating curve observed previously, so-called de-rating events. Such an event is illustrated on the Figure 6, where the data of the 2018 melting season is shown and color-coded with the calendar week corresponding to the date of the measurement. For this season, a flood event occurred during the calendar week 31 (first days of August) and resulted in a de-rating event

illustrated by the departure of the measured data from the expected rating curve. In such an event, the cross-section is subject to substantial changes due to the interplay of hydromorphologic processes such as erosion and sedimentation, so that for similar water levels as previously measured, the obtained flow values are significantly different. On Figure 6, note the dashed-line which is the original rating curve on which the data of the season 2018 is falling until the flood event of week 31. The bathymetry of the measurement site was recalibrated upon the de-rating event and the resulting data is the one presented in the Figure 5. With this updated bathymetry, the data is again more similar to the original rating curve measured.

For every measurement performed, a so-called proof image showing the measured water-level and surface-velocity field measured is stored. In the case of the de-rating event mentioned, the proof-image can be assessed a posteriori to ensure that the anomaly detected is in fact the consequence of an extreme event and not the consequence of a measurement error. Warnings can be configured so that the user is informed as soon as such events occur.

An interesting feature of this technology is that the measurements can be performed without having any instrument directly in contact with the water. Such non-contact measurement techniques are particularly of interest in the alpine context where the river bed is subject to important hydromorphological processes, so that material installed in the river bed or its vicinity could be damaged upon extreme events such as floods or landslides. This is particularly true in the present case, as for example the boulder present in Figure 2 B and not visible in any images of Figure 3 attests of the instability of the river bed. Again, real-time access is of interest here as it allows to visually inspect the occurrence of such events.

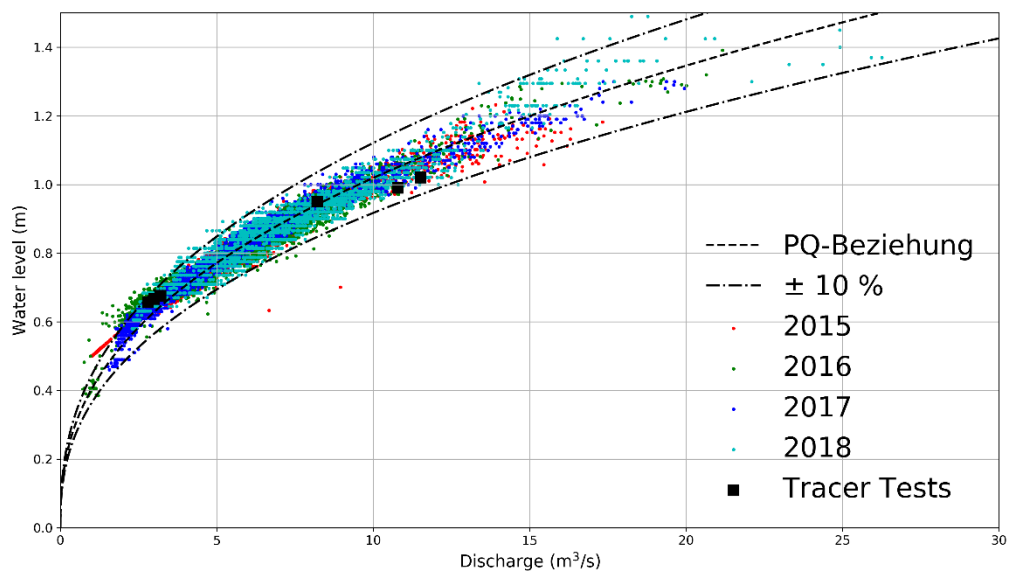


**Figure 5. Measured water level plotted as function of the measured discharge for the melting seasons 2015 to 2018, as well as several tracer tests performed (black dots). The black dashed-line presents a possible rating-curve and the dot-dashed lines represent 10 percent intervals.**

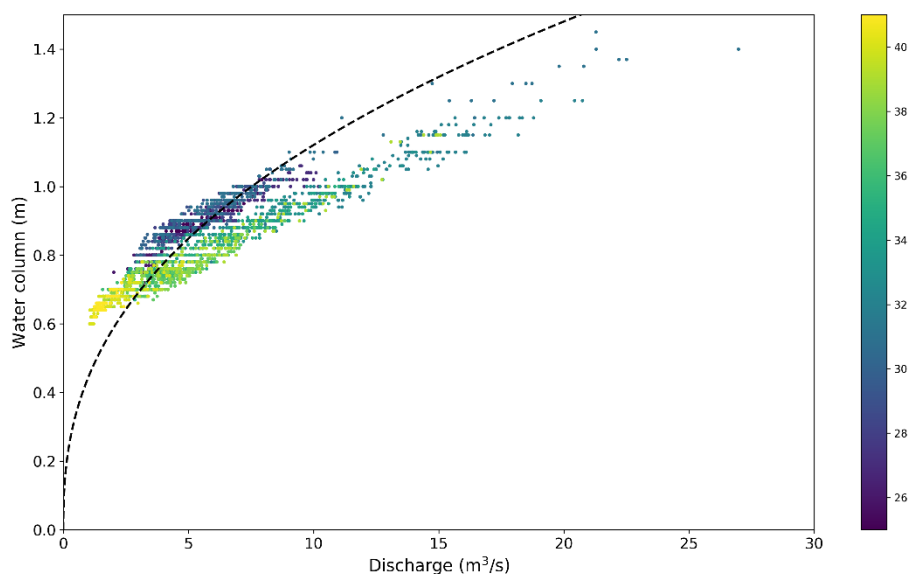


**Figure 6. Water level and discharge data measured for the 2018 melting season color-coded with the calendar week before the correction for the de-rating event. Note the de-rating event occurring at the beginning of the calendar week 32.**

## Conclusions

The results presented in this study underline the potential of non-contact image-based approaches for flow measurements in remote areas. Thereby, one very interesting feature of the technology introduced is that it allows real-time access to the measurement system, providing some interesting information to monitor flow and the vicinity of the river bed. Additionally, early warning can easily be implemented in such measurement system, informing the user in case of extreme events and the plausibility of these early warnings could be checked in real-time.

## References

- Absi, R. (2006). "A roughness and time dependent mixing length equation." *Journal of Hydraulic, Coastal and Environmental Engineering*, Japan Society of Civil Engineers 62 (4): 437-446.
- Adrian R.J. (1991). Particle-imaging techniques for experimental fluid mechanics. *Annual Review of Fluid Mechanics* 23.
- Bandini F., Lüthi B., Bauer-Gottwein P. (2019). Unmanned aerial systems (UASS) for monitoring water surface elevation, bathymetry, surface velocity and discharge in streams. *Drone Special, Hydrolink* (1).
- Carrel M., Detert M., Peña-Haro S., Lüthi B. (2019). Evaluation of the DischargeApp: a smartphone application for discharge measurements. *Hydrosensoft 2019*, Madrid, Spain.

Fujita I., Muste M. and Kruger A. (1998). Large-scale particle image velocimetry for flow analysis in hydraulic engineering applications. *Journal of Hydraulic Research* 36(3).

Leitão J.P., Peña-Haro S., Lüthi B., Scheidegger A., Moy de Vitry M. (2018). Urban overland runoff velocity measurement with consumer-grade surveillance cameras and surface structure imaging velocimetry. *Journal of Hydrology* (565) 791 – 804.

Muste M., Fujita I., Hauet A. (2008). Large-scale particle image velocimetry for measurements in riverine environments. *Water Resour. Res.*, 44.

---

# Regobs – an open geohazards-related data hub used in citizen science, warnings, preparedness and crisis management

Rune Verpe Engeset<sup>1</sup>, Ragnar Ekker<sup>2</sup>, Priska Hiller<sup>3</sup>, Tore Humstad<sup>4</sup>

**Keywords:** Field data; Crowd sourcing; natural hazards; modelling; machine learning

## Abstract

The Regobs system enables all stakeholders to submit and share data on geohazards in real-time using web applications. Users include Norwegian warnings services for floods, landslides, snow avalanches and lake/river ice problems, transportation authorities and companies, rescue services and the military. This paper presents the 2019 improvements, which includes an English version and international maps. We describe how the system is being used in forecasting and management of geohazards, and how it enables crowd sourcing and citizen participation. We also discuss opportunities for machine learning and modelling using the system.

## Introduction

Observing current conditions and sharing data with several stakeholders in real-time, are crucial for management of geohazards. In order to effectively manage data, the Norwegian Water Resources and Energy Directorate (NVE) has developed the Regobs system (Fig. 1) to manage floods, landslides, snow avalanches and lake/river ice problems – in close collaboration with the National Public Roads Administration (NPRA) and the Norwegian Meteorological Institute (MET). Regobs is short for **register observations**. The system just recently has become available in English with universal functionality, thus the aim of this presentation and paper is to give an overview of the system, provide some examples of use and to discuss associated opportunities and challenges.

---

<sup>1</sup> Dr., Head of section, Norwegian Water Resources and Energy Directorate, Middelthunsgate 29, Oslo, Norway (rue@nve.no)

<sup>2</sup> Siv.Ing., Norwegian Water Resources and Energy Directorate

<sup>3</sup> M.Sc., Norwegian Water Resources and Energy Directorate

<sup>4</sup> Siv.Ing., National Public Roads Administration

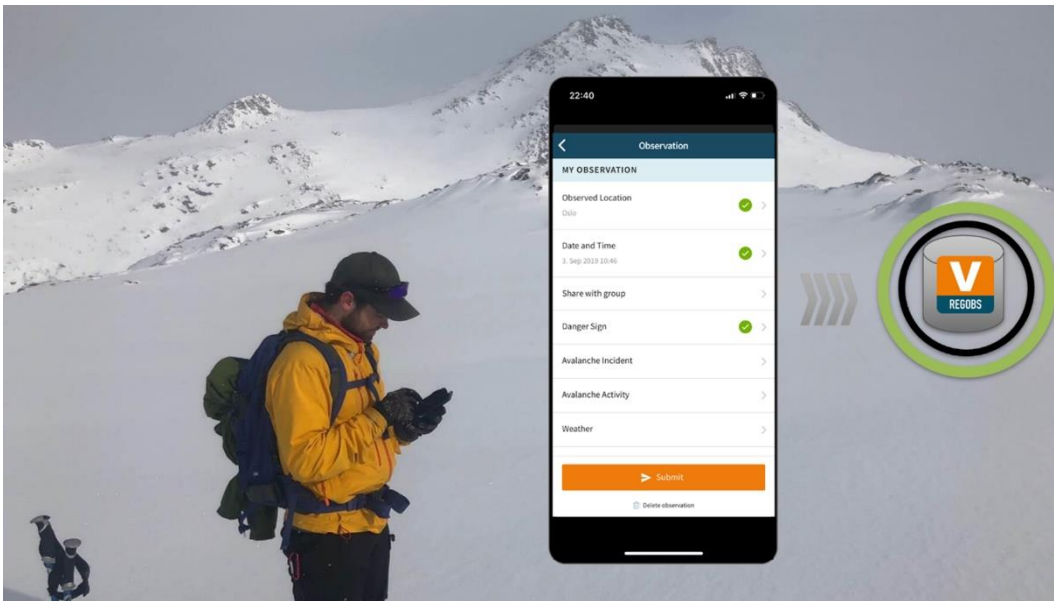


**Figure 1. A professional observer submitting data from the field in order to be immediately available to the avalanche forecasting.**

Regobs is part of the Varsom portfolio (Johnsen, 2013), which is shown in Fig. 2. The purpose of Varsom is to prevent loss of life and values due to avalanche, floods, landslides and weakened ice conditions in Norway. When developing the system, we aimed at making a tool for efficiently gathering of data, data such as snow conditions, avalanches, landslides, floods, ice conditions and images. We wanted to ensure that data are available to everybody for immediate use.

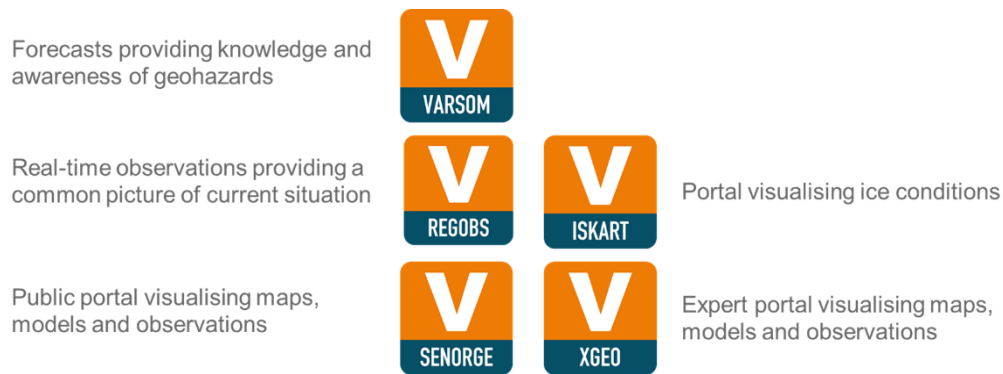


**Figure 2. The Varsom family. All modules are available on the web with the .no postfix. Varsom Regobs is also available as an app.**

The four categories of observations in Regobs are snow, ice, soil and water. Observations of weather, danger signs, avalanche events, avalanche activity, snow cover, tests, snow profiles, avalanche problems, avalanche danger assessments, accidents/incidents and notes are available in the snow category, while danger signs, ice cover, ice thickness, accidents/incidents, and notes in the ice category, danger signs, landslide events and notes in the soil category, and water levels, damages and notes in the water category. Several parameters may be recorded in each observation.

## Methods

Regobs is a web-based system, which includes a smartphone app, open data on Application Programming Interfaces (API's), databases and a webpage (Engeset et al., 2018). The app has both online and offline capacity, and includes relevant supporting thematic maps and data. We have an open and free policy for data access and users. Development started in 2011 (Ekker et al., 2013) in support of establishing the Norwegian Avalanche Warning Service (Engeset, 2013) and Landslide Warning Service (Krøgli et al., 2018). The Norwegian Flood Warning Service, which has been operational since 1989, started to publish warnings on Varsom and use Regobs for manual field observations in 2013.

Regobs enables crowdsourcing and citizens participate by submitting observations, provide feedback on forecasts or share information with others (Hiller et al., 2019). This way citizens gain knowledge and awareness of the geohazards at hand, and get better at managing risk. Most participants are preparedness/crisis managers for companies/organisations, or individuals traveling in the backcountry on their own or in groups. Thus, preparedness and crisis management stakeholders and the public share data on the current situation and interact with the forecasting services.

All data in Regobs is licenced under the Norwegian licence for public data (NLOD), which is compatible with the Creative Commons licence for public use by attribution (CC BY 4.0). This ensures that data submitted and thus shared in Regobs is for all to use equally. In order to make data use effective, we developed API's to gives other applications access to our applications and data. API's are used to connect the Varsom systems and between Varsom and third-party systems (Fig. 3), such as the reporting system ELRAPP used by NPRA and all road management contractors.

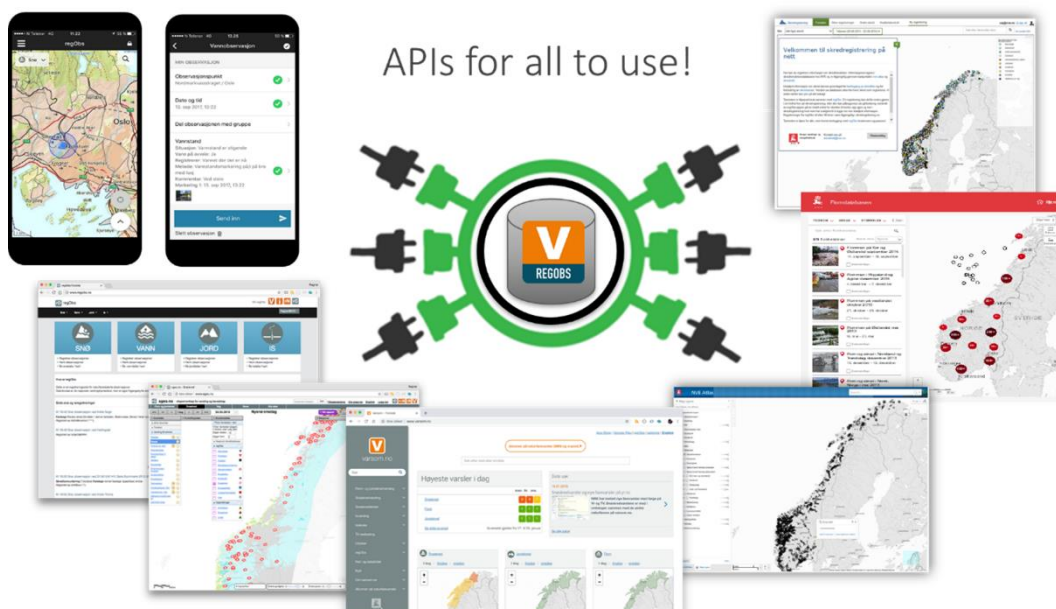


**Figure 3. Illustration of interconnectability between systems using API's. Both the Regobs app and webpage use the open API's, as do other systems: data delivery from ELRAPP and the road managements**

companies, Xgeo data visualisation, Varsom.no data visualisation and Regobs data sharing with the national databases for avalanche, landslide and flood events.

The data are provided and displayed on Regobs “as is” and unvalidated. However, users are assigned a competence level (from 1 to 5 stars) if known to the administrator of the system. If not the user and observations are tagged by “Competence unknown”. The competence levels are assigned based on observer experience and education. It is very useful information for the users of data in order to assess which observers and observations to trust. An explanation of the levels is provided on <https://www.varsom.no/regobs/kompetanse/> (in Norwegian).

## Results and discussion

By autumn 2019, more than 100 000 observations have been submitted in Regobs since it was launched at the end of 2012. The use has increased every year. Most observations are submitted during the winter seasons. 67 % of the observations are snow related and 22 % ice related (Fig. 4).

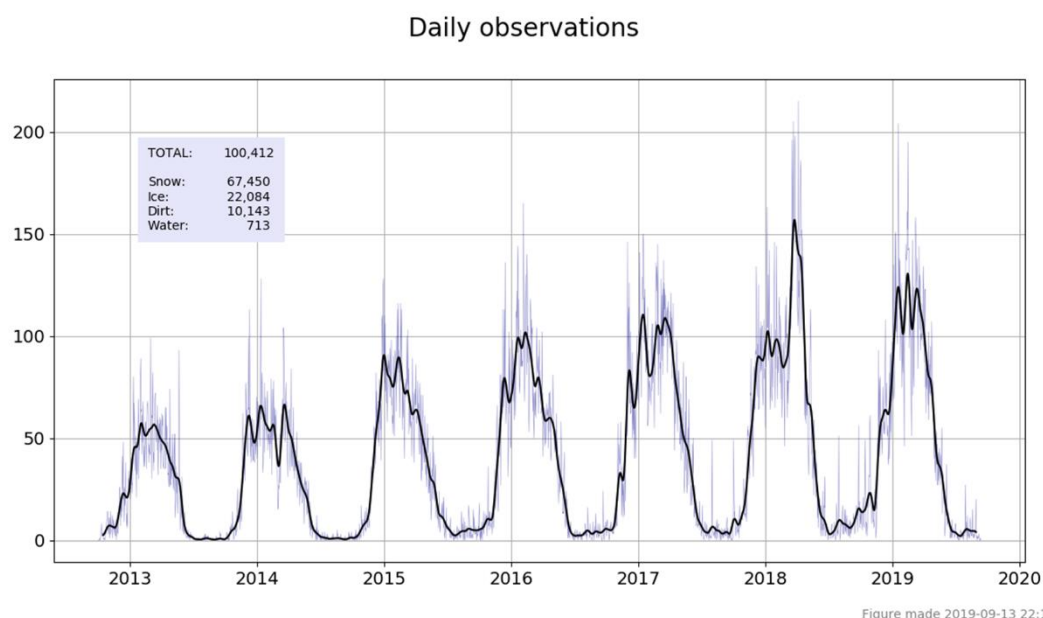


**Figure 4. Data statistics for Regobs. Blue shine show number of observations per day, while the black line shows a smoothed weekly average.**

How can observations help prevent problems caused by floods, landslides, avalanches and ice, now and in the future? Our experience is that observations of incidents, danger signs, events and damages shared in Regobs improve forecasting, crisis management and planning.

The value of Regobs for crowdsourcing increases every year, as more and more citizens become aware of the system and its value. During Easter 2018 (Saturday 24th March to Tuesday 2nd April), Regobs received 1 393 snow observations. 14 % of the submissions were from professional observers, 32 % from public partner organisations (MET, NPRA and the military), and as many as 54 % were from other professionals and the public. In fact, the public provided a large and important volume of observations and hence improved

the quality and reduced the uncertainty of the avalanche forecasts during this period with heavy activity in the mountains.

Collaboration and data sharing are also important for managing other geohazards. Regobs will be integrated as the first-stop observing service for the national flood event documentation system, as illustrated in Fig. 5. Geolocation and image data from events are very useful to get in real-time using Regobs, as illustrated in Fig. 6.



Figure 5. Illustration of the data flow and interaction between stakeholders.

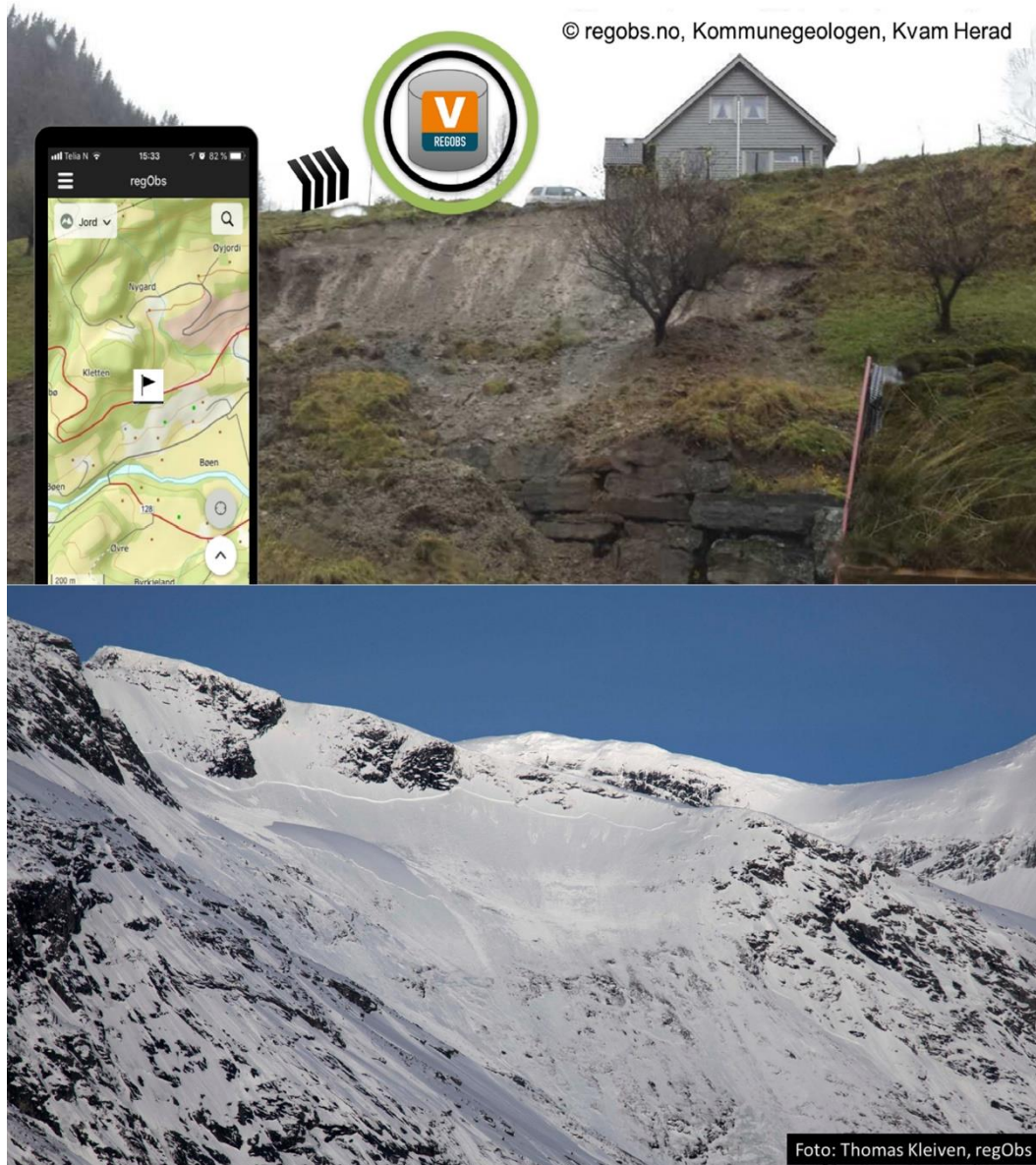


**Figure 6.** Geolocated and time-stamped pictures of events (landslide at the top and avalanche at the bottom) are very useful to understand triggering mechanisms, size and (potential) damages.

In 2019, we introduced support for English language and international use (universal maps, time and positioning) in the app, previously it was in Norway/Norwegian only. Other languages (German, Slovenian and Italian) are in the pipeline. The website was internationalized during 2019. Recording and plotting of snow profile is another feature introduced in 2019. It was a great success; during the first season, 1700 snow profiles were submitted. Fig. 7 shows the English version of the Regobs app and the Regobs web, as well as the relation between maps, observations and the warnings.

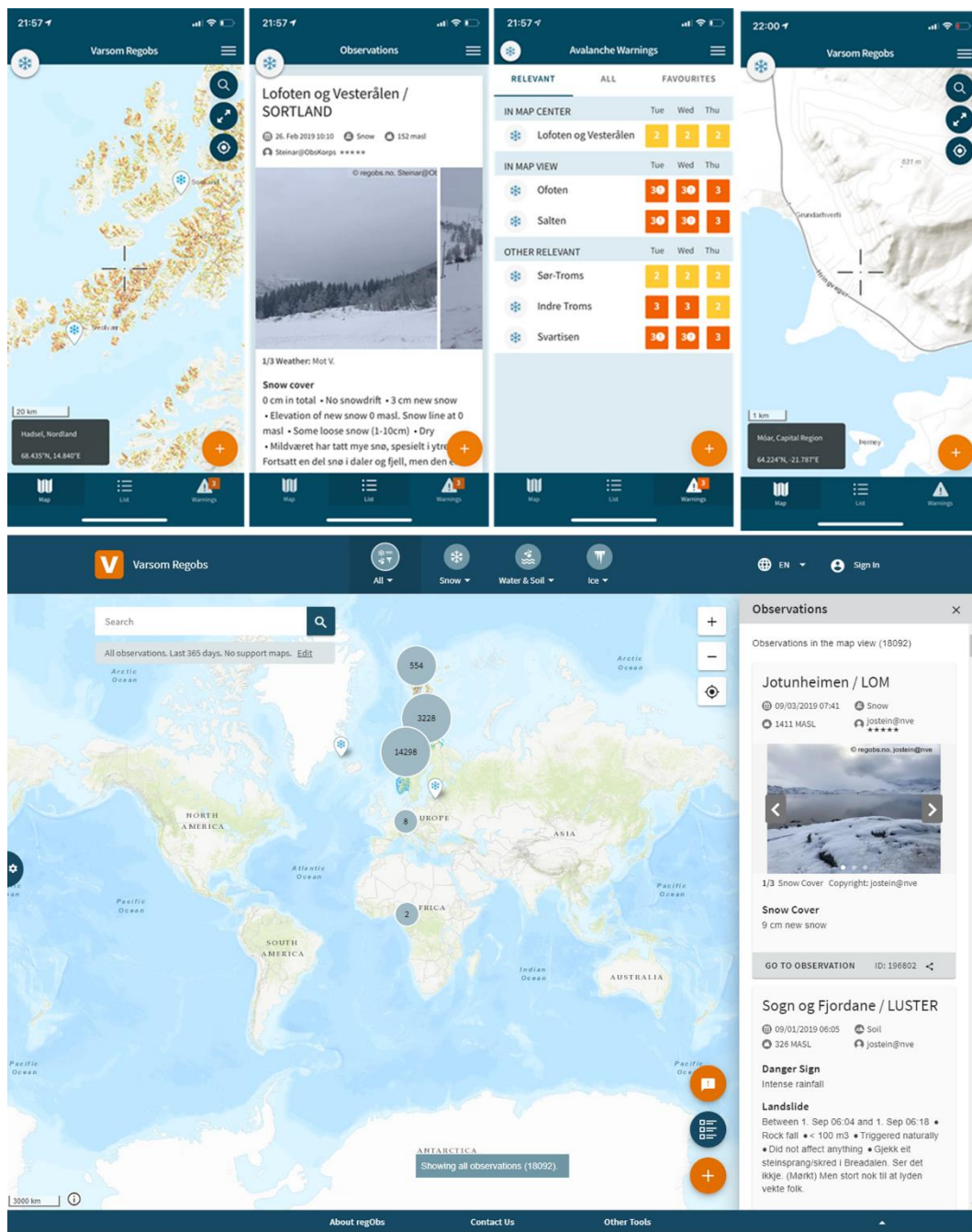


Figure 7. Upper panels shows screenshots from the Regobs app (map, observations, forecasts and detailed maps) and bottom panel shows screenshots from the Regobs webpage.

The Regobs policy for free open data and crowdsourcing has a number of advantages; Data in real time, a lot of observations and combination with relevant background maps and data. However, there are also some challenges: Unfiltered publication, need for evaluation of quality, and coming up with incentives for getting more professional and public users. The open approach offers a number of opportunities: Increased number of observations, common contribution to public safety and awareness, and a community-based development based on experience. So far, the advantages have outweighed the challenges by far.

Regobs contains data, which support geoscientific modelling and artificial intelligence. For example, snow profiles may be used to model the development of snow properties relevant to weak layers and avalanche release, by using an online snow model and weather prediction data. The evolution of ice on lakes may be modelled using a fresh water ice model and weather data. Field observations of snow and avalanches may be used as one of the data sources for machine learning and thus contribute to the automatization of the avalanche forecasting process. Field observations of water levels in rivers, lakes or urban areas may be used to drive or validate hydrological and hydraulic models in order to improve our management of floods and water damages. These applications are currently topics for research and development at NVE. As data are openly available on API's, also other users are free to explore the potential in the system and its data.

## Conclusion

Regobs has become the working horse for collecting and sharing observations of snow, avalanches, floods, landslides, weather and ice in Norway. Its crowdsourcing appeal multiplies observations and use: 1 observation from 100 users, gives 100 observations to 100 users! Regobs structures observations well for use in forecasting, planning, research and education. The in-situ observations are useful when managing critical events and Regobs helps in communicating the current situation to and between stakeholders including the public. Historical events are useful in handling critical events, as they help in learning from previous events. Current research and development explore the potential of machine learning and modelling, in order to make use of the data to improve forecasting and crisis management in the future.

Regobs may be used in other countries, as international maps and support for other language are available. If necessary in the future, Regobs may also be extended to include other hazards, such as strong wind, fires, droughts, lightening and earthquakes.

Professionals, the public, students and academia can use and support Regobs on web at [www.regobs.no](http://www.regobs.no) and as app at [App Store](#) and [Google Play](#).

## References

- Ekker, R., Kvaerne, K., Os, A., Humstad, T., Warttinen, A., Eide, V., Hansen, R.K., 2013: RegObs – Public Database for Submitting and Sharing Observations. Proceedings of the International Snow Science Workshop, 7–11 October, Grenoble, France, 461–465, 2013.
- Engeset, R.V., 2013: The Norwegian Avalanche Warning Service. Proceedings of the International Snow Science Workshop, 7–11 October, Grenoble, France, 301–310, 2013.
- Engeset, R. V., Ekker, R., Humstad, T., Landrø, M., 2018: Varsom:regobs – A common real-time picture of the hazard situation shared by mobile information technology. Innsbruck, International Snow Science Workshop: 1573-1578, 2018.
- Hiller, P.H., Midttømme, G.H., Ekker, R., 2019: regObs, a tool to share observations in safety management. In Tournier, J.-P., Bennett, T., Bibeau, J., Sustainable and safe dams

around the world: Proceedings of the ICOLD 2019 Symposium, (ICOLD 2019), June 9-14, 2019, Ottawa, Canada.

Johnsen, E., 2013: Modern forms of communicating avalanche danger – A Norwegian case. Proceedings of the International Snow Science Workshop, 7–11 October, Grenoble, France, 423–427, 2013.

Krøgli, I. K., Devoli, G., Colleuille, H., Boje, S., Sund, M., and Engen, I. K.: The Norwegian forecasting and warning service for rainfall- and snowmelt-induced landslides, *Nat. Hazards Earth Syst. Sci.*, 18, 1427–1450, <https://doi.org/10.5194/nhess-18-1427-2018>, 2018.

---

# Dynamics and geomorphological analysis of the Taan Fiord 2015 tsunamigenic landslide

Andrea Franco<sup>1</sup>, Andreas Huber<sup>2</sup>, Jasper Moernaut<sup>3</sup>, Barbara Schneider-Muntau<sup>4</sup>, Markus Aufleger<sup>5</sup>, Michael Strasser<sup>6</sup>, Bernhard Gems<sup>7</sup>

**Keywords:** Tsunamigenic landslide; Digital Elevation Models; Geomorphological analysis; Cascade hazard; Mountain hazards.

## Abstract

Landslide-generated impulse waves in water bodies can have devastating effects on surrounding areas. The recent tsunami event in the Taan Fiord (Alaska) in October 2015 presents a good opportunity to analyse the landslide dynamics and its characteristics. Based on multi-temporal digital elevation models from different sources we provide a geomorphological analysis to interpret the processes and give an estimate of changes in the landslide volumes before the final failure. Based on these results, displacements in the landslide source area before the 2015 event have been observed in the same order of magnitude as the final collapse. These pre-collapse movements are related to the glacier advances and retreats, influencing the slope stability and probably causing the landslide failure in response to a sudden retreat after 2013. This work underlines the importance of investigating pre-collapse slope movements and forms a good data base for future efforts to back calculate the tsunami event in the Taan Fiord.

## Introduction

Tsunamigenic landslides can present a serious threat to human lives and infrastructure in affected areas. Climate change and environmental variations like glacier retreat can have a significant influence on stability of steep slopes (Higman et al., 2018). In many cases a lack of observations with high temporal resolution impedes the study of these processes. The landslide-induced tsunami event in the Taan Fiord (Fig.1) on 17 October 2015 presents an exceptional case in terms of data availability. At this date, a huge landslide (tens of Mm<sup>3</sup>, Haeussler et al., 2018) impacted the sea (and partially the glacier) at the head of the fiord

---

<sup>1</sup> M.D., PhD., Unit of Hydraulic Engineering, University of Innsbruck, AUSTRIA, ([Andrea.Franco@uibk.ac.at](mailto:Andrea.Franco@uibk.ac.at))

<sup>2</sup> D.I., Unit of Hydraulic Engineering, University of Innsbruck

<sup>3</sup> Dr., Institute of Geology, University of Innsbruck

<sup>4</sup> Dr., Unit of Geotechnical and Tunnel Engineering, University of Innsbruck

<sup>5</sup> Dr., Unit of Hydraulic Engineering, University of Innsbruck

<sup>6</sup> Dr., Institute of Geology, University of Innsbruck

<sup>7</sup> Dr., Unit of Hydraulic Engineering, University of Innsbruck

(Fig. 1c), triggering a tsunami that propagated along the bay for more than 20 km and reached a maximum run-up of 193 m on the headland in front of the landslide source (Haeussler et al., 2018). George et al. (2017) numerically modelled the tsunami event. The authors recreated most of the features of the landslide process and wave inundation starting from their own reconstruction of the pre-event failure surface, the bay head and bathymetry configuration. Dufresne et al. (2017) and Higman et al. (2018) recognised the landslide as a rotational slide and described the wave dynamics observing geological records onshore after the event. Haeussler et al. (2018) provided results from geophysical investigations that took place in summer 2016, focusing on topographical changes, bathymetric observations and seismic stratigraphy for submarine depositional processes. They estimated a volume for the subaerial source of about 75.7 Mm<sup>3</sup> comparing their results with the IFSAR DEM of 2012.

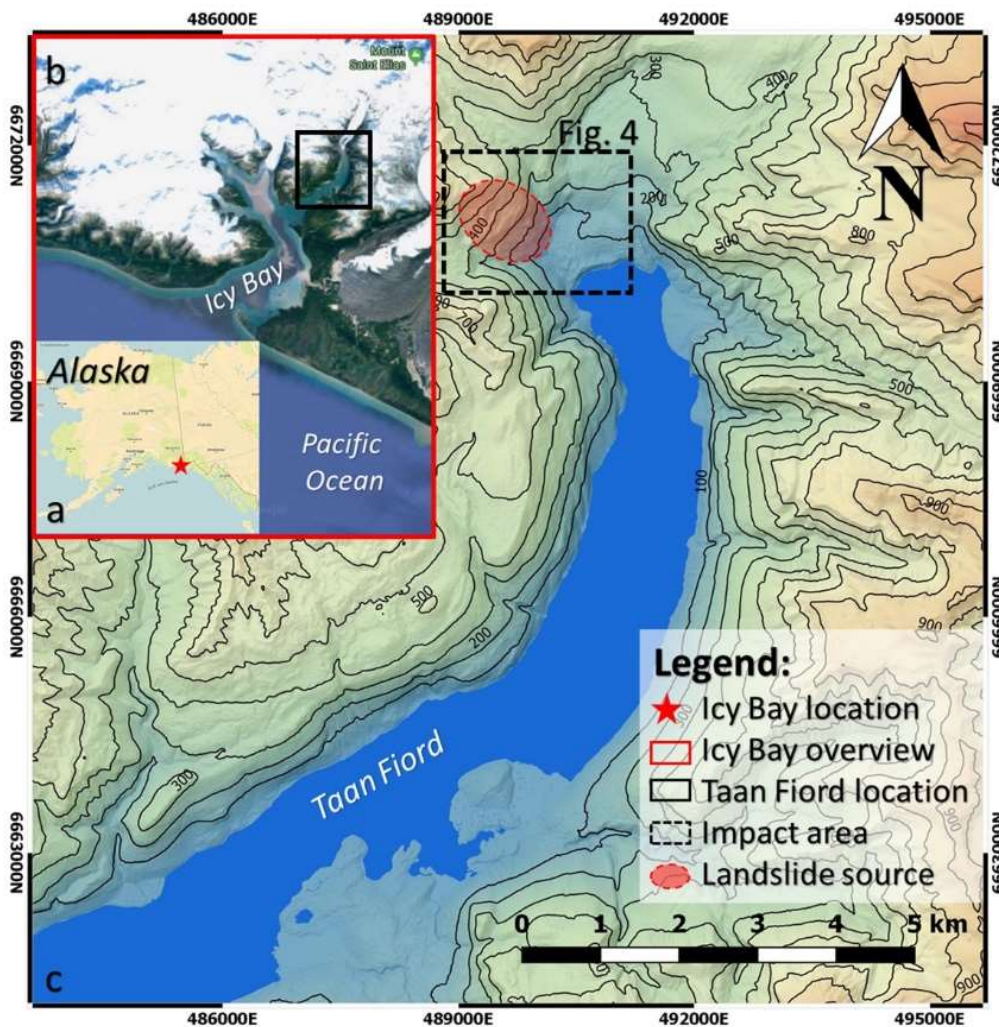


Figure 1: Case study location. a) Location of Icy Bay, south of Alaska. b) Location of Taan Fiord. c) View of Taan Fiord in 2012 (DEM provided by Elevation Portal of Alaska – DGGS). The landslide source at the head of the bay (red circle) is highlighted (satellite image from © Google Earth Pro 7.3.2.5776). Coordinate reference system: WGS84/UTM zone 7N.

For this work, several digital elevation models (DEMs), from 2000 to 2016, have been compiled (available from different sources, see Tab. 1). Since 2017, a new dataset for the Icy Bay (Arctic DEM AK V.2 - 2014) is available on the Elevation Portal of Alaska – DGGs. This gives us the possibility to observe the landslide position one year before the catastrophic event and to update the estimate of the landslide volume before final collapse.

The main aims of this study are:

- to analyse the landslide displacements with time and to establish possible relations to the glacier movements utilizing open-source GIS-software (QGIS, SAGA GIS);
- to quantify the volume involved in the displacements before the final collapse (Tab. 2) and the volume of the landslide that actually induced the tsunami in 2015 (Tab. 3).

Name	Publication Date	Acquisition Date	Resolution (m)	Method	EPSG	Source
Icy Bay 2000	30/08/2000	18-26/08/2000	5	Intermap STAR-3i airborne interferometric synthetic aperture radar (SAR) system mounted in a LearJet 36A aircraft.	32607	DGGs Elevation Portal of Alaska
Mt Saint Elias 2002	30/12/2002	03-05/08/2002	10	Intermap Technologies airborne interferometric SAR data acquisition system.	32607	DGGs Elevation Portal of Alaska
IFSAR	08/04/2015	14/08-08/09/2012	5	IFSAR data	3338	DGGs Elevation Portal of Alaska - USGS National Map
Arctic DEM AK (5m Mosaic) V2	21/05/2017	01/03/2014	5	Optical stereo imagery, high-performance computing, and open source photogrammetry software.	3413	DGGs Elevation Portal of Alaska
taan_topobathy_1m_UTM7_WGS84	11/10/2018	01/08/2016	1	Lidar data set, collected using a system based on a Riegl LMS-Q240i Pulsed Scanning Altimeter	32607	Haeussler et al. (2018)

**Table 1. DEM catalog**

Time interval	Resolution	Negative $\Delta V$ (Mm <sup>3</sup> )	Mapped area (m <sup>2</sup> )	Positive $\Delta V$ (Mm <sup>3</sup> )	Mapped area (m <sup>2</sup> )
2012-2014	5	-28.50 ± 1.66	817000	3.51 ± 0.76	373000
2014-2016	5	-27.50 ± 1.52	824000	1.75 ± 0.34	183000

**Table 2. Volumes estimations**

Data	Symbol	Dimension	Value	References
Landslide width	sw	m	915	From this study
Landslide max. vertical thickness	sh	m	105	From this study
Landslide length	ls	m	1450	From this study
Landslide impact velocity	vs	m/s	36-45	Highman et al. (2018)
2015 landslide volume onshore	-	Mm <sup>3</sup>	23.5	Haeussler et al. (2018)
2015 landslide volume entered in the fiord	-	Mm <sup>3</sup>	26.0	From this study
2015 total landslide volume	Vs	Mm <sup>3</sup>	49.4	From this study
Density (weakly lithified sandstone)	$\rho$	kg/m <sup>3</sup>	2150-2650	Highman et al. (2018)
Impact slope angle	$\alpha$	degrees	10-20	From George et al. (2017) Icy Bay pre-event reconstruction

**Table 3. Landslide properties**

## Methods

The Elevation Portal of Alaska – DGGS provides several DEMs for the Icy Bay area, from 2000 to 2014 (Tab. 1). A reconstructed model of the Taan Fiord head in October 2015 as a pre-collapse configuration, based on the IFSAR DEM of 2012, is available from the work of George et al. (2017). Haeussler et al. (2018) produced a detailed bathymetry and a topographic surface of the fiord after the tsunami event, providing a high resolution DEM of 1 meter. Where necessary, a re-projection to a common Coordinate Reference System (CRS) has been performed. The Arctic DEM-2014 shows significant vertical and horizontal offsets compared to the DEMs of 2012 and 2016. In order to compare the different DEMs, a co-registration (correction in offset differences) of the digital models of 2014 and 2016 to the DEM of 2012, using the method presented by Nuth and Kääb (2011), was performed. For this step we utilized demcoreg, a collection of python and shell scripts for DEM co-registration (Shean et al., 2016). Afterwards, a Root Mean Square Difference (RMSD) between the DEMs of 2014 and 2012 and between 2016 and 2014 was found to be 2.03 m and 1.85 m respectively. RMSDs were obtained for “stable terrain features” present in all DEMs. Taking into account the high geomorphological dynamics of this area and the high variability in snow cover during the year, these statistics seem reasonable for the purpose of this study. For further geomorphological analysis, to allow a better visual interpretation of the topographic surfaces, all available DEMs were resampled to the resolution of the most recent terrain model (1m) using the bicubic spline interpolation method available in SAGA GIS. Changes in the shoreline and glacier position in time are highlighted and fluctuation of the glacier limit along a pre-defined cross-section G-G’ (Fig. 2) has been estimated based on the available DEMs and satellite images (Landsat 7, Landsat 8). Scarps in the landslide area are manually identified for different DEMs (Fig. 3a). Deformations in time are noticed along cross-section A-A’ (Fig. 3b). Mass movements, elevation difference distributions and related volumetric changes are given through a raster difference utilizing the raster calculator method implemented in QGIS. For these estimations, the resolution of 5 m has been adopted.

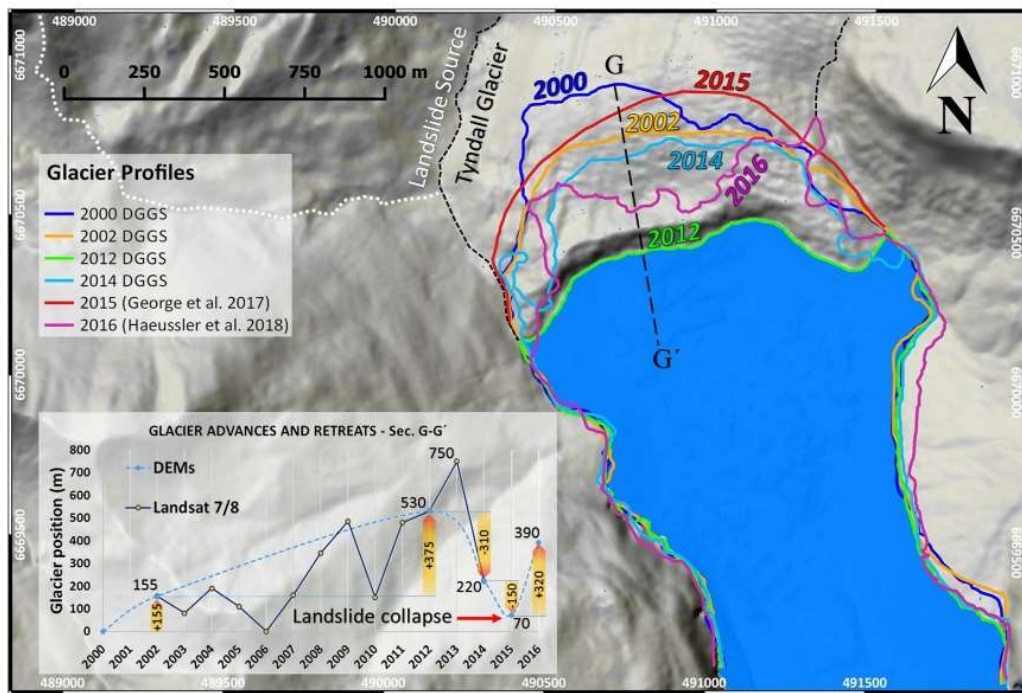


Figure 2: Glacier movements. Shoreline changes in time at the head of the bay. The glacier and the delta fronts variation are shown from 2000 to 2016. The shoreline of 2015 is taken from the reconstruction of George et al. (2017) as bay head pre-event configuration. The graph shows the glacier position in time for the available DEMs and satellite images from Landsat 7 and Landsat 8 - USGS. Orange columns highlight the associated glacier movements for the available DEMs.

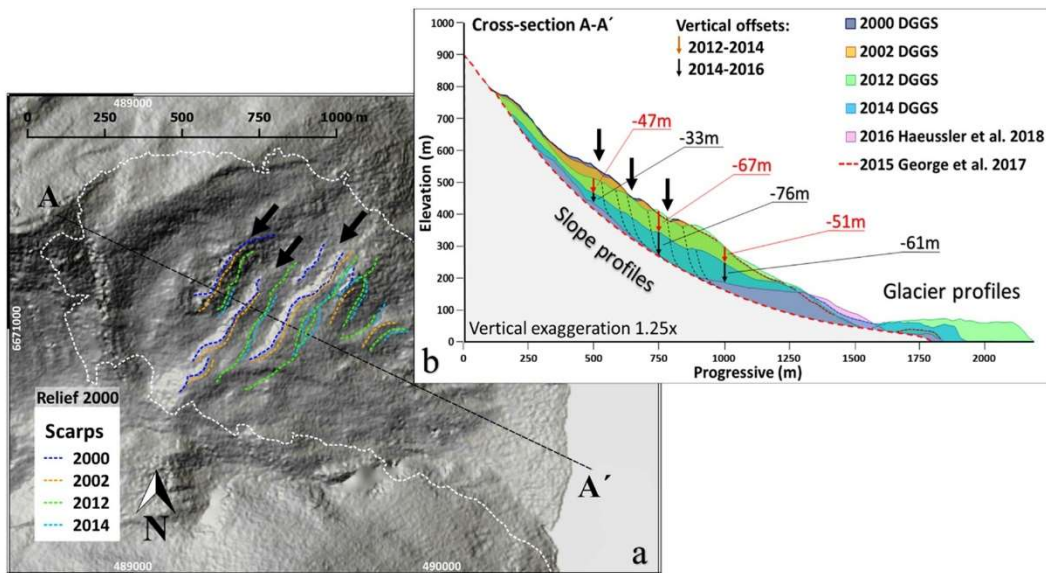
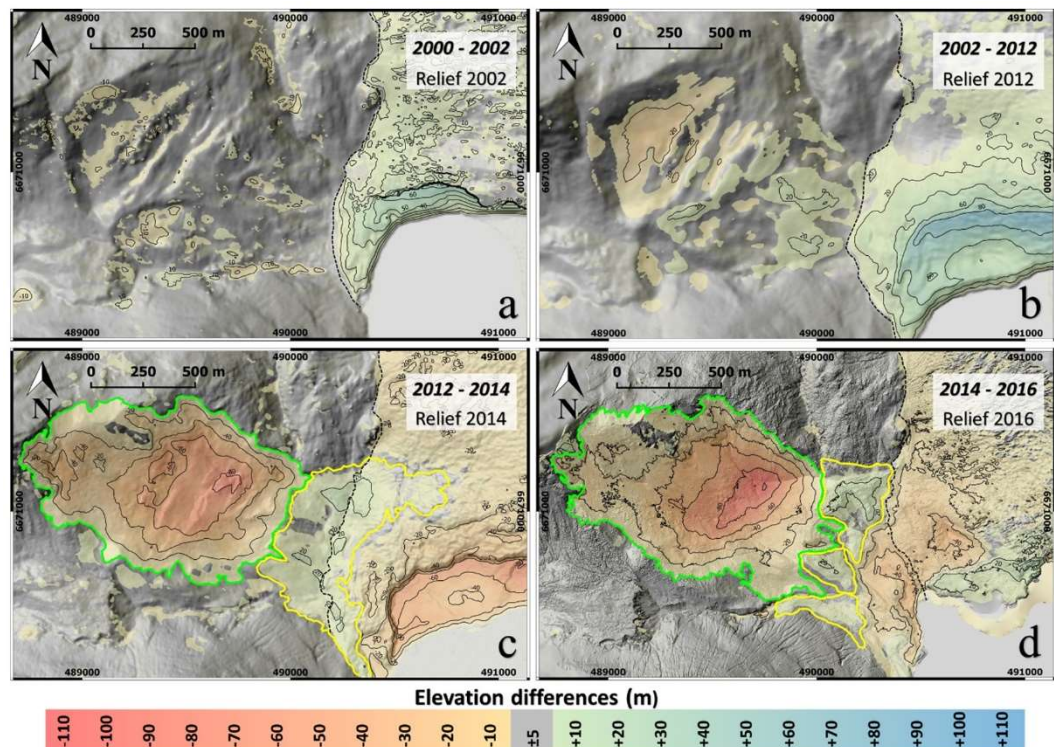


Figure 3: Landslide profile. a) Recognized scarps in the landslide area (white dashed line) from 2000 to 2016. The black dashed line represents the cross-section A-A'. b) Different landslide profiles in time along section A-A'. Vertical displacements between 2012-2014 (red) and 2014-2016 (black) are estimated. The black arrows indicate the position of the observed grabens. Sub-vertical discontinuities (black dashed lines) in the landslide body are hypothesized since the presence of scarps and the considerable vertical displacements. The red dashed line in section shows the failure surface interpreted by George et al. (2017).

## Results and discussion

From the interpretation of the different DEMs (Tab. 1) and additional sources as Landsat 7 and 8, it appears that the Tyndall Glacier front at the head of the fiord had advanced and retreated several times in the last decades (Fig. 2). Along the line G-G' the glacier front advanced more than 500 m up to 2012 compared to the 2000-position. After its greatest advance in 2013 (about 750 m), the front retreated again by around 500 m in 2014 and another 150 m up to the time of the documented landslide in 2015. As reconstructed from George et al. (2017), in October 2015 the glacier is located very close to its position in 2000. After the event, in 2016 the glacier advanced again around 320 m. These glacier movements can be related to the landslide displacements. In Figure 3a several upslope facing scarps noticed from 2000 to 2014 are highlighted. Most of them are still recognizable until the year 2014, with a variable horizontal displacement of 30-100 m in the slide direction. Through a cross-section (Fig. 3b), it is possible to observe the slope and glacier profile in time. Grabens in the upper part of the landslide body are present in the year 2000 (black arrows in Fig. 3). These were already noticed from aerial photos taken in 1996 (Meigs et al., 2006). Vertical offsets at progressive distance of 500-750-1000 m from the landslide crest are provided for the intervals 2012-2014 and 2014-2016, showing the large change for the landslide body position (Fig. 3b). George et al. (2017) defined a possible failure surface (red dashed line in Fig. 3b) that seems to be well representative for the lower part of the scar area, under the remaining accumulated material. Along this surface, the landslide could have deformed several times during the last decades. In Figure 4 these movements and their relative elevation difference distributions are shown. Between 2000 and 2002 (Fig. 4a) vertical displacements of maximum -15 m on the upper part of the slide body and small increases in the centre are noticed. The glacier advanced, keeping a thickness of 70 m. In the time interval of 2002-2012 larger displacements are recognizable in the upper part of the landslide with a negative maximum offset of -40 m and a maximum positive one of about 25 m (Fig. 4b). In 2012 the glacier reached a thickness of 100 m. Between the years of 2012 and 2014 a considerable displacement is noticed (Fig. 3b), with a maximum vertical offset of -90 m resulting in about -28.5 Mm<sup>3</sup> of volume changes (Fig. 4c area in the green line). At the base of the landslide and on the glacier (that retreated about 500 m from 2013 with a lack of -80 m in thickness at the head of the fiord) a positive volume change (Fig. 4c, area in the yellow line) resulting in an additional volume of 3.5 Mm<sup>3</sup> and up to 35 m in thickness can be observed. On 17 October 2015 the landslide collapsed and impacted into the water body (and part of the glacier) triggering a giant tsunami that devastated the forest along the fiord. The exported volume from the difference between the years 2014-2016 results in approximately -27.5 Mm<sup>3</sup>. Maximum negative vertical displacements are estimated in the range of -105 m (Fig. 4d). An amount of additional accumulated material up to 35 m is still observed in the slide scar, resulting in 1.75 Mm<sup>3</sup> (Tab. 2). According to George et al. (2017) the glacier had a varying thickness between 50-20 m in front of the slide source from north to south at the moment of the collapse. Afterwards, the glacier results completely disintegrated from the landslide.



**Figure 4: Displacements distribution. Landslide evolution and involved displacements distribution. The difference in elevation for the landslide area and glacier body are shown for the time interval a) 2000-2002, b) 2002-2012, c) 2012-2014 and d) 2014-2016 representing the final collapse. The black dashed line separated the landslide source from the glacier body. Green and yellow lines in c) and d) refer to negative and positive vertical changes areas respectively.**

The glacier movements seem to have an effect on the landslide body stability, since several displacements are noticed while the glacier moved. Between 2012 and 2014 the scarps are still visible and no evidences of exported or accumulated material are noticed. This interval could represent an important phase of a creeping-motion of the landslide, where the pressure at the base induces a bulge of part of the glacier. As a trigger of the final collapse, the sudden retreat after 2013 and the lack of ice thickness in front of the sliding mass might have destabilized the slope since a lower slope buttress was missing. Moreover, as reported in Higman et al. (2018), in September and October 2015 precipitation records at the gage in Yakutat (110 km away) were about 10 % higher than normal (graphics available on <https://nwis.waterdata.usgs.gov>; <https://www.wunderground.com>). Even though these deviations were noticed also in the years prior to the landslide collapse, rain events combined with the fast glacier retreat could have influenced the underground water table and water saturation inside the landslide body, reducing its stability until the failure. Considering the landslide position after March 2014 and the glacier position in 2015, it is plausible that the landslide acted like a sub-horizontal piston (10-20° slope, Tab. 3), disintegrating a part of the glacier and inducing the wave impacting the sea with a velocity estimated between 36-45 m/s (Tab. 3, Higman et al., 2018). Haeussler et al. (2018) estimated a volume remaining in the scar of about 21.9 Mm<sup>3</sup> and 1.5 Mm<sup>3</sup> on the glacier (for a total of 23.4 Mm<sup>3</sup>, Tab. 3). Assuming these values, the final volume involved in the

final collapse is estimated to be approximately 49.4 Mm<sup>3</sup> (Tab. 3). While this is the total amount of material involved in the landslide, 26 Mm<sup>3</sup> entered in the fiord and possibly triggered the tsunami (Tab. 3).

From the findings of this work and a review of previous literature, a short table summarizing the main landslide properties and information for the collapse process is compiled (Tab. 3). These data provide a base for future works, to perform detailed slope stability analyses, assess landslide dynamics and links between the landslide and glacier dynamics, to eventually model the tsunami event towards advanced understanding of landslide-induced tsunamis and its cascade hazards effect.

## Conclusion

The tsunamigenic landslide event of October 2015 in Taan Fiord presents a case where the landslide dynamics can be analysed in more details since a large dataset of DEMs from 2000 to 2016 is available. The availability of multi-temporal pre- and post-event datasets allows an analysis of the landslide body prior to the final collapse. The use of open source software as QGIS and SAGA GIS is suitable for this geomorphological analysis and DEM elaboration, where insights about the deformation process and estimation of the involved volumes are provided. Utilizing the co-registration method proposed by Nuth and Kääb (2011) we could reasonably compare DEMs from different sources. RMSDs estimations, assuming stable areas in the DEMs, were in the range of 2 m, which was adequate for the purpose of this analysis given the large displacement volumes and significant morphological and nivological dynamics of the study area.

The method adopted for this study represents a suitable and easy approach to analyse qualitatively and quantitatively a moving landslide body, where limitations are mostly represented by the availability and quality of multi-temporal data as DEMs. Statistics are recommended to verify the reliability of DTMs co-registration. However, with the presented approach it is not possible to predict a possible time for the landslide collapse or to define any failure mechanism. Such information requires monitoring systems, supported by stress-strain analysis.

In the following the main findings are listed:

- several previous smaller and larger pre-failure displacements, scarps and creeping-motion on the upper part of the landslide are noticed between 2000 and 2012;
- a significant vertical displacement has been observed between 2012 and 2014 (about -90 m) where a negative change in volume (about -28.5 Mm<sup>3</sup>) is recognizable in the landslide area and a positive one on the glacier;
- it is noticed that this creeping-motion of the landslide can be related to the glacier reprise and its migrations. This has probably influenced the slope stability at the head of the bay and triggered its collapse after a fast sudden retreat between 2013 and 2015;
- the final landslide collapse in 2015 is estimated with a volume of 49.4 Mm<sup>3</sup>. Of this amount, 26 Mm<sup>3</sup> entered in the fiord and triggered the tsunami.

With this work, we highlight the importance to collect as much time series data as possible for a better comprehension of a tsunamigenic landslide event, and how a detailed 4D geomorphological analysis gives fundamental insights of the slide collapse and provides findings that are essential for future works. An even higher time-resolution data set would be needed to compensate missing seasonal information (especially concerning the glacier behaviour).

## References

Dufresne A., Geertsema M., Shugar D. H., Koppes M., Higman B., Haeussler P. J., Stark C. P., Venditti J. G., Bonno D., Larsen C., Gulick S. P. S., McCall N., Walton M., Loso M. G., Willis M. J. (2017) Sedimentology and geomorphology of a large tsunamigenic landslide, Taan Fiord, Alaska. *Sedimentary Geology*, 364, 302-318.

George D. L., Iverson R. M., Cannon C. M. (2017) New methodology for computing tsunami generation by subaerial landslides: Application to the 2015 Tyndall Glacier landslide, Alaska. *Geophysical Research Letters*, 44, 7276-7284.

Higman B., Shugar D., Stark C. P., Ekström G., Koppes M.N., Lynett P., et al. (2018) The 2015 landslide and tsunami in Taan Fiord, Alaska. *Scientific Reports*, 8, 12993.

Haeussler P. J., Gulick S. P. S., McCall N., Walton M., Reece R., Larsen C., Shugar D. H., Geertsema M., Venditti J. G., Labay K. (2018) Submarine deposition of a subaerial landslide in Taan Fiord, Alaska. *Journal of Geophysical Research: Earth Surface*, 123, 2443-2463.

Meigs A., Krugh W. C., Davis K., Bank G. (2006) Ultra-rapid landscape response and sediment yield following glacier retreat, Icy Bay, southern Alaska. *Geomorphology*, 78(3-4), 207-221.

Nuth, C. and Kääb A. (2011) Co-registration and bias corrections of satellite elevation data sets for quantifying glacier thickness change. *The Cryosphere*, 5, 271-290.

Shean D.E., Alexandrov O., Moratto Z. M., Smith B. E., Joughin I. R., Porter C., Morin P. (2016) An automated, open-source pipeline for mass production of digital elevation models (DEMs) from very-high-resolution commercial stereo satellite imagery. *ISPRS Journal of Photogrammetry and Remote Sensing*, 116, 101-117.

## Acknowledgement

We thank Mario Crevato (Limes – Arheologija prostora/Archaeology for the territory) for the preliminary informatics and geomorphological elaborations support.

---

# Swiss surface runoff risk map

Roberto Loat<sup>1</sup>, Andy Kipfer<sup>2</sup>, Natascia von Wattenwyl<sup>3</sup>, Antoine Magnollay<sup>4</sup>

**Keywords:** surface runoff; surface runoff map; heavy precipitation; Hazard mapping; modelling

## Abstract

Since 2018, Switzerland has a surface runoff risk map covering the whole of the country. It shows which areas may be affected by surface runoff during a rare heavy precipitation event. The map is based on modelling without verification in the field. The modelling was undertaken using high-resolution land cover data, terrain models and regional hyetographs, among other sources. Sensitivity analyses were performed to investigate the influence of the input parameters. Up to half of all flood damage in Switzerland is caused by surface runoff. It is likely that climate change results in more frequent and intense events in future. The map helps to strengthen the prevention. The risk map was developed as a public-private partnership project between the Swiss federal authorities and the insurance industry.

## Background

Analysis of damage to buildings following rainstorms has repeatedly shown that a significant part of the damage is not caused by overflow from watercourses (fluvial flood) but by surface runoff, i.e. water that flows over the land surface (Fig. 1) caused by heavy precipitation (pluvial flood). The proportion of overall damage caused by surface runoff varies greatly from one event to another. According to insurance industry estimates, it accounts for on average between 25 % and 50 % of all flood damage.

Such damage is mainly caused by short, intense rainfall events as it was the case in Zofingen in 2017, Lausanne in 2018 and Geneva in 2019. The rainwater gathers on slopes and in depressions and passes through openings into buildings, where it can cause extensive damage to chattels and the building shell. There is little danger to people while outside buildings, but the risk in basements is very real. The new climate scenarios for Switzerland forecast a 10–20 % increase in intensity and frequency of extreme precipitation by the middle of this century (NCCS 2018).

---

<sup>1</sup> Dipl. Geograph., Hazard Prevention, Federal Office for the Environment (FOEN), SWITZERLAND, ([roberto.loat@bafu.admin.ch](mailto:roberto.loat@bafu.admin.ch))

<sup>2,3</sup> geo7 AG

<sup>4</sup> Federal Office for the Environment (FOEN)



**Figure 1: Damage caused by surface runoff. Surface runoff is the part of the precipitation that does not infiltrate into the soil but flows over open ground or roads. It occurs primarily during heavy precipitation (Mobiliar Lab für Naturrisiken, Christophe Lienert / CC BY-SA 4.0, 2016).**

Until now, the basic information needed to assess runoff risks has been lacking. The Switzerland-wide available water hazard maps only show areas prone to flooding as a result of the overflowing of watercourses.

## Objectives

The aim of the Federal Office for the Environment (FOEN) in developing the surface runoff risk map was to provide a 1:12,500 hazard map covering the whole of Switzerland, showing the areas that could be affected by this natural hazard process and the water depth that might be expected (Fig. 2). By choosing a standardised methodology, it can be ensured that equivalent and comparable results are available throughout Switzerland.

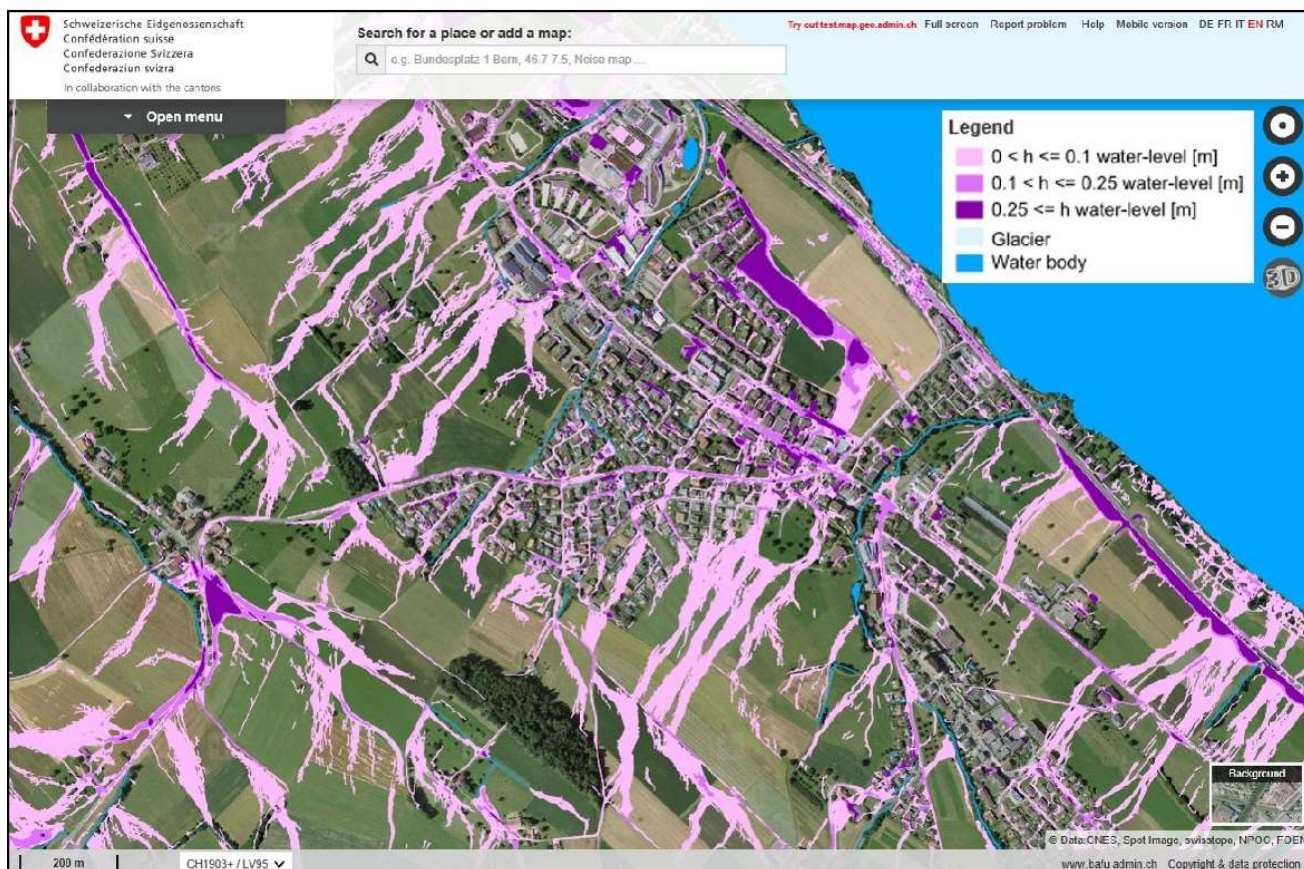


**Figure 2: Surface runoff risk map (BAFU, SVV, VKG, 2018, [www.bafu.admin.ch/surface-runoff](http://www.bafu.admin.ch/surface-runoff))**

The primary aim of the surface runoff risk map is to raise awareness of this so far neglected natural hazard. It is of great practical benefit to building and infrastructure owners, architects, builders, planners/designers, emergency services and insurers, helping them to identify the hazard, assess risks and take appropriate steps to prevent damage.

The map can for instance be used as a basis for:

- the designation of hazard areas by planning authorities and the formulation of conditions/requirements;
- the design of object- and surface protection measures;
- emergency planning;
- awareness raising and advice for building owners by insurance companies;
- the design of urban drainage systems;
- the implementation of soil protection measures in the agriculture sector;
- the assessment of hillslope debris flows and landslides.

## History of the surface runoff risk map

Surface runoff as a hazard process has been known long ago. However, the amount of damage it caused has long been underestimated. In 2009, the Gebäudeversicherung Kanton Zürich commissioned consultants geo7 to model surface runoff in the region of Langnau am Albis. The results of the mapping exercise were compared with the company's actual claims records. This showed a good correlation.

In 2011, the FOEN commissioned the same consultants to test and further develop the methodology in other regions, to figure out whether it was suitable for other topographical and geological conditions (Kipfer et. al. 2012). Once again, the mapping correlated closely with known damage events.

This prompted the FOEN to develop a national surface runoff risk map in partnership with the Swiss Insurance Association (Schweizerischer Versicherungsverband SVV) and the Association of Public Insurance Companies for Real Estate (Vereinigung Kantonalen Gebäudeversicherungen VKG). Work began in 2016 and was completed in 2018. It was assisted by about 80 experts from a range of fields including natural hazards, insurance, infrastructure, urban drainage and agriculture, as well as professional associations. The project was implemented as a public-private partnership (PPP).

The Swiss surface runoff risk map was published on 3 July 2018 and made available online (see Fig. 2).

## Modelling

### Study area

The study area encompasses the whole of Switzerland. Given the significant regional differences in topography, geology, soil and climatic conditions, the country was divided into over 250 modelling regions, each with its own precipitation scenario. The size of each modelling region varied from around 10 km<sup>2</sup> to 500 km<sup>2</sup>.

### Basis for modelling

The modelling of the surface runoff risk map was based on three main factors:

- Terrain model
- Precipitation
- Runoff coefficients

Figure 3 shows the procedure used in the simulation for the surface runoff risk map.

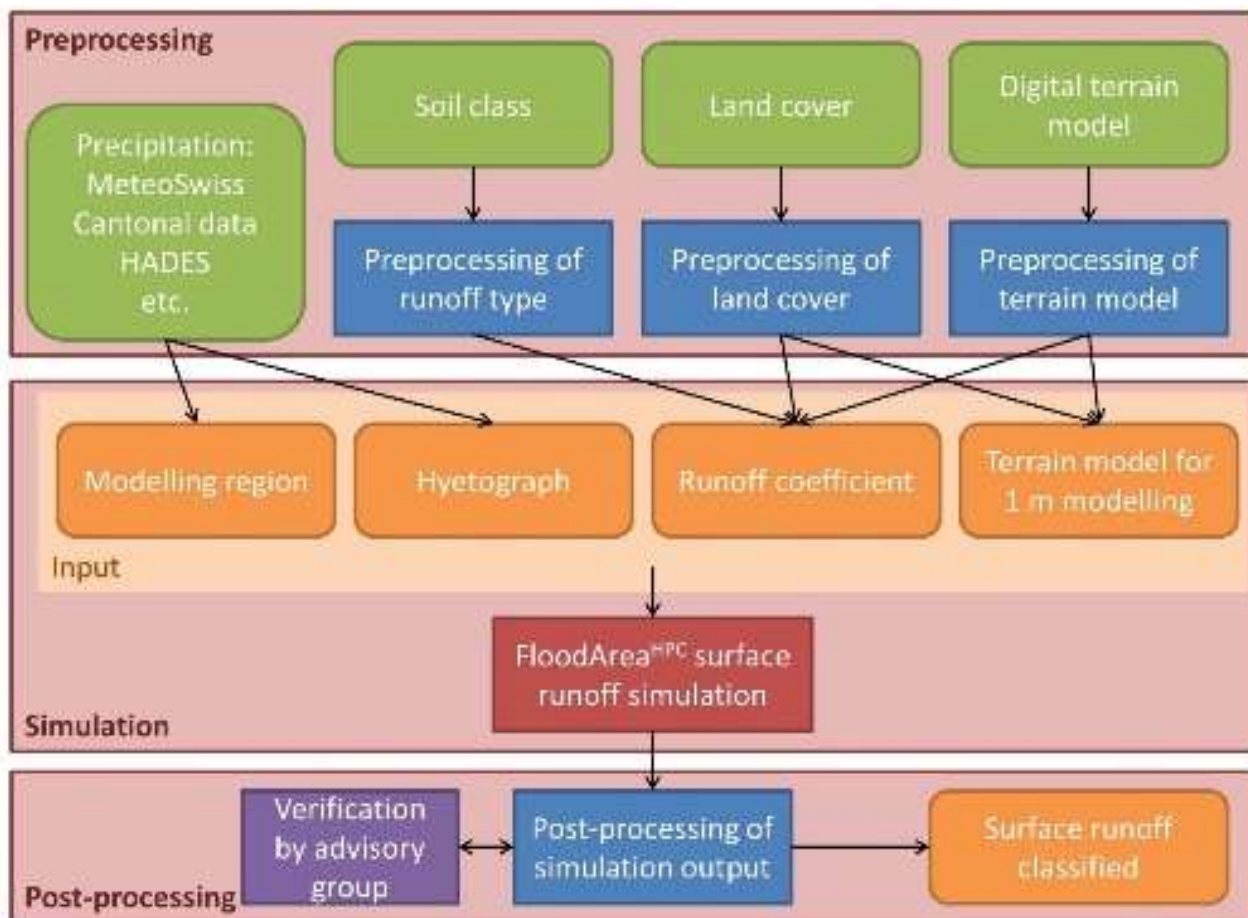


Figure 3: Schematic representation of the procedure used for the surface runoff simulation (geo 7, 2018a).

To preprocess the terrain model and determine the disposition to surface runoff, information about land cover was needed. This was provided by data from the official cadastral survey, which have a very high degree of positional accuracy. Since these data are not available for the whole surface area of Switzerland, swisstopo's Topographic Landscape Model (TLM), which is based on aerial images, was used for the remaining areas.

For the preprocessing of the land cover component, the land classifications were grouped into land cover types, the data were supplemented with hydrographic network information and paved surface areas updated where necessary. All the data were then combined to form a classified land cover data set (see table 1).

**Table 1: Land cover types.**

<b>Number</b>	<b>Type</b>
1	building
2	paved surface (for instance traffic infrastructure)
3	agricultural area
4	high moor / low moor
5	garden / surrounding of house
6	watercourse
7	forest
8	glacier
9	rock
10	foreign ground

By default the digital terrain model (DTM) used for the modelling was swisstopo's swissALTI3D with a grid size of 2 m. Where higher-resolution cantonal terrain models were provided, they were used instead.

The terrain models were converted to a grid size of 1 m for the modelling and preprocessed. This includes eliminating noise in the DTM as well as making adjustments around buildings, watercourses and transport routes in particular (see table 2).

**Table 2: Main working steps for preparing the terrain model.**

<b>Working step</b>	<b>Description</b>
Smoothing	The height values of the raster cells were smoothed taking into account all neighbouring raster cells.
Resampling	The terrain models were converted to a grid size of 1 m
FillSink	Grid cells, which represent sinks (surrounding grid cells all have a higher value), were filled up to 1m.
Building	Since buildings are not included in the terrain model, all building footprints have been increased by 5 m. The building floor areas were taken from land cover (see table 1). In the canton of Basel-Stadt, the buildings were already integrated into the terrain model and were therefore not raised additionally.
Watercourse	Water that is fed into a watercourse is no longer relevant for modelling surface runoff. Therefore all watercourse were lowered by 500 m. This excludes Suonen / Bisses (irrigation channels), they were only lowered by 1 m. Culverted watercourses were generally not taken into account. The water body areas were taken from the prepared land cover (see table 1).
paved surface	Paved surfaces often form important lead structures for flow paths but are not perfectly mapped in all terrain models. Therefore all paved areas were lowered by 0.25 m. The paved areas were taken from the prepared land cover (see table 1).

Heavy precipitation with a return period of approximately 100 years was used as a basis for the modelling. For each modelling region, a precipitation amount was determined in consultation with the cantonal representatives and taking into account MeteoSchweiz (2017) and other inputs. The percentage distribution of precipitation over one hour was identical for all regions (Fig. 4). The synthetic rainfall was specified in accordance with the FOEN.

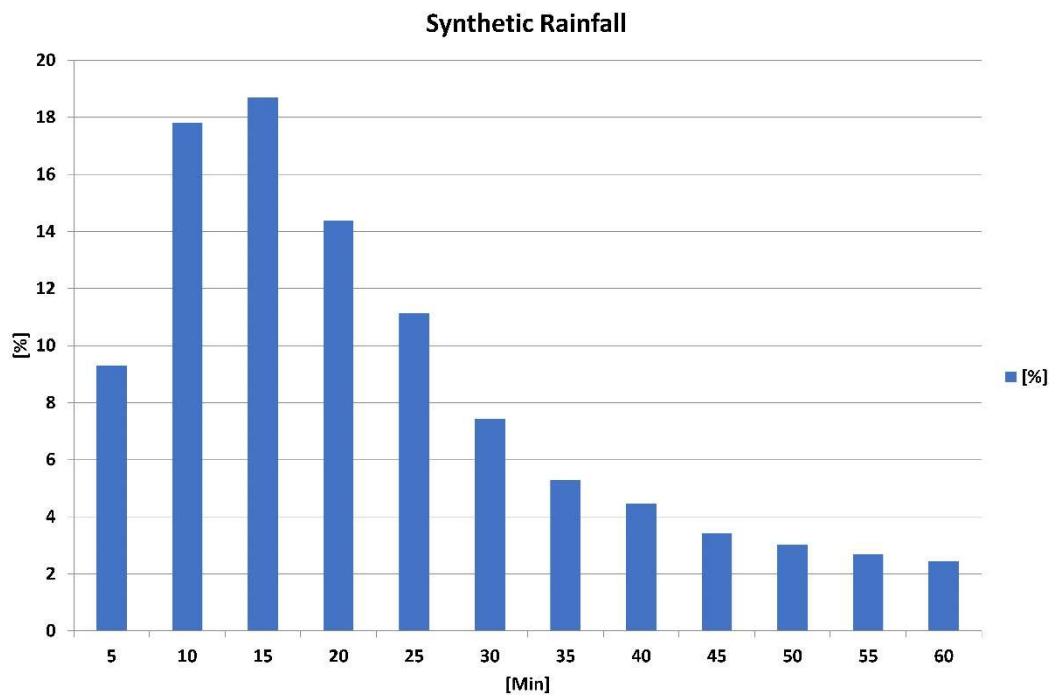


Figure 4: Percentage distribution of precipitation in the synthetic rainfall used for the modelling (geo7, 2018a).

The infiltration of rainwater is an important factor in determining the runoff coefficient. Paved surfaces prevent infiltration whereas in forests larger volumes of water can often infiltrate into the ground. Based on their different runoff propensity characteristics, each land cover type was assigned a basic value for the runoff coefficient  $\psi$  according to Rickli and Forster (1997) and Dobmann (2009).

This basic value was then modified in various preprocessing steps (geo7, 2018a). The resulting runoff coefficient  $\psi_{def}$  was put into the modelling as a weighting grid. For example, a coefficient of 1 in a given grid cell means that all precipitation becomes runoff (paved and/or steep areas). With a coefficient of 0.4, only 40 % of the precipitation turns into runoff (see table 3).

Table 3: Land cover types according to table 1 and the runoff coefficient  $\psi$  which was used for the simulation (derived from Rickli and Forster, 1997 and Dobmann, 2009).

Land cover type	Basic value
Building, watercourse, foreign ground	0
paved surface, rock	1
agricultural area	0.45
high moor / low moor	0.45
garden, glacier	0.5
forest, scree	0.35

Surface roughness was not taken into account, as its influence on the classified result is limited and the uncertainties are considerably.

#### Post-processing, sensitivity analysis and validation

The raw data from the modelling were then post-processed. The main steps involved consolidating small surface areas, classifying the water depth  $h$  into various categories ( $0 \text{ cm} < h \leq 10 \text{ cm}$ ,  $10 \text{ cm} < h \leq 25 \text{ cm}$  and  $25 \text{ cm} < h$ ), integrating watercourses and vectorising the grid data.

A modelling result depends on the quality of the input data, the modelling algorithms used and the settings applied. When modelling on a large scale, it is particularly important that small changes in the input data do not lead to substantially different results. Therefore, the influence of precipitation amounts, development and duration as well as the terrain model and their preprocessing on the modelling results was investigated.

The results of the sensitivity analysis show that the terrain model and its preprocessing have a greater influence on the modelling result than, for example, the choice of the precipitation amount or the hyetograph (Fig. 5). With the latter factors, the model results are only affected by large adjustments and can therefore be considered robust in relation to the precipitation input.

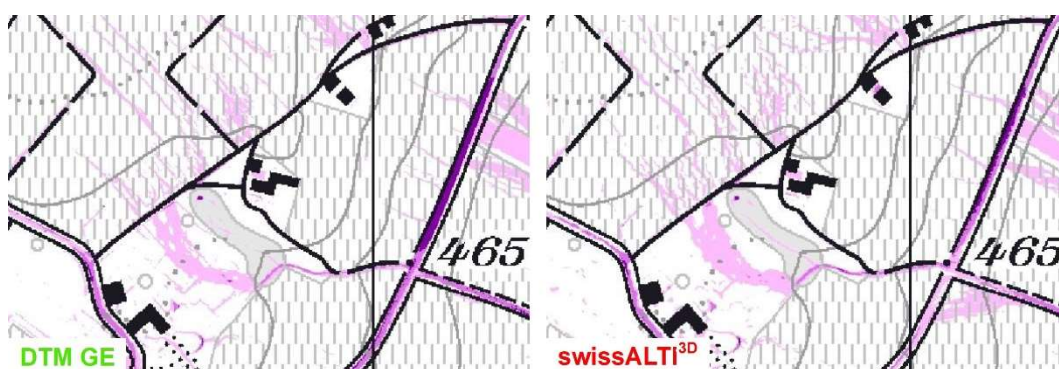


**Figure 5: Different modelling results obtained using different terrain models (sources: Federal Office of Topography, Direction de la mensuration officielle Genève and geo7 2018a).**

To verify the results, the surface runoff map is compared with real events and resulting damage on an ongoing basis, such as the storms that hit Zofingen in 2017 (geo7, 2018b) and Lausanne in 2018. The evaluations show that the surface runoff risk map results in plausible designations of areas and buildings potentially affected by surface runoff and is a qualitatively good supplement to the existing water hazard maps.

#### Significance and limitations of the results

The surface runoff risk map shows the flow paths of surface runoff, the affected areas and the expected water depths (classified) on a scale of 1:12,500. The map is accurate in terms

of indicating potential risks. With a view to correct interpretation, it should be noted that the following aspects are not considered into the modelling:

- Urban drainage systems, because these are assumed to be overloaded during rare events.
- The effect of culverts and underpasses, because standardised data sources are not available.
- Water that has been discharged into a watercourse is no longer considered as surface runoff.
- Water escaping from watercourses.
- Underground water flows and groundwater outcrop.

## Practical application of the map

With around two thirds of buildings in Switzerland potentially affected by surface runoff, the surface runoff risk map helps to raise awareness of a so far underestimated natural hazard. Several cantons have already included the map in their official hazard data and documentation and published it online.

Until recently, the map was responsible for some heated discussions as it highlighted the fact that responsibilities for this hazard process had not been defined, despite current events indicating an urgent need for action. It has now been clearly established that surface runoff falls under the Federal Act on Hydraulic Engineering and so has to be treated on a par with all other water hazard processes. The cantons receive up to 45% in federal subsidies for the implementation of surface protection measures.

However, object protection measures on buildings are more important than technical surface protection measures. Spatial planning measures, such as requiring a proof of object protection, can ensure that new structures are built to withstand the hazard. For existing buildings, owners need to be encouraged to take their personal responsibility. It is often possible to protect a building with simple and affordable measures. In many cantons, cantonal building insurance companies and private insurers advise their policyholders and offer financial incentives to implement object protection measures (Imhof et. al. 2020).

Events have repeatedly shown that urban drainage systems become overloaded during heavy precipitation. A newly launched project called 'Heavy precipitation in urban areas' initiated by the Federal Office for the Environment (FOEN) and the Federal Office for Spatial Development (ARE) develops recommendations for action, planning principles and practical measures to adapt to the increasing frequency and intensity of heavy precipitation. This project is aimed particularly at drainage network operators, urban and landscape designers as well as architects. Its purpose is to establish stakeholder networks and create synergies with other topical issues such as urban heat.

In the field of emergency planning the map is used to detect risk hotspots and to plan responses. In the 'Heavy precipitation and response planning' project run by the Bundesamt für Bevölkerungsschutz BABS (2019) could be shown that 75 % of the 16,000 flood-related emergency responses in the canton of Zurich between 2005 and 2018 were triggered by surface runoff.

## Conclusion

The Swiss surface runoff risk map was modelled nationwide following a uniform procedure. Runoff paths and the depressions in which rainwater accumulates are accurately mapped, even in urban areas, as comparisons with real events have demonstrated. However, it must be borne in mind that changes in microtopography (new buildings, roads, walls, etc.) can have a major effect on flow paths so checks must be carried out in the field before practical measures are implemented.

Covering the whole of Switzerland, the surface runoff risk map is a useful and high-quality damage prevention tool. This is all the more important given that climate change will result in more frequent and intense rainfall in the future. Homeowners in particular can make a substantial contribution to damage reduction by implementing object protection measures. Close cooperation between planners/designers, architects, natural hazard specialists, construction professionals and insurance experts is the key in this regard.

## References

- BABS Hrsg. (2019). Starkniederschläge und Einsatzplanung von Schutz & Rettung Zürich Studie im Rahmen des National Centre for Climate Services NCCS. Bundesamt für Bevölkerungsschutz (BABS), Bern.  
<https://www.babs.admin.ch/de/publikservice/downloads/gefrisiken.html#ui-collapse-698>  
> Bevölkerungsschutz und Klimawandel.
- BAFU, SVV, VKG (2018). Gefährdungskarte Oberflächenabfluss Schweiz. Im Auftrag von Bundesamt für Umwelt BAFU, Schweizerischer Versicherungsverband SVV, Vereinigung Kantonalen Gebäudeversicherungen VKG, Bern.  
[www.bafu.admin.ch/surface-runoff](http://www.bafu.admin.ch/surface-runoff)
- Bundesamt für Meteorologie und Klimatologie MeteoSchweiz (2017). Extremwertanalysen (Version 2016). Zürich.  
<https://www.meteoswiss.admin.ch/home/climate/swiss-climate-in-detail/extreme-value-analyses.html>
- Dobmann J. (2009). Hochwasserabschätzung in kleinen Einzugsgebieten der Schweiz. Interpretations- und Praxishilfe. Dissertation, Universität Bern, Bern.
- geo7 (2018a). Gefährdungskarte Oberflächenabfluss, Technischer Bericht. Im Auftrag von Bundesamt für Umwelt BAFU, Schweizerischer Versicherungsverband SVV, Vereinigung Kantonalen Gebäudeversicherungen VKG. Bern, 59 Seiten.

geo7 (2018b). Oberflächenabfluss in Zofingen, Analyse der Gefährdungskarte Oberflächenabfluss in Bezug auf das Schadenergebnis vom 08.07.2017. Im Auftrag von Bundesamt für Umwelt BAFU, Schweizerischer Versicherungsverband SVV, Vereinigung Kantonalen Gebäudeversicherungen VKG. Bern, 31 Seiten.

Imhof M., Staub B., Marti A., Niederbäumer G., Loat, R. (2020). Building protection against surface runoff. Interpraevent 2020, Bergen / Norway.

Kipfer A., Kienholz Ch., Liener S. (2012). Ein neuer Ansatz zur Modellierung von Oberflächenabfluss. In: 12th Congress INTERPRAEVENT 2012 – Grenoble / France, Conference Proceedings, Band 1, S. 179-189

NCCS (2018). Heavy precipitation. National Centre for Climate Services NCCS. Zurich. <https://www.nccs.admin.ch/nccs/en/home/climate-change-and-impacts/swiss-climate-change-scenarios/key-messages/heavy-precipitation.html>

Rickli Ch., Forster F. (1997). Einfluss verschiedener Standorteigenschaften auf die Schätzung von Hochwasserabflüssen in kleinen Einzugsgebieten. In: Schweiz. Zeitschrift für Forstwesen, Volume 148, Issue 5:367–385. Illnau.

---

# The interaction between flood and morphology

Lars Fredrik Lund<sup>1</sup>, Gerard Dam<sup>2</sup>

**Keywords:** flood mapping; Morphologic model; Slow/fast morphodynamic changes

## Abstract

In this paper we look at the ability of a morphodynamic model to accurately predict morphologic changes in rivers, and whether such predictions are beneficial in flood mapping. Two examples from real events are presented; an extreme flood in a scenario with fast changes in a steep catchment, and a slow build-up of sediment in a delta. The model FINEL2D was used to simulate these scenarios. We found that the model is able to predict morphologic changes in both instances, and the use of a morphodynamic model as opposed to a model using only hydrodynamics, can be beneficial in flood mapping.

## Introduction

Floods can cause massive damage to human infrastructure. Norway has since 2007 been under the European Union's flood directive. In accordance with this directive, The Norwegian Water Resources and Energy Directorate (NVE) has developed guidelines for planning and development in risk-areas along watercourses (NVE, 2011). Damage done due to floods has yearly insurance claims on the scale of hundreds of millions Norwegian crowns (Finans Norge, 2019). NVE's guidelines for planning and development considers safety classes F1, F2 and F3, which correspond to 20, 200 and 1000-year floods, respectively.

However, flood mapping in Norway nowadays is limited to hydrodynamics only. In these calculations the riverbed is assumed to be fixed, even though it is obvious that the riverbed-level changes (Neuhold et al., 2009). Over time, morphodynamics change the bed due to erosion and sedimentation, which causes the water levels and inundation-area to change. This makes a flood map's validity limited in time. Depending on the available sediment and build-up of a river channel, these flood maps can be obsolete after hours, years or decades. Calculating morphological changes of the riverbed during peak flows, may provide a basis to estimate water surface levels and inundations lines, which can be used in flood hazard assessment (Neuhold et al., 2009).

Sediment transport is a power function of the flow velocity. Empirical transport formulae have a power function between 3 to 5 (Engelund & Hansen 1967). That means that an increase in flow velocity of 15-25% results in a doubling of the sediment transport. Most of the sediment transport is therefore limited to floods where the flow velocity is large. In

---

<sup>1</sup> Department of Mathematics, Universitetet i Bergen, NORWAY, ([lars.fredrik.lund@hvl.no](mailto:lars.fredrik.lund@hvl.no))

<sup>2</sup> Ph.D., Asplan Viak, ([gerard.dam@asplanviak.no](mailto:gerard.dam@asplanviak.no))

Norway we assume an increase of extreme discharges under flood conditions of around 20-50% due to climate change depending on the size and characteristics of the catchment (NVE, 2011). This means that we can expect more than linear reaction of the sediment transport amount, making the subject of this paper more and more relevant in the future.

The central question of this article is to examine whether morphodynamic changes are predictable and useable in flood mapping. We will refer to the works of Dam (2017, 2018), where the author claims that morphodynamics are predictable with a morphodynamic model.

When looking at morphological changes, it is important to distinguish between different timescales. During pluvial extreme floods, the morphological changes occur over a very short period of time in steep terrain and small catchments. Extreme floods are usually not contained in their original river channels, and they can leave a significant geological footprint. Depending on the available sediment supply in the river, floods can carry a massive amount of sediment, morphologically changing the original channel and its hydrodynamics (Guam et al., 2016). Often, sedimentation in the original river channel leads to increased water levels at the points where the river cannot contain the water within its banks. The river then finds new paths through the terrain that often was not included in the original flood maps. This leads to excessive damage to infrastructure since nobody anticipated flooding there. In contrast, a river delta can gradually build up over time. This build-up is due to the reduced flow velocity at the outlet, such that there is not enough kinetic energy to carry the sediment further along the river- or seabed.

To explore the differences between these timescales, and the ability of the model to predict the morphological changes, we will look at two examples; the extreme flood in Utvik (fast timescale), and the sedimentation in Namsen (slow timescale).

NVE has mapped flood zones of several high-risk rivers and streams in Norway. This map gives cities and municipalities a basis for area-planning and damage-prevention. However, it is the municipalities' responsibility to have an accurate flood mapping of their local building- and development-areas. NVE has issued guidelines for these mappings in line with civil engineering regulations (TEK). To develop these flood maps a hydrodynamic numerical model is used, without a sediment transport module. Such models require geometrical data of the river and knowledge of constructions such as bridges, culverts and sluices along the watercourse.

The severity of the flood is set by its recurrence. The recurrence is the average number of years between floods of a similar magnitude occur. The method of calculating this average can be based upon; observed water flow, the data of nearby stations where no such measures are available, historical regional flood frequency and precipitation/run-off models (Nie et al., 2012).

As mentioned, there are three flood safety classes for area planning; F1, F2 and F3. By TEK regulations, these areas can be developed with a different set of buildings.

F1 has a recurrence of 20 years, or a 5% yearly likelihood. Areas with a F1 safety class is for buildings with low human activity and little economic or societal consequences.

F2 has a recurrence of 200 years, or a .5% yearly likelihood. Areas with a F2 safety class is for residences, offices, schools, agricultural buildings and industry. The economic consequences of damage to these buildings can be great, but critical societal functions are not disabled.

F3 has a recurrence of 1000 years, or a .01% yearly likelihood. Areas with a F3 safety class are for buildings and facilities with critical societal functions such as hospitals, fire stations, and police stations.

The TEK regulations are not as well-defined when an event is involving large amounts of sediment and water which is being carried downstream. Such an event could either fall under the flood or landslide/debris category (S1, S2, S3). These include slides triggered by water, or slides ending up in a watercourse. Slides ending up in a steep watercourse could make a particularly dangerous flood. The mass and water will have high velocities and force, making damage to human life and infrastructure more devastating. These masses will deposit where the river flattens or meets a choke point. This buildup of deposits may lead to over-flooding and formation of new river channels through the terrain. Typically, human infrastructure and settlements are around the flatter regions of a river, which makes it more probable that these new branches of the river will affect such areas (NVE, 2011).

## Methods

The model used to simulate the events at Utvik and Namsen below is FINEL2D, developed by Technical University of Delft and Dutch company Svašek Hydraulics (Dam et al., 2016). The model uses the finite element method, and the governing equations are based on the shallow-water continuity- and momentum-equations. In addition to a hydrodynamic module, the model also has a sediment transport module, allowing for estimations of morphologic changes over time.

The morphologic changes of a river are dependent on the erosion and sedimentation. Morphologic changes of the river also affect velocity; thus, velocity and morphology create a feedback loop. A morphodynamic model uses morphodynamics to calculate the changes in the flow. This flow is then used to calculate the sediment transport, before the bed-level in the grid-cell is updated. This loop continues with the flow being updated with the updated bed-level.

The sediment transport module uses the sediment balance equation (1), where  $z_b$  is the bed level (m),  $q_x, q_y$  are the components of the sediment flux in the x- and y-direction ( $m^2/s$ ). The Engelund and Hansen transport formula (Engelund & Hansen, 1967) is used to determine the non-cohesive sediment fluxes, where first a dimensionless equilibrium concentration is calculated from equation (2), where  $c_e$  is the equilibrium concentration,  $S$  is the magnitude of the equilibrium sand transport according to Engelund & Hansen ( $m^2/s$ ).

Next the depth averaged sediment concentration  $c$  is calculated from equation (3), where  $d$  is the water depth (m),  $u$  and  $v$  are the horizontal components of flow velocity ( $m/s$ ) and  $TA$  is a characteristic timescale. This equation shows that if the concentration is lower than the equilibrium concentration, erosion will occur, and if it is higher, sedimentation occurs. The timescale coefficient  $TA$  is related with the settling velocity of the sand particles. In

relatively shallow areas the time scale is small, and the concentration adjusts quickly to the equilibrium concentration.

In the modelling of the flood in Utvik a grain size of 1000  $\mu\text{m}$  was assumed, which is a large simplification, but the assumption is that changes in bed level were caused primarily by this sediment fraction. In the simulation of Namsen, grain size sampling was done for more accuracy. The results were not sensitive with respect to such parameters; the sedimentation and erosion occurred in the same locations, but with different magnitudes. In the simulation of Utvik a layer thickness of 2.5-4.0m is available for erosion, dependent on location. Other assumptions such as bridges to be non-erodible were also applied.

On July 24th, 2017 there was an extreme flood event in Utvik (Sogn og Fjordane), occurring from the two rivers Storelva and Brulandselva. As a result of heavy precipitation, the rivers flooded, creating new channels through the small town, causing severe damage to buildings and infrastructure. After the flooding, an analysis by DAM engineering (Dam engineering, 2017) simulated the flood using the FINEL2D model.

Figure 1 compares the morphodynamic simulation of Storelva and the laser-data in the river from 2013-2017, where the flow direction is upwards towards the sea. One can see that there is significant sedimentation and erosion along the river. The model also shows large amounts of sediment being carried into the sea, as seen on the top on the right figure. This sedimentation causes the water levels in the river to rise, causing more spread. According to the simulation, the water rise due to sedimentation alone is around 1.3 meters (Figure 2) at the point indicated by the yellow dot in Figure 1. The model also predicts new channel branches formed during the flood.

Of note is the ability of the model to simulate the build-up of sediment at Bridge A, which was completely blocked off with sediment during the flood. This was caused by a decrease in flow velocity under the bridge. Because of this, the flood diverted around the bridge instead of under it. A hydrodynamic model would not be able to predict such blocks, leading to the flood taking unexpected routes.

Namsen river discharges into the fjord at Namsos. We have two measured bathymetries from 2005 and 2018. Clearly visible in the surveys is that the delta front moves down toward the fjord with massive sedimentation in the lower part of the river. A simulation of the river's morphodynamics was done with FINEL2D. The model was calibrated with the changes in bed-level over the 13-year period. The figure below (Figure 3) compares the measured change in bed level with the simulated model. The model corresponds well with the observed changes.

A flood map of this area would certainly become worse over time (with higher water levels) due to this sedimentation effect and seaward expansion of the delta, since sedimentation takes the place of the water and pushing water levels up.

## Results and discussion

The results of the two examples indicates that morphology is predictable, and that flood mapping with a morphological model is useful. During a flood where a river overflows, the water might take on a new path, which happened in Storelva. Due to the incorporation of elevation and terrain being put into the model, these changes can be predicted. The reason for this predictability is that erosion and sedimentation is mostly dependent on gradients in the velocity. Deceleration leads to sedimentation, and acceleration leads to erosion. The model is also able to predict morphologic changes over a slow time scale, shown in the simulation of Namsen. In comparison with a strictly hydrodynamic simulation, this adds a significant value to the predicted outcomes. Predicting morphologic changes during a flood such as that in Utvik can help in taking preventative measures. One important question is whether the correct predictions by the model were done simply by adjusting parameters to make it fit with reality. Then the modelling can be seen as an advanced form of curve-fitting. Will the model make accurate predictions into the future, where there is not already a set answer to calibrate for?

## Conclusion

The examples discussed have shown that the model FINEL2D has accurately predicted morphologic changes, both over fast and slow timescales. In producing a flood map, such a model can be an important tool. Compared to hydrodynamic models, it has clear advantages both in predicting floodpaths, the long-term changes in a river delta and the changes in flood mapping over time.

## References

- Dam Engineering (2017). Simulating the flooding in Utvik on 24 July 2017 using a high resolution 2D hydro- and morphological model. *Unpublished report*.
- Dam et al. (2018). Sedimentasjon i Namsen. *Unpublished report*.
- Dam et al. (2016). Modeling centuries of estuarine morphodynamics in the Western Scheldt estuary. *Geophysical research letter*, 43.
- Finans Norge (2019). <https://www.finansnorge.no/statistikk/skadeforsikring/nokkeltall/naturskade/>
- Guan M. et al. (2016). Quantifying the combined effects of multiple extreme floods on river channel geometry and on flood hazards. *Journal of Hydrology* 538 (2016). 256-268.
- Engelund, F., and E. Hansen (1967). A monograph on sediment transport in alluvial channels. *Teknik Forlag, Copenhagen*.
- Neuhold C., Stanzel P., and Nachtnebel H. P. (2009), Incorporating river morphological changes to flood risk assessment: uncertainties, methodology and application, *Natural Hazards and Earth System Sciences*, 9, p. 789-799, 2009

Nie L., Selseth S., Sægrov S., Vagle O. A., Andrianov A. (2012). Flomfrekvensanalyse og flomvannlinjeberegninger for byvassdrag. *Vann 1*, 2012

NVE, Guidelines 2011

[http://publikasjoner.nve.no/retningslinjer/2011/retningslinjer2011\\_02.pdf](http://publikasjoner.nve.no/retningslinjer/2011/retningslinjer2011_02.pdf)

---

# Active sediment control with a shutter and monitoring of sediment runoff in Jo-Gan-Ji River

Koso Mikami<sup>1</sup>, Tomoyuki Noro<sup>2</sup>, Takahiko Nagayama<sup>3</sup>, Tomohiko Furuya<sup>4</sup>, Masaharu Fujita<sup>5</sup>, Takahisa Mizuyama<sup>6</sup>, Takahiro Itoh<sup>7</sup>

**Keywords:** sediment monitoring; bedload monitoring; hydrophone; sabo dam with shutter; robust-type senso

## Abstract

Continuously measuring sediment runoff along a main river is necessary to know both the propagation of sediment volume and the sorting to appropriately evaluate temporally and spatially sediment yielding/transportation for sediment management in the basin. Appropriate methods are selected and applied to monitoring in the river, using a Reid-type bedload slot sampler, robust-type hydrophones and velocity meters on the bed for bedload and turbidity meters for washload. To actively control sediment runoff in floods, a sabo dam with shutter was developed and installed, and pilot operations were tried to conduct in flood to flood. On 4th July in 2017 and 5th July in 2018, floods took place with the magnitude of flow depth over the top of the dam, and sediment controls were carried out with/without shutter operations during floods. Differences of those sediment transport characteristics with/without the shutter operations were also shown through the sediment monitoring along Jo-Gan-Ji River.

## Introduction

Relationships between sediment and water runoff through monitoring show discontinuous relations in mountainous regions, and this shows necessity of sediment monitoring. Following sensors are selected/installed as appropriate tools such as a set of pipe-hydrophones for bedloads, pressure sensors for the flow depth, turbidity meters for washloads and an electro-magnetic velocity meter on the bed for bed shear stress [Mikami et al., 2014]. In Jo-Gan-Ji River, longitudinal sediment monitoring is also carried out using robust-type sensors, that prevent from collisions by boulders.

---

<sup>1</sup> Ministry of Land, Infrastructure, Transport and Tourism (MLIT)

<sup>2</sup> Tateyama Sabo Office, Hokuriku Regional Bureau, MLIT

<sup>3</sup> General Manager, Hokuriku office, NIPPON KOEI CO.,LTD., 1-43,Eki Nishihon-machi 5-chome, Kanazawa-shi, Ishikawa, Japan (a4619@n-koei.co.jp)

<sup>4</sup> Nippon Koei Co., Ltd.

<sup>5</sup> Dr., Prof., Disaster Prevention Research Institute, Kyoto University

<sup>6</sup> Dr., Professor emeritus, Kyoto University

<sup>7</sup> Dr., PhD., Engineering, Center for Advanced Research and Development, Nippon Koei Co., Ltd.

A sabo dam with a movable shutter is installed for smoothing sediment runoff with a slit dam. An effective control of sediment runoff can be carried out and evaluated measured data with sensors installed around dams [Mikami et al., 2014]. Pilot operations were tried to conduct in flood to flood. On 4th July in 2017 and 5th July in 2018, sediment controls were carried out with/without shutter operations during floods. Differences of those sediment transport characteristics with/without the shutter operations are shown in present study.

## Monitoring for bedload and washload

Figure 1 shows the observation stations and Fig. 2 are the longitudinal bed profiles. Bedload monitoring at Hongu sabo dam ((F) in Fig.1) using a pipe hydrophone and pressure meter for the flow depth started on 15th December in 2009 and added turbidity meter began on 17th December in 2012 [Nagayama et al., 2019]. At Hongu sabo dam, width of spillway is 85 m, flow width is 52 m, bed slope is 1/90 and drainage area,  $A$ , is 193.1km<sup>2</sup>. Water discharge is calculated using a relation between flow depth,  $H$ , and discharge,  $Q$ , estimated by surface velocity measurements in floods. Bed sediment has a range of diameters such as  $d_{60}$ = 30 mm and  $d_{95}$ = 150 mm.

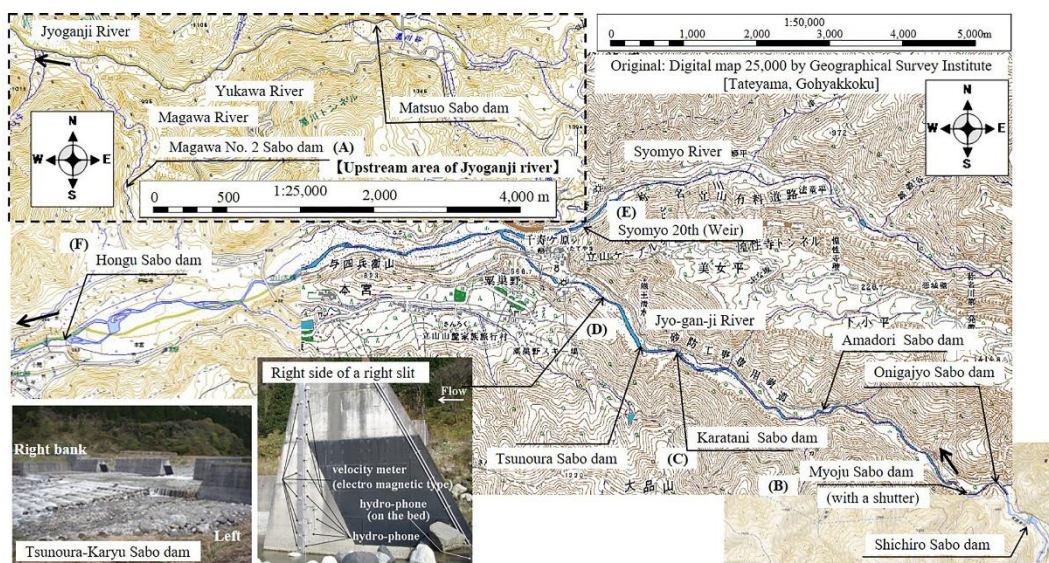
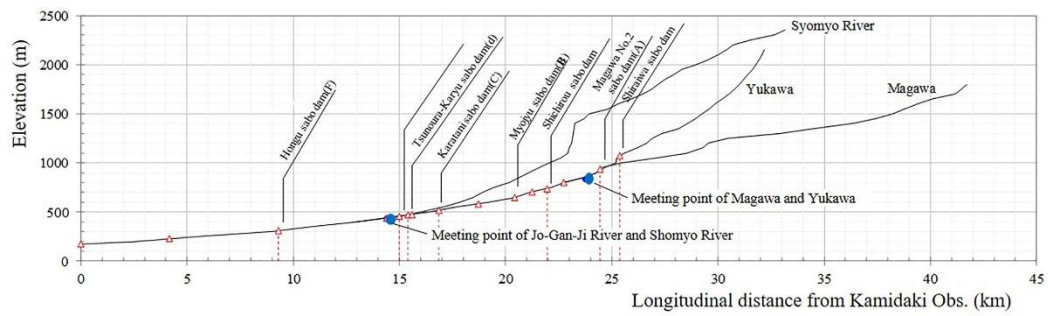


Figure 1. Sabo dams and monitoring sections along Jo-Gan-Ji River.



**Figure 2. Longitudinal bed profiles along Jo-Gan-Ji River.**

At Tsunoura-Karyu sabo dam ((D) in Fig. 1), concentrated monitoring was conducted at the slit of the sabo dam since June in 2001. The catchment area of the dam,  $A$ , is 139.49 km<sup>2</sup> and the bed slope near the dam is 1/56 which is measured in 2007. Flow width is 110 m and bed sediment have a range of diameters such as  $d_{60}$ = 20 mm and  $d_{95}$ = 200 mm. Rainfall is measured at Senjyu-ga-hara Station. Sediment monitoring started with a combination of Reid-type bedload slot there, that was installed in January of 2008 and the size is 2.0m X 2.0m in plane, 1.5m in deep and slit is 0.6m on the bed, pressure meter and a pipe hydrophone. The calibration line is obtained between impulses of the hydrophone and bedload discharge by the bedload slot [Nagayama et al., 2019], and the line is used for estimation of bedload discharge at several observatories.

Figure 3 shows the relationship between water discharge and bedload discharge at Hongu sabo dam. Several equilibrium bedload formulas for  $d_{60}$  are compared with previously measured data [e.g., JSCE, 1999]. Fig. 4 shows the relation between water discharge and fine components of sediment discharge measured by a turbidity meter and direct water sampling at several observatories at Jo-Gan-Ji River. The linear calibration line is obtained between turbidity meter output (Voltage) and volumetric concentration with Kaolin and water mixture. The two dashed lines identify the range of fine components of sediment discharge in Japan [JSCE, 1999] to compare with the monitored data in Jo-Gan-Ji River. Data of Imagawa Bridge is sampled near the river mouth, and measured value is close to the sampling data at relatively large river in Japan.

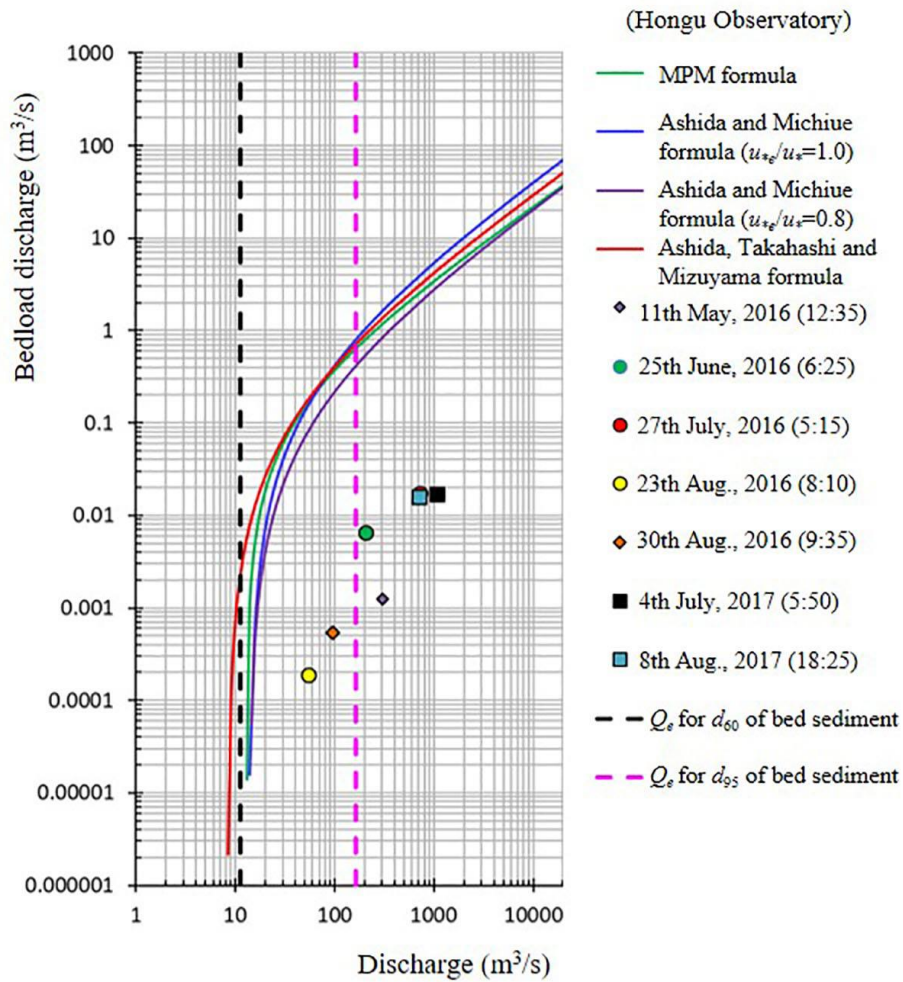


Figure 3. Relationship between water discharge and bedload discharge estimated using impulses of 16 times amplifier and bedload slot.

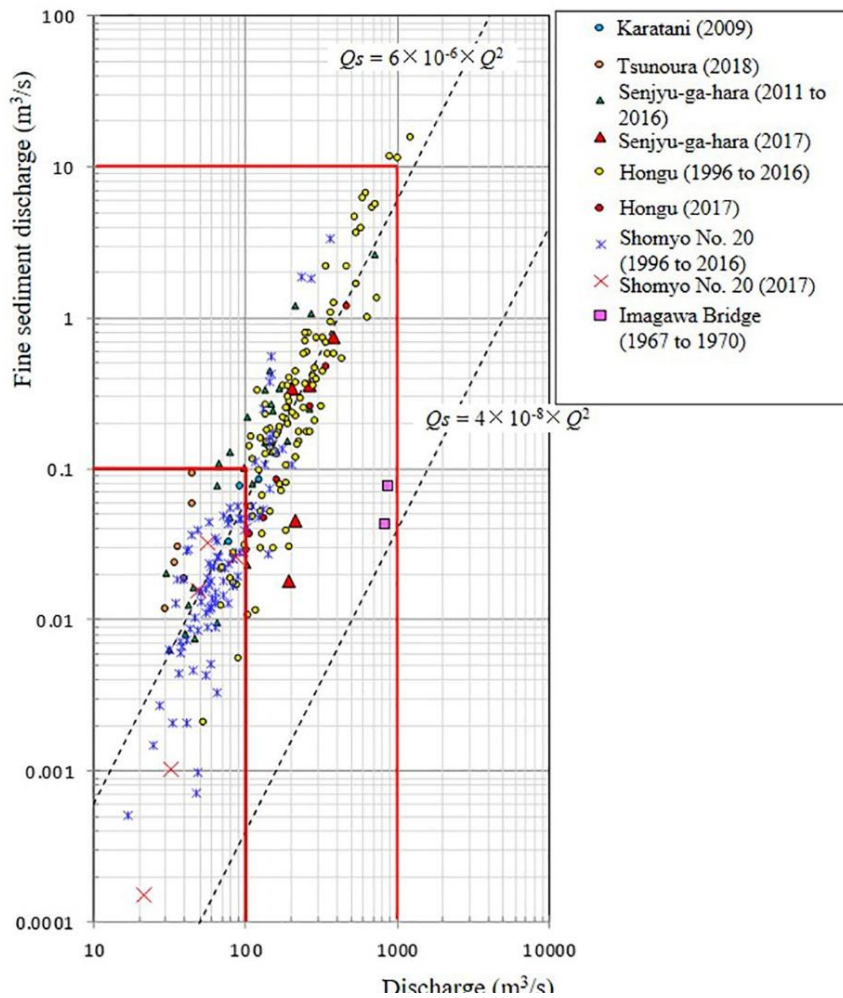


Figure 4. Relationship between water discharge and fine components of sediment discharge measured by turbidity meter and direct water sampling.

## Effective sediment control with a shutter

A sabo dam with a shutter is installed at Myoju sabo dam. The shutter has a structure in which the lower part of the slit dam is opened and closed by oil hydraulic pressure [Mikami et al., 2014]. The width and height of the slit of the dam is 7.5m, 8.5m, respectively. A shutter operation has almost two roles, one is active sediment runoff control and the other is shutter movement control during operations. Trial attempts were conducted during floods and the preferable timing of the operation tried to be found, as shown in Fig. 5, in decreasing stage of floods.

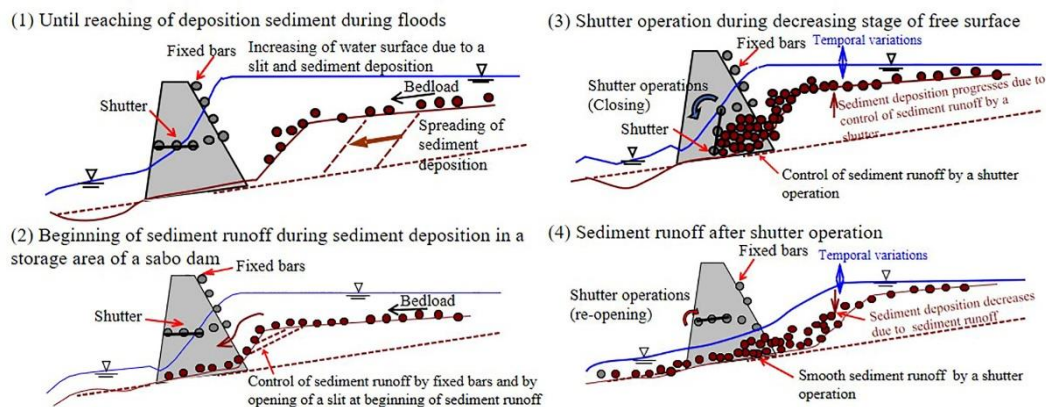
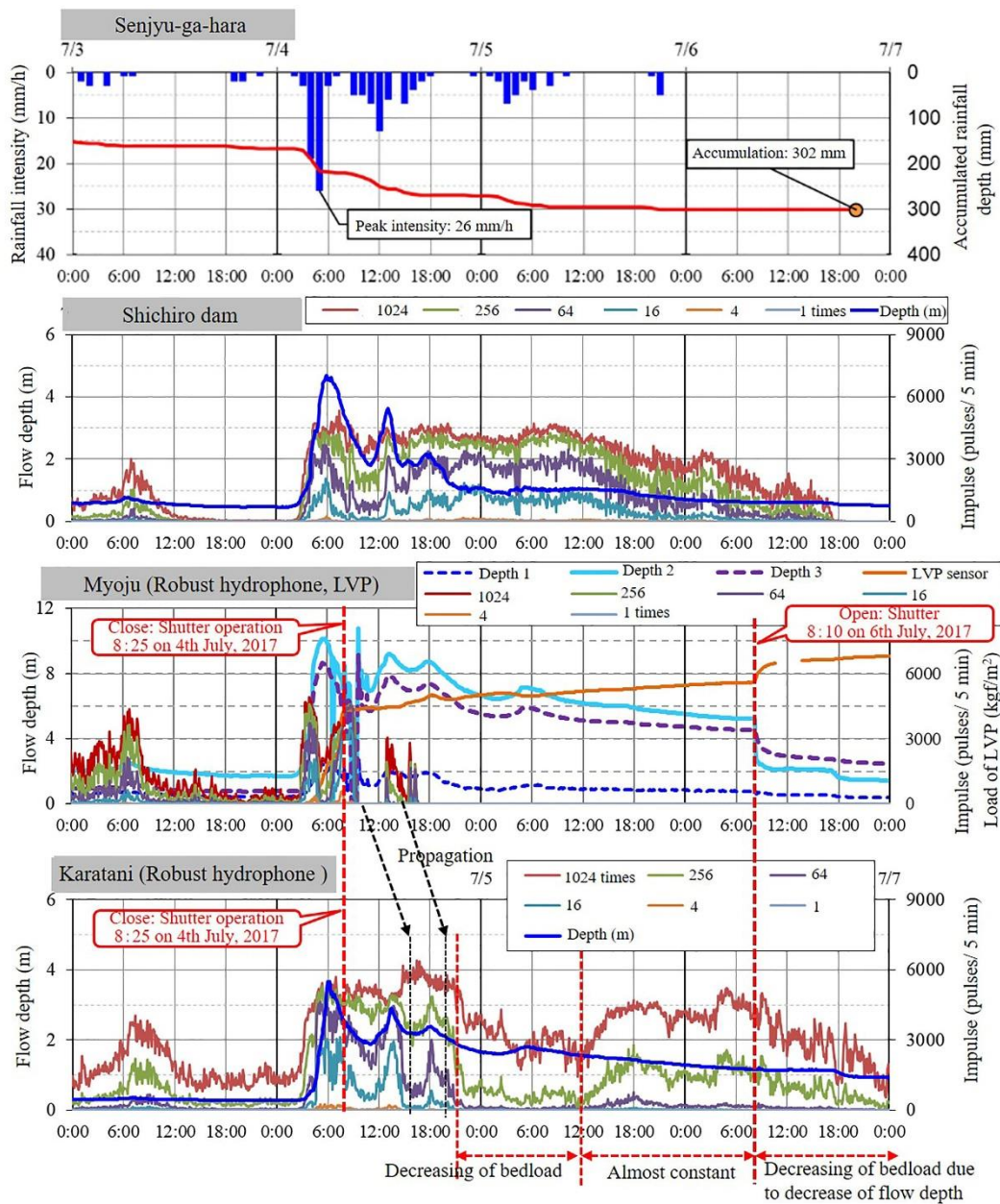


Figure 5. Trial operations for sediment control by a movable shutter.

### Floods on 4th July in 2017 and on 5th July in 2018

There were rainfall events on 4th to 5th July in 2017: Maximum rainfall intensity was 26 mm/h at 5:00 on 4th July and accumulated rainfall depth was 302 mm. Maximum the top of spillway of the sabo dam and the maximum flow depth was 10.2 m over the top of spillway of the dam and peak discharge was estimated as 500m<sup>3</sup>/s using relation between flow depth and discharge, obtained by flume tests. During decreasing stage of the flow depth, the closing shutter was operated at 8:25 on 4th July in 2017. At 8:10 on 6th July in 2017, the opening operation was carried out at around 5m in depth of the storage area of the dam. There were no troublesome such as closeness/meshing of sediment particles between the shutter and side wall, during those operations.

Figure 6 shows measured data including the shutter operation during 4th to 6th July in 2017, at Shichiro and Karartani sabo dam which is located at 1,540 m upstream and at 3,465 m downstream of Myoju sabo dam.



**Figure 6. Longitudinal measured data in the shutter operation during 4th to 6th July in 2017 (with shutter operation).**

Rainfall events continued during 5 to 8th July in 2018, and maximum rainfall intensity was 30.0 mm/h at 16:00 on 5th July, and accumulated rainfall depth was 341 mm. Maximum flow depth was around 9.0 m and estimated peak discharge was 330 m<sup>3</sup>/s as well as floods on 4th in July. Bed sediment were excavated to maintain the storage area of the dam before flood, and deposition of sediment was almost passed through without the shutter operation.

Figure 7 shows measured data in the shutter operation during 5th to 8th July in 2018, as well as in Fig. 6.

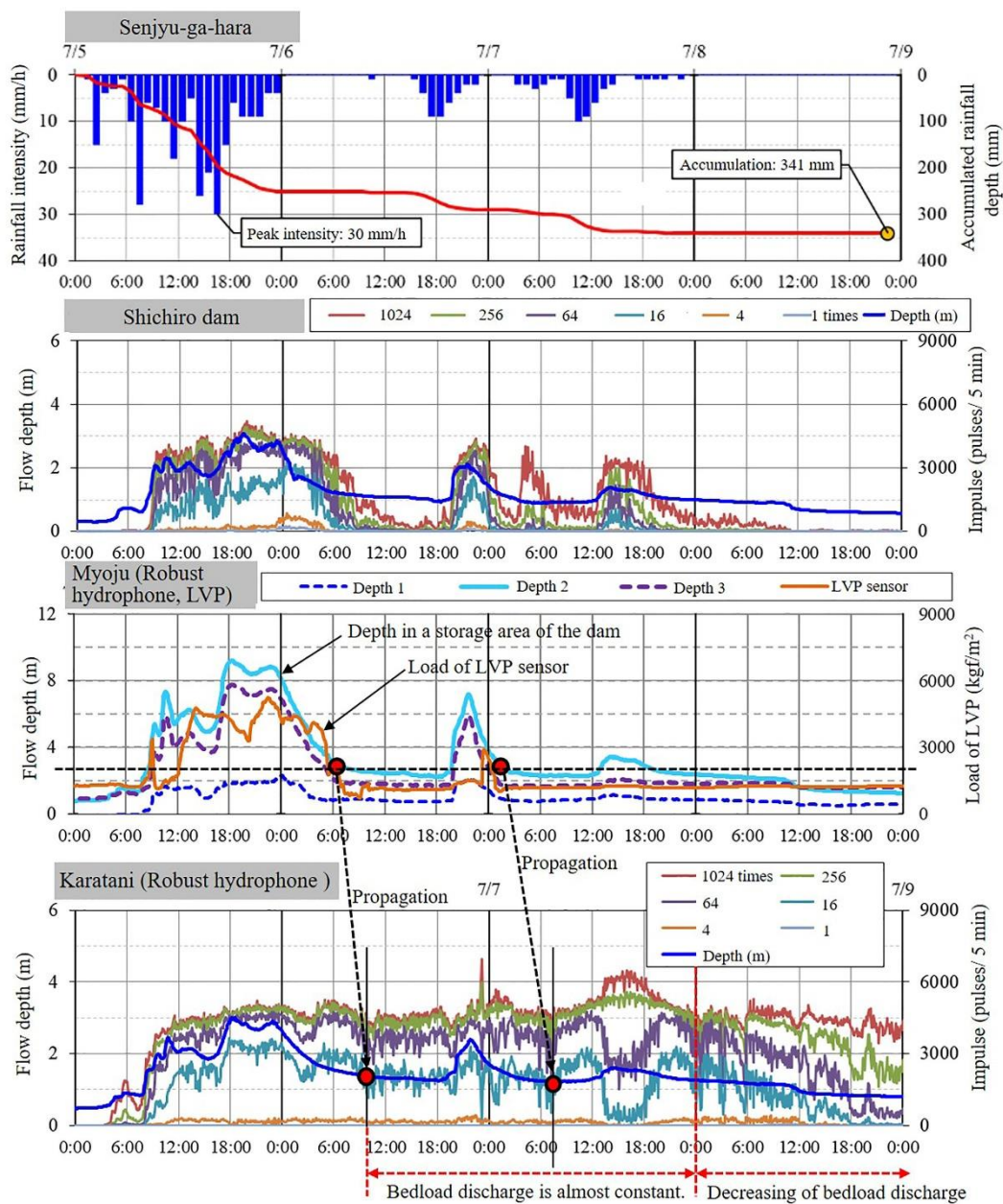


Figure 7. Longitudinal measurements during floods on 5th to 8th July in 2018 (without shutter operations).

### Sediment control by a movable shutter

Sediment discharge of bedload and washload can be calculated using sensors such as robust-type hydrophone and turbidity meter, and the values passing through monitoring sections are obtained at Shichiro, Myoju and Karatani sabo dams. In addition, a loadcell also tries to be installed for measuring the weight of sediment deposition in the storage area of the dam.

Figures 8 show temporal changes of flow conditions around Myoju sabo dam during shutter operations for floods in 2017 and 2018 as shown in Figs. 6 and 7. Notation of (A) and (B) means flood events in 2017 and 2018, respectively. Pictures of camera from peak to

decreasing stage of the flow are shown at several timing in 2018 as same as that in 2017. The notation of circles shows top of the iron bar in the storage area of the dam and the height is 1.1 m above on the top of a spillway of the dam. Numbers of 1 to 8 shows time progressing during floods. Pictures of 1 & 2, 3 & 4, 5 & 6 and 7 & 8 are same time, respectively. The timing of 3 & 4, 5 & 6 means closing and opening operation of the shutter in 2017, respectively. The pictures of B3 & B4, B5 & B6 in floods in 2018 mean time with almost same depth as floods in 2017 to compare flow conditions.



**Figure 8. Temporal changes taken by CCTV camera during shutter operations and comparison of sediment runoff passing through the sabo dam with/without shutter operation ((A) shows floods in 2017 with shutter operations and (B) shows floods in 2018 without shutter operation; e.g., pictures (A1) to (A8) show time progressing during the flood in 2017).**

Let us discuss floods in 2017 referring to Figs. 6 and 8. Closing operation at 8:25 on 4th July has better control function of sediment deposition in decreasing stage of the flood. After closing operation, sediment runoff decreasing in downstream reach during around two days, until opening operation of the shutter. Effects of opening operation on sediment runoff might be a little small during a flood, because of delaying the opening timing.

Next, floods in 2018 are discussed referring to Figs. 7 and 8. Effects of the opening of a slit on sediment runoff are observed during flood events. Vertical opening of the shutter is almost 3.0 m and sediment trapping is effective over 3.0 m of the flow depth in a storage area of the dam (See depth 2 in Fig. 7). Sediment deposition in the storage area of the dam took place during 15 hours from 9:00 on 5th to 0:00 on 6th July in 2018. Sediment runoff took place during 6 hours of decreasing stage and the flow depth is decreasing with around 0.83 m/s. Bedload controlled by a slit is transported to downstream and observed at Karatani sabo dam., as shown in Fig. 7 using the circle notation and broken line.

Figures 9 show the relation of the flow depth versus sediment discharge at Karatani sabo dam for floods in 2017 and 2018. Measured raw data are impulses of 16 times amplifier for bedload and mVolt of output of turbidity meter for washload, respectively.

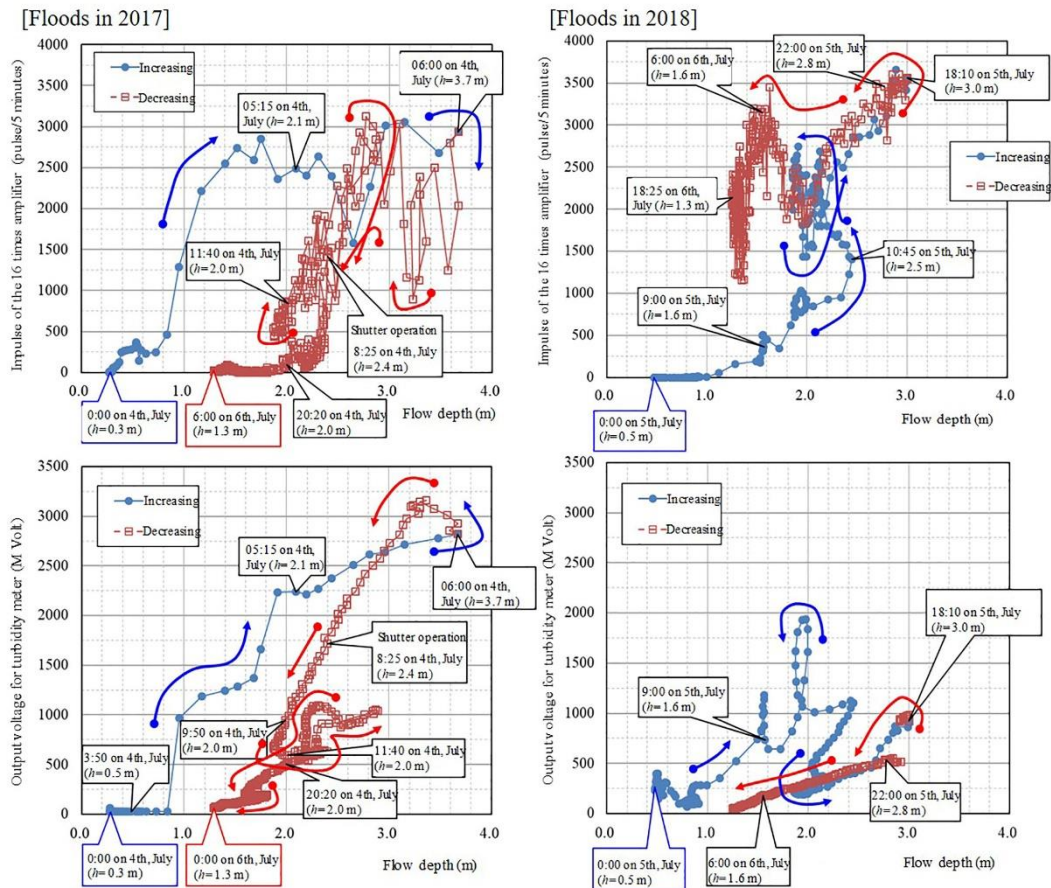


Figure 9. Relationship of flow depth versus sediment runoff for bedload and washload observed at Karatani sabo dam.

Relation of the flow depth versus bedload takes clockwise curve with shutter operations during floods. Washload also takes clockwise curve, because it is not affected by the shutter operation. On the other hand, relation of the flow depth versus bedload takes counter-clockwise curve in floods without shutter operation, though washload take clockwise curve. Because sediment runoff from Myoju sabo dam would affect the bedload discharge in downstream reach of the sabo dam without shutter operations.

Table 1 shows sediment runoff volume passing through dams and erosion/deposition in the reach between dams. Those data collections can give us effective materials for discussions about sediment control by the shutter.

**Table 1. Sediment movements estimated by monitoring tools during shutter operations**

Methods/ Floods	Sediment runoff volume passing through Shichiro sabo dam (m <sup>3</sup> )	Deposition in the storage area of the sabo dam (B) (m <sup>3</sup> )	Runoff volume passing through the dam (B) (m <sup>3</sup> )	Bed variations between (B) and (C) of sabo dams (m <sup>3</sup> )	Runoff volume passing through the dam (C) (m <sup>3</sup> )
Tools for evaluating sediment volume	Robust type pipe hydrophone and correlation relation using impulses	Field measurements and image analyses using CCTV camera	Robust type pipe hydrophone and correlation relation using impulses	Differences in sediment volume between (B) and (C) of dams	Robust type pipe hydrophone and correlation relation using impulses
July in 2017	12,200 (100 %)	+9,400 (75 %) (Deposition)	2,800 (25 %)	-6,300 (-50 %) (Erosion)	9,100 (75 %)
July in 2018	9,561 (100 %)	-976 (10 %) (Erosion)	10,537 (110 %)	-4,413 (-46 %) (Erosion)	14,950 (156 %)

## Conclusion

Trial operations were carried out for the movable shutter at Myoju sabo dam and differences of sediment control with/without the shutter were compared using two floods events in 2017 and 2018. Sediment control with shutter operations can be well for smoothing sediment runoff from the open-type sabo dam. There can be also several control functions for sediment runoff by a slit dam and by a controlled slit height with horizontal iron bars, without shutter operations.

Trial operation will be continued for sediment runoff control and basin management. Effective operation by the shutter can be evaluated using measured data by sensors for monitoring water and sediment movements.

**Acknowledgement:** Authors should be thankful for Tateyama Sabo Office, MLIT, Japan for data usage and for Hydrotec Co., Ltd. for useful development of sensors.

## References

- Japan Society of Civil Engineering (JSCE) (1999): Handbook of Hydraulic Engineering, Maruzen (in Japanese).
- Mikami, K. et al. (2014): Install of a Movable shutter in Myo-Jyu Sabo Dam and Longitudinal Bedload Monitoring in Jyo-Gan-Ji River, Proceedings of the Interpraevent 2014 Pacific Rim (edited by Fujita, M. et al.), November 25-28, Nara, Japan, 2014, P-36.pdf in DVD.
- Nagayama. T. et al. (2019): Monitoring of sediment runoff and observation basin for sediment movements focused on active sediment control in Jo-Gan-Ji River, Proceedings

of 7th international Conference on Debris-flow Hazards Mitigation, Golden, Colorado, USA, June 10-13, 2019: 170-176.

---

# River morphology and sediment transport processes numerical modeling applied to the fluvial environment of the Rhône River in Valais

Francesc Molné<sup>1</sup>, Giovanni de Cesare<sup>2</sup>, Jose Luis García Rodríguez<sup>3</sup>, Azin Amini<sup>4</sup>, Jean-Noël Saugy<sup>5</sup>

**Keywords:** River morphology; Hydraulics; Numerical modeling; Physical modeling; 3rd Rhone Correction

## Abstract

Within the frame of the Third Rhône Correction, the river bend in Martigny is considered a top priority measure for flood protection. During the preliminary project, physical and numerical modeling tests were considered necessary. For the latter, the software BASEMENT has been employed, using the Shallow Water Equations and the Meyer-Peter and Müller transport equations. The scenario simulated consists of a 10-year return period flood applied during 19 days and 20 hours to force the formation of a natural bed, which will be used as an initial state for further scenarios. The results show the morphological evolution of the river and confirm the heterogeneity of the flow. Moreover, a cross-comparison with a physical model has been carried out for a better understanding and with the objective to validate the numerical model for its application at other areas of the Third Rhône Correction project.

## Introduction

With its source in the Rhône Glacier in the Swiss Alps and its mouth in the Lake Léman, the Swiss Rhône once was a dynamic braided river flowing through the Valais Valley. However, as a result of two river corrections to reduce the impact of floods and allow the development of intensive agriculture, urban and commercial zones in the former floodplains, most parts of the river were constrained in a straight, unique channel surrounded by high levees and embankments, completely modifying the hydromorphological and ecological behavior of the river (Fig. 1).

---

<sup>1</sup> Ecole Polytechnique Federale de Lausanne, Switzerland, (francesc.molne@icloud.com)

<sup>2</sup> Dr., Supervisor, Ecole Polytechnique Federale de Lausanne, Switzerland

<sup>3</sup> Dr., Supervisor, Universidad Politecnica de Madrid, Spain

<sup>4</sup> Dr., Research assistant, Ecole Polytechnique Federale de Lausanne, Switzerland

<sup>5</sup> MSc., Research assistant, Ecole Polytechnique Federale de Lausanne, Switzerland

The First Rhône Correction (1863-1893) consisted on a channelization and fixation of the course, by building two parallel dikes and deflectors across the river, to assure an increased safety in a certain extent of the plain. However, the corrected river was unable to carry the millions of cubic meters of sediments to the lake, resulting in an unexpected and most dangerous rise of the riverbed.

The Second Rhône Correction (1930-1960) was aimed to increase the carrying capacity, narrowing the course by filling with rocks the space between deflectors. At the same time, the dikes were reinforced and raised. Not only the works were not sufficient as the gravel loading was still bigger than the carrying capacity but they resulted in a deterioration of the fluvial ecosystem.

The floods of 1987, 1993 and 2000 revealed serious security deficiencies and confirmed the vulnerability of the plain. In October 2000 occurred the highest flood of the century, with a maximum discharge of 1380 m<sup>3</sup>/s. The dikes failed and several dams broke, causing flooding and sediment coverage on 1100 hectares of the plain. People were evacuated and main services and supplies were affected. The damages were quantified in nearly half a billion Swiss francs and have led to a current state suffering deficits in security, environment and socio-economy.



**Figure 1: Left: Napoleon map in St. Léonard (1802) (Centre historique des archives nationales, CHAN). Right: Ortophoto of the same zone (2019) (Swisstopo).**

A Third Rhône Correction is currently being planned with the objective to increase the space available for the river and approach its natural regime, increasing the protection against floods and improving its ecological state at the same time. One of the top priority measures is located in the river bend in Martigny, where the plain upstream is very vulnerable to floods. The planned river training works include: a general widening of the river, a lowering of the bed in the river bend, a construction of a ramp upstream of the river bend, a construction of two local widenings and a widening and optimization of the Dranse confluence.

Modeling tests were considered necessary to optimize the hydraulic design, as well as to gain a better knowledge of the hydro and morphodynamics of the Rhône and the confluence of the Dranse. Hydraulic physical and numerical models have been already developed, cross compared and validated by the EPFL's Platform of Hydraulic Constructions (PL-LCH) in a previous phase. The next step is to include the sediment transport processes and assess the morphological evolution of the river. The aim of this study is to set up a 2D numerical model and cross compare it with the results of the physical model.

## Methods

### Physical model

A physical model has been built in a scale of 1:52 ( $\lambda = 52$ ) in a 1350 m<sup>2</sup> laboratory. The aim is to observe the fluvial processes in a reduced time-frame while collecting a set of data that can be used to validate the numerical model, allowing further long-term simulations to be carried out numerically and provide valuable know-how not only for the modeled perimeter but for all the third Rhone correction project. The measurement instruments include a Leica P20 laser scanner, automatic ultrasonic probes and ultrasonic velocity profilers (UVP) among others.

### Similarity and scale effects

A model is said to be similar to its real-world prototype if it meets geometric, kinematic and dynamic similarities (Yalin, 1971). The design of the physical model was done accordingly. Next, it has been necessary to upscale its dimensions to obtain a comparable numerical model, using the physical model as the prototype.

Geometric similarity refers to the similarity in length, area and volume and kinematic similarity implies constant ratios of time, velocity and discharge. The determination the physical parameters in the modeled scale has been done according to Froude's similitude, requiring that the Froude number in the model is the same as in the prototype. The mathematical formulation is written as follows:

$$\mathbb{F} = \sqrt{\frac{F_i}{F_g}} = \frac{u}{\sqrt{gh}}$$

$\mathbb{F}$  : Froude number     $F_i$  : Inertial forces     $F_g$  : Gravitational forces  
 $u$  : Flow velocity [ $ms^{-1}$ ]     $g$  : Gravitational acceleration [ $ms^{-2}$ ]

$h$  : Flow depth [m]

Dynamic similarity indicates a constant ratio of masses and forces. As it is impossible to scale all these parameters at the same time, models are built by properly scaling the relevant forces and parameters and proving that the effects of all other forces can be neglected according to the Reynolds and Weber's criteria.

The behavior of sediments used in the model must as well be similar to the prototype. If the grain size distributions of the prototype sediments are converted by the geometric scale, scale effects may appear. In order to avoid that, the particle size is scaled using the friction velocity similitude:

$$\frac{u_{*P}}{u_{*M}} = \lambda^{1/2}$$

$u_{*P}$  : Friction velocity (prototype) [ $ms^{-1}$ ]

$u_{*M}$  : Friction velocity (model) [ $ms^{-1}$ ]

$\lambda$  : Geometric scale factor

## Numerical model

The software BASEMENT 2.8, developed by the ETH Zürich, has been used for the numerical modeling. The 2D model, included in a subsystem called BASEplane, is based on the Shallow-Water (SWE) and the Exner-Hirano Equations for the hydrodynamics and morphodynamics respectively.

The validity of the SWE implies assuming that vertical accelerations are negligible (hydrostatic distribution of pressure), the slope for the channel bottom is small and the steady-state resistance laws are applicable for unsteady flow. These conditions permit to reduce the 3D flow into 2D. The vertical dimension is removed by the integration of the Navier-Stokes equations over the flow depth, which results in the Shallow Water Equations. The lateral slope and curvature effects have not been considered in this phase.

The transport formula of Meyer-Peter and Müller (1948) has been used to determine the bed load and an extension of the formula by Hunziker (1995) is utilized in the model. In the case of a sloped bed in the flow direction or transverse to it, the stability of the grains can either be reduced or increased due to gravity. This is also considered in the model by the implementation of correction factors as suggested by van Rijn (1989).

Some of the most interesting morphological features are formed by 3D processes. Although only 2D models are performed with BASEMENT, it is also useful to study the vertical eddies (Fig. 2) that will cause the creation of bedforms (dunes and ripples) which will indeed be observed in the physical model. These deformations on the bed will in turn affect the hydraulics and cause stationary waves. This aspect has also been studied considering a quasi-uniform and bi-dimensional flow in the Verney widening, obtaining a maximum dune height of 0.47 m. Variations of this order of magnitude can therefore occur between the physical and numerical models.

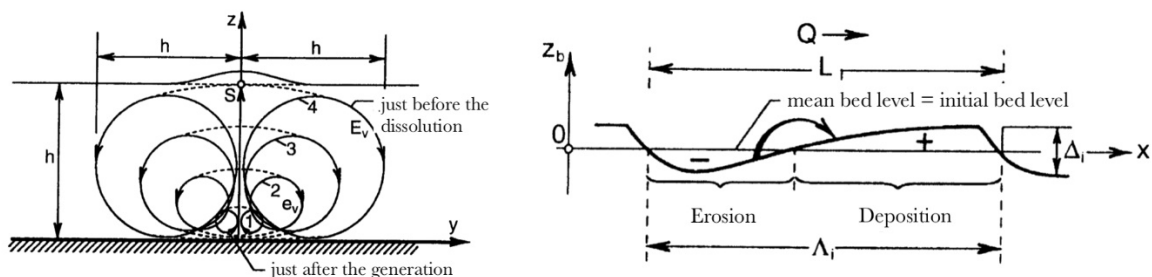
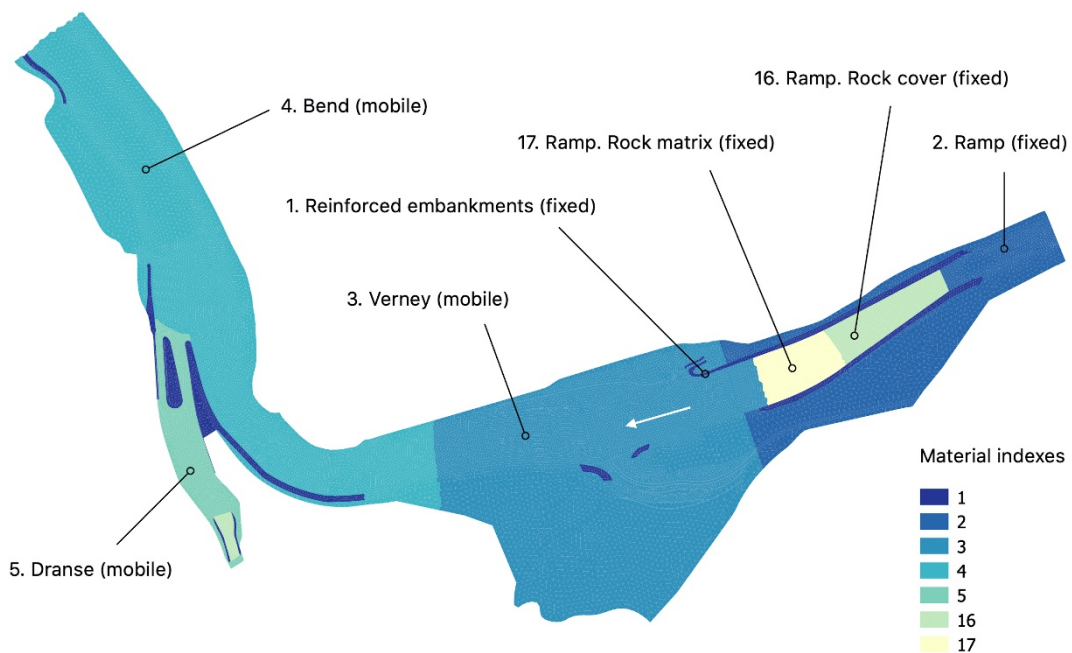


Figure 2: Vertical eddies and conceptual representation of the bedforms they produce (Schleiss, 2018).

## Variables and conditions

In BASEMENT the topography is discretized into an unstructured grid composed of triangulated cells. The mesh was built based on the transversal profiles of the project in AutoCAD. The terrain model was densified by doing a linear interpolation using the HEC-RAS software and the final grid was obtained using the “paving” method in SMS software. The mesh consists of 18399 nodes and 36097 elements. The roughness coefficient is defined using the Strickler coefficient, and was determined according to the soil cover and the grain size distribution, distinguishing 7 different zones or material indexes:



**Figure 3: Material indexes of the mesh and bed mobility.**

As seen in the previous hydraulic studies, the flow is sub-critical at the upper and lower ends of the channel, thus it is influenced from upstream and downstream. The modeled scenario in this study corresponds to a 10-year return period flood in which the characteristic water and bed load discharges remain constant until the input sediments reach the downstream boundary. The aim is to build an heterogeneous bed in a faster way, that will be used afterwards as initial condition for further simulations and scenarios. Therefore, the upstream boundary conditions for the Rhône and the Dranse have been defined with their characteristic  $Q_{10}$  water (669 and 95  $m^3/s$  respectively) and solid discharges (0.0596 and 0.0302  $m^3/s$  respectively).

The data from the river grain size distribution analysis was downscaled to the physical model scale according to the friction velocity similitude. To avoid cohesive forces, the grains with a diameter below 0.063 mm were removed from the mixtures. Very similar sediment mixtures were supplied by a specialized company from Valais. These mixtures were then upscaled to the numerical model scale according to the critical velocity similitude in order to perform comparable simulations.

## Results and discussion

The target results were obtained after 19 days and 20 hours in the numerical model scale. The discussion focuses on the bed changes ( $\Delta Z$ ), bed elevation, depth, velocity and water surface elevation. The increased space given, makes the river to approach its natural regime, developing a new bed with its characteristic bedforms until a new quasi-equilibrium state is reached. This is especially clear in Verney, where it can be observed the typical pattern of a local widening. The ramp upstream the widening prevents the upstream scour that can appear at the beginning caused by a temporary flow acceleration towards the widening, and even the deposits ascend over the ramp. It can also be seen how the longitudinal slope within the widening increases in order to ensure enough transport capacity to deliver the entire bed load discharge downstream. As a consequence, the water surface elevations also increase compared to the initial state, but the risk of overflow is properly prevented. Furthermore, the new bathymetry increases the heterogeneity of the flow, diversifying the velocity magnitudes and directions and offering as well an enhanced habitat variability.

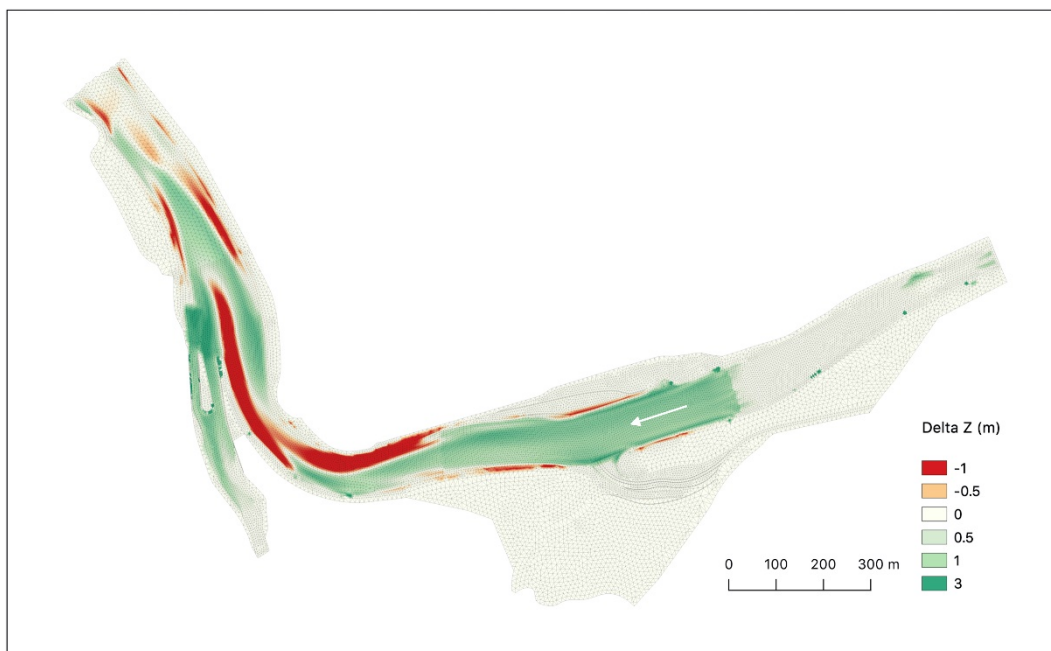


**Figure 4: 2D results of the bed changes (erosion and deposition).**

A cross-comparison with the physical model has been carried out quantitatively with the results of the water surface elevation and qualitatively with visual observations and tests of water recirculation in order to analyze the morphological evolution and its effects on the flow. In Fig. 5 it can be seen the longitudinal profile in which the water surface elevation measurements from the ultrasonic probes are represented by green crosses. Most of them show a very good accordance between the physical and numerical results. However, at probes 5 and 6, in the Verney widening, a slight difference of around 30 cm is observed, the same order of magnitude than the calculated regime bedforms' dimensions. This is due to the fact that the bedforms in the vertical plane developed by 3D processes are ignored in the numerical model. Some deviations are also observed in probes 7 and 8, at the river

bend. In this case, it has to be understood that in river bends a non-uniform vertical distribution of velocities and non-horizontal water level, caused due to tangential and centrifugal forces along a radial path, can generate secondary currents and require the application of 3D models. Even though, the time series plots at each probe show similar trends for the two models.

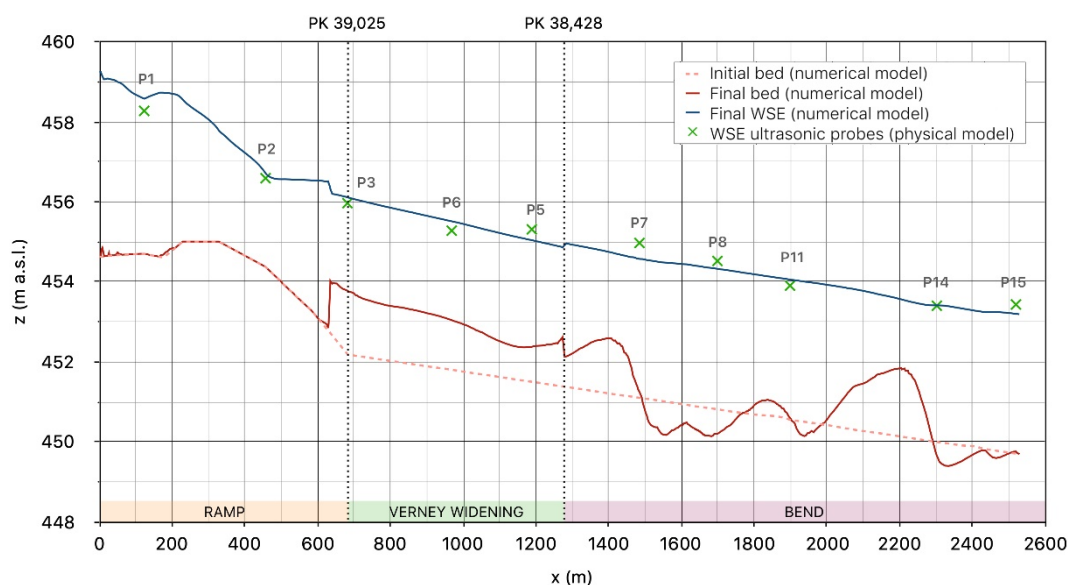


**Figure 5: Longitudinal profile with the WSE results from the physical and numerical models.**

During a flood event in the restored channel, the presence of new floodplains will make the river react firstly by increasing the width, which might be followed with an increase in depths and velocities as well, but in a more slowly and peacefully manner, containing the volume of water without risk of overflow and reducing the shear stress over the banks and riverbed.

## Conclusion

For the modeled scenario, taking into consideration the sediment transport processes, the results have shown coherence between the 2D numerical and the physical models. However, the understanding of their limitations has been key for a better interpretation of the results. The possibility to have had data from the two models is a great advantage as it permits to complement the information available and obtain more trustable results. The numerical model has proved to be very useful for testing simple river engineering problems, showing very accurate results in accordance with the ones of the physical model even for the morphodynamics. Furthermore, it constitutes a cost-effective methodology to be applied in a bigger extent. Yet, the fact that the 3D processes are ignored reveals its weaknesses in certain cases. A good knowledge of the assumptions made by the model and the real processes that occur in nature, permit to criticize the results and squeeze the huge potential of these tools. The validation of the model requires additional simulations, but the results obtained and the understanding of its limitations suggest that the possibilities of this tool applied to the Third Rhône Correction are promising.

## References

- ASCE (American Society of Engineers). (2000). *Hydraulic modeling: Concepts and practice*.
- Canton Valais. (2014). *Plan d'aménagement (PA-R3). Rapport de synthèse*.
- Rey, Y. & Bureaux partenaires. (2014). *Rapport d'impact sur l'environnement Ire étape du Plan d'aménagement de la 3e correction du Rhône adopté le 2 mars 2016 par le Conseil d'Etat valaisan*.
- Schleiss, A. (2018). *Polycopiés du cours "Eco-morphologie fluviale". Laboratoire de Constructions Hydrauliques (LCH). EPFL*.
- Vetsch D., Siviglia A., Caponi F., Ehrbar D., Gerke E., Kammerer S., Koch A., Peter S., Vanzo D., Vonwiller L., Facchini M., Gerber M., Volz C., Farshi D., Mueller R., Rousselot P., Veprak R., Faeh R. (2018). *System Manuals of BASEMENT. VAW, ETH Zurich*.
- Yalin, M. S. (1971). *Theory of hydraulic models. Springer*.

---

# Image-based flow measurements in wide rivers using a multi-view approach

Salvador Peña-Haro<sup>1</sup>, Robert Lukes<sup>2</sup>, Maxence Carrel<sup>3</sup>, Beat Lüthi<sup>4</sup>

**Keywords:** Discharge, Wide rivers, Cameras, SSIV

## Abstract

A multi-view image based system has been developed to measure the discharge in large rivers using Surface Structure Image Velocimetry. In large rivers the image resolution might not be enough to allow for a proper characterization of the flow surface patterns. To get more detailed surface patterns, a Pan-Tilt-Zoom camera was used, which has the capability to move and zoom into smaller areas of the river on the spanwise direction. The system has been installed in the Zollbrücke on the Rhine river where it is around 100 meters wide during low flow conditions. The system records videos with a duration of 5 seconds in each one of the views every 5 minutes. One month of data was compared against the reference values. The mean discharge during that period was of 190 m<sup>3</sup>/s and the Root Mean Square Error was found to be 8.4 m<sup>3</sup>/s compared to the official values.

## Introduction

Knowing the volumetric flow in rivers is essential to analyze hydrological process, and for many applications ranging from flood forecasting to water resources management. And at the same time it is one of the most difficult variables to measure. Discharge is normally estimated by using stage-discharge curves which are established by having some measured discharges at different stages and then a curve is fitted to those measured values. Latter on, only river stage is continuously measured, for instance with pneumatic gauges (Creutin et al., 2003, Turnipseed and Sauer, 2010).

During the last years several image based methods for measuring the surface velocity in rivers and channels have being proposed (Fujita et al., 2007, Patalano, et al., 2017, Jodeau et al., 2017, Leitão et al., 2018, Tauro et al., 2018). Image based discharge measurements posses several advantages, one of them being that the sensor (camera) is not in contact with the water and its mounting position is very flexible and there is no need of expensive structures to mount it. Beside environmental factors, the performance of image based discharge measurements depends on the image resolution. In large rivers the image resolution at the far field can be very poor (Muste et al., 2011). To overcome this problem we used pan-tilt-zoom (PTZ) cameras which are capable of moving and zooming.

---

<sup>1</sup> Photrack AG, Switzerland, (pena@photrack.ch)

<sup>2</sup> Swiss Federal Office for the Environment, Switzerland

<sup>3</sup> Photrack AG, Switzerland

<sup>4</sup> Photrack AG, Switzerland

Herein we present a new implementation of an image based discharge measurement using PTZ cameras, this feature allows to look at a smaller parts of the river by zooming in. Several videos are recorded and processed individually to obtain the surface velocity. Later the calculated surface velocities of each of the views are assembled and the discharge is computed.

## Methods

Traditional camera calibration in Large Scale Image Velocimetry (LSPIV) methods require to have visible Ground Control Points (GCP) on the river shores (Creutin et al, 2003, Kim et al., 2006, Jodeau et al, 2008) which should be visible on the image. When measuring the discharge in large rivers using a PTZ camera, it can be zoomed into smaller parts of the river. By doing this, it can happen that a camera view would only contain water with no visible shores, hence we developed a new camera calibration methodology which does not need to have any visible GCP on the image which is going to be processed.

From PTZ cameras it is possible to extract information related to the pan and tilt angles as well as the zoom factor. The PTZ camera calibration consisted on finding the camera mount orientation and on establishing a relation between the zoom factor and focal length of the camera. To do this, GCP have to be placed in any place which is visible to the camera and the pan/tilt values of the camera have to be read for each of the GCPs. This information was used to estimate the camera mount once this is known, it is possible to move the camera to any location with any zoom level and calculate the world coordinates of a given pixel of the view (for a given water level).

After camera calibration, the discharge is calculated as follows. The water level is measured optically by segmentation of images of a view located on the right shore of the river (see Figure 2 A). The surface velocity measurements are obtained by applying the Surface Structure Image Velocimetry (SSIV) method (Leitão et al., 2018) to the recordings of the remaining views, yielding a surface velocity field spanning over the entire width of the river. It is assumed that the cross-section of the river remains constant for the portion considered. A fit is applied to the stream-wise components of the surface velocity yielding a surface velocity profile. The fit is done using a least square regression with a model function which depends on the cross section.

The average vertical velocity for discrete sections over the width of the river is obtained by applying the ISO norm 748:2007, which is a standard expressing the average velocity of a river section as a function of its depth and roughness coefficient. For each discrete section the discharge is calculated by multiplying the average velocity and the area of that section. Finally, the total discharge is then obtained by integrating the discharge of all the discrete sections.

## Case study

The measurement system presented in this study is installed on the Zollbrücke on the Rhine river, at the border between Switzerland and Austria. At this location the river width is of approximately 100 meters under low flow conditions, while the width of its floodplain is of about 200 m (Figure 1, left).

At the site there is an official station from the Swiss Federal Office for the Environment (FOEN), where there is a SOMMER RQ-30 radar sensor under the bridge. The river stage and a rating-curve are used to get the reference current discharge.

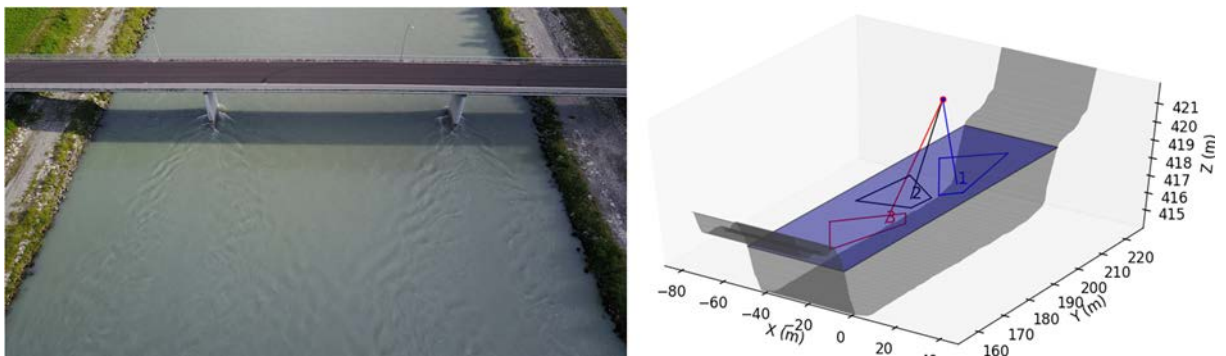


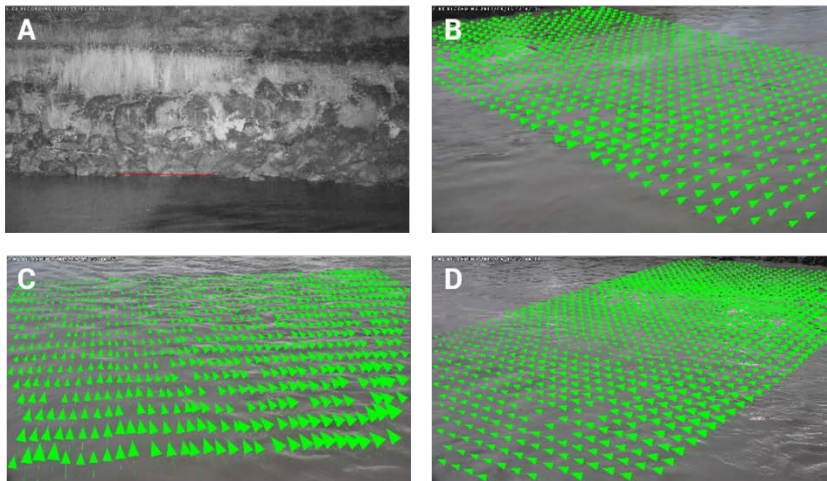
**Figure 1** Aerial view of the Rhine river and the bridge where the camera is mounted (left). Camera position and different camera views where the surface velocity measurements are performed (right).

In order to measure the surface velocity field over the whole river width, a PTZ camera was installed (Vivotek SD9364-EH, which also has an integrated IR light), and 3 views were defined in order to cover the whole river width (Figure 1 right). An additional view was defined for the level measurement. The camera records videos of 5 seconds in each one of the views every 5 minutes. The videos are recorded with HD resolution and a frequency of 30 fps.

The system is also running during night, for this end the camera used is equipped with an infrared light whose zoom is synchronized with the one of the camera. Making use of this feature, it is possible to measure optically the water level on the right shore of the river over night (Figure 2A). The infrared projector is too weak to allow to measure the surface velocity fields in all views, therefore during night the surface velocity measurements are performed only in the vicinity of the bridge, close enough to ensure a good infrared illumination.

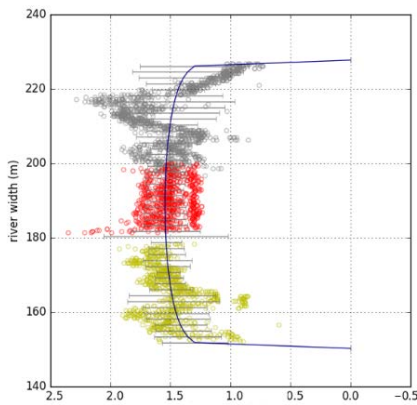
## Results and discussion

Figure 2 shows the results of a single measurement, it comprises the level detection (Figure 2A) and the surface velocity for the 3 views (Figure 2B, 2C and 2D).



**Figure 2 (A) View used for the automatic water level detection (red line). Surface velocity fields measured for the views located on the left (B), middle (C) and right (D) of the river.**

After the surface velocities are independently calculated for each view, the measured stream-wise velocity components are assembled and a velocity profile is fit to them over the whole river surface width (Figure 3). Then, for the surface velocities obtained with the fit, an average velocity is calculated using the ISO standard. The discharge is computed by integrating the average velocities and corresponding depths over the entire river width.



**Figure 3 Stream-wise velocity components measured on the left (yellow), middle (red) and right (grey) sides of the river as well as the fit applied to these velocities (blue).**

Discharge time series of a month obtained with the camera-based system were compared to the reference values. Figures 4 and 5 show the unfiltered time series of water level and discharge obtained by means of SSIV for a time period between January 10<sup>th</sup> and February 10<sup>th</sup>, 2018 with time intervals of 10 minutes. At first glance, the water level and measured discharge with the PTZ camera look fairly similar to the official values. All time series show important daily fluctuations reflecting the effect of the hydro-power facilities located upstream. This is quite interesting for this study because these daily fluctuations mean that

the variables measured cover an important range allowing an extensive comparison of both measurement systems.

The root mean square error (RMSE) was used in order to perform a qualitative comparison between the reference data and SSIV. For the water level an RMSE 0.068m was calculated and for the discharge 8.487 m<sup>3</sup>/s.

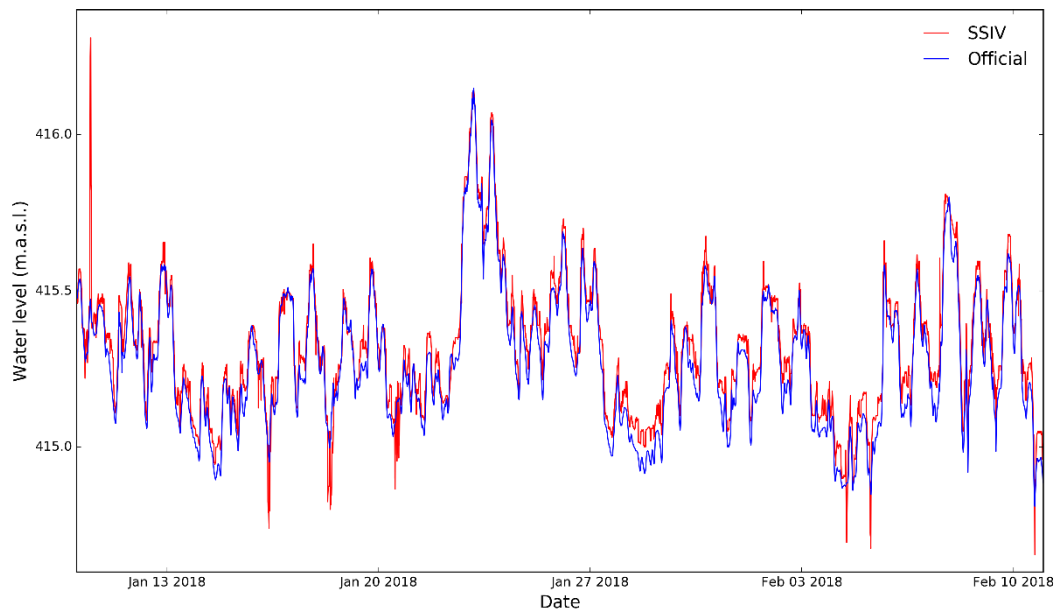


**Figure 4** Time series of water level measurements by the camera-based system and the official ones.

The water level expressed as a functions of the discharge is often referred to as rating curves, and for our case it is shown in Figure 6. Also in this graph it can be seen the good agreement between the reference and the measured values.

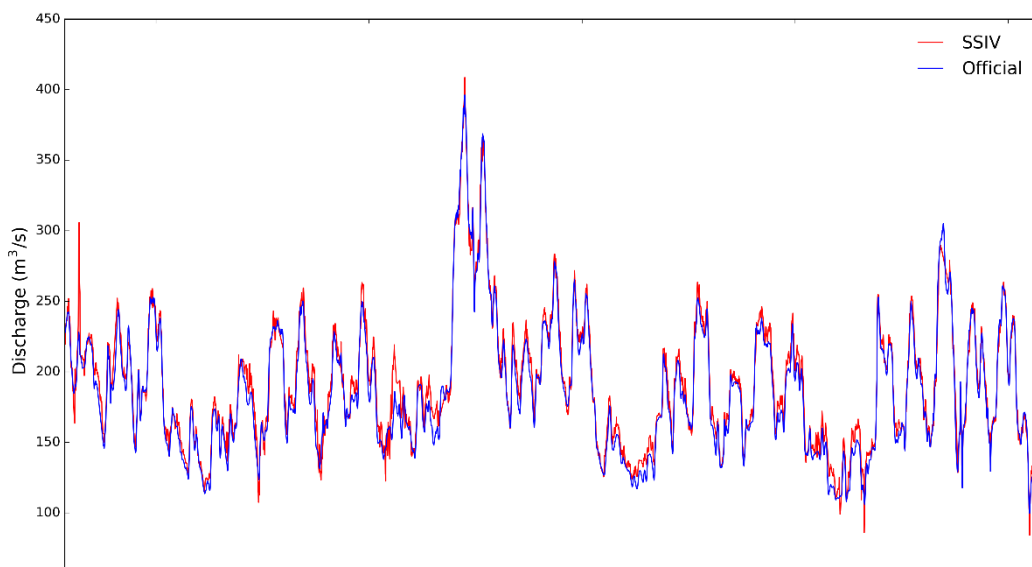


**Figure 5** Time series of discharge measurements by the camera-based system and the official ones.

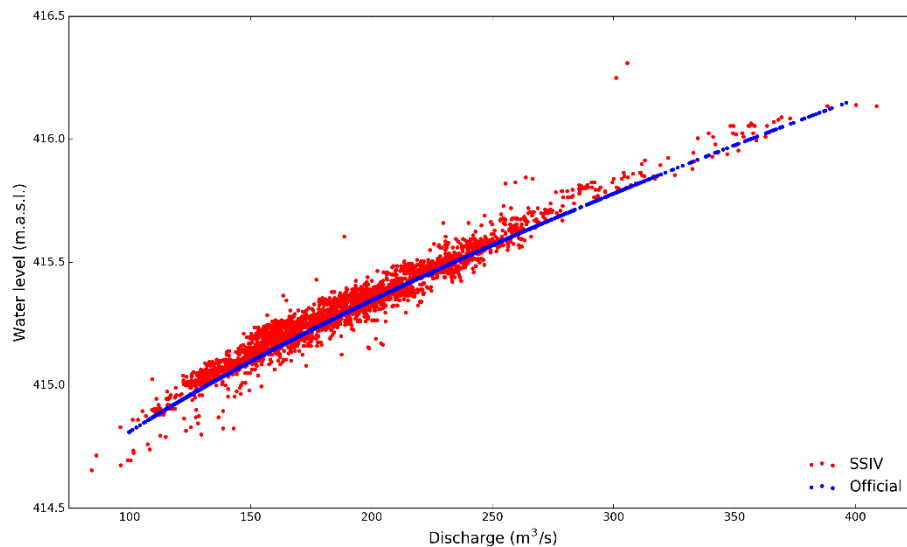


**Figure 7 Stage-discharge curve. Red dots are the ones from the SSIV + PTZ camera. Blue dots are the official values.**

Within this setup there are some factors that can affect the surface velocity measurement accuracy, like the camera potential to always come back to the same predefined position, and the influence of the bridge vibration on the recorded videos. Regarding the first point, the used camera can pan and tilt with steps of 0.016072 degrees, which allows to accurately go back to the predefined positions. As mentioned before, the camera was mounted under a bridge which is open to vehicles. Therefore the camera is subject to vibrations, however it was observed that the vibrations did not have any visible influence on the surface velocity measurements. This is, the direction and magnitude of the vector are in correspondence with the flow direction. However further research is needed to quantitatively determine the vibration influence on the measured surface velocity.

One interesting feature of the image based methods is that every measurement comes with a proof-image so that the plausibility of the results can be checked directly by the operator. Additionally, it is possible to access the measurement system in real-time, or even to take control of the camera and to make use of the PTZ functionality to monitor the surroundings. This is a function that is in particular of interest for locations where natural elements (e.g. floods, landslides, drift wood) potentially can cause important hazards to habitations, bridges, hydraulic structures etc.

## Conclusions

This study introduced an image-based measurement system relying on the use of a PTZ camera for performing water level, surface velocity and discharge measurements in a wide river. The mean discharge during that period was of 190 m<sup>3</sup>/s and the RMSE was found to

be 8.437 m<sup>3</sup>/s. The system has proved to perform well and has the potential to measure even wider rivers.

## References

Creutin, J. D., M. Muste, A. A. Bradley, S. C. Kim, and A. Kruger. "River Gauging Using PIV Techniques: A Proof of Concept Experiment on the Iowa River." *Journal of Hydrology* 277, no. 3–4 (2003): 182–94. [https://doi.org/10.1016/S0022-1694\(03\)00081-7](https://doi.org/10.1016/S0022-1694(03)00081-7).

Fujita, Ichiro, Hideki Watanabe, and Ryota Tsubaki. "Development of a Non-intrusive and Efficient Flow Monitoring Technique: The Space-time Image Velocimetry (STIV)." *International Journal of River Basin Management* 5, no. 2 (2007): 105–14. <https://doi.org/10.1080/15715124.2007.9635310>.

Hauet, Alexandre, Jean-Dominique Creutin, and Philippe Belleudy. "Sensitivity Study of Large-Scale Particle Image Velocimetry Measurement of River Discharge Using Numerical Simulation." *Journal of Hydrology* 349, no. 1–2 (2008): 178–90. <https://doi.org/10.1016/j.jhydrol.2007.10.062>.

Jodeau, M., A. Hauet, A. Paquier, J. Le Coz, and G. Dramais. "Application and Evaluation of LS-PIV Technique for the Monitoring of River Surface Velocities in High Flow Conditions." *Flow Measurement and Instrumentation* 19, no. 2 (2008): 117–27. <https://doi.org/10.1016/j.flowmeasinst.2007.11.004>.

Jodeau, Magali, Alexander Hauet, Jerome Le Coz, Yvan Bercovitz, and Franck Lebert. "Laboratory and Field Lspiv Measurements of Flow Velocities Using Fudaa-LSPIV a Free User-Friendly Software." Madrid, 2017.

Leitão, João P., Salvador Peña-Haro, Beat Lüthi, Andreas Scheidegger, and Matthew Moy de Vitry. "Urban Overland Runoff Velocity Measurement with Consumer-Grade Surveillance Cameras and Surface Structure Image Velocimetry." *Journal of Hydrology* 565 (2018): 791–804. <https://doi.org/10.1016/j.jhydrol.2018.09.001>.

Muste, M., H. -C. Ho, and D. Kim. "Considerations on Direct Stream Flow Measurements Using Video Imagery: Outlook and Research Needs." *Journal of Hydro-Environment Research* 5, no. 4 (2011): 289–300. <https://doi.org/10.1016/j.jher.2010.11.002>.

Patalano, Antoine, Carlos Marcelo García, and Andrés Rodríguez. "Rectification of Image Velocity Results (RIVER): A Simple and User-Friendly Toolbox for Large Scale Water Surface Particle Image Velocimetry (PIV) and Particle Tracking Velocimetry (PTV)." *Computers & Geosciences* 109 (2017): 323–30. <https://doi.org/10.1016/j.cageo.2017.07.009>.

Tauro, Flavia, Fabio Tosi, Stefano Mattoccia, Elena Toth, Rodolfo Piscopia, and Salvatore Grimaldi. "Optical Tracking Velocimetry (OTV): Leveraging Optical Flow and Trajectory-Based Filtering for Surface Streamflow Observations." *Remote Sensing* 10, no. 12 (2018): 2010. <https://doi.org/10.3390/rs10122010>.

Turnipseed, D. Phil, and Vernon B. Sauer. "Discharge Measurements at Gaging Stations." Reston, Virginia: U.S. Geological Survey, Techniques and Methods book 3, chap. A8, 87 p., 2010.

---

# Documentation of Natural Events and its Importance for the Integrated Risk Management. Review, current use and new developments in Switzerland

Wolfgang Ruf<sup>1</sup>, Mathias Zesiger<sup>2</sup>

**Keywords:** event documentation; past event data; StorMe; rapid mapping; Switzerland

## Abstract

The documentation of natural events has a long tradition in Switzerland and has a great potential for the use in the hazard assessment, planning of protective measures, and in the risk dialogue. This article about event documentation highlights, which data are available and collected in Switzerland, their added value and how they are used. Furthermore, recent developments are described, such as the newly implemented database StorMe 3.0 as well as the use of geodata within the federal Rapid Mapping service.

## Introduction

### History of documentation of natural events

The documentation of natural events has a long tradition in Switzerland, but information is widely spread. Since hundreds of years, people were aware of the possible occurrence of natural hazards and collected information about catastrophic events, which is now stored in numerous different historic archives. In the Euro-Climhist database (University of Berne), natural events data were gathered mainly from the time period between 1501 and 1863 by evaluating historic sources. For avalanches that caused damage to persons or property, an inventory database with more than 15'000 events has been run by the WSL Institute for Snow and Avalanche Research SLF since 1936. Since 1972, for inundation, debris flow and landslides and since 2002 for rock fall processes, the Swiss Federal Institute for Forest, Snow and Landscape Research WSL has collected data from over 20'000 events by evaluating newspaper articles in the so-called "Unwetterschaden-Datenbank". Only Euro-Climhist is open to the public.

---

<sup>1</sup> Dr., scientific collaborator, Hazard Prevention, Federal Office for the Environment (FOEN), Postfach, Bern, Switzerland ([wolfgang.ruf@bafu.admin.ch](mailto:wolfgang.ruf@bafu.admin.ch))

<sup>2</sup> Federal Office of Topography swisstopo

## **Legal Basis, StorMe Database and Guidelines**

Triggered by some severe events in the second half of the 20th century, new laws were enacted in 1994, with the obligation for the cantons to run an inventory of natural events. To facilitate this process, the federal authorities provided them the nationwide database application StorMe in 1998 for the collection of event data (with today over 43'000 recorded events). The cantons mandated specific persons or consulting offices to systematically collect information in the field and record it in StorMe after the occurrence of an event. Additionally, during the hazard assessment process, further information about past events was collected and then recorded in StorMe by asking witnesses or searching through communal or cantonal archives.

Between 1998 and 2002, the guidelines “Documentation of Mountain Disasters” (Hübl et al., 2002) were elaborated by different international associations in order to set common standards for recording event data, based on the recording forms used in StorMe. After two decades, the application StorMe was further developed (see chapter *New web-GIS application StorMe 3.0*). The experience showed that the existing guidelines were not sufficient to collect information in a uniform and unambiguous way. The recently developed new recording guidelines (“Erfassungsrichtlinien”, BAFU, 2020a) will now provide a more precise guidance and clear definitions for a better data acquisition and interpretation.

## **Use and benefits of event documentation**

The documentation of past events satisfies different purposes within the integrated risk management. It is an important basis for hazard and risk assessment, increases the understanding of natural processes, helps to understand the past and to learn for the future, improves the planning of measures, and is an important information for the risk dialogue.

### **Basis for hazard and risk assessment**

The hazard assessment for the settlement areas within Switzerland is now complete, but in future, a periodic re-assessment must be carried out. For its scenario building and modelling purposes, a good process understanding of past natural events was and will be essential. The questions, what can happen, how often, and what are possible future evolutions of events, must be answered, which would be more difficult and less reliable without the observation-based scenarios and the knowledge supported by past event data.

For hazard assessment, the collection of information about past events starts with a scan through the “StorMe” inventory, additionally in archives of communes, cantons, insurance companies and others. The map of the phenomena (containing the so-called “silent witnesses“ that are still visible in the field today) is equally essential as a data source to get a full picture of what has happened in the past. In any case, the collected information must be verified in the field.

The following paragraphs explain more in detail, how these data are used in hazard assessment, structured according to the various natural processes. Representative for

numerous cases, selected examples are shown, where the benefit of event documentation data could be attested (oral communication by the persons responsible for the documentation of natural event and hazard assessment in the cantons St. Gall, Berne and Lucerne).

*Inundation:* Small catchments suffer mostly from a lack of recorded runoff data. Models are used for the estimation of runoff with a given return period. Past event data are used for plausibility checks. If time series are too short to catch also very rare events, the peak over threshold values for the extreme event analysis can be prolonged using historic documented event data (see e.g. Scherrer et al., 2011) by reconstructing the runoff peak.

Regarding the extent of flooding, historic pictures, documented water levels or mapped inundation areas help to estimate the water pathways within areas affected by inundation. The cases of Hohenrain (Canton Lucerne) or Kien (Canton Berne) show that modelling assumptions for the hazard assessment had to be revised, because the flow paths during a real event - obtained by photos and event documentation - differ from the modelled ones, which are based on the DTM, thus underestimating the possible inundated areas remarkably.

*Overland flow:* A Swiss-wide indicative hazard map of overland flow was recently produced. Investigations showed reasonable results also within built environments. This has been approved till now by the documentation of several heavy rainfall events, such as in Zofingen (July 2017) or Lausanne (June 2018). However, small differences between the real altitude and elevation model data such as tiny structures on the ground or smoothed surface roughness may cause distinct flow pathways compared to the model. Therefore, improvements of the model are needed in order to proceed from a hazard indication map towards a precise hazard map. Documentation of observed inundated areas and overland flow paths is still necessary in the future to bring this procedure an essential step forward.

*Landslides:* In order to assess the susceptibility of a hillslope for spontaneous landslide processes, the past occurrence of landslides with comparable geological, vegetation and soil conditions in an area of interest is essential as a decisive criterion. This procedure is recommended in the federal guidelines about mass movements (BAFU, 2016). A good inventory reduces also in this case the degree of uncertainty of the hazard assessment.

*Rock fall / rock slide:* Knowledge about the frequency and size of detached rocks and stones is the key information for defining the scenarios. While the estimation of the relevant rock size is already difficult to assess in the field, the corresponding frequency can hardly be assessed only by visual inspection. With a comprehensive inventory of past events, the frequency of rock falls with a given rock size can be estimated, leading to the relevant scenarios.

The location of the deposited stones and rocks in the field are real realizations of acceleration tracks, as they are also mimicked in numerical models. Silent witnesses and documented past events must be used for the validation of these models. If the properties in the translation zone have not changed considerably, the observed deposited rocks must lay within the assessed hazard zone, otherwise, the model parameters have to be adapted.

The documentation and analysis of a rock slide event from the Guschakopf in Bad Ragaz (SG) attested, for the existing hazard assessment, the quality of the numerical model in itself, but showed that the scenario assumptions for the block size and frequency were too optimistic. The hazard maps are thus being revised. In Weggis (LU), the documentation of a rock fall event confirmed the existing hazard map and lead to building codes for a new house, which was planned just at the edge of zones of different hazard levels.

*Avalanches:* The assessment of the released snow volume is challenging. For a given frequency, it depends on the depth and the extent of the released snow package. The transition process depends further on the snow condition. In the case of flow avalanches, the extent of the deposition zone can be estimated for events of high and mean frequency, provided that inventory data of good quality and with long-time-series are available.

In the Canton Berne, e.g., the avalanche inventory is always consulted for the assessment of building applications outside of the settlement areas, where no hazard maps are available. For an alpine cabin in Adelboden, e.g., additional modelling results confirmed the conclusion from the inventory data.

*Benefits independent from the process type:* In some cases, extreme events might have been documented events in the past, not being considered by the hazard assessment modelling. In these cases, these events must be included in the scenario definition. Past event data are furthermore helpful to detect unexpected process chains being overlooked in the scenario building process. Failure points during past events, who give hints also for nowadays scenarios, can also be identified.

## **Improving the planning of measures**

The dimension of technical protective structures depends on reliable assumptions about the corresponding expected load. After problems with floating wood in the river Kleine Emme in July 2008, the new wood retention system in Ettisbühl was designed to a large extent on the basis of event documentation data. The new weir at the river Reuss in Lucerne was designed as well based on the real data of the flood event documented in August 2005.

For intervention measures, emergency services profit from the a-priori knowledge about possible scenarios in order to be better prepared for the real case (e.g. by establishing interventions maps). Additionally, road managing services make use of a good inventory for current risk assessment and decision making about road closure (example of Guttannen, Canton BE: avalanche risk during heavy snowfall situations).

## **Research and Process understanding**

A good general understanding of the processes is essential for a reliable future hazard assessment. Here, the case of hillslope debris flow is addressed as an example, i.e. a process where the triggering factors are still not sufficiently understood. The event analysis of 2005 (Bezzola et al., 2018) could already improve the knowledge of the susceptibility of slopes to landslides. In 2019, the WSL installed a new database for hillslope debris flow events. Starting from numerous landslide events in August 2005 in Switzerland, the new database

will continue to integrate such events to provide the fundamental information for future applied research about the triggering of landslides.

## **Learning from the past through event analysis**

The analysis of hazard events, which relies on a profound documentation of the related events, plays an important role in the integrated risk management in Switzerland. First examples were the avalanche events of 1887/88 or 1950/51. Numerous other event analysis followed, both at the federal and cantonal level. The objective is always to learn from the past for the future. Deficiencies in the scientific knowledge, process understanding, dealing with the hazards and risks, protective measures or the clarity of responsibilities must be detected in these types of analysis. The event analysis of the avalanche events in 1999 led to measures, which reduced the risk situation successfully, as it could be proved by the analysis after the avalanche events in 2018 (Bründl et al., 2019). The event analysis of the large flood events of 2005 led to a whole bundle of measures especially related to the optimization of the warning and altering system in Switzerland, the one of 2007 to an improved regulation procedure of the Lake of Biel.

## **Convincing information within the risk dialogue**

The risk dialogue is important for the success of the integrated risk management. Risk awareness is crucial for the acceptance and enforceability of measures and for a risk adapted behaviour of the population. Often it was observed that the past natural events are forgotten after one generation at the latest. Only by showing inventory data, documentation and photographs, people may be convinced that events had already occurred in the past.

## **New developments**

### **New web-GIS application StorMe 3.0**

After about 20 years of experience, a working group consisting of representatives of different cantons, the federation and other stakeholders examined, whether the data collected so far were adequate and useful for the objectives described above. The basic structure and content of the data collected was attested to be useful. Some attributes, however, will be neglected in the future because of their low added value. Some essential features or structures were missing in the past: 1. the spatial differentiated and clearly delineated description of the events using GIS-data, 2. the attachment of photographs, and 3. the attachment of supplementary or complementary documents.

These deficiencies are overcome by the completely new web GIS database application StorMe 3.0, which is operational since 2019 (for more information see BAFU, 2020b). Besides this, not only the cantons, but also the Federal Roads Office and the Swiss Federal Railways will now use StorMe for the recording of events, thus improving the collaboration between the different stakeholders. Additionally, this application serves as a national platform making accessible basically all available information about natural events in the past by integrating data or establishing interfaces to the other nation-wide databases, namely the ones already mentioned above: avalanche database of SLF,

Unwetterschadendatenbank and hillslope debris database of WSL, Euro-Climhist, as well as two glacier related research databases. Reading access can be granted by the cantonal or federal responsible persons. Furthermore, thanks to new legislation about geoinformation, enacted in 2007/08, the cantonal data itself, which are originally recorded in StorMe, will be publicly available as WMS and download on the intercantonal geodata infrastructure (geodienste.ch).

Additional features of the new application data are the recording in the field using a tablet, and an optional first notification application. The latter will allow the responsible persons in the communes, but also the public, to easily record their observations in the field during an event (fig. 1). On an open access website, a short description of an event including some photos directly taken by a mobile phone can be uploaded. An e-mail is automatically sent to the StorMe responsible persons. This information will be evaluated in terms of its relevance for StorMe. In the easiest case, the information can simply be integrated as it is into a StorMe database. In the regular case, someone will be mandated to undertake an additional field survey. As a side effect, the first notification can also be used for triggering immediate intervention measures.

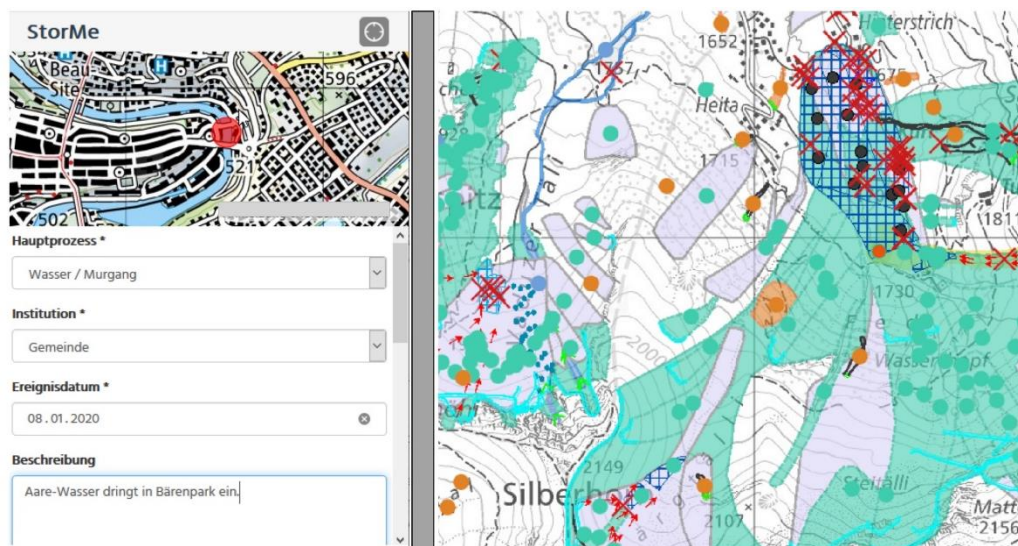


**Figure 1. Fig. 1: Examples of the recording of natural events in StorMe 3.0 illustrating the different levels of complexity.**

**Left: first notification recorded by a responsible person of the city; only one single point is set, followed by a very short description. Right: ensemble of different StorMe objects; the various signatures show the numerous possibilities of differentiated recording.**

The structure of a recorded StorMe event, a so-called StorMe object, is very flexible with respect to the degree of detail both in terms of geometry and attributes. Therefore, the different user needs and the importance and complexity of an event can be considered. A valid StorMe object can consist just of a single location point, the date and type of the natural process. On the other hand, a very complex event can be described by several distinct and distributed process areas enriched with numerous attributes describing the physical properties of the process, meteorological information, lots of cartographic

elements (named “observations”), photographs, geofotos, documents, videos, and geographically distributed and detailed information about damages. As different process types can be united within a single StorMe object, process chains can also be represented. Examples of the geographic representation of different StorMe events recorded in high detail are shown in fig. 1.

In addition to this, several single StorMe objects can be combined to “collective events” on a cantonal level, indicating the same hydro-meteorological origin and containing collective information for all of the related StorMe objects, such as an event analysis, radar pictures and others. This allows also to categorize and to find large events within the huge amount of small StorMe events. Similarly, “collective events” can be aggregated to so-called “large events”.

## **The federal Rapid Mapping service: fast acquisition and provision of geodata**

New technological developments in the field of remote sensing led to new collaboration practice and products of event documentation in case of events with a large extent. This information will also be a future data source for the event inventory.

The earliest possible recording of large natural disasters is very important for event documentation. That is why the federal service Rapid Mapping was established. It collects and provides geodata such as aerial or satellite imagery for event management and documentation following natural disasters.

In case of large-scale or nationally significant events, the Federal Office for the Environment (FOEN), together with the National Emergency Operations Centre (NEOC), coordinates the requirements of federal offices and cantonal agencies as well as any other stakeholders. The Federal Office of Topography swisstopo acquires the required image data and makes the processed data available as Rapid Mapping products. In addition to the newly recorded (post-disaster) data, swisstopo also provides the periodically updated basic geodata (pre-disaster) as a basis for comparison. The data is made available via the Federal Spatial Data Infrastructure (FSDI). The products can be viewed publicly and freely on its map viewer [map.geo.admin.ch](http://map.geo.admin.ch) (pre- and post-disaster data), making it easy for even inexperienced geodata users to visualize and compare the situation before and after the event.

Rapid Mapping offers a range of so-called basic products. This comprises digital image data from various acquisition platforms (e.g. satellites, aeroplanes or helicopters) and sensors, the choice of which is made according to the request and availability. The subsequent image interpretation is carried out by natural hazard specialists. The following basic products are defined:

- Single images (oblique or vertical): quickly available, minimal geolocation.  
Main purpose: general overview
- Quick Orthophoto: quickly available, loss in accuracy and aesthetics.  
Main purpose: event management

- Orthophoto: fully processed orthophoto, time-consuming to produce.  
Main purpose: event documentation

Rapid Mapping produces single images and orthophotos in the required quality. A tight timeframe and unfavourable weather conditions can additionally influence the quality of the images.

## Conclusion

The long tradition of the documentation of natural events in Switzerland proved to be a treasure on which we can be grateful to our ancestors. These data have a remaining value for the future, especially for hazard assessment, process understanding and risk communication. Some effort has still to be made in order to make full use of the entire value of the data. Future open access to the data and technological developments in geoinformatics will support this process. The new structure of the StorMe database and the new guidelines will increase the data quality in the future. Data gathering after the occurrence of natural events will however remain a persistent task for the future in order to collect the necessary information needed for the integrated management of risks.

## References

- BAFU (Hrsg.) (2016). Schutz vor Massenbewegungsgefahren. Vollzugshilfe für das Gefahrenmanagement von Rutschungen, Steinschlag und Hangmuren. Bundesamt für Umwelt, Bern. Umwelt-Vollzug Nr. 1608: 98 p.
- BAFU (2020a). Erfassungsrichtlinien StorMe 3.0, Bern. (available at: [www.bafu.admin.ch/storme](http://www.bafu.admin.ch/storme))
- BAFU (2020b). Naturereigniskataster StorMe (website). [www.bafu.admin.ch/storme](http://www.bafu.admin.ch/storme).
- Bezzola G.R., Hegg C. (Ed.) (2008): Ereignisanalyse Hochwasser 2005, Teil 2 – Analyse von Prozessen, Massnahmen und Gefahrengrundlagen. Bundesamt für Umwelt BAFU, Eidgenössische Forschungsanstalt WSL. Umwelt-Wissen Nr. 0825: 429 p.
- Bründl M. et al., Hafner E., Bebi P., Bühler Y., Margreth S., Marty C., Schaer M., Stoffel L., Techel F., Winkler K., Zweifel B., Schweizer J. (2019). Ereignisanalyse Lawinensituation im Januar 2018. WSL Berichte, 76: 162 p.
- Hübl J., Kienholz H., Loipersberger A. (2002). DOMODIS – Documentation of Mountain Disasters, State of Discussion in the European Mountain Areas. Interpraevent, Klagenfurt.
- Scherrer S., Frauchiger R., Naef D., Schelble G (2011). Historische Hochwasser: Weshalb der Blick zurück ein Fortschritt bei Hochwasserabschätzungen ist. Wasser Energie Luft, 103. Jahrgang, 11: 7-13.

---

# Third correction of the Rhône River in Switzerland: physical and numerical modelling of the “Martigny bend” priority measure

Jean-Noël Saugy<sup>1</sup>, Azin Amini<sup>2</sup>, Giovanni De Cesare<sup>2</sup>, Stéphanie André<sup>3</sup>, Pierre Bourqui<sup>3</sup>, Khalid Essyad<sup>4</sup>, Irene Samora<sup>4</sup>, Tony Arborino<sup>5</sup>

**Keywords:** flood; study case; numerical model; physical model; Rhone river

## Abstract

The Rhône River, second largest in Switzerland, has already been corrected twice (1863-1893; 1930-1960) to ensure safety and economic development in the Rhône valley. However, in October 2000, the highest flood of the century occurred showing the limitations of the two first corrections and the need for a third one. The Rhône bend, located near the city of Martigny, is a priority project because of the high damage potential. Given the complexity of the hydraulic and morphological phenomena, physical and numerical modelling are used to validate and optimize the project design. To obtain the best results, the two models must be used together and the results cross-compared. Hence, they are checked and adjusted in parallel. The first tests, which were purely hydraulic, showed a good agreement between them. The extreme flood succeeded to pass through the enlarged cross-section with an acceptable water level. After these encouraging results, the morphodynamic tests are ongoing.

## Introduction

Floods represent a major risk for the Rhône valley (Switzerland) despite two former corrections. The dikes are tall, old and fragile. In case of overflow or dike failure, the plain located 4 m below the dike level will be flooded. In certain parts, the water level can rise up to 2 m (figure 1).

---

<sup>1</sup> Project Engineer, Platform of Hydraulic Constructions, Ecole Polytechnique Federale de Lausanne Faculte Environnement Naturel Architectural et Construit, EPFL ENAC IIC Platform of Hydraulic Constructions GC A3 504 (Bâtiment GC) Station 18, Lausanne, Switzerland (jean-noel.saugy@epfl.ch).

<sup>2</sup> Platform of Hydraulic Constructions EPFL

<sup>3</sup> Stucky Ltd, Switzerland

<sup>4</sup> BG Consulting Engineers Ltd, Switzerland

<sup>5</sup> Service de la protection contre les crues du Rhône, Canton du Valais



**Figure 1. Saillon village during the flood of October 2000 (source: [www.vs.ch](http://www.vs.ch)), flood return time period slightly less than 100 years.**

The 3<sup>rd</sup> correction of the Rhône River is the largest flood protection project in Switzerland so far. Covering a length of 162 km, it aims to protect 100,000 people and prevent flood damages, which could rise up to 20 billion francs per event. The target includes the increase of protection against floods in the valley while ensuring sustainable conditions for the Rhône River ecosystem by making it more natural. This project is expected to span over several decades.

Due to the high flood hazard risk and related potential damages, the correction of the "Martigny bend" has been defined as a priority measure (Canton of Valais, 2016). The concept combines widening of the bed, lowering the bottom, the construction of a ramp and bank protections over a length of 4.5 km. It also includes the revitalization of drainage channels and of the mouths of two main tributaries (the Dranse and the Trient Rivers).

The complexity of the section justifies the development of physical and numerical models. This involves the building, setting up and calibration of instruments as well as some key parameters. The models are also used to simulate bedload transport. Despite a separated design, the interoperability of these two models is key to create a powerful tool for observing and understanding the future behaviour and development of the river.

## Data

Near the city of Martigny (canton of Valais), the Rhône River bends sharply on the North-North West. This section is commonly termed the Rhône bend (Figure 2). The limits of the Martigny bend priority measure are set between kilometre 35 and km 39.5. The physical

model is shorter and thus does not include the complete river reach, unlike the numerical one.



**Figure 2. Limits of the different models. In red: the 2D numerical model In yellow: the physical model**

The canton of Valais is the project client of the Platform of Hydraulic Constructions (PL-LCH) of the Ecole Polytechnique Fédérale de Lausanne (EPFL) but also the project owner of the 3<sup>rd</sup> Rhône correction. The models are built upon the design and project drawings from the Groupement Coude du Rhône (GCR). Stucky Ltd and BG Consulting Engineers Ltd ensure the supervision of the modelling procedure for the GCR. The hydraulic and granulometric data come from NIPO Ltd, HZP Ltd and iDEALP Ltd (table 1). These are the only field measurements that have been made and on which the model development can be based. Moreover, they determine the boundary conditions and a roughness range for specific reaches. However, the numerical model, once validated, gives the downstream conditions of the shorter physical model.

**Table 1. Scale factors.**

Physical parameter		Scale ratio	Scale factor
Length Pressure	[m] [m water column]	$\frac{L_p}{L_m} = \frac{P_p}{P_m} = \lambda$	52
Velocity Time	[m/s] [s]	$\frac{V_p}{V_m} = \frac{t_p}{t_m} = \lambda^{1/2}$	7.2
Discharge	[m <sup>3</sup> /s]	$\frac{Q_p}{Q_m} = \lambda^{5/2}$	19'499

## Methods

In order to optimize the hydraulic design in the phases of the project work and execution, as well as having a better understanding of the future hydraulic and morphodynamic behaviour of the Rhône and the confluences, the following parameters have to be assessed during the simulations:

- Hydraulics: water level, energy losses and shear stress on the riverbanks and the widened bed.
- Bedload transport: sediment transport, estimation of the bedload regime in the widened riverbed and the sediment supply from the Dranse River.
- Morphology: variety of morphology, dynamics of the confluences and widened areas.

The physical model is located in Martigny in an industrial hall of 1'500 m<sup>2</sup> (figure 3). A physical model is an excellent means to communicate to the affected people and other stakeholders concerned by the 3<sup>rd</sup> correction. This explains the fact that the model was constructed close to the study site.



**Figure 3. Physical model of the Martigny bend.**

Once the hall was chosen, the drawings of the physical model were developed. The first parameter to be set was the scale factor depending on the available space in the hall and the river reach to model. The downscaling factor is 52 (table 2). The 2 km of the project zone, which is modelled physically, represents a length of about 38 m at the physical model scale.

**Table 2. Measurement instruments installed on the physical model.**

Physical variable	Instruments	Model scale precision	Prototype scale precision
Water level	23 ultrasonic probes	1 mm	5 cm
Bathymetry	Leica Scanstation P20	3mm	15 cm
Discharge	3 electromagnetic flow meter	1 - 2 % of max discharge	-
Velocity	Ultrasonic Velocity Profiler (UVP) Micro propeller current meter Particle Image Velocimetry (PIV)	1 mm/s 1 mm/s 1 cm/s	5 cm/s 5 cm/s 0.5 m/s
Solid discharge	Sediment feeders (sediment input) Downstream scale (sediment output)	10% 10%	- -

Besides the geometric scale factor, the model is based on the Froude similarity, meaning that the Froude number is the same at prototype and model scale. As a reminder, if a scaling factor is too large, viscosity and surface tension cannot be ignored. This point was considered during the elaboration of the model.

Based on the Froude similarity, the velocity factor corresponds to the square root of the scale factor, i.e. 7.21. By combining the scale factor with the velocity factor, the discharge factor is easily determined. It equals to 19'899 which means that the modelled flood discharge is about 20'000 less than the real discharge.

To ensure a similar behaviour of the scaled sediments with the prototype ones, a sensitivity analysis based on the Shields sediment transport similarity was conducted. Furthermore, the finest part of selected sands has been removed in order to prevent cohesion effects that would lead the model to be clogged.

Once built, the following measurement instruments were installed (table 3): 23 ultrasonic water level probes, a Leica ScanStation P20, 3 electromagnetic flow meters, 3 sediments feeders and a calibrated scale situated at the downstream boundary. Besides these instruments, temporary ones were also used like a micro propeller current meter, Particle Image Velocimetry (PIV) and Ultrasound Velocity Profiler (UVP).

**Table 3. Discharge and solid discharge data for the Rhône and the Dranse Rivers.**

Return time [year]	Discharge				Solid discharge			
	Rhône River		Dranse River		Rhône River		Dranse River	
	Prototype scale [m <sup>3</sup> /s]	Model scale [L/s]	Prototype scale [m <sup>3</sup> /s]	Model scale [L/s]	Prototype scale [kg/s]	Model scale [g/s]	Prototype scale [kg/s]	Model scale [g/s]
10	669	34.3	95	4.9	80	3.4	64	2.7
50	885	45.4	99	5.1	113	4.8	70	3.0
100	1'260	64.6	144	7.4	169	7.2	152	6.6
Extreme flood	1'600	82.1	204	10.5	220	9.3	310	13.4

As already mentioned, a 2D numerical model (figure 4) has been developed for the entire priority measure at prototype scale. Simulations are performed using BASEMENT software (BAsic Simulation EnvironMENT) of the ETHZ School, which allows to couple hydraulic equations with bedload transport equations over a mobile bed. Pre- and post-processing are performed using Aquaveo's Surface-water Modeling System (SMS) software. It is for instance on this software that the 2D mesh is built.

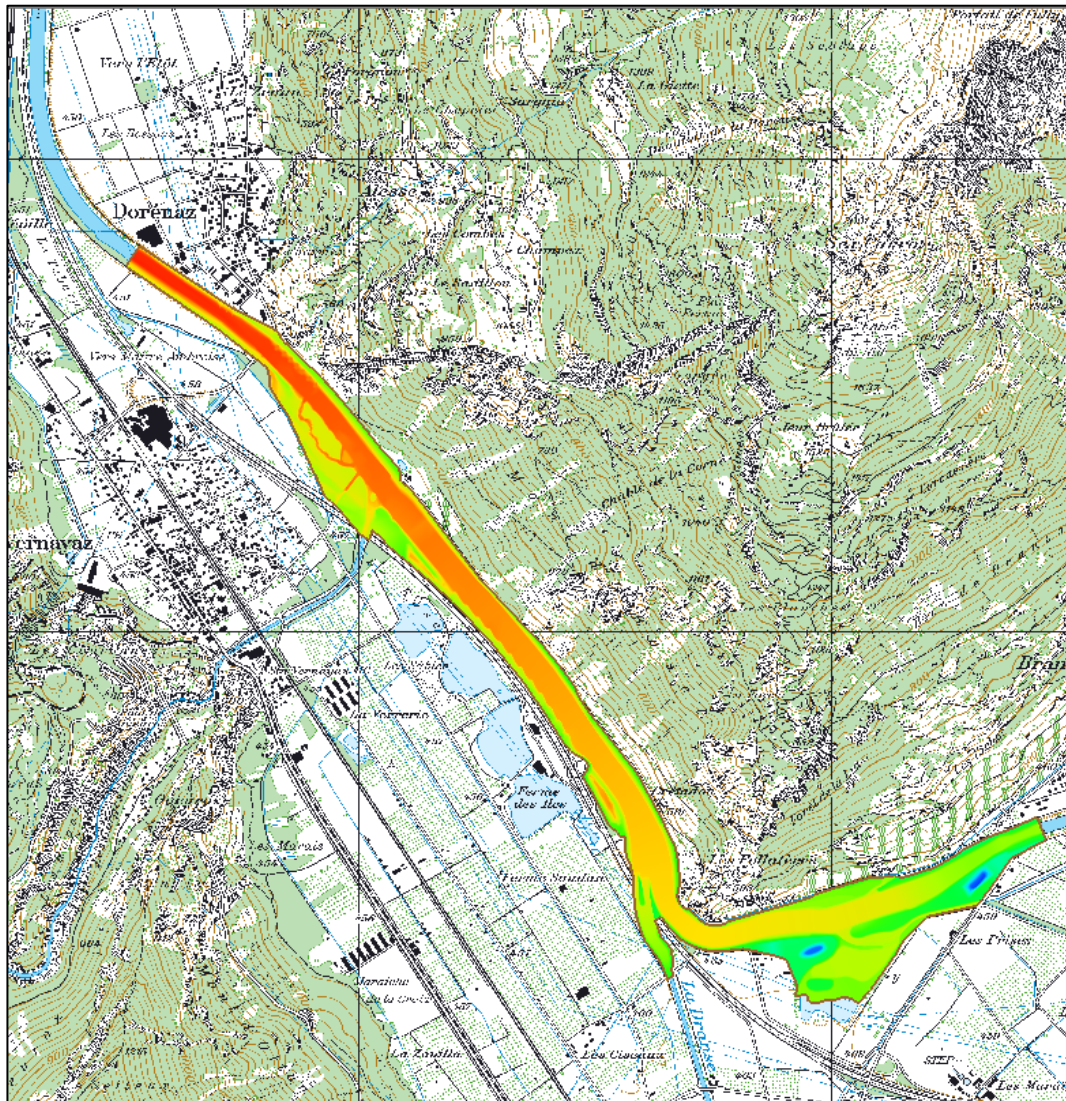


**Figure 4. Bathymetry and limits of the 2D numerical model. Initial topography of the numerical model.**

Building the 2D geometry is an important step. The mesh is irregular but keep the break lines. The cells density depends on the expected local phenomena. For every grid change, a sensitivity analysis consisting of one hydraulic simulation and one morphodynamic must be performed. After that, parameters like the bedload transport equation, the parameters of the gravitational transport or the presence of a pavement layer are set in order to get results corresponding to those of the physical model.

One of the goals is to ensure a synergy between the two models to create a reliable numerical tool, which can be used to simulate any modification of the project once the physical model is disassembled. At all times, the results are cross-compared. It enables each model to be validated, optimized or to highlight its limits using the other. In the last case, some adjustments can be made.

Another strength of this synergy is to extend the hydraulic results of the physical model with the ones of the numerical model (measurement point ratio: 23/15'000). However, this

ratio changes for the bathymetry. With more than 70 million points taken on the physical model with the Laser scan station, it easily outmatches the 15'000 grid nodes.

## Results and discussion

The first phase of the project is to adjust both models together using purely hydraulic, the so called clear water tests. The latter are also a means of controlling the preliminary design of 100-year and extreme flood events by water level and velocity profiles measurements. Therefore, these tests aim at assessing the hydraulic behaviour and ensure safety from future Rhône and Dranse floods. This phase allows observing and analysing hydraulic phenomena in specific sections with potential for optimization. The clear water phase also aims to compare the results with the preliminary design water lines resulting from the 1D HEC-RAS numerical model. The tests are carried out on a fixed bed without bed load supply. Roughness of the 2D numerical model is used as the main corrective factor to adjust to the physical one. The boundary sections are also subject to adjustments.

Before the advancement of the morphological tests involving mobile bed and bedload transport, the two models have been subjected to a significant geometric modification following a project variant. This implied repeating the hydraulic tests. Parallel to these changes, the Rhône and Dranse ramps have been optimized while the technical elements necessary for the morphological tests have been put in place.

After all these optimizations, the hydraulic results show good agreement between the two models. Including the results of 1D numerical model, the water surface elevations are similar (figure 5). These first results show also some limitations which will be considered later. For example, the 2D numerical model is not able to reproduce the secondary flow field, a 3D phenomenon, in the bend. As an improper result, higher velocities are observed inside the curve instead of outside. This limitation is well-known by the software engineers. The PL-LCH team has to find a solution for driving the flow in line with the results of the physical model. Another known limit of physical models at small scale is that they become too smooth. In this case, it affects the results from the upstream boundary of the Rhône River and the ramps. It is why the results of the probe N°1 are lower than the other models (figure 5).

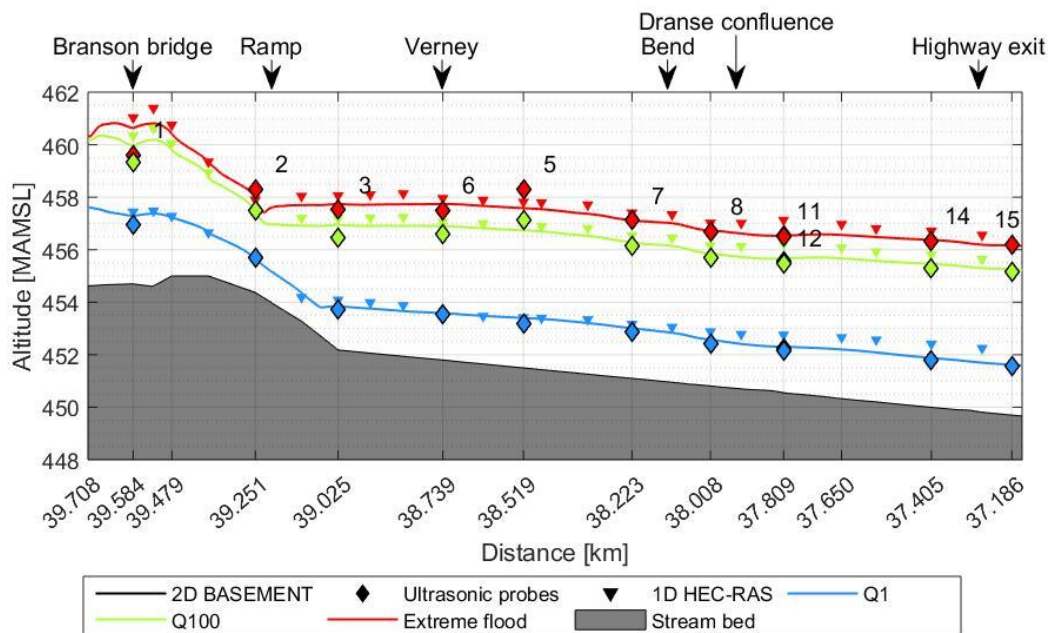


**Figure 5. WSE results between 3 models. Initial topography of the numerical model. Water surface elevation along the Rhone river for three different scenarios and models: 1D numerical model (HEC-RAS; values given by the engineering companies), 2D numerical model (BASEMENT) and the physical model (ultrasonic probes).**

Based on the valuable results of the first phase, the two models have been set up for the morphological tests. They can be divided into two different groups: the long tests and the short ones.

The aims of the long tests are to create a first river bed morphology, observing the erosion sectors and the deposits as well as checking the water surface elevations. Indeed, before these tests, morphologic data is unknown. Instead of simulating 10 times a 10-year morphogenic flood event, it was decided to test a steady state 10-year flood during several days. It means a steady discharge and a steady sediment supply until sediment equilibrium is reached. This method is reapplied for a 50-year flood. In order to simulate significant scenario and regardless of sediment equilibrium, short simulation times are set for a 100-year flood and an extreme one

There are two ways for checking the equilibrium of the sediment transfer in the physical model. The first one is by using the laser survey (figure 6) and the 23 ultrasonic probes. In a steady case, the bed and the water level do not change. The second way is to compare the overall sediment balance, associating the weighted output with the feeder input.

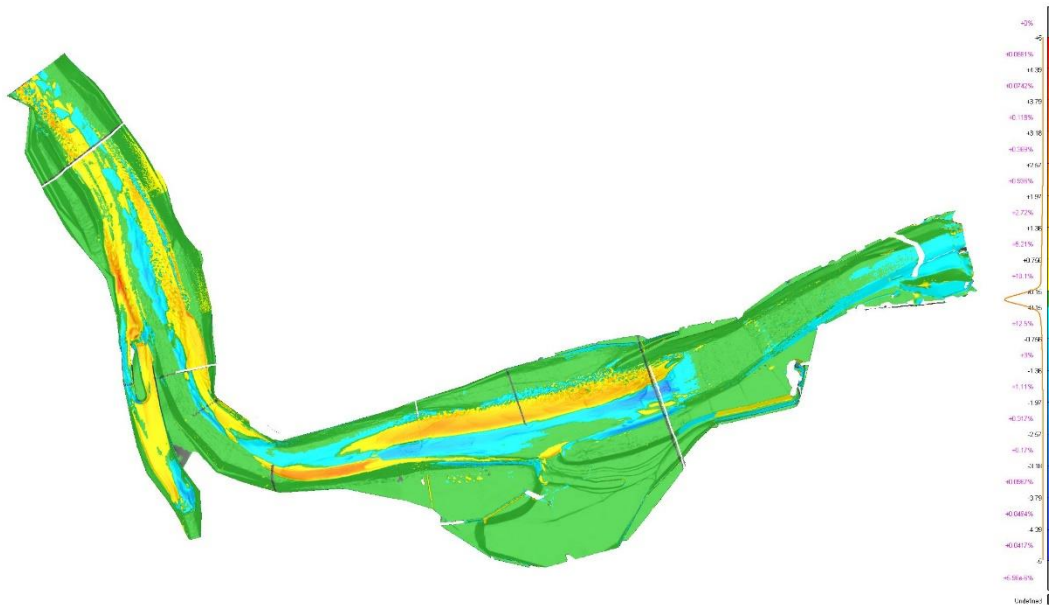


**Figure 6. Bathymetry evolution for a 100-year flood between  $t = 0$  day and  $t = 5.7$  days. Comparison between the Lidar scans taken before the 100 years flood test and after 5.7 days prototype**

The 10-year flood has been simulated for more than 50 days (prototype scale). The three next scenarios have already been simulated but only on the physical model. Indeed, even though the morphogenic simulations performs well on the numerical model and produce some valuable results, matching these two models is a long and complex task.

Short tests will be conducted after the long ones. They are based on some reference events like the October 2000 flood or on some specific scenarios, for example, testing the return flow from upstream controlled flooded areas or compartments back into the Rhône River (the residual risk or beyond the expected scenario).

## Conclusion

In conclusion, the modelling tools developed and optimised by the Platform of Hydraulic Constructions of EPFL have proven to give satisfactory results throughout the hydraulic phase. The extreme flood can pass safely through the Rhône River bend reducing considerably the potential damage cost. The morphological parameters (bed load transport, erosion and deposition) are currently being tested. Depending on these results, some protection measures can be reduced, increased, added or even removed. They will also serve optimising the initial excavation volumes, which may drastically reduce the project costs.

## References

Canton of Valais (2016), Development plan of the Rhône River, adopted in March 2016

---

# Groundwater recharge and discharge in the Åknes rockslide – constraining uncertainties for the development of a numerical groundwater flow model

Clara Sena<sup>1</sup>, Alvar Braathen<sup>1</sup>, José Acuna<sup>2</sup>, Frida Biørn-Hansen<sup>1</sup>, Stig Runar Ringstad<sup>1</sup>, Halvor Bruun<sup>1</sup>, Gustav Pless<sup>3</sup>, Mark Mulrooney<sup>1</sup>

**Keywords:** Rockslide; Groundwater recharge; Laminar and turbulent flow; interconnected fracture network; steep topography

## Abstract

In 2008, groundwater springs were reported in the Åknes rockslide at three main elevations; Lower, Middle and Upper Spring Horizons. The flow-rate and water chemistry of these springs were monitored in the Spring-Summer of 2018 and 2019. In addition, detailed structural geology mapping was done in the area above the backscarp to assess the groundwater recharge processes. Results indicate that groundwater recharge occurs indirectly through infiltration of surface runoff and subsurface flow produced above the backscarp, and directly through infiltration of precipitation and snowmelt from the backscarp to the toe zone. On the East side of the unstable slope, perched aquifers and surface runoff feed the ephemeral Eastern Stream. To the West and South, the discharge regime and water chemistry reveal a groundwater reservoir with an important storage capacity discharging at the bottom of the fastest moving rock mass (West part of the Middle Spring Horizon). An even larger reservoir feeds the Lower Spring Horizon, at the rockslide's toe zone.

## Introduction

Norwegian rock-slope failures have been studied systematically since the late 1990's, meeting public demands to address natural hazards for the local population. A comprehensive mapping program (step 1) and subsequent monitoring (step 2) of selected, hazardous slope-failures have been carried out by the Norwegian Water and Energy Directorate (NVE), the Geological Survey of Norway (NGU), institutes (NGI, Sintef), private engineering companies, and research undertaken at the universities of Tromsø, Trondheim and Oslo. The hydrogeology (step 3) of Åknes rock slide is being investigated, as a fundamental tool to support the design of water-intercepting structures to increase slope stability. This is the first site to be investigated in Norway for this purpose (Blikra, 2012), and will with time form the foundation for similar studies elsewhere. Here, we

---

<sup>1</sup> Department of Geosciences, University of Oslo (UiO), Oslo, Norway

<sup>2</sup> Department of Geoscience and Petroleum, NTNU, Trondheim, Norway

<sup>3</sup> Landslide Department, Norwegian Water and Energy Directorate (NVE)

present the results of the first two years of the NVE-UiO collaboration that aims to characterize and quantify the groundwater recharge, discharge and flow patterns, and ultimately develop a hydrogeological model of the Åknes rockslide.

Åknes rockslide is made of gneisses which were altered and reworked during the Caledonian Orogeny. These vary from granitic gneiss to biotite bearing granodioritic gneiss, and up to 20 cm-thick layers of biotite schistose gneiss. Sub-vertical joints occur predominantly in the granitic gneiss while undulating foliation surfaces, sub-parallel to the mountain slope, prevail in the biotite schistose gneiss. The unstable rock mass is bounded by an 800 m-long backscarp at 900 masl (meters above sea level); a NNW-SSE trending strike slip fault to the West; a fault dipping 35-45° west to the East; and, a toe zone at 120 masl (Figure 1), where the basal sliding surface daylights at the topographic surface (Ganerød et al., 2008 and references therein).

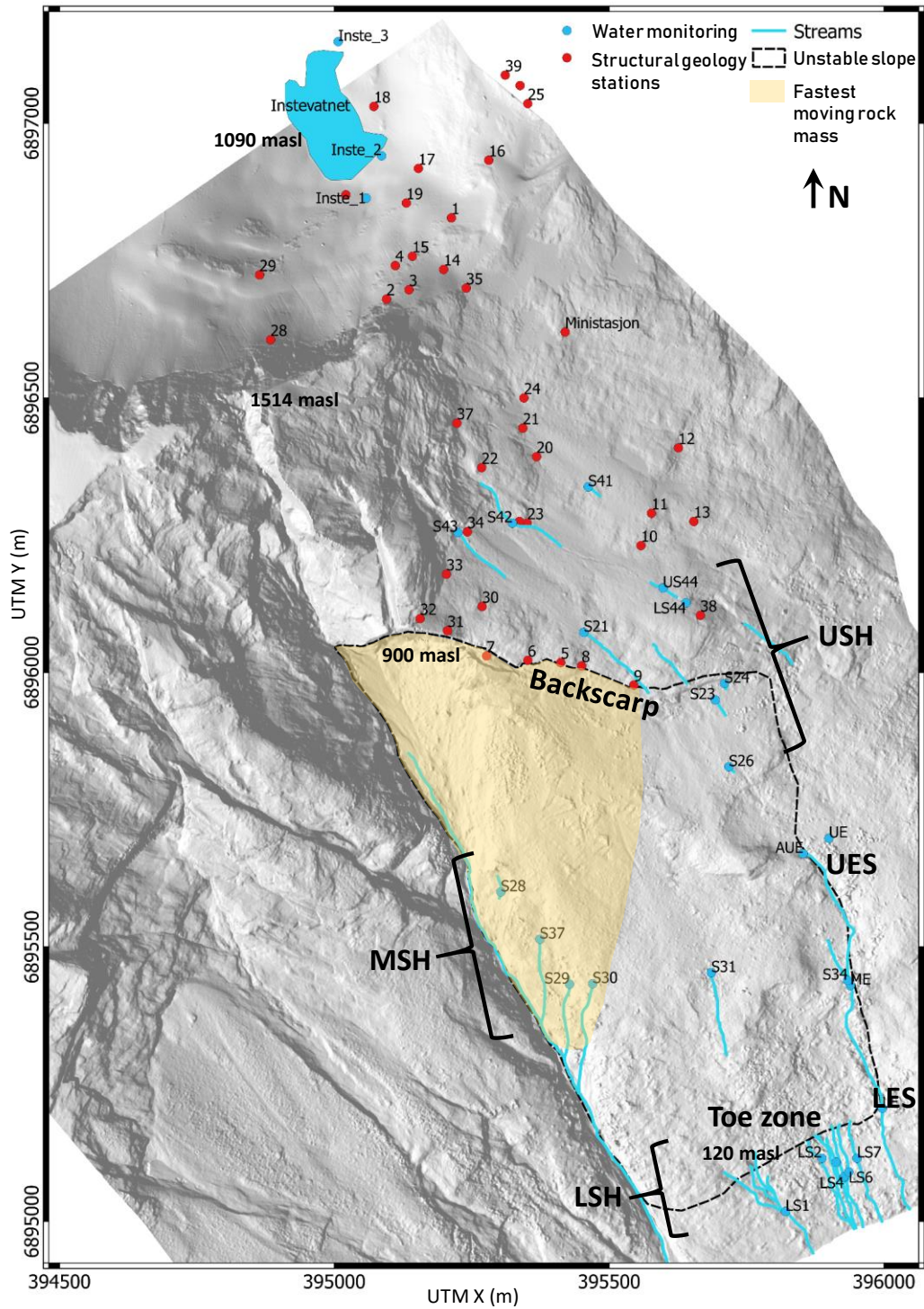


Figure 1. Location of the hydrogeology and structural geology monitoring points on a hillshade map. LSH, MSH & USH: Lower, Middle and Upper Spring Horizons; LES, UES: Lower and Upper Eastern Stream.

## Methods

Åknes rockslide, located in Storfjorden (Møre and Romsdal County), has been monitored since 1986. By 2004, NVE installed an automated monitoring system. Instrumentation includes extensometers, fixed station GPS, boreholes recording displacement, groundwater levels, microseismic activity, and a meteorological station. Groundwater springs were identified in the slope at different elevations (Frei, 2008): the Lower Spring Horizon (LSH, 100-120 masl); the Middle Spring Horizon (MSH, 360-460 masl); and the Upper Spring Horizon (USH, 640-840 masl). In addition, along the Eastern boundary there is a stream; the Eastern Stream (ES).

Monitoring of springs and streams (1) discharge (measured manually by converging the flowing water into a controlled volume); (2) physico-chemical parameters (pH; Electrical Conductivity, EC; temperature measured with portable HANNA probes); and, (3) dissolved inorganic components (analysed at the UiO laboratory) took place in the Spring-Summer of 2018 and 2019 (Biørn-Hansen, 2019). In addition, detailed structural geology mapping of the area above the backscarp was carried out in the Summer 2018 (Bruun, 2019; and Ringstad, 2019) (Figure 1), in conjunction with a drone photographic campaign and subsequent photogrammetric model design.

## Results and discussion

### Groundwater flow

The groundwater peak velocities attained in Frei (2008), 17.4 m/h, are clearly higher than the values typically observed in fully water-saturated fractured or porous media with laminar flow. The groundwater flow in Åknes is therefore laminar to turbulent, partially occurring along perched aquifers above the local water table. Contributing to this high-velocity groundwater flow regime are:

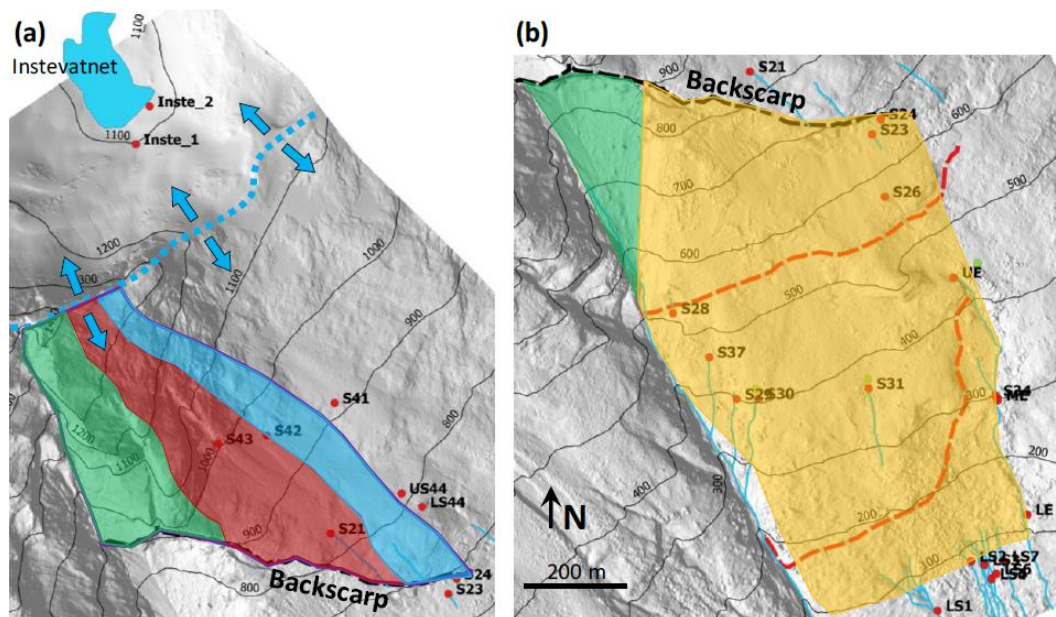
- a) the permeable structures of the rock mass: slope cover (soil and rock debris), steep fractures interconnected to slope-subparallel undulating fracture corridors in biotite-rich and feldspar-rich gneiss, and crushed rock membranes (i.e. layers along shear fractures or sliding surfaces that are formed by crushing of the host rock); and,
- b) the high steepness of the topographic slope (30-40°).

Since the slope-subparallel undulating fracture corridors dip less than the topographic slope, hosting a dense fracture network, groundwater seepage is observed from these fractures where they daylight in outcrops, namely in the Lower Spring Horizon and the West area of the Middle Spring Horizon.

### Groundwater recharge

From the surface water divide to the backscarp, the scarcity and tightness of the fractures indicate that precipitation and snowmelt lead primarily to evapotranspiration and surface runoff (Biørn-Hansen, 2019) (Figure 2a). Nonetheless, the occurrence of ephemeral springs

(Upper Spring Horizon and the streams S41 to S43, Figure 1) indicates that there is a shallow and thin aquifer between the surface water divide and the backscarp. Here, the main permeable structures are: (i) the exfoliation, hosting a small aquifer with high groundwater velocity (corresponding to subsurface flow); (ii) regional fracture corridors with low groundwater velocity; and, (iii) the background fracture system with a very low groundwater velocity.



Groundwater recharge processes (modified after Biørn-Hansen, 2019):

- Surface runoff that feeds surface runoff in the Western Gully (no groundwater recharge)
- Surface runoff that feeds focused infiltration in the backscarp (graben and open cracks)
- Surface runoff that bypasses the backscarp cliff infiltrating diffusely further downstream
- Direct infiltration of rain and snowmelt

**Figure 2. Identification of groundwater recharge processes (a) above, and (b) below the backscarp. Blue arrows and dashed line indicate surface water divide. Elevation contours in black, and hydrogeology monitoring points in red.**

On the opposite side of the surface water divide, the Instevatnet lake stands at a higher elevation than the unstable slope (Figure 1). The similar aspect of the fractures around Instevatnet indicates that this is most likely hydraulically disconnected from the unstable slope (Biørn-Hansen, 2019; Bruun 2019; and Ringstad, 2019).

Groundwater recharge in the unstable slope is derived primarily from precipitation and snowmelt. It occurs indirectly through focused infiltration of surface runoff and subsurface flow in the open section of the backscarp (bottom of red area in Figure 2a), and through dispersed infiltration below the closed section of the backscarp, in the upper NE part of the unstable slope (below the blue area in Figure 2a). Direct groundwater recharge between the backscarp and the toe zone occurs through infiltration of precipitation and snowmelt (yellow area in Figure 2b).

The fraction of the slope highlighted in green in Figure 2 indicates the areas where precipitation and snowmelt lead solely to surface runoff and evapotranspiration, meaning that no groundwater recharge occurs in this part of the slope.

Estimates of potential evapotranspiration in the area above the backscarp, indicate that on average 88% of precipitation and snowmelt occurring in the red and blue areas in Figure 2a produce surface runoff and subsurface flow that infiltrates in and below the backscarp, leading to groundwater recharge in the unstable slope (Biørn-Hansen, 2019). This corresponds to 1197 mm/year, for the normal period 1960-1990. Estimates of groundwater recharge below the backscarp are being conducted now. Preliminary results indicate that for the whole unstable slope (0.580 km<sup>2</sup>), focused infiltration of surface runoff in the backscarp may represent 38 to 53% of the total groundwater recharge. If only the fastest moving rock mass is considered (0.217 km<sup>2</sup>, Figure 1), focused infiltration of surface runoff in the backscarp may represent up to 80% of the groundwater recharge to this area.

### **Groundwater discharge and chemistry**

In all the field-campaigns of the Spring-Summer 2018, the flow-rate of the springs increases going downslope; with an average of 0.8 l/s in the USH, 1.3 l/s in the MSH, and 4.7 l/s in the LSH (Figure 3). This agrees with the findings by Ganerød et al. (2008) and Frei (2008). During these field-campaigns, the lowest flow-rates were registered in the beginning of June and mid-July 2018 which were extremely hot and dry. The MSH and LSH had measurable groundwater discharge (0.4 and 3.4 l/s, respectively) while the UES was almost dry (flow-rate too low to measure). This indicates the presence of a groundwater reservoir with an important storage capacity feeding the MSH and LSH, while the USH and Easter Stream are ephemeral. The highest flow-rates were registered in September 2018 which was characterized by intense rainfall events.

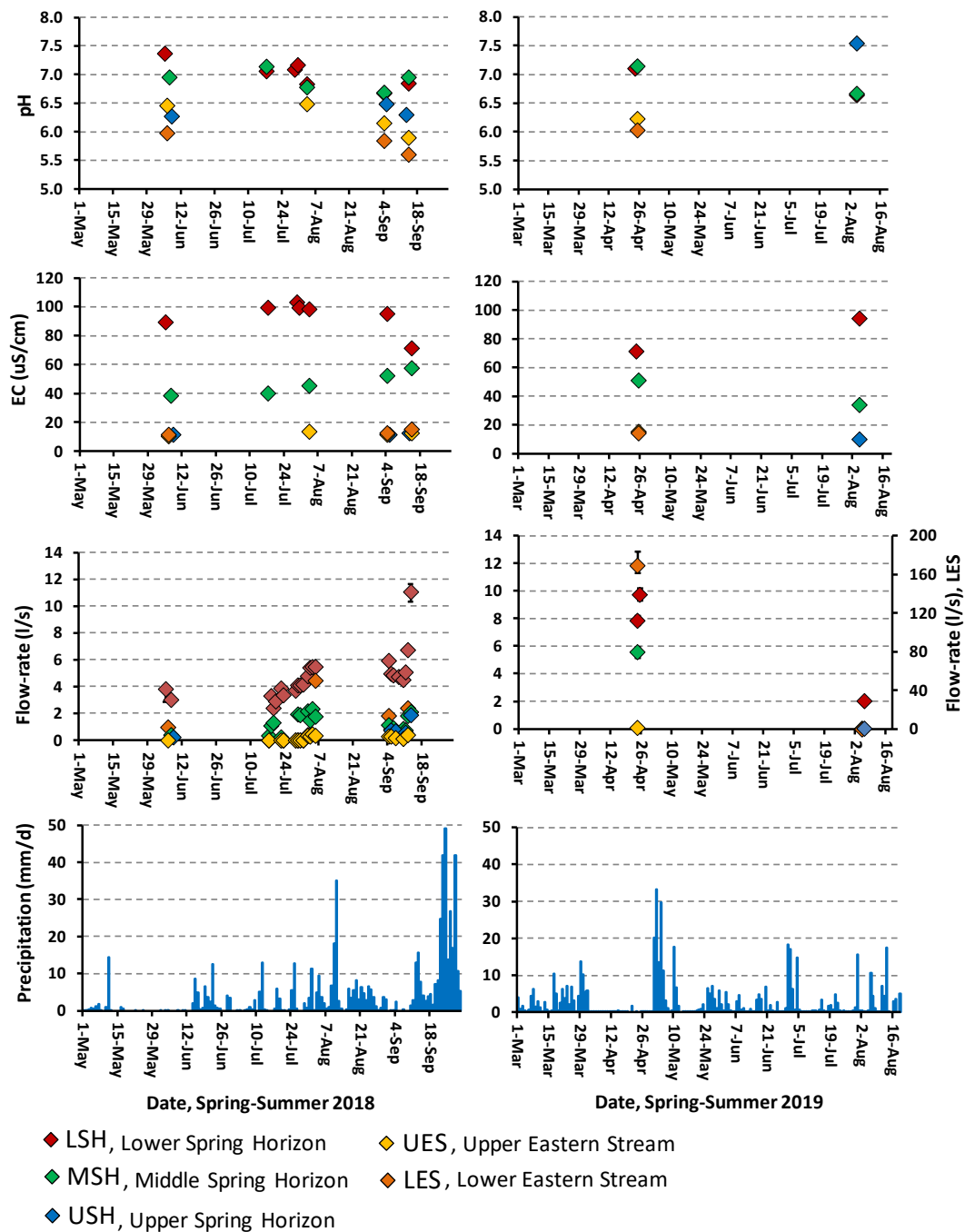


Figure 3. pH, EC and flow-rate of the springs and streams in Åknes, in the Spring-Summer of 2018 and 2019. Daily precipitation in blue bars, at the bottom.

At the beginning of the Spring-Summer 2019, the flow-rate at the Lower Eastern Stream (LES) was extremely high (170 l/s) reflecting the considerable amount of surface runoff collected in the Eastern Stream due to the snowmelt occurring in April 2019. Snowmelt in groundwater is also evidenced by the lowest EC value registered at the LSH in this month. In August 2019, the Lower Eastern Stream was dry, reflecting its strong dependency on precipitation and snowmelt (Figure 3).

pH varies from circum-neutral at the Lower Spring Horizon (7.4) to more acidic in the Upper Spring Horizon and Lower Eastern Stream (6.3 and 5.6, respectively). More acidic groundwater, i.e. closer to rainwater pH (5.8, on 11/09/2018), is characteristic of a short residence time, while circum-neutral pH in a granitic-gneissic setting reveals dissolution of feldspar by the naturally occurring carbonic acid in the infiltrating rainwater and snowmelt. As higher the residence time of the groundwater in the rock-slope, higher the content of dissolved solids, and therefore, higher is the Electrical Conductivity (EC). This is clearly seen by the higher EC values recorded in the LSH and MSH throughout the sampling campaigns, and agrees with the findings by Ganerød et al. (2008), and Frei (2008).

## Conclusions and future work

The groundwater flow in Åknes is laminar to turbulent, partially occurring along perched aquifers above the local water table. The turbulent flow regime is controlled by the occurrence of wide underground openings, a connected fracture network, and a steep topographic slope. Perched aquifers occur mainly in the Eastern side of the unstable slope where the ephemeral Eastern Stream occurs. Important obstacles to the groundwater flow occur to the West and South.

Groundwater recharge occurs indirectly through focused infiltration of surface runoff and subsurface flow in and below the backscarp, and directly through infiltration of precipitation and snowmelt in the area below the backscarp. Preliminary calculations indicate that the surface runoff infiltrating in the backscarp is a major source of groundwater recharge to the fastest moving rock mass.

Groundwater discharge occurs at three main spring horizons; Lower, Middle and Upper. The discharge regime and water chemistry reveal a groundwater reservoir with an important storage capacity (therefore, longer residence time) discharging at the bottom of the fastest moving rock mass (West part of the Middle Spring Horizon). An even larger groundwater reservoir feeds the Lower Spring Horizon, at the rockslide's toe zone.

The recently installed multi-level borehole in Åknes (October 2018) indicates a clear and significant stratification of the groundwater flow, with an increase in water pressure at 100 m depth. Future work will focus on this, other borehole data and meteorological data to further constrain the boundary conditions and hydrogeological parameterization of the groundwater flow model at Åknes.

## References

- Biørn-Hansen, F. (2019). The Hydrogeochemistry and Water Balance of Åknes Rock Slope. Master thesis. University of Oslo.
- Blikra, L. (2012). Evaluering av drenering som risikoreduserende tiltak ved Åknes. Åknes/Tafjord Beredskap, Energikonsernet Tafjord, (893).
- Bruun, H. (2019). An analysis of bedrock fracture networks based on outcrop data to establish a baseline discrete fracture network model – Åknes rockslope in western Norway. Master thesis. University of Oslo.

Frei, C. (2008) Groundwater Flow at the Åknes Rockslide Site (Norway) Results of a Multi-Tracer Test. MSc thesis, ETH Zurich, Switzerland

Ganerød, G., Grøneng, G., Steinar, J., Dalsegg, E., Elvebakk, H., Tønnesen, J., Eiken, T., Blikra, L., Braathen, A. (2008). Geological model of the Åknes rockslide, western Norway. *Engineering Geology*, 102(1–2), 1–18.

Ringstad, S.R. (2019). The influence of structural discontinuities on the stability of the Åknes rockslide. Master thesis. University of Oslo.

---

# Examination of shape efficacy of steel pipe open sabo dam according to Impulsive Load of Debris Flow

Osamu Shimakawa<sup>1</sup>, Toshiyuki Horiguchi<sup>2</sup>, Yoshiharu Komatsu<sup>3</sup>, Satoshi Katsuki<sup>4</sup>

**Keywords:** bouldery debris flow, open sabo dam, impulsive load, discrete element method

## Abstract

A steel pipe open sabo dam have mainly been constructed in debris flow section since 1990s. Recently, the geology hit torrential rain happen to the unexpected debris flow, and the evaluation method of impact load is required against the open sabo dam. The shape of an open sabo dam is normally more complicated than a closed sabo dam, and it is difficult to predict the bearing capacity performance. We have already conducted the preliminary experiment to evaluate the impulsive load of debris flow, and the load that the open sabo dam received is decreased due to front inclination angle that represent the shape of a dam. However, the load reduction effect is uncertain. The study reproduced load time relation using discrete element method, and investigated the mechanism of the load reduction effect. Therefore, the ‘dead zone’ that mean the ceased gravel zone was spread due to the front inclination angle after gravel collide with the dam, and it was found to decrease the impact load that the subsequent gravels possessed.

## Introduction

Although the latest statistics indicate a decrease in the number of victims of natural disasters in Japan, the number of debris flow or sediment disasters has increased. Especially, the bouldery debris flow has a large impact force. In Japan, human settlement is close to mountainous area, and the conservation region is instantly reached from debris flow prone torrent. Also, a torrential rain is increasing due to abnormal climate, and then, debris flow disasters are likely to occur. In especially, bouldery debris flow is directly hit the human settlement. Therefore, concerning the impulsive load, it is necessary to construct sabo works. Anyway, the steel pipe open sabo dam (hereafter, open sabo dam) is basically built in current design (NILIM, 2016). Recently, the measurement of open sabo dam is incredible because of an increasing tendency of woody debris (Mizuyama, 2008). The

---

<sup>1</sup> Master, National Defense Academy

<sup>2</sup> Ph.D, Associate Professor, Civil Engineering, National Defense Academy, 1-10-20 Hashirimizu, Yokosuka, Kanagawa, Japan (debrissegregation@gmail.com)

<sup>3</sup> Master, National Defense Academy

<sup>4</sup> Professor, National Defense Academy

feature of an open sabo dam always control routine sediment transport and have a large trapping capacity of debris flow, and the sediment normally pass through in concerning of environment. When generating debris flow, the dam entrap the front part of debris flow, and successively block subsequent sediment flow due to closed spacing intervals (Mizuyama. 2008). Because the trapping capacity of open sabo dam is always vacant, it is not necessary to remove the sediment or gravel. Therefore, it is assumed that debris flow directly collide with the steel pipe.

There are lots of research of impulsive load or debris flow fluid force (Ishikawa et al. 2018). The impulsive load of debris flow is classified as compressive fluids and incompressive fluid. The phenomenology is organized, and the equation of debris flow fluid force was proposed based on the concept, and the safety factor is calibrated on basis of a lot of empirical data, and Japanese design is compiled. We focused on interaction between the shape characteristic of open Sabo dam and the impulsive load of debris flow. It was examined to reduce impulsive load of debris flow due to the front inclination angle of open Sabo dam experimentally. It was thought that the load by friction with the gravel that crashed into the dam thought experimental efforts but, quantitatively verified research has not been conducted and the reduction effect of the load is unclear. In addition, it is suggested that the load is reduced by the influence of the sediment which slowed down and stopped after the flexible facilities entrapped sediment or gravels. (Song et al., 2019) The effect is obtained also in the open Sabo dam about this reduction effect (dead zone), and it is necessary to elucidate it analytically (Horiguchi et al., 2018). The study reproduces load-time relation using discrete element method, and the efforts investigate the mechanism of the load reduction effect. We examine about the effect of dead zone formed by front inclination angle.

## Outline of Experiment

The experimental cases include five repetition for each dam model. Globally, experiment measures the impulsive load of debris flow for four kinds of Sabo dam model. Each sabo dam changes the front inclination angle ( $\theta_{LS}$ ). The channel slope, as shown in **Fig.1a**. The gravel model and sabo dam model are placed in the slope. The sabo dam models are show in **Fig.1b,c**. Also, the experiment fixed at gradient of  $11.3^\circ$ . The used material includes 3 kinds of gravel size that is 10, 20, 30 mm, respectively, for a total weight of 35 kg for each and a discharge of  $0.06 \text{ m}^3$ . It was observed the maximum impact load decreases as the front inclination angle increases. In the results, the impact load of debris flow is reduced 30 % by the front inclination angle of the dam model. In addition, the impact load is reduced utilizing the front inclination angle of the sabo dam (Horiguchi et al., 2018).

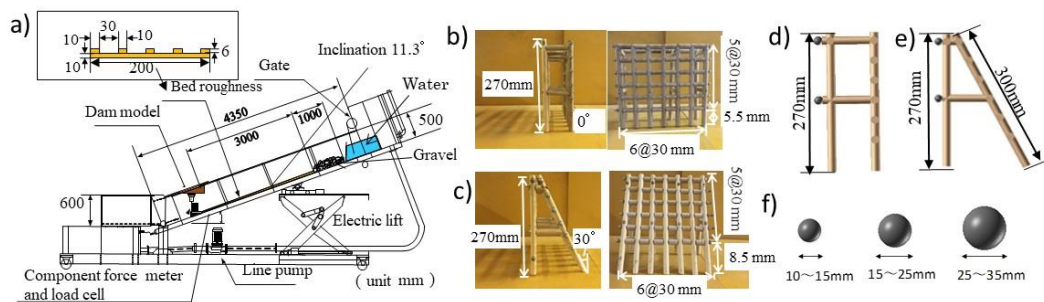


**Figure 1. Outline of channel flume and analysis model; a) channel flume, b) Lateral view of the sabo dam having a front inclination angle is 0 degree, c) The front inclination angle is 30 degrees, d),e) Each analysis model, f) gravel modelled by DEM form 10 to 35mm**

## The applied DEM ANALYSIS: Model Description

In this study, the numerical simulation analyzes the reduction effect mechanisms of the front inclination angle in two cases ( $\theta_{LS} = 0^\circ, 30^\circ$ ). The initial water depth is 0.15 m, and debris flow velocity is 2.0 m/s referred to experimental movie, and water was poured from the rear side of gravel, and the debris flow was generated. **Fig. 1d, e** describe each open sabo dam model and gravel model. The  $\theta_{LS} = 0^\circ, 30^\circ$  dam models are made by combining cylindrical elements. The gravel model use a spherical model (**Fig.1f**). The diameter size of the spherical element based on grain size distribution of experiment, and the gravel size utilizes a random number, is fit total weight of 35 kg. It is confirmed that the gravel size distribution in experiments and analysis is the same. The channel model constitute six plane elements. The front shape of the sabo model arrange 7 cylindrical elements at equal intervals of 30 mm along vertical member. Herein, each front inclination angle have different length of front shape. This almost gives the same dimensions as the shape of the experiment. In addition, initial position of gravels is randomly arranged 3.0 m of upstream from the dam model. The arrangement method is drop method as experiment condition. The debris flow model is reproduced to flow from backside of accumulation gravel using water flow distribution model (Horiguchi et al., 2017). The numerical simulation computes contact force obtained from permanent connect spring between the dam model and spherical elements, and the obtained value is determined as load-time relation. This connect spring can reproduce compress load and tension force. The analysis utilize the water flow distribution model on the dam and confirms that the fluid force is measured for load evaluation. In addition, the element for evaluating the contact force was fixed.

## DEM ANALYSIS Results

**Fig.2** describe the comparison of the accumulation process of experiment and analysis. Firstly,  $t = t_0$  is determined as initial time, and it is almost the same state in the experiment and the analysis (**Fig.2a,e**). This time can be considered also as initial time for the load evaluation. In case of  $t = t_0 + 0.3$  s, the sedimentary of the gravel at  $\theta_{LS} = 30^\circ$  is lower than one at  $\theta_{LS} = 0^\circ$ , and the gravel is delayed by covering the entire dam model (**Fig.2b,f**). A similar trend is seen in the analysis.  $t = t_0 + 0.6$  s or later, the analysis can be reproduced the experimental sedimentary shape. (**Fig.2c,g**). Comparing the final accumulation process,

experiments deposit in a convex and analysis forms almost straight shape (**Fig.2d,h**). This is because spherical elements are used as gravel models. However, the process from collision to stable gravel and the sedimentary shape can be reproduced. **Fig.2i** indicated in load-time relation of experiment and analysis. In experiment in case of  $\theta_{LS} = 0^\circ$ ,  $t = t_0 + 0.5$  s is the maximum impact loads 198 N, and controversially, In  $\theta_{LS} = 30^\circ$ ,  $t = t_0 + 0.6$  s, the maximum impact load is 143 N. The maximum load decreases 30 % by the front inclination angle, and the time to reach the maximum load is delayed by about 0.1 s. On the other hand, in the DEM analysis, load is 209 N, for  $\theta_{LS} = 0^\circ$ ,  $t = t_0 + 0.5$  s, and maximum load is 149 N for  $\theta_{LS} = 30^\circ$ ,  $t = t_0 + 0.6$  s. Although the load is highly evaluated compared to the experiment. Both the effects of reducing the load by the front inclination angle and to delay the time before the maximum load occurs are reproduced roughly. In addition, for the case of  $\theta_{LS} = 30^\circ$ , the sediment load results smaller. From this, we can reproduce the process from the impact load to the sedimentary load.

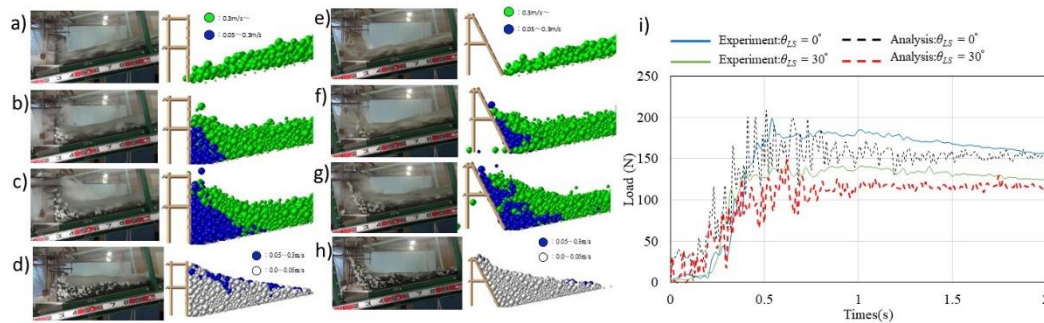


Figure 2. Experiment and analysis results; a)  $t = t_0$ , b)  $t = t_0 + 0.3$  s, c)  $t = t_0 + 0.6$  s, d)  $t = t_0 + 3.0$  s at the front inclination angle  $\theta_{LS} = 0^\circ$ , e)  $t = t_0$ , f)  $t = t_0 + 0.3$  s, g)  $t = t_0 + 0.6$  s, h)  $t = t_0 + 3.0$  s at the front inclination angle  $\theta_{LS} = 30^\circ$ , i) Each result is load time relation.

## The loading mechanism for impact load

**Fig.3** describes the load reduction mechanism of experiment and DEM analysis. Mainly, it is compared with simplification description of experiment and velocity vector distributions of analysis. The comparison between experiment and numerical analysis is computed taking in consideration a qualitative simplified description for the experiment, while for the DEM results the vector distribution of the velocity is considered. The velocity of each element is in fact displayed as a green vector, and the length of the vector represents the degree of speed. Each result compares the individual motion shape at the time of analysis with the one observed in the experiment. Firstly, in **Fig.3a,e,i,m**, it is observable how the tip of the debris flow is approaching the dam. At this time, the impact load doesn't occur in both of cases, and the debris flow becomes the same state. **Fig.3b,f** show the gravel flowing at the front part straightly colliding with the dam. The velocity vector of each gravel can be observed in numerical analysis outcomes. The gravel elements that reached the dam lose velocity and becomes red. Simultaneously, an impact load is generated against the dam. On the other hand, in case of  $\theta_{LS} = 30^\circ$ , the results have already fitted shape of the front inclination (**Fig.3j,m**), and the sedimentary shape is different from  $\theta_{LS} = 0^\circ$  (**Fig.3b,f**). A lot of gravel that has already stopped is represented in case of **Fig.3c,e** using

red color, while the gravel which gets over the ceased ones spreads. Comparing with  $\theta_{LS} = 0^\circ$  (Fig.3 c,g) and  $\theta_{LS} = 30^\circ$  (Fig.3 k,o), the red zone of  $\theta_{LS} = 30^\circ$  is clearly larger than that of  $\theta_{LS} = 0^\circ$ . Fig.3d,h shows when the mass of gravels reach the half height of sabo dam. At this time, the gravel mass is divided into two groups. The first group has already reached the dam and it is stopped. The second group is moving over the gravel mass of the first group. Comparing the cases of the two fronts of inclination angle of the sabo dam in Fig.3 l, p, the differences occur in the formation of the dead zones. Also, it is thought that the movement energy of the gravel is lost, and the collision load is reduced. This situation shows a similar tendency in the analysis result, and it can be seen that the following gravels have overcome the stopped ones. This makes it hard for the gravel to overcome by increasing dead zone. Therefore, the collision velocity is slowed down. The effect is reduced for the gravel, which passes through the dead zone. Comparing with the velocity vector, the velocity of the gravel is lost due to the front inclination angle. Moreover, it is suggested that the impact load that the debris flow gives is reduced.

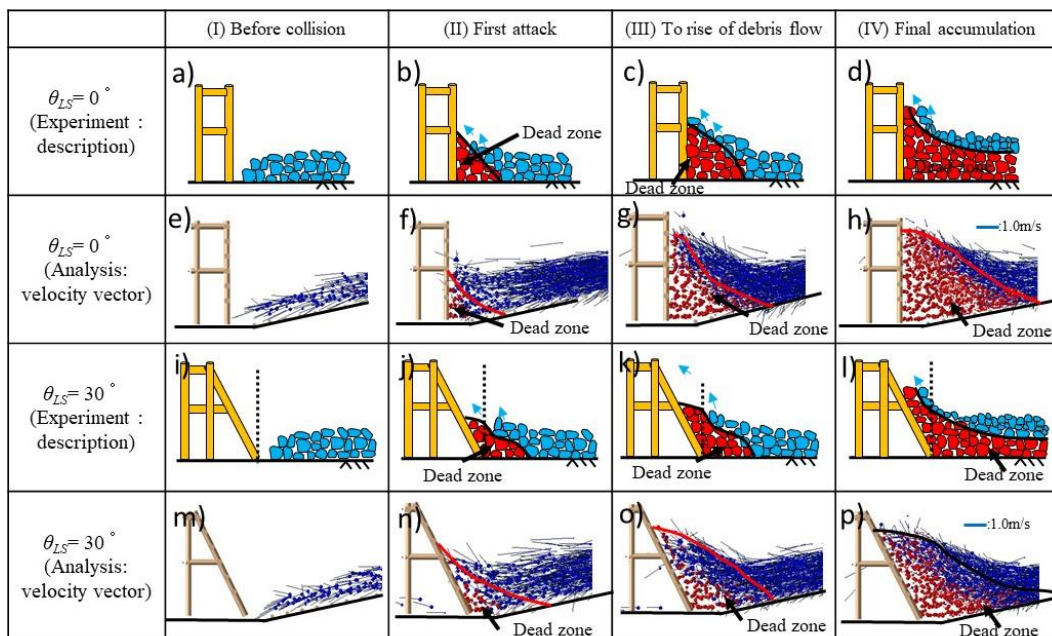


Figure 3. The reduction load mechanism; I) state before the debris flow collide with the dam, II) the head of debris flow contact the dam, III) the main debris flow contact the dam, IV) the subsequent sediment flow get over the entrapped debris flow at experiment description. and, a)-d) at experiment,  $\theta_{LS} = 0^\circ$ , e)-h), at analysis,  $\theta_{LS} = 0^\circ$ , i)-l) at experiment,  $\theta_{LS} = 30^\circ$ , m)-p) at analysis,  $\theta_{LS} = 30^\circ$

## Discussion: Reduction Mechanism of Impact load of bouldery debris flow

This study investigated both fluid force and boulder collision load using the interaction of DEM and water flow distribution model (Horiguchi et al., 2019). In near future, it is necessary to improve the analysis model, and comparing the motion mechanism and the impact load estimation method by repeating the experiment; further, the reproducibility of

the phenomenon and the applicability of the design method are requested. Particularly, because the impact load directly hits the open sabo dam, it is not realizable to actually predict impact load of debris flow, and also, it is important to mitigate the impact function of boulder. In addition, it is observed that the load reduction mechanism effect reduced the load due to debris flow entrapped in flexible structures (Song et al. 2019), and afterwards it is important to examine the optimal shape characteristics that can form the ‘dead zone’.

## Conclusion

The aim of the study investigated the influence of an impact load of debris flow against an open sabo dam characterized by a particular front inclination angle. The load reduction mechanism was organized through results of the experiment and the analysis, and the numerical simulation was examined considering the movement process of each elements. The results reproduced load-time relation of experiment, and comparing with  $\theta_{LS} = 0^\circ$  and  $\theta_{LS} = 30^\circ$ , it was visible that the maximum loads were reduced about 30 % due to the front inclination angle. The load reduction mechanism induced the ‘dead zone’ and impact load of debris flow was largely influenced. The effect of the dead zone was useful to reduce the impact load. On basis of the examination, the optimal shape of steel pipe open sabo dam may be built in near future.

## Acknowledgements

The authors would like to express deepest appreciation for the help and support of Steel Pipe Sabo Dam Facility Association.

## References

- Mizuyama, T. 2008. Structural Countermeasures for Debris Flow Disasters. *International Journal of Erosion Control Engineering* 1, 38–43.
- Hübl, J., Nagl, G., Suda, J. Rudolf-Malklau, F. 2017. Standardized stress model for design of torrential barrier under impact by debris flow (According Austrian Standard Regulation 24801), *International Journal of the Japan Society of Erosion Control Engineering*, Vol.10, No.1, 47–55.
- Horiguchi, T. & Katsuki, S. 2017. DEM analysis on impact load of boulders on open type steel frame dam, *Journal of the Japan Society of Erosion Civil Engineering*, 70(3), 51–57.
- Horiguchi, T., Takahashi, T., Takamori, K., Katsuki S. 2017. Evaluation of load-carrying capacity of full-scale falling protection net using distinct element method, *International Journal of Protective Structure*, Vol.8, No.1, 1–20.
- Horiguchi T. & Komatsu Y. 2018. Method to evaluate the effect of inclination angle of steel open type check dam on debris flow impact load, *International Journal of Protective structure*, 10(1), 95–115.

Horiguchi T., Katsuki S., Ishikawa N., Mizuyama T. 2019. Method for Evaluating the Trapping Effects of Woody Debris Using a Distinct Element Method International Journal of the Japan society of Erosion Control Engineering, Vol.12, No.1, 1–12.

Ishikawa N., Shima J., Matsuzawa R., Mizuyama T. 2018. Safety verification of Sabo dams against large-scale debris flow, *Symposium Proceedings of the INTERPRAEVENT 2018 in the Pacific Rim*, 145–152.

National Institute for Land and Infrastructure Management, Ministry of Land, Infrastructure and Transport. 2016. Manual of Technical Standard for designing Sabo facilities against debris flow and driftwood, technical note of national institute for land and infrastructure management, No905.

Song D., Gordon G., D., Xu M., Choi G., E., Li S., Zheng Y. 2019. Quantitative analysis of debris-flow flexible barrier capacity from momentum and energy perspectives, *Engineering Geology* Vol.251, 81-92.



# HAZARD AND RISK ASSESSMENT (HRA)

---

# Comparing nets and forests for rockfall risk reduction along the Gotthard highway using cost-benefit-analysis and net present values

Luuk Dorren<sup>1</sup>, Christine Moos<sup>2</sup>, Martin Nussbaumer<sup>3</sup>, Steve Vogel<sup>4</sup>, Philippe Arnold<sup>5</sup>

**Keywords:** rockfall, protection forest, net, cost-benefit-analysis, NPV

## Abstract

Rockfall events occur frequently along the Gotthard highway and cause high costs. The most common rockfall risk reduction measures used there are forests, flexible rockfall nets and dams. For a realistic long-term economic assessment of such risk reduction measures, all costs and benefits must be adjusted to a common point of time, which can be done by calculating the Net Present Value (NPV). In this study, we economically assess the performance of a forest and of flexible nets, as well as combinations thereof, which protect a section of the Gotthard highway against rockfall. We show that the variant “current forest with maximal nets” provides the highest risk reduction but has a highly negative NPV and a low benefit-cost ratio. The variant current forest is the only one with a positive NPV. Our study shows that the combination of forests and nets can significantly increase the risk reduction capacity of nets.

## Introduction

In June 2006, two persons were killed by a direct rockfall impact while driving on the Gotthard highway in Switzerland. Although rockfall events occur frequently in mountainous areas (cf. Volkwein et al., 2011), fortunately such accidents are rare. In many cases, rockfall events remain unnoticed since they invoke little or no damage. Nevertheless, rockfall blocks end up almost yearly on the mountain side driving lanes of the Gotthard highway, leading to road closures during the time needed to assure that no additional rock mass falls might impact the highway. These closures lead to detours and delays and consequently additional costs. Dorren and Arnold (2016) showed that road closures after blockfall and rock mass falls represent approximately 28% of the total yearly expected damage induced by gravitational natural hazards (i.e. snow avalanches, floods, bank erosion, landslides and rockfall). The most common rockfall risk reduction measures along the Gotthard highway are forests, flexible rockfall nets and dams. More information on

---

<sup>1</sup> Prof., Dr., HAFL, Bern University of Applied Sciences, Zollikofen, SWITZERLAND, ([luuk.dorren@bfh.ch](mailto:luuk.dorren@bfh.ch))

<sup>2</sup> Dr., CIRM - Univ. Lausanne UNIL Switzerland

<sup>3-4</sup> CIRM - Univ. Lausanne UNIL Switzerland

<sup>5</sup> Federal Roads Office FEDRO 3003 Bern Switzerland

rockfall protection forests can be found amongst others in Moos et al. (2017), Yang et al. (2019) present details on the functioning of nets and Lambert et al. (2018) on rockfall dams.

The protective effect of forests and the subsequent rockfall risk reduction is a direct benefit of trees covering the transit and deposit areas of rockfall slopes. On top of that, if combined with structural protective measures, the maintenance costs of the latter are generally reduced, and in the best case the installation costs as well, due to the reduction of rockfall rebound heights and impact energies by previous impacts on trees. To support decisions on risk prevention measures, consisting of single measures or variants of combinations of different types of measures, a cost-benefit-analysis (CBA) is a method that provides standardised and quantified information on the efficacy and efficiency of the analysed measures. For natural hazard risk reduction measures, such a CBA typically includes the equivalent annual costs (annual cost of installation, operation and maintenance) of the measure versus the yearly avoided damages. These damages thereby concern buildings, infrastructure and goods, as well as loss of human life. For a realistic long-term economic assessment of risk reduction measures, all costs and benefits must be adjusted to a common point of time, which can be done by calculating the Net Present Value (NPV), being the sum of all future expected benefits and costs discounted to today.

In this study, we aim to economically assess the performance of a forest and of flexible nets, as well as a combination thereof, which protect a section of the Gotthard highway against rockfall. To achieve this, we determine the net present value (NPV) of:

- the current forest with a management scenario that aims to promote regeneration using gap cuttings (variant 1)
- a combination of variant 1 and the currently installed flexible nets (200 & 500 kJ; variant 2)
- a combination of variant 1 and maximal flexible nets (5000 kJ energy capacity; variant 3)
- only currently installed flexible nets, no trees (variant 4)

To be able to determine the benefit (risk reduction) of these three measure variants, we compare each of them with a situation without protective measures (no trees and no nets). This is the “baseline” variant.

## Methods

The chosen study area is the Gotthard highway section between Meitschligen and Stotzigwald in the Canton of Uri, Switzerland (cf. Fig. 1). This highway section, which has an altitude of approx. 670 m a.s.l. is continuously endangered by rockfall originating from cliff faces below the Vreniberg that stretch stepwise from approx. 750 to 1100 m (a.s.l.). During the last registered rockfall event on the 8th of January 2009 (with a release volume of 10 m<sup>3</sup>), two blocks with a volume of approx. 1 m<sup>3</sup> arrived on the highway. Other than damages to the road guard rails and a highway closure for 36 hours nothing happened. An identical event occurred almost one year before on the 8th of February 2008. At that time, 4 cars collided with the deposited rocks, but nobody got hurt.

To calculate the NPV of the four defined variants, we modelled the propagation of three block volumes for the four described risk reduction measure variants. These were single rectangular blocks with a maximum volume of 1, 2 and 15 m<sup>3</sup> with a uniform random volume variation of +/- 20% for each trajectory simulation. The rock type is gneiss and we defined its density as 2700 kg/m<sup>3</sup>. The used block volumes were defined by Berwert et al. (2011). The attributed onset probabilities (detachment probability at the rockfall cliffs) for these defined blocks were 0.067 (10-year return period: 1 m<sup>3</sup>), 0.023 (30-year return period: 2 m<sup>3</sup>), 0.007 (100-year return period: 15 m<sup>3</sup>) and 0.003 (300-year return period: 15 m<sup>3</sup>). The difference between the 100- and 300-year return period lies in the number of individual blocks that descend the slope, which is set to 2-5 blocks for the 100- and 4-8 blocks for the 300-year return period. The 10-year return period is a fixed 1-block scenario, while the 30-year return period is a randomised 1-3 block(s) scenario.

Our risk calculation is based on FEDRO (2012) and accounts for the damage types “direct impact” (only for regular fluid traffic conditions), “collision” (with rock deposits on the road or other vehicles), “infrastructure damage” and “road closure after a hazard event”. The Gotthard highway is also precautionary closed for snow avalanches and debris flows, but not for blockfall and rock mass fall on our study section.

The NPV for all four measure variants, based on the defined return periods, was calculated following:

$$NPV = \sum_1^{100} \frac{[I(w) + I(rr)] - [O(n) + O(m) + O(f)]}{[1 + i]^t}$$

where:  
*I(w)* = revenue from wood sales  
*I(rr)* = risk reduction (i.e., risk of protection variant – risk of baseline variant)  
*O(n)* = Costs for installing flexible nets  
*O(m)* = Operation and maintenance costs for the flexible nets  
*O(f)* = Costs for forest interventions  
*i* = discount rate  
*t* = year

Values for the variables we used for the calculation of costs and risks that are not provided in FEDRO (2012), as well as those needed for calculation the NPV, are presented in Table 1. Further information on the NPV calculation is provided by Moos et al. (2019). Although the cantonal road lies directly below the highway, in this study we focused on the highway only.

**Table 1. List of variables and values used for the calculation of costs and risks in this study.**

Variable	Value	Unit	Source
Mean daily traffic (MDT)	22'500	vehicles/day	www.astra.admin.ch
Indicated maximum speed on the highway section	100	km/h	Field observation
Forest intervention costs (harvesting + preparation, road maintenance)	110	CHF/m <sup>3</sup>	Starke et al. (2017)
Revenue from wood sales	75	CHF/m <sup>3</sup>	idem.
Net installation costs (200 kJ)	1200	CHF/m	Moos et al. (2019)
Net installation costs (500 kJ)	1500	CHF/m	idem.
Net installation costs (5000 kJ)	4500	CHF/m	idem.
Discount rate (mean value last 30 years in CH)	2	%	idem.
Road closure costs	87'000	CHF/day	FEDRO (2012)

For the rockfall simulations, we used Rockyfor3D, which is a probabilistic, process-based 3D rockfall model (Dorren, 2012). Parameter maps that characterize the slope surface roughness, the damping of the subsoil, as well as the forest (if present) are required. The topography must be defined by a digital elevation model (DEM) in ESRI ASCII raster format. For that, we used the 2 x 2 m SwissAlti3D raster from Swisstopo. The surface roughness indicates the dimension of obstacles in the form of previously deposited stones and blocks. To characterise this roughness, Rockyfor3D needs values for size distribution of the blocks that are encountered by the falling block (measured normal to the slope). The surface roughness is divided into Rg70, Rg20 and Rg10, which represents the height of an obstacle the falling block encounters during 70%, resp. 20% and 10% of the rebounds within a defined homogeneous area (see Dorren, 2012). The soil type represents the damping of the subsoil and distinguishes between seven different categories, which lead to different energy dissipations of the falling block.

We mapped the current forest stands (cf. Fig. 1) by using orthophotos and field inventory plots. For each stand, a random sample was carried out on an area of 20 by 20 metres. All trees with a stem diameter at breast height (DBH) larger than 8 cm were recorded. Subsequently, the mean BHD, the standard deviation of the BHD, the number of stems per hectare and the proportion of coniferous trees were calculated for each stand (see Table 2). RockyFor3D uses this data to create a forest model consisting of individual trees with their position and DBH, which are saved in a treefile.txt. We assumed that every 20 years, 25% of the total standing volume would be removed in the denser stands by using cable crane lines and lateral regeneration gap cuttings of 20 by 30 m. In QGIS (QGIS Development Team, 2019). QGIS Geographic Information System. Open Source Geospatial Foundation Project. <http://qgis.osgeo.org>) we removed the trees in the cut regeneration gaps from the generated treefile to be able to simulate rockfall trajectories and calculate the change in risk reduction after a forest intervention. The current mean standing volume per ha is 575 m<sup>3</sup> (i.e., almost 6000 m<sup>3</sup> on 10.4 ha). The net costs of a single forest intervention add up to 165'808 CHF (intervention costs) – 113'098 CHF (revenue of wood sales) = 57'710 CHF.

**Table 2. Key data on the forest stands covering the study area.**

Stand number	Stem density [/ha]	Mean DBH [cm]	Stddev. DBH [cm]	% Conif. trees
1	350	11	3	79
2	350	45	16	100
3	200	46	6	100
4	675	25	11	96
5	400	40	17	88
6	500	36	9	100
7	0	-	-	-
8	125	12	3	60

Rockfall nets can be included directly in Rockyfor3D. These need to be characterised by their height measured normally to the slope surface [in m], the energy that the net can dissipate [in kJ] and a net number [-]. Currently, approx. 220 m of 500 kJ nets with a height of 4 or 6 meters and approx. 380 m of 200 kJ nets with a height of 3 meters are installed (see also Fig. 1). The costs of these current nets added up to ~690'500 CHF installation costs and ~13'500 CHF operation and maintenance costs in the following years. We designed a maximal net variant in which we virtually installed 1125 m of 5000 kJ nets with a height of 9 m (see figure 1). The costs of those "maximal" nets added up to ~5'062'500 CHF installation costs and ~101'250 CHF operation and maintenance costs in the following years. The service life of the nets is defined as being 50 years (FEDRO, 2012).

Along the highway we placed a virtual control screen, which can be defined in Rockyfor3D as a net with a height of 0 m and an energy capacity of 0 kJ. This screen allows recording all relevant data for the risk calculation (number of passed rocks, energy distribution, passing height distribution). The density, shape and three dimensions (height, width and depth) of the falling block can be defined in the user interface RockyFor3D. For each defined block volume and variant, we simulated 1000 trajectories per release cell.

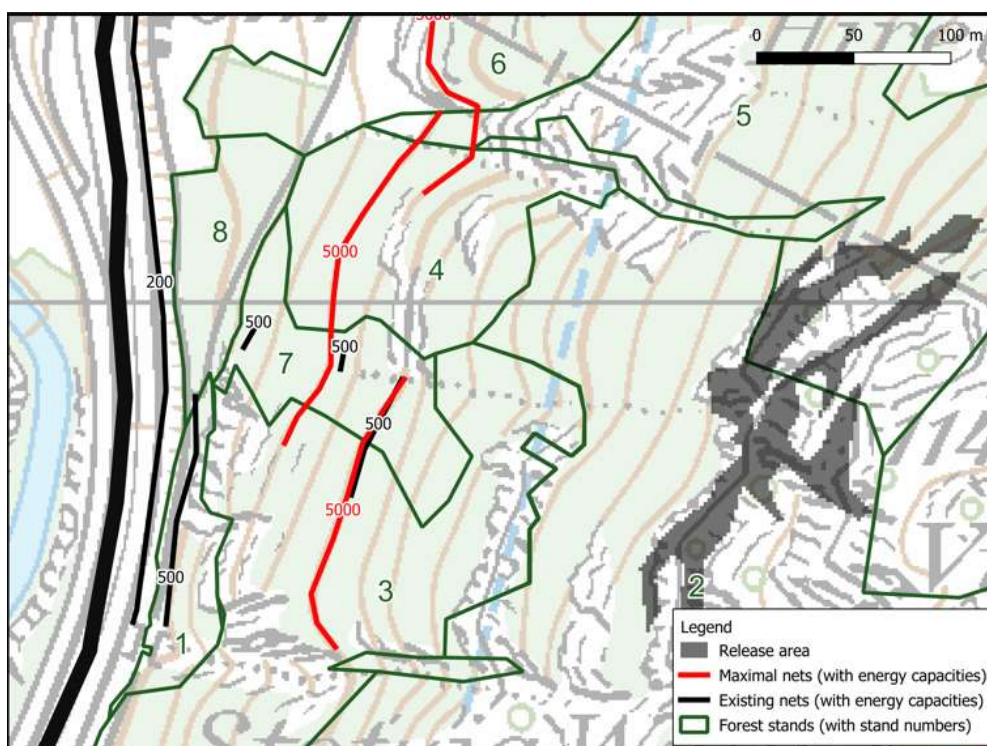


Fig. 1. Map of the study area showing the location of the used nets and forest stands as well as the virtual control screen along the Gotthard highway as thick black line on the left side of the map.

## Results and discussion

The total risk per year (sum of the risk for the four defined rockfall return periods) for the 5 variants is given in table 3. As expected, it shows that the variant forest + maximal nets provides the highest risk reduction in comparison to the baseline variant (10'904 CHF/yr risk reduction). The lowest risk reduction (957 CHF/yr) is provided by the variant 4 (current nets without forest). An interesting effect of the forest can be seen when comparing variants 1, 2 and 4, which shows a significant increase of the efficacy of the current nets with an increase of the risk reduction of more than 400%.

Table 3: Summary of the key results.

Variant	Total risk [CHF/yr]	Difference with baseline variant [CHF/yr]	NPV [CHF]	Benefit-cost ratio [-]
“Baseline” (no trees, no nets)	30'647	-	-	-
1 (current forest with management, no nets)	25'493	5'154	85'922	1.96
2 (variant 1 + current nets)	23'464	7'183	-1'404'000	0.21
3 (variant 1 + maximal nets)	19'743	10'904	-10'565'000	0.05
4 (current nets, no trees)	29'690	957	-1'672'000	0.03

Although the variant forest + maximal nets provides the highest risk reduction, its NPV is highly negative (ca. -10 million CHF over a period of 100 years) and its benefit-cost ratio is 0.05. Variant 1 (forest with management and no nets) is the only one with a positive NPV. This variant is also the only one with a benefit-cost ratio larger than 1.

With none of the studied protective measures, the risk could be reduced to a value below 10'000 CHF/yr, which is the defined threshold for high-risk hot spots along the Swiss national roads (FEDRO, 2012). To do so, additional measures such as regular monitoring of the source area and where possible rock cliff cleaning (trundling) could help reducing the risk further. It needs to be evaluated, however, if these measures would suffice to reach risk values smaller than the set threshold.

## Conclusion and outlook

Our study shows that the combination of forests and nets can significantly increase the risk reduction capacity of nets. Moreover, before deciding to construct nets for rockfall protection, one should not only carefully look at the benefits and costs, but also at the net present value. None of the studied protective measures sufficed to reach risk values smaller than the threshold set by the FEDRO. We are currently improving our work by better accounting for the future dynamics and related uncertainties of the forest ecosystem.

## References

- Dorren L. (2012). Rockyfor3D (v5.2) revealed. Transparent description of the complete 3D rockfall model. ecorisQ Paper ([www.ecorisq.org](http://www.ecorisq.org)): 33 p.
- Arnold Ph., Dorren L. (2015). The Importance of Rockfall and Landslide Risks on Swiss National Roads. In: G. Lollino et al. (Eds.) Engineering Geology for Society and Territory 6, Springer Int. Publishing: 672-675.
- Berwert J., Burkard A., Gertsch E., Liniger M., Mischler A., Thali U., Tobler S., Winkler C., Chiapolini A., 2011. Gefahrenbeurteilung und Risikoanalyse betreffend Naturgefahren auf Nationalstrassen - Los 1: Uri. Technischer Bericht - Teil Gefahrenbeurteilung. Bericht Bundesamt für Strassen ASTRA: 23 p. (excl. annexes).
- FEDRO (2012) Natural hazards on national roads: Risk concept. Methodology for risk-based assessment, prevention and response to gravitative natural hazards on national roads. Documentation 89001, V2.1. Federal Roads Office, Bern: 106 p.
- Lambert S., Kister B., Loup B. (2018) Literature-based expedient criterion for assessing the impact strength of Switzerland's rockfall protection embankment inventory. Proceedings INTERPRAEVENT 2018 in the Pacific Rim: 208-214.
- Moos C., Dorren L., Stoffel M. (2017) Quantifying the effect of forests on frequency and intensity of rockfalls. Natural Haz. Earth Syst. Sciences 17: 291-304.
- Moos C., Thomas M., Pauli B., Bergkamp G., Stoffel M., Dorren L. (2019). Economic valuation of ecosystem-based rockfall risk reduction considering disturbances and comparison to structural measures. Science of the Total Environment 697: 134077.

QGIS Development Team (2019). QGIS Geographic Information System. Open Source Geospatial Foundation Project. <http://qgis.osgeo.org>.

Starke M., Menk J., Thomas M., Keel A., Ziesak M. (2017). Abschlussbericht Mobilisierung von Holz mit geringem Deckungsbeitragspotenzial. BFH-HAFL / Bundesamt für Umwelt BAFU (unpublished), Zollikofen: 129 p.

Volkwein A., Schellenberg K., Labiouse V., Agliardi F., Berger F., Dorren L., Gerber W., Jaboyedoff M. (2011) Rockfall characterisation and structural protection - a review. *Natural Haz. Earth Syst. Sciences* 11: 2617 - 2651.

Yang J., Duan S., Li Q., Liu C. (2019) A review of flexible protection in rockfall protection. *Natural Hazards*: <https://doi.org/10.1007/s11069-019-03709-x>

---

# Automated delineation of large-scale landslides based on high-resolution digital terrain models

Bernhard Elsner<sup>1</sup>

**Keywords:** Delineation; Large-scale landslides; Airborne laser scanning; Automatisations; Tyrol

## Abstract

This methodology for the automated linear delineation of large-scale landslides from high-resolution digital terrain models, generated from airborne laser scan data, consists of two automated steps. Based on curvature values of the terrain surface, linearly describable landforms of large-scale landslides are first detected, and then classified. As a basis for the two automated steps used to identify landslides, reference data are manually created by experts. This comprehensive dataset contains various indicator landforms of large-scale landslides (larger than 10 ha). The application of this methodology to the entire study area, the Austrian province of Tyrol, shows that linear delineation is possible to a large extent, even if complete area boundaries cannot be generated. The precisely located results therefore provide a comprehensible and helpful basis for subsequent manual examination and final completion.

## Introduction

Due to their long-lasting permanent, but imperceptible movement rates, large-scale landslides such as mountain slope deformations, pose a rather treacherous hazard, especially for infrastructure – but also for human life, when parts of these landslides suddenly accelerate (MOSER et al., 2017). Thus, for the purpose of consistent and sustainable natural hazard management within the project "WLV-MB: Tyrol-wide detection of large-scale landslides from high-resolution digital terrain models in the torrent and avalanche cadastre", a methodology is to be developed, which allows an area-wide linear delineation of large-scale landslides to be automatically carried out for the entire study area, the Austrian province of Tyrol.

The data basis for this is a province-wide, high-resolution (1 m) Digital Terrain Model (DTM), generated from airborne laser scan data (LAND TIROL, 2011). Therefore, the detection of landslides, which due to the lack of multi-temporal datasets is carried out purely through the identification of indicator landforms, can be done quite precisely even in areas covered by dense mountain forests.

---

<sup>1</sup> M.Sc., Universität Innsbruck, AUSTRIA, [Bernhard.Elsner@uibk.ac.at](mailto:Bernhard.Elsner@uibk.ac.at); [BernhardElsner@gmx.de](mailto:BernhardElsner@gmx.de)

Based on the methodology presented here, the results generated should serve as a reproducible and comparable basis for subsequent final manual examination and delineation of large-scale landslides, and thus provide more objective and more precise data for hazard and risk assessment, and resultant preventive measures.

In general, only large-scale landslides that have an area of more than 10 ha are considered. Although other characteristics, such as deepness, cannot be determined purely on the basis of the remote sensing method, in most cases, the landslides are likely to be deep-seated gravitational slope deformation, rock flexural topple or a hybrid of both types of landslide. In this way, only the characteristic landforms of these – according to HUNGR et al. (2014) – purely large-scale landslide types, which are generally deep-seated and characterised by slow, permanent movements, are considered.

## Methods

Figure 1 shows that the development of the automated methodology, which is described in detail in ELSNER (2019), consists of three sub-steps, all of which are based on the high-resolution DTM. The definition of linearly describable, relevant landforms for the detection of large-scale landslides, such as scarps, is fundamental for the reference dataset, which represents the necessary basis for developing the two automated steps of this methodology (step 1). This dataset contains so-called mapped landslide lines, which are localized structures representing landforms that are indicators for landslide processes and provide information on two levels. On the one level, the mappings show the directly visible characteristics of the structure through the specific forms of its surface curvature. These curvature lines are detected by a method which extracts such lines from the high-resolution DTM, in step 2 referred to as automated structure detection. Based on this, on the second level, the relevance of structures as indicator landforms and therefore as a part of large-scale landslides, is considered, by building a classification model, in step 3 referred to as automated classification. The area-wide application of this automated methodology, developed in accordance with the reference data, generates the classified landslide lines as the result. Subsequently to this entire procedure described here these lines form the basis for final, manual delineation of large-scale landslides.

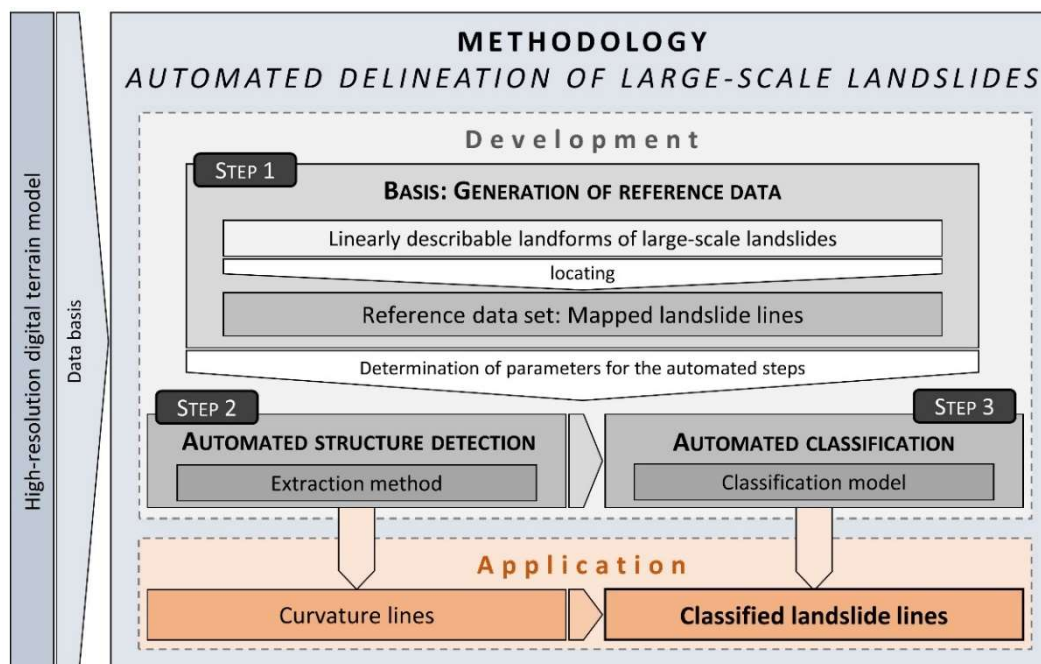


Figure 1: Steps in the development and application of the methodology.

Generation of reference data: For the most comprehensive detection of landslides possible, not only delineating indicator landforms such as double-crested ridges and main scarps are considered, but also indicator landforms within the landslide surface, such as counterscarps and secondary scarps. The landslide lines for the reference dataset are manually mapped by ten experts from the research fields of geology and geomorphology, on a specific mapping basis and taking into account special mapping rules. Derived from the DTM, the terrain is diffusely illuminated onto these maps and thus a similar assessment of the terrain situation across all exposures is possible. In five mapping areas, each being approximately 2.5 km<sup>2</sup> and having existing evidence of landslides, landslide lines are drawn over the entire area, in the maximum convexly curved surface area of the visible indicator landforms. Thus, main, lateral and secondary edges of the scarps, the ridge lines of the double-ridge-, trench- and counterscarp-structures, as well as the convex edges of tension cracks are mapped. In order to obtain a dataset as representative as possible for Tyrol, the mapping areas were selected in such a way, that each of the different geological units is represented by one of the proportionally largest coarsely combined areas (carbonate rock, crystalline, greywacke zone, Bündner schist and quartz phyllite), and that from a geomorphological point of view, as many different indicator landforms as possible are present. In the post-processing, the individual maps are digitised, and the experts' knowledge is combined to a mean and therefore more objective overall assessment, forming the final reference dataset. This process takes place over many steps, at a much higher resolution, to minimise inaccuracies that occur for example during manual mapping and georeferencing. Nevertheless, existing errors are taken into account by averaging the areas of inaccuracy of the manually mapped landslide lines.

Automated structure detection: Following the modified method of RUTZINGER et al. (2007), convex curved surfaces are automatically extracted on the basis of curvature values derived from the DTM, and thus linearly describable landforms are detected. These so-called curvature lines should then be able to correctly and completely reproduce the mapped landslide lines – to the extent to which this is possible when solely taking the curvature into consideration. In order to obtain the optimum adaptation to the reference data, the level of agreement of the extracted curvature lines and mapped landslide lines, for all parameter combinations of the methodology, and therefore the best setting for the calculation, is determined by using the F-measure quality measure (ELSNER, 2019). In the course of this, it is additionally calculated whether, and if so, how often the study area should be subdivided into areas (generated on the basis of an unsupervised cluster analysis), which have mutually different land surface properties. The slope and the roughness (in different scales) are also taken into account here, which are all derived from the DTM. Thus, in the final determination of the best parameter combination for the study area, a spatially differentiated approach is followed. The result of the area-wide application of the automated structure detection therefore consists of pixels of individual curvature lines, which will be classified in the following automated step, according to whether or not they are part of a large-scale landslide. For the development of this last methodological step (see next paragraph), the reference dataset is adjusted to include this new information, as a so-called selected reference dataset, by transferring the values of the reference dataset to the generated pixels of the curvature lines.

Automated classification: Based on the results of the automated structure detection, a supervised pixel-based classification is carried out by applying the Random Forest classifier, which is very well-suited and often used for remote sensing data of this extent (BELGIU et al., 2016). As in the cluster analysis, but in much larger numbers, many Land Surface Parameters (LSPs) are also derived from the DTM and are used to characterise the indicator landforms of large-scale landslides, and thereby distinguish them per pixel from other natural or anthropogenic convex landforms. In addition to the local LSPs already used in the previous methodological step, the 28 different LSPs also include regional LSPs, such as distances to channels or geomorphological structures like ridges, as well as visibility parameters. In many cases, these parameters are calculated at various scales, using different resolutions and sizes for the calculation environment, so that close to 300 LSPs per observation point of the selected reference dataset can serve as features for the classification. In order to speed up the calculation process with regard to a high-resolution, area-wide application, very strongly correlated features of the same LSP, with different scales, are sorted out in the course of the classification, according to specific rules (ELSNER, 2019). Whilst building the classification model, a further selection of features is made, in which the importance of the features for the classification is recognized by the frequently used permutation importance (BELGIU et al., 2016). Consequently, the unimportant LSPs are deleted using recursive feature elimination (GREGORUTTI et al., 2017). In the subsequent fine-tuning of the most important model parameters, the best parameter combinations from the random forest classifier are individually calculated for four different sets of most important features (ELSNER, 2019). This then roughly determines an almost optimal number of features, and thus the best model with the best settings, with independent data previously separated from the rest of the reference dataset.

These settings are subsequently used for the final creation of the prediction model and therefore also for applying the classification method to unknown, automatically generated curvature lines outside of the mapping areas of the reference data. The data points classified as being part of a large-scale landslide are then selected and connected, in a concluding step, to the so-called classified landslide lines, which represent the final result of the entire methodology for automated delineation of large-scale landslides.

## Results and discussion

When generating the reference data, it should be noted that the mappings created by the individual experts were done at different levels of detail, but generally in the area of the main structures these lines were mapped almost exactly congruently, which can be determined by the concurrence in the combination of landslide lines. The difference between the experts' mappings, and thus the variability of the experts' individual errors, generally seems to be low.

The interim results of the methodology, collected by applying the automated structure detection, show that, for the optimal combination of parameters, the mapped landslide lines of the reference dataset (especially the less prominent ones) could not continuously be detected as curvature lines by the automated process. By using the spatial differentiation approach in five regions with different land surface properties, an optimisation of the detection of smaller indicator landforms, such as tension cracks, is possible. The use of multi-scale methods, which can directly detect different convex, linearly describable landforms for each surface, equally, by combining different scales, could most likely bring further improvements. In general, however – as can be seen by the two pronounced landslides on the orographic left in the upper left image in Figure 2 – it can be stated that at least all the more prominent indicator landforms, such as scarps, and therefore the structures most relevant for the linear delineation of the landslide surface, are well represented. Besides the curvature lines that represent landslide lines, numerous natural landforms that are not directly connected to large-scale landslides are also shown, such as in areas of rugged, rocky terrain and in torrent valleys, as well as anthropogenically created edges such as forest roads (see the bottom left in Figure 2). The mapping areas of the reference data also show these mentioned observations regarding the curvature lines. Therefore, through the multifaceted and widespread representation of landslide lines and non-landslide lines, the selected reference dataset provides a comprehensive basis for the development of a classification model which represents the real-world situation most accurately.

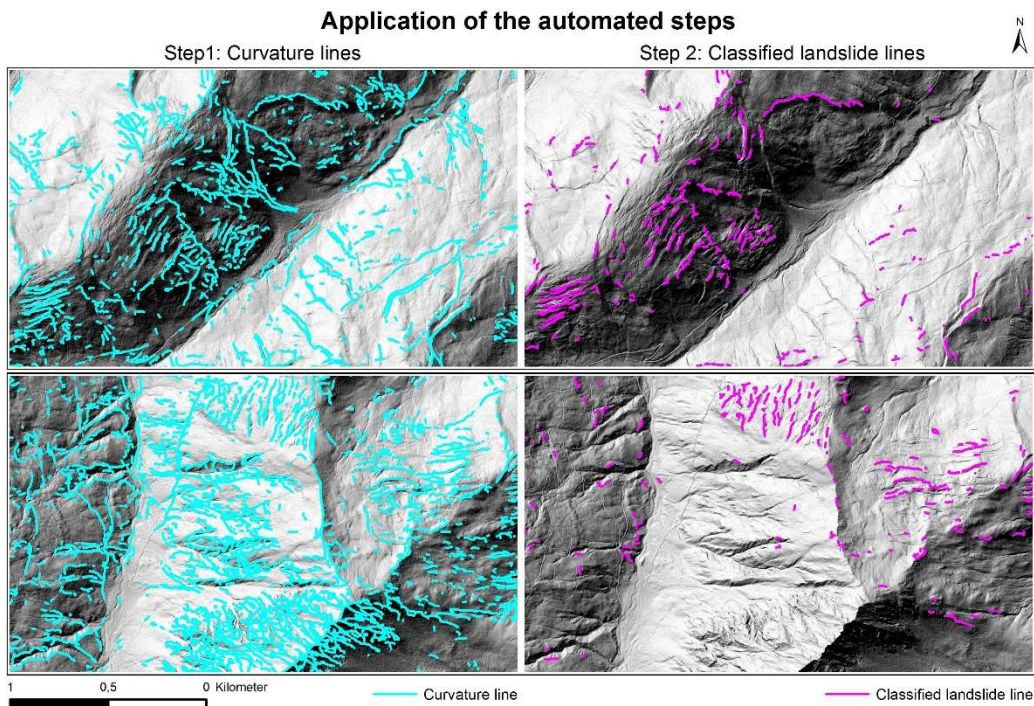


**Figure 2: Results of the two automated steps for two selected areas of Tyrol near Kitzbühel: curvature lines (left); classified landslide lines (right) (ELSNER, 2019; based on LAND TIROL, 2011).**

The optimisation processes in the context of the automated classification show that even when using the default settings of the model parameters of the random forest classifier, similar results can already be achieved. The number of features also does not have a decisive influence on the quality of the model (ELSNER, 2019). The minimal best model (with an F-Measure of 0.96) contains the 50 most important features, which are dominated by roughness LSP and especially by LSP presenting height difference or distance to channels calculated on a smaller scale. The slope itself does not matter here. In future calculations for creating further improved models, the focus could thus be specifically placed on the more important roughness and distance LSPs, and the computing time could significantly be reduced by determining the optimal settings of only a few sensitive model parameters (ELSNER, 2019).

The validation of the automated methodology was carried out by comparing the results of applying the classification model to the area of Tyrol with results from existing manual mapping (ELSNER et al., 2015, HEINISCH et al., 2015). This qualitative comparison shows that classified landslide lines can be found mainly and in every mapped area, but a complete linear delineation could not be achieved anywhere. This is probably above all due to the object of investigation itself, namely the complex interaction of natural processes and the thus very different manifestations of the indicator landforms. The small reference dataset, in relation to the study area, and the sources of error within this dataset, as well as the remote sensing data basis, which could detect smaller landforms with an even higher resolution, are other factors which can be influenced. Furthermore, from the very large number of curvature lines in Figure 2, it can be observed that a notable filtering is carried out in the area of anthropogenic edges and natural structures which are not connected to

large-scale landslides, by the selection according to the classification. Especially curvature lines in the areas of rugged, rocky terrain are almost completely separated out (see the bottom of Figure 2). As already observed in the results of the automated structure detection, however, the less clearly visible and thus also less frequently automatically detected tension cracks, or other only slightly pronounced structures on the sliding mass, are very poorly detected, or are in part not detected and so are not classified as landslide lines at all. As can be seen on the right in Figure 2, the classified landslide lines are thus mainly landforms of prominent indicator landforms and, therefore, in addition to counterscarps, predominantly include delineating structures such as main scarps.

## Conclusion

On the basis of the methodology presented here, the automated detection and linear delineation of large-scale landslides from a high-resolution DTM is possible, as shown for the Province of Tyrol. Although no complete area boundaries are generated, convex, linearly describable landforms of large-scale landslides are automatically detected to a large extent, not only in the area of the boundary lines. Due to the automated procedure, the results form a more replicable and objective basis for natural hazard management than purely manual mappings do, even though these classified landslide lines still have to be manually examined and the area boundaries of large-scale landslides need to be completed to form polygons. Therefore, the fragmentary detection and precise location can be seen as clear simplification measures on the level of indication that remote sensing data analysis generally provides. Thus, in addition to increased transparency and replicability, more efficient detection in the future is made possible through the overall semi-automatic approach of the WLV-MB project.

## Acknowledgement

Sincere thanks go to the very dedicated experts PD Dr. Florian Haas, Dr. Michael Lotter, Dr. Gertraud Meißl, Mag. Michael Mölk, Prof. Dr. Michael Moser, Dr. Marc Ostermann, Dr. Thomas Sausgruber, Prof. Dr. Johann Stötter, Dr. Thomas Strauhal and Dr. Thomas Zieher, whose mappings were used as the basis for generating the reference data, which is vital pre-requisite for developing this methodology.

## References

Belgiu M. and Drăguţ L. (2016). Random forest in remote sensing: A review of applications and future directions. *ISPRS Journal of Photogrammetry and Remote Sensing* 114: 24-31.

Elsner B. (2019). Methodik zur automatisierten Erfassung und Abgrenzung großdimensionaler Massenbewegungen aus hochaufgelösten Geländemodellen für Tirol. Master-Thesis. Leopold-Franzens-Universität Innsbruck.

Elsner B., Mölk M., Jenner A., Küfmann C. (2015). Erfassung und Bewertung großdimensionaler Massenbewegungen aus hochauflösenden digitalen Geländemodellen –

Entwurf zur Integration in den Wildbach- und Lawinenkataster (WLK). Journal - Verein der Diplomingenieure der Wildbach- und Lawinenverbauung Österreichs 175: 48-63.

Gregorutti B., Michel B., Saint-Pierre P. (2017). Correlation and variable importance in random forests. *Statistics and Computing* 27: 659-678.

Heinisch H., Pestal G., Reitner J. M., Ahl, A. (2015). Geologische Karte der Republik Österreich 1: 50 000 - 122: Erläuterungen zu Blatt 122 Kitzbühel. Geologische Bundesanstalt Wien.

Hungr O., Leroueil S., Picarelli L. (2014). The Varnes classification of landslide types, an update. *Landslides* 11: 167-194.

Land Tirol – Amt der Tiroler Landesregierung, Abteilung Geoinformation (2011). ALS-DGM der Gesamtbefliegung 2006-2010 mit der Auflösung von 1m. ASCII-Raster.

Moser M., Amann F., Meier J., Weidner S. (2017). Tiefgreifende Hangdeformationen der Alpen – Erscheinungsformen – Kinematik – Maßnahmen. Springer Spektrum.

Rutzinger M., Maukisch M., Petrini-Monteferri F., Stötter J. (2007). Development of algorithms for the extraction of linear patterns lineaments from airborne laser scanning data. *Geomorphology for the Future*: 161-168.

---

# Driftwood and Hybrid Debris Barrier Interactions: Process of Trapping and Prevention of Releases during Overtopping

Toshiyuki Horiguchi<sup>1</sup>, Guillaume Piton<sup>2</sup>, Muhammad Badar Munir<sup>3</sup>, Vincent Mano<sup>4</sup>

**Keywords:** debris flood, hybrid barrier, open Sabo dam, trapping effect, Discrete Element Method

## Abstract

This study presents a new concept of debris barrier based on an experimental application to the Combe de Lancey stream (Villard-Bonnot, France). In 2005, 20,000 m<sup>3</sup> of gravels and large wood (LW) were transported and deposited. A debris basin was designed to trap sediment and LW supplied by extreme events while letting routine bedload transport to pass through. Here, hybrid barrier was successfully tested to achieve this dual objective. A short description of the catchment and proposed barrier is presented. Its trapping efficacy was also examined with a small-scale model. These laboratory observations were used to calibrate a numerical Discrete Element Model that to study processes driving LW entrapment and release. It highlights that a high accumulation of LW may occur on barriers. When water overflowed the barrier above a critical depth, the overtopping of massive LW was observed. To prevent it, a rack was tested and proved sufficient.

## Introduction

During extreme debris flow and debris flood events, large wood (hereafter, LW), i.e., wood pieces longer than 1 m and thicker than 0.1 m, are often recruited along with high volumes of sediment. Such wood- and sediment-laden high discharges regularly damage downstream settlements. Closed Sabo dams had long been used as a preferred counter-measure for trapping sediment (Mizuyama 2008). However, a lot of LW may overflow such structures during disastrous events (Piton and Recking 2016). More recently, open Sabo dams, i.e., permeable structures, are increasingly implemented. They are supposed to possess better selectivity on sediment trapping, better trapping efficacy of LW and lower maintenance cost because of their ability to transfer fine sediment naturally (Shima et al. 2016). However field surveys report that some structures did not work as expected, e.g., slit dams did not self-cleaned because of large wood jamming at the openings (Mizuyama 2008). Although debris basins are created mainly for sediment trapping, LW regularly

---

<sup>1</sup> Dr., National Defense Academy, Japan, ([debrisregregation@gmail.com](mailto:debrisregregation@gmail.com))

<sup>2</sup> Dr., Univ. Grenoble Alpes, INRAE, ETNA, France

<sup>3</sup> Univ. Grenoble Alpes, INRAE, ETNA, France

<sup>4</sup> Dr., ARTELIA Eaux Et Environnement, France

affects the functionality of these hydraulic structures (Shima et al. 2015, Piton and Recking 2016). LW may be trapped by hydraulic structures during the rising limb of hydrograph, disrupting its functioning. In addition, a massive part of LW may eventually be released by overtopping the structures.

This paper is based on a case study of the Ruisseau de la Combe de Lancey, located in the Isère valley, north of Grenoble (France). The stream's alluvial fan is fully occupied by the Villard-Bonnot municipality, particularly by an old paper mill where the development of a new residential area is in progress. Protection of the whole area is mandatory before the construction of new settlements. Past studies demonstrated that a retention basin was the best option (SOGREAH 2006). Its best location would be slightly downstream of the fan apex (Fig. 1a), where most of the deposit occurred in 2005 during a large flood. Designing a retention basin in a city center needed a detailed analysis which has been performed using small scale modelling (ARTELIA and IRSTEA 2018). A particular challenge addressed in this case study was to design a debris basin with robust functioning regarding capacity to transfer small events and prevention of LW overtopping. Piton et al. (2019) demonstrated that the selected design achieved satisfying sediment trapping efficacy.

The main objective of this paper is to examine trapping effect on LW by the barrier and the drivers of potential release of LW downstream. Two design events were tested in the small-scale model with different peak discharges. LW releases were observed during the higher peak discharge. A rack was added on the initial barrier to prevent the release (compare Fig. 1c & d) and it gave satisfactory results. After a short description of the case study, this paper first reports the small scale experiment results. These results were secondly used to calibrate a Discrete Element Model (hereafter, DEM) of the barrier to finally examine which parameters drive trapping and release of LW at a barrier through virtual repetitions of the flume experiment.

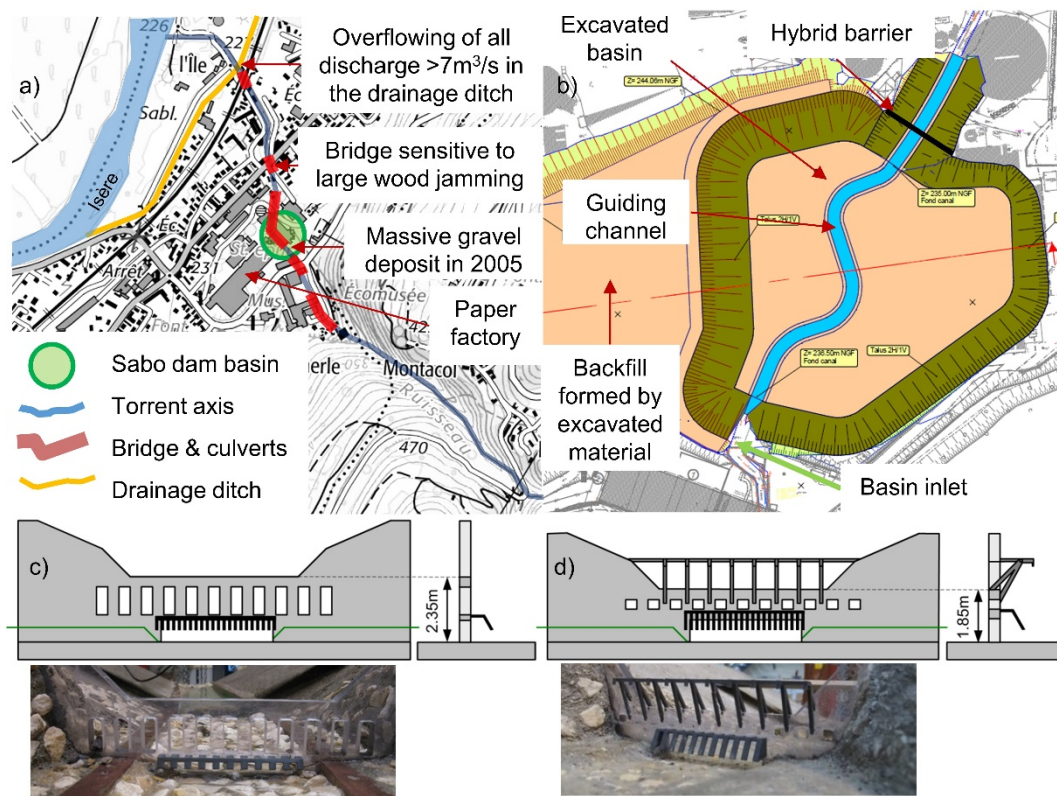


Figure 1 a) map of the alluvial fan and main hazardous points, b) zoom on the retention basin and location of the main structure, c) first version of the hybrid barrier called “initial barrier” (drawing and scaled version pictures) and, d) improved version of the hybrid barrier called “improved barrier” (drawing and scaled version picture), structure lowered but equipped with a rack

## Case study description

A full description of the rarely active, 18 km<sup>2</sup> catchment can be found in Piton et al. (2019). On Aug. 21st and 22nd, 2005, a long lasting flood transported and deposited 20,000 m<sup>3</sup> of sediment onto the fan (Fig.1a). SOGREAH (2006) demonstrated that sediment and LW trapping was required to protect the village: downstream channel has insufficient hydraulic capacity and several bridges are prone to be jammed by LW. The debris basin should ideally be a large excavated basin located where debris deposition occurred in 2005 (Fig.1b). State-of-the-art hydrology enabled to define peak discharges:  $Q_{30\text{years}} \approx 22 \text{ m}^3/\text{s}$  and  $Q_{100\text{years}} \approx 35 \text{ m}^3/\text{s}$  (SOGREAH 2006). The extraordinary long duration of the 2005 event was studied by Piton et al. (2019). They concluded that although the peak discharge was close to the 1:30 years return period, the bivariate statistical analysis of peak discharge and duration falls within the  $\pm 20\%$  uncertainty range around the 1:100 year exceedance probability when accounting for decreasing discharge for increasing duration, i.e., the bivariate time return for both events was somewhat equivalent. Several flood scenarios were thus defined: (i) the 2005's disaster, hereafter referred to as “Q100L” with peak discharge 22 m<sup>3</sup>/s and a long duration of 30 h, as well as (ii) a shorter and more typical 1:100 years return period of debris flood, “Q100s”: peak discharge 35 m<sup>3</sup>/s and duration of 18 h. Both events were tested using small scale model and then reproduced in DEM.

Other events with higher solid concentration, bigger sediment supply or coarser grain sizes were also tested in the flume to check the robustness of the structure functioning regarding varying events or return periods. The barrier proved very robust to the variability of events (Piton et al. 2019).

## Flume experiments: model description

A 1:40 scaled model of the basin with a length and width of about 3.0 m was built (Fig. 1c-d). A 56 mm high hybrid barrier was installed at the outlet. Its detailed design is presented in Piton et al. (2019). The sediment mixture was composed of poorly sorted sand and gravels of diameter 1-13 mm. Multiple high waterfalls and pools are located in the gorge immediately upstream of the alluvial fan. Flow energy in this area is capable to break tree crowns, trunks and root wads. Field survey demonstrated that only LW of a few meters, i.e., no whole trees, was found approaching the fan. Archived pictures from 2005 and another event in 1939 confirmed this point. LW was consequently added to both runs as mixture of thin (diameter: 1 mm, length: 40 mm, number: 764) and the thick wooden logs (diameter: 5 mm, length: 40 mm, number: 122). Logs were fresh branches and needles of pine tree. LW was not soaked prior to experiment. LW was introduced manually during the rising limb of the hydrograph, starting when discharge overpassed the 10 years return period (15 m<sup>3</sup>/s at prototype scale).

## Flume experiments: model results

Flow depth was measured directly upstream of the barrier. It reached  $h_w = 81$  mm above bed at peak flows during run Q100L and  $h_w = 86$  mm during run Q100s. In both runs, sediment filled the basin progressively. The deposited front eventually reached the barrier at the end of the runs demonstrating full entrapment of sediment. At the beginning of both runs LW was efficiently transported and accumulated against the barrier. It progressively clogged the orifices thus increasing water depth at the barrier; as a consequence the flow rapidly overflowed the spillway.

As shown in Fig. 2a, nearly all LW was trapped by the barrier during run Q100L, even at peak discharges (22 m<sup>3</sup>/s at prototype scale). LW formed a thick jam, tightly entangled at the barrier and kept piling up even though overflowing depth (20-25 mm) was much higher than average log diameter (1 or 5 mm). Under such conditions, the average velocity of the approaching flow was 0.10 m/s.

The close packing against the barrier was also observed during the first steps of run Q100s. The cross sectional average velocity was approximately 0.17 m/s. When discharge approached 34 m<sup>3</sup>/s at prototype scale, i.e., nearly peak flows of 35 m<sup>3</sup>/s, most of the LW jam was suddenly released in two bursts (Fig. 2d, f & h).

Such sudden releases of most of LW should be prevented because bursts of LW flowing in congested mode increase dramatically the likelihood of bridge jamming (Gschritzer et al. 2017). An improved design with a rack added on the spillway was thus proposed (compare Fig. 1c for initial barrier and Fig. 1d for improved barrier). Racks on open SABO dams have usually an angle below 90° with horizontal (Piton & Recking. 2016). This enables

drag forces to push LW forward, thus giving room to flow to pass through the rack. However, it somehow prevents the tight entanglement between pieces and the barrier, which, in the present case, is desirable because it holds the LW in the structure. Therefore, the rack was designed with a negative slope (angle with horizontal  $113^\circ$ , see Fig. 1d) with sort of hooks on top. Its function is to keep LW in the basin even when water depth overtopped it. The negative slope angle has the twofold advantage to better stabilize the LW jam and to have a 20% higher surface, thus hydraulic capacity, than a vertical structure.

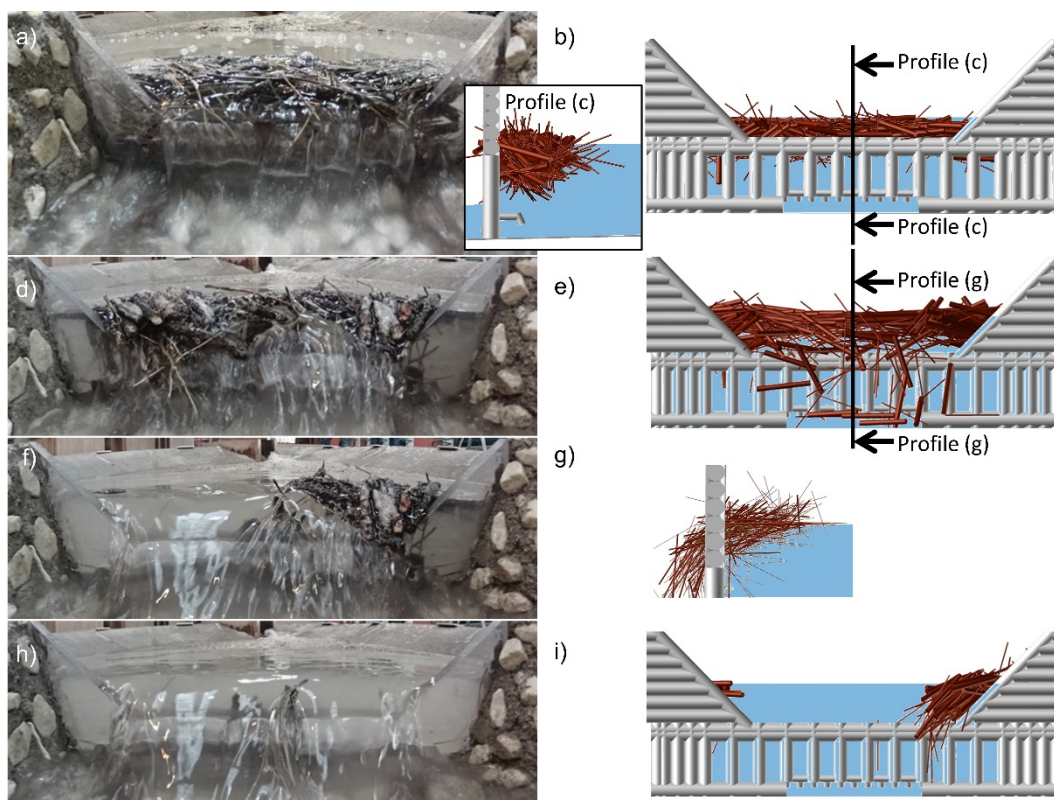


**Figure 2** a) LW accumulation at the peak flow for the run Q100L, overflowing but no overtopping of log pieces, b) same situation modelled by DEM with linear free surface model, c) side view of image (b), d) LW accumulation just before release during run Q100s, e) starting of release during run Q100s modelled by DEM with horizontal free surface model, f) more than half of the accumulated wood was released, fast flow overtopping the barrier, g) side view of image (e), h) full release of floating elements in run Q100s and i) same situation modelled by DEM

Run Q100s was repeated with the improved barrier demonstrating that although a few pieces eventually passed through the rack, no more massive releases were observed and trapping conditions became satisfactory.

## DEM analysis: model description

A numerical analysis was performed to understand the process of LW over topping at the barriers. It was calibrated on the small-scale model and then a parametric study was performed. The coupled DEM-fluid model developed by Horiguchi et al. (2015) was used to reproduce the initial and improved barriers (Fig. 3a & c). Logs were computed as cylindrical elements with same size as LW used in the flume experiment. The model solves

the Newton equations for LW, including drag forces. The flow model is a simplified fluid dynamics model where the free surface profile is forced according to measurements performed in the flume. Two free surface models were used: in a first step, the free surface profile was simplified as horizontal until the barrier (Fig.3b). In a second step, a linearly decreasing free surface profile was incorporated (Fig. 3d). In the present work, velocity is uniform in the section, computed based on water discharge and wetted section and sediment is not included.

## DEM analysis: parametric sensitivity analysis

Run Q100L was repeated only for the initial barrier. Run Q100s was tested for both the initial and the improved barrier (Table 1). Logs were initialized in random arrangement in the reach immediately upstream of the barrier. The approaching flows dragged the logs toward the barrier and reproduced their entanglement (Fig. 2).

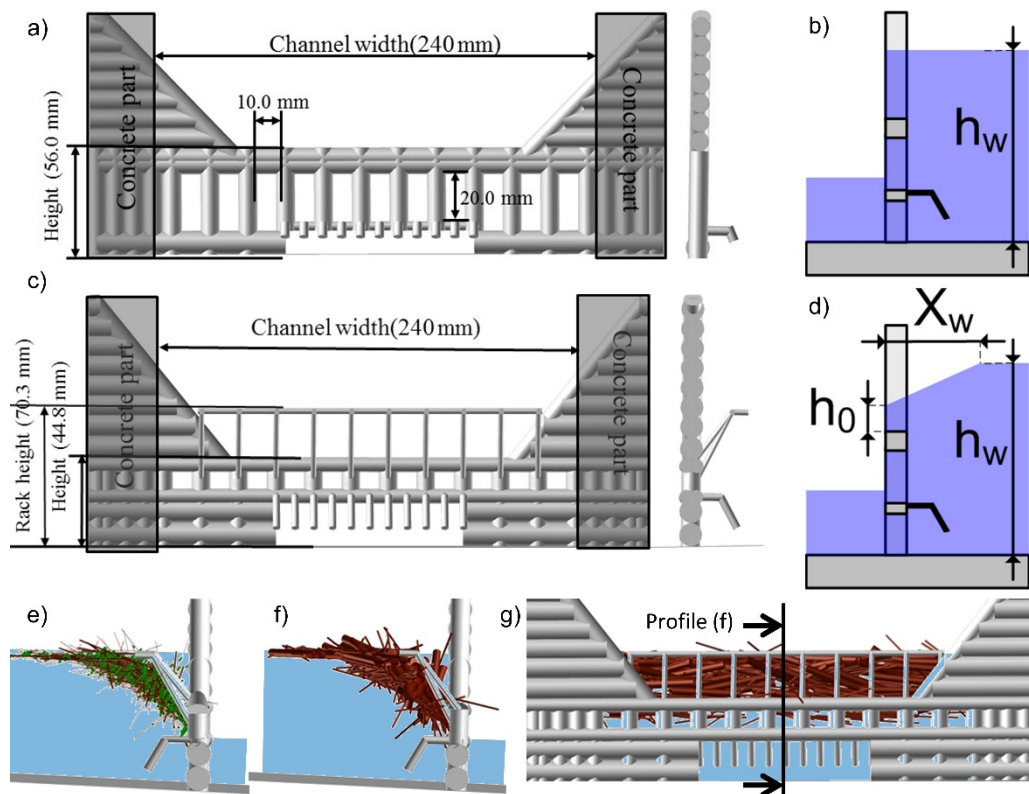


Figure 3 a) upstream and side view of the initial barrier, b) concept of simplified hydraulic free surface longitudinal profile with horizontal hypothesis, c) upstream and side view of the improved barrier, d) concept of longitudinal profile of hydraulic free surface with linear hypothesis, e) side view of contact points within the accumulation for run Q100s, f) side view of accumulation, trapped by improved design for same instant and, g) downstream view for same instant.

As shown in Figure 2, the numerical model accurately reproduced the accumulation arrangement. The overtopping of LW for run Q100s occurred first centrally and secondly near wings, consistently with flume experiment. However, the lack of overflowing during run Q100L was correctly reproduced for water depth  $h_w \leq 76\text{mm}$ , for  $h_w > 76\text{mm}$  LW

overtopped the barrier (Table 1) when using the horizontal flow model, i.e., for a water depth 4 mm lower than in the flume. A parametric analysis with virtual runs (herein, called V\_Q\*\*) was undertaken to find how to improve the model. Numerical values of tested parameters are provided in Table 1. The next section describes the results qualitatively.

**Table 1** Analysis case and outline of result

Run name	Barrier design	$h_w$ water height [mm]	$V_w$ water velocity m/s	$\rho_w$ (LW density)	Objective of the run	Outline of result
Q100L low	Initial	66-76	0.10	0.5	<i>Calibration: Check consistency of DEM with flume</i>	<i>DEM similar to flume</i>
Q100L	Initial	77-81	0.10	0.5		<i>DEM overtopping of LW: inconsistent with flume</i>
Q100s	Initial	86	0.17	0.5		<i>DEM similar to flume</i>
V_Q100L.Fast	Initial	76	<b>0.17</b>	0.5	<i>Check influence of approaching mean water velocity</i>	<i>No influence (no overtopping)</i>
V_Q100s.Slow	Initial	<b>86</b>	0.10	0.5		<i>No influence (overtopping)</i>
V_Q100.Heavy	Initial	86	0.17	<b>0.7,0.9,1.06</b>	<i>Check how wood density influences wood overtopping</i>	<i>Density of less than 1.0 had no influence. Logs with density of 1.06 sink and cannot overtop the barrier.</i>
V_Q100L.linear	Initial	81	0.10	0.5	<i>Check influence of approaching velocity profile</i>	<i>DEM similar to flume</i>
V_Q100s.linear	Initial	86	0.17	0.5		<i>DEM similar to flume</i>
Q100s	Improved	86	0.17	0.5	<i>Validation: Check consistency of DEM with flume</i>	<i>DEM similar to flume</i>
V_Q100s.linear	Improved	81	0.10	0.5	<i>Check influence of approaching velocity profile</i>	<i>DEM similar to flume</i>

One possible hypothesis was that LW overflowed in run Q100s as well as in run Q100L because of the excess in drag force related to the approaching flow velocity. Two cross-control virtual runs were launched to check it. During run V\_Q100L.Fast, flow velocity was forced as same value of run Q100s, nonetheless no log release was observed demonstrating that velocity is of secondary importance. A symmetric case was tested with run V\_Q100s.Slow where velocity was decreased to the value of run Q100L, nonetheless LW were released as the previous result in Q100s. We concluded that although approaching velocity increases drag force and probably accumulation density, it is not the main triggering factor of the LW release.

Another possible parameter to drive LW overflow can be their floatability that is controlled by the density (Furlan, 2019). Runs with increased densities (Table 1 run V\_Q100.Heavy) demonstrated that floating logs i.e. LW with density  $<1$ , gave similar results as in the previous cases with density of 0.5. Thus, density also appears of secondary importance in our case study with high amount of logs tightly entangled.

For the sake of simplicity, the free surface model was initially set horizontal until passing the barrier (Fig. 3b). This hypothesis could be responsible of our overestimation of LW overtopping by overestimating buoyancy force at the crest. Additional flume runs were performed to measure more precisely the free surface profile. It was later simplified in a linear model (Fig. 3d) with parameter  $X_w$  set at 0.033 m and  $h_0$  at 0.010 m. Once implemented in the DEM, it computed the overtopping of LW for  $h_w = 81$  mm consistent with the flume (Table 1 runs V\_Q100L.linear). LW were also correctly released for run Q100s. DEM approach was then considered reasonably calibrated.

Finally, when the crest rack of the improved barrier (Fig. 1d) was numerically tested (Fig. 3e-g), it achieved similar results as the small-scale model, i.e., a few logs passed through the rack but the LW mostly remained trapped by the barrier.

## **Discussion: driving processes of LW accumulation and release**

This section discusses the preliminary lessons learnt from this dual analysis with small-scale modelling and DEM. It is interesting to note that Furlan (2019) demonstrated that when flow depth is more than 1-2 times log diameters, LW is usually not trapped on reservoir dam spillways. Conversely, we observed LW jams are stable until flow depth reached 5-6 times log diameter. Compared to the experiments by Furlan (2019), we used higher volumes of LW and a time-dependent overflowing related to hydrographs. LW jams were progressive with partial passing through the openings. When trapped through openings, logs are very stables and become fixed points upon which the jam piles up. Friction between logs in the flume and in DEM, where friction angle between logs is set to  $22^\circ$ , stabilized the jam. DEM computes and enables us to draw contact forces, i.e., interactions between LW pieces. Very complicated chain force networks emerged when several logs slid and piled up on each other. Fig. 3e displays for instance a side view of the central barrier cross-section. Chain forces are highlighted by LW thickness: the thicker the log, the more numerous are contact points with other logs or with the barrier. The resulting load of LW on barrier had a downward direction. Further works should be dedicated to study the magnitude, location and direction of the resulting loading and stress concentration.

For run Q100s with the initial barrier, the accumulated LW overflowed the structure. Before accumulated LW burst and overtopped the barrier, flume experiment showed that LW slowly and progressively migrated over the barrier. Small rearrangements of LW resulted from distinct downward flow, increasing the accumulation compactness and pulling the logs towards the bottom and impacts of upstream approaching logs. The chain forces thus kept on varying randomly. Increase in flow depth also decreased LW contacts

and load transfer with the barrier due to LW buoyancy. At some point, friction between logs and load transfer on the barrier no longer exceeds buoyancy plus flow drag and the accumulation bursts downstream (Run Q100s: Fig. 2).

The rack on the crest prevents this progressive overtopping and rearrangement by providing solid supports to any LW approaching the crest. Massive amount of LW was thus gathered above the barrier. The rack also holds part of LW buoyancy force and drag force. Loading is different in both the initial and improved design. Further works will be dedicated to study load diagram, stress distribution as well as resulting forces and structural design.

It is worth stressing that simple cylindrical elements were used in both the small-scale model and the DEM to model LW for the site-specific reasons as explained above. In field applications where LW with branches, crowns and root wads may be encountered, one should expect higher stability of jams but also denser jam because of small particles like leaves and small branches, which can result in higher head losses and overtopping depth for same discharges.

## Conclusion

We analyzed trapping effect of LW and its release at open Sabo dams. Results from a small-scale physical model enabled calibrating a DEM approach. In both models, it was observed that LW might accumulate in jams with thickness equivalent up to 5 times log diameters. Their entanglement, interactions between elements and with the barrier crest hold them upstream of the barrier. At some point, when discharge and head losses are such that flow depth over the crest reaches a critical value, LW jams may burst and be suddenly released. Adding a rack at the crest enabled to prevent such releases.

## Acknowledgements

The authors would like to thank the Villard-Bonnot municipality for allowing the study results to be re-used in this paper as well as the two anonymous reviewers who provided very constructive comments and helped us improving this manuscript.

## References

- ARTELIA & IRSTEA. 2018. Etude de l'Aménagement d'une Plage de Dépôt sur le Torrent de la Combe De Lancey - Site des Anciennes Papèteries de Villard Bonnot - Rapport de Modélisation Physique. Ville de Villard-Bonnot.
- Furlan, P. 2019. Blocking probability of large wood and resulting head increase at ogee crest spillways. PhD dissertation, EPFL (Lausanne) and IST (Lisboa), 160 p.
- Gschnitzer et al. 2017. Towards a robust assessment of bridge clogging processes in flood risk management. *Geomorphology*, 279:128-140
- Horiguchi et al. 2015. A Basic Study on Protective Steel Structures against Woody Debris Hazards. *International Journal of Protective Structures* 6:191–215.

Mizuyama. 2008. Structural Countermeasures for Debris Flow Disasters. *International Journal of Erosion Control Engineering* 1(2):38–43.

Piton et al. 2019. Design of a debris retention basin enabling sediment continuity for small events: the Combe de Lancey case study (France). Proc. 7th Int. Conf. on Debris-Flow Hazards Mitigation: Mechanics, Prediction, and Assessment, 1019-1026

Piton & Recking. 2016. Design of sediment traps with open check dams. II: woody debris. *Journal of Hydraulic Engineering* 142:1–17.

Shima et al. 2015. Consideration on boulders & members' interval of open type steel sabo dam for capturing debris flow. *Journal of the Japan Society of Erosion Control Engineering* 67(5):3-11

Shima et al. 2016. Prevention and mitigation of debris flow hazards by using steel open-type sabo dams. *International Journal of Erosion Control Engineering* 9(3):135–144.

Sogreah 2006. Etude de Diagnostic et d'aménagement Hydraulique du Bassin Versant du Ruisseau de la Combe De Lancey. Technical report. Commune de Villard-bonnot

---

# Evaluation of river Gail flood retention system after the flood 2018: experiences and limits

Gernot Koboltschnig<sup>1</sup>, Erwin Schumi<sup>2</sup>, Christian Kopeinig<sup>3</sup>

**Keywords:** event documentation, flood retention, practical recommendations

## Abstract

In this paper we would like to report on the analysis and evaluation of a flood event in October 2018 at river Gail in Austria (total catchment area 1.400 km<sup>2</sup>) with a focus on the experiences, advantages but also the limits of flood retention. As flood retention already has a long tradition at river Gail and the last conceptual adaptation took place after huge floods in the 1960ies, the flood event in October 2018 was the first practical test. The October 2018 flood is of interest as it on the one hand has shown that retention can massively lower peak runoff downstream and therefore is substantial to protect settlements with the highest damage potential along the river Gail. On the other hand, the event has shown the limits in the case of an overload. Furthermore we can confirm that assumptions for hazard mapping were correct, especially concerning scenarios of tributaries' runoff contribution and assumptions concerning the consideration of bedload.

## Introduction

As several devastating floods happened in the past, already in 1935 it was started to adapt classical linear protection measures to a retention system with several basins. After huge floods in 1965 and 1966 the flood retention system has again been re-adapted from the 1970ies on and still nowadays retention is the primary structural measure for flood protection (Poglitsch et al., 2001). The retention system comprises 26 basins with retention volumes between 0,13 and 6,76 Mio. m<sup>3</sup> at HQ30 and 0,21 and 12,94 Mio. m<sup>3</sup> at HQ100. All in all, the potential retention is 24,5 Mio. m<sup>3</sup> at HQ30 and 57,5 Mio. m<sup>3</sup> at HQ100. These volumes have been calculated using a 2d-hydraulic model based on a 1x1 m laser-scan and 50 m cross-section terrestrial surveys (Porzer, 2017). Earlier calculations, which have been applied during a study in the mid 1990ies, were modelled with a 1d-hydraulic model based on terrestrial surveys, have shown a total retention volume of only 38 Mio. m<sup>3</sup> at HQ100. Besides retention pools, the flood protection system furthermore consists of longitudinal dams along the stream to avoid an early filling of basins, of ring-dams around villages and transverse dams at sensitive sections to revert flood plain flows into the riverbed. All basins are designed to be filled via bypasses from downstream up against

---

<sup>1</sup> Dr., Regional Government of Carinthia, Austria, (Gernot.Koboltschnig@ktn.gv.at)

<sup>2</sup> Ing., Regional Government of Carinthia

<sup>3</sup> Dipl.-Ing., Regional Government of Carinthia

normal flow direction without technical equipment. The emptying – after the flood event – happens generally automatically.

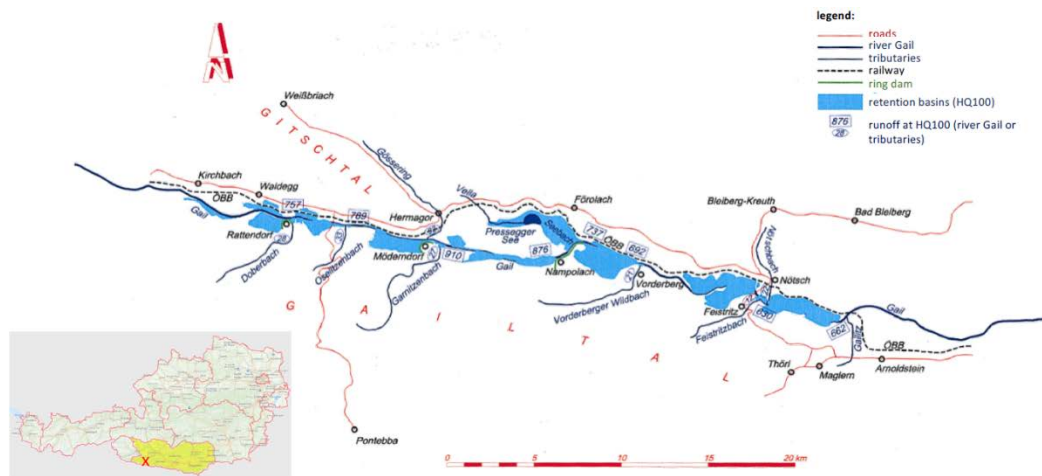


**Figure 1: Flood retention system at river Gail.**

Within a cost-benefit analysis (Prettenthaler et al., 2009) it was shown that during 40 years (from 1971 to 2008) the investment of 60 Mio. Euro - which is the capital stock of all structural measures including maintenance – induced a protection and development (increase of building value, industry and production in flood protected area) of 570 Mio. Euro. The main positive effect of the flood retention was gained downstream for the city of Villach.

## The flood in October 2018

In October 2018 a huge flood event was triggered in Carinthia (the southernmost region of Austria) by a rainfall event with up to 800 mm precipitation within five days (Moser et al., 2019). As the precipitation was driven and combined by strong warm winds from the south all catchments received (untypical for the late fall season) only rainfall without snow even in the elevated more than 3000 m a.s.l. high catchment areas. Luckily, snowmelt did not contribute to runoff, as catchments were nearly snow free. As the catchments were quite dry at the beginning of the precipitation, runoff reacted quite slowly and e.g. at the gauging station Rattendorf at river Gail (350 km<sup>2</sup> catchment area) HQ<sub>1</sub> (147 m<sup>3</sup>/s) was reached one day after rainfall started. Within this time already up to 270 mm of precipitation were observed (rainfall gauge at Plöckenpass).

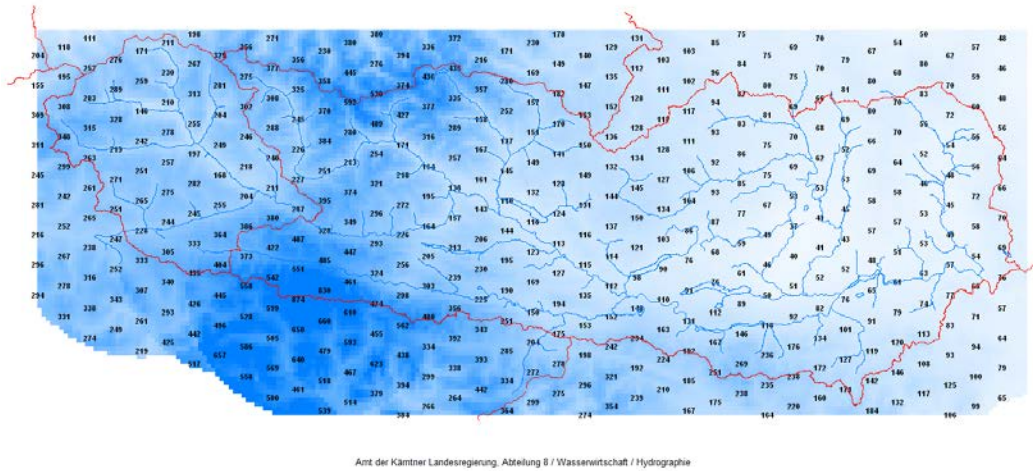


Figure 2: Map of 5-day precipitation between 26 and 31 October 2018 (Moser et al., 2019).

The huge amount of rainfall triggered at one section a flood peak of about 820 m<sup>3</sup>/s, which reached more than HQ100. As the flood wave has been reduced by retention, downstream close to the mouth of river Gail, peak runoff was only 640 m<sup>3</sup>/s (HQ12). The Water Management Administration of the Regional Government of Carinthia is running a flood forecast system, in which the river Gail catchment is implemented. As in such small catchments a hydrologic model is very much dependent on good precipitation forecasts, a flood forecast is quite tricky. But nevertheless already 1,5 days before the event a peak runoff of HQ30 has been forecasted for river Gail. The second part of the rainfall event was triggered by a foehn storm. Therefore, the rainfall amount was complicated to be forecasted but the most intensive rainfall happened only regionally.

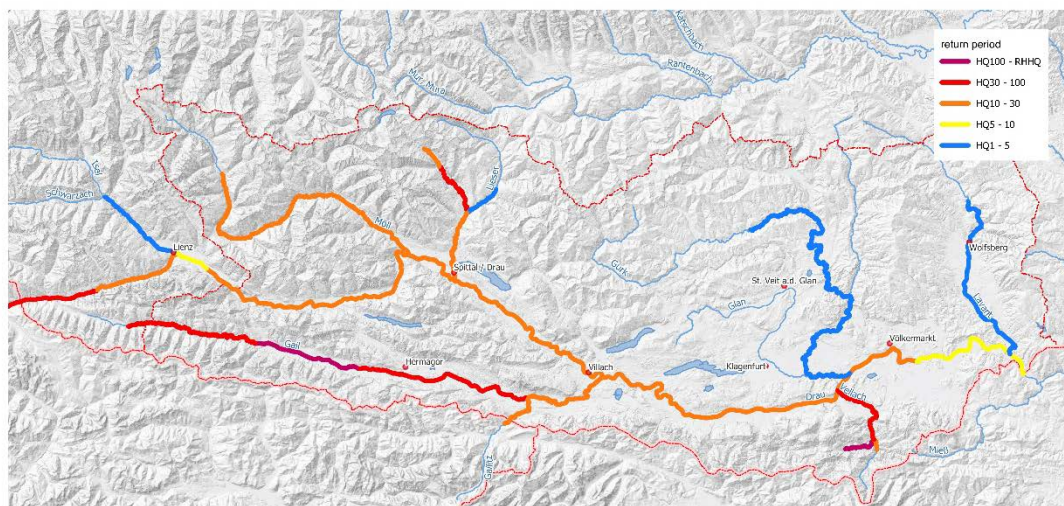


Figure 3: Map of main rivers in the region of Carinthia showing the return period of the flood in October 2018 (Moser et al., 2019).

## Case Study 1 – best practise retention

The biggest retention basin along river Gail is a natural lake (Pressegger See, see map in Figure 1), which is filled during floods via its draining creek in the opposite flow direction. The potential retention volume at HQ100 was calculated as 12,94 Mio. m<sup>3</sup>. At the flood event in October 2018 the retention basin Pressegger See was filled with 5,55 Mio. m<sup>3</sup> water coming from river Gail and additionally 2,45 Mio. m<sup>3</sup> coming from the catchment area around the basin (about 50 km<sup>2</sup>). This led to an increase of the water level of 2,6 m above normal water level. A hydrologic and hydraulic recalculation (based on a 2d numeric model, Kirnbauer, 2019) has shown that during 18 hours more than 50 m<sup>3</sup>/s with a maximum of 90 m<sup>3</sup>/s flew into this retention basin.

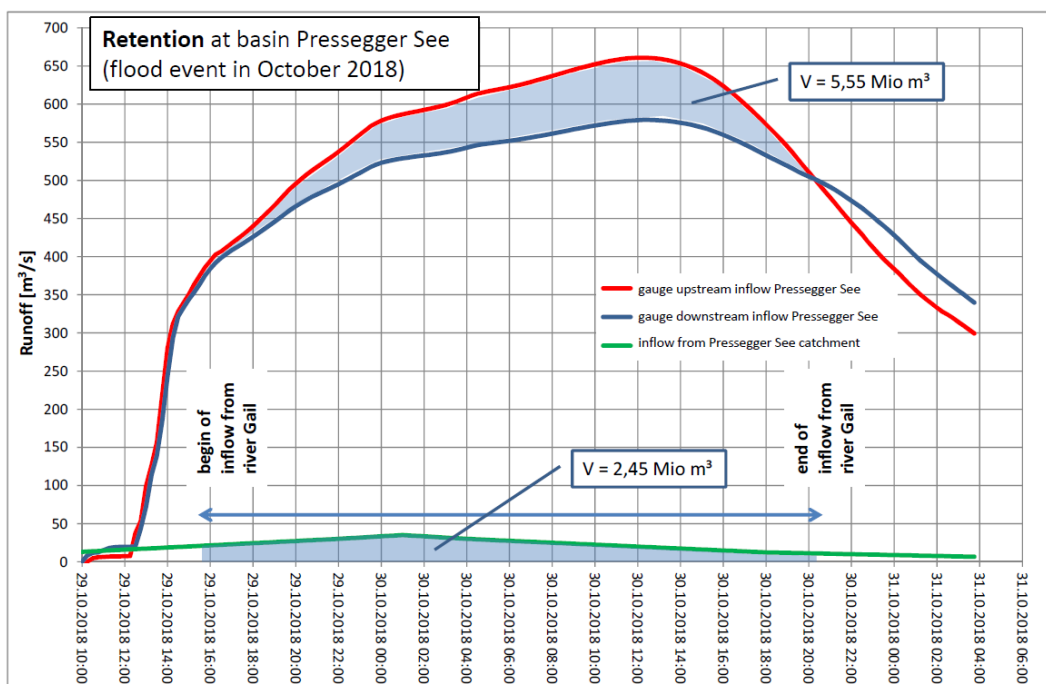


Figure 4: Retention volume at basin Pressegger See during the flood in October 2018.

Just a few years ago a new weir was installed at the outlet of the retention basin Pressegger See to accelerate the outflow after a flood event. The inflow happens over a long dam section and the outflow was originally designed to go through pipes added with floodgates. After the re-design the weir is regulated by gauges up- and downstream. Despite of smaller damages due to the intensive hydraulic load at the inflow section, this retention basin worked exactly as it was planned. Although we faced a huge flood event in October 2018 at the retention basin Pressegger See, additional 5 Mio. m<sup>3</sup> retention volume would have been available for further flood water.



Figure 5: Filling and emptying of the retention basin Pressegger See during the flood event in October 2018.

## Case Study 2 – limits of retention system

Another retention basin is situated at the village of Rattendorf (see map in Figure 1). It has a calculated retention volume of nearly 2 Mio. m<sup>3</sup> at HQ100 and has been designed to be filled by a channel (Cerim creek), which under mean flow conditions of river Gail would drain the area. Hence, as at the inflow section no further technical equipment is installed, the filling already starts at floods far below HQ10. During the flood wave in October 2018 the retention basin Rattendorf has already been filled partly in the foreseen way by the Cerim creek. Nevertheless, at a runoff of about 690 m<sup>3</sup>/s in the Gail river bed a 150 m long section of the longitudinal dam upstream, which encloses the retention basin, broke due to the massive hydraulic load so that a huge amount of water went directly into the retention basin (see Figure 6). During the event analysis it was found out (Tschernutter, 2019), that the dam brake did not happen because of an over flow. Drift wood accumulated at a bridge and led the main stream directly towards the dam. Although the lower dam section was enforced with rocks, which reached below the river bed, the shear stress was too big and eroded the dam. The breach went stepwise bigger during the flood. The maximum runoff through the breach was calculated as nearly 470 m<sup>3</sup>/s, whereas the runoff in the riverbed locally reduced massively. The hydraulic recalculation (based on a 2d-numeric model, Kirnbauer, 2019) resulted that the maximum runoff of river Gail at the section upstream of

the dam breach was about 820 m<sup>3</sup>/s. Consequently, the retention basin was filled with about 5,5 Mio. m<sup>3</sup> water. As the volume of water was more than the double volume compared to the designed volume, the ring dam, which was built to protect the village of Rattendorf was overtopped. 35 houses were flooded and about 400.000 m<sup>3</sup> of bed-load were deposited in the retention area. This not foreseen retention reduced the flood wave downstream with a maximum of about 300 m<sup>3</sup>/s. Nevertheless, to reduce further damage in the village, another longitudinal dam next to the village had to be opened by caterpillars to lead the flood water back into the Gail river-bed.

As we furthermore were interested, what would have happened if the longitudinal dam upstream of Rattendorf did not break, we recalculated this scenario using the 2d hydraulic model calibrated for the flood event in October 2018. For this scenario a part of the flood wave would have been retained in the left bank retention basin (opposite of Rattendorf). The main volume would have been flown into basin Presseegger See and another part of this volume into the downstream retention basin at Vorderberg. Already at the village of Nötsch, which is about 30 km downstream of Rattendorf, peak runoff would already have been at the same level as observed.

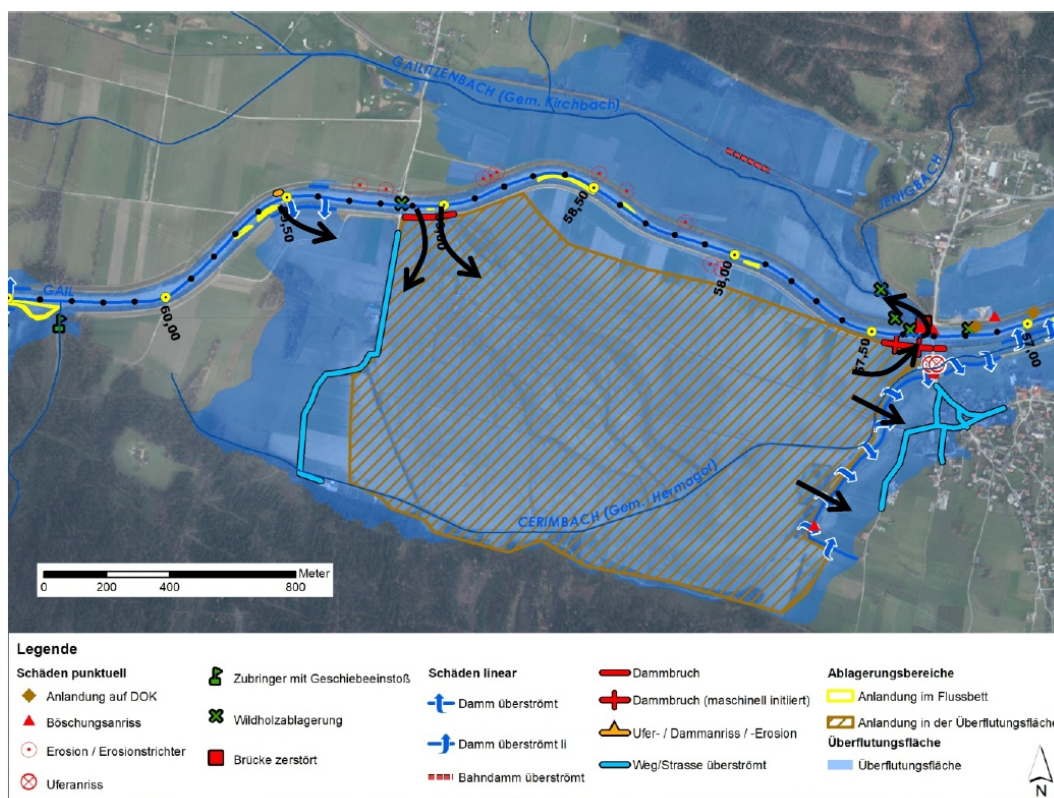


Figure 6: Retention basin Rattendorf.



**Figure 7: Flight image a few hours after the flood maximum.**

Using a hydrologic model, which was implemented in Carinthia for flood forecasts, we recalculated the flood event from October 2018. We then switched off the entire static retention a long river Gail. With that we wanted to find out what would have happened if in the past the flood protection system along river Gail would have been applied without retention but only with linear protection measures. For sure, this is not a realistic protection scenario, because an entirely channelized river would not be possible, but it was of interest to at least get an impression of negative effects downstream if no-retention was considered. For the city of Villach, which is situated downstream at the mouth of river Gail (39 km downstream of Pressegger See), the peak flow at the October 2018 flood event would have been  $1.200 \text{ m}^3/\text{s}$  without retention, which is nearly the double of the observed runoff (HQ300 instead of HQ12 observed).

## Conclusion

Right after the flood the Federal Water Management Administration began with immediate measures to repair the dam breaches. The deposited bed-load material and drift-wood had to be removed. Within a study the flood scenario has been hydraulically modelled to find solutions how to improve dams to guarantee safety and to keep the retention system. Within a detailed event documentation, it was possible to proof that water levels and flooded area simulated earlier with a 2d-hydraulic model were correct. We also found out that assumptions for hazard mapping were correct, especially concerning scenarios of tributaries' runoff contribution and assumptions concerning the consideration of bedload.

Although further dam sections and two bridges were destroyed along river Gail, only one village was directly affected by the flood but luckily without any casualties. Therefore, we

assume that retention as a central part of the river Gail flood protection system is still up-to-date and we will continue working to improve it.

## References

Kirnbauer R. (2019): Hydraulic recalculation of the flood event in October 2018 at river Gail. Report as contribution to the event documentation. Regional Government of Carinthia, Austria

Moser J., Kopeinig Ch., Gutschi E., Malle H., Koboltschnig G., Schober St., Kulterer K., Schabus V., Hofer W. (2019). Final hydrological report on the flood events at the rivers Drau, Möll, Gail and tributary rivers on 28-31 October 2019. Regional Government of Carinthia, Austria. <https://www.ktn.gv.at/Themen-AZ/Details?thema=11&subthema=58&detail=383>.

Poglitsch H. (2001). 125 years of flood protection at river Gail (125 Jahre Gailregulierung). Regional Government of Carinthia. 160 pp.

Porzer W. (2017). River development plan Gail (GEK Gail) - Analysis and Optimization of Retention. Regional Government of Carinthia, Austria.

Prettenthaler F., Amrusch P., Habsburg-Lothringen C., Köberl J. (2009). 40 years of flood protection at river Gail: determination of the protentional economical development. Report commissioned by BMLFUW, Regional Government of Carinthia and Interpraevent.

Tschernutter P. (2019): Detailed analysis of dam failures due to the flood event in October 2018 at river Gail. Report as contribution to the event documentation. Regional Government of Carinthia, Austria

---

# Meteorological and Hydrological Service in risk assessment and management of forest fire hazards in Croatia

Tomislav Kozaric<sup>1</sup>, Marija Mokoric<sup>2</sup>, Tanja Renko<sup>2</sup>

**Keywords:** forest fire protection; risk assessment; weather and climate

## Abstract

The most important role of the Croatian Meteorological and Hydrological Service (DHMZ) is the risk assessment of dangerous weather and hydrological events, such as floods, heat waves, forest fires etc. Forecasts and warnings are among the main products and responsibilities of the service. In the risk management of these natural hazards DHMZ cooperates with the Ministry of the Interior, mainly its Civil Protection Directorate, the Ministry of Defence, the Croatian Firefighting Association and other organisations participating in the protection and rescue of people and property.

This paper gives an overview of the key elements of cooperation between DHMZ and organisations involved in the protection and rescue. Special focus is given on the current activities of the service in the forest fire protection system, future cooperation in the risk management as well as on the development of meteorological tools for the forest fire risk assessment in order to mitigate the effects of this natural hazard.

## Introduction

Meteorological and Hydrological Service (DHMZ) is the official institution in Croatia that deals with risk assessment of dangerous weather or weather related disasters. One of the key roles of the service is issuing forecasts for the early warning system on dangerous weather phenomena. In case of extreme weather DHMZ cooperates with the Ministry of Interior, mainly its Civil Protection Directorate, the Ministry of Defence, the Croatian Firefighting Association and other organisations participating in the protection and rescue of people and property. With this organisations DHMZ has made a cooperation agreements and defined standard operating procedures (SOPs).

The climate analysis shows that the mean temperature in Croatia has been increasing with prominent positive trend since 1990s (Gajić-Čapka et al., 2010). Also, the extreme meteorological events, such as longer dry spells and heat waves, as well as higher

---

<sup>1</sup> Head of Weather Analysis and Forecast Verification Division, Croatian Meteorological and Hydrological Service, Ravnice 48, Zagreb, Croatia (tomislav.kozaric@cirus.dhz.hr)

<sup>2</sup> Croatian Meteorological and Hydrological Service

maximum air temperatures have been recorded more frequently in Croatia, particularly in the Adriatic area since 1990s but also from the beginning of the last century (Gajić-Čapka et al., 2010). These conditions particularly affected the change in meteorological forest fires indices which tend to be higher and show positive trends (Figure 1). According to climate change scenarios and modelling performed at DHMZ and in co-operation with international joint initiatives and projects on regional climate modelling (e.g. CORDEX, EURO-CORDEX, ENSEMBLES), these extreme weather events will be even more frequent and stronger in the Mediterranean and Croatia in the future (Branković et al., 2012), leading to further increase in forest fire danger in the next decades. Unfortunately, there are still no efforts made to adapt forest fire danger system used at DHMZ (Van Wagner, 1987) to climate change.

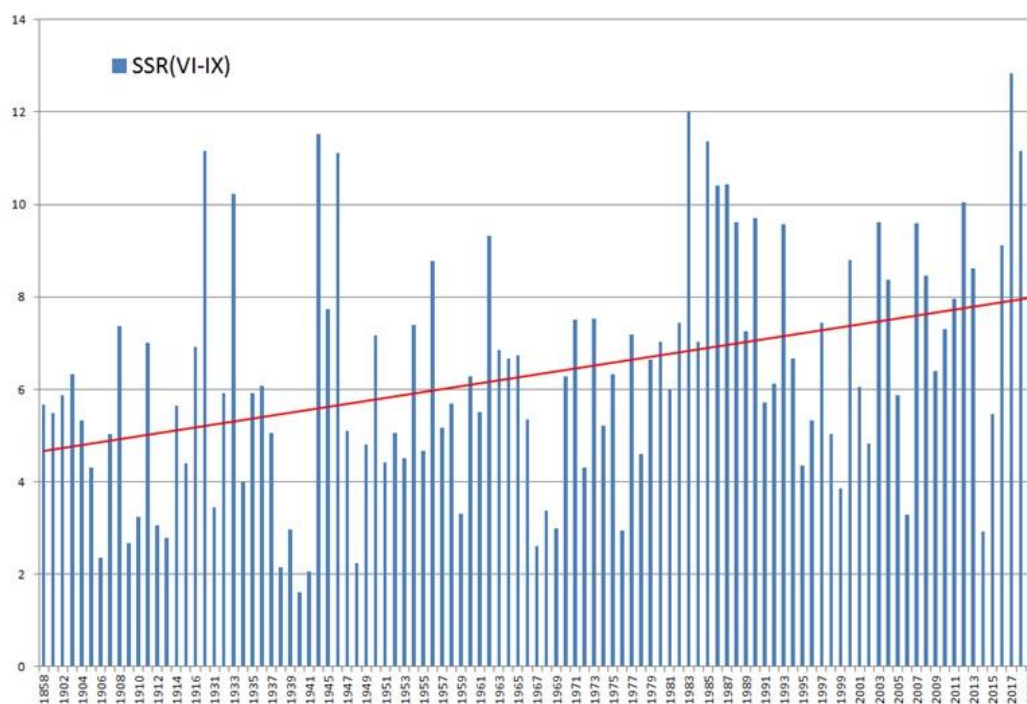


**Figure 1. Historical time series of the Seasonal Severity Rating (SSR) as one meteorological index derived from the Fire Weather Index (Van Wagner, 1987). Data range from 1858 to 2019.**

Forest fires are the most common natural disaster in the warm part of the year on the Adriatic coast of Croatia causing extensive damage and sometimes even a true ecological disaster (Figure 2). There were also cases of heavy precipitation following large forest fires and resulting in severe soil erosion.

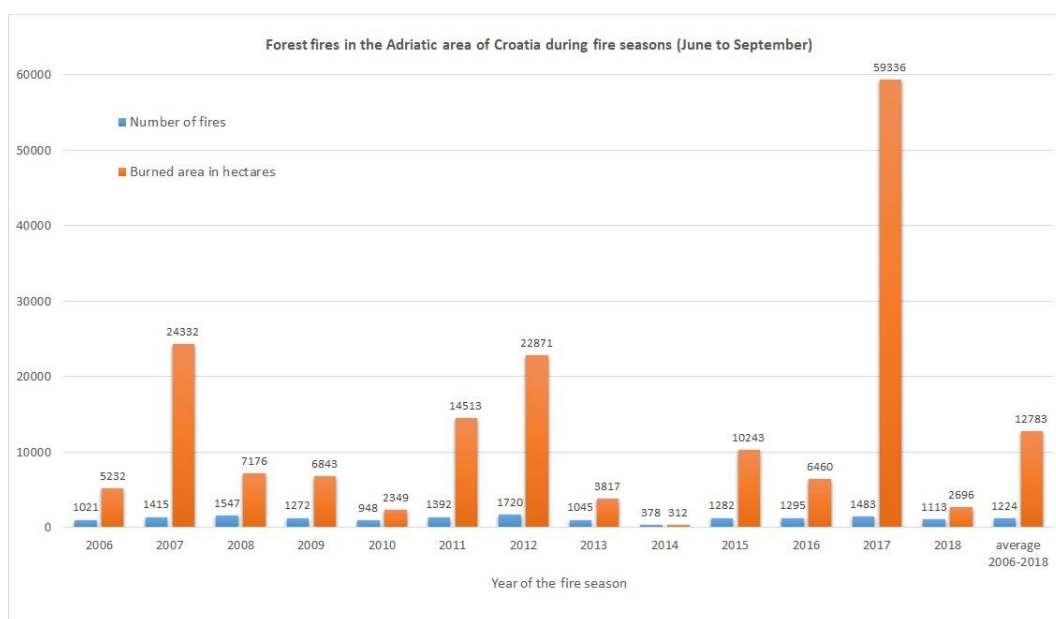


**Figure 2. Evolution of forest fires (number and burned area) in the Adriatic area of Croatia in the fire seasons from 2006 to 2018 (June to September). Average number and burned area in this period are shown in last two columns.**

Therefore, forest fire protection and related activities are conducted from spring to autumn, usually from the beginning of May until the end of October. On the national level Meteorological and Hydrological Service of Croatia (DHMZ) is acting as advisory body in fire suppression system providing specialized meteorological information to the stakeholders, the Civil Protection Service and local fire departments with focus on meteorological conditions favoring fire ignition, rapid fire spread potential and fire severity rate (Vlada Republike Hrvatske, 2019).

Several high temperature and drought extremes were recorded in the Adriatic area in the last decade causing extremely high forest fire risks in fire seasons of 2011, 2012 and 2017. Consequently, this resulted in an increased number of forest fires and very large burned areas (Figure 2). Forest fires information were obtained from the Croatian Firefighting Association on DHMZ's demand. There are also other forest fire databases maintained by other organisations, e.g. the Ministry of Interior.

## Time horizons of forest fire risk assessment

Long-term meteorological risk assessment in Croatia is based on the seasonal and monthly forecasts provided mainly by European Centre for Medium-Range Weather Forecasts (ECMWF). It is adapted at DHMZ for the needs of fire protection program and has been used for the last 10 years. In that period some upgrades of the products were made as well, particularly regarding climatology.

Seasonal forecast describes mean quarterly anomalies of precipitation, air temperature and sea level air pressure expected for the next three months with corresponding accuracy of forecast. It is issued once a month for the whole country in the format of text document mainly in order to assess the possible onset of the fire season and its probable severity.

Typically, fire seasons in the Adriatic region last from June to August with peak in July or August. The negative precipitation anomaly particularly when associated with positive temperature and positive pressure anomalies could lead to a more severe fire season than normal. If this occurs also in spring months fire season will possibly start earlier than normal.

Monthly forecasts describe mean weekly anomalies of precipitation and air temperature in the next four weeks with corresponding accuracy of forecast. It is provided for three different areas of the Adriatic coast region as well as mountainous area inland. Also daily probabilities for different precipitation thresholds and air temperature plume (i.e. chart showing forecast median, interquartile range and extremes) are shown for same month and for one particular place representing the given area. Monthly forecast is issued two times per month in format of text and charts. It is primarily used to assess possible meteorological forest fire risk at the monthly scale and in general to specify the peak month of the fire season.

Medium-term meteorological risk assessment for forest fires in the Adriatic region of Croatia is mainly based on the weather prediction model guidance from ECMWF global model, both high resolution and ensemble (ECMWF, 2019) and ALADIN mesoscale model run at DHMZ (Tudor et al., 2016). It consists of a general weather outlook up to seven days ahead and a more detailed forecast up to four days ahead specifically written for fire protection purposes. These two types of forecasts are issued at DHMZ twice a week from April to November, in text and tabular format, and have a long history of dissemination starting in 1990s.

7-days outlook qualitatively describes expected precipitation, wind and air temperature to assess general fire weather conditions (e.g. dry or wet, windy or not, warmer or cooler), separately for the north Adriatic (including Istria inland), Dalmatia (including middle and south Adriatic as well as the inland) and mountainous area.

The special 4-days forecast gives daily quantitative assessment of rain amount and probability, wind speed and direction, maximum temperature range and lightning potential for the north Adriatic and Dalmatia and thus describes fire weather conditions more precisely.

The use of medium-term forecasts is for the fire management planning functions, giving fire managers time to evaluate potential demands on fire suppression resources, such as pre-positioning of means and personnel in the areas with increased risk of forest fire ignition or spread.

Meteorological risk assessment based on short-term forecast for heavy precipitation, strong wind, high and low air temperature, freezing rain and other possible dangerous meteorological events is issued 2-3 days ahead in form of image and textual forecast. These forecasts are based on numerical prognostic models: ECMWF model, Croatian ALADIN model and model of German meteorological service (DWD, 2019).

A short-term assessment of the meteorological risk for forest fire ignition and spread is the primary activity of DHMZ in the program of fire protection. It is based on a meteorological

index of the Canadian Forest Fire Danger Rating System (CFFDRS) known as Canadian Forest Fire Weather Index (FWI) which relates the state of biomass and weather conditions (Van Wagner, 1987). This methodology has been used in Croatia since the early 1990s, for almost 30 years. Occasion-related warnings introduced in 2012 are issued when one of the following weather phenomena is expected: a strong or stormy wind (usually from NE or SE direction), a passage of a cold front with little or no rain but accompanied by lightning (i.e. dry cold front), a low level jet and an unstable dry air mass with weak winds (i.e. high value of Haines Index). If one of these phenomena is expected and the fire danger class of FWI is high or very high at the same time, a textual warning is issued with an indication of the phenomenon, area and period of validity, until the end of the next day. The aim of occasion-related warnings is to draw fire managers' attention to extremely dangerous fire weather conditions in the short-range which may cause many new ignitions or strongly affect ongoing forest fires.

In Figure 3 the DHMZ's methodological approaches to the different forecast horizons are shown in a form of a detailed flowchart. The chart explains a flow of the meteorological risk assessment information from DHMZ to forest fire protection services operating in accordance with the Governmental program and SOPs. Short-term forecasts (FWI and occasion-related warnings) serve as an operational early warning giving precise and prompt information about times and areas of increased risk of forest fire ignition, spread and intensity. This warning leads to fire management decision and actions in terms of more intense surveillance or quick pre-positioning of fire protection personnel and fire suppression means. The performance of the meteorological forecasts presenting risk information against forest fires number and burned areas has not been quantitatively evaluated at DHMZ. Due to specific nature of forest fire ignitions (i.e. mainly human cause), actions of surveillance and suppression (both strongly influencing burned areas) this kind of quantitative verification is not easily performed, frequently giving misleading results. However, there is a positive feedback from forest fire managers about the value of DHMZ's forecasts, particularly those of shorter-terms. Something different approach to the evaluation of short-term meteorological risk (i.e. FWI classes) is performed at DHMZ and will be shortly presented later in this paper.

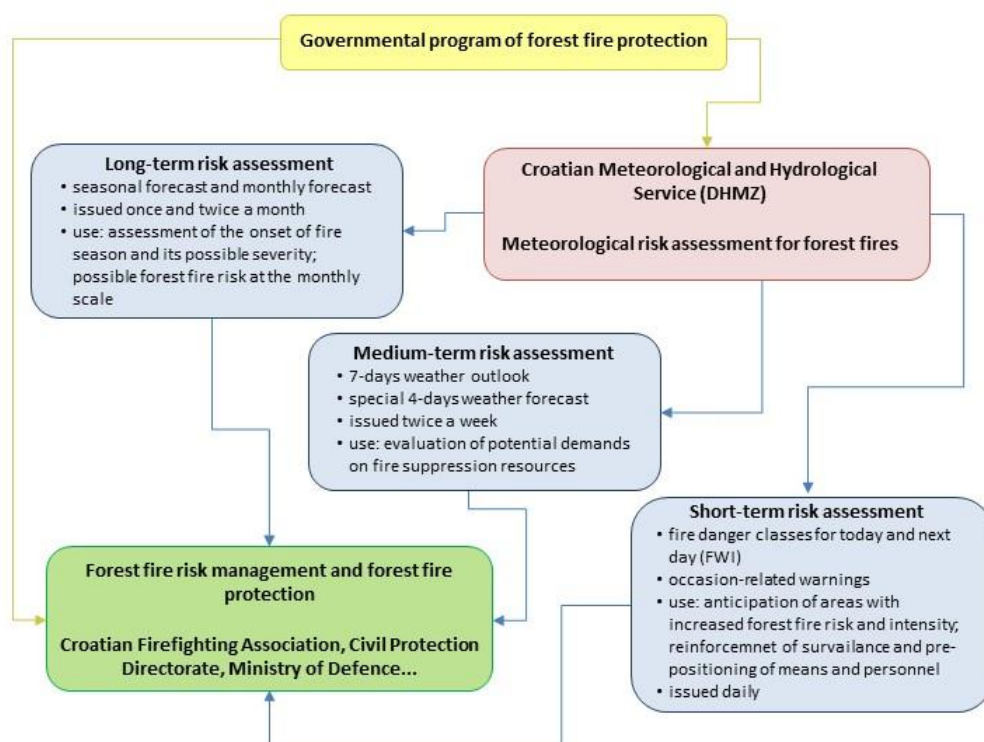


Figure 3. Flowchart of the DHMZ's methodological approaches in the risk assessment of forest fires hazards in Croatia.

## Methods

The Canadian Forest Fire Weather Index (FWI) System detailed structure and development can be found in Van Wagner (1987). The FWI refers primarily to a standard pine fuel type but is useful as a general measure of forest fire danger. Basically, FWI consists of six standard components - three fuel moisture codes and three fire behavior indices which provide numeric ratings of relative potential for forest fire. Numeric ratings of the moisture content are the Fine Fuel Moisture Code (FFMC) for litter and other dried fine fuels, the Duff Moisture Code (DMC) for loosely compacted organic layers of moderate depth (duff) and the Drought Code (DC) for deep, compact organic layers. Two intermediate fire behavior indices represent fire spread rate and amount of available fuel. The Initial Spread Index (ISI) is a numeric rating of the expected rate of fire spread, which combines the effects of wind and FFMC. The Buildup Index (BUI) is a numeric rating of the total amount of fuel available for combustion, which combines DMC and DC. Described moisture codes and fire behavior indices are functions of temperature, relative humidity, wind and rain. The final fire behavior index, the Fire Weather Index (FWI), combines ISI and BUI to represent the intensity of a spreading fire as energy output rate per unit length of fire front. FWI ranges between 0 and 200, and BUI ranges between 0 and 400, both dimensionless.

At DHMZ the FWI components have been calculated on daily basis. Corresponding classes of fire danger have also been derived, by combining FWI and BUI. Generally, linking FWI with BUI proved to be the best way for defining fire danger classes in Croatia (Dimitrov,

1987). The classes can be: very low (1), low (2), moderate (3), high (4) and very high (5). Figure 4 shows mean monthly FWI classes for the fire season of 2012 (June to August). The observed and prognostic fire danger classes are calculated from weather observations at 12 UTC and from forecast data at 12 UTC next day, respectively. In Croatia 12 UTC means CET or CET+1h when daylight saving time is used. According to the requirements of the program of fire protection in the calculation of the observed classes, 40 main meteorological stations throughout Croatia have provided data from April to November. Yet, for most of the Croatian inland stations, except the mountainous Lika, FWI is not calibrated, so these stations will not be taken into consideration in this paper. Also, in the inland of Croatia forest fires are much less frequent and less intense than in the Adriatic region. Nevertheless, these calculations are used by fire managers for orientation purposes only. For the same reason prognostic classes have been calculated for only 22 stations in the Adriatic region and Lika from May to October at the basis of ALADIN model. In any case the observed and prognostic FWI classes are used to assess the meteorological risk of the forest fire intensity for the current and the following day. The classes are disseminated daily to fire managers in tabular and graphical form. A simple verification of prognostic FWI classes is carried out seasonally, using a five-by-five contingency table made of all cases of the prognostic classes and the corresponding observed classes for 22 stations in the Adriatic region and Lika. The chart in Figure 5 was plotted from sums of rows and columns of the contingency table for the fire season in 2013 when all five FWI classes occurred. A comparison between number of cases of observed and prognostic classes clearly shows that forecast was skillful for each FWI class.

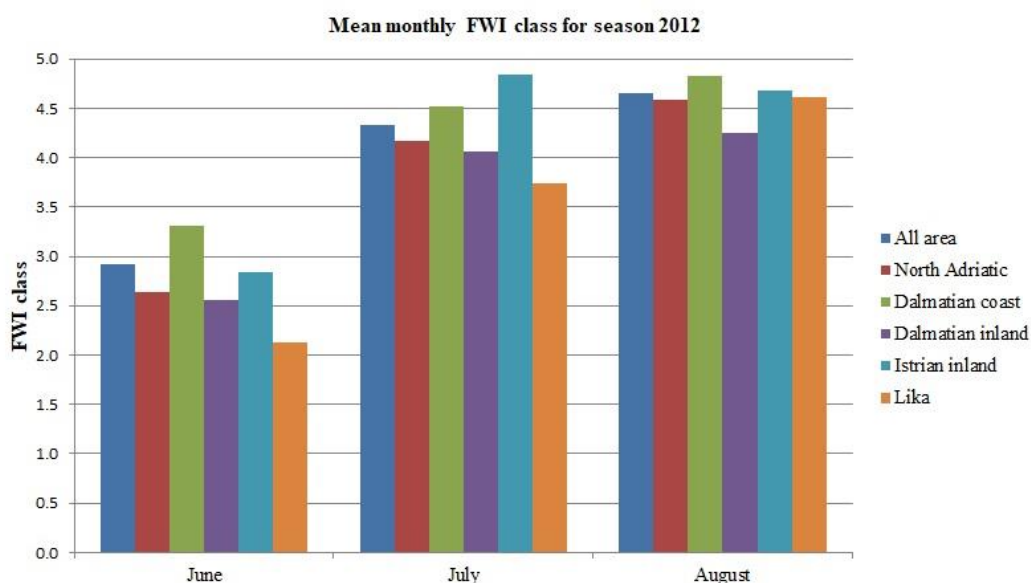


Figure 4. Mean monthly FWI classes for the fire season of 2012 (June to August). Monthly means are shown for individual subareas and the all areas together.

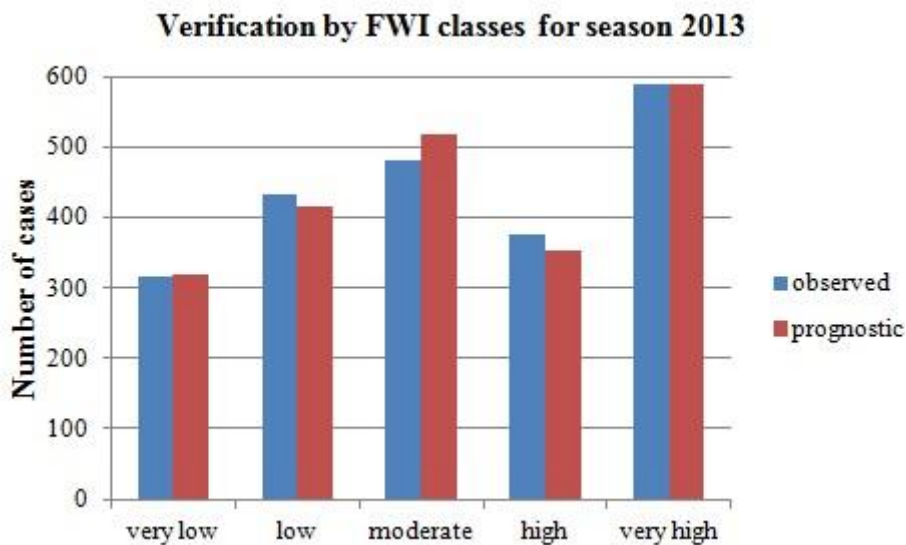


Figure 5. Comparison between number of cases of observed and prognostic FWI classes as a simple verification method.

In extremely severe fire seasons when high and very high daily classes of fire danger were most frequent, additional meteorological tools were needed for better temporal and spatial assessment of short-range meteorological risk of forest fire spread and behavior.

In this manner the Haines Index (Haines, 1988) was first introduced at DHMZ in the year 2013 as a measure of atmospheric humidity and stability. It is known that the unstable and dry air has an impact on the forest fire behavior, particularly in weather situations with a weak wind. The highest values of Haines Index correlate well with the burned area and number of fires. This is also the case at the Adriatic region of Croatia as shown in Kozaric and Mokoric (2014). Values of the Haines Index range from 2 to 6 and measure the potential for large forest fire growth. Values 6 and 5 correspond to very high and high potential, respectively. Otherwise, potential for large forest fire growth is moderate, low or very low.

At DHMZ the analytical and prognostic Haines Indices are used and calculated on a daily basis from two meteorological models, ALADIN and ECMWF. Indices are calculated for three ranges of altitude (low, middle and high) depending on the terrain elevation. Analytical index is calculated from model analysis at 00 UTC and 12 UTC and the prognostic is calculated from the model forecast at 3-hourly timesteps for three days in advance. Haines Index is used in combination with FWI fire danger classes for issuing special warnings as described in the text.

## Results

Figure 6 is an example of the visualisation of the Haines Index (HI) and at the same time shows the mean analytical index for the fire season of 2013. Mean values of index were highest in some parts of Dalmatia (red color referring to a HI of 5). These parts also experienced the highest number of days with Haines Index equaling 6 (approximately 20

days per season). In the regions coinciding with these parts the actual number of forest fires and associated burned area turned out to be the highest.

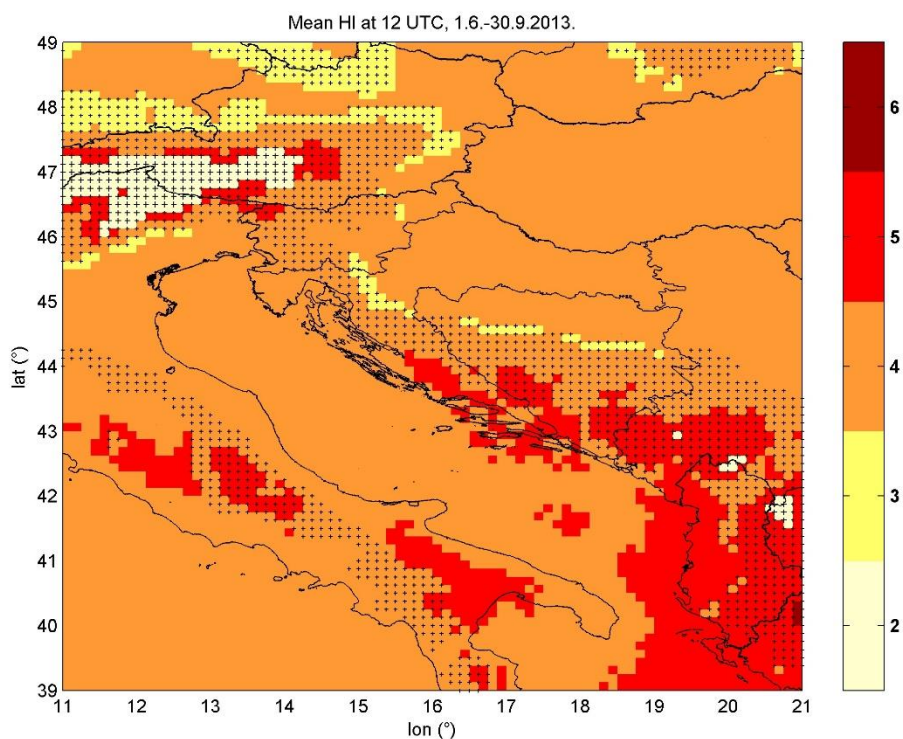


**Figure 6. Mean analytical Haines Index at 12 UTC for fire season of 2013. Black dots represent topography higher than 500 m.a.s.l. where middle or high variants of index are used.**

## Conclusion and outlook

This paper presented numerous activities and efforts at the Meteorological and Hydrological Service of Croatia (DHMZ) to assess the meteorological risk for forest fires, mainly in the Adriatic region of Croatia. The risk assessment is required by the governmental program of fire protection. Further development is needed as a part of the activities.

In long- and medium-term risk assessment, some improvements are planned regarding method and issuing form, particularly in seasonal forecast and special 4-days fire weather forecast.

In the short-term assessment, a calibration of Fire Weather Index is needed for Croatian inland with different kind of vegetation. A calculation of prognostic index at the basis of ECMWF model is planned for the fire season 2020. Special occasion-related warnings on extreme fire weather, seem to be satisfactory according to feedback from fire protection community. The verification of warnings has not been done yet because of a very small sample.

Regarding additional tools, Haines Index has been used and so far appears to be a helpful tool also in the Adriatic region of Croatia. However, there is need for improvement and further research.

Two more tools have recently been calculated from the ALADIN meteorological model for experimental reasons. One estimates the height and speed of the wind maxima in the lower troposphere (i.e. low level jet) and another is the so called “Richardson number” (i.e. the dimensionless number that expresses the ratio of the buoyancy to the flow shear). There is no validation of these two tools yet.

Also in order to better assess the meteorological risk for forest fires a turbulent kinetic energy (TKE) is experimentally introduced in operational forecast, mainly for the purpose for developing better warning system for unexpected forest fire behaviour.

## References

Branković Č., Patarčić M., Güttler I., Srnc L. (2012): Near-future climate change over Europe with focus on Croatia in an ensemble of regional climate model simulations, *Climate Research*, 52, 227-251, available at [https://www.int-res.com/articles/cr\\_oa/c052p227.pdf](https://www.int-res.com/articles/cr_oa/c052p227.pdf)

Dimitrov T. (1987). Šumski požari i sistemi procjene opasnosti od požara, in: S. Bertović, T. Dimitrov i dr. (Eds.), *Osnove zaštite šuma od požara*, Centar za informacije i publicitet, Zagreb, pp. 181-251 (in Croatian)

DWD (2019). ICON (Icosahedral Nonhydrostatic) Model, available at [https://www.dwd.de/EN/research/weatherforecasting/num\\_modelling/01\\_num\\_weather\\_prediction\\_modells/icon\\_description.html?nn=484268](https://www.dwd.de/EN/research/weatherforecasting/num_modelling/01_num_weather_prediction_modells/icon_description.html?nn=484268)

ECMWF (2019). IFS documentation CY46R1, available at <https://www.ecmwf.int/en/publications/ifs-documentation>

Gajić-Čapka M., Zaninović K., Cindrić K. (2010). Climate Change Impacts and Adaptation Measures – Observed Climate Change in Croatia, in: *Fifth National Communication of the Republic of Croatia under the United Nation Framework Convention on the Climate Change*, Ministry of Environmental Protection, Physical Planning and Construction, 137-151, available at [https://unfccc.int/resource/docs/natc/hrv\\_nc5.pdf](https://unfccc.int/resource/docs/natc/hrv_nc5.pdf)

Haines D.A. (1988). A lower atmosphere severity index for wildland fire, *Natl. Wea. Dig.* 13, 23–27

Kozaric T., Mokoric M. (2014). Haines Index and the forest fires in the Adriatic region of Croatia, in: D.X. Viegas (Eds.), *Advances in Forest Fire Research*, Imprensa da Universidade de Coimbra, Coimbra, 1175-1181. doi:10.14195/978

Van Wagner C.E. (1987). Development and Structure of the Canadian Forest Fire Weather Index System, Canadian Forestry Service, Forestry Technical Report 35

Vlada Republike Hrvatske (2019). Program aktivnosti u provedbi posebnih mjera zaštite od požara od interesa za Republiku Hrvatsku u 2019. godini, NN 35/2019, DOC NO 735,

available at [https://narodne-novine.nn.hr/clanci/sluzbeni/2019\\_04\\_35\\_735.html](https://narodne-novine.nn.hr/clanci/sluzbeni/2019_04_35_735.html) (in Croatian)

Tudor M., Ivatek-Šahdan S., Stanešić A., Horvath K., Hrastinski M., Odak Plenković I., Bajić A., Kovačić T. (2016). Changes in the ALADIN operational suite in Croatia in the period 2011-2015, *Hrvatski meteorološki časopis* 50, 71–89

---

# Slope collapses along the southern Åfjorden cliff (Hyllestad municipality-Sogn og Fjordane, Norway)

Ivanna Penna<sup>1</sup>, Vegard Nes<sup>2</sup>, Reginald Hermanns<sup>3</sup>, Marie Bredal<sup>4</sup>, Lene Kristensen<sup>5</sup>, Pierrick Nicolet<sup>6</sup>

**Keywords:** Unstable slope, Displacement waves, Hazard

## Abstract

Landscape evolution, and geologic conditions have led to the development of hundreds of unstable slopes on valleys and fjord slopes in Norway. In the last 100 years, slope collapses caused important life and economic losses in counties such as Møre og Romsdal and Sogn og Fjordane, mainly by triggering displacement waves when impacting water bodies. In this work we map unstable slopes along the southern cliff of Åfjorden (Sogn og Fjordane), estimate their potential recurrence interval, and their hazards. We produced two inventories, one of the past slope collapses lying on the fjord floor and one containing current unstable slopes along the cliff. Around 25 deposits have been identified by interpreting bathymetric data, and nine current unstable slopes were identified on field work. Current instabilities and past events have similar dimensions. A recurrence interval of 334 years for events higher than 20 000 m<sup>3</sup> and of 2900 years for events higher than 250 000m<sup>3</sup> was obtained. Further work is planned to be conducted on determining the magnitude of potential displacement waves, and on the delimitation of hazard zones based on displacement waves analyses.

## Introduction

The landscape in Norway has been strongly shaped by glaciers that carved deep valleys, that later flooded and formed fjords. The landscape evolution, in combination with structural and lithologic conditions led to the development of large slope instabilities. In the last ten years, the Geological Survey of Norway and the Norwegian Water Resources and Energy Directorate has conducted along Norway a systematic mapping and monitoring of unstable slopes. So far 580 instabilities have been identified in the country. Hazards and risk assessments are conducted for those unstable slopes, following the criteria described in Hermanns et al. (2013). Finnmark, Troms, Møre og Romsdal and Sogn og Fjordane are the counties that count with most of them. In the last 100 years, several events took around

---

<sup>1</sup> Dr., The geological survey of Norway, Norway, (ivanna.penna@ngu.no)

<sup>2</sup> NTNU: Norwegian University of Science and Technology, Norway

<sup>3</sup> The geological survey of Norway, Norway

<sup>4</sup> The geological survey of Norway, Norway

<sup>5</sup> The Norwegian Water Resources and Energy Directorate, Norway

<sup>6</sup> The geological survey of Norway, Norway

170 people's lives (Blikra et al., 2006). Several of the losses were not caused by the direct impact of the rock mass but the secondary hazard that constitute the displacement waves created when rock mass propagates into water bodies. In this work we focus on identifying unstable slopes along the southern cliff of Åfjorden, their potential recurrence interval, and the hazard level. The cliffs in Åfjorden experienced slope collapses triggering significant displacement waves in 1992 (Lifjellet Øst) and in 1998 in Katlanova (Harbitz et al., 2001; Figure 1).

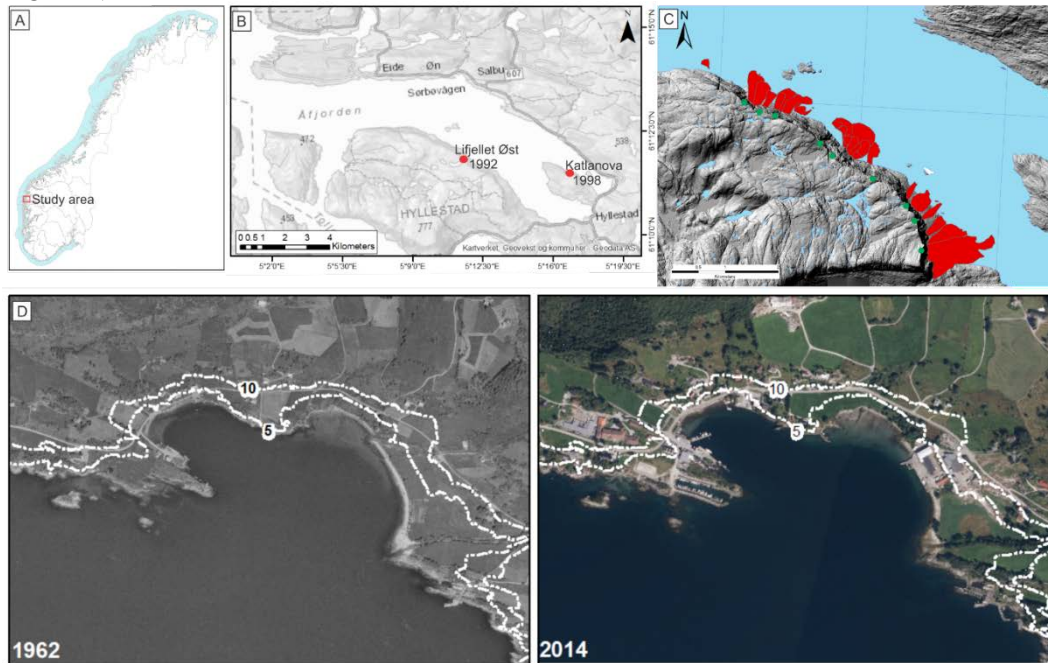


**Figure 1** A) Map of Norway showing the location of the study area. B) Map showing the extension of Åfjorden and the recent slope collapses that have triggered displacement waves. C) Hillshade map with indication of the unstable slopes detected (green dots) and the extension of landslides deposits lying on the fjord (red polygons). D) Aerial photographs of Sørbovågen showing the population growth close to the shoreline between 1962 and 2014. White dashed lines: contours at 5 and 10 m a.s.l.

## Methodology

*Mapping of unstable slopes and past collapses:* Interpretation of aerial photos, high resolution airborne lidar DEM and field work allowed to identify the unstable slopes, as well as the dip and dip direction of the structures controlling their development. Because of the topography of the area (mountain plateau ending in a cliff), the DEM lack of important data on the cliff, which is needed to place and measure the lower limit of the instabilities. To overcome this issue, we conducted a photogrammetry survey from a boat that allowed us to obtain a detailed 3D photogrammetric model. 1102 pictures were taken for the model, and 902 of those were finally used to build a dense cloud containing around 216 million points. In addition, high resolution bathymetric data allowed us to map on the fjord floor deposits of past slope collapses. The DEM combined with the photogrammetric model of the front cliff and the bathymetry allowed us to have a full overview of the spatial distribution and extension of the hillslope processes that occurred in the past and that are still ongoing.

*Magnitude of events:* The potential consequences of slope collapses relate to the magnitude of the slope collapses. Therefore, we estimated their volume of past events and present unstable slopes using different methods. For the present unstable slopes, as they are structurally controlled, we delimited the unstable rock mass by reconstructing the planes that act as boundaries (backscarp, flanks and sliding surface). The subtraction between the current topography (DEM) and the one obtained with the structural analyses results in the volume of unstable rocks. In the case of the deposits lying on the fjord, we used the SLBL method (Jaboyedoff et al., 2018) implemented as an ArcGIS tool (developed at NGU). This method allows to reconstruct the pre-depositional surface and the volume results from the subtraction of the pre and post-depositional surfaces.

*Hazard levels:* The hazard classification on the identified unstable slopes and their respective scenarios was done following the methodology described in Hermanns et al. (2013). The hazard assessment requires data with displacement rates and acceleration. Because we lack data for most of the sites, standard values were used.

## Results

Two inventories were made, one containing the present unstable slopes along the cliff and one of the past slope collapses lying on the fjord floor.

*Past events:* Around 25 deposits have been identified. Volumes range between  $7000 \text{ m}^3$  to  $2 \times 10^6 \text{ m}^3$ . They mostly have well preserved morphologies, which allows to differentiate events on areas with high superposition of events. The longest run out is observed in a deposit from the SE end of the cliff (Figure 1). No dating of the deposits has been made, however the area was deglaciated ca. 11 500 years ago, which means an average recurrence rate of 460 years. It is known that larger events are less frequent than the smaller ones and therefore we corrected the recurrence rate using volume classes. A recurrence rate of 334 years was obtained for events larger than  $20\,000 \text{ m}^3$  and of ca. 2900 years for events larger than  $250\,000 \text{ m}^3$ .

*Current instabilities:* Nine unstable slopes were identified, and among these, 14 scenarios of failure were defined. Volumes range from  $2.6 \times 10^6 \text{ m}^3$  to  $6000 \text{ m}^3$ . In all these cases, the potential angle of reach (Scheidegger, 1973) is lower than the angle between the backscarp of the events and the shoreline, meaning that in case of collapse the rock mass would propagate into the fjord.

The hazard assessment conducted shows 12 scenarios that fall into the medium hazard class, with an annual probability between 1/1000 to 1/5000 and 2 on low hazard class with an annual probability of less than 1/5000. Two of the most relevant medium hazard sites (Lifjellet Øst and Lifjellet Vest) are currently being monitored. GPS and extensometer measurements show up to 3 mm/y horizontal displacement in Lifjellet Øst and 2 mm/y in Lifjellet Vest (Figure 2). For the remaining seven sites, the hazard assessment is uncertain, because of the lack of accurate displacement rates.



Figure 2 Lifjellet Vest unstable slope. Main morphologic features related to the instability are displayed.

## Discussion and conclusion

A recurrence interval of 334 years for events higher than 20 000 m<sup>3</sup> and of 2900 years for events higher than 250 000m<sup>3</sup> was obtained. However, as many authors showed (Evans and Clague, 1994; Blikra et al. 2006, Cossart et al., 2008; Ballantyne and Stone 2013) most of the collapses tend to cluster close after deglaciation and their occurrence decreases with time. In addition, Harbitz (1999) showed that 5 collapses occurred in a period of 6 years in the '90s, therefore, it seems there was also a sort of period of “crisis”. Even if their recurrence decreases with time after deglaciation, the events of 1996 in our study area, or the ones in 1998 in Katlanova show that rockslide events are ongoing processes and their assessment and follow up is key for protecting society. Absolute dating of deposits will shed light on the recurrence of the past events in our study area.

Current instabilities have the same dimensions as past events; therefore, their back analysis would lead to build accurate models of future scenarios. The magnitude of the displacement waves will depend on the volume collapsed, the fragmentation degree and shape of the rock mass impacting the water, as well as fall height. Therefore, further work is planned to be

conducted on this aspect, and on the delimitation of hazard zones based on displacement waves analyses.

## References

Ballantyne, C. K. and Stone, J. O. (2013) Timing and periodicity of paraglacial rock-slope failures in the Scottish Highlands, *Geomorphology*, 186, pp. 150-161. doi: <https://doi.org/10.1016/j.geomorph.2012.12.030>.

Blikra, L. H., Longva, O., Braathen, A., Anda, E., Dehls, J. F. and Stalsberg, K. (2006b) Rock slope failures in Norwegian fjord areas: Examples, spatial distribution and temporal pattern in Evans, S. G., et al. (ed.) *Landslides from Massive Rock Slope Failure*. Netherlands: Springer, pp. 475-496.

Cossart, E., Braucher, R., Fort, M., Bourlès, D.L., and Carcaillet, J., 2008, Slope instability in relation to glacial debuitting in alpine areas (Upper Durance catchment, southeastern France): Evidence from field data and <sup>10</sup>Be cosmic ray exposure ages: *Geomorphology*, v. 95, no. 1–2, p. 3–26, doi: 10.1016/j.geomorph.2006.12.022.

Harbitz, C. B., 1999. Vurdering av skredfare og bølgehøyder i Åfjorden. (981014-1): Norwegian Geological Institute.

Harbitz, C. B., Domaas, U. and Varlid, E. (2001) Rockslide generated tsunamis – probability and hazard zoning in Åfjorden, western Norway., *Fjellsprenningsteknikk - bergmekanikk - geoteknikk*. Oslo 2001. Pp. 27.1 - 27.13.

Hermanns, R. L., Oppikofer, T., Anda, E., Blikra, L. H., Böhme, M., Bunkholt, H., Crosta, G. B., Dahle, H., Devoli, G. and Fischer, L., 2013. Hazard and risk classification for large unstable rock slopes in Norway, *Ital J Eng Geol Environ*. doi, 10, pp. 2013-2006.

Jaboyedoff, M., Chigira, M., Arai, N., Derron, M.-H., Rudaz, B., and Tsou, C.Y., 2018. Testing a failure surface prediction and deposit reconstruction method for a landslide cluster that occurred during Typhoon Talas (Japan). *Earth Surf. Dynam. Discuss.*, <https://doi.org/10.5194/esurf-2018-61>

NGU, 2019. Nasjonal database for ustabile fjellparti. Available at: [http://geo.ngu.no/kart/ustabilefjellparti\\_mobil/](http://geo.ngu.no/kart/ustabilefjellparti_mobil/)

NVE, 2019. Skredhendelser. Available at: <https://temakart.nve.no/link/?link=SkredHendelser>

---

# Mapping of the protective function of forests in Austria against shallow landslides

Frank Perzl<sup>1</sup>, Monika Rössel<sup>2</sup>, Elisabeth Lauss<sup>3</sup>, Michael Neuhauser<sup>4</sup>

**Keywords:** object-protection forest; shallow landslides; susceptibility modelling; runout-modelling; damage potential

## Abstract

We performed the first approach of shallow landslide hazard and damage potential modelling throughout Austria in order to map object-protection forests. Landslide susceptibility mapping was done regionally by frequency ratio method (FRM) and binary logistic regression (BLR) based on two landslide inventories compiled from random archive data and area plot sampling. As predictions from regional models cannot be compared directly, we tested two approaches of trans-regional adjustment. In total, adjusted results show similar prediction-rates with a slightly lower performance of BLR. However, the two versions show quite different prediction patterns with higher plausibility of FRM. We used the travel-angle method to approximate runout of hillslope debris flows. The algorithm implies functionality to back-calculate zones from potentially affected infrastructure to locations of slope instability. The intersection of these hazard zones with forest area indicates object-protection forests against landslides.

## Introduction

An object-protection forest is a forest with an object-protective function against natural hazards (Brang et al. 2001). The concept of forest function mapping strictly distinguishes functions (tasks) and effects of forests. Protective functions of forests are not limited to forested terrain. They depend on site conditions and the position of objects to be protected. Protective effects of forests result from forest cover conditions and are not considered. Woody vegetation offers the opportunity to mitigate the risk of damage caused by gravitational natural hazards, if it is located within potential hazard zones with damage potentials to assets like settlements and infrastructures. The hazard zones include areas susceptible to hazard initiation and subsequent runout zones, which may impact an asset.

---

<sup>1</sup> Dipl.-Ing., senior scientist, Department of Natural Hazards, Austrian Research Centre for Forests, Rennweg 1, A-6020 Innsbruck, Tyrol, Austria ([frank.perzl@bfw.gv.at](mailto:frank.perzl@bfw.gv.at); [frank.perzl@chello.at](mailto:frank.perzl@chello.at))

<sup>2</sup> Bacc. techn., MSc (GIS), Austrian Research Centre for Forests

<sup>3</sup> Austrian Research Center for Forests

<sup>4</sup> Dipl.-Ing., Austrian Research Centre for Forests

They spatially define a direct object-protective function of forests, which poses societal demands regarding safety to woody vegetation.

Previously, landslide susceptibility maps have been created with different methods for selected federal provinces of Austria or parts of them (e.g. Petschko et al. 2014, Proske & Bauer 2015, Poltnig et al. 2016). The landslide susceptibility map GHK-RU200 of entire Austria generated by Schindlmayr et al. (2016) is an expert assessment of the landslide susceptibility of lithostratigraphic units on an ordinal scale (high, medium and low susceptibility) based on geological maps 1:200.000. The map does not consider crucial factors such as the slope gradient. Hence, existing geoinformation about landslides were not completely sufficient for mapping the protective function of forests, e.g. with regard to runout zones with a damage potential.

Perzl & Huber (2015) generated maps, giving forest managers hints on areas with an object-protective function of forests against rockfall and avalanches. As no appropriate map was available for landslides, Austrian Federal Ministry of Sustainability and Tourism (BMNT) requested a spatial modelling of landslide hazard and damage potentials (GRAVIMOD II).

Modelling considered the following types of shallow (depth  $\leq 5$  m) spontaneous landslides: a) slides (planar) and slumps (rotational) in regoliths without flow type mass movements, b) hillslope debris ("earth" or debris) flows without and with abrasion of the soil in the flow path. Debris flows and floods originating from fluvial erosion in existing gullies and channels were not a topic of hazard modelling.

The objective of this paper is to introduce a fast mapping approach of protective functions of forests against landslides for large areas based on archive and geomorphologic landslide inventories.

## Methods

Figure 1 shows the concept of automatic determination of object-protective functions of forests. The first step is to identify locations within forests or unwooded land prone to slope failures (landslide susceptibility modelling). Step 2 is the calculation of the runout zones (C, D), which may result from these failures. However, runout analysis is not sufficient in order to map the object-protective function of forests. It is also necessary to identify the hazard zone C1 automatically, as it may damage infrastructures (E). Finally, the area of direct object-protection forest (G) results from the intersection of C1 with the forest area. Zone F is not an object-protection forest, but an area with an object-protective function of forest, since afforestation could reduce the risk of damage at E.



Figure 1. Mapping concept of direct object-protective functions of forests: (1) Identification of locations prone to slope failures (A, B), (2) mapping of runout zones (C, D) and of hazard zones with damage potential to the infrastructure (C1) inside (3 G) and outside of forest (3 F).

## Data and concept of landslide susceptibility modelling

Figure 2 shows the concept of data preparation, model formulation and validation. We applied two statistical methods (DISPOA, DISPOB) and two trans-regional adjustment factors (LITHKF, LITHRDKF). The combination of statistical approaches and adjustment factors results into four adjusted susceptibility models (DISPOA\_LITHKF, DISPOB\_LTHKF, DISPOA\_LITHRDKF, DISPOB\_LITHRDKF).

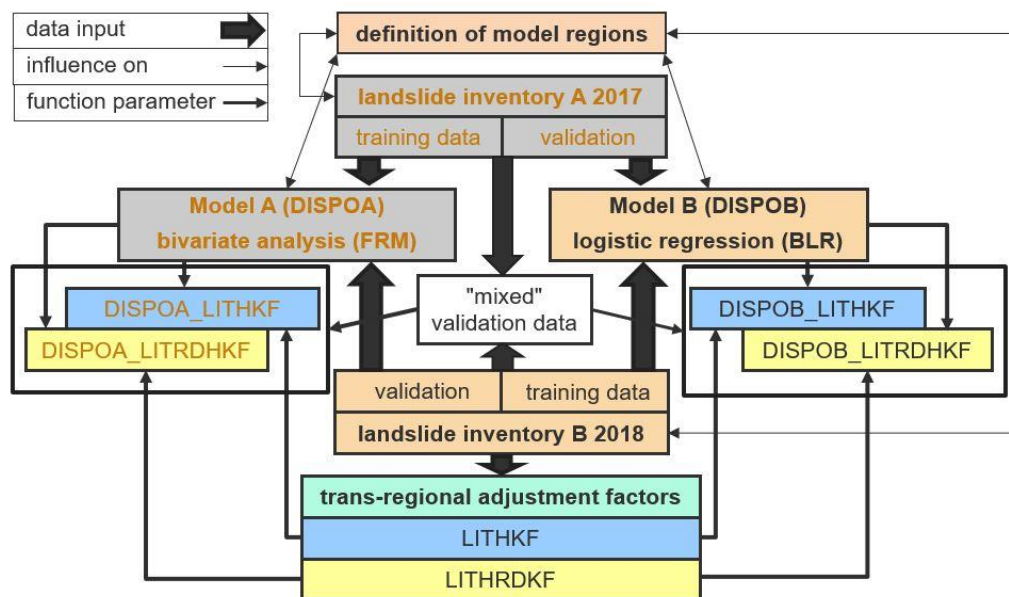


Figure 2. Concept of landslide susceptibility modelling: Statistical methods (DISPOA, DISPOB), trans-regional adjustment factors (LITHKF, LITHRDKF) and the adjusted susceptibility models (DISPOA\_LITHKF, DISPOB\_LITHKF, DISPOA\_LITHRDKF, DISPOB\_LITHRDKF).

## Basic geodata and data preparation

We used digital terrain models (DTM) with a resolution of 1 x 1 m derived from airborne laser-scanning provided by the data centre (LFRZ) of the BMNT. On base of this DTM, we generated a multi-directional relief image to enable landslide inventories and landscape analysis. We corrected distortions and resampled the DTM to the resolution of modelling (10 x 10 m). LFRZ also provided the GHK-RU200 and time-series of orthophoto-mosaics

which were used for landslide inventories. The units of the GHK-RU200 do not cover the southern part of Tirol. Therefore, we completed the GHK-RU200 using the geological map 1:500.000. We also completed the geotechnical susceptibility assessments by expert, as ranking of some lithologies was missing. Finally, we had to correct topology, since the map tiles are not adjusted to each other. Maps of infrastructures to be protected and of forest area had be compiled by Perzl & Huber (2015).

## **Model regions**

Statistical landslide susceptibility modelling for large areas have to consider the different geomorphic and geotechnical characteristics of landscapes, which are connected to change in lithology (Petschko et al. 2014). Therefore, we defined 21 landscape regions by visual interpretation of the relief image overlaid with the lithological map. Because of the results of the landslide inventories, we combined them into 16 and 17 model domains (U) for DISPOA and DISPOB.

## **Landslide inventories**

Statistical methods require mappings of landslide scars for training and validation. A representation of a slope failure with a point in the scar is the most effective method (Petschko et al. 2016).

Schindlmayr et al. (2016) compiled a dataset of 30,138 landslide points from different archive sources. Landslide dataset A was generated by random sampling of 3,750 points (at least about 100 points within each domain) from this collection in a stepwise procedure. Additionally, we implemented sample plots with a radius of 300 m around each landslide point. We used three time-series of orthophoto maps and the relief image to verify the selected landslide points by correction of the position (to the centre of the scar), standardized classification and detection of redundancies. Moreover, we amended slide scars in the plots, which are not in the archive data collection. We only accepted landslides visible in the aerial image or with clear traces of the process in the relief image. If we could not verify at least one spontaneous debris slide within a sample plot, we scanned a maximum of two other randomly selected substitutes in order to obtain a sufficient quantity of scar points. As many points from archives could not be verified, the number of plots increased to 8,304 (213,817 ha in total).

The sample plots of the inventory B are a two-step random selection of 37,350 tiles from a 400 x 400 m grid throughout Austria. The sample covers each domain by the same density (587,765 ha in total). Plots of both inventories may overlap to avoid a bias.

## **Statistical susceptibility mapping**

Spatial landslide prediction DISPOA was made with the frequency ratio method (FRM). The slope failure probability is the sum of the weighted and standardized frequency ratio (FR) values of the explanatory variables. Standardizing implies limitation of FR to values from zero to one. Figure 3 shows the derivation of regional FR values for the slope gradient in domain U2 ("Flysch Zone in Vorarlberg"). Distribution of slopes in relation to slope failures indicates classes of disproportionate occurrence of failures in relation to class

occurrence in the terrain (Fig. 3 A). FR is the ratio of the share of the scar points' count and the share of the area of the predictor's class. Effects of sampling cause outliers and deviations in FR distributions. Hence, we smoothed values stepwise by moving average method in order to get a plausible FR curve (Fig. 3 B). The method delivered characteristic FR curves for each domain (examples in Fig. 3 C). A FR of 1.0 indicates an indifferent effect of the predictor's value on landslide occurrence. Hence, the mean of the absolute difference of FR values to 1.0 in case of n classes regionally occupied by slopes shows the predictor's information value. The proportion of an explanatory variable in the total sum of all predictors' information values indicates the relative signal power and is a weighting factor (Fig. 3 D).

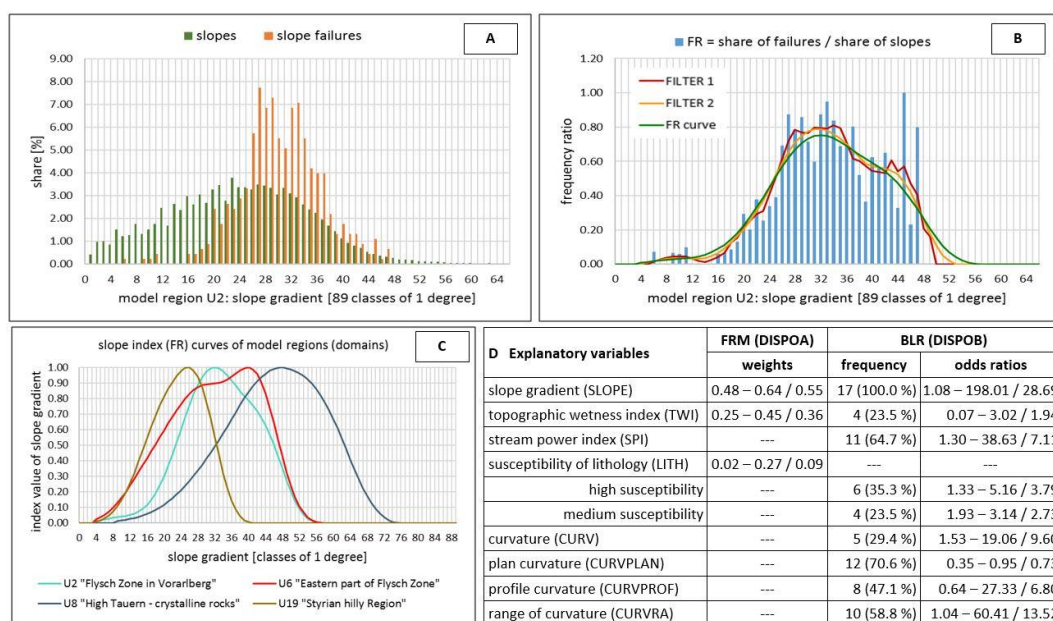


**Figure 3. (A) Frequency Ratio (FR) of the slope gradient - share of slopes and slope failures, (B) smoothing of FR, (C) examples of FR curves, (D) explanatory variables of statistical approaches.**

Spatial landslide prediction DISPOB was made by BLR based on landslide inventory B. We compiled 1:1 event to non-event samples by random sampling of non-event points within the plots of each domain.

Table D in Figure 3 shows the explanatory variables of FRM and BLR. FRM was limited to three variables, since we could hardly detect clear patterns of landslide occurrence for others. Variable selection of DISPOB was done automatically for each domain by backward likelihood ratio method. We used combinations of direct, FR forms and non-linear smoothed forms of predictors in BLR to consider the functional shape of the relationships of slope failure occurrence and explanatory variables. The decision about the input form was made on base of higher specificity in univariate logistic regression (ROC-analysis).

We interpolated FR values and weighting factors of predictors class by class as well as intercepts and coefficients of BLR to avoid breaks of slope failure probability at the borders of the domains.

## **Trans-regional adjustment, validation and classification of landslide susceptibility**

Statistical landslide predictions derived from different regional models do not express the same slope failure probabilities. The adjustment of odds would require knowledge about all landslides in Austria. We tested two multiplicative adjustment factors on base of inventory B to approximate the relative landslide susceptibility of the domains. LITHKF is the landslide probability calculated from ranks of lithological susceptibility by BLR. LITHRDKF also considers the landslide density of the domains. Statistical validation was done by prediction-rate curve method from Chung & Fabbri (2003) for each method and domain (unadjusted) as well as for all adjusted versions. We divided the landslide susceptibility into four classes by the mean of trans-regional and regional quantiles (Q5, Q25, Q75) of the unadjusted and adjusted slope failure probabilities of sampled landslides.

## **Modelling of landslide runout-lengths and damage potentials**

We approximated the potential runout lengths of debris flows from areas susceptible to slope failures using the energy line algorithm developed by Huber et al. (2017) and a travel-angle of 22 degrees. The inventory data are in line with the literature indicating that less than 25 % of the slope failures have smaller travel angles. As visual map analysis is too time-consuming, and simple intersection of infrastructures and potential hazard zones as well as calculations of upslope areas by watershed functionalities may result in too large areas without any importance for hazard control, the algorithm implies functionality of back-routing relevant hazard zones (Fig. 1, 2 C1). We divided hazardous areas with a damage potential into four zones based on the value of the assets and the susceptibility to slope failures according to the scheme of forest landuse planning (BMLFUW 2012).

## **Results and discussion**

Our approach of mapping the landslide-protective function of forests was customer-oriented. The approach aimed at a fast delivery of maps of the landslide susceptibility and damage potential in Austria within eight person months. Hence, we decided to implement statistically approaches.

A major challenge was to create an appropriate landslide dataset for training and validation. Landslide data from archives are often of varying quality and biased from unsystematic recording of landslide hazards. However, the archive data made it possible to generate a dataset of 5,302 debris slides by scar point editing based on a random sample within four months (inventory A).

We started to predict spatial landslide susceptibility by FRM (DISPOA), as FRM does not need a non-event sample which may be biased within the sample plots around scar points from archive data. According to forest services, the map of the classified hazard susceptibility well depicts the terrain prone for landslide hazards within the domains. However, the relation of slope failure susceptibility inter the domains does not represent the observed landslide occurrence in Austria. This was to be expected, and results from unadjusted slope failure probabilities and biased landslide densities in archive data. Hence,

customer agreed to generate a second dataset of 5,652 scar points (inventory B) with less distortions for validation, and for training of a second model (DISPOB). The landslide densities of the domains from inventory A and B differ significantly.

DISPOA resulted in area under the curve values (AUC) of model domains from 0.71 to 0.97 (area weighted mean 0.83). In DISPOA, landslide susceptibility is controlled by SLOPE (Fig. 3 D). There are also clear patterns and effects of the modified TWI (the relation of  $\tan(\text{SLOPE})$  to the upslope drainage area) in all domains. The weights correspond to our expectations with a rather small effect of LITH. DISPOA may overestimate soil instability in some steep and rocky areas rather susceptible to rock slides, as information of geological maps about regolith cover is not sufficient. Despite training data and explanatory factors do not consider channel bank failures triggered by undercutting, slope breaks and adjacency to rivers, the FRM well depicts inner gorges which couple areas of hillslope and channel processes.

AUC values of DISPOB (BLR) range from 0.71 to 0.85 (mean 0.80). SLOPE is also the most effective predictor and was included in all model domains (variable frequency 100 %, Fig. 3 D). Odds ratios are remarkably high with an average of 28.69. Only in two domains we decided to use the unsmoothed form which resulted in lowest effect sizes of SLOPE. The second most common predictor is CURVPLAN. However, univariate ROC-analysis indicates low sensitivity. SPI and CURVRA have above-average variable frequencies and high odds ratios. BLR indicates higher explanatory power of SPI than TWI and rather low influence of LITH-classes.

In total, the adjusted versions show quite different prediction images but similar AUC in the range of 0.82 to 0.87. Hence, model selection was done by geomorphological validation and considerations of expediency. We used DISPOA\_LITHRDKF for processing the finally map of object-protection forests as 1) FRM achieved a good separation of inner gorges, and 2) models from BLR with automated variable selection suffer from overfitting and very fragmented susceptibility zones. Additionally, FR-curves (Fig. 3 A, B, C) are useful to communicate slope failure susceptibility for forest management.

Slopes of high and medium landslide susceptibility cover 22.7 % of Austria and 29.8 % of the forest area (Fig. 4) as slopes in forest are steeper. 8.4 % of the forest is object-protection forest located in hazard zones with a considerable damage potential for major infrastructures.

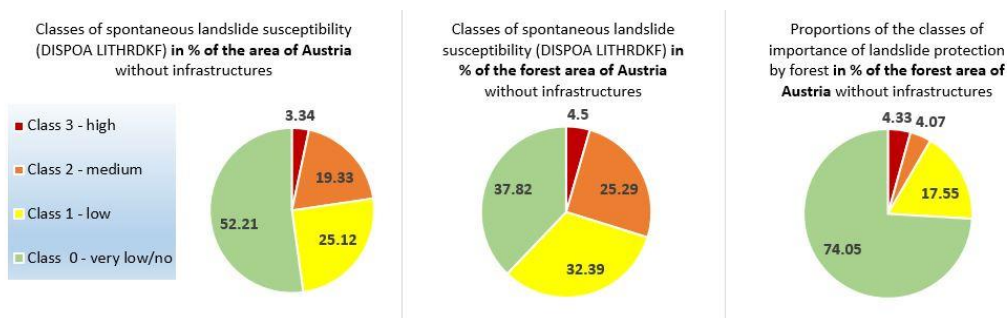


Figure 4. Proportions of classes of landslide susceptibility and object-protecting forest.

## Conclusion

Mapping of landslide hazard and damage potentials by statistical susceptibility modelling and runoff analysis in order to map protection function of forests can be realized for large areas in a relatively short time. If there is no complete map of landslide occurrence, landslide data may be collected on random area plot samples from aerial and relief images. Delineation of landscape units and trans-regional adjustment of relative landslide susceptibilities is crucial. Simple methods like FRM and selection of predictors by expert may outperform multivariate analysis and automated selection techniques.

## References

- BMLFUW (2012): Waldentwicklungsplan. Richtlinie über Inhalt und Ausgestaltung – Fassung 2012. Bundesministerium für Land- und Forstwirtschaft, Umwelt und Wasserwirtschaft (BMLFUW), Wien.
- Brang P., Schönenberger W., Ott E., Gardner B. (2001): Forest as Protection from Natural Hazards. In: *The Forest Handbook: Applying Forest Science for Sustainable Management*, Volume 2: 53-81
- Chung Ch-J.F., Fabbri A.G. (2003): Validation of Spatial Prediction Models for Landslide Hazard Mapping. *Natural Hazards* 30: 451-472.
- Huber A., Kofler A., Fischer J.-Th., Kleemayr K. (2017). Projektbericht DAKUMO. Bundesforschungszentrum für Wald (BFW), Innsbruck.
- Perzl F., Huber A. (2015). GRAVIPROFOR. Verbesserung der Erfassung der Schutzwaldkulisse für die forstliche Raumplanung. Synthese und Zusammenfassung: Ziele, Grundlagen und Ergebnisse der Modellierung von Waldflächen mit Lawinen- und Steinschlag-Objektschutzfunktion. Technische Hilfe im Rahmen des österreichischen Programms LE 07-13. Hauptbericht V2 2015. Bundesforschungszentrum für Wald (BFW), Innsbruck.
- Petschko H., Brenning A., Bell, R., Goetz J., Glade T. (2014): Assessing the quality of landslide susceptibility maps – case study Lower Austria. *Natural Hazards and Earth System Sciences* 14: 95-118.
- Petschko H., Bell R., Glade T. (2016): Effectiveness of visually analyzing LiDAR DTM derivatives for earth and debris slide inventory mapping for statistical susceptibility modeling. *Landslides* 13 (5): 857-872.
- Poltnig W., Bäk R., Berg W., Keršmanc T. (2016). Runout-modelling of shallow landslides in Carinthia (Austria). *Austrian Journal of Earth Science* 109,1: 59-67.
- Proske H., Bauer Ch. (2015). Methodik zur Erstellung einer Gefahrenhinweiskarte für Rutschungen in der Steiermark. In: *Gefahren am Hang – Schutz vor Massenbewegungen*. Wildbach- und Lawinenverbau, Heft 175: 84-93.

Schindlmayr A., Haunschmid B., Heidenreich A., Holzer R., Kreslyer D., Montag O., Poscher G., Ribis M., Sommer P., Stadlmann T., Kendlbacher D. (2016). Gefahrenhinweiskarte Rutschungen 1:200.000 der Österreichischen Bundesländer. Im Auftrag des BMLFUW in Kooperation mit dem Versicherungsverband Österreich. ARGE Gefahrenhinweiskarte Rutschungen.

---

# Impact of groundwater accumulation on slope failure initiation: A simulation of slope failure due to rainfall

Xin Qin<sup>1</sup>

**Keywords:** slope failure; water level change; slope stability; laboratory experiment

## Abstract

In Japan, precipitation events have increased in frequency and intensity, in turn increasing the risk of sediment disasters such as slope failures and debris flows. In this study, we examined the impact of groundwater level changes due to heavy rainfall on slope failure characteristics. We performed experiments using a rectangular flume containing a slope model formed of decomposed granite soil; drainage conditions were varied to investigate the relationship between groundwater level and the slope failure mechanism. We used a rainfall simulator to produce artificial rainfall events and installed groundwater level pressure gauges within the flume to record groundwater level changes. Our results indicate a clear relationship between drainage conditions and the initial time of failure.

## Introduction

Following climate predictions by the Japan Meteorological Agency, precipitation events in Japan have already increased in frequency and intensity (Japan Meteorological Agency, 2009). The number of precipitation events with rainfall intensity exceeding 50 mm/h has increased continually. Frequent intense precipitation events are expected to become a significant new hazard and are now recognized as a major antecedent of sediment disasters, such as slope failures and debris flows. During the annual rainy season in Japan, rainfall intensity can reach 100 mm/h within short periods, dramatically increasing the risk of such disasters. The annual mean cost of sediment damage due to typhoons and heavy rain in Japan was approximately 100 million USD over the past decade (Kawagoe et al., 2014). Due to the impact of global climate change on sediment disasters, providing information about infrastructure vulnerability to hydrological events is necessary for damage control in the face of such hazards, particularly in Japan, where geological conditions can be unstable.

Field studies have shown that most failed slopes had several common features, including a failure depth < 2 m, slope ranging from 30–50°, and slope material consisting of permeable residual layers on relatively firm rock foundations (Anusron, 2018). Slope failures occur

---

<sup>1</sup> M2, Student, civil and environmental engineering, Ritsumeikan Daigaku - Biwako Kusatsu Campus, nojihigashi 1-1-1, kusatsu-shi, Japan (rd0059ek@ed.ritsumei.ac.jp)

according to the water content and soil conditions; in particular, rainfall is a severe threat to soil stability due to pore pressure and changes in seepage force. Rapid and intermittent soil movement can occur without warning, within a matter of seconds. Even a single disaster of this type can cause heavy economic losses and casualties. To improve the accuracy of disaster prediction, it is necessary to understand the contributory factors and warning signs.

Many studies have investigated the mechanisms of slope failure, and landslide predictions have been established based on theories of soil creep. However, the slope failure initiation process remains poorly understood and studies of sliding initiation time are scarce.

In this study, we assessed the effects of groundwater level changes due to rainfall, which represents the most important factor in slope failure, on the initial stage of slope failure under consistent soil conditions. We also conducted laboratory experiments using the same slope model, but with different drainage conditions, to determine the effects of groundwater level changes during rainfall on slope failure initiation and progress.

## Methods

### Experimental equipment

To investigate how groundwater levels change over time during slope failure due to rainfall, we used a rainfall simulator to produce an artificial rainfall event and installed groundwater level gauges (OYO S&DL mini 5m) at three locations along the slope. Gauges No.1, No.2, and No.3 were installed 10, 30, and 50 cm, respectively, from the front edge of the slope. A schematic diagram of the experiment is provided in Figure 1.

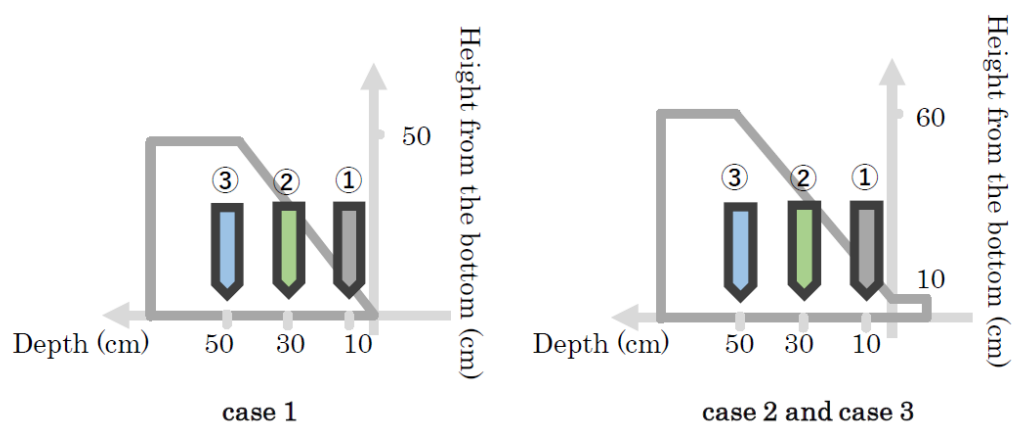


**Figure 1. Schematic diagram of the experiment.**

To simulate Japanese landforms, which are mainly composed of weathered granite, the slope model was constructed from decomposed granite, which has a dry density of 1.6 g/cm<sup>3</sup>. To reproduce the process during which dry, compact soil layers collapse due to heavy rainfall in natural environments, we set the initial water content to 10%. The slope had a length of 71 cm, a height of 50 cm, and a wide of 50 cm. Because slope failure occurs most frequently on slopes ranging from 30 to 50°, we set the slope gradient of the model

to the average of this range (45°). Although the rainfall intensity threshold for sediment disasters is unknown, we used a large value (120 mm/h) to simulate an extreme amount of precipitation within a short period. To maintain uniform soil characteristics, the slope model soil was compacted uniformly in approximately 10-cm-thick layers using a tamper. The full experimental conditions are listed in Table 1.

**Table 1**

w (%)	Dry density (g/m <sup>3</sup> )	Material	Length (cm)	Height (cm)	Wide (cm)	Gradient (°)	Rainfall intensity (mm/h)
10	1.6	Decomposed granite	71	50	60	45	120

## Experimental cases

To investigate the effects of groundwater level changes on the slope failure process, we conducted three experiments, which differed in terms of drainage conditions. In both cases, water was released on the slope model directly from above, and saturated water could drain only from the front of the model. The sides and bottom of the slope model remained undrained. The shape, size, and gradient of the slope were the same between cases; only the drainage conditions at the front of the slope differed.

In case 1, no barriers were placed in the model, such that saturated water could drain freely from the front edge. In case 2, an impervious plate with a height of 10 cm was placed directly on the bottom front edge of the slope model, and drainage holes were made to cover 10% of the total area of the impervious plate. In case 3, we installed an impervious plate without drainage holes under the same conditions under the assumption that following saturation, only groundwater exceeding a height of 10 cm in the slope model would be discharged. Drainage conditions for both cases are shown in Figure 2.

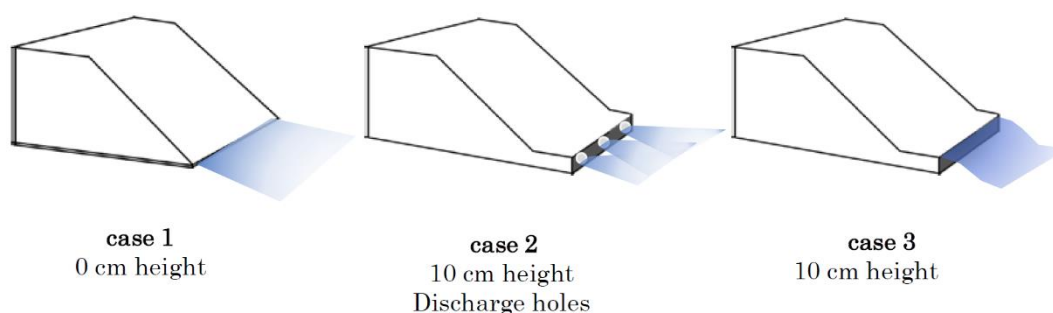


**Figure 2. Schematic diagram of the experiment**

## Results and discussion

Based on visual inspection of video recordings acquired during the experiments, we determined the amount of time that passed between the onset of rainfall and significant displacement of the slope surface (failure initiation). We designated the period from the onset of rainfall until the collapsed area exceeded 2/3 of the surface as the time to total

failure (Figure 3). The slope conditions and time to slope failure initiation and total slope failure for each case are provided in Table 2.

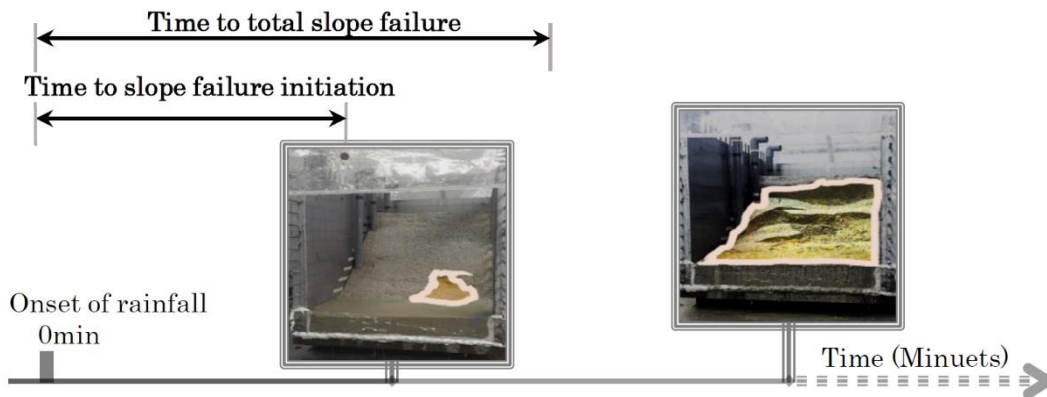


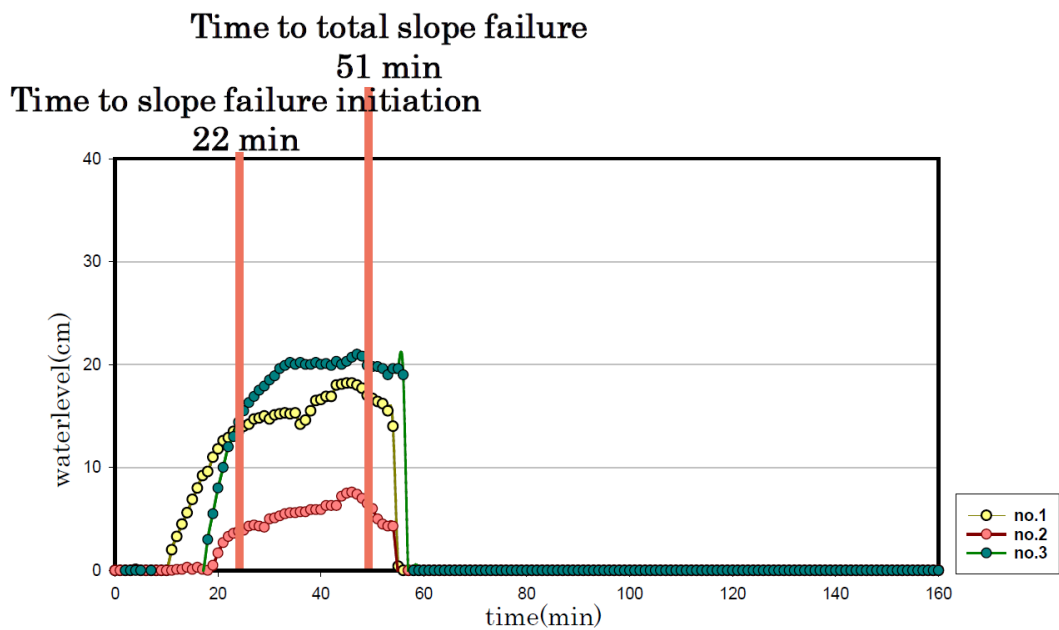
Figure 3. Initiation Failure Time & Total Failure Time

Table 2

	case 1	case 2	case 3
Drainage Conditions	0cm height	10 cm height & discharge holes	10 cm height
Time to slope failure initiation	22 min	44 min	27 min
Time to total slope failure	51 min	100 min	145 min

The sudden collapse was observed in cases 1 and 2, starting from the front edge of the slope following an increase in moisture content, because the reduced shear strength was insufficient to retain the mass of the upper part of the slope. A new collapse then began from the bottom of the slope, propagating to the top. Under the drainage conditions for case 2, the collapse was observed within a longer rainfall duration, indicating a lower collapse speed than observed for case 1.

Video recordings of the experiment confirmed that in case 1, the most transient and rapid collapse process was observed, loss of integrity occurred rapidly with continuous erosion of the front section of the slope. The initial collapse occurred 22min after the start of rainfall, and the collapse process took 19 minutes. (Figures 4)



**Figure 4. Groundwater level changes (Case 1).**

The impervious plate installed in case 2 was originally intended to change the drainage conditions of the slope while keeping all other conditions consistent with those of case 1. The plate also acted as a counterweight fill, providing an opposing force to the outflow of water and soil, although saturated groundwater was discharged from the drainage holes. The plate supported the bottom of the slope to some degree, thus maintaining the stability of the entire slope. Therefore, the total collapse time and duration of each stage were longer for case 2 than for case 1, which lacked an impervious plate.

In case 3, we observed the longest and slowest collapse process. The initial collapse occurred 27 min after the start of rainfall, but soil movement and changes in the slope surface then slowed considerably. Although the water was observed on the surface and at the toe of the slope, indicating that saturation was imminent, a slow slide associated with liquefied soil was observed instead of sudden collapse, as observed in case 2. In case 3, initiation failure occurred earlier than in case 2, but the time to total failure was longer than in case 2. All three groundwater gauges indicated a rise in groundwater level early in the rainfall period, and faster than in case 2. Initiation failure was observed when the gauges detected the maximum groundwater level at all three points.

Comparing groundwater levels between case 2 and case 3 (Figures 5 and 6, respectively), the collapse occurred as the groundwater level rose to that of the gauge installed at the toe of the slope model. A previous study, conducted by Tohari et al., 2007, concluded that sudden collapse was expected to occur as the toe of the slope model approached saturation even if other parts of the model were unsaturated. During rainfall, the water table approaches the surface; slope failure is ultimately caused by pore pressure and seepage forces, which increase due to reduced shear strength. Following the collapse, the water table continues to change due to rainfall, and its new shape will affect the seepage face and infiltration rate; without shear force, the inside of the slope becomes unstable, and a feedback loop occurs, causing the collapse to propagate outwards from its point of

inception. In case 2, the groundwater level rose continuously at all three gauge positions as the propagate of collapse occurred.

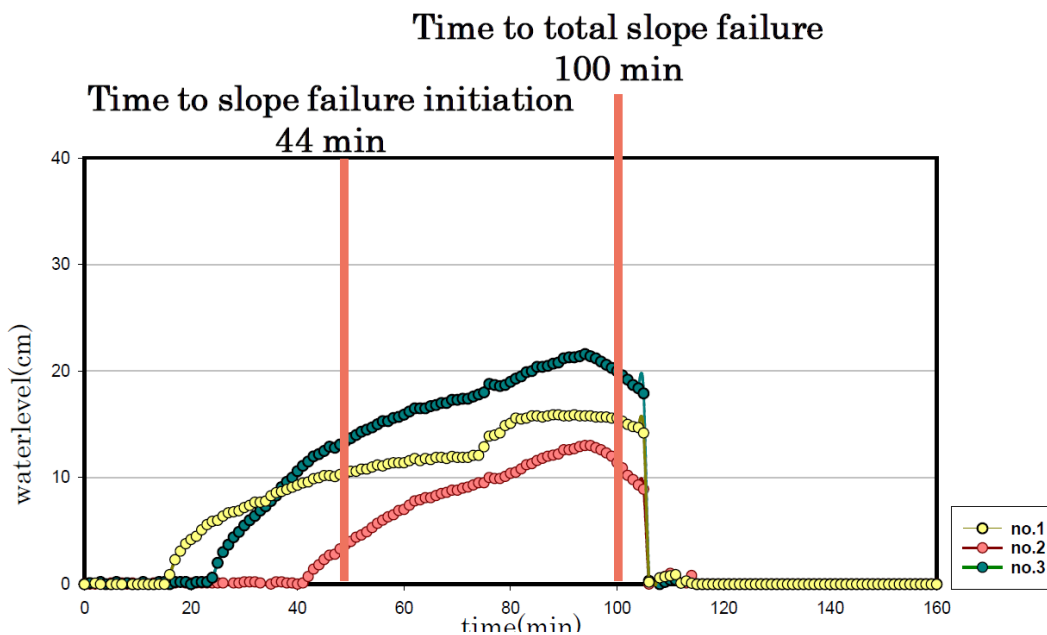


Figure 5. Groundwater level changes (Case 2)

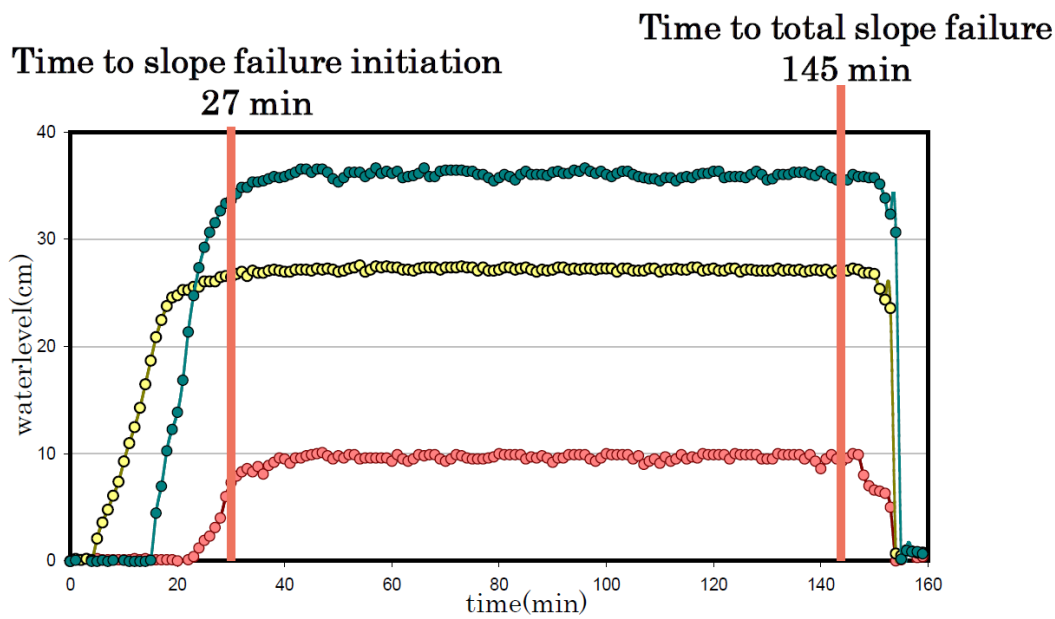


Figure 6. Groundwater level changes (Case 3).

In case 2, we imposed drainage and bottom resistance simultaneously, to lengthen the time to initial slope failure. Since the balance of forces within the slope changes constantly due to drainage, the slope model continued to collapse and the time to total slope failure was shorter than that of case 3. In case 3, forces at the bottom of the slope resisted collapse; however, groundwater rose to exceed 10 cm. Under such drainage conditions, groundwater,

which is considered to be the most important factor affecting slope stability, rose rapidly, but with relatively consistent infiltration and outflow. Thus, the groundwater level and saturation degree did not change, allowing the soil to remain more stable.

## Conclusion

In this study, we conducted three experiments to investigate the mechanism of slope failure initiation due to frequent, intense precipitation.

In case 1, no impervious plate was present and the slope was completely drained, such that the lower part of the slope quickly reached saturation after the onset of rainfall; collapse was sudden and dramatic. In case 2, the presence of an impervious plate allowed forces on the slope to maintain its stability, thereby lengthening the failure process than case 1. And the collapse process of case 2, occurs on a continuum, have also caused the groundwater within the slope to rise.

In case 3, we imposed a 10-cm drainage condition, such that the groundwater level within the slope rose rapidly to approach saturation; infiltration and outflow remained constant. This equivalent condition between input rainfall and discharge of outflow may lead to taking the longer time of total slope collapse compared to the case2.

We speculate that there may be a correlation between groundwater zone formation and evolution during rainfall and slope collapse. In conclusion, at the same rainfall intensity, differences in the shape of the slope and drainage conditions affected the progression of collapse.

## References

- Japan Meteorological Agency. (2009) Watching report of meteorological changes 2009, 29–30 (Chapter 1).
- Kawagoe, S., Esaka, Y., Ito, K., Hijioka, Y. (2014) Estimated sediment hazard damage using general circulation model outputs in the future. *Journal of the Japan Society of Civil Engineers, Ser. G (Environmental Research)* 70 (5), 167–175
- Anusron C., Toshikazu H., Hirotaka S., Tomotaka S., Y. (2018) Experimental tests of slope failure due to rainfalls using 1g physical slope models. *Soils and Foundations* 58 (2018), 290–305
- Tohari, A., Nishigaki, M., Komatsu, M., 2007. Laboratory rainfall-induced slope failure with moisture content measurement. *J. Geotech. Geoenviron. Eng.* 133 (5), 575–587

---

# Evaluation and adaption of existing protection measures to the Austrian Standards at the Poellinger Torrent

Claudia Sauermoser<sup>1</sup>

**Keywords:** existing technical protection measures; Austrian Standards; protection goal; design event; monitoring

## Abstract

In the catchment of the Poellinger Torrent various technical protection measures exist with different construction states. A main check dam is partly destroyed and cannot fulfil its function any longer, which means a high risk for the downstream village in case of a break down. The aim of this paper is to show a practical example of how to adapt existing protection measures to the Austrian Standards. Therefore all structures were visually evaluated. A detailed hydraulic calculation was carried out for the downstream channel. With the gained data from the field and the modeling, different variants were checked. To find a realizable solution - from economical and technical point of view - the protection goal had to be adjusted.

## Introduction

The Austrian Service for Torrent and Avalanche Control is a federal institution aimed at protecting settlement areas and infrastructures against natural hazards. One of the main tasks is planning, building and maintaining technical protection measures against torrents, avalanches and rockfall. In total, 64,160 transverse structures against torrent hazards exist in Austria. These structures were implemented during the last hundred years with an average age of the check dams of nearly 50 years [Fink, 2018]. The state of the art has been continuously developed within the last decades due to intensive research and practical experience in the field of natural hazards. Until the beginning of the 21<sup>st</sup> century, there were no clear technical standards about functional or structural attributes, which led to many different types of protection structures in different conservation status nowadays. Many of them do not fulfil modern standards and there is a reason to doubt that they might not all work in case of a design event. This unsatisfying situation led to the elaboration of common standards in torrent control. The standardization process started 10 years ago with the aim to unify and harmonize planning, design, construction and maintenance of torrent protection constructions. Currently it is mandatory to consider the Austrian Standards (ONR) in the planning and building of technical protection measures. The big challenge, however, is to adapt the already existing constructions to these standards. This is necessary

---

<sup>1</sup> Claudia Sauermoser, DI Austrian Service for Torrent and Avalanche Control  
Villach, Austria (claudia.sauermoser@die-wildbach.at)

to guarantee the function of old constructions in case of a design event and to guarantee safety from torrent hazards. This paper aims to show a practical example how to adapt existing protection measures to the Austrian Standards at the Poellinger Torrent in the municipality of Treffen in Carinthia, Austria.

## Methods

In general, different steps are necessary to renew constructions in a torrent:

- Definition of a modern protection goal based on the present hazard zone map and the ONR.
- Analysis of the existing constructions, e.g. the construction state or function against the design event.
- Variation studies of protection concepts under consideration of the protection goal and the analysis of existing constructions.

Based on the analysis it has to be decided, whether the existing constructions can be integrated into the new protection concept, perhaps with adaptations, or have to be replaced by new protection measures.

The catchment of the *Poellinger Torrent*, with an area of 10.36 km<sup>2</sup>, is located in the westernmost part of the Gurktal Alps in Carinthia, Austria. Paragneis and mica schist with moraines in the middle part dominate in the catchment. The annual precipitation rate at the nearest weather station (715 m above the Adriatic Sea level) is 1005 mm (1896-2015) and the maximum one-day-precipitation is 127.7 mm (29/08/2003). The catchment area is covered 70 % by forest, mainly by spruce. 26.4 % of the area is used for agriculture and the remaining area is with 3.6 % settled area at the debris cone. In the past, several debris flows occurred. An event in 1948 was marked because of its high intensity with about 20.000 m<sup>3</sup> of debris deposition at the alluvial fan.

The former events led to an implementation of 146 structural measures in total from 1910 to 1988. In addition, the middle and upper part of the catchment was afforested. In 2018, all of these longitudinal and transverse structures were visually evaluated and classified in their construction state according to the Austrian Standards [ONR 24803]. Apart from the technical, also other factors concerning the surrounding and the function of protection measures, e.g. the sedimentation degree or the ability of migration for fish, were assessed. The ONR 24803 defines seven construction state classes as follows (for key function constructions “S” is used in front of the number):

0: Construction is dispensable

1: Very good condition

2: Good condition

3: Sufficient condition

4: Insufficient condition

5: Bad condition

6: Destroyed

The classes include a forecast of the development of the structural stability and the functionality depending on the expected events. The classification is based on the ability to fulfil the protection function at the time of evaluation, after the next 30-year event, the next design event (150-year event) or in long term. With the probable development a differentiation between the classes, e.g. class 4 and 5 is possible. Furthermore, the damages are classified in “uncritical”, “critical” and “urgent need for action”. [Suda and Mehlhorn, 2013].

In addition, the functionality was evaluated with a focus on the design, the expected process and if the construction has full, limited or no function against a design event.

In the hazard zone map, the design runoff at the debris cone is defined with 50 m<sup>3</sup>/s including debris. The debris discharge is estimated with approximately 15,000 m<sup>3</sup> at the debris cone. For a design event, it is expected that the debris blocks the channel and the water run-off and debris can spread over wide areas of the debris cone and harm the village of Treffen. The potential amount of woody debris was estimated based on empirical values with 20 % of the total expected debris.

In a next step, the protection goal for the village of Treffen was determined to define a protection concept based on the ONR 24802. The decisive factor was the hydraulic system at the downstream section between hectometer (hm) 6.00 and hm 0.00. The critical cross-sections were first determined by empirical formulas. After that, a detailed modelling of the hydraulic system and the bedload transport was carried out using an online bed-load discharge tool and HEC-RAS. Both tools calculated the capacity of the existing channel.

The online bed-load discharge tool is a one-dimensional tool using different formulas. For the *Poellinger Torrent*, the formula of Smart & Jäggi (1983) was used due to the slope up to 10 %. For the one-dimensional tool, the roughness coefficients were estimated with  $k_{st} = 50 \text{ m}^{1/3}/\text{s}$  [Naudascher, 1992]. The cross-sections were calculated with steady and unsteady flow including debris.

Besides, HEC-RAS was used to verify the results calculated with the one-dimensional tool. The existing channel was integrated into the digital evaluation model with CIVIL-3D. A geodetic survey was not conducted. For the modelling, an unsteady flow with a roughness of 60 m<sup>1/3</sup>/s was used.

After the protection concept was determined, the new and existing structures were dimensioned based on the ONR 24801 which defines the static and dynamic actions on structures.

## Results and discussion

The protection goal is to protect the village of Treffen against the impact of the defined design event in the hazard map, which is classified as a 150-year-event. Based on this goal further analysis and the variation study were conducted.

In Table 1, the most important constructions are summed up with their construction state, their functionality and if the construction is taken into account in the future protection concept. Figure 1 gives an overview of where the measures are situated in the catchment area. The numbers in Figure 1 correlate with the numbers in Table 1.

**Table 1: Summary of the existing constructions with their construction state according to the ONR 24803, their functionality and the consideration in the future protection.**

No.	Position	Construction type	Year	Construction state	Functionality	Consideration in protection system
1	hm 31.13 – hm 25.57	check dam chain	1990 - 2000	2	limited function, gaps between dams with sliding	considered, remaining debris expected
2	hm 24.26	bed load sorting dam	1990	S2	limited function, too small volume	not considered;
3	subbasin	check dam chain	1950	3	full function	considered
4	subbasin	bed load sorting dam	2007	S2	full function	considered
5	hm 22.17 – hm 18.76	check dam chain	1948-1951; 1992	2	full function	considered
6	hm 17.25	check dam	1938; 1992	S5	no function, filled up with sediment	removed
7	hm 16.27	check dam	1950; 1992	3	full function	considered
8	hm 14.00	Curve dam	1950-1951; 1990	S3	limited function; too small volume (3.000 m <sup>3</sup> )	considered
9	hm 10.21 - hm 6.26	15 concrete sills	1931-1933; 1952-1953; 2003	2	full function	considered
10	hm 10.57 – hm 6.0	concrete channel	1930-1935; 1938-1958; 1989-2007	2	full function	considered
11	hm 6.00 – hm 0.00	concrete/ cement mor-	1961-1971	2	limited function, too small	adapted

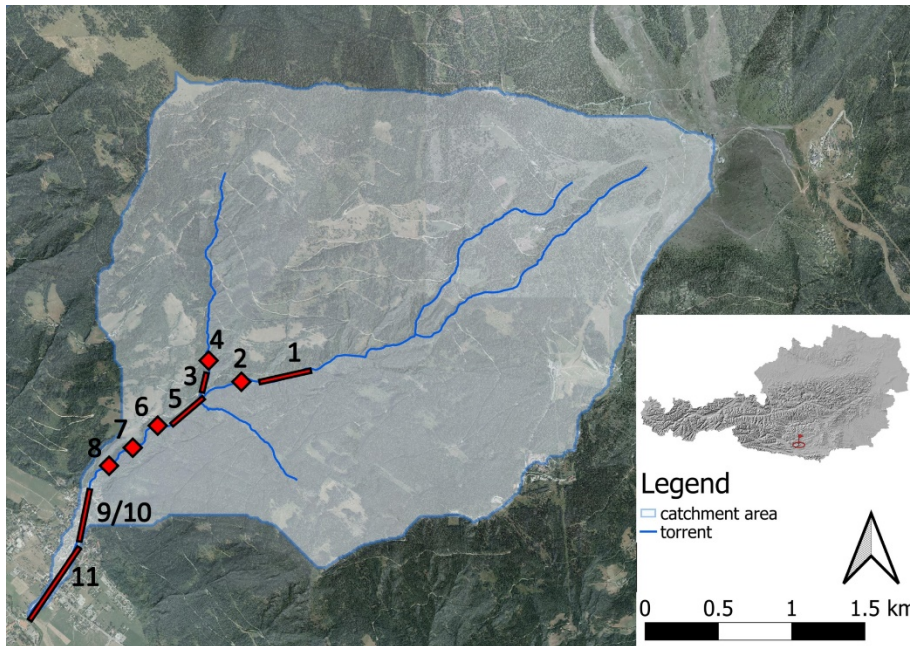


**Figure 1: Location of the existing constructions in the catchment area of the Poellinger Torrent. The numbers in Figure 1 correlate with the numbers in Table 1.**

A main bed load-retention dam in hm 17.25 (Table 1; No. 6), built in 1938 out of cement mortar and adapted in 1988 with concrete, is partly destroyed at the right wing and cannot fulfil its function any longer, which means a high risk for the village in case of a break down. The dam was designed as a consolidation check dam but was used as a bed load-retention dam during the last decades. The check dam has no openings to allow fine-grained sediment passing through. Due to the old structure no static proof of the check dam exists. Therefore, a further adaption is very complex and difficult. Figure 2 shows the destroyed wing of the check dam in hm 17.25.



**Figure 2: Partly destroyed check dam in hm 17.25 built in 1938 and adapted in 1988.**

The check dam chain in the middle reach (Table 1; No. 1, 3 and 5) is in a good structural and functional condition. For the channel, the visual evaluation shows a good constructional state but a too small hydraulic dimensioning. Both methods confirm that the channel can transport a design event of 50 m<sup>3</sup>/s until hm 5.30. From hm 5.30 until the receiving water, the slope is constantly decreasing. Table 2 shows the transport capacity of the lower channel calculated with the online bed-load discharge tool. The weakest point is at hm 3.80, where the channel has only a capacity of 23 m<sup>3</sup>/s and buildings are the closest to the torrent (Figure 3). At hm 2.60, where a bridge of the main road exists, the channel has a capacity including freeboard of 40 m<sup>3</sup>/s. With the bed-load discharge tool the bed load transport capacity was calculated with 1,100 m<sup>3</sup>. The calculations with HEC-RAS confirm that the weakest point of the hydraulic system is at hm 3.80. This is equal to a 50-year flood.

**Table 2: Results of the online bed-load discharge tool for different cross-sections at the Poellinger Torrent Channels.**

Position	Cross section area [m <sup>2</sup> ]	Slope [%]	Roughness	Velocity [m/s]	Capacity [m <sup>3</sup> /s]
hm 5.30	4.9	7.5	50	6.2	30
hm 3.80	4.5	5	50	5.2	23
hm 3.60	5.2	5	50	5.6	29
hm 2.60	8.2	3	50	5.2	40
hm 1.20	4.5	2	50	3.5	16



**Figure 3: Weakest point of the channel regarding the hydraulic dimensioning and limited space between existing buildings.**

The field surveys and the hydraulic calculations show that the protection measures at the *Poellinger Torrent* are not able to handle a design event. Even though numerous structural measures exist at the *Poellinger Torrent*, 15,000 m<sup>3</sup> of debris are still expected to reach the alluvial fan due to the high number of unstable slopes in between the measures. Regarding the whole protection system at the *Poellinger Torrent*, measures with key function according to the Austrian Standards are located in the middle reach but not at the neck of the alluvial fan in front of the village to directly protect it.

Based on the gained data and results the following protection measures were planned under consideration of technical and economical aspects:

- Bed-load sorting dam in hm 17.25 with a total capacity of 10,000 m<sup>3</sup> instead of the destroyed check dam.
- A net barrier in hm 11.32 to filter remaining debris and woody debris (1,000 m<sup>3</sup>).
- Enlargement of the channel between hm 0.30 and hm 5.80 with vertical concrete walls.

Instead of the destroyed check dam, a bed-load sorting dam according to the state of the art is planned. The old one will be removed as further adaption would have been difficult due to the static proof. The bed load sorting dam is designed as a reinforced concrete structure with two openings and a steel construction to deposit debris and wood and let fine-grained material pass through. Driftwood is taken into account with a steel construction designed to avoid blockages of the openings and to keep them open as long as possible.

At the neck of the alluvial fan, a net barrier is planned to filter the remaining debris and woody debris originated on a distance of about 600 m between hm 17.25 and hm 11.32. Log- or driftwood jams will be avoided with this measure in the downstream channel. The net is situated directly at the beginning of the settled area to have the best possible effect. With a volume of 1,000 m<sup>3</sup> the deposition area is large enough for the remaining woody debris.

Between the planned bed load sorting dam and the net barrier an existing curve dam at hm 14.00 adapted to a bed load sorting dam in 1990 is able to deposit about 3,000 m<sup>3</sup> of debris and woody debris.

Even though the problem of debris and wood is solved with the bed-load sorting dam and the net barrier, the calculations of the hydraulic system of the channel show that the design event can only be transported until hm 5.30. The runoff of 50 m<sup>3</sup>/s including debris was reduced to a water runoff with only fine-grained material of 46 m<sup>3</sup>/s for the further planning due to the retention of debris. This led to a discussion, how to handle the situation at the debris cone considering a balance between protection and economical aspects. During the planning process, three variations were proofed in detail for the channel:

Variation A: This alternative contains no measures along the channel at the debris cone. The focus is on the management of the debris in the middle reach. This means an outburst of the *Poellinger Torrent* at cross-section hm 5.30 and a high remaining risk for the village. The protection goal will not be reached. An advantage would be lower costs for the implementation.

Variation B: The existing channel will be enlarged to a capacity of a 50-year flood (40 m<sup>3</sup>/s). This would imply that the bridge of the main road must not be reconstructed. Two small bridges at the weakest point would have to be replaced for this, however. Even though the space is very limited, an enlargement to 40 m<sup>3</sup>/s is technically realizable. The remaining risk is lower than before when the channel has only a capacity of 23 m<sup>3</sup>/s.

Variation C: This variation contains an enlargement to the design event of 50 m<sup>3</sup>/s. In this case, the reconstruction of the main bridge and two other bridges is necessary. The limited space demands high technical development and the existing channel must be removed totally. As a consequence of this variation, hazard zones should be reduced along the channel. Nevertheless, the costs would not stand in relation to the reduction of the hazards zones.

After several discussions variation B is, regarding technical and economic aspects, considered as the best solution for the downstream channel. The enlargement of the channel to a design event is limited by the main road, several buildings and would only be possible with enormous technical and financial effort. The enlargement of the downstream channel to the 50-year event will be implemented with concrete walls on both sides of the channel. An additional deposition of debris is not expected because the profile of the cross section remains same.

## Conclusion

The in Austria usually defined protection goal could not be achieved for the downstream channel as the field survey and the calculations of the existing measures demonstrated. An adaption to a 150-year event is hardly realizable. Therefore, the protection goal was adapted to the found situation. Flooding with shallow flow depth further down hm 6.0 had to be expected and accepted.

The planned and existing structural measures are able to deposit about 14,000 m<sup>3</sup> of debris. As the calculations show, the remaining 1,000 m<sup>3</sup> of debris should be transported to the receiving river. In the awareness of failures of the hydraulic system in reality, such as a lack of maintenance, a residual risk will remain even after the realization of the project.

In general, one of the main problems is that old structures cannot absorb the static and dynamic actions according to the ONR 24801. Technical structures were erected mainly without reinforcement that might be critical especially by the impact of debris flows.

For the Austrian Service of Torrent and Avalanche Control the existing technical protection measures mean continuous effort in monitoring, control and maintenance together with the municipalities. Further analysis of the concrete status is necessary. With modern calculation methods according to the state of the art, the proof of the functionality is possible and this must be the basis for the decision of renovating or removing. Old and insufficient dimensioned constructions mean a high potential risk because they simulate a safety that is not true. As the example of the *Poellinger Torrent* illustrates, even insufficient dimensioned channels lead to settlement activities too close to the channel. The later necessary widening is therefore not possible or difficult. An alternative might be to adapt the protection goal in the lower parts of the torrent and to focus on the sediment management to reduce damages because of debris and woody debris.

Using the example of the *Poellinger Torrent* an adaption of the protection goal was necessary to find a realizable solution. Even though a residual risk will exist after the implementation, which is delineated in the hazard map and communicated to the municipality, the planned protection measures provide an essential improvement for the village.

## References

Fink T. (2018) State of Affairs: Transverse Structures and WLK. Journal of Torrent, Avalanche, Landslide and Rock Fall Engineering 181. 26 -32.

Naudascher, E. (1992): Hydraulik der Gerinne und Gerinnebauwerke, Springer-Verlag, Wien, New York, 2<sup>nd</sup> Edition.

ONR 24801:2013: Protection works for torrent control – Static and Dynamics actions on structures. Austrian Standards Institute – 2013-08-15

ONR 24802:2011: Protection works for torrent control – Design of structures. Austrian Standards Institute – 2001-01-01

ONR 24803:2008: Protection works for torrent control – Operation, monitoring, maintenance. Austrian Standards Institute – 2008-02-01

Smart G., Jäggi M. (1983): Sedimenttransport in steilen Gerinnen. Mitteilung der Versuchsanstalt für Wasserbau, Hydrologie und Glaziologie der ETH Zürich Nr. 103

Suda J., Mehlhorn S., (2013): Schutzbauwerke der Wildbachverbauung. Handbuch zur Durchführung einer Bauwerkskontrolle. Fassung 15.10.2013. Publisher: BMLFUW, Wien.

---

# The PermaRisk project - Emerging hazards due to mountain permafrost degradation in the French Alps

Philippe Schoeneich<sup>1</sup>, Xavier Bodin<sup>2</sup>, Ludovic Ravanel<sup>3</sup>, Pierre-Allain Duvillard<sup>4</sup>, Marco Marcer<sup>5</sup>, Thomas Echelard<sup>6</sup>, Raphaèle Charvet<sup>7</sup>, André Revil<sup>8</sup>, Diego Cusicanqui<sup>9</sup>

**Keywords:** mountain permafrost; degradation; rock glaciers; thermokarst; infrastructure

## Abstract

The PermaRisk project was devoted to the study and assessment of hazards linked to mountain permafrost degradation in the French Alps, resulting from rock glacier destabilization, thermokarst lakes and infrastructure on permafrost. It provided several datasets covering the entire French Alps: a new permafrost map, an inventory of rock glaciers, an inventory of destabilized rock glaciers and an assessment of their sensitivity to degradation, an inventory of thermokarst lakes, an inventory of infrastructure built on permafrost and an assessment of their vulnerability, as well as several case studies. These data will be made available to local authorities and to hazard managers.

## Introduction

Mountain permafrost is considered as highly sensible to climate change and is expected to experience degradation due to atmospheric warming. Many signs of ongoing degradation are already observed for more than twenty years throughout the Alps, especially an increase of rockfalls in high mountain rock faces, or an acceleration of rock glacier motion which can lead to complete destabilisation. These phenomena generate direct (rockfalls) or indirect hazards (through debris flow generation or thermokarst outflow). In order to assess these emergent hazards in the French Alps, the EU POIA *PermaRisk* project was launched in 2016. We present here the results and products of the project.

---

<sup>1</sup> Université Grenoble Alpes, France, ([philippe.schoeneich@univ-grenoble-alpes.fr](mailto:philippe.schoeneich@univ-grenoble-alpes.fr))

<sup>2</sup> Université Savoie Mont Blanc, France

<sup>3</sup> Université Savoie Mont Blanc, France

<sup>4</sup> Université Savoie Mont Blanc, France

<sup>5</sup> Université Grenoble Alpes, France

<sup>6</sup> Université Grenoble Alpes, France

<sup>7</sup> Université Savoie Mont Blanc, France

<sup>8</sup> Université Savoie Mont Blanc, France

<sup>9</sup> Université Grenoble Alpes, France

## The Permarisk project

The *PermaRisk* project is conducted by a consortium of researchers from the Institute for Urban Planning and Alpine Geography – Univ. Grenoble Alpes, and the EDYTEM lab – University Savoie Mont Blanc, in association with the French service for mountain hazard management (RTM). It is co-funded by the Region Auvergne Rhône Alpes, the IMSrn engineering company, the ERDF through the EU POIA interregional program and the French National Fund for territorial development (FNADT).

The *PermaRisk* project focuses on emergent hazards due to mountain permafrost degradation in superficial deposits. This includes rock glaciers, debris-covered ice affected by thermokarst evolution and infrastructure built on either of these environments. The project is therefore structured into three thematic work packages:

- rock glaciers and related direct and indirect hazards;
- thermokarst lakes and related hazards;
- infrastructure on permafrost and related vulnerability and damages.

For each of these topics, the following objectives were intended:

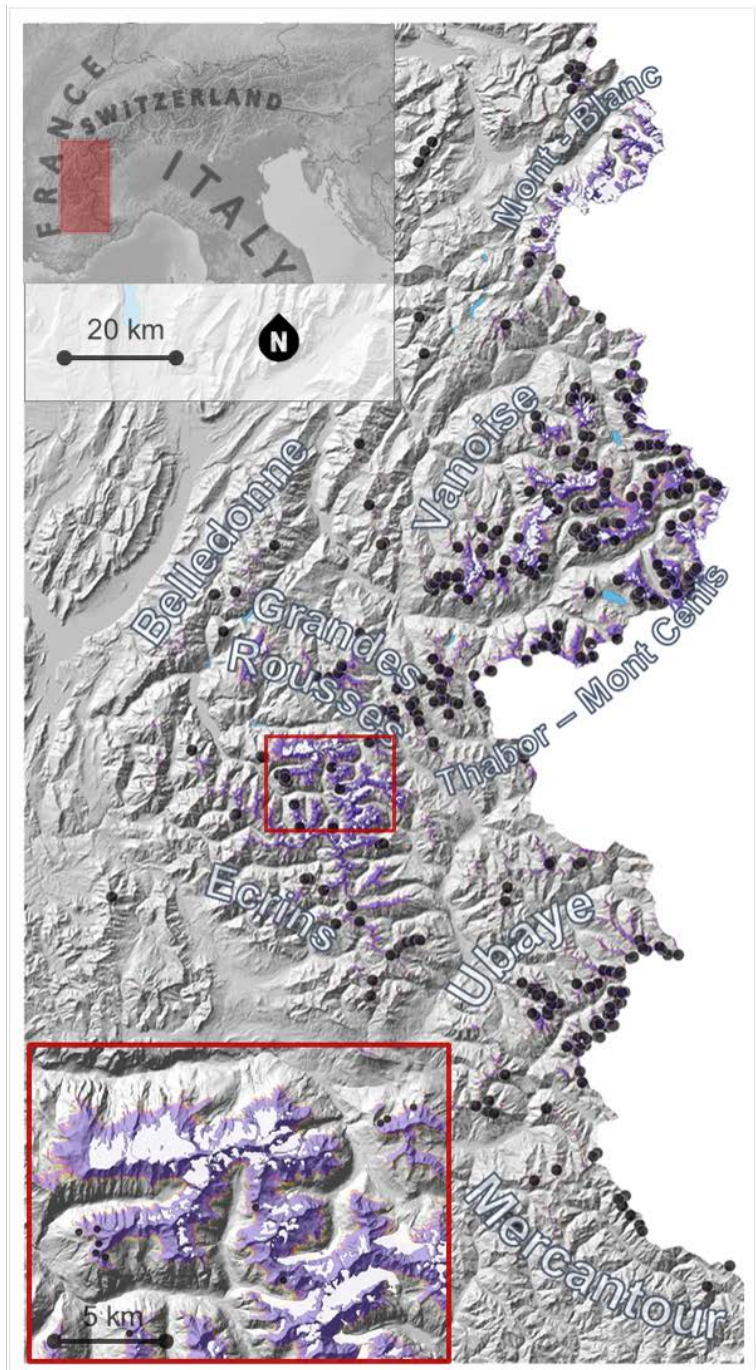
- mapping and creating inventories over the entire French Alps, including sensitivity and vulnerability assessments;
- local case studies of representative examples;
- elaboration of recommendations for hazards assessment, prevention and mitigation.

## Results and products

The main products are detailed below. Some are already published as scientific papers, and most of them will be made available online.

A first set of data includes GIS layers covering the entire French Alps:

- A new permafrost distribution map for the French Alps (Fig. 1, Marcer *et al.*, 2017): this map follows a similar approach as the previously existing *Alpine Permafrost Index Map* (APIM), but was calibrated on an extensive inventory of rock glaciers and revised climate data. It considers rooting zones of rock glaciers for calibrating the permafrost favourability index.



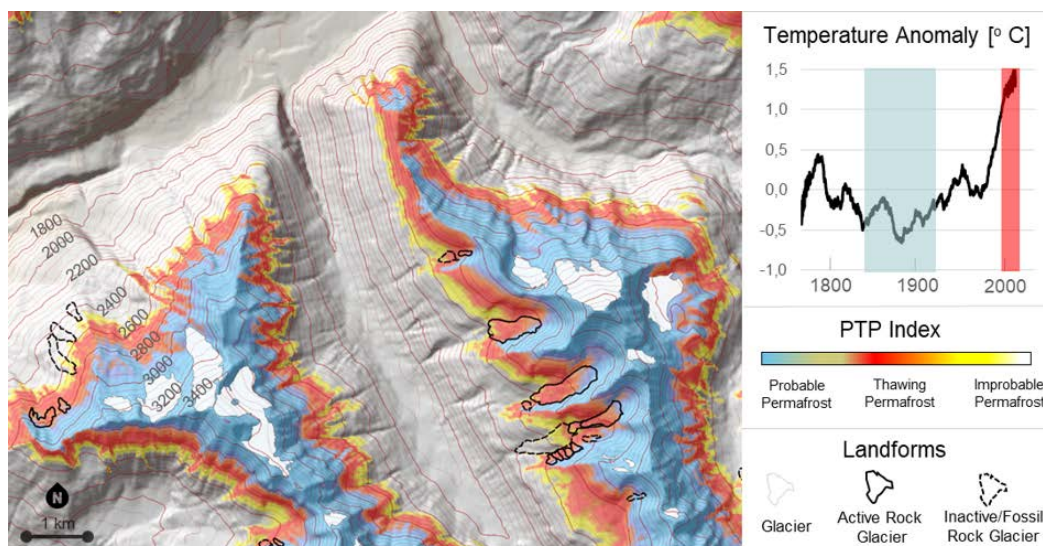
**PFI**  
Permafrost Favourability Index

Figure 1 Permafrost Favourability Index map of the French Alps (from Marcer et al. 2017). Interpretation according to color scale: purple = very favourable to permafrost in all conditions, yellow = unfavourable to permafrost in almost all conditions. Black dots represent active rock glaciers used for calibration. Box in the lower left: zoom on the Ecrins massif.

- A complete rock glacier inventory, conducted since 2013 in collaboration with RTM: a total of 3261 rock glaciers were identified throughout the French Alps above 2000 m a.s.l., from which 814 are classified as active, 671 as inactive, and 1776 as fossil. The activity rate of all active rock glaciers was checked by diachronic aerial photograph comparison, and is going to be updated by InSAR data.

- An inventory of destabilized rock glaciers: this inventory is based on the identification of destabilisation indices on aerial photographs like cracks, crevasses and scars indicating extensive stress, and on surface velocity time series, derived from historical aerial photographs. This inventory included 46 rock glaciers showing signs of destabilisation, of which 19 experienced a strong acceleration during the two last decades (Marcer *et al.*, 2019; Marcer *et al.* 2021).

- A map of “Potential Thawing Permafrost” (PTP), indicating the sensitivity of permafrost to climate induced degradation, based on the increased mean annual air temperature since the end of Little Ice Age (Fig. 2, Marcer *et al.*, 2019).



**Figure 2** Map of Potential Thawing Permafrost (PTP). The red fringe indicates the altitudinal belt where permafrost is still observed, but no longer in favourable climatic conditions (from Marcer *et al.* 2019).

- An assessment of the susceptibility of rock glaciers to destabilization based on topographic and climatic parameters. Based on this, a map of susceptibility for the destabilization of ice-rich permafrost was created, which identifies the rock glacier areas that may encounter destabilization (Fig. 3, Marcer *et al.*, 2019).

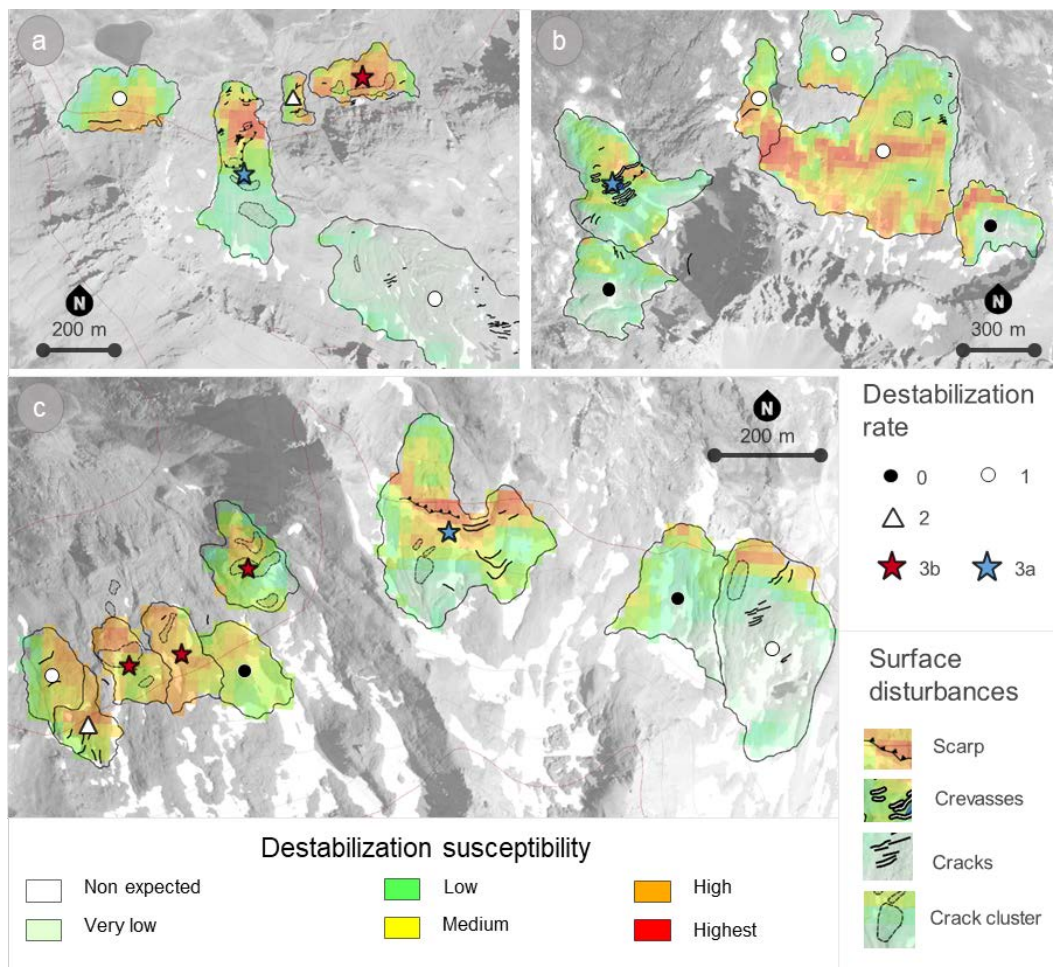


**Figure 3 Destabilization susceptibility of rock glaciers (from Marcer et al. 2019). Color scale indicates the modelled susceptibility to destabilization. Linear symbols indicate observed destabilization signs that served for calibration of the model. Dots and stars indicate the destabilization classes inferred from observed signs.**

- An inventory of thermokarst lakes: this includes lakes forming either on rock glaciers or on zones of debris covered dead ice bodies, but outside of known glacier extents. These ephemeral features were only rarely considered, but several observations indicate that their occurrence could increase and generate a hazard potential in form of outburst floods. In order to complete and update this first inventory, a participative tool (a smartphone app) was developed in order to encourage mountain practitioners to communicate their observations.

- An inventory of infrastructure built on permafrost areas according to the permafrost distribution map for the French Alps, mainly on superficial deposits, but also on frozen bedrock, revealed approximately 1000 infrastructure elements (pylons, lower or top stations, huts, ...) built on permafrost, sometimes on rock glaciers (Duvillard *et al.*, 2019a). Most are elements of ropeway transport systems.

- An assessment of the sensitivity of infrastructure to permafrost degradation: this includes an inventory of damages to infrastructure, with reconstruction of the history of damages and remediation, and the construction of an infrastructure vulnerability index (Fig. 4, Duvillard et al. 2015, revised version in review).

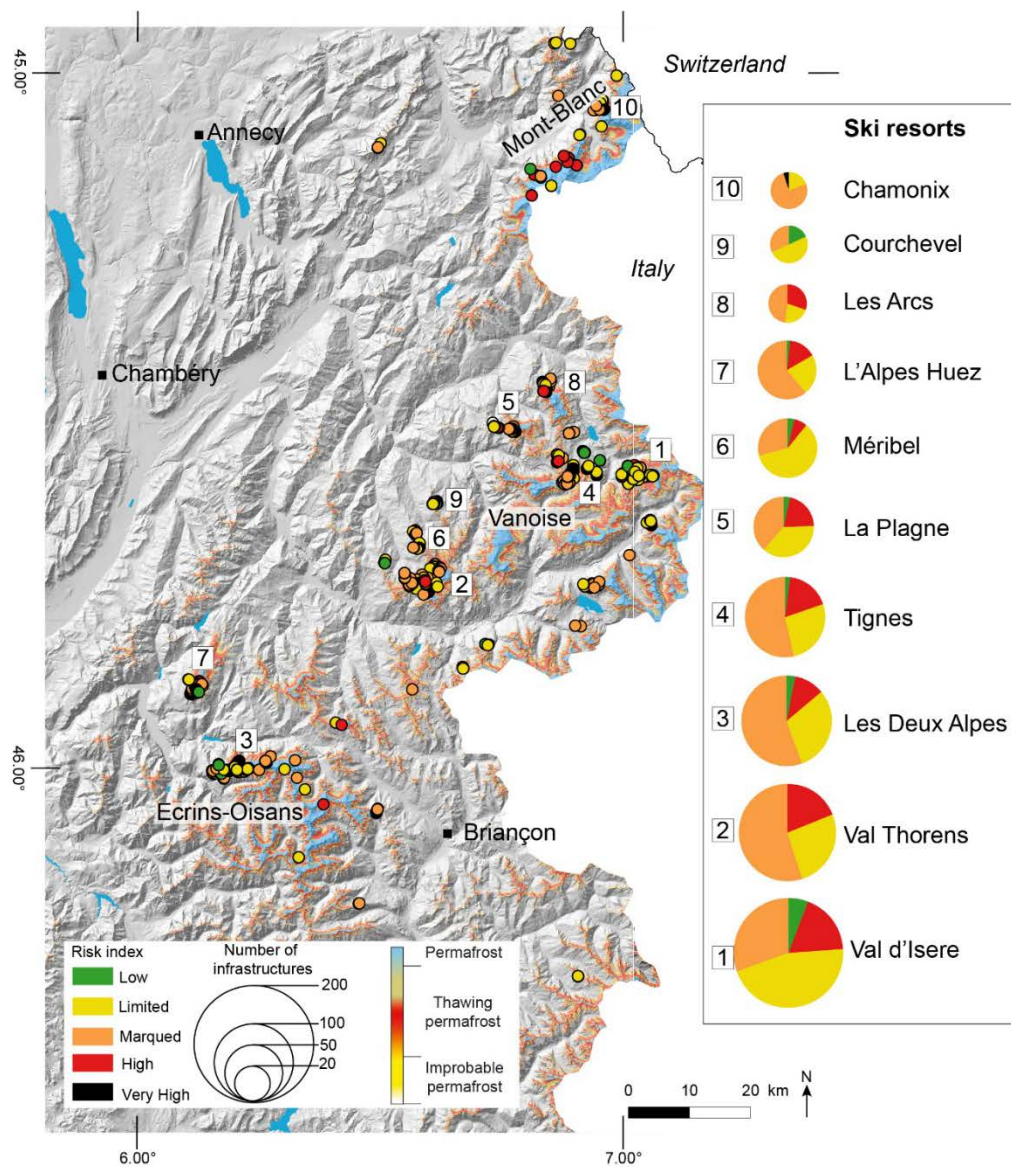


Figure 4 Distribution of infrastructure elements on permafrost in the French Alps, rated according to the risk index (from Duvillard, in review). Base map: PTP map, see figure 2.

A second dataset includes detailed local case studies, conducted on representative examples or on cases where an event occurred just before or during the project:

- For destabilized rock glaciers, the main case study concerns the Col du Lou rock glacier, where two frontal failures induced a debris flow in August 2015, causing extensive damage at Lanslevillard (Savoie). The results show that the event resulted from the combination of progressive acceleration since the 1990's, an early snow melt, a strong heat wave in early summer, and a rainy period and strong thunderstorms as final trigger (Marcer *et al.*, 2020). Other case studies concern rock glaciers showing strong destabilization signs and/or a strong acceleration in the last decades (Marcer *et al.* 2021).

- For thermokarst, the main case study concerns the area of Col des Vés-Pramecou above Tignes (Savoie), where successive thermokarst lakes form at least since the 1950's, and drain after a few years (Duvillard *et al.* submitted). The area allows to study the life cycle of such lakes. Geophysical investigations show that the lakes form on a very thick dead glacier ice body. The ice is potentially much older than Little Ice Age. Similar conditions were described for the Lac Chauvet (Haute Ubaye) (Cusicanqui *et al.* in prep.).

- For infrastructure, the main case study concerns a destabilised cableway pylon built on a rock glacier at Val Thorens (Savoie). Field investigations show that the modification of melt water drainage patterns by ski track planation works may have played the main role in the destabilisation process, by enhancing locally the permafrost degradation and inducing suffosion under the pylon foundations (Duvillard *et al.*, 2019b).

Finally, recommendations for stakeholders were elaborated. They contain guidelines for the identification of potential hazards due to mountain permafrost and to its degradation, for the evaluation of the hazard, for monitoring identified cases, and for possible prevention and mitigation measures. They include also proposals for the information of concerned populations.

## Conclusion

The *PermaRisk* project provides a whole set of homogenous and comprehensive datasets covering for the first time the whole alpine territory of a country. The data include maps and inventories of permafrost distribution, permafrost sensitivity to climate change, rock glacier destabilization, infrastructure on permafrost, vulnerability of infrastructure elements to permafrost-induced destabilisation, and thermokarst occurrence. They will provide a valuable base for stakeholders for the management of permafrost-induced hazards. They constitute a major contribution to the governmental action plan for the prevention of hazards of glacial and periglacial origin, which is being implemented by the French ministry of environment.

## References

- Cusicanqui D., Rabatel A., Vincent C., Bodin X., Francou B. (in review). Interpretation of volume and flux changes of the Laurichard rock glacier between 1952 and 2019, French Alps. *Journal of Geophysical Research*.
- Cusicanqui, D., Bodin, X., Rabatel, A., Duvillard, P.A., Schoeneich, P., Berthet, J., Revil, A. (in prep.). Investigating the multi-decadal (1948-2020) thermokarst dynamics of the Chauvet glacial and periglacial complex, Southern French Alps. *The Cryosphere*.
- Duvillard P.A., Ravel L., Deline P. 2015. Risk assessment of infrastructure destabilisation due to global warming in the high French Alps. *Journal of Alpine Research*, 103-2. DOI:10.4000/rga.2896
- Duvillard P.-A., Ravel L., Deline P., Dubois L. (2018) Paraglacial Rock Slope Adjustment Beneath a High Mountain Infrastructure—The Pilatte Hut Case Study (Écrins Mountain Range, France). *Front. Earth Sci.* 6:94. doi: 10.3389/feart.2018.00094
- Duvillard, P. A., Revil, A., Qi, Y., Soueid Ahmed, A., Coperey, A., & Ravel, L. (2018). Three-dimensional electrical conductivity and induced polarization tomography of a rock glacier. *Journal of Geophysical Research: Solid Earth*, 123. <https://doi.org/10.1029/2018JB015965>
- Duvillard P.-A., Ravel L., Marcer M., Schoeneich P. (2019a). Recent evolution of damage to infrastructure on permafrost in the French Alps. *Reg. Environ. Change*, 19:1281–1293. DOI:10.1007/s10113-019-01465-z
- Duvillard P.A., Ravel L., Schoeneich P., Marcer M., Piard J.F. (2019b). Analyse multi-méthodes de la déstabilisation d'un pylône de remontée mécanique implanté sur un glacier rocheux des Alpes françaises. *Géomorphologie. Relief. Processus. Environnement*, 25/1:21-36. DOI:10.4000/geomorphologie.12945
- Duvillard, P.-A., Magnin, F., Revil, A., Legay, A., Ravel, L., Abdulsamad, F., Coperey, A., 2021. Temperature distribution in a permafrost-affected rock ridge from conductivity and induced polarization tomography. *Geophysical Journal International* 225, 1207–1221. <https://doi.org/10.1093/gji/ggaa597>
- Duvillard P.A., Ravel L., Schoeneich P., Deline P., Marcer M., Magnin F. (in review). Qualitative risk assessment and strategies for infrastructure on permafrost in the French Alps. *Cold Regions Science and Technology*.
- Duvillard, P.A., Cusicanqui, D., Charonnat, B., Marcer, M., Revil, A., Menard, G., Schoeneich, P. (submitted). Evolution of thermokarsts over seven decades in an Alpine ice-rich rock glacier / dead ice complex. *Arctic, Antarctic and Alpine Research*.

Marcer, M., Bodin, X., Brenning, A., Schoeneich, P., Charvet, R., Gottardi, F. (2017). Permafrost Favorability Index: Spatial Modeling in the French Alps Using a Rock Glacier Inventory. *Frontiers in Earth Science*, 5:1–17. <https://doi.org/10.3389/feart.2017.00105>

Marcer, M., Serrano, C., Brenning, A., Bodin, X., Goetz, J., Schoeneich, P. (2019). Evaluating the destabilization susceptibility of active rock glaciers in the French Alps. *The Cryosphere*, 13:141–155. <https://doi.org/https://doi.org/10.5194/tc-13-141-2019>

Marcer, M., Nielsen, S. R., Ribeyre, C., Kummert, M., Duvillard, P. A., Schoeneich, P., Bodin, X., Genuite, K. (2020). Investigating the permafrost slope failures at the Lou rock glacier front , French Alps. *Permafrost and Periglacial Processes*, 31:15-30. DOI: 10.1002/ppp.2035

Marcer, M. (2020). Rock glaciers automatic mapping using optical imagery and convolutional neural networks. *Permafrost and Periglacial Processes*, 31: 561– 566. <https://doi-org.proxy.findit.dtu.dk/10.1002/ppp.2076>

Marcer, M., Cicoira, A., Cusicanqui, D., Bodin, X., Echelard, T., Obregon, R., Schoeneich, P. (2021). Rock glaciers throughout the French Alps accelerated and destabilised since 1990 as air temperatures increased. *Communications Earth & Environment*. <https://doi.org/10.1038/s43247-021-00150-6>.

---

# WoodFlow project – large wood management in rivers

Nicolas Steeb<sup>1</sup>, Alexandre Badoux<sup>2</sup>, Robert M. Boes<sup>3</sup>, Eric Gasser<sup>4</sup>, Dieter Rickenmann<sup>2</sup>, Christian Rickli<sup>2</sup>, Virginia Ruiz-Villanueva<sup>5</sup>, Isabella Schalko<sup>6</sup>, Lukas Schmocker<sup>7</sup>, Massimiliano Schwarz<sup>4</sup>, Markus Stoffel<sup>8</sup>, Volker Weitbrecht<sup>3</sup>

**Keywords:** large wood; floods; natural hazards, wood accumulations

## Abstract

This contribution summarises the most important practical findings from the WoodFlow research project. The main goal was to improve understanding of the processes governing large wood (LW) dynamics in watercourses and to provide practitioners with suitable tools to help assess LW-related hazards. The results provide a basis for estimating potential LW quantities, modelling wood transport during floods and describing the associated hazards due to wood accumulations. The resulting recommendations can be used by specialists as a basis for silvicultural and river-engineering measures.

## Introduction

Rivers are not only carrying clear water during floods. Especially in mountain areas, significant amounts of sediment (both suspended and bedload) and large wood (LW) from forested parts of the basins are mobilized and transported as well. The deposition of LW may reduce the river's cross-sectional area, triggering backwater effects with possible inundation of adjacent areas, together with aggradation or scouring. All these processes may cause damage to river infrastructures. This eventually results in an increased flood hazard and risk, as witnessed for example during the 2005 flood in Central Switzerland (Bezzola & Hegg, 2007). Therefore, the analysis of the processes involved in LW dynamics (i.e., wood recruitment from hillslopes and fluvial corridor, transport and deposition) is of high interest when it comes to mitigating potential wood-related hazards as well as to preserving the fluvial ecosystem, thus requiring an integrated management approach. The goal of the *WoodFlow* project supported by the Swiss Federal Office for the Environment (FOEN) was to develop know-how and methods to analyse LW dynamics in Prealpine and

---

<sup>1</sup>Gebirgshydrologie und Massenbewegungen, Eidg. Forschungsanstalt für Wald, Schnee und Landschaft, Switzerland ([nicolas.steeb@wsl.ch](mailto:nicolas.steeb@wsl.ch))

<sup>2</sup> Swiss Federal Research Institute WSL, Zürich, Switzerland

<sup>3</sup> Laboratory of Hydraulics, Hydrology and Glaciology (VAW), ETH Zürich, Switzerland

<sup>4</sup> University of Applied Sciences (BFH), School of Agricultural, Forest and Food Sciences (HAFL), Bern, Switzerland

<sup>5</sup> Laboratory of Hydraulics, Hydrology and Glaciology (VAW), ETH Zürich, Switzerland (formerly at University of Geneva)

<sup>6</sup> Massachusetts Institute of Technology, Cambridge, MA, USA (formerly at VAW)

<sup>7</sup> Basler & Hofmann AG, Consulting Engineers, Esslingen, Switzerland (formerly at VAW)

<sup>8</sup> Institute for Environmental Sciences, University of Geneva, Switzerland Department of Earth Sciences, University of Geneva, Switzerland

Alpine rivers. This contribution presents an overview of the practical tools and results of this project.

## Methods

The main questions of the project *WoodFlow* were divided in three blocks (Figure 1):

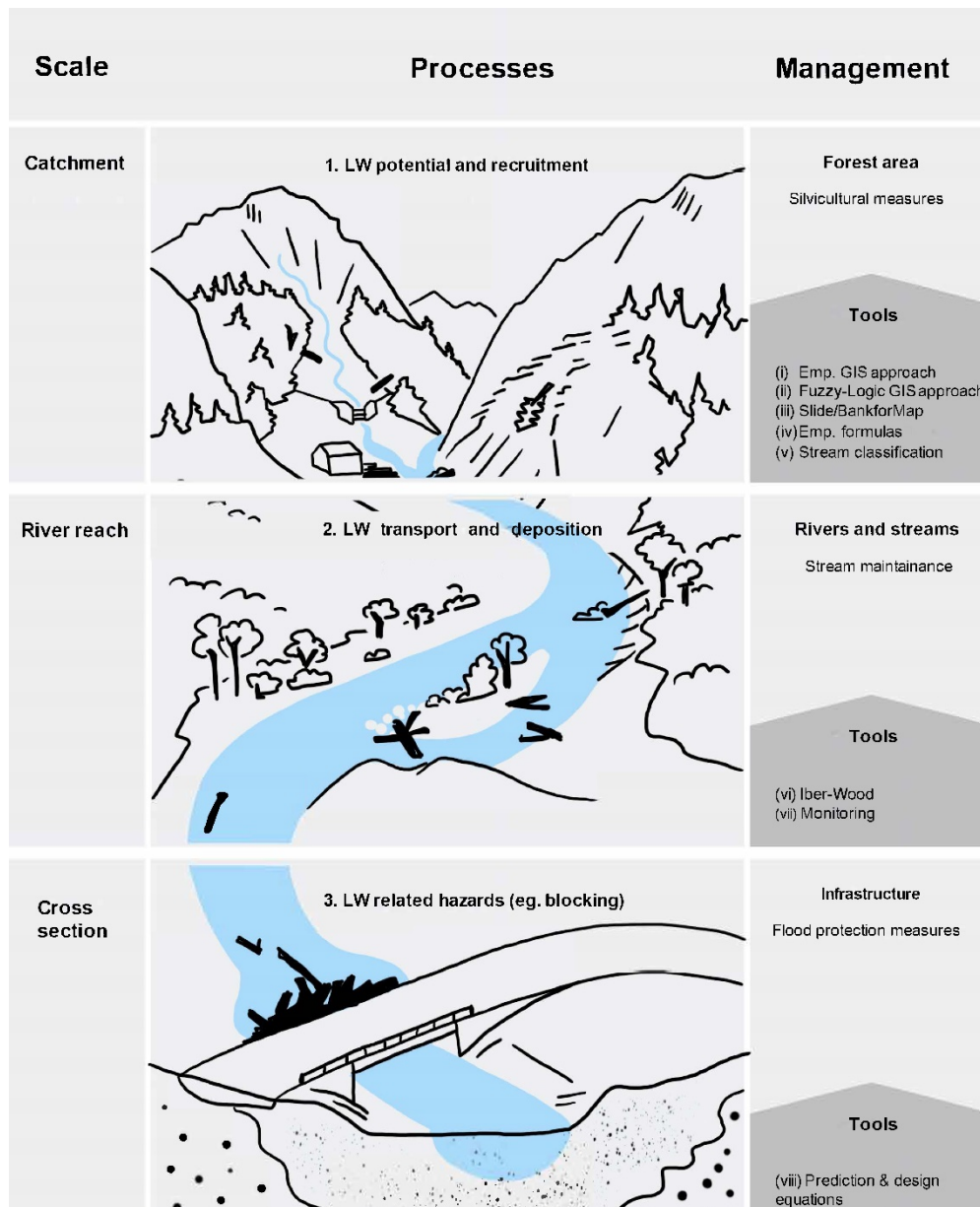


Figure 1: Thematic structure and overview of the tools developed in WoodFlow (illustration by L. Pfister).

- *Block 1* focused on the analysis of wood recruitment processes and the estimation of wood loads: the main processes responsible for controlling the amount of wood

within a stream reach were identified, exploring driving variables (climate, forest stand and morphological factors of the catchments) and input processes (shallow landslides, debris flows, bank erosion, fluvial transport of stored LW). Data collected during previous flood events in Switzerland formed the basis for these investigations (Steeb et al., 2019b). Wood supply was estimated with empirical, process-based and physically-based approaches. Different GIS (Geographic Information System) methods were developed to estimate LW volumes that may potentially be delivered to streams during a flood event. Large wood recruitment processes were partly modelled with SilvaProtect-CH data (Losey & Wehrli, 2013), which is based on topographic, geotechnical and rainfall distribution maps. Another important aspect analysed within Block 1 was the role of vegetation patterns and their mechanical effects on recruitment process. The fundamental dynamics of the recruitment processes such as bank erosion and shallow landslides were also analysed in more detail on the basis of physically-based numerical models (Schwarz et al., 2010) in which the mechanical effects of vegetation (root reinforcement, flow resistance, and wind-load) were implemented with state-of-the-art methods (Gasser et al., 2019).

- *Block 2* focused on the entrainment, transport and deposition of wood in rivers. It aimed to understand the processes involved in the wood dynamics, how wood pieces evolve when transported (i.e., breakdown), their travel distance and to recognise and predict potential depositional areas. The transport of LW in rivers was numerically simulated using the recently developed *Iber-Wood* model (Ruiz-Villanueva et al., 2014b). This tool is fully coupled with a two-dimensional hydrodynamic model (*Iber*) based on the finite volume method with a second-order Roe scheme. Further, the monitoring of wood fluxes in rivers was also carried out in Block 2. In addition to field surveys and remote sensing techniques, the monitoring of wood transport in rivers by both using existing video cameras and installing new devices was an important activity. To complement such monitoring, network home videos in which wood-laden flows have been recorded were analysed. Post-processing of these videos provided quantitative information about this type of multiphase flows and the dynamics of the fluxes during floods (Ruiz-Villanueva et al., 2019a).
- *Block 3* focused on the interactions between wood and river infrastructures on cross-section scale. Hazards due to wood accumulations were identified using a combined approach of physical and numerical modelling (Schalko, 2018). The main objectives were to predict (1) accumulation probability of logs at bridge piers (Schalko et al., 2019a), (2) backwater rise (Schalko et al., 2019b) and local scour (Schalko et al., 2019c) due to wood accumulations at racks and to (3) derive countermeasures at bridge piers to ensure the safe downstream conveyance of wood.

## Results and discussion

The following chapter provides an overview of the practical tools developed within *WoodFlow*, as shown in Figure 1.

### (i-iii) GIS approaches for the estimation of LW potential and transported wood volumes

Three different GIS approaches were developed to estimate LW volumes within a catchment during a flood event, namely:

- (i) *Empirical GIS approach (EGA)*: The model is based on nationwide homogenous data for Switzerland (SilvaProtect-CH) regarding possible trajectories of shallow landslides and debris flows, allowing for regional comparison of results. Bank erosion is determined by buffer widths from empirical channel widening ratios. The focus lies specifically on mountain rivers and torrents in alpine environments where most of the LW recruitment happens. Because only parts of the potential wood sources are being recruited and mobilized during a flood event, empirically derived volume correction factors are applied to estimate the actual wood load (Steeb et al., 2019a; Steeb et al., 2020).
- (ii) *Fuzzy-Logic GIS approach (FGA)*: Recruitment processes and source areas of LW are modelled similarly to the EGA. The main difference between the two methods lies in the estimation of actual wood load. FGA was implemented with a method proposed by Ruiz-Villanueva et al. (2014a) who used a regional scenario on multi-criteria evaluation and fuzzy logic principles.
- (iii) *Slide/BankforMAP*: The process probabilities of shallow landslides, geotechnical and hydraulic bank erosion are modelled with these two tools. Fuzzy process boundaries are considered to a certain degree by using probabilistic approaches. In addition, when estimating the LW potential and the actual wood load, specific characteristics of the vegetation (spatial distribution of root reinforcement) are taken into account, which have a direct influence on the input processes.

The three GIS approaches allow a spatially explicit analysis, whereby (a) potential LW source areas are identified (Figure 2), (b) the LW potential is calculated using wood stock data and (c) the effective LW load within streams is estimated by different correction methods. Each model calculates three different scenarios ( $LW_{\langle 30 \rangle}$  |  $LW_{100}$  |  $LW_{\langle 300 \rangle}$ ) equivalent to the probability of occurrence or return period of the processes involved. Comparing the modelling results of the three GIS approaches with empirical data from previous flood events showed that the estimated LW loads and input areas are in the same order of magnitude as the observed values from past floods. In general, EGA and FGA show good results for catchment sizes ranging from approx. 5-200 km<sup>2</sup>. In smaller catchments (<5 km<sup>2</sup>) wood loads tend to be underestimated, whereas in larger catchments (>200 km<sup>2</sup>) the model results often show an overestimation. Because of large computation time, the probabilistic Slide/BankforMAP approach is most suitable for small-scale

modelling (catchment size 1-30 km<sup>2</sup>). From a practical point of view, the GIS tools can serve as a basis for flood protection and/or silvicultural measures as well as for the reconstruction of past flood events (event analyses).

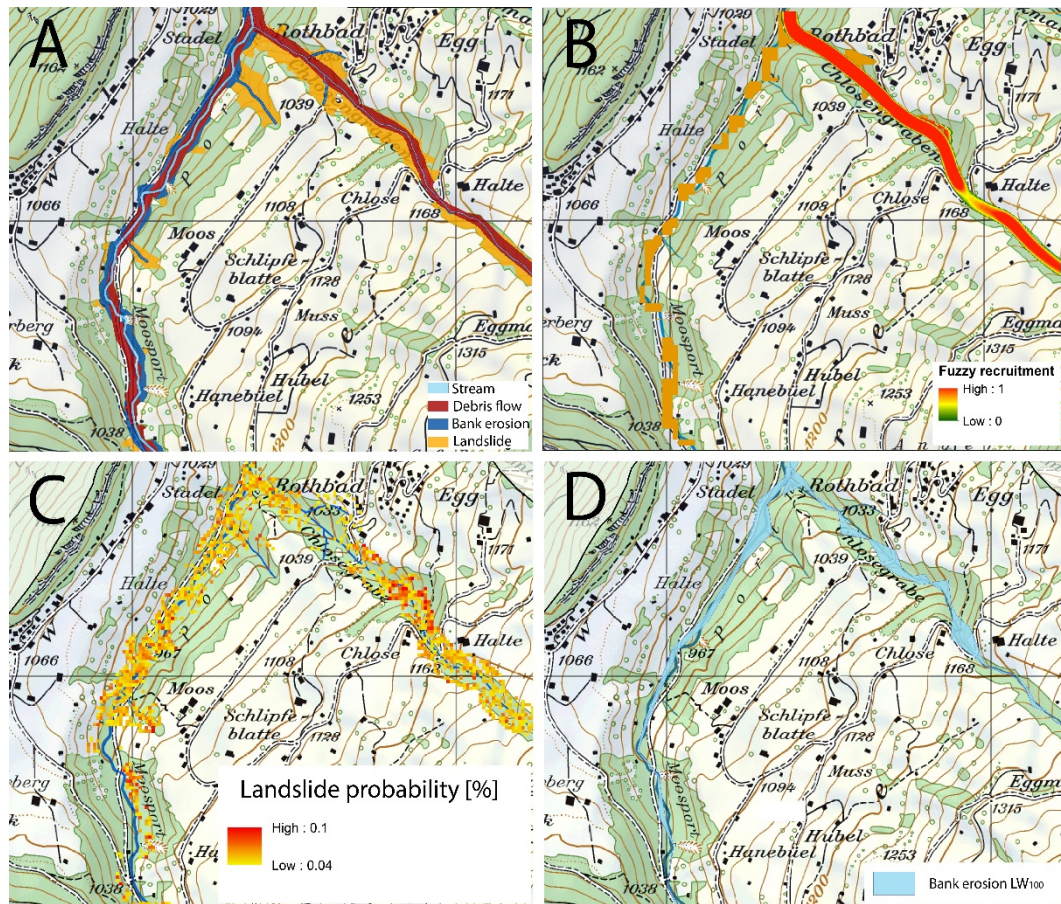


Figure 2: Comparison of the three GIS approaches for modelling the LW potential (location: confluence of the tributary Chlosegrabe with the Chirel near Rothbad, canton Bern). (A) Empirical GIS approach, (B) Fuzzy-Logic GIS approach, (C) SlideforMAP and (D) BankforMAP.

#### (iv) Empirical formulas for the estimation of observed LW volumes

In the context of the *WoodFlow* project, an extensive database was developed which documents recruited and transported quantities of LW together with the associated catchment and flood-specific parameters. Transported LW volumes were related to catchment area, forest cover, (forested) stream length, peak discharge, runoff volume, sediment load, and precipitation. Using these parameters and various statistical methods, the ten best empirical estimation formulas for quantifying LW load were defined (Steeb et al., 2019b). In addition, the wood piece length reduction (i.e., breakage) of transported logs was analysed for several events. The average reduction factor is about 0.21 (Steeb et al., 2019c).

### (v) Stream classification based on vegetation influence

A flow chart was formulated that uses specific criteria to define conditions in which forest management should be performed to mitigate potential LW recruitment without drastically removing all trees (Gasser et al., 2019). In particular, a distinction is made between the following conditions: (a) vegetation contributes in any case to reducing the recruitment of large wood; (b) vegetation influences the recruitment process only if specific (forest) maintenance measures are taken; (c) the effects of vegetation on the supply of large wood are in any case negligible. This approach supports the choice of possible measures within the framework of a risk-based assessment.

### (vi) LW transport modelling with *Iber-Wood*

*Iber-Wood* is a two-dimensional Euler-Lagrange model that couples the transport of individual LW pieces with hydrodynamics (Ruiz-Villanueva et al., 2014b), as shown in Figure 3. *Iber-Wood* can be used to model both the transport and the deposition of LW. *Iber-Wood* has been used to reconstruct patterns of wood deposition and to identify sites with a high clogging probability, to analyse factors controlling wood transport, deposition and blockage probabilities. During the *WoodFlow* project, *Iber-Wood* was enhanced to improve model reproduction of logs with roots, the interactions between logs and the river bed (e.g., when logs are transported sliding and not just floating); and the formation of log jams (i.e., accumulations of > 3 logs; Ruiz-Villanueva et al., 2019b).



Figure 3: Example of simulation results with *Iber-Wood*: Deposit pattern of LW pieces (brown lines) and identification of a channel section (red rectangle) with high retention capacity (Ruiz-Villanueva et al., 2017).

### (vii) Monitoring of LW processes

Three LW monitoring approaches were used during the *WoodFlow* project, namely:

- *Field surveys*: Field surveys focused on the quantification of wood deposits, the identification of the source areas and recruitment processes as well as a description of the channel morphology and the vegetation near the river. As part of the *WoodFlow* project, a field protocol was proposed such that the most important wood parameters can be recorded directly in the field.
- *Video surveillance*: Post-processed videos and time-lapse photographs are useful to extract quantitative data related to wood transport and wood fluxes. Ground control points were used to extract metrics from the video frames, such as flow depth, flow velocity (estimated based on time and distance travelled by the flow mass or single pieces), size of logs, stream gradient, width and height of the

bankfull channel (Ruiz-Villanueva et al., 2019a). As part of *WoodFlow*, we provide guidelines how to install and analyse such video surveillance systems.

- *Systematic drone and aerial photo analyses:* As part of *WoodFlow* we applied remote sensing techniques (both satellite and unmanned aerial vehicle imagery) for detailed inventory of the LW stored in the channel, enabling spatial and temporal changes in the wood deposits to be analysed. Time series can be used to observe the changes before and after a flood event. The volume of alluvial wood can be derived from the area of eroded vegetation with known forest density.

### **(viii) Prediction/design equations for LW related hazards**

Physical model tests were performed to investigate LW accumulation probability at bridge piers for varying flow conditions, LW and pier characteristics, and a movable bed (Schalko et al., 2019a). LW accumulations at rack structures were modelled to analyse resulting backwater rise and local scour (Figure 4). The experiments were conducted for three model scales using different wood characteristics, including branches and leaves (organic fine material *FM*). For small-scale model tests, plastic fir tree was added to the LW accumulation to model branches and leaves. For close-to-prototype tests, willow and fir branches were used as model *FM*. In addition, the effect of varying LW volume on backwater rise and local scour was considered (Schalko et al., 2019b and c). The efficiency of LW fins and bottom sills to reduce accumulation probability at bridge piers was studied for various approach flow conditions and LW characteristics. For model validation, selected tests on accumulation probability and backwater rise were simulated using the 2D numerical program *Iber-Wood*. The main results of this work are prediction equations for

- LW accumulation probability at bridge piers for uncongested and semi-congested LW transport as a function of flow velocity, log length, and pier diameter, and
- Backwater rise and local scour due to wood accumulations at rack structures based on flow conditions, and sediment and wood characteristics.

This study adds to the process understanding of LW accumulations at river infrastructures and contributes to an improved design of LW retention structures.



Figure 4: Flume experiment of LW accumulation at a retention rack with a movable bed (Schalko, 2018).

## Conclusion

*WoodFlow* focused on the integrated management of instream wood dynamics in mountain and foothill rivers. It was directed towards an effective reduction of instream wood-related hazards and risks while taking into account the requirements of the fluvial ecosystem. Tools were developed to analyse and predict hazardous processes associated with instream wood, which contribute to the development of a federal management strategy to evaluate and modify established protection concepts.

## References

- Bezzola G.R., Hegg C. (Eds.) (2007). Ereignisanalyse Hochwasser 2005, Teil 1 – Prozesse, Schäden und erste Einordnung. Umwelt-Wissen Nr. 0707. Bundesamt für Umwelt BAFU & Eidg. Forschungsanstalt WSL, Bern.
- Gasser E., Schwarz M., Simon A., Perona P., Phillips C., Hübl J., Dorren L. (2019). A review of modeling the effects of vegetation on large wood recruitment processes in mountain catchments. *Earth-Science Reviews* 194: 350–373. doi: 10.1016/j.earscirev.2019.04.013
- Losey S. and Wehrli A. (2013). Schutzwald in der Schweiz. Vom Projekt SilvaProtect-CH zum harmonisierten Schutzwald. Bundesamt für Umwelt, Bern. 29 S. und Anhänge.
- Ruiz-Villanueva V., Mazzorana B., Bladé E., Bürkli L., Iribarren-Anacona P., Mao L., Nakamura F., Ravazzolo D., Rickenmann D., Sanz-Ramos M., Stoffel M., Wohl E. (2019a). Characterization of wood-laden flows in rivers. *Earth Surface Processes and Landforms* 44: 1694-1709. doi: 10.1002/esp.4603
- Ruiz-Villanueva V., Gamberini C., Bladé E., Stoffel M., Bertoldi W. (2019b). Numerical modelling of instream wood transport, deposition, and accumulation in braided

morphologies under unsteady conditions: sensitivity and high-resolution quantitative model validation. *Water Resources Research* 56 (7). doi: 10.1029/2019WR026221

Ruiz-Villanueva V., Díez-Herrero A., Ballesteros, J.A., Bodoque J.M. (2014a). Potential Large Woody Debris recruitment due to landslides, bank erosion and floods in mountain basins: a quantitative estimation approach. *River Research and Applications* 30: 81-97. doi: 10.1002/rra.2614.

Ruiz-Villanueva V., Bladé-Castellet E., Sánchez-Juny M., Martí B., Díez Herrero A., Bodoque J.M. (2014b). Two dimensional numerical modelling of wood transport. *Journal of Hydroinformatics* 16.5: 1077-1096. doi: 10.2166/hydro.2014.026

Schalko I., Schmocker L., Weitbrecht V., Boes R.M. (2019a). Laboratory study on wood accumulation probability at bridge piers. *Journal of Hydraulic Research*. doi: 10.1080/00221686.2019.1625820

Schalko I., Lageder C., Schmocker L., Weitbrecht V., Boes R.M. (2019b). Laboratory flume experiments on the formation of spanwise large wood accumulations Part I: Effect on backwater rise. *Water Resources Research* 55: 4854-4870. doi: 10.1029/2018WR024649.

Schalko I., Lageder C., Schmocker L., Weitbrecht V., Boes R.M. (2019c). Laboratory flume experiments on the formation of spanwise large wood accumulations Part II: Effect on local scour. *Water Resources Research* 55(6): 4871-4885. doi: 10.1029/2019WR024789.

Schalko I. (2018). Modeling hazards related to large wood in rivers. VAW-Mitteilung 249, (R.M. Boes, ed.), ETH Zürich, Schweiz.

Schwarz M., Preti F., Giadrossich F., Lehmann P., Or D. (2010). Quantifying the role of vegetation in slope stability: the Vinchiana case study (Tuscany, Italy). *Ecological Engineering* 36(3): 285-291. doi: 10.1016/j.ecoleng.2009.06.014

Steeb N., Badoux A., Rickli C., Rickenmann D. (2020). GIS modelling of large wood recruitment and estimation of wood volumes. *Earth Surface Processes and Landforms* (Special issue on 'Wood in Rivers'; under review).

Steeb N., Badoux A., Rickli C., Rickenmann D. (2019a). Detailbericht zum Forschungsprojekt WoodFlow: Empirischer GIS-Ansatz. Eidg. Forschungsanstalt WSL, Birmensdorf.

Steeb, N. Badoux A., Rickli C., Rickenmann D. (2019b). Detailbericht zum Forschungsprojekt WoodFlow: Empirische Schätzformeln. Eidg. Forschungsanstalt WSL, Birmensdorf.

Steeb N., Badoux A., Rickli C., Rickenmann D. (2019c). Detailbericht zum Forschungsprojekt WoodFlow: Verkleinerung von Schwemmholz. Eidg. Forschungsanstalt WSL, Birmensdorf.

---

# Xgeo.no – A decision-support tool for assessing geohazards

Heidi Bache Stranden<sup>1</sup>, Graziella Devoli<sup>2</sup>, Rune Engeset<sup>3</sup>, Tuomo Saloranta<sup>4</sup>, Jess Andersen<sup>5</sup>, Søren Boje<sup>6</sup>, Kjetil Melvold<sup>7</sup>, Tore Humstad<sup>8</sup>, Knut Inge Orset<sup>9</sup>, Nils Kristian Orthe<sup>10</sup>, Ragnar Ekker<sup>11</sup>

**Keywords:** xgeo.no; natural hazard assessment; geohazard forecasting; Sentinel satellite; threshold maps

## Abstract

Xgeo.no is one of the most important tool used in Norway in the daily hazard assessments, performed by the regional forecasting and warning services. Xgeo.no includes a variety of meteorological and hydrogeological model simulations daily updated, data from automatic stations (from national networks in Norway and Sweden), field observations, satellite images and more. The application is a unique collaboration between governmental agencies.

## Introduction

Natural hazards forecasters need to access relevant, real-time, data from multiple sources, in order to carry out hazard assessments. This includes data from: automatic stations (e.g. meteorological and hydrological stations); visual inspections and field observations from professionals and citizens (e.g. snow profiles and stability tests); satellites images (e.g. Sentinel 1-3 image data); outputs from model simulations (hindcasts, nowcasts and forecasts of daily or hourly precipitation, temperature, snow, runoff, groundwater, etc.); observations from terrestrial cameras (e.g. web cams); information about occurred events, like snow avalanches, landslides, floods or information about geohazards-related traffic restrictions (e.g. road closures or restrictions, railway interruptions, etc.). Besides these data, forecasters need also static geographical data (e.g. release areas, runout areas, susceptible areas, slope maps, land cover, administrative boundaries, river network and hydropower system).

---

<sup>1</sup>M.D., The Norwegian Water Resources and Energy Directorate, Norway, (hrb@nve.no)

<sup>2</sup> The Norwegian Water Resources and Energy Directorate

<sup>3</sup> The Norwegian Water Resources and Energy Directorate

<sup>4</sup> The Norwegian Water Resources and Energy Directorate

<sup>5</sup> The Norwegian Water Resources and Energy Directorate

<sup>6</sup> Previously at The Norwegian Water Resources and Energy Directorate

<sup>7</sup> The Norwegian Water Resources and Energy Directorate

<sup>8</sup> The National Public Roads Administration (NPRA)

<sup>9</sup> The National Public Roads Administration (NPRA)

<sup>10</sup> The Norwegian Water Resources and Energy Directorate

<sup>11</sup> Previously at The Norwegian Water Resources and Energy Directorate

The Norwegian forecasters working daily to predict hazards like floods, snow avalanches, landslides, weather-related and ice conditions in lakes and rivers, need such data to analyse the current situation and the future development of the specific hazard, to be able to issue warnings to the public and authorities. Also, other professionals, responsible for preparedness, emergency response and crisis management require similar information, as well as students and researchers who investigate geohazards processes and their management.

Thus, we saw the need to develop an open access decision-support tool to assist forecasters and geoscience professionals and provide them with relevant and up-to-date information. The Xgeo.no decision-supporting tool has been developed in Norway since 2013 as a result of a joint collaboration among the Norwegian Water Resources and Energy Directorate (NVE), the National Public Roads Administration (NPRA), the Norwegian Meteorological Institute (MET), the National Rail Administration (Bane Nor) and the Norwegian Mapping Authority (NMA).

Xgeo.no include a web portal and modules where data are stored. Most of its data are open access, to let the public and other users benefit from the efforts to develop and maintain such a system and in order to enable collaboration between all stakeholders involved in preparedness and crisis management (e.g. different government agencies, local administrations, private companies and organisations with volunteers), as well as the public. Xgeo.no is available in both Norwegian and English languages.

The tool has been partially described in previous works (Barfod et al., 2013, Devoli et al., 2014, Krøgli et al., 2018) and examples of how the tool is applied in the daily hazard assessments have been presented in works like Saloranta (2012, 2016), Lussana et al. (2018a, 2018b) and Devoli et al. (2018).

This paper presents an overall and updated description of the tool. While the focus in previous papers was primary the specific warning services, this paper describes the different modules and present an overall view of how the different warning services use the application in the daily assessments. In this paper we also describe the recent integration of satellite images as a new module in the tool including functionality where satellite data visually can be compared with model data or multitemporal data.

## **Xgeo.no modules**

The Xgeo.no tool is composed of a web portal and a host of data modules with distributed implementation and application programming interfaces (API) (figure 1). The modules include:



Figure 1: The different modules in Xgeo.no and their sources. <sup>1</sup>Numeric Weather Prediction.

**Gridded maps module:** This module includes gridded maps of meteorological data, simulated hydrological, glaciological and hydrogeological conditions and thresholds of 1 km<sup>2</sup> spatial resolution, and 24h and 3h temporal resolution.

- a) Meteorological maps: includes both forecasted and historical data. The first version of the gridding algorithms became operational in 2004 (Engeset et al., 2014). There have been significant improvements in algorithms and available data since then (Lussana et al., 2018a, Lussana et al., 2018b). The forecasted data are divided in short-term and medium-term. The short-term forecasts are obtained from running a numerical weather prediction model (The MetCoOp Ensemble Prediction System (MEPS), see <https://www.met.no/en/projects/metcoop>) for the next 66 hours used in the Scandinavian region. The medium-term forecast data are obtained from the European Centre for Medium-Range Weather Forecasting (ECMWF) model. These gridded maps of forecasted precipitation, temperature and wind are visualized as separate maps at Xgeo.no, and they are also input to the other maps. The historical meteorological data are obtained from interpolation of

rainfall- and temperature observations from meteorological stations (Lussana et al., 2018a and 2018b). The meteorological dataset from this module acts also as input to different hydrological models that run outside Xgeo.no, i.e. different hydrological models used by the flood forecasting service or the lake-ice model used by the forecasters that predict ice conditions.

- b) Hydrological maps: The gridded maps of the forecasted meteorological data are sent as input data in the different snow-, hydrological- and hydrogeological models as previously mentioned. The output is a series of hydrological and hydrogeological parameters also in form of gridded maps of 1 km<sup>2</sup> spatial resolution and 24h and 3h temporal resolution. These gridded maps include a variety of snow themes (e.g. snow water equivalent, new snow depth, snow wetness and many more, described in e.g. Saloranta (2012) and Saloranta (2016)), hydrogeological maps, obtained as output parameters from the distributed precipitation-runoff model, described in Beldring et al. (2003) (e.g. runoff from rain and snowmelt, ground water level, subsurface water content, degree of soil saturation, water feed capacity, drought and more). In the same way, gridded maps of historical meteorological data acts as input to the same snow-, hydrological and hydrogeological models and the results are historical hydrological and hydrogeological maps continuously updated.
- c) Threshold maps: The meteorological, hydrological and hydrogeological data are combined with historical observations to produce different type of thresholds maps and geohazards indication maps to be used in the early warning assessment. The forecasting services uses at the present time the following threshold maps with 1km<sup>2</sup> spatial resolution:
- Rainfall threshold: The rainfall threshold map shows the amount of precipitation in % of the value expected for a 5 year return period.
  - Landslide threshold: The landslide threshold map, called Hydmet (Hydro-meteorological index), shows in which area the landslide threshold will be exceeded (looking at forecasts) or has been exceeded in the past. The map shows where the relative water supply and the relative soil water content will exceed a certain level and a landslide can occur. This threshold was obtained by combining statistically parameters like rainfall and temperature, as well as simulated parameters like rainfall and snowmelt, water supply, degree of soil saturation, groundwater level, etc., with historical landslide data to find the best combination of parameters that trigger landslides (Krøgli et al., 2018).
  - Slushflow threshold: The map of estimated runoff from snowpack is used for slushflows assessment. The map shows the amount of water added to the snow pack to snow when the snowdepth is above 40cm.

- Amount of new snow as a possible hazard. Knowing the amount of new snow is of great importance not only for the snow avalanche forecasting service but also for the road and railway authorities for the maintenance of both infrastructure elements.

**Stations:** This module includes all real time data recorded at automatic stations, like meteorological stations (mainly owned by the Norwegian Water Resources and Energy Directorate (NVE), the National Public Roads Administration (NPRA), the Norwegian Meteorological Institute (MET), the National Rail Administration (Bane Nor) and others). Data from the different stations are continually updated and visualized in several ways in a separate graph-application. Over the past 7-8 years, nearly 100 new stations have been established (Brækkan et al., 2018), and a large number of stations from other owners have been made accessible through the systems of MET and NVE for public use.

**Events:** this module includes a layer of geohazard events, marked as clickable points at the maps in the tool. The points might be historical landslides and snow avalanche events from the national mass movement's database ([www.skredregistrering.no](http://www.skredregistrering.no)) and from Regobs.no (which is a registration of geohazards events and field observations in an open geohazard-related datahub), in addition to points representing field observations reported at Regobs.no. This module also includes information on in situ traffic restrictions from the NPRA.

**Supporting data:** This module includes several different data and thematic maps from different sources, e.g. administrative boundaries of regions and municipalities, snow avalanche warning regions, steepness, landslide susceptibility maps, river network, dams as well as live web cams images.

**Warnings:** Maps showing the areas and the levels where a warning has been issued are not a separate module in Xgeo.no, but they are visualized directly from the webpage [varsom.no](http://varsom.no). This illustrates the interaction between the two web portals. The boundaries of the warning areas and colour representing the warning levels are in accordance to the specific hazards and the colour schemes proposed by the different forecasting services. The warning level and headlines are shown directly in Xgeo.no while the full bulletins and warning levels are published at [varsom.no](http://varsom.no).

**Satellite images:** In this module, images from Sentinel 1, 2 and 3 satellites are collected. This module was recently added in October 2019 and is based on a process chain developed by Norwegian Computing Centre (NR) for NVE. The work has also been supported by the Norwegian Space Agency' Copernicus-program. The module includes both natural colour images used for visual inspection and visual comparison, false colour images special designed to detect i.e. snow covered area, lake ice and glacier extend and multiday combination images to be used in i.e. flood and landslide forecasting. In addition, while introducing the satellite module, a function that enables visual comparison of data from different dates was implemented (figure 2). This function enables comparison of different satellite images, satellite images against hydrological maps and among the different hydrological maps. The purpose of this function is to more easily discover temporal changes, or analyse how the current situation differs from previous years or previous events. More details on the satellite images available are described below:

- a) Sentinel 1: Downloading of images from Sentinel-1 is activated automatically on days with flood warning level at level 2-yellow or higher. The processed image is a multi-temporal map showing the differences in flooded area between two different Sentinel 1-images. The spatial resolution is 20m.
- b) Sentinel 2: Images from Sentinel 2 includes both natural colour pictures, and false colour images designed to easily detect snow covered area, glacier extent and lake ice. The spatial resolution is 10m, and during spring, summer and early autumn, pictures covering part of the country are available nearly every day except during wintertime when the solar angle is low.
- c) Sentinel 3: Images from Sentinel 3 include both pictures taken from the Ocean and Land Colour Instrument and the Sea and Land Surface Temperature Radiometer, resampled to 250 m and 500 m resolution, respectively. In addition to natural colour images, false colour images designed to easily and visually detect snow and ice are available nearly every day (except during the dark wintertime when only data from the radiometer sensor can be used).

The different satellites are further described in:

<https://sentinel.esa.int/web/sentinel/missions>

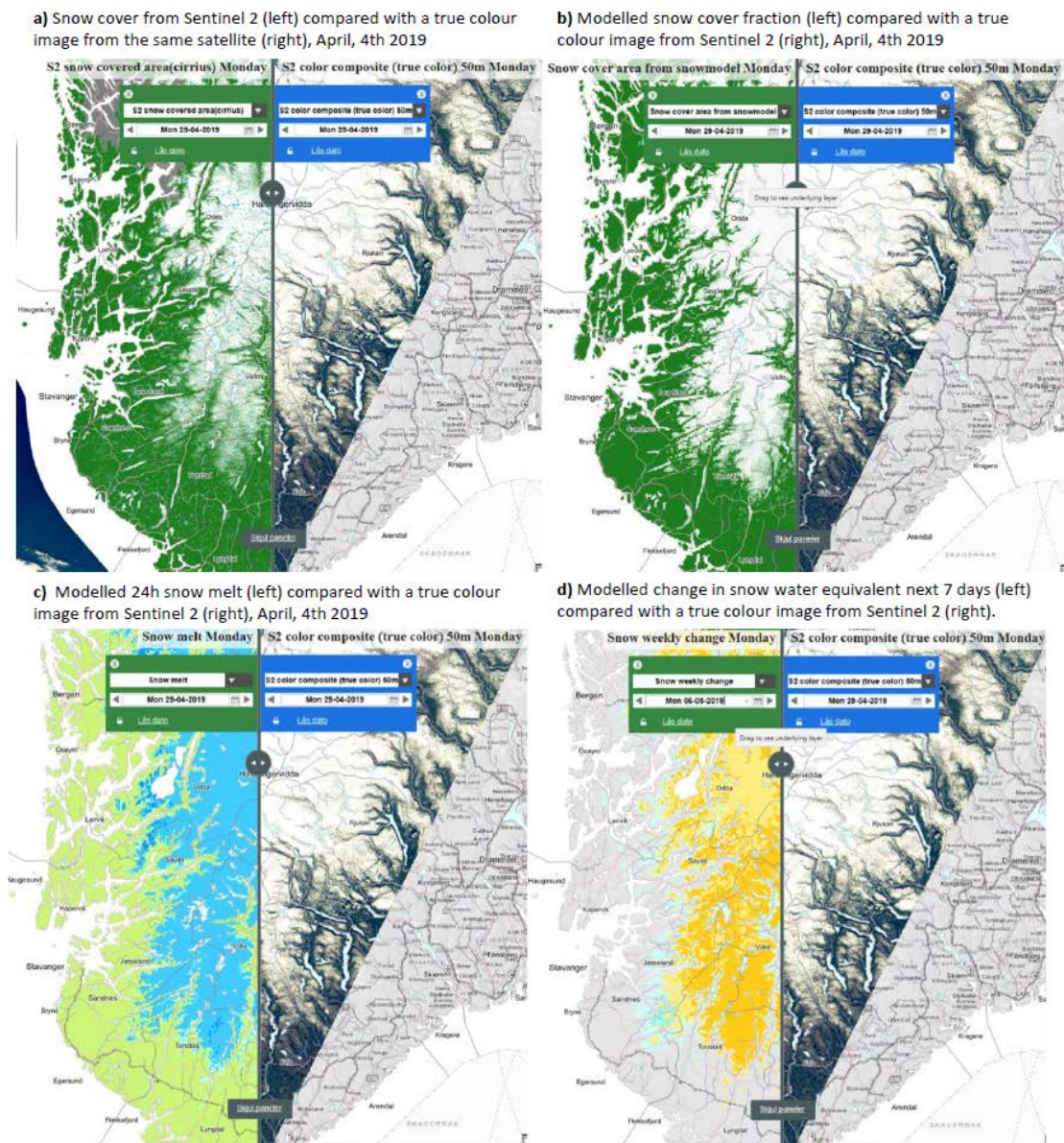


Figure 2: Examples of dual data visualization of satellites images, where the vertical line may be slid left or right in order to compare the two data sets.

## Practical use of the tool

Forecasters working at the national warning services (floods, landslides, avalanches, ice and weather) are using Xgeo.no tool daily, while other geoscience professionals e.g. the NPRA are using the tool periodically, during specific investigations. The use of the Xgeo.no tool and its modules may be different among the different groups of users, but all groups use the tool for decision purpose, before the hazardous events occur and for evaluation after the events has occurred. In particular, the data contained in the different modules are used by all services for the following purposes: a) definition of thresholds derived from different meteorological and hydrological parameters, b) daily hazard assessments (figure 3, last page) and c) evaluation of warning performance (last column in

figure 3, last page). In addition, the different forecasting services have grouped their favourite maps and layers in predefined groups (such as “Flood and landslides”, “Snow Avalanches”, “Road”, “Railway” and “All data”, “Satellite”).

## Conclusion

Xgeo.no tool has been used for forecasting flood-, landslide-, ice- and snow avalanches since 2013 at NVE, and its data and functionality have been gradually improved during this period. Its main strength is to display the most recently available observations and model simulations from multiple sources, integrated in a GIS-based web application. Another strength is the ability to display historical information back to 1957 and to manage and analyse point and gridded time series data. The recently added satellite module provides easy access to satellite imagery and derived geophysical products, as well as a time- and parameter-dependent slider for making comparisons. The creation of other thematic maps is an ongoing process driven by the different needs from forecasters and other users.

The data from Xgeo.no are also sometimes presented by the national broadcasting television, NRK, to illustrate the snow or the climatic situation. Private companies, power production companies, municipalities, universities and colleges use also these data during research projects.

## References

- Barfod E., Engeset R., Müller K., Saloranta T., Andersen J., Orthe N.K. and Humstad T. (2013): The expert tool XGEO and its applications in the Norwegian avalanche forecasting service. Proceedings ISSW, Grenoble.
- Beldring, S., Engeland, K., Roald, L. A., Sælthun, N. R., and Voksø, A.: Estimation of parameters in a distributed precipitation runoff model for Norway, *Hydrol. Earth Syst. Sci.*, 7, 304–316, <https://doi.org/10.5194/hess-7-304-2003>, 2003.
- Brækkan R., Nygård H. D., Orset K. I. and Stranden H. B. (2018): Automatiske værstasjoner til skredvarsling. Oppbygging av værstasjonsnettet for skredvarsling. MET report no. 11/2018. ISSN: 2387-4201. Available at [https://www.varsom.no/media/2079/rapport-skredprosjektet\\_17122018.pdf](https://www.varsom.no/media/2079/rapport-skredprosjektet_17122018.pdf) (last access: 19. September 2019)
- Devoli G., Kleivane I., Sund M., Orthe N.-K., Ekker R., Johnsen E., Colleuille H., (2014): Landslide early Warning System and Web tools for real-time Scenarios and for Distribution of warning Messages in Norway. G. Lollino et al. (Eds), *Engineering geology for Society and territory – Volume 2*, Springer international publishing Switzerland 2015
- Devoli G., Tiranti D., Cremonini R., Sund M. and Boje S., (2018): Comparison of landslide forecasting services in Piedmont (Italy) and Norway, illustrated by events in late spring 2013. *Nat. Hazards earth Syst. Sci* 18, 1351-1372.

Engeset R., Tveito O. E., Alfnes E., Mengistu Z., Udnæs H.-C., Isaksen K., and Førland E. J., (2004): Snow map system for Norway, XXIII Nordic Hydrological Conference, 8–12 August 2004, NHP report 48(1).

Krøgli K. I., Devoli G., Colleuille H., Boje S., Sund M. and Engen I.K. (2018): The Norwegian forecasting and warning service for rainfall- and snowmelt-induced landslides. *Nat. Hazards earth Syst. Sci* 18, 1427-1450.

Lussana C., Tveito O., and Uboldi F. (2018): Three-dimensional spatial interpolation of two-meter temperature over Norway, *Q. J. Roy. Meteor. Soc.*, <https://doi.org/10.1002/qj.3208>. (last access: 25. September 2019)

Lussana C., Saloranta T., Skaugen T., Magnusson J., Tveito O. E. and Andersen J. (2018): seNorge2 daily precipitation, an observational gridded dataset over Norway from 1957 to the present day. *Earth Syst. Sci. Data* 10, 235–249. <https://doi.org/10.5194/essd-10-235-2018> (last access: 25. September 2019)

Saloranta T. M. (2012): Simulating snow maps for Norway: description and statistical evaluation of the seNorge snow model, *The Cryosphere*, 6, 1323-1337, <https://doi.org/10.5194/tc-6-1323-2012> (last access: 25. September 2019)

Saloranta T. M. (2016): Operational snow mapping with simplified data assimilation using the seNorge snow model, *J. Hydrol.*, 538, 314–325.

		Daily hazard assessment					Evaluation of performance	
		Threshold maps	Gridded maps		Stations	Events and field observations		Supporting layers
			Meteorological maps	Hydrological maps				
Landslide forecasting	"Hydmet" maps; Runoff from snowpack (for slushflows); Precipitation in % of 5 years return period	Precipitation, Temperature, wind	Combination maps (rain & snowmelt, rain&snow), modelled maps (i.e. snowmelt, degree of soil saturation, ground water level, changing in ground water level, soil water soil capacity, snow depth, snow water equivalent, snow wetness conditions).	Meteorological- and hydrogeological stations	Events and field observations from regobs.no and NPRA traffic restrictions	Landslide susceptibility maps at different scales, slope angle map, web cams, among others	To verify snow cover: Sentinel 2 - true colour and colour composite; Sentinel 3 - true colour and snow cover	Comparison of maps of warning areas and levels; Hydmet threshold maps with the number of landslides and slushflows events recorded at regobs.no and from NPRA traffic restrictions. To identify the correct location of landslides satellite images from Sentinel 2 - true color and color composite.
Flood forecasting	Precipitation in % of 5 years return period, "hydmet" and runoff from snowpack	Precipitation, Temperature, In addition gridded meteorological data as input to hydrological models outside the Xgeo.no	Combination maps (rain & snowmelt, rain&snow), modelled maps (i.e. snowmelt, degree of soil saturation, ground water level, snow depth, snow water equivalent, snow wetness conditions and more).	Meteorological- and hydrological stations	Events and field observations from regobs.no and NPRA traffic restrictions	Among others: river network and catchment areas, administrative boundaries, hydro power	To verify snow cover: Sentinel 2 - true colour and colour composite; Sentinel 3 - true colour and snow cover	Maps of precipitation, temperature and snow. Threshold maps. Data from meteorological and hydrological stations, Events and data from regobs.no and NPRA, different supporting data e.g. river network and catchment areas, administrative boundaries, hydro power. <b>Satellite images</b> (Sentinel 1 - flooded area)
Snow avalanche forecasting	Precipitation in % of 5 years return period, amount of new snow.	Precipitation, Temperature, wind	Combination maps (rain & snowmelt, rain&snow), modelled maps (i.e. new snow, snow depth, snow water equivalent, snow wetness conditions and more).	Meteorological stations (precipitation, temperature, (new-) snow, wind, surface temperature	Events and field observations from regobs.no and NPRA traffic restrictions	Among others: warning region boundaries and steepness, web cams.	To verify snow cover: Sentinel 2 - true colour and colour composite; Sentinel 3 - true colour and snow cover	Maps of precipitation, temperature, wind and snow. Data from meteorological stations, events and data from regobs.no and NPRA, different supporting data e.g. warning region boundaries.
Lake- and river ice forecasting		Precipitation, Temperature, wind. In addition gridded meteorological data as input to lake ice models outside the Xgeo.no	Modelled maps (i.e. new snow, snow depth, snow water equivalent and more snow related maps).		Field observations from regobs.no	Web cams	To verify ice extend: Sentinel 2 - true colour and colour composite Sentinel 3 - true colour and lake ice extend	Optical satellite images (Sentinel 2 and 3), classified images for lake ice extend and lake temperatures from Sentinel - 3. <b>Field observations</b> from regobs.no and <b>supporting data</b> like web cams.

Figure 3: Synthesis of the most frequently used modules and maps by the different forecasting services (a high resolution image might be downloaded separately if necessary)

---

# A field experimental study of a landslide dam outburst following progressive failure in the Ashiaraidani basin

Shoki Takayama<sup>1</sup>, Shusuke Miyata<sup>2</sup>, Masamitsu Fujimoto<sup>3</sup>, Yoshifumi Satofuka<sup>3</sup>

**Keywords:** field experiment; landslide dam; outburst; progressive failure

## Abstract

The failure mechanisms behind dam outbursts are classified into three types: overtopping, instantaneous slip, and progressive failures. Several experimental studies have suggested that the highest peak flood discharge rate results from progressive failure. However, these experiments were conducted on small-scale structures with indoor channels, and under ideal conditions. Here, we present the results of relatively large-scale experiments on the progressive failure of a landslide dam in a mountainous stream. We created 1-m-tall dams in a stream bed and conducted dam-outburst experiments with four different initial conditions, among which the inflow discharge and dam shape were varied. In all experiments, partial collapse was initiated at the dam toe and propagated upwards until the reservoir overflowed the dam. The subsequent overtopping quickly eroded the dam and triggered large flood runoffs. Through comparison with previous field experiments, we found that differences in failure mode did not have a significant effect on the peak flood discharge rate, and the reservoir water volume at the moment of overtopping was the predominant factor affecting the discharge.

## Introduction

Large-scale landslides into rivers can block flow and form a landslide dam that increases the water volume upstream, and can cause catastrophic flooding downstream if an outburst occurs. Following the formation of a landslide dam, effective damage-reduction planning requires prediction of the areas that may be flooded in the event of an outburst.

Many experimental studies have been conducted to clarify the landslide dam deformation process. Takahashi and Kuang (1988) showed that the processes leading to dam outburst can be described by one of three failure modes. Overtopping failure occurs when an overtopping flow rapidly erodes a landslide dam, instantaneous slip failure is a process in which a large-scale slip occurs from the top of a dam, and progressive failure results from a partial collapse at the dam toe that proceeds upward. Awal et al. (2008) suggested that

---

<sup>1</sup> D2, Ritsumeikan University, Japan, (rd0036pr@ed.ritsumei.ac.jp)

<sup>2</sup> Ph.D., Disaster Prevention Research Institute, Kyoto University, Japan

<sup>3</sup> Ph.D., College of Science and Engineering, Ritsumeikan University, Japan

peak discharge rate associated with progressive failure was the greatest of the three failure modes. However, data and understanding of progressive failure mechanisms are still limited, as most experiments have been conducted on a small scale, in ideal conditions, using indoor channels.

The purpose of this study is to clarify the process of a landslide dam deformation and a flood runoff when a progressive failure occurs. Thus, we conducted large-scale field experiments on the progressive failure of a landslide dam.

## Methods

The experimental site was located in the catchment of Hirusudani stream in the Ashiaraidani basin, Takayama City, Gifu Prefecture, Japan (Figure 1a). Figure 1b shows topographical maps of the experimental site before and after the landslide dam was constructed. Construction of the dam required a dry streambed; thus, as shown in Figure 1c, the inflowing water was drained using a sandbag weir, drainage hose, permeable layer, and drainage pipe. The temporary weir was constructed from sandbags positioned 35 m upstream from the construction site, and the inflow was drained using the hose. The permeable layer was built on the channel bed, and the drainage pipe was laid underneath it. The landslide dam was constructed on the permeable layer, and the experiment began by closing the drainage hose and pipe valves.

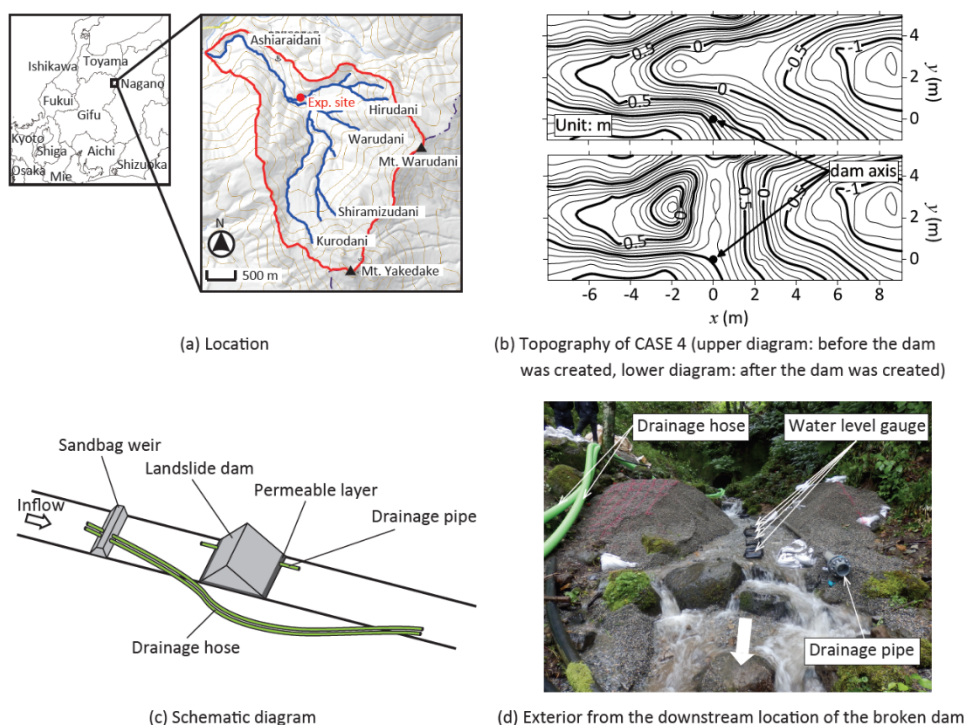


**Figure 1: Overview of the experimental site.**

The inflow discharge was measured at the check dam located 50 m upstream from the landslide dam. The dam deformation process was recorded using video cameras. The reservoir and ground water levels were measured using pressure water level gauges (S&DL

mini; OYO Corporation) installed at the bottom of the reservoir and dam, respectively. The gauges were fixed to concrete blocks, and measurements were taken every 5 seconds. The outflow discharge was calculated by subtracting the temporal change of the water volume in the reservoir from the inflow discharge, where the water volume in the reservoir was calculated based on the measured reservoir level and topographical data (Figure 1b). Figure 1d shows the exterior view of the experimental site, as seen from downstream of the broken dam.

Figure 2 shows the geometry of the landslide dam, which was constructed from cohesionless soil with a mean particle diameter of 5 mm. The permeable layer was built using cohesionless soil with a mean particle diameter of 14 mm (Figure 3a). A constant head permeability test showed that the saturated hydraulic conductivity of the dam material was 0.00115 m/s. The soil water retention curve of the dam material was obtained by fitting the Tani equation (Tani, 1982) to the result of the soil water retention test, as shown in Figure 3b.

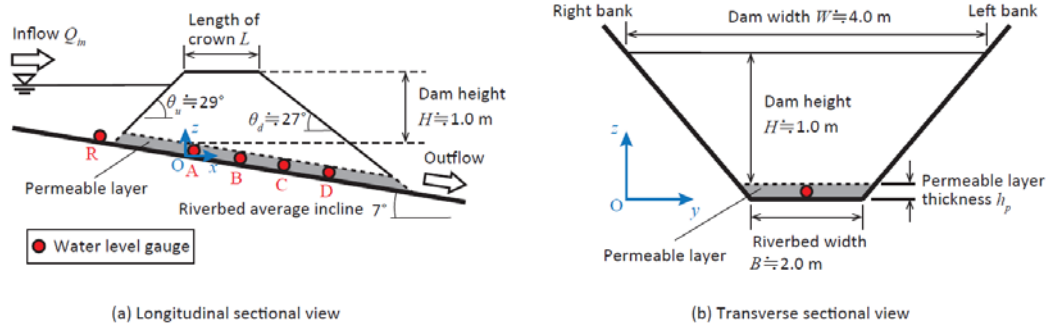


Figure 2: Schematic of the landslide dam.

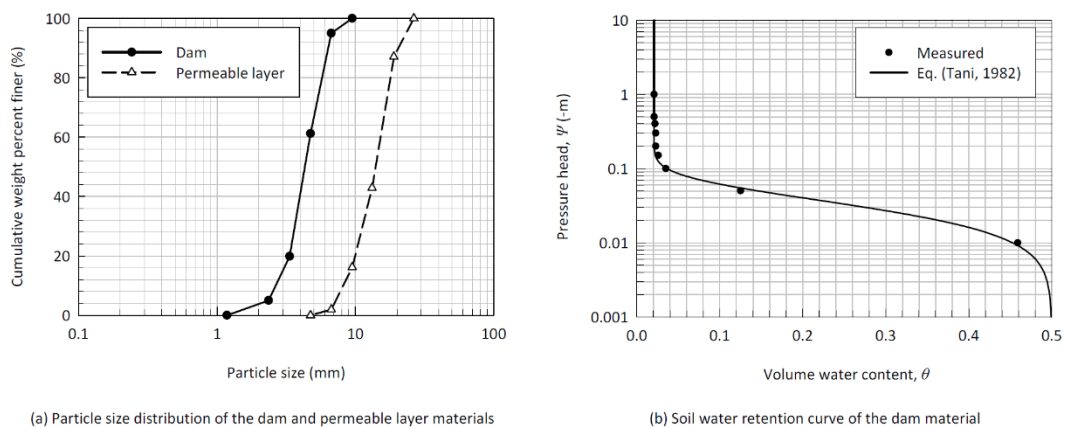


Figure 3: Results of the dam and permeable layer soil tests.

The experimental conditions are summarized in Table 1. The experiments were conducted under four different conditions, where the inflow discharge rate and initial dam shape were varied. A triangular dam was used in cases one to three, and a trapezoidal dam was built for case four. In cases three and four, the permeable layer thickness was increased because it was difficult to drain the inflow water through the thinner layer used in cases one and

two. The landslide dam was constructed using dry materials in cases one to three, and from material with 10% water content in case four.

**Table 1: Experimental conditions.**

	Inflow discharge, $Q_{in}$ ( $m^3/s$ )	Length of crown, $L$ (m)	Permeable layer thickness, $h_p$ (m)
CASE 1	0.028	0.0	0.05
CASE 2	0.037		
CASE 3	0.062		0.15
CASE 4	0.052	0.8	0.20

## Results

The results of the dam deformation process in case two are shown in Figure 4. Seepage started at the dam toe, but dam deformation was not visually apparent before 0 s. At approximately 50 s, the center of the dam toe partially collapsed due to the rising phreatic surface. This small-scale collapse propagated upward until 302 s, when the reservoir water started to overflow from the lowest point in the transverse direction. The subsequent overtopping flow quickly eroded the landslide dam, triggering a large flood runoff. The dam deformation process in all cases was similar to that shown in Figure 4.

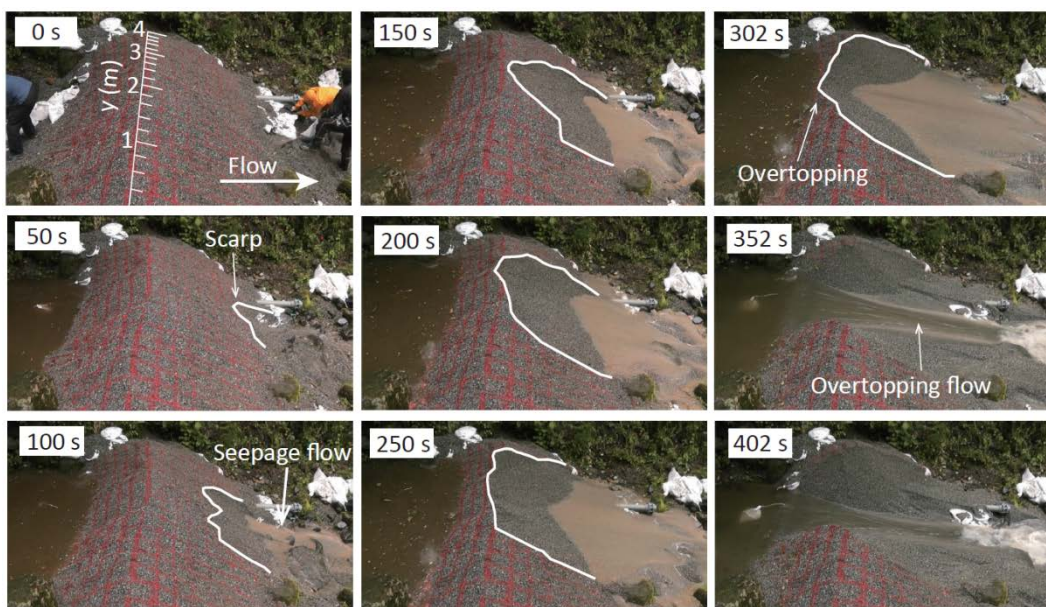


**Figure 4: The dam deformation process observed for case two, where 0 s is the time when the reservoir level started to increase.**

The temporal changes of the reservoir and ground water levels are shown in Figure 5. The levels rose until the reservoir water overflowed the landslide dam, and then dropped suddenly due to the erosion of the dam caused by the overtopping flow. The time-dependent

variation in the groundwater level was similar to that of the reservoir, because a rise in the reservoir level caused an increase in the groundwater level.

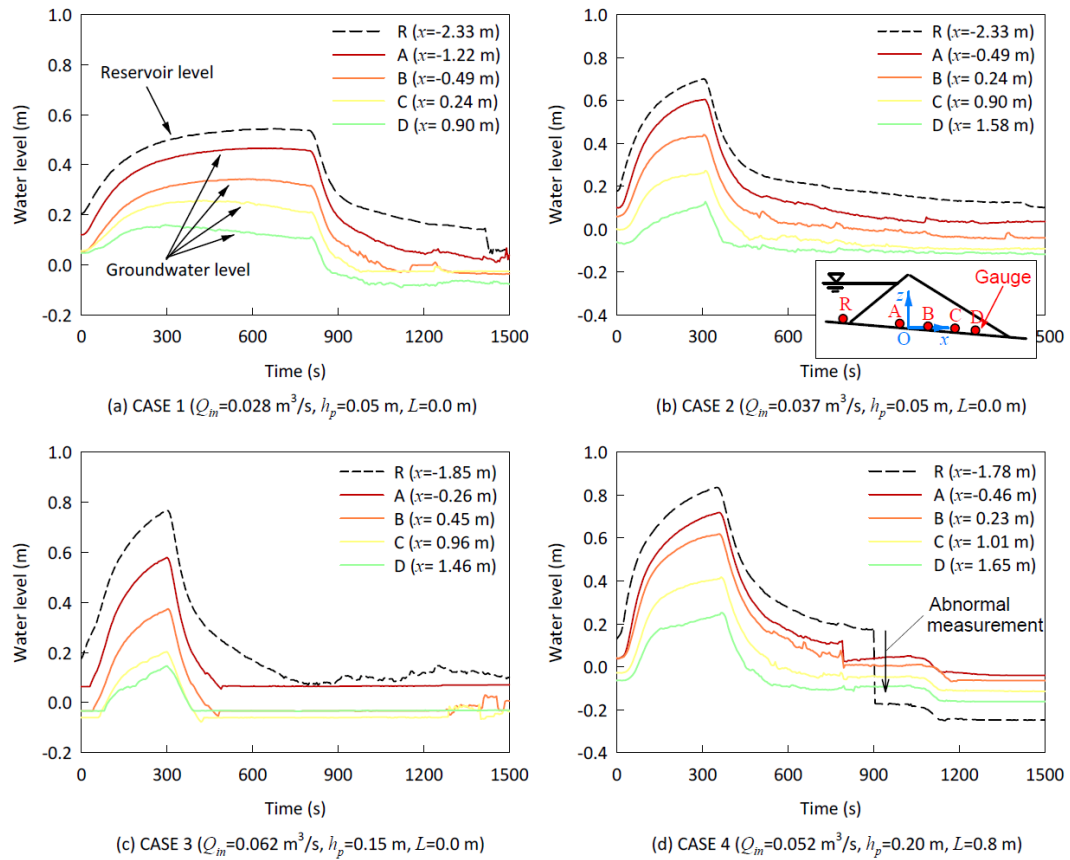


**Figure 5: Temporal changes of the reservoir and groundwater levels; 0 s is the time at which the reservoir level started to rise. The reference water level is the dam axis shown in Figure 2. The solid lines are the reservoir water levels, and the dashed lines indicate groundwater levels.**

Figure 6 shows a hydrograph of the outflow. The peak discharge occurred when the reservoir water overflowed the landslide dam. The peak discharge rates of cases one to four were  $0.053$ ,  $0.086$ ,  $0.126$ , and  $0.160 \text{ m}^3/\text{s}$ , logged after 820, 320, 320, and 370 s, respectively. The times at which the peak discharge rates were recorded depended on the time at which overtopping occurred.

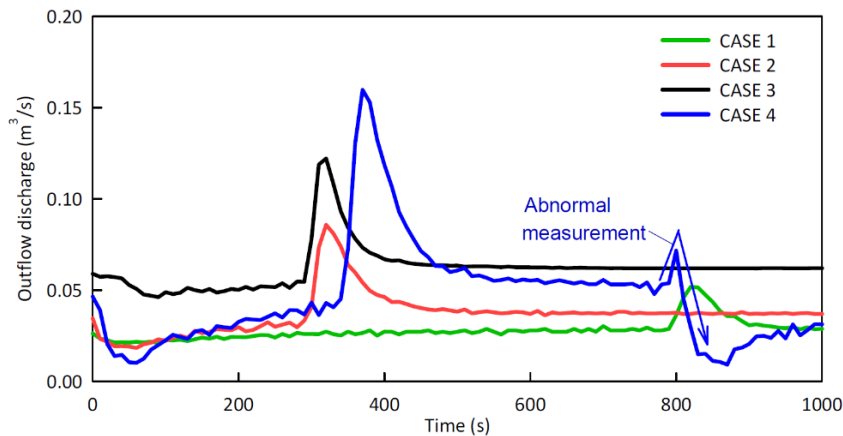


Figure 6: Outflow hydrograph, where 0 s is the time when the reservoir level started to rise.

## Discussion

Measurements of the dam deformation prior to overtopping are presented in Figure 7. In cases one to four, dam deformation started at 70, 30, 40, and 80 s, respectively. The rate of dam deformation was similar between cases two and three, whereas in case one deformation was slower and in case four it was faster. Figure 8a shows the groundwater levels at the crown of the dam over time, until the overtopping process started. Figures 8b, 8c, and 8d show the phreatic surface of the dams at 150, 200, and 250 s, respectively. The phreatic surface rose at a similar rate between cases two and three, while it was lower in case one and higher in case four. These results suggest that a dam deforms more quickly when the phreatic surface level is high. Therefore, they imply that the difference in the dam crest length has a smaller effect on the rate of dam deformation than the difference in the phreatic surface level.

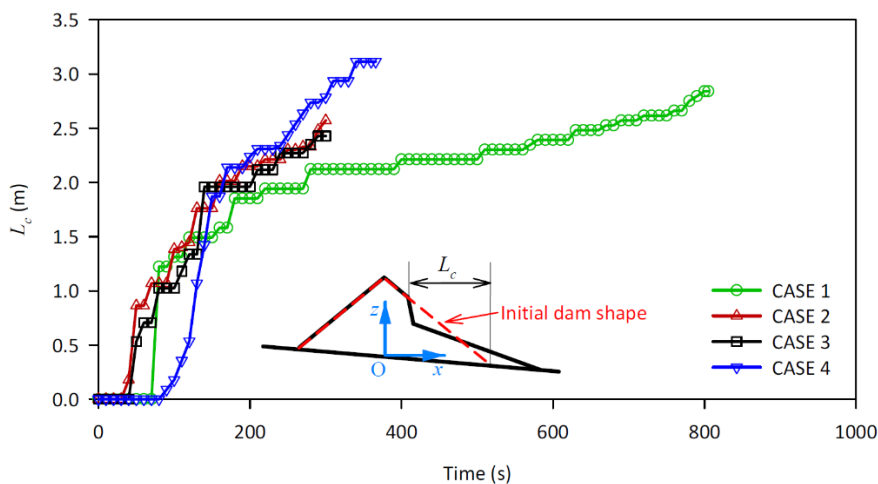
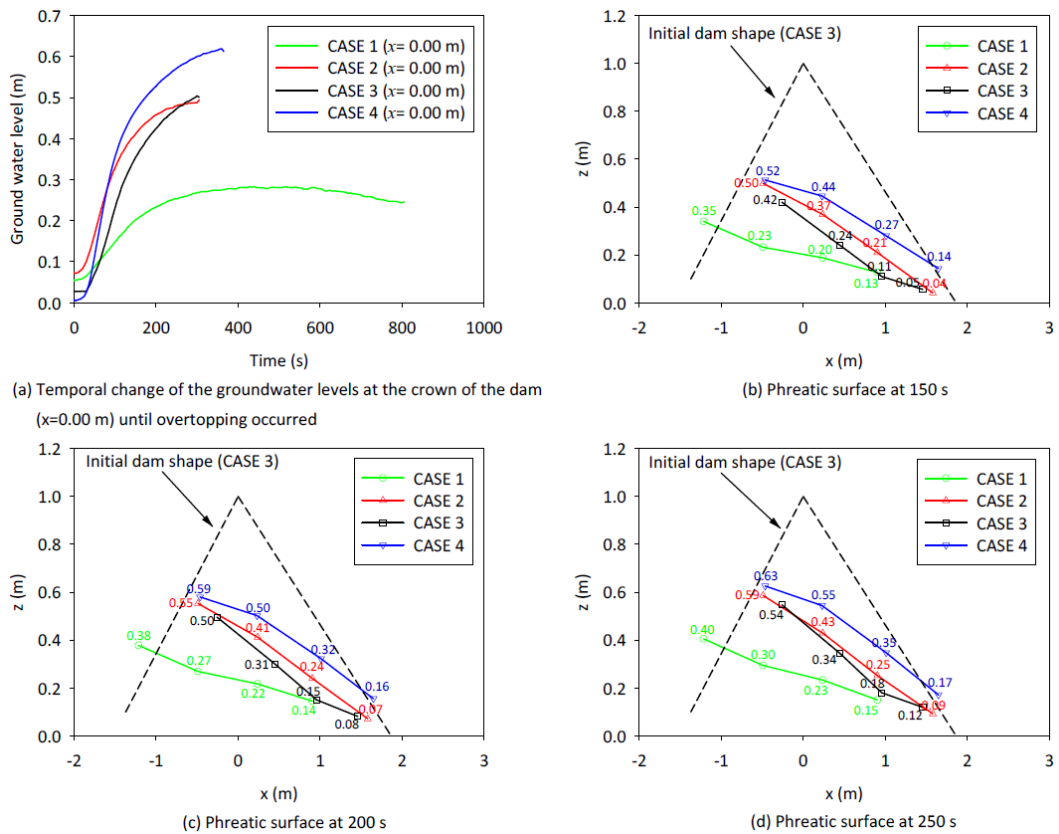
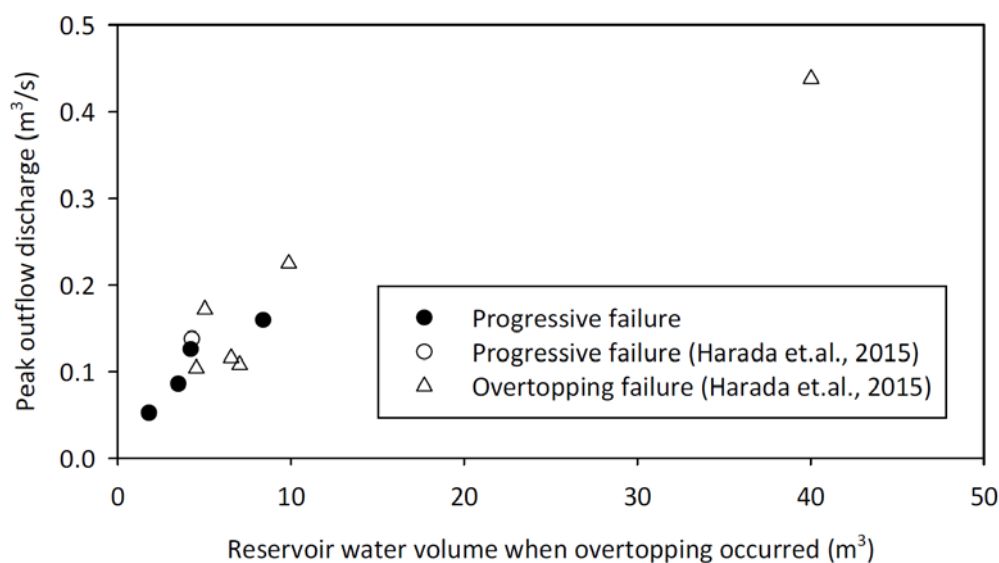


Figure 7: Comparison of dam deformation until overtopping occurred among the four cases ; 0 s is the time at which the reservoir level started to rise.  $L_c$  is defined as the horizontal distance from the toe of the initial dam shape to the crown of the landslide.



**Figure 8: Comparison of the rising groundwater levels among the four cases, where 0 s is the time at which the water started to rise. The levels at  $x = 0$  m in (a) were obtained by linear interpolation in the  $x$ -direction.**

Figure 9 shows the relationship between the reservoir volume at the time of overtopping and the peak discharge rate, and includes the results attained by Harada et al. (2015). The peak discharge rate tended to be greatest when a large volume of water was in the reservoir when overtopping started; therefore, this suggests that differences in failure mode did not have a significant effect on the peak discharge rate. However, measurements on small-scale channels carried out by Awal et al. (2008) indicated that the peak discharge rate associated with progressive failure was greater than that associated with failure due to overtopping. The authors inferred that peak discharge following progressive failure became the greatest because the large-scale slip of the dam produced the instantaneous release of the water in the reservoir. On the other hand, no large-scale slip of the dam was observed in our experiments; therefore, differences in failure mode had no significant effect on the peak discharge rate. We considered the main reason why no large-scale slip of the dam occurred in our experiments is that the impact of the cohesion on the occurrence of the slip was relatively small because of the large experimental scale. We concluded that peak discharge following progressive failure is not always greater than overtopping failure and depends on whether the large-scale slip observed in the channel experiment occurs or not.



**Figure 9: Relationship between the reservoir water volume when overtopping occurred and the peak discharge rate. This figure includes our results and those obtained by Harada et al. (2015).**

## Conclusion

We performed field experiments on the progressive failure of a landslide dam, to study the processes of dam deformation and flood runoff. Inflow discharge, dam deformation, reservoir level, the groundwater level in the dam and outflow discharge were measured. In all experiments, the dam collapsed partially at the dam toe, and the failure propagated upward until the reservoir overflowed the dam. The subsequent overtopping flow quickly eroded the dam and triggered large flood runoffs. Measurements of the deformation and groundwater levels suggest that the rate of deformation is greatest when the phreatic surface is highest. Comparison between our results and those of previous field experiments suggested that differences in failure mode had little effect on the peak flood discharge rate, as the reservoir water volume was the rate-determining factor. We conclude that the reservoir water volume is the most important parameter to be considered when predicting the flood areas most at risk from landslide dam outburst. However, in the case of progressive failure, large-scale slip of the dam body can increase the peak discharge rate. Therefore, further study of this process is required to accurately predict the flood areas resulting from a dam outburst.

## References

Awal, R., Nakagawa, H., Kawaike, K., Baba, Y., Zhang, H. (2008) Experimental study on prediction of failure mode of landslide dams. Proceedings of Fourth International Conference on Scour and Erosion (ICSE-4), 5.-7. November 2008, The Japanese Geotechnical Society: 655–660.

Harada, N., Akazawa, F., Hayami, S., Yanagisaki, G., Satofuka, Y., Fujimoto, M., Tsutsumi, D., Miyata, S., (2015) Field experiment of deformation processes of a landslide-dam in the Ashiarai Basin. Journal of the Japan Society of Erosion Control Engineering 67(6): 41–48.

Takahashi, T. and Kuang, S.F. (1988) Hydrograph prediction of debris flow due to failure of landslide dam. *Annals of the Disaster Prevention Research Institute* 31(B-2): 601–615.

Tani, M. (1982) The properties of a water-table rise produced by a one-dimensional, vertical, unsaturated flow. *J. Jpn. For. Soc.* 64: 409–418.

---

# Deciphering sediment Connectivity Index and erosion pattern in a debris flow catchment

Loris Torresani<sup>1</sup>, Vincenzo D'Agostino<sup>2</sup>, Guillaume Piton<sup>3</sup>

**Keywords:** Connectivity Index; protection measures; debris flow, GIS, hazard assessment, geomorphic analysis

## Abstract

Understanding sediment connectivity and erosion pattern are fundamental in order to assess in a proper way actual and potential future hazard in debris flow prone areas. In this work, we propose a novel way to analyse and decipher the Connectivity Index (CI) applied in the Saint Antoine catchment, located in the French Alps. We conceptualised a procedure for the extraction of each variable involved in the CI computation along the thalweg profile. This new way to analyse CI helps to understand how this index is affected by past debris flow events and presence or absence of protection measures, also comparing protected reaches against non-protected reaches. This method opens new opportunity to use the Connectivity Index as an effective instrument to catch present or future hazard and support the planning of hazard mitigation measures.

## Introduction

In Alpine regions, the occurrence of torrential processes is one of the major driving factors in morphology changes and sediment relocation as well as in threats endangering human assets. The availability of sediment and the capacity of a given stream to deliver it in areas at risk plays a leading role in the assessment of debris flow (DF) or debris flood risks. Thus, assessing sediment sources and sediment delivery processes is a crucial step to plan proper hazard mitigation measures.

However, this is a complex and challenging task, and it is specifically time-consuming at large scale, i.e., for catchments of 10-50 km<sup>2</sup>. Many non-linear processes are involved in slope erosion and sediment transport (Ferro and Minacapilli, 1995; López-Vicente et al., 2015). Furthermore, anthropogenic activities are affecting sediment dynamics. Changing in flow paths related to roads and tracks on hillslopes, terraces, urbanisation over fan areas and agricultural expansion are examples of human impacts on the landscape with potential

---

<sup>1</sup> Dr., Department of Land, Environment, Agriculture and Forestry, University of Padova, Agripolis, Viale dell'Università 16, 35020, Legnaro (PD), Italy (loris.torresani@phd.unipd.it)

<sup>2</sup> Prof., Department of Land, Environment, Agriculture and Forestry, University of Padova, Agripolis, Viale dell'Università 16, 35020, Legnaro (PD), Italy

<sup>3</sup> Dr., Univ. Grenoble Alpes, INRAE, UR ETNA, 38000 Grenoble, France

complex side effects on geomorphology and hydrology. As a consequence, the change in landscape and land-use combined in some cases by climate changes, are accelerating the dynamics of slope erosion and degradation (Brown et al., 2016). This makes the task of geomorphic analysis even more challenging, and effects need to be addressed in order to have a complete perspective on sediment dynamics in a studied catchment.

To evaluate sediment dynamics, GIS-based indices have been developed since the 1970s (Atkinson, 1995; Dietrich and Dunne, 1978). Researchers have recently shown an increasing interest in studying the existing connection between sediment sources and channels.

The Connectivity Index (CI) is one morphometric index that for instance computes the existing degree of linkage between sediment sources (e.g. eroded areas on hillslopes) and sinks areas (outlet, hydrologic network, lakes). It was initially introduced in a work of Borselli et al. (2008) and then modified by Cavalli et al. (2013). Two concepts are the fundamentals of CI assessment: sediment delivery across the whole drainage system and sediment coupling/decoupling along the travel path from the source to the nearest sink. The CI is computed as the logarithm of the ratio between (i) an “upslope component”, which is the product of square root of catchment area by mean slope by a mean value of upslope weighting factor; and (ii) a “downslope component” which is the sum of distance to downstream sink divided by the weighting factor and the slope of each pixel:

$$CI_k = \log_{10} \left( \frac{\overline{W_k} \overline{S_k} \sqrt{A_k}}{\sum_{i=k, \dots, n_k} d_i / W_i S_i} \right) \quad (1)$$

Where  $k$  is the pixel index for which the CI is computed,  $W_i$  is the weighting factor of pixel  $i$  and  $\overline{W_k}$  is the mean value of  $W_i$  of all pixels located upstream of pixel  $k$ ,  $S_i$  is the slope of pixel  $i$  and  $\overline{S_k}$  is the mean value of  $S_i$  of all pixels located upstream of pixel  $k$ ,  $A_k$  is the drainage area of pixel  $k$ , i.e., the contributing area;  $k, \dots, n_k$  are the indexes of all pixels on the path from pixel  $k$  down to the target sink, and  $d_i$  is the path length in pixel  $i$ . The weighting factor ( $W$ ) represents the impedance to sediment flows that can be based on different characteristics of the area. It can be computed from land use (using c-factors of the USLE-RUSLE model or Manning’s  $n$ ), or also from topography (Roughness Index).

The connectivity index (CI) varies in the interval  $[-\infty, +\infty]$ . In essence, CI increases with increasing sediment supply related to erosion rate proxy (weighting factor of upstream and downstream areas), upstream and downstream slope and catchment size, and decreases with distance to a downstream target.

Cavalli et al. (2013) adapted the CI to the alpine environment and to the use with high-resolution digital terrain models (HR-DTM) by introducing modifications that in essence (i) bounds to slopes in the range 0.5%-100% to focus on torrential flows and prevent bias-related to HR-DTM, (ii) uses the residual topography, i.e., standard deviation of the roughness height of the terrain as Weighting factor, to avoid using empirical parameters and because erosion processes tend to generate “noisy” topographies where flows are confined and thus transport more sediment and (iii) compute the contributing area with an algorithm that accommodates flow spreading on flat areas rather than artificially concentrating flow in one single lower pixel (D-infinity algorithm).

The CI computation, as described in Cavalli et al. (2013), is consequently fast and easy to use, requiring only an HR-DTM and the implementations of some GIS procedures. The same authors developed a specific GIS toolbox and a standalone application called SedInConnect that allows estimating the CI in a semi-automatic way (Crema and Cavalli, 2017).

Given this state of the art, there still exists a gap in this framework to be used in planning and designing hazard mitigation structures. In this context, a recent work by Cucchiaro et al. (2019) started to analyse the interaction of mitigation measures with CI but circumscribed to qualitative map interpretations. A quantitative interpretation of CI and changes provided by protection measures remain poorly unexplored.

This work seeks consequently to introduce a new quantitative way to analyse the CI, and highlights how the presence/absence of mitigation structures affects CI in the studied catchments. In general, we aim to apply for the first time this method and understand its potential to become an effective complementary tool for hazard assessment and mitigation measure planning in debris flow/flood-prone catchments. A French catchment, the Saint-Antoine torrent at Modane, is used as an application case after the occurrence in summer 2014 of a large DF event.

Assuming that check dams are mostly built to stabilise channel beds, while the open check dams aim at trapping debris flows, if CI analysis makes sense, we can hypothesise that (H1) connectivity index should be lower in the stabilised reaches than in the untrained reaches and (H2) that erosion rates should be lower where check dams are present, and deposition should obviously be concentrated in retention structures as open check dams.

CI is supposed to be lower on average with a regular drop of values in trained reaches. This because of the increased likelihood to flow diversion due to the new bed line (thalweg) induced by the presence of check dams. The component capturing this behaviour is the “upslope component” that encapsulates flow dispersion through the D-infinity algorithm used for drainage area computation. Also, the height drop at the check dam location will induce a certain degree of slope variation. The same attitude is expected to be visible from a DEM of Difference analysis (DoD) performed after the last DF event: more regular and moderate erosion rates are expected in reaches that are protected with check dams. Concerning non-protected domains in the Saint Antoine catchment, a consistently higher CI is expected due to the lower flow dispersion caused by higher flow confinement in the gorge. Besides, the channel is supposed to be more susceptible to randomly localised higher erosion or deposition rates.

In this work, the main stem of the Saint Antoine catchment (France) is studied. More precisely, the effects of the 2014 debris flow are analysed in the light of CI and of erosion/deposition assessment using LiDAR data taken before and after the event.

## Methods

The Saint Antoine torrent is a tributary of the Arc River in the Western French Alps, located in the Community of Modane, Maurienne Valley. The drainage area of the catchment is 5.10 km<sup>2</sup>, and ranges from 3065 m a.s.l. at Belle Plinier summit, to 1160 m a.s.l. at the outlet in the Arc River. The average slope is of 22%, and the Melton Index is 0.88. This catchment is prone to produce debris flow events; the oldest record dates back to 1489. In the last decades, two DF events occurred. One in 1987 with 55 000 m<sup>3</sup> to 80 000 m<sup>3</sup> of sediment deposited, and one in August 2014, with an estimated deposition of about 40 000 to 60 000 m<sup>3</sup>. This catchment is characterised by the presence of 112 check dams and a unique open check dam located at the fan apex. The DTMs used in this work come from two different LiDAR surveys performed on 14<sup>th</sup> September 2010 and on 20<sup>th</sup> October 2014. As to the longitudinal analysis, the main channel was divided into five homogeneous domains (from A to E): (A) Upper trained reach, (B) untrained gorge, (C) trained gorge, (D) Open check dam, (E) Fan (Figure 1a).

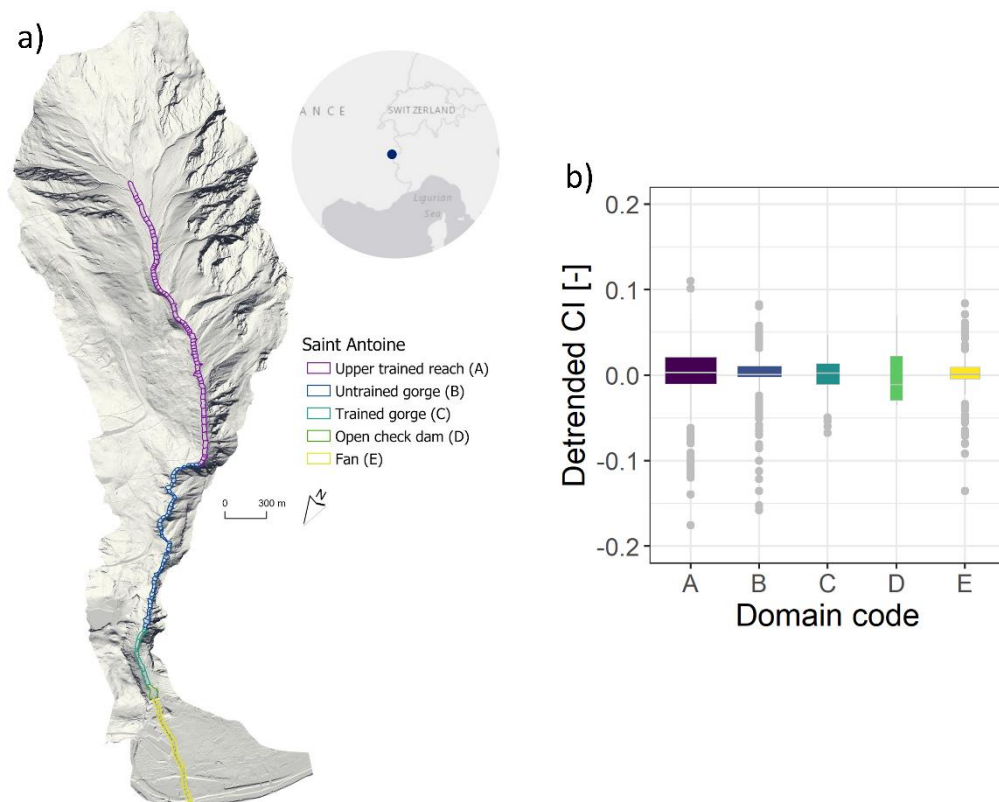


Figure 1. a) Map of the Saint Antoine catchment and alluvial fan and main domains: (A) upper main stem trained with more than 100 check dams, (B) intermediate reach, untrained, (C) lower main stem, trained by 5 check dams, (D) open check dam and (E) alluvial fan channel, embanked by dykes and b) boxplot of detrended connectivity index in the five main domains.

The method we propose is based on the longitudinal analysis of CI applied to a selected reach, e.g., the main channel or a tributary. The analysis was performed at two scales: at the pixel scale (5 m) for the extraction of CI, and at reach scale, i.e., integration on polygons

that are as wide as the active channel and roughly 30 m long, i.e., same distance as between check dams. This resolution allowed to segment the channel bed in coherent units, i.e., reaches between check dams or reaches of equivalent length, for the extraction of erosion and deposition patterns and for comparison with reach-averaged CI values. The weighting factor ( $W$ ) used in the CI computation was the topographic Roughness Index (RI). In particular, we choose to compute “ $W$ ” on the 1m resolution DTM to highlight better Check-dam influence on surface roughness. This is achievable by the fact that the  $W$  computation is estimated by the standard deviation of residual topographic between the original DTM and a smoothed version over a 5 X 5 moving window. This results in a smoothing window size of 25 m<sup>2</sup> using the 1 m DTM, and 625 m<sup>2</sup> using the 5 m DTM. This aggregated  $W$  has then be used as a “Custom” Weighting factor in the second iteration of SedInConnect for the final estimation of the CI. There is a negative relationship between RI and CI: higher roughness corresponds to lower connectivity because terrain roughness affects sediment transfer capacity. It is worth stressing that extremely planar surfaces could invite flow spreading, resulting in reduced transport capacity, while rough surfaces could quickly develop confined flow paths with high transport capacity. However, this effect related to flow confinement is computed by the D-infinity algorithm and accounted for in the computation of the contributing area. For its use as Weighting factor, an inverse normalisation is needed to obtain values from zero (high RI) to one (low RI).

The first phase of the procedure is the production of the shapefile containing the sampling points needed for the longitudinal extraction of each variable composing the Connectivity Index. An easy way to obtain the point sampling layer was to convert a flow accumulation raster (using the D-8 algorithm) and filtered according to the drainage area of the reach under analysis, into a point shapefile. A quality check of this stream-line map was performed and proved to be a crucial step, which supported the choice to work with an aggregate 5 m pixel rather than the original 1 m pixel size. After that, the analysis was carried out on rasters with a pixel size of a coherent dimension with the investigated channel and process. This operation was necessary to reduce the micro-topography noise on the longitudinal analysis of CI and to focus only on the relevant geomorphic characteristics of a DF channel.

For the reach scale analysis, the integration with the(FluvialCorridor) toolbox presented in Roux et al. (2015) helped to extract riverscape features and aggregate them into homogeneous reaches using a semi-automatic procedure. The variables analysed at reach scale, mean and standard deviation values of CI, were derived from an aggregation of all cells within each reach.

The computation of the DEM of Differences (DoD) for sediment budgeting was obtained using multi-temporal DTM analysis derived from two LiDAR surveys. To improve results, a proper point cloud registration has been performed on assumed stable areas using the Iterative Closest Point (ICP) tool included in CloudCompare. This step was necessary to perform an accurate uncertainty estimation, and to filter noise and false-positive signals in elevation change.

An R script was produced for processing all the extracted variables and relate them with the geomorphic features of the investigated segments. Moreover, to better highlight check

dam induced geomorphic variations over CI, an analysis of a linearly detrended CI was performed. This operation was based on removing the linear base trend (grey line on Figure 2) related to increasing catchment scale (on upslope component) and decreasing distance to the target (on downslope component).

## Results and discussion

The first application of a longitudinal analysis on CI applied in Saint Antoine catchment allowed the understanding of the interaction between CI and the protection measures located along the main channel (Figure 1, 2).

The boxplot reported in Figure 1b displays the value of the detrended CI. It enables us to compare the variability of CI between each domain and the influence induced by the presence of hazard mitigation structures. We can see that CI varies markedly in the protected domains (“A” and “C”), i.e., boxplots have a wider interquartile range (IQR) than in the unprotected domains (“B” and “E”).

Outliers are slightly wider in domain A than in domain B, mainly due to spreading near structure crest (Figure. 2e). Conversely, domains “B” and “E” (unprotected) show lower variability (lower IQR) in the CI value due to a more confined flow and the absence of protection measures. This is also visible in the detrended Upslope component on Figure 2e, is showing fewer drops and more stable stability in unprotected areas. This consistently higher connectivity should be considered more prone to transfer and to recruit sediment in the case of a DF due to the higher probability of the flow to incise or deposit material in this un-protected domain. Hence, we concluded refining hypothesis H1, that connectivity index is not specifically lower in the stabilised reaches than in the untrained reaches but clearly shows more varied distribution with low values in correspondence of consolidation structures and higher values far from check dams. In this work, we pushed further the CI analysis by understanding how it behaves quantitatively over different channel management conditions.

According to the CI analysis, erosion–deposition patterns displayed in Figure 2g are different for each specific domain. The protected domains “A” and “C” reported diffuse but regular values of erosions, generally lower than 1 m (as mean  $\pm$  St. D,  $-0.43 \text{ m} \pm 0.24 \text{ m}$  for domain A;  $-0.59 \text{ m} \pm 0.44 \text{ m}$  for domain C), if compared with the non-protected domain B. Here reach-averaged erosion rate exceeded 2 m in some location but remained on average only slightly higher ( $-0.57 \text{ m} \pm 0.72 \text{ m}$ ). As to the domain “D” of the open check dam, is the domain with the highest deposition rate (1.83 m). In domain “E”, the fan channel experienced low erosion rates in the upper part, followed by some sediment depositions near the outlet with the Arc River; this is consistent with the usual behaviour of debris flows on fans. Our working hypothesis H2 is here validated since erosion rates are lower where check dams are located, and deposition is concentrated in the open check dam. It is worth stressing that the trends on domains “A” and “B” are however extremely oriented toward erosion caused by the August 2014 DF. Conversely, reports from ONF RTM archive relates major deposition in the downstream part of domain “A” during the event of 1987 and let presume that basin behaviour is massively variable.

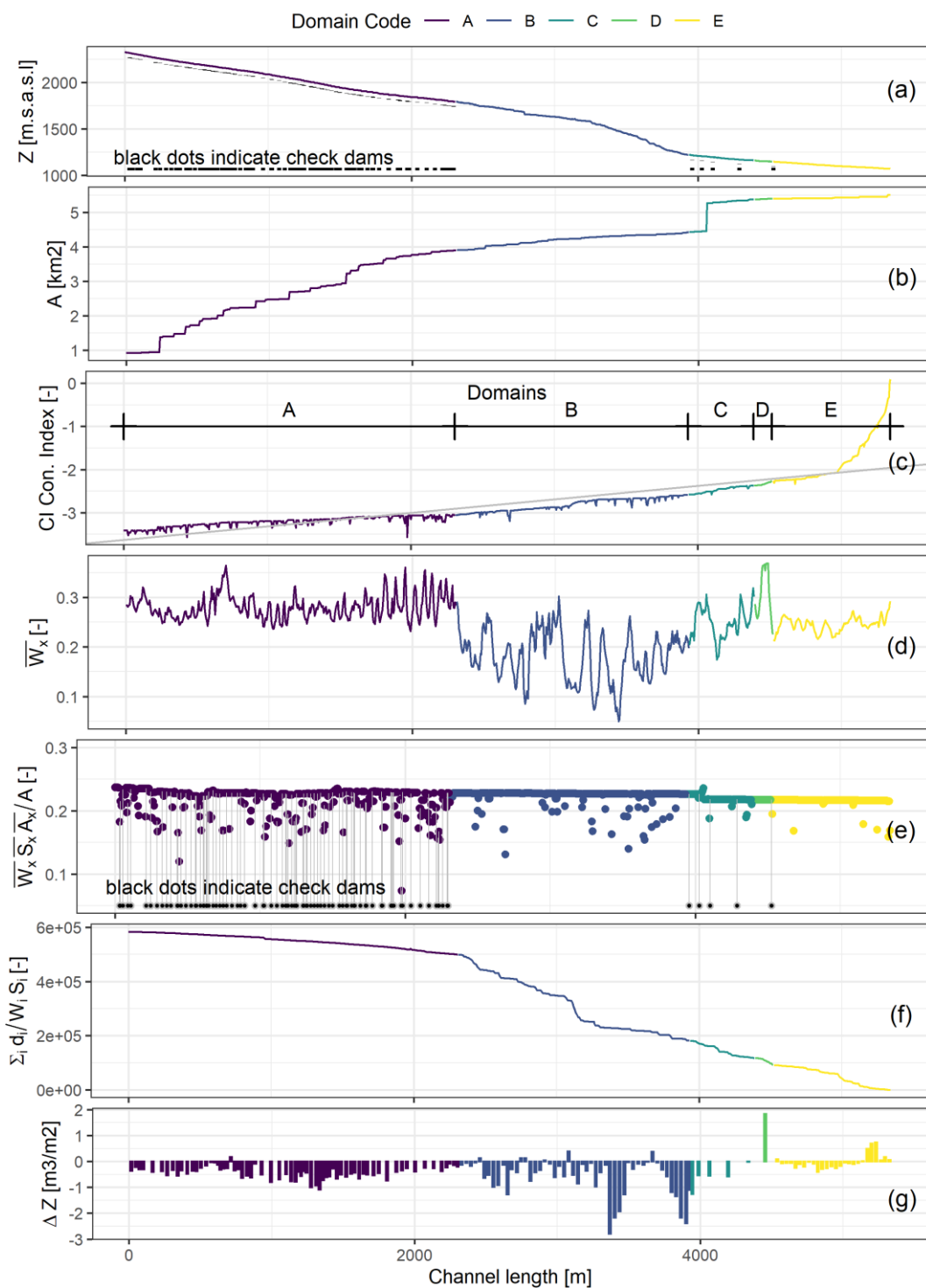


**Figure 2. Longitudinal analysis of the Saint Antoine main stem according to our procedure: a) longitudinal profile highlighting the domain and location of check dams, b) upstream catchment area, c) connectivity index, d) Weighting factor, e) detrended upslope component, i.e., upslope component divided by square root of contributing area, f) downslope component and g) erosion and deposition rate ( $m^3/m^2$ ) aggregated at reach length (30 m long) from DoD**

The catchment size increases gradually (Figure 2b) as well as the CI (Figure 2c) except for a fast increase in the more distal part of the fan where the downslope component drops to

zero (Figure 2f), and thus CI increases markedly. The drop in the downslope component is mainly related to the regular decrease in distance since the weighting factor oscillates between 0.15 and 0.6 (Figure 2d). Regarding the weighting factor, in domain “A” is fluctuating rhythmically between 0.3 and 0.6. The lower point of each swaying cycle falls in the area where a Check Dam is located. In domain B (un-trained) the weighting factor varies greatly inside the range 0.15 to 0.6, but with a lower mean value. The weighting factor variable explains a moderately higher roughness in domain B, which can be explained by the higher confinement of flow and higher irregularities in the topography induced by a gorge morphology.

The upslope component detrended by the square root of the contributing area is rather stable except for local drops that are more numerous in domain “A” than in other downstream domains (Figure 2e). Visual inspection of the maps demonstrated that flow spreading on the reaches located directly upstream of check dams is responsible for these drops.

In a global perspective of Figure 2, the relation between elevation changes and all the other variables appear interesting. In particular, it is possible to see how each variable has different patterns according to the analysed domain.

## Conclusion

From the results, we can conclude that this first quantitative analysis of CI along the main channel opens new opportunities for the interpretation and use of the Connectivity Index as a tool for geomorphic features analysis of a selected catchment. It also enables us to understand how each factor encapsulated in the CI framework is affected by the long-term presence of protection structures. Moreover, we observed that some interesting correspondence appears between different statistical distributions of CI and geomorphic changes in case of a debris-flow event. Advanced analyses on the previous point are ongoing extending the application of this novel method to tributaries. This will help to test the global versatility of the approach on heterogeneous mountain catchments.

Through this new procedure, we are opening a new way to analyse the connectivity index and its possible use during hazard mitigation planning and hazard assessment. In particular, after further applications, we might deliver an easy-to-use procedure for CI interpretation that can be used to understand sediment dynamics in mountain torrents.

## Acknowledgement

The authors would like to thank the ONF RTM for providing data on the torrent. The work of G.P. was funded by the H2020 NAIAD project [grant no. 730497] from the European Union’s Horizon 2020 research and innovation program.

## References

Atkinson, E., 1995. Hydrological Sciences Journal Methods for assessing sediment delivery in river systems. *Hydrol. Sci. J.* 40(4), 273–280. DOI:10.1080/02626669509491409

- Borselli, L., Cassi, P., Torri, D., 2008. Prolegomena to sediment and flow connectivity in the landscape: A GIS and field numerical assessment. *Catena* 75, 268–277. DOI:10.1016/j.catena.2008.07.006
- Brown, A.G., Tooth, S., Bullard, J.E., Thomas, D.S.G., Chiverrell, R.C., Plater, A.J., Murton, J., Thorndycraft, V.R., Tarolli, P., Rose, J., Wainwright, J., Downs, P., Aalto, R., 2016. The geomorphology of the Anthropocene: emergence, status and implications. *Earth Surf. Process. Landforms*. DOI:10.1002/esp.3943
- Cavalli, M., Trevisani, S., Comiti, F., Marchi, L., 2013. Geomorphometric assessment of spatial sediment connectivity in small Alpine catchments. *Geomorphology* 188, 31–41. DOI:10.1016/j.geomorph.2012.05.007
- Crema, S., Cavalli, M., 2017. SedInConnect: A stand-alone, free and open-source tool for the assessment of sediment connectivity. *Comput. Geosci.* DOI:10.1016/j.cageo.2017.10.009
- Cucchiaro, S., Cavalli, M., Vericat, D., Crema, S., Llena, M., Beinart, A., Marchi, L., Cazorzi, F., 2019. Geomorphic effectiveness of check dams in a debris-flow catchment using multi-temporal topographic surveys. *Catena* 174, 73–83. DOI:10.1016/J.CATENA.2018.11.004
- Dietrich, W.E., Dunne, T., 1978. Sediment budget for a small catchment in mountainous terrain. *Z. Geomorph. N. F., Suppl. Bd. 29*, 191–206.
- Ferro, V., Minacapilli, M., 1995. Sediment delivery processes at basin scale. *Hydrol. Sci. J.* 40, 703–717. DOI:10.1080/02626669509491460
- López-Vicente, M., Quijano, L., Palazón, L., Gaspar, L., Navas, A., 2015. Assessment of soil redistribution at catchment scale by coupling a soil erosion model and a sediment connectivity index (central Spanish pre-Pyrenees). *Cuad. Investig. Geográfica* 41, 127. DOI:10.18172/cig.2649
- Roux, C., Alber, A., Bertrand, M., Vaudor, L., Piégay, H., 2015. “FluvialCorridor”: A new ArcGIS toolbox package for multiscale riverscape exploration. *Geomorphology* 242, 29–37. DOI:10.1016/j.geomorph.2014.04.018

---

# Comparison of techniques for estimating soil drainage for the assessment of empirical rainfall thresholds - a case study of ash-fall pyroclastic soil mantled slopes of southern Italy.

Rita Tufano<sup>1</sup>, Pantaleone De Vita<sup>2</sup>, Thomas Glade<sup>3</sup>

**Keywords:** ash-fall pyroclastic soil, flood hydrograph, recession limbs, physically-based modelling, infiltration rate

## Abstract

The *d*-factor for the “Antecedent Daily Rainfall” index definition represents an estimate of the effect of soil moisture drainage in the antecedent period to landslide occurrence. To determine the *d*-factor, two techniques were adopted in this paper for identifying the most performing one in view of the definition of rainfall thresholds based on rainfall recorded in the day of the landslide event (*P*) and that cumulated in an antecedent period (*P<sub>a</sub>*). The study is focused on the well-known case study of shallow rainfall-induced landslide involving ash-fall pyroclastic soils mantling steep slopes in the Campania region (southern Italy). At this scope, the first technique is based on the analysis of flood hydrographs of Sarno river, whose catchment comprehends mountain slopes prone to rainfall-induced shallow landslides. The second approach is based on modelling infiltration process through soil horizons forming ash-fall pyroclastic series. The results of first analysis are conditioned by hydrogeological setting and strong urbanisation, making more plausible the results of the second one.

## Introduction

Shallow landslides triggered by rainfall events are extremely diffused in mountain areas and potentially exerting catastrophic impacts on urbanized zones located along footslopes. Therefore, this type of geohazard is a geomorphological process well-known worldwide and studied by the scientific community. In Italy, a special case is represented by shallow landslides involving ash-fall pyroclastic soils mantling steep mountain slopes that surround

---

<sup>1</sup> Ph.Student, DISTAR, Università degli Studi di Napoli Federico II, Cupa Nuova Cintia, 21, Naples, Italy ([rita.tufano@unina.it](mailto:rita.tufano@unina.it))

<sup>2</sup> University of Naples "Federico II"

<sup>3</sup> University of Vienna

the Somma-Vesuvius volcano, which initiate as small debris slides and often evolve downslope as deadly debris avalanches or debris flows (Hungri et al., 2014). Due to the volume of the depleted mass, debris flows induced by shallow, often translational landslides, are more dangerous than those resulting from continuous erosive processes (Malet et al., 2005).

One of the most recent catastrophic events, occurred on 5-6 May of 1998 in Sarno Mountains (Campania Region, southern Italy), caused the loss of 160 lives and the destruction of some infrastructures in the municipalities surrounding the mountains involved (De Vita et al., 2013). Sarno Mountains are formed by Mesozoic carbonate platform series covered by ash-fall pyroclastic deposits derived by the explosive volcanic activity of the Somma-Vesuvius and Phlegrean Fields volcanoes. These deposits are characterized by alternated pumiceous lapilli and pedogenized horizons, frequently involved by erosional processes, such as debris slides – debris flows events (De Vita et al., 2013). In such a geomorphological framework, many studies have been focused on estimating reliable relationships among the onset of shallow landslides and the amount and duration of rainfall events, to define or estimate landslide-triggering rainfall thresholds.

In particular, several authors developed empirical thresholds, such as those based on the correlation of rainfall intensity (I) and duration (D) (Bogaard & Greco, 2018) or on the relationship between the rainfall recorded in the day of the landslide event and that cumulated in an antecedent period (P-P<sub>a</sub>) (e.g. Mirus et al., 2018) as well as deterministic thresholds (Godt & McKenna, 2008) based on a physical-conceptual modelling of hillslope hydrological processes.

In order to investigate the role played by antecedent hydrological conditions on the stability of the ash-fall pyroclastic soil mantle, by the recognition of P-P<sub>a</sub> thresholds, Crozier and Eyles (1980) introduced the “Antecedent Daily Rainfall” index. Aiming at taking into account soil hydrological conditions pre-existing the rainfall event, this index determines the soil water status preceding each daily rainfall by estimating the water storage of soils through the soil drainage rate. It is calculated as (Eq. 1):

$$r_a = r_1 k + r_2 k^2 + \dots + r_n k^n \quad (1)$$

where  $r_a$  is antecedent daily precipitation index (mm) for day 0,  $k$  is a constant representing the average outflow from the regolith (conventionally equal to 0.84), and  $r_n$  is the maximum regional precipitation (mm) on the  $n^{\text{th}}$  day before 0. Subsequently, Glade et al. (2000) proposed a factor which reflects the soil moisture drainage more appropriately. This is the runoff-derived decay factor ( $d$ -factor), generally estimated through the analysis of the hydrograph recession limb. Introducing this runoff characteristic to equation (1), the “Antecedent Daily Rainfall” index becomes (Eq. 2):

$$r_a = r_1 + 2^d r_2 + 3^d r_3 \dots + n^d r_n \quad (2)$$

where  $n$  is number of days before the day 0 (Glade et al., 2000).

In this work, two techniques are investigated for estimating the  $d$ -factor. The first is based on the classic calculation derived by the analysis of hydrograph recordings. The second approach is based on physical modelling and, in particular, the soil drainage is estimated by the infiltration rate of a simulated rainfall through the ash-fall pyroclastic soil deposits. Results of both analyses were compared in order to identify the most performing approach for the application of the “Antecedent Daily Rainfall”.

## Methods

### Runoff-derived decay factor

To estimate the  $d$ -factor, the analysis of flood hydrograph of Sarno River was carried out considering time series of river discharge measured at the San Valentino Torio hydrometric station (Fig. 1). The latter was identified due to the inclusion in its catchment of a sector of ash-fall pyroclastic soil mantled slopes of Sarno Mountains along which deadly debris flows occurred in May 1998. Data were available by printed annals published by the *Servizio Idrografico e Mareografico Nazionale* (SIMN) until 1994. Unfortunately, time series was discontinuous, thus limiting us to consider the following available sub-series: 1981, 1982, 1983, 1985, 1991 and 1994. Instead, for the following period, from 2014 to 2017, hydrometric height time series measured by the *Centro Funzionale* at the San Marzano sul Sarno hydrometric station were available and considered for the estimation of the  $d$ -factor. From discharge and hydrometric heights time series, various recession limbs with varying durations were analysed. The analysis was focused on recession limbs recognized in time series not influenced by contemporaneous rainfall, to ensure that rates of hydrograph recession accurately reflect drainage from the catchments. Moreover, rainfall data was derived by the Sarno rain gauge located inside the mountain catchment analysed (Fig. 1).

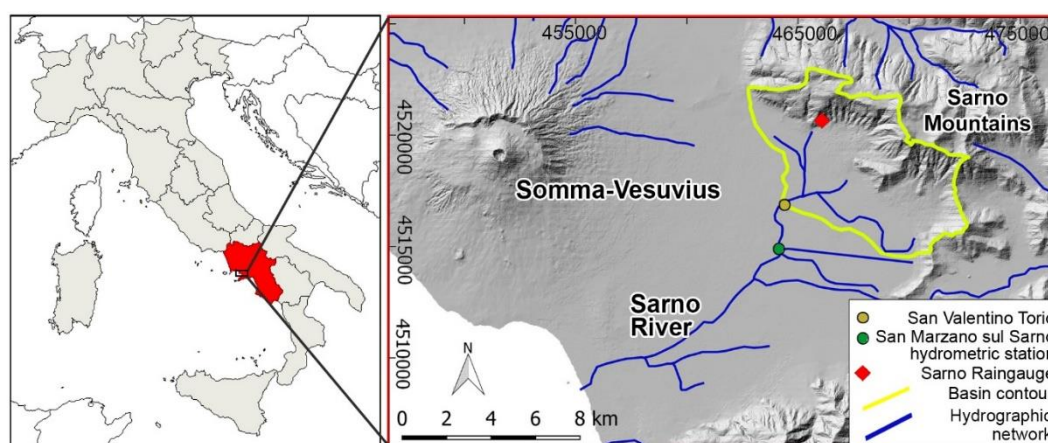


**Figure 1. Hillshade of the mountain catchment considered for hydrometric analysis, ubication of hydrometric station of discharge measurements and rain gauge considered.**

All hydrological data, including rainfall, were analysed at the daily scale as shown in Figure 2. Hydrograph recession limbs are best represented with a power trend line. The general power equation for these recession limbs takes the form (3):

$$y = c n^d \quad (3)$$

Where  $y$  is the discharge ( $\text{m}^3/\text{s}$ ) or the hydrometric height (cm) at any point in the recession limb,  $c$  is the peak of streamflow,  $n$  is the time in days, and  $d$  the slope of the recession limb on a logarithmic scale.

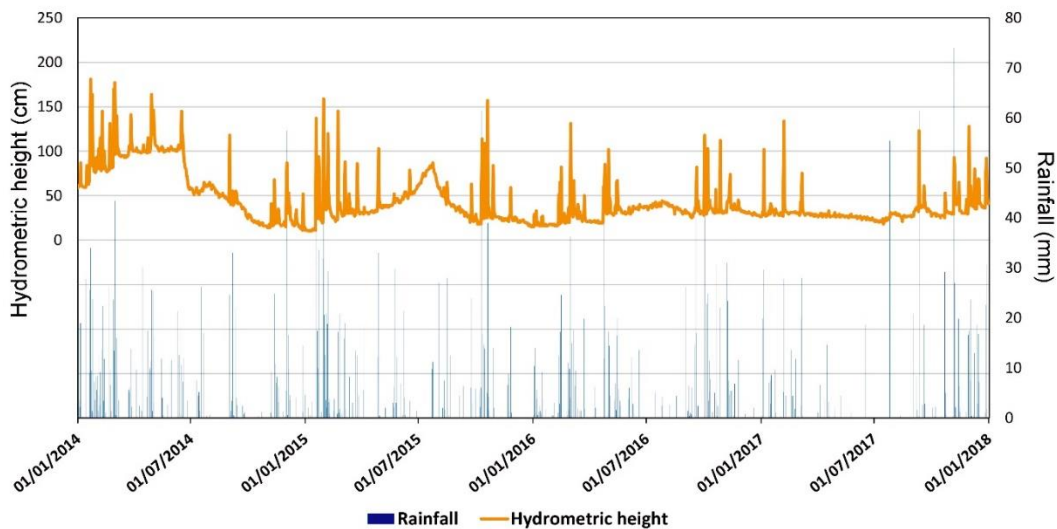


Figure 2. Trend of hydrometric height of Sarno river from 2014 to 2017 measured to San Marzano sul Sarno station and rainfall data by Sarno rain gauge.

## Physically-based modelling for soil drainage estimation

Physically-based modelling was performed to estimate the physical trend of infiltration rate, using the numerical code VS2DTI (Hsieh et al., 2000), which is a physically-based model of variably saturated subsurface flow in two dimensions. The model setup was based on a representative stratigraphic setting of ash-fall pyroclastic deposits in the Sarno Mountains area, formed by three pedogenized soil horizons (B, Bb and Bb<sub>basal</sub>), classified as SM (USCS), which are alternated to two unweathered pumiceous soil horizons (C and Cb), classified as GP-GW (USCS) (Fig. 3a). Unsaturated and saturated hydraulic properties of materials forming the model were assigned by considering fitting parameters of the van Genuchten (1980) SWRC model and saturated hydraulic conductivity ( $K_{\text{sat}}$ ), provided by literature data (Tab. 1) (De Vita et al., 2013). The A horizon (organic soil) has been neglected due to its reduced thickness. The initial pressure head values used for the simulations were set equal to 0,0 m (saturation condition), for each horizon. Observation points were located close to the upper boundary. Finally, the modelling was carried out in a transient state and considering a time step of simulation of 0,5 sec for a variable duration, depending on the hydraulic properties of investigated horizon.

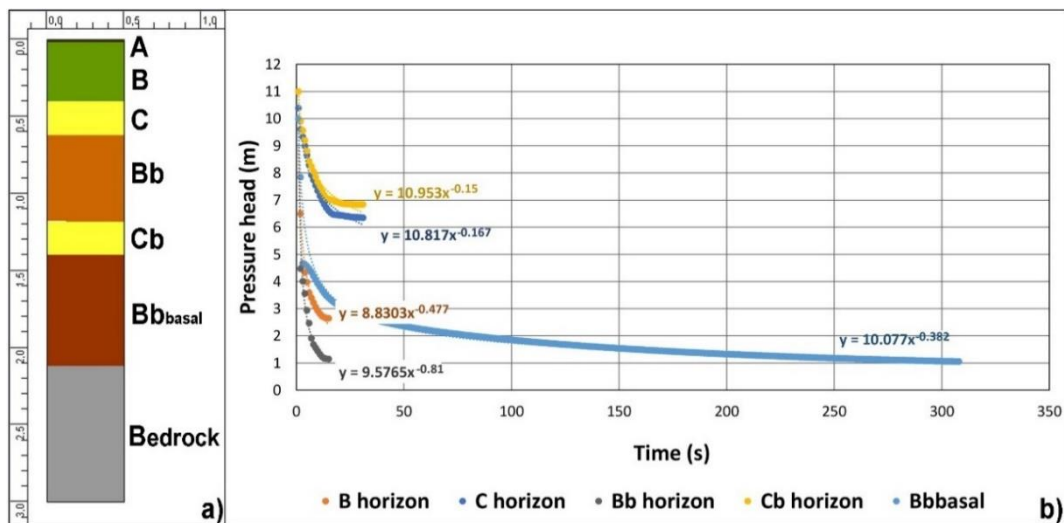


Figure 3. a) Representative stratigraphic setting of ash-fall pyroclastic deposits used for the physical modelling (A horizon was not considered because of its low thickness); b) infiltration rate trend (pressure head vs time) and dashed power line fitting the equation for each horizon of ash-fall pyroclastic series.

Table 1. Unsaturated hydraulic and mechanical parameters considered for the VS2DTI hydrological modelling.

	Horizon B	Horizon Bb	Horizon Bbasal	Horizon C
$\gamma_{dry}$ (kN/m <sup>3</sup> )	10.22	10.33	6.83	8.42
$\gamma_{nat}$ (kN/m <sup>3</sup> )	12.09	11.64	10.09	10.57
$\gamma_{sat}$ (kN/m <sup>3</sup> )	15.85	16.16	13.82	14.94
$\theta_s$ [-]	0.500	0.560	0.590	0.630
$\theta_r$ [-]	0.080	0.200	0.001	0.001
Perc 25% < $K_{sat}$ <	$4.8 \times 10^{-5} < K_{sat}$	$6.0 \times 10^{-6} < K_{sat}$	$2.4 \times 10^{-7} < K_{sat}$	$2.8 \times 10^{-3} < K_{sat}$
Perc 75% (m/s)	$< 1.2 \times 10^{-4}$	$< 2.6 \times 10^{-5}$	$< 6.8 \times 10^{-6}$	$< 1.2 \times 10^{-2}$

## Results and discussion

In this paper, the runoff-derived decay factor (*d*-factor), derived by the analysis of recession limbs of river discharge and hydrometric height time series (related to Sarno River basin), and the infiltration rate, estimated using the physically-based modelling, were considered as the “Antecedent Daily Rainfall” index calculation (Glade et al., 2000). Both results describe soil drainage processes, useful for understanding the hydrological state of soil in the antecedent period to landslide occurrence.

The results of the recession limb analysis of Sarno River hydrographs and hydrometric heights are shown in Table 2. The average values of the two data series, equal to n-0.10 and n-0.12 respectively, indicate a significant regional drainage rate. In particular, using these *d*-factors in the Eq. (2), the “Antecedent Daily Rainfall” index will not give a correct

indication of the antecedent rainfall to be considered for the estimate of P-P<sub>a</sub> thresholds. In fact, it indicates a fast drainage of water from the soil and a low amount of retention water of pyroclastic soils. However, this result could be explained by the complex hydrogeological setting of Sarno Mountains with high permeable karst rocks, the presence of large summit endorheic or flat areas that favour the direct infiltration and groundwater recharge processes, and at least five basal springs that feed the water flow to the river (De Vita et al., 2018). Moreover, discharge regime of Sarno river is also conditioned by an extensive agricultural and industrial activity responsible of spills or artificial inflows of wastewater. These considerations make understandable the very low value of *d*-factors estimated and open the way to physically-based modelling of the infiltration process in the ash-fall pyroclastic series.

**Table 2.** calculated exponential *d*-factor derived from hydrograph recession limbs by discharge and hydrometric height data for Sarno basin, and annual *d*-factor standard deviation.

<b>Discharge</b>	<b>1981</b>	<b>1982</b>	<b>1983</b>	<b>1985</b>	<b>1991</b>	<b>1994</b>
Exponential <i>d</i> -factor	-0.04	-0.15	-0.14	-0.09	-0.03	-
Standard deviation of <i>d</i> -factor	0.03	0.14	0.12	0.08	0.03	0.07
<b>Hydrometric Height</b>	<b>2014</b>	<b>2015</b>	<b>2016</b>	<b>2017</b>		
Exponential <i>d</i> -factor	-0.11	-0.15	-0.11	-0.11		
Standard deviation of <i>d</i> -factor	0.08	0.08	0.05	0.08		
<b>Numerical modelling</b>	<b>Horizon B</b>	<b>Horizon C</b>	<b>Horizon Bb</b>	<b>Horizon Cb</b>	<b>Horizon Bb<sub>basal</sub></b>	
Exponential <i>d</i> -factor	-0.48	-0.17	-0.81	-0.15	-0.38	

Physically-based modelling represents the second approach tested in this paper to assess the soil drainage capability. In particular, we analysed soil water pressure head during an infiltration process which was simulated for soil horizon. Results are represented by curves, well described by a general power equation (Fig. 3b). By these curves an average *d*-factor was determined, equal to n-0.40, less than those determined by the previous one (n-0.10 and n-0.12). Table 2 shows the *d*-factor estimated for each soil horizon. In particular, the high hydraulic conductivity due to large macropores of the two pumiceous horizons (C and Cb) determines a value of the *d*-factor lower than that estimated for the three pedogenized horizons (B, Bb and Bb<sub>basal</sub>), for which saturated hydraulic conductivity is lower. In fact, hydrological properties of such pedogenized soil horizons allow to retain a soil water amount which is drained more slowly. As a consequence, by using the *d*-factors derived by physically-based modelling, the “Antecedent Daily Rainfall” index enhances more the effect of those rainy days immediately preceding the landslide event than the antecedent others. Numerical comparison between results obtained using the two techniques identifies the physically-based approach as the most suitable. Such a technique can be conceived as more adaptable to simulate the soil drainage rate in mountain catchments to which a not hydrogeologically homogeneous catchment, subtended by a hydrometric station, can be associated.

## Conclusion

The analysis of  $d$ -factor, estimated by two different approaches, shows a better performance of results obtained by the physically-based modelling. In fact, results obtained by this second method show more properly the hydrological ability to store water of soils involved. Moreover, the  $d$ -factor obtained by the simulation of the infiltration process is strictly related to infiltration and drainage processes occurring in soil coverings potentially affected by shallow rainfall-induced landslides begin not influenced by geological and hydrogeological heterogeneities occurring at the scale of an extended catchment including parts of urbanized territory.

## References

- Bogaard T., and Greco R. (2018). Invited perspectives: Hydrological perspectives on precipitation intensity-duration thresholds for landslide initiation: proposing hydro-meteorological thresholds. *Natural Hazards and Earth System Sciences*, 18(1), 31-39.
- Crozier M. J., and Eyles, R. J. (1980). Assessing the probability of rapid mass movement. In *Third Australia-New Zealand conference on Geomechanics: Wellington, May 12-16, 1980* (p. 2). Institution of Professional Engineers New Zealand.
- De Vita P., Napolitano E., Godt J.W., and Baum R. (2013). Deterministic estimation of hydrological thresholds for shallow landslide initiation and slope stability models: case study from the Somma-Vesuvius area of southern Italy. *Landslides*, 10, 713–728.
- De Vita P., Fusco F., Tufano R., and Cusano D. (2018). Seasonal and event-based hydrological and slope stability modeling of pyroclastic fall deposits covering slopes in Campania (southern Italy). *Water*, 10(9), 1140-1162.
- Glade T., Crozier M., and Smith P. (2000). Applying Probability Determination to Refine Landslide-triggering Rainfall Thresholds Using an Empirical “Antecedent Daily Rainfall Model”- *Pure Appl. Geophys.* 157, 1059–1079.
- Godt J. W., and McKenna J. P. (2008). Numerical modeling of rainfall thresholds for shallow landsliding in the Seattle, Washington, area. *Reviews in Engineering Geology*, 20, 121-136.
- Hsieh P.A., Wingle W., and Healy R.W. (2000). VS2DI: A Graphical Software Package for Simulating Fluid Flow and Solute or Energy Transport in Variably Saturated Porous Media. U.S. Geological Survey. *Water-Resources Investigations Report 9-4130*.
- Hungr O., Leroueil S., and Picarelli L. (2014). The Varnes classification of landslide types, an updated. *Landslides*, 11, 167–194.
- Malet J. P., Laigle D., Remaître A., and Maquaire O. (2005). Triggering conditions and mobility of debris flows associated to complex earthflows. *Geomorphology*, 66(1-4), 215-235.

Mirus B., Morpew M., and Smith J. (2018). Developing hydro-meteorological thresholds for shallow landslide initiation and early warning. *Water*, 10(9), 1274-1293.



# HAZARD AND RISK MITIGATION (HRM)

---

# Building protection against surface runoff

Markus Imhof<sup>1</sup>, Benno Staub<sup>2</sup>, Alain Marti<sup>3</sup>, Gunthard Niederbäumer<sup>4</sup>, Roberto Loat<sup>5</sup>

**Keywords:** surface runoff; heavy rain; protection of buildings; building damage; urban drainage

## Abstract

Surface runoff is responsible for a considerable proportion of flood damage to buildings. It affects many buildings in Switzerland, including those far away from any lake or river. In view of insufficient advance warnings of heavy local rainfall, these buildings can be protected only by permanent measures. There is a broad range of possible protection strategies, from landscaping to targeted water diversion and waterproofing measures for the building envelope, including protections for openings and access points.

## Introduction

The fire service is familiar with the unsatisfactory situation in which, just a few minutes after being called out, they are ready for action on site but the flood damage has already happened, and with the exception of inundated cellars and underground car parks, the water has already drained away. The only thing to do in such cases is to pump out the remainder, yet protection measures could have prevented the situation in the first place. This is a description of the typical progression of surface runoff caused by heavy rain in a sloping location (Fig. 1, right).

---

<sup>1</sup> Ph.D., Bereichsleiter Naturgefahren, APIRE, Bundesgasse 20, Bern, Switzerland  
(markus.imhof@vkg.ch)

<sup>2</sup> Dr., APIRE Association of Public Insurance Companies for Real Estate, Bundesgasse 20, CH-3001 Bern, Switzerland

<sup>3</sup> Mr., APIRE Association of Public Insurance Companies for Real Estate, Bundesgasse 20, CH-3001 Bern, Switzerland

<sup>4</sup> Dr., SIA Swiss Insurance Association, C.-F.-Meyer-Strasse 14, CH-8022 Zurich, Switzerland

<sup>5</sup> DR., FOEN Federal Office for the Environment, Worblentalstrasse 68, CH-3063 Ittigen, Switzerland



**Figure 1. Extract from the surface runoff risk map, and actual loss event (legend: pale pink: < 10 cm / dark pink: 10 – 25 cm / purple > 25 cm flow depth; red circle: building in the photo to the right). Map: FOEN / Swisstopo; photo: GVL claim files.**

Surface runoff is defined as the part of the precipitation that flows over the land directly towards a stream channel or lake (Loat & Meier, 2003). In other words, it is a type of flooding which does not originate from permanent bodies of water, such as streams, rivers and lakes, but which occurs spontaneously as the result of localised heavy rain. In the case of permanent water bodies, gauge measurements can be accomplished and a threshold for water level can be set at which an alert is triggered. Ideally, this provides several hours' advance warning of flooding. Meanwhile, surface runoff can be forecast at best only minutes ahead, if at all, on the basis of rainfall radar data. It is therefore impossible to have any reliable early warning system.

The cantons' conventional natural hazard maps depict the risks posed by permanent bodies of water. By contrast, the potential occurrence of surface runoff is shown at best schematically, if at all, on the basis of known events. However, since July 2018 it has been possible to make a realistic assessment of the risk affecting every building in Switzerland using the Swiss 'Surface runoff risk map' (FOEN, 2018; Loat et al., 2020). On a scale of 1:12,500, it shows where surface runoff is likely in the event of heavy rain, and also indicates the expected water depth (Fig. 1, left). According to this map, almost two-thirds of Switzerland's building stock is potentially at risk.

## Significance of surface runoff

As a natural hazard, surface runoff was underestimated until just recently. Its significance is nonetheless underscored when the building damage claims paid out over the past 20 years by the 18 cantonal Public Insurance Companies for Real Estate (PIRE), are extrapolated to cover the whole of Switzerland. This shows that, on average, over 3,000 buildings nationwide are damaged by surface runoff each year, resulting in costs of just under CHF 30 million. This corresponds to almost half of all flood-related claims, and to around a quarter of the corresponding costs (Bernet et al., 2018). The total building damage caused by surface runoff thus clearly exceeds that resulting from landslides, rock falls, snow pressure and avalanches combined.

## **The role of urban drainage**

In urban areas, drainage systems generally ensure that rainwater is discharged swiftly. As a rule, these systems are designed to cope only with precipitation events with return periods of five or ten years (Maurer et al., 2012). However, assuming a useful life of (at least) 50 years, any given building has a 40 per cent probability of being exposed to a centennial heavy rainfall event. For both technical and economic reasons, urban drainage systems are simply not designed to deal with such volumes of water. Even in the case of more minor events, leaves, hailstones, mud and hydrodynamic processes (such as vortexes) prevent much of the water entering the sewers at all. In many cases, some of the water within the drainage system will be forced up out of manholes further downhill, or will enter buildings directly via the drains as a result of backflow.

## **The risk posed by surface runoff**

Buildings in sloping locations and at the foot of slopes are at particular risk of surface runoff, especially if the slope is concave (i.e. forming a channel or bowl). The same is true of buildings located at topographical low points. The problem is often exacerbated by the artificial channels formed by roads and paths, kerbs, edgings, underground car park entrances and steps, all of which guide the water towards the building itself. Although the flow depth of surface runoff is generally low, once it penetrates a building the water level on basement floors can quickly rise as far as the ceiling – with the corresponding damage to property and, in the worst case, danger to life. Electrical systems are a further hazard, not only for those already within the building, but also for the emergency services.

The quality of the building envelope is the primary factor determining whether or not damage will be incurred. Water is almost bound to find any weak points. In most cases, these will be pedestrian and vehicle entrances at low levels, as well as windows, doors, light wells and ventilation shafts. Water can also enter the building via the sewerage system (backflow) and non-watertight cable feed-throughs or walls within the building. The water is mostly polluted to a greater or lesser degree, thus bringing mud, faecal matter or heating oil into the building. This increases the damage caused within and to the building, and also poses an environmental risk to the surrounding area. Capillary action (i.e. the way in which moisture rises through walling or insulation) and high humidity mean that damage typically extends above the level of the actual flood.

## **Building protection measures**

### **Integrated risk management strategy**

A whole variety of parties are involved in creating the building envelope and surroundings as part of a construction project, such as developers, architects and specialist planners. They should thus all be aware of the problems that surface runoff can cause, as well as the ways in which they can avoid future building damage and the action that they should take.

The integrated risk management strategy issued by the Swiss National Platform for Natural Hazards (PLANAT, 2014) sets out guidelines in this regard. It seeks to answer three key questions:

**'What can happen?'** – All action planning begins with a risk analysis, i.e. an evaluation of the situation at hand and the potential dangers it poses. The 'Surface runoff risk map' is used to determine whether or not any risk actually exists. The map also offers initial indications of the paths the water might take, as well as the water depth. However, since the foundations on which modelling is based lack granularity (small structures such as edging, kerbs or sills in front of vehicle entrances may not be shown on the digital terrain model), it is essential that actual flow paths are subsequently verified in a site visit. This must also establish whether people are at risk in the building, and if so, how many, the openings through which water might enter the building, the sections of the building and systems which are sensitive to water, any building contents (such as furnishings or stored goods) that might be affected, and whether or not the building can continue to be used (for residential or business purposes) after the event of flooding.

**'What is allowed to happen?'** – The answer to this question determines the effectiveness requirements that protection measures must fulfil. The task is to establish which consequences of a loss event are deemed tolerable, and which not. The individual needs of the developers and/or users of the building take precedence here, although there are also statutory requirements that must be satisfied, such as those concerning human safety.

**'What has to be done?'** – When implementing defence measures, there is seldom a single, one-size-fits-all solution. Rather, those measures which are most appropriate to the situation (new build / conversion, building type and usage) must be selected (see also the online natural hazards check at [www.schutz-vor-naturgefahren.ch](http://www.schutz-vor-naturgefahren.ch) [in German and French] as well as SIA, 2019). The owner of the building will, of course, restrict themselves to object protection measures. Meanwhile, the authorities (the commune and canton) are responsible for action to protect larger areas within towns and villages.

Measures to protect buildings against surface runoff are naturally also effective against flooding originating from permanent bodies of water (and vice-versa). It is therefore recommended that measures are planned not in isolation, but taking overall risk into account. This means factoring in the cantonal natural water hazards map in addition to the 'Surface runoff risk map'.

Broadly speaking, property protection measures fall into three categories: landscaping, protection measures outside the building and measures inside the building.

## Landscaping

As a general rule, the surrounding area should be designed so that water flows away from the building. Depressions neighbouring the building should be avoided or filled in, or used specifically as retention areas. In this way, the building envelope will ideally not even come into contact with any surface runoff. Collecting channels, edging and diverting walls (Fig. 2) can also be used to keep surface water away from the building. With all diversion measures, care must be taken to comply with Article 689 of the Swiss Civil Code (CC):

*"No person may alter the natural course of flow [of water] to his or her neighbour's detriment".* Furthermore, entry points to the drains on the property must be checked regularly and cleaned if necessary.



**Figure 2. A diverting wall takes the water past the building. Photo: APIRE.**

Specific drainage corridors are important to prevent the risk being shifted on to other properties. In the case of major and growing developments, surface water drainage must be planned at an early stage in a coordinated approach. If all of the relevant parties are involved in planning how to deal with large volumes of rainwater, entire neighbourhoods can be protected against surface runoff, while also meeting environmental requirements for sustainable rainwater management.

### **Protection measures outside the building**

There are a multitude of ways of preventing water penetrating a building. Elevating the ground floor – and building entrances in particular – to above flood level can lift potential weak points out of the vulnerable area. Especially where new builds are concerned, this solution is as effective as it is cost-efficient. It is also worth elevating the upper edges of light well and ventilation shaft openings (Fig. 3). Meanwhile, underground car parks can be protected by creating a counter slope with a sill in front of the entrance (Fig. 4). Where this is not possible, flip-up flood barriers or (automatically closing) flood gates may help to solve the problem. Sections of the building which remain within the flood zone can be secured by means of watertight doors and windows, and watertight walls constructed of non-hygroscopic materials. Certain types of insulation and plaster are particularly sensitive to water, which is why conversion and renovation work should also be planned carefully.



Figure 3. Light well and ventilation shaft openings elevated above flood level. Photo: APIRE.



Figure 4. A counter slope at the entrance to an underground car park prevents it flooding. Photo: APIRE.

A thorough, considered approach is key when planning what measures to institute. A single weak point anywhere in the building is all it takes for damage to result. Therefore, it is not enough simply to address the 'major' weak points, but forget the cat flap, for example. It takes more than defensive action to solve the problem, however. Moveable elements of the building, and those prone to wear and tear, require special care and maintenance. Part of ensuring good drainage is the regular checking and cleaning of guttering and downspouts, as well as entry points to drainage on the property. This reduces the volume of water that might potentially collect around the building.

## **Protection measures inside the building**

Technical facilities such as electrical sockets, electrical control panels, washing machines, tumble dryers, freezers, lifts, heating systems and computer servers, etc., as well as items of value, should all be installed or stored above the expected flood level. Anchor points prevent heating oil tanks floating up in the water and contaminating it. Protecting all electrical installations is also key to personal safety. Backflow prevention devices such as non-return flaps and anti-flooding valves also prevent water from the sewerage system entering the building. Care must be taken to ensure that the points at which pipes and cables feed through to the interior of the building are watertight.

## **Permanent or temporary measures?**

Experience has shown that surface runoff happens so quickly that there is no time for defensive action. Measures to shield buildings, divert water and waterproof installations must therefore be permanent, and function independently, i.e. without human intervention. By contrast, temporary measures require those entrusted with deploying them to be ready at all times. Equipment such as sandbags, flexible barriers, flood barriers, mobile barriers, manual flood gates and door and window shields, which first have to be put into position or at least operated by hand, are thus of little value as a means of protecting property against surface runoff.

A further factor against such temporary property protection measures is that they generally require individuals to be operating within the danger zone. An adult on a wet and slippery surface (mud!) risks being pulled over in water as shallow as 25 cm, with a flow velocity of as little as 0.5 m/s (AWEL & GVZ, 2017). However, concentrated surface runoff can easily reach flow velocities of 2–3 m/s, and much faster on tarmac if the flow depth is sufficient.

## **Dimensioning of property protection measures**

The 'Surface runoff risk map' offers some initial pointers as to the scale that defensive measures should take. It distinguishes between three categories of flow depth: 0 – 10 cm / 10 – 25 cm / > 25 cm. These are only a rough guide, however. It is therefore essential to have an on-site assessment conducted by an expert. An appropriate allowance must also be made over and above the expected depth of water flow (SIA, 2019: 27f). This is particularly important in the case of surface runoff, as the relatively shallow flow depth means that the percentage allowance is more important than at greater depths.

## Cost of property protection measures

Compared with watercourses prone to flooding, the intensity (runoff depth  $\times$  flow velocity) of surface runoff is relatively low. Effective action to protect property can therefore often be taken at modest cost, and also generally has a positive cost-benefit ratio. If measures are planned at the early stages of a project, they can be integrated more flexibly and cost-efficiently, and as a more attractive part of the design. By contrast, measures that are incorporated into an existing building or at a later stage in the planning process are more expensive, and generally limited in scope. In addition, they frequently appear to jar aesthetically with the rest of the building.

Contractors are essentially expected to guarantee a certain degree of safety. PLANAT (2015: 63) and APIRE (Information platform on building protection against natural hazards) have thus formulated the recommended objective that, *in the event of surface water events with 100-year return periods, no water should enter the building, and underground spaces should also remain dry*. This recommendation applies to normal residential and commercial buildings. Depending on the function and use of a building, higher requirements are also justified, e.g. in the case of a school building or a hospital.

## Approach based on the current state of knowledge

Switzerland recognised a number of years ago that surface runoff posed a serious risk, and is taking steps to counter it. As a result, the Swiss federal authorities, the cantons, the cantonal Public Companies for Real Estate, as well as private-sector insurance firms, have combined their expertise in dealing with natural hazards, and initiated a PPP (public-private partnership) project (Loat et al., 2020). The project partners commissioned an external firm specialised in modelling natural hazards to draw up a nationwide map showing the risk situation attached to surface runoff (FOEN, 2018). The 'Surface runoff risk map' achieved the objective of being able to evaluate the real risks in greater detail. It is a further milestone in the way in which Switzerland handles future challenges posed by natural hazards.

## Acknowledgements

The authors would like to thank the Lucerne Public Insurance Company for Real Estate (Kantonale Gebäudeversicherung Luzern GVL) for their permission to use the illustration shown in this document.

## References

APIRE (Association of Public Insurance Companies for Real Estate): Information platform on building protection against natural hazards. (German / French) <https://www.schutz-vor-naturgefahren.ch>.

AWEL & GVZ (2017). *Verhältnismässigkeit von Gebäudeschutzmassnahmen bei Umbauten* [Proportionality of building protection measures for conversions]. Working aid

8 from the Office for Waste, Water, Energy and Air and the Zurich Public Insurance Company for Real Estate. Zurich, 4 p. (German)

Bernet, D. B., Sturny, R. A., Berger, C., Kipfer, A., Prasuhn, V., Staub, B., Stoll, S. & Thomi, L. (2018). *Werkzeuge zum Thema Oberflächenabfluss als Naturgefahr – eine Entscheidungshilfe* [Instruments for surface runoff as a natural hazard – a decision-making aid]. Articles in The Hydrology of Switzerland, No. 42. Bern, 94 p. (German)

FOEN (2018). Swiss surface runoff risk map. Federal Office for the Environment, Bern. <https://www.bafu.admin.ch/bafu/en/home/topics/natural-hazards/naturgefahren--fachinformationen/naturgefahrensituation-und-raumnutzung/gefahregrundlagen/oberflaechenabfluss.html>.

Loat, R. & Meier, E. (2003). Dictionary of Flood Protection. Federal Office for Water and Geology (Eds.). Haupt-Verlag, Bern, 424 p.

Loat, R., Kipfer, A., von Wattenwyl, N. & Magnollay, A. (2020). Swiss surface runoff risk map. Full paper, Interpraevent 2020, Bergen / Norway.

Maurer, M., Chawla, F., von Horn, J. & Stauffer, P. (2012): *Abwasserentsorgung 2025 in der Schweiz* [Sewage disposal 2025 in Switzerland]. Schriftenreihe der Eawag (Swiss Federal Institute of Aquatic Science and Technology), Nr. 21, Dübendorf: 232 p. (German) <https://www.dora.lib4ri.ch/eawag/islandora/object/eawag%3A10831/datastream/PDF/view>.

PLANAT (2014). Security Level for Natural Hazards. National Platform for Natural Hazards PLANAT Bern, 15 p. [http://www.planat.ch/fileadmin/PLANAT/planat\\_pdf/alle\\_2012/2011-2015/PLANAT\\_2014\\_-\\_Security\\_Level\\_for\\_Natural\\_Hazards.pdf](http://www.planat.ch/fileadmin/PLANAT/planat_pdf/alle_2012/2011-2015/PLANAT_2014_-_Security_Level_for_Natural_Hazards.pdf)

PLANAT (2015). *Sicherheitsniveau für Naturgefahren – Materialien* [Security Level for Natural Hazards – Materials]. National Platform for Natural Hazards PLANAT Bern, 68 p. (German) [http://www.planat.ch/fileadmin/PLANAT/planat\\_pdf/alle\\_2012/2011-2015/PLANAT\\_2015\\_-\\_Sicherheitsniveau\\_fuer\\_Naturgefahren.pdf](http://www.planat.ch/fileadmin/PLANAT/planat_pdf/alle_2012/2011-2015/PLANAT_2015_-_Sicherheitsniveau_fuer_Naturgefahren.pdf)

SIA (Eds.; 2019). *Entwerfen & Planen mit Naturgefahren im Hochbau* [Designing & planning with natural hazards in the construction industry]. Documentation D 0260. Swiss Society of Engineers and Architects. Zurich, 78 p. (German)

---

# A Virtual Reality Tool for Hazard and Risk Mitigation of Landslides through Serious Gamification

Shafaq Irshad<sup>1</sup>, Gebray H. Alene<sup>2</sup>, Nitesh Godara<sup>3</sup>, Oddbjørn Bruland<sup>4</sup>, Vikas Thakur<sup>5</sup>, Andrew Perkis<sup>6</sup>

**Keywords:** Quick Clay landslides; Virtual Reality; Risk mitigation

## Abstract

Immersive technologies such as virtual reality (VR) can offer new opportunities to communicate vital information about natural hazards and climate change to both experts and the public. In order to address this issue, researches at NTNU are working on a project titled World of Wild Waters (WoWW) that aim to help people foresee the potential danger of Natural Hazards (NH) and risk mitigation by immersing in VR environment through digital story telling. The VR tool presented in this paper is based on Digital Elevation Model (DEM) and flow simulations based on Newtonian fluids using blender (for 3D modelling and flow simulation) and unity (for virtual reality prototyping). The VR prototype depicts the landslides happened in Byneset, Norway. The aim is to educate general public on coping with NH. Another purpose is to inform the stakeholders about the potential damage and effects of NH in a particular area so that they can take preventive measures and make more effective policies for mitigation of these NH.

## Introduction

Information about potential hazards are often complex and uncertain, making it difficult to convey potential risk to the public. Risks such as extreme weather events, natural disasters and failure of climate change mitigation and adaptation have the highest likelihood of occurrence and largest global impact [1]. Over the last ten years, direct compensations due to Natural Hazards (NH) have costed Norway a sum of 27 Billion NOK according to the Natural Perils Pool. The responsibility for adaption strategies, to map the risks and prevent or reduce the threat and damages, are scattered. Events over the recent year have shown that there is an urgent need for developing technologies that can depict and showcase a holistic perspective and coordination across sectorial boundaries. Further research is needed to create a holistic understanding of cause and effect of natural hazards (NH) by creating an immersive user experience based on real data, realistic scenarios and simulations. Stakeholders, planners, decision makers and emergency agencies can use these

---

<sup>1</sup> Research Fellow, Norges teknisk-naturvitenskapelige universitet (NTNU), NORWAY,  
[shafaq.irshad@ntnu.no](mailto:shafaq.irshad@ntnu.no)

<sup>2-6</sup> NTNU

experiences and measures to base their preventive and emergency evaluations to save life and costs.

Immersive technologies allow for powerful and compelling experiences, thus helping people to foresee the potential danger that can be caused by these natural hazards [2]. However, there are many challenges in depicting realistic and scientifically valid scenarios. In the past few years, several tools have been introduced to produce immersive experiences. Some prominent tools include Unity3D and Unreal game engines for VR, ARKit and ARCore for AR, Mapbox and ESRI's City Engine for 3D geospatial visualization. However, using this technology for serious gaming remains a challenge. Much of the software for creating immersive experiences does not interface with traditional spatial data tools or data types, requiring time consuming and often ad-hoc adaptations. The purpose of WOWW is to overcome these shortcomings and present people with hands on immersive experience of natural hazards in the form of digital story. It was achieved by simulating the landslide happened in 2012 in Byneset, Norway. The outcome from the simulation was gamified to produce virtual reality tool for landslide visualization.

## Background and overview

Landslide is a down slope movement of mass of rock, debris, earth or generally soil. Landslides occur when shear stress within a slope exceed the shear strength (resistance to shearing) of the materials that form the slope. The primary source of the shear stress in the slope is gravity. There are many factors which can affect landslides either by increasing the shear stress due to gravity or by reducing the shear strength of the slope. Depending on the mode of movement, landslides can be categorized as slide and flow.

In general, flow landslides travel far, very rapidly and cause a threat to life, property and environment. Run-out analyses are needed to identify the elements at risk and to make decisions on the optimum mitigation measures. Several numerical modelling methods and tools exist to predict landslide run-out. The immediate output results of the analyses are flow depth, velocity and impact pressure represented by thousands, if not millions, of rows and columns of a table. As handling of such bunch of numbers as they are is impossible and human beings are visual creatures, visually represented data should be more easily understood compared to the numbers or written words.

Visualization in natural hazards such as floods and landslides is mostly associated with geographical information. Therefore, the data to be visualized might lay on top of a map, terrain model or an image representing the landform of the area. It is not uncommon to see different governmental and non-governmental organizations working on prevention and mitigation of natural hazards using colour codes to identify the level of susceptibility of an area to the occurrence of the hazards. Such kind of visualizations are only understandable to the corresponding experts. [3] and [4] have developed visualization of landslides by focusing on the architecture of the landscape of the area vulnerable to landslide which do not include any numerical computations. Unlike landslides, the current developments in visualization of floods is one-step further by including numerical computations and simulations in 3D ([5], [6] and [7]).

Several types of researches have been done in the past years focusing on gamification of immersive experiences for natural hazards. For example, researchers at the Red Cross Red Crescent Climate Centre[8] are working to explore Virtual Reality (VR) to blend playful interactivity with innovative approaches to data visualization for risk management. Researchers have been working on simulating various emergency scenarios such as typhoons, earthquakes, tsunamis, and fires in a 4-wall immersive VR environment. EON Reality's interactive VR platform allow the visitors to experience the effects of different emergency scenarios in actual scale while in a safe environment. Reyes [9] has worked on a storm surge flooding animation system using three-dimensional (3D) visualization of the real-life Geographic Information System (GIS) data. Putting together ground elevation with building information provided by Open Street Maps (OSM), they recreated real-life cities in a 3D environment.

Massaabi et al. [10] worked on an immersive system for 3D floods visualization and analysis. They develop an analytical tools that evaluated the threats of floods and investigated the influence of mitigation and adaptation measures, such as adaptive spatial planning, and flood disaster plans. They presented a flood management system that aims to model and visualize floods. However, there is a lack of research on visualization of real time data and simulations in VR. Our research focuses on creation of VR tool incorporating sensor based digital storytelling targeting natural hazards through interactivity and feedback for mitigating risks in Norway. This will be done by creating an immersive and participatory user experience for deeper understanding of the natural hazard through the use of new digital media, especially virtual reality (VR) and using gamification and natural user interfaces (NUI) for understanding. After the development of VR, we will learn the impact of natural hazard events on end users. Stakeholders, planners, decision makers and emergency agencies will be able to use these experiences and measures to base their preventive and emergency evaluations to save life and costs.

## Methods

### Flow landslide

Blender, an open source 3D modelling software, was used to model the landslide event occurred in Byneset, Norway in 2012 (see Figure 1). The digital elevation model (DEM) of Byneset covering the area of the landslide was imported using BlenderGIS plugin. The DEM is then meshed to the size of 1.0 m and made ready for visualization and flow simulation.

The flow landslide was simulated using the fluid physics, which enables the user to define the fluid properties specifically kinematic viscosity and the boundary conditions of the flow. Blender uses Lattice-Boltzman as a numerical scheme for simulating fluid flows and modeling physics in fluids. As the only available rheology in blender is newtonian fluid, the landslide material in this case the quick clay is assumed to follow a newtonian rheology having kinematic viscosity as a sole material property input while in reality it follows a non-linear rheology. The flow is initiated by giving a primary flow velocity, and then it follows the DEM slope downhill (Figure 2).



**Figure1: Documentation of the landslide in Byneset in 2012.**

### Visualisation

The main objective of this paper is how to create a visual impression in stakeholders and the public about natural hazards. The flow simulation depicted in Figure 2 might still be not understandable to the ordinary people. Hence, the DEM was textured with an orthographic photo taken from the landslide area after the occurrence of the landslide. Similarly, the flowing material was textured by choosing a colour, which looks like the colour of quick clay (Figure 3). Note that both the DEM and the orthographic photo were geo-referenced to the same coordinate and projection system using ArcMap. The DEM and the flow simulation along with their corresponding texture were then exported to Unity3D for further enhanced visualization and VR implementation.

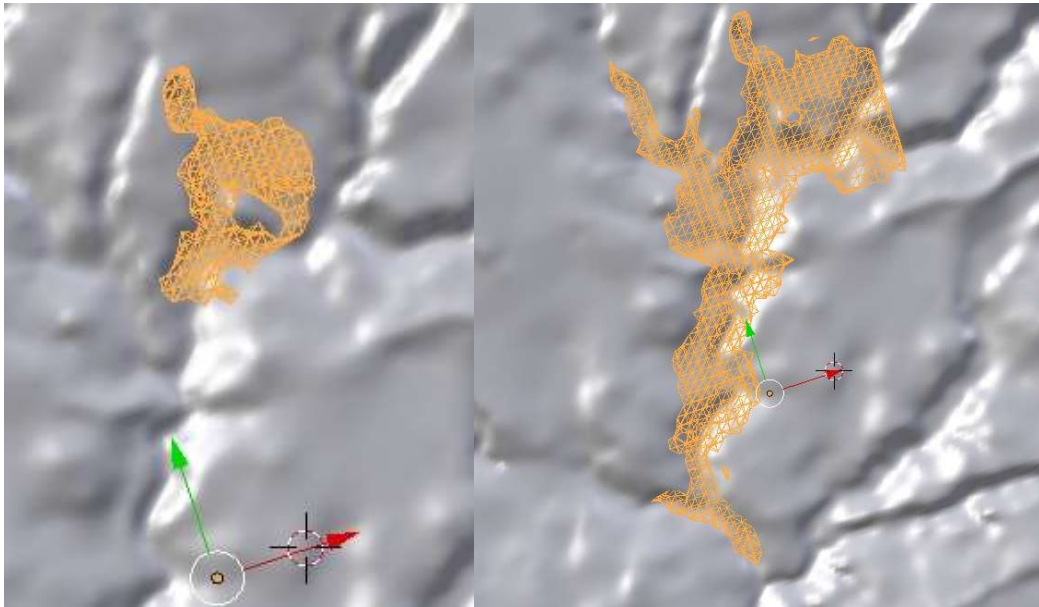


**Figure 2: Simulation of landslide in Blender a) during the initiation of the landslide b) at the end of the landslide. The white color refers to the DEM raster of the area while the yellow color is the flowing material.**



**Figure 3: Visualization of the landslide in Blender a) during the initiation of the landslide b) at the end of the landslide after the surrounding area is texture with orthophoto and the flowing material with clay material.**

### Virtual Reality Gamification

After exporting the DEM and the fluid simulations along with the textures, the whole setup was imported to Unity gaming engine. Unity was used to develop a 3D Virtual Reality environment using DEM and fluid simulation as the foundation. The VR environment was

made interactable where the user can move and view the landslide. Figure 4 shows the experimental setup for developing the VR prototype.

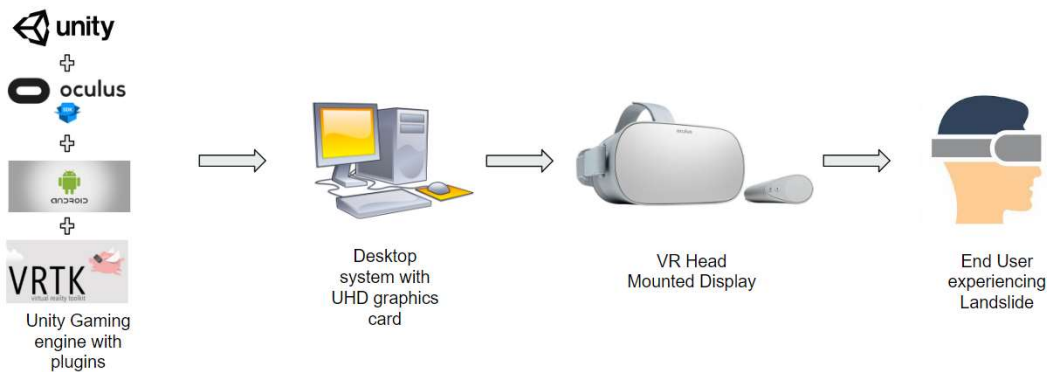


**Figure 4: Experimental setup for developing the VR prototype.**

Several plugins were used inside the unity i.e. oculus integration for unity [11], android studio and Virtual Reality Toolkit (VRTK) [13]. The Oculus Integration for Unity package adds scripts, prefabs, and other resources to supplement Unity's built-in support. Furthermore, android studio was used which is an official Integrated Development Environment (IDE) for Android app development [12]. Ultra-High Definition graphics card was used on a desktop computer along with oculus go to deploy the prototype. The final VR output is shown in Figure 5.

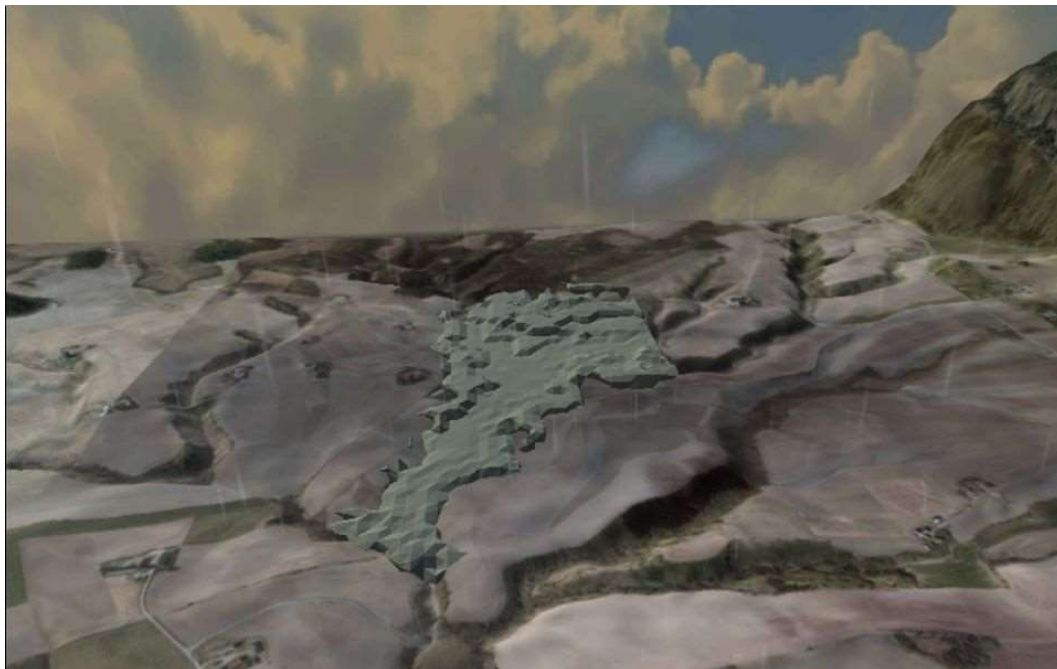


**Figure 5: VR visualization of landslide based on real data and realistic scenario in Oculus Go.**

## Future work and conclusion

In the future, we aim for producing relatively more realistic flow simulations improving the visualization and adding functionality in VR scenarios based on digital story telling so that general public and stakeholders can interact and experience the severity of hazards inside the VR game. This will help them in better decision making by practicing different NH scenarios first hand in VR. We will also include flash floods which is mainly the triggering event for landslides [14]. The groundwork for effective stakeholder involvement in risk management will be conducted from the early stages. Future versions of the tool will include a gamified version of the risk scenario analysis, which will enhance the understanding for the complex interaction of the hazard factors and the effects of risk mitigation options.

This research aims at presenting a virtual reality tool for natural hazards by simulating real time data. The purpose is to allow the citizens and stakeholders to be better prepared because they will be able to experience the effects of different emergency scenarios while in a safe environment. The VR environment based on real time simulations and realistic scenarios will allow the people to quickly and effectively react to emergencies. This will also allow the stakeholders to better manage and mitigate the consequences.

## References

- [1] World Economic Forum. The global risks. Report, World Economic Forum, 2018.
- [2] Stephen Burt. Playful floods. <http://blogs.reading.ac.uk/flooding/2017/12/08/the-ffir-annual-conference/>, 2019. [Online; accessed 13-january-2019]
- [3] Kun Zhang and Songlin Zhang. 3d visualization of landslide deformation. *Geospatial Information Science*, 10(1):67–70, Mar 2007
- [4] Daxi Ma and Xiaohong Liu. Three-dimensional modeling and visualization of landslide based on gtp. In 2011 International Conference on Remote Sensing, Environment and Transportation Engineering, pages 914–917. IEEE, 2011
- [5] Xinxin Li, Wanggen Wan, Li Li, Ximin Zhang, Chao Gan, and Xiaoqing Yu. Realization of flood simulation visualization based on opengl. In 2012 International Conference on Audio, Language and Image Processing, pages 1151–1154. IEEE, 2012
- [6] Fanghong Ye, Huibing Wang, Sida Ouyang, Xinming Tang, Zhong Li, and Mahesh Prakash. Spatio-temporal analysis and visualization using sph fordam-break and flood disasters in a gis environment. In 2012 International Symposium on Geomatics for Integrated Water Resource Management, pages 1–6. IEEE, 2012.
- [7] Keqi Zhang, S-C Chen, Peter Singh, Khalid Saleem, and Na Zhao. A 3d visualization system for hurricane storm-surge flooding. *IEEE Computer Graphics and Applications*, 26(1):18–25, 2006
- [8] Pablo Suarez et al. Virtual reality for a new climate: Red cross innovations in risk management. *Australian Journal of Emergency Management*, 32(2):11, 2017.

- [9] Maria E Presa Reyes and Shu-Ching Chen. A 3d virtual environment for storm surge flooding animation. In 2017 IEEE third international conference on multimedia big data (BigMM), pages 244–245. IEEE, 2017.
- [10] Marwa Massa<sup>^</sup>abi, Olfa Layouni, Wided Ben Moussa Oueslati, and Fahad Alahmari. An immersive system for 3d floods visualization and analysis. In International Conference on Immersive Learning, pages 69–79. Springer, 2018.
- [11] <https://developer.oculus.com/downloads/package/unity-integration/>
- [12] <https://developer.android.com/studio/intro>
- [13] <https://vrtoolkit.readme.io/>
- [14] Faccini, Francesco & Piana, Pietro & Sacchini, Alessandro & Lazzeri, Riccardo & Paliaga, Guido & Luino, Fabio. (2017). Assessment of heavy rainfall triggered flash floods and landslides in the Sturla stream basin (Ligurian Apennines, northwestern Italy). *Jokull*. 67. 44.

---

# Avalanche- and Slush-Flow Dam Vallabøen, Ørsta Municipality, Western Norway

Árni Jónsson<sup>1</sup>, Peter Gauer<sup>2</sup>, Marius S. Lianes<sup>3</sup>, Marius Mathisen Søvik<sup>4</sup>

**Keywords:** Ørsta; Vallabøen; slush-flow; avalanches; catching dam

## Abstract

Vallabøen residential area Ørsta municipality, Western Norway, is located below the 835 m high Vallahornet mountain. Snow avalanches release almost every year from Vallahornet mountain but most of these have only short runouts and stop above the tree line. Three avalanches are known to have reached or went into the area of present residential area. West of the residential area runs Vikeelva river. Slush-flows are registered in the river and some of them have reached far into today's residential area. One school, a kindergarten as well as over one hundred residential units are inside hazard zones. To mitigate the avalanche and slush-flow danger it was proposed to build a combined catching- and deflecting dam above today's residential area. One of the challenges during preliminary design was the dimensioning of a culvert for Vikeelva river; that is estimating the volume flux of slush-flow permitted to pass it and how to delay or stop the rest of the slush-flow. The combined avalanche- and slush-flow dam was built between 2017 and summer 2019.

## Introduction

Snow avalanche and slush-flow hazards have been known for long time at and near Vallabøen residential area in Ørsta municipality Western Norway, Figure 1. The residential area is located between Vikeelva river at west and Skytjeåna river at east. Vallahornet, (835 m asl) is above Vallabøen residential area.

The Engeset avalanche on February 10, 1979, which ran along Skytjeåna river and is ranked one of the largest avalanches in modern time in Norway, hit the Engeset residential area and the east part of Vallabøen residential area. It claimed three lives and destroyed or damaged 11 buildings (Humstad, 2019; Siem, 2019). Avalanches release every year below Vallahornet but are usually small and stop above a planted forest belt. Three avalanches are known to have reached into today's residential area and few others have terminated in the forest above it. Slush- and debris flows along or in Vikeelva river are also mentioned

---

<sup>1</sup> Civ. Eng., HNIT Consulting Engineers, ICELAND, ([arni@orion.is](mailto:arni@orion.is), [arni@hnit.is](mailto:arni@hnit.is))

<sup>2</sup> PhD., Norwegian Geotechnical Institute

<sup>3</sup> Civ. Eng., OSE Engineering

<sup>4</sup> Civ. Eng., Norwegian Geotechnical Institute

in old records and during hazard mapping in 1971 an information on a slush-flow to the church was registered.

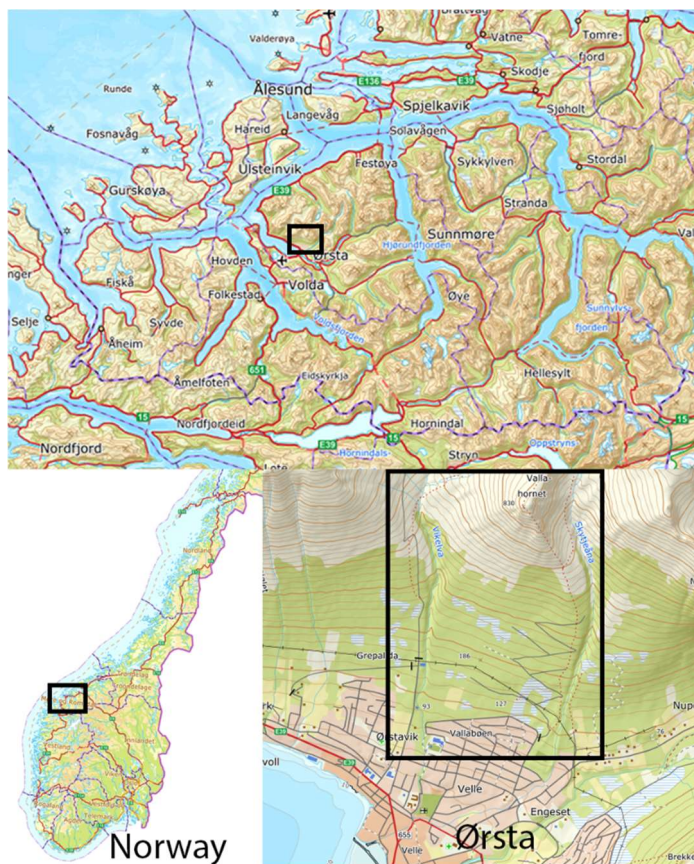


**Figure 1: Location**

In 1979, the Norwegian Geotechnical Institute (NGI) proposed approx. 100 m long and 5 m high deflecting dam along the west side of the river to protect planned residential area and a approx. 50 m long deflecting dam at the east side of it to protect the school and kindergarten (NGI, 1979). The height of the shorter dam was not suggested in the report. The location was planned some 50-70 m above the residential area. In 1980, NGI (NGI, 1980) proposed a new catching dam to protect future residential area at the west side of the river slightly further down from the deflecting dam mentioned earlier. The height was suggested to be 5 m and length some 80 m from the river to west. Neither of these proposals were realized.

In 1987 it was legislated that the probability of an avalanche hitting and damaging planned residential buildings should be less than 1/333. Today the legislated probability has been reduced to 1/1000 for planned residential buildings and 1/5000 for schools and other places where more than 25 persons gather (TEK17 (Dibk, 2017)). During the first phase of this work in 2011/2012 TEK10 was still valid but during the final phase in 2017 TEK17 had been adopted by the authorities. However, there is no practical difference between TEK10 and TEK17 for the work in Ørsta.

In 2011, Ørsta municipality asked for an update and revision of the work from 1979 and 1980. This paper describes the work performed after 2011 to the final stages of the construction phase in 2019.

## Hazard Assessment

Vallahornet mountain side that threatens Vallabøen residential area has a triangular shape and faces SSE. Potential release area can be divided in two, the topmost part and steepest from approx. 680 masl. to 825 masl. with an area of approx. 5 ha, and the lower part with a gentler slope from approx. 600 masl. to approx. 680 masl. with an area of 4.2 ha. The steepness of the top part is between 30° and 40°. It is assumed that the design avalanches can release in these areas. Vikeskåla bowl is the catchment area for Vikeelva river and is approx. 3.0 km<sup>2</sup> large. Both areas are covered with low vegetation (bushes in the lower part and grass) and partly with bare rock in the upper part. During the 1979 avalanche cycle most of the Vikeskåla bowl released and the avalanche ran along Vikeelva and stopped just above the residential area. NGI report (NGI, 1979) does not indicate any size or volume but discusses the possibility that there might have been more than one release area with uncertain release times. A comparison to the Engeset avalanche reveals many similarities such as the avalanche profile and runout distance. Prior to the avalanches there were several weeks with little precipitation and cold weather. Weak surface crystals formed and approx. a week before the accident heavy snowfall in combination with strong winds accumulated the snow in the starting zones.

The hazard assessment "Skredfarevurdering" (NGI, 2011) is based on historical reports, observations from site, empirical and dynamical models such as the alfa/beta-model (Lied and Bakkehøi, 1980) and RAMMS (Christen and others, 2010) and a "similarity model" (Bakkehøi and Norem, 1999). The avalanche paths from Vallahornet are open and they do have parabolic forms, which favors long runouts under similar snow conditions as in the 1979 Engeset avalanche. It is uncertain how much effect the present forest will have on the runout and more important, will there be continuously forest in future? The density of the forest varies considerably especially from top and down and there are openings within. In our calculations the effect of the forest is ignored.

The forest is owned by local inhabitants and forest harvesting can increase the runout of snow avalanche considerably. Restrictions on forest harvesting were proposed during this work. The hazard zones for all processes are shown on Figure 2.



Figure 2: Vallabøen residential area. Red dotted line depicts annual probability of 1/300, orange 1/1000 and yellow 1/5000 prior to any measures. Cyan line depicts the boundary of mapped area. Map: [wms.geonorge.no/skwwms1/wms.norgebilder](https://wms.geonorge.no/skwwms1/wms.norgebilder), accessed 2011-04-17.

## Preliminary design

The aim of mitigation measures ordered by the Ørsta municipality was to protect the school and the residential area at Vallabøen to the highest safety class or S3 (1/5000 annual probability) for the school and S2 (1/1000) for residential buildings. The Norwegian government through The Norwegian Water Resources and Energy Directorate (NVE) partly funds mitigation measures of this kind. However, the funding is limited to existing buildings and to avalanche events that are considered to have annual probability of more of 3/1000. In the presented work, this meant down scaling “full size” mitigation measures to measures fitting the annual probability of 3/1000. If the municipality wanted “full” protection, it had to fund the differential cost.

Several alternatives of mitigation scenarios were studied in the "Forprosjektering" (NGI, 2015). The “zero” option was to maintain existing routines of avalanche forecasting and warning services for the area. This method is considered not enough and only suitable for short periods. The second option was a removal of exposed building inside the hazard zones. This option is only relevant if the monetary value of buildings is less than the costs of erection of structural mitigation measures. Rough estimates of the value of buildings indicated that the cost of structural measures would be less than the monetary costs of existing buildings.

Supporting structures in the starting zone were considered but the estimated total length of structures is over 5000 m and preliminary costs estimated to be too high. Furthermore, supporting structures do not protect against slush-flows in Vikeelva river and therefore additional structures would have to be built in the course of Vikeelva anyhow.

The option considered to give enough protection against dry snow avalanches and slush-flows is a catching dam located just above the residential area. The challenges with this concept are to build a dam crossing the Vikeelva river so it can catch or delay the slush-flows and still to be open enough for the regular water discharge.

The criteria for available funding from NVE for this project was limited to annual probability 3/1000. The municipality choose to down scale “full” mitigation measures to 3/1000 due to financial constraints. The consequences of this down scaling are fully understood by the municipality.

Dry avalanche velocities were calculated for the whole stretch of Vallabøen area in the design report (NGI, 2015) but they were reconsidered with respect to knowledge of similar terrain conditions in Norway. Figure 3 shows RAMMS velocity example calculations for two scenarios. The scenario on the right was chosen as velocity criteria in this work.

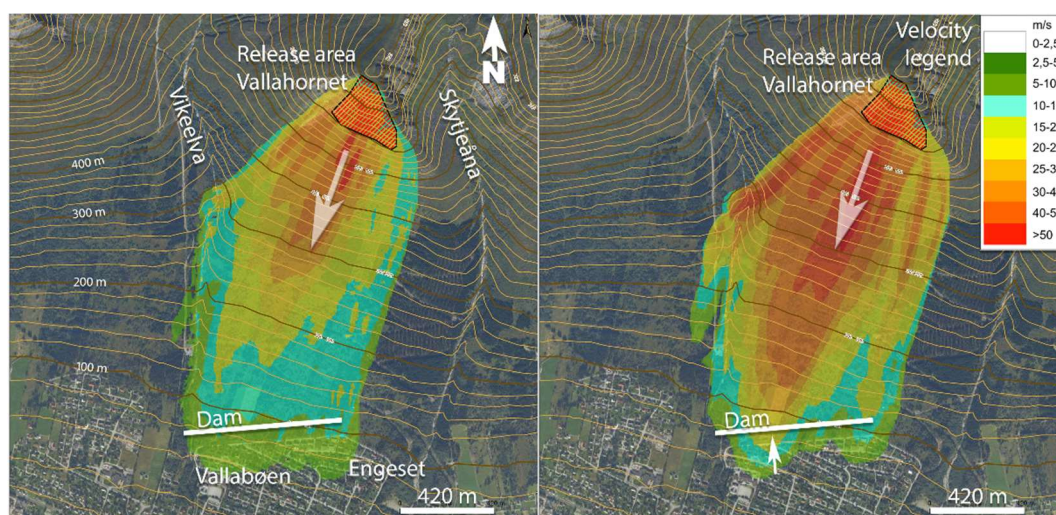


**Figure 3: Avalanche velocity distribution for two RAMMS setups. Left figure: SLF standard parameter set L300; fracture depth  $D = 1.50$  m and max erosion depth  $e = 0.5$  m. Right figure: more Coulomb type-friction  $\mu = 0.25$  and  $\xi = 30000$  m/s<sup>2</sup>; fracture depth= $D$  1.50 m and max erosion depth  $e = 0.5$  m. Volume is approx. 105000 m<sup>3</sup>. The velocity distribution to right is considered to represent annual probability of <1/1000. White line represents the location of the catching dam above the residential area. White arrow at the dam depicts the location of the loading example in next chapter. White arrows below release area depicts flow direction.**

Velocity distribution along the catching dam varies, 16 m/s is here considered to be representative for the stretch from station 70 to station 340 east of Vikeelva (station 0 is on the west bank) and 8 m/s from station 440 to station 600 east of Vikeelva. The stretch between is linear interpolated from 16 m/s to 8 m/s. The stretch west of station 70 is designed for slush flow. New RAMMS velocity calculations were not performed for down scaling but expert judgement was used. Velocities considered are 13 m/s and 7 m/s for the respective stretches.

Evaluation of necessary dam height is done according to (Jóhannesson and others, 2009). Estimated height of avalanche core in motion is approx. 2 m and snow on ground 2-3 m.

The dam height set to 13 m for the west part and 9 m for the east part. The dam height changes linearly between the stretches mentioned earlier.

Nothing is known about velocities of slush flows in Vikeelva river and general knowledge about slush flow behavior was not well understood at the time of this work. Therefore, we looked at three different velocities 15, 20 and 25 m/s which we considered could be realistic.

One important aspect in the design was how to minimize the chance of slush-flow damming up in the river and eventually flow over and continue down into the residential area. Therefore, the dam was designed to act as a deflecting dam (curved form) from the west bank, over the river to the catching dam east of it, to a basin. The radius of the curve is 60 m. The method of calculating climbing height to curved surfaces is described in (NGI, 2002). Calculated height is 6.5 m for 15 m/s, 7.0 m for 20 m/s and 9.0 m for 25 m/s. The velocity chosen is 15 m/s as it is considered the most realistic for the location of the dam. Climbing height is set to 6.5 m, the thickness of the flow is chosen 3 m and the dam height is set to approx. 10 m at an impact angle of 30°. Density of slush flow is set to 700 kg/m<sup>3</sup>. The dam height, however, varies between 8 and 10 m as the terrain from the west bank to the catching dam varies.

As no information is available of the optional volume in slush-flow in Vikeelva the approach here is to account for a volume of 2000-4000 m<sup>3</sup> in several releases. The volume of the basin is approx. 25000 m<sup>3</sup>.

A culvert through the dam was planned for the daily river discharge. The opening of the culvert was planned approximately the same as the opening of a bridge over the river further down in the residential area. That for limiting the risk of slush-flow to stow up above the bridge and flood the closest properties.

The basin will not only act as an area for slush-flow debris but also for surface and ground water, which is collected from the canal above the catching dam. A culvert drains the water from the basin (the pond) through the dam into the river below the dam. A safety culvert is located approx. one meter above the main culvert in case this will get plugged by tree branches or other loose material.

The impact face of the catching dam is typically 4:1 to 6:1 and a foundation or base height of approx. 3 m with relatively gentle slope of 1:1.5 in the canal. The inclination of the downhill side is typically 1:1.5 to 1:1.8. The planned width of the top is at least 3 m for most of the dam, but it is wider over the Vikeelva river as excavators or other machines must be able to access the river area.

To prevent Vikeelva river during normal discharge to flow into the basin a concrete wall of approx. one meter must be built some tens of meters upriver. However, in flood situations water can flow into the basin if the discharge of the main culvert in the river is not enough. In this case, it is important that the culverts, either the main or safety culvert from the pond (basin), are not plugged. This is extremely important as the dam is not designed to withstand water levels in the pond/basin higher than approx. 2 m.

To the west, the dam is connected to an existing road and to the river embankment further up Vikeelva river. The inclination of the eastern end is relative gentle as machines for maintenance must be able to drive to the top. A path for maintenance machines is at the downhill side and there is also a walkway to the top of the dam. Due to its location and height it will provide a nice view to the Vallabøen residential area and the rest of Ørsta town.

Ørsta municipality concluded late 2017 that they would call for a turnkey contract. The contract was awarded to Aurstad Maskin AS with OSE engineers as subcontractor for the geotechnical design.

## Detail design

The avalanche catching dam is designed to withstand the design force of a snow avalanche from Vallahornet (NGI, 2018). Examples of the loadings for the center of the dam (Figure 3) are  $P_0=88$  kN/m,  $P_1=588$  kN/m and  $P_2=12$  kN/m, Figure 4.

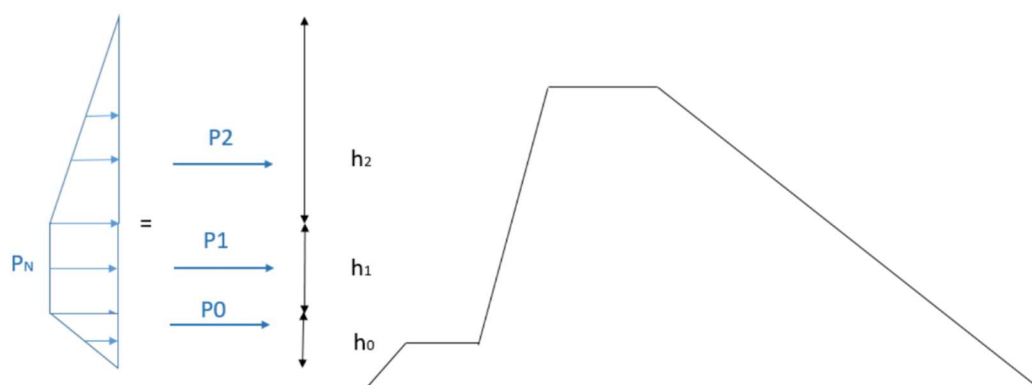


**Figure 4: Principal of load distribution on the center of the dam from snow avalanches.**

The embankment consists of a core material of blasted rock ( $\gamma=19$  kN/m<sup>2</sup>,  $\phi=38^\circ$ ), with an overlaying layer of on-site moraine. The two layers are separated with a geotextile fabric that prevents mix up between the layers. To ensure enough drainage of the embankment (supporting fill,  $\gamma=19$  kN/m<sup>2</sup>,  $\phi=36^\circ$ ) several thin drainage layers consisting of blasted rock are laid out in the moraine. The catching dam is strengthened using reinforced earth and is checked for stability and shear capacity during an avalanche impact.

Geotechnical investigation consisted of 15 “total” soundings and sampling at three locations (Norconsult AS, 2013). Observed ground conditions show relatively thin layers of loose material, on the average approx. 2.75 m (between 1.8 and 3.5 m).

The slope stability of both sides of the catching dam and the internal stability of the georeinforcement is calculated with the geotechnical software Plaxis 2D (Bentley Systems, 2020) and GEOSLOPE (Geoslope, 2020).

The facing material of the impact side is a dry-stone wall ( $\gamma=19$  kN/m<sup>2</sup>,  $\phi=40^\circ$ ). The stability of the dry-stone wall was designed for a snow avalanche impact, in addition to holding the embankment without the force of an avalanche. The decision to use dry-stone

as the facing material was based on the contractor's experience in building similar constructions in road work in Norway, and because of the way a dry-stone structure blends into nature.

A part of the project there was also to build a small concrete bridge over Vikeelva river several tens of meters above the catching dam. The bridge is supported by a dry-stone wall on each side. Furthermore, the bridge is designed to collapse during slush-flow event, to prevent it from blocking the culverts downstream. The catching dam crosses Vikeelva river and to ensure undisturbed flow of the river a culvert of concrete was built over it. The walls/foundations are bolted into rock in the riverbed.

All structures are designed according to current national design standards (Norsk Standard, 2016a; b) and other acknowledged practice.

For maintenance purposes a road was built alongside the foot of the embankment at downhill side and the top of the catching dam (crown) is wide enough for machines to operate there.

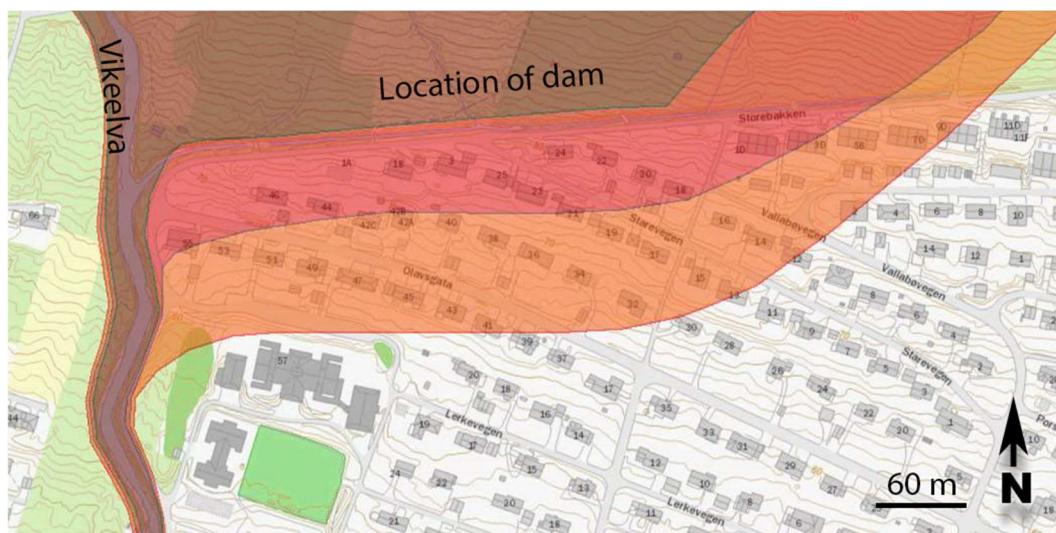
The catching dam is a towering structure in the middle of Ørsta, and the structure is visible from wherever you are in the central parts of the municipality, Figure 5. The landscaping architect focused on preserving nature, a natural look of the constructions and reuse of existing material as much as possible. A trail is located on top of the embankment and it ties trails from the residential area of Vallabøen and the mountain trails up to Vallahornet and Saudehornet. After some years the embankment, the dry-stone wall, and the surrounding area, will be overgrown with grass, and will blend into the previous untouched mountain side.



Figure 5: Vallabøen catching dam after completion summer 2019. A view to east. Vikeelva river at bottom of photo. ©Gunnar Ingvald Frøholm/Aurstad.

The construction work was completed during summer 2019.

The down scaling of the mitigation measures means that the residential area below the measures is not fully protected but the safety has been improved considerably. A proposal for the revised hazard zones is shown on Figure 6, for comparison see Figure 2.



**Figure 6: A proposal for the reduced hazard zones after completion of mitigation measures. Brown area depicts annual probability of 1/100, red area 1/1000 and orange 1/5000. The catching dam is at the border of brown/red area.**

## References

Bakkehøi S and Norem H (1999) Comparing topographical and dynamical runout model by ideas of 'nearest neighbor' method. *Wildbach- und Lawinenverbau (Zeitschrift des Vereins der Diplomingenieure der Wildbach- und Lawinenverbauung Österreichs)* 63, 39–50

Bentley Systems (2020) Plaxis. <https://www.bentley.com/en/products/brands/plaxis>

Christen M, Kowalski J and Bartelt P (2010) RAMMS: Numerical simulation of dense snow avalanches in three-dimensional terrain. *Cold Reg. Sci. Technol.* 63, 1–14 (doi:10.1016/j.coldregions.2010.04.005)

Dibk (2017) TEK17. <https://dibk.no/byggereglene/byggteknisk-forskrift-tek17/>

Geoslope (2020) Geoslope. <https://www.geoslope.com/>

Humstad T (2019) 40 år sidan Engesetfonna. *Nordskred* <https://norskred.wordpress.com/2019/02/10/40-ar-sidan-engesetfonna/>

Jóhannesson T, Gauer P, Issler D and Lied K (2009) The design of avalanche protection dams. *European Commission*

Lied K and Bakkehøi S (1980) Empirical calculations of snow-avalanche run-out distance based on topographic parameters. *J. Glaciol.* 26(94), 165–177

- NGI (1979) Snøskredfare Engeset-Hagen-Vikeskåla-Vikeelva. 79414–1. Norges Geotekniske Institutt, Oslo
- NGI (1980) Snøskredfare Engeset-Hagen. Sikringstiltak Vikeskåla Vikeelva. 79414–03. Norges Geotekniske Institutt, Oslo
- NGI (2002) Klatrehøgder av skred på krumma leievoll. 581200–36. Norges Geotekniske Institutt, Oslo
- NGI (2011) Vikeelva , Ørsta kommune-Vurdering av skredfare. 20100968-00-2-R. Norges Geotekniske Institutt, Oslo
- NGI (2015) Forprosjekteringsnotat: Sikringstiltak mot snø- og sørpeskred. 20111024-01-TN. Norges Geotekniske Institutt, Oslo
- NGI (2018) B003 Stabilitetsberegninger av jordarmert voll. 20180383-02-TN. Norges Geotekniske Institutt, Oslo
- Norconsult AS (2013) Skredsikring. Vallabøen, Ørsta. Grunnundersøkelser. 5136178–1. Norconsult AS, Molde
- Norsk Standard (2016a) NS-EN 1990:2002+A1:2005+NA:2016. Eurokode 0: Grunnlag for prosjektering av konstruksjoner. Norway
- Norsk Standard (2016b) NS-EN 1997-1 :2004+A 1:2013+NA:2016. Eurokode 7: Geoteknisk prosjektering Del1: Allmenne regler. Norway
- Siem B (2019) Gløymer aldri rastragedien - smp.no/nyheter – Nyheter fra Ålesund, Sunnmøre og Nordvestlandet, Page 1 of 5. Sunnmørsposten (September 2012), 1–5 <https://www.smp.no/nyheter/soere/article148847.ece>

# Rapid revision of the hazard maps for debris flow and snowmelt-type mud flow caused by volcanic eruptions of unexpected magnitudes and from unexpected vents

Norihisa Kumai<sup>1</sup>, Takashi Kurogi<sup>2</sup>, Shin-ichiro Shimomura<sup>3</sup>, Keishi Saito<sup>4</sup>, Yuya Aoyagi<sup>5</sup>, Shun'ichi Niwa<sup>6</sup>, Shusaku Shiiba<sup>7</sup>, Shin-ichiro Hayashi<sup>8</sup>, Marino Hiraoka<sup>9</sup>, Yusuke Yamazaki<sup>10</sup>, Yasuo Ishii<sup>11</sup>, Yoko Tomita<sup>12</sup>, Jun Minagawa<sup>13</sup>

**Keywords:** debris flow, snowmelt-type mud flow, volcanic eruption, numerical simulation, hazard map

## Abstract

In Japan, while the hazard maps for volcanic eruption to ensure evacuation based on probable scenarios of volcanic eruption have been prepared and published for 49 major active volcanoes, rapid revision of these hazard maps is essential in case of volcanic eruptions of unexpected magnitudes and from unexpected vents such as the eruptions of Mt. Unzen 1991 and Mt. Kusatsu-Shirane 2018. This report shows the framework and the operational design of the revision system, which we have established for the rapid revision of hazard maps for debris flows and snowmelt-type mud flows caused by volcanic eruptions of unexpected magnitudes and from an unexpected vents.

## Introduction

Debris flow and snowmelt-type mud flow derived from the explosive volcanic eruptions can cause damage to the residents and the infrastructures in the downstream areas (Pierson and Major, 2014; Major and Newhall, 1989). Japan Meteorological Agency (JMA) has designated 111 volcanoes as active volcanoes. These were the volcanoes that have erupted within the last 10,000 years or with vigorous fumarolic activity. The Coordinating

---

<sup>1-2</sup> Kyushu Technical Office, Kyushu Regional Development Bureau, Ministry of Land, Infrastructure, Transport and Tourism

<sup>3-4</sup> Kyushu Regional Development Bureau, Ministry of Land, Infrastructure, Transport and Tourism

<sup>5-7</sup> Ministry of Land, Infrastructure, Transport and Tourism

<sup>8</sup> Dr., Deputy director, Ministry of Land, Infrastructure and Transport and Tourism (MLIT), JAPAN, ([hayashi-s23b@mlit.go.jp](mailto:hayashi-s23b@mlit.go.jp))

<sup>9-12</sup> Dr., Public Works Research Institute

<sup>13</sup> Kokusai Kogyo Co., Ltd.

Committee for Prediction of Volcanic Eruption has selected 50 major active volcanoes for which 24-h monitoring is being conducted (JMA, 2019). Hazard maps have been prepared for eruption of the active volcanoes to ensure evacuation. This includes debris flow and snowmelt-type mud flow, and is based on the most probable scenarios of volcanic eruption, which have been prepared and published for 49 major active volcanoes (except Ioto Island) till the end of March, 2019 (e.g. Cabinet office, Government of Japan, 2015; National Research Institute for Earth Science and Disaster Resilience, 2016). The most probable scenarios of volcanic eruption were decided by historic records of past eruptions and observation data. Volcanic Disaster Management Councils of each active volcano, lead by the prefectural governmental office and/or the municipality office control the preparation of hazard maps in case of an eruption (Nakamura et al., 2013). Ministry of Land, Infrastructure, transport and tourism (MLIT) provides the results of numerical simulation of the inundation area of debris flow and snowmelt-type mud flow based on the Act on special measures for active volcanoes.

Rapid revision of the hazard maps may be needed due to volcanic eruptions of unexpected magnitudes and from unexpected vents such as the eruptions of Mt. Unzen 1991 (Ikeya, 2008) and Mt. Kusatsu-Shirane (Mt. Motoshirane) 2018 (Takahashi, 2019). In the eruption of Mt. Unzen 1991, a gigantic lava dome was formed, and pyroclastic flows and debris flows occurred intermittently during the eruption. In Mt. Kusatsu-Shirane 2018, the eruption occurred from an unexpected vent not marked in the hazard map and the target area of 24-h monitoring. As above examples, when an eruption of an unexpected magnitude, from an unexpected vent of eruption, or a deformation occurs in a volcano, it may be difficult to use the hazard map published to ensure evacuation, and to carry out urgent structural measures and monitoring as planned in the Sabo Plan for Urgent Measures (structural and non-structural for sediment-related disaster) for Volcanic Disaster Reduction (Nakamura et al., 2013), for the disaster reduction/mitigation during an eruption. Therefore, for the rapid revision of the hazard map, a system has been proposed which will consider the location of the vent and the deformation of the volcano. This report shows the framework and the operational design of the system for rapid revision of hazard maps for debris flows and snowmelt-type mud flows caused by volcanic eruptions of unexpected magnitudes and from unexpected vents called the Volcanic eruption Real-time Hazard Map System (VRHMS) by MLIT (MLIT, 2018).

## Framework of the system for rapid revision

VRHMS (Fig. 1) has two components, a database module (DM) and a numerical simulation module (NM). DM stores the results, boundary conditions, and parameters of 2D numerical simulation for debris flow and snowmelt-type mud flow based on the probable scenarios of volcanic eruption other than the most probable scenarios adopted in the hazard map. When a volcanic eruption of an unexpected magnitude and from an unexpected vent other than the ones adopted in the hazard map and stored in the DM occurs, The NM conducts 2D numerical simulations based on the J-SAS model developed by Sabo & landslide Technical Center, Japan. It considers location of the vent, defamation of the volcano, and the variation in the boundary conditions, and the parameters for numerical simulation such as the hydrograph and the representative grain-diameter. In addition, the VRHMS stores

the 2D numerical simulation results in the DM and conducts 2D numerical simulation using the NM for lava flow and pyroclastic flow.

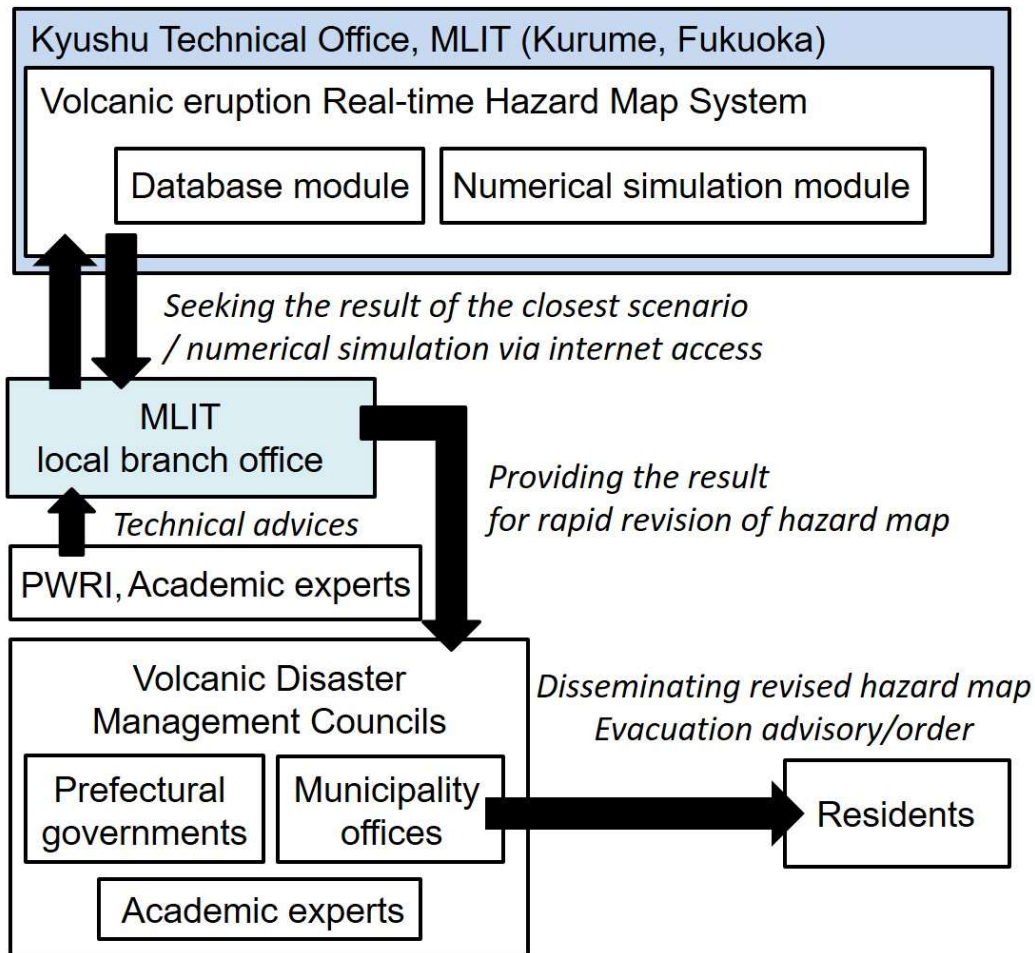


**Figure 1: VRHMS related operation and information flow after the detection of signs of eruption**

In NM, base map for the numerical simulation is a 10m mesh DEM provided by the Geospatial Information Authority of Japan. NM considers the location of the vent and the starting point of inundation of the debris flow and snowmelt-type mud flow, and can designate them on the base map. If the deformation of the volcano is considered, the elevation of base map can be change. Boundary conditions and parameters for numerical simulation can be changed and reused for another numerical simulation. The above operations can be conducted using a web-based graphical user interface.

The server on which VRHMS is installed is FUJITSU RX2530 M2 (CPU: Intel Xeon E5-2667V4 3.2GHz 8core, Memory: 8GB x 2). VRHMS is located at Kyushu Technical Office, MLIT (Kurume City, Fukuoka Prefecture), and connected to the MLIT local branch offices throughout Japan by the internet. MLIT local branch offices can help the affected areas by operating a web-based VRHMS alternatively.

## Operational design of the system for rapid revision

After detection of the signs of an eruption, which is of unexpected magnitude or from an unexpected vent, the MLIT local branch office seeks the DM to find the scenario closest to the present eruption about the location of vents, the type and magnitude of the eruption. If the closest scenario can be found, the MLIT local branch office provides it to the Volcanic Disaster Management Councils. On the other hand, if no result is found, the MLIT local branch office calculates the inundation area of the debris flow and the snowmelt-type mud flow considering the location of the vent, deformation of the volcano, variation in the boundary conditions, and the parameters obtained from field survey. Additionally, the information provided by the volcano-related organizations and/or shared in the Coordinating Committee for Prediction of Volcanic Eruption is used in the calculation. After the numerical simulation, the MLIT local branch office provides the result to the Volcanic Disaster Management Councils.

After receiving the result of the closest scenario or the numerical simulation provided by the MLIT local branch office, the Volcanic Disaster Management Councils revises the hazard map based on them with the inputs from the volcano-related academic experts such as volcanology and sediment and erosion control rapidly. Based on the revised hazard map, the municipality office in charge of the resident protection disseminates it along with the evacuation advisory/order for the residents.

Because the frequency of eruption of one volcano is very low generally, it is difficult for the MLIT local branch officers, primarily the ones in charge of design, building, and management of the sediment and erosion control facilities such as check dams, to operate the VRHMS. When the MLIT local branch office operates the system during an eruption, Public Works Research Institute (PWRI) and volcano-related academic experts give technical advices for setting the boundary conditions and the parameters for numerical simulation. Moreover, when the MLIT local branch office conducts the training for operation of the system as a preparation for volcanic eruptions, officers from Kyushu Technical Office serve as instructors.

Fig.2 shows the demonstration example of inundation areas in the DM (a) and calculated by the NM (b) for debris flow. In this case, a stream (catchment area of the upstream side from starting point of inundation: approximately 0.4km<sup>2</sup>) has a ground deformation with 5 m rise due to the uplift and/or accumulation of the volcanic ash. The inundation area is calculated based on hydrograph corresponding to precipitation of 100-years recurrence interval (933mm/24h) and the concentration of sediment (Cd) corresponding to the volume of sediment that can be transported in the stream. Comparing Fig.2 (a) and (b), the larger inundation area appeared in (b) in the northeast direction. As a results, the affected area and residents to be evacuated were changed when an unexpected ground deformation caused by a volcanic eruption changes the direction of the debris flow and the inundation area based on calculation of the NM. The NM indicates the maximum flow depth, distribution of the sediment deposit at the end of the calculation, and the arrival time of flow. The calculation result of inundation area in Fig.2 was obtained in 15 minutes by NM.

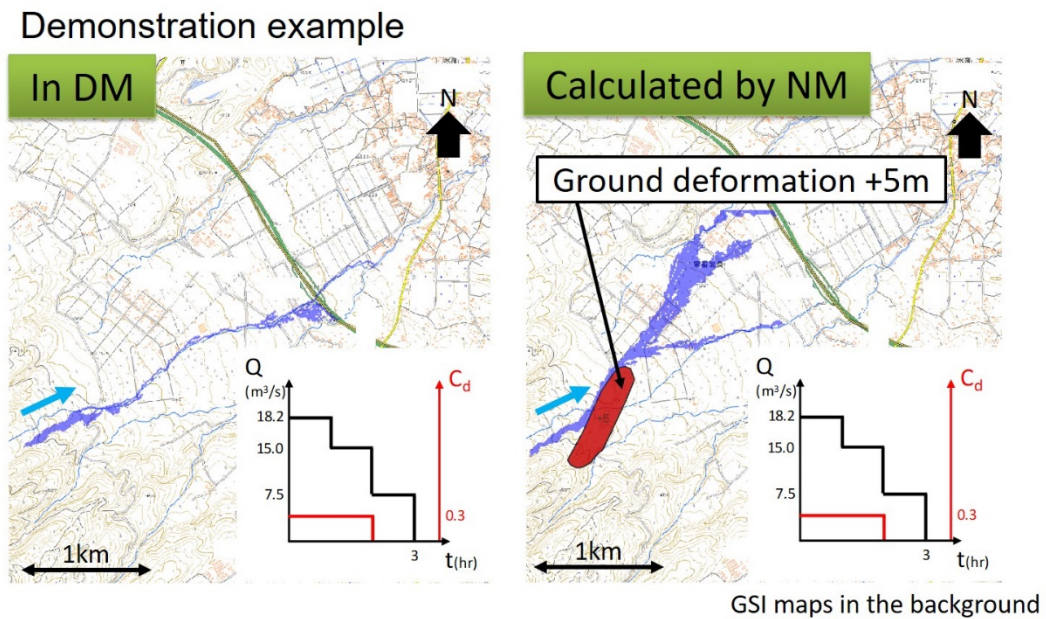
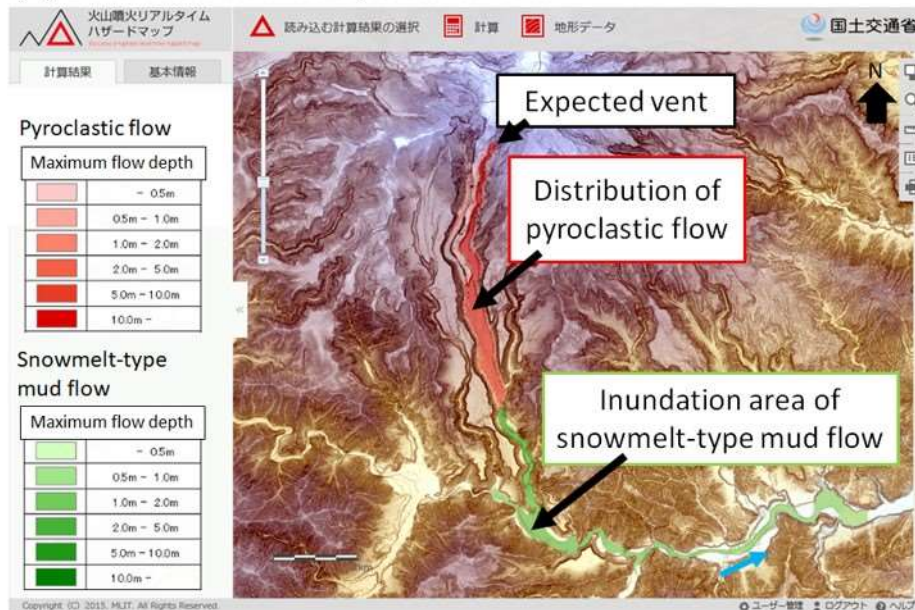


**Figure 2: Demonstration example of inundation areas for debris flow in the DM and calculated by the NM (Q: flow rate of debris flow,  $C_d$ : concentration of sediment).**

Fig.3 shows the demonstration example of the inundation areas in the DM (a) and calculated by the NM (b) for the snowmelt-type mud flow. In this case, a 10 million  $m^3$  pyroclastic flow, at  $800^\circ C$ , continues for 500 seconds and melts snow (165cm depth and  $400kg/m^3$  density), from expected (a) and unexpected (b) vents and causes a snowmelt-type mud flow. The inundation area of the snowmelt-type mud flow calculated based on the hydrograph calculated by the kinematic wave model, corresponds to a water discharge five times more than melted snow (Miyamoto et al., 1989). In Fig.3 (b), the valley where the pyroclastic flow and snowmelt-type mud flow flow down was changed to the valley adjacent to the west. The inundation area based on calculation of the NM for rapid revision of hazard map and for evacuation is spread upstream. The calculation result of inundation area in Fig.3 was obtained in 13 minutes by NM.

(a) Demonstration example in the DM



(b) Demonstration example calculated by the NM

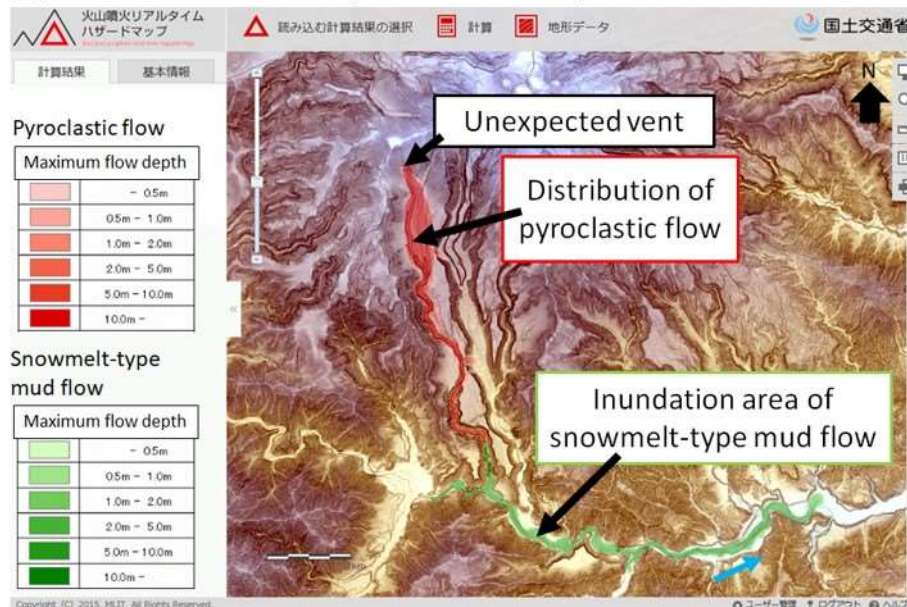


Figure 3: Demonstration example of the inundation areas for snowmelt-type mud flow in the DM (a) and calculated by the NM.

## Conclusion

In this report, the framework and the operational design for rapid revision of the hazard maps for debris flow and snowmelt-type mud flow caused by volcanic eruptions of unexpected magnitudes and from unexpected vents. Until August 2019, the system has been installed for five major active volcanoes namely Mt. Asama, Mt. Fuji, Mt. Ontake, Mt. Kirishima and Mt. Sakurajima. The system will be installed for other major active

volcanoes. For further improvement of the calculation of inundation area against the debris flow, consideration of the distribution of volcanic ash, pyroclastic flow and/or the precipitation observed and forecasted has been planned.

## References

Cabinet office, Government of Japan (2015) Disaster management in Japan, [http://www.bousai.go.jp/info/pdf/saigaipamphlet\\_je.pdf](http://www.bousai.go.jp/info/pdf/saigaipamphlet_je.pdf)

Ikeya H. (2008) The Heisei eruption of Mt. Unzen-Fugendake and measures against volcanic disasters, *Journal of Disaster Research*, Vol.3, No.4, pp.276-283

Japan Meteorological Agency (2019) Active volcanos in Japan, [https://www.data.jma.go.jp/svd/vois/data/tokyo/STOCK/kaisetsu/katsukazan\\_toha/katsukazan\\_toha.html#kanshikazan](https://www.data.jma.go.jp/svd/vois/data/tokyo/STOCK/kaisetsu/katsukazan_toha/katsukazan_toha.html#kanshikazan)

Major J.J and Newhall C. G. (1989) Snow and ice perturbation during historical volcanic eruptions and the formation of lahars and floods, *Bulletin of Volcanology*, Vol. 52, pp.1-27

Nakamura Y., Tanada T., Aramaki S. (2013) Volcanic hazard maps of Japan, second Edition, Technical Note of the National Research Institute for Earth Science and Disaster Prevention, No. 380, 186pp.

National Research Institute for Earth Science and Disaster Resilience (2016) Database on volcanic hazard maps and reference material, <http://vivaweb2.bosai.go.jp/v-hazard/index-e.html>

Ministry of Land, Infrastructure, Transport and Tourism (2018) Demo movie for “Volcanic eruption real-time hazard map system”, [http://www.mlit.go.jp/river/sabo/movie/rthmsystem\\_gaiyo.mp4](http://www.mlit.go.jp/river/sabo/movie/rthmsystem_gaiyo.mp4)

Miyamoto K., Suzuki H., Yamashita S., Mizuyama T. (1989) Reconstruction of the Volcanic Mud Flow at Mt. Tokachi in 1926, *Proceedings of the Japanese conference on hydraulics*, Vol.33, pp.361-366

Pierson T.C and Major J.J (2014) Hydrogeomorphic effects of explosive volcanic eruptions on drainage basins, *The Annual Review of Earth and Planetary Sciences*, Vol.42, p.469-507

Takahashi S. (2019) Countermeasures conducted by Tone river system sabo work office after the eruption of Mt. Motoshirane, Kanto skill up seminar 2019, [http://www.ktr.mlit.go.jp/ktr\\_content/content/000746685.pdf](http://www.ktr.mlit.go.jp/ktr_content/content/000746685.pdf)

---

# Forest stands from high elevation afforestation in the Austrian Alps – past, present and future at a glance

Christian Norbert Scheidl<sup>1</sup>, Micha Heiser<sup>2</sup>, Veronika Lechner<sup>3</sup>, Frank Perzl<sup>4</sup>, Silvio Schueler<sup>5</sup>, Georg Frank<sup>6</sup>, Thomas Thaler<sup>7</sup>, Gerhard Markart<sup>8</sup>

**Keywords:** high-elevation afforestation, Austrian Alps, protective forest

## Abstract

Mountain forests protect people, infrastructure and resources from natural hazards including snow avalanches, floods, debris flows and rockfalls. For such natural hazards the probability of occurrence and magnitude is essentially coupled to the protective effects of vegetation - especially in forested landscapes. In the 50s of the last century after two years of catastrophic avalanche events, the Austrian Forest-Technical Service for Torrent and Avalanche Control (WLV) acknowledged the importance of forest stands as active mitigation measurements against natural hazards and started with an extensive high-elevation afforestation campaign throughout the Austrian Alps. Recently, about 30% of the forested area of Austria has a major control function on avalanches, runoff, but also on erosion and rockfall. From a global perspective, high-elevation afforestation is a typical nature-based solution for managing natural hazards and resulting risks. Their advantages may include low environmental impacts, multiple benefits due to the ecosystem-based approach, and relatively low investment costs and higher adaptability to changing conditions.

This contribution is intended to recall the theoretical and practical effort that was put into reforestation at high altitudes (mainly situated within the timberline ecotone, acting as absolute limits for the existence of upright trees so far) and tries to make the future challenges of forest stands from high elevation afforestation tangible.

## Introduction

Since the 19th century, European countries in Alpine regions are historically leader in managing protective forests. Those ecosystems and management techniques can be seen as part of European natural and technical heritage, whereas high-elevation afforestation and

---

<sup>1</sup> Dr., PD. PhD., Institute of Mountain Risk Engineering, University of Natural Resources and Life Sciences, Vienna, AUSTRIA, ([christian.scheidl@boku.ac.at](mailto:christian.scheidl@boku.ac.at))

<sup>2</sup> Dr., Institute of Mountain Risk Engineering, University of Natural Resources and Life Sciences

<sup>3</sup> DI., Department of Natural Hazards (BFW-Innsbruck)

<sup>4</sup> DI., Department of Natural Hazards (BFW-Innsbruck)

<sup>5</sup> Dr., Department of Forest Growth and Silviculture (BFW-Vienna)

<sup>6</sup> Dr., Department of Forest Growth and Silviculture (BFW-Vienna)

<sup>7</sup> Dr., Institute of Mountain Risk Engineering, University of Natural Resources and Life Sciences

<sup>8</sup> Dr., Department of Natural Hazards (BFW-Innsbruck)

regeneration of protective forests are of highly public interest throughout the Alpine areas of Europe. This is because mountain forests are a major factor in reducing risk on people, infrastructure and resources from natural hazards including floods, debris flows, debris flows, snow avalanches and rockfalls (e.g.: Brang et al., 2008; Sidle and Ochiai, 2013). In Austria as well as South-Tyrol (Italy) about 30%, in Switzerland about 40% (Duc and Brändli, 2010) and in Bavaria even 60% (Binder et al., 2019) of the forested area is designated to forests for which the prevention of gravity-driven natural hazards is the major control function.

In Austria, the relative high proportion of protective forests was not always existing. Caused by an extensive reforestation project in the late 1960's (WIFO, 1963) devastated forests have been restored. Great attention was paid to high-elevation afforestation (c.f. Figure 1) merely either within avalanche release zones - aiming to supplement or even substitute technical avalanche mitigation structures (Heumader, 2000; Schönenberger, 2001) - or to reduce strong runoff events because of increased rainfall interception and increased transpiration during dry periods (e.g.: Andréassian, 2004; Hewlett, 1982)

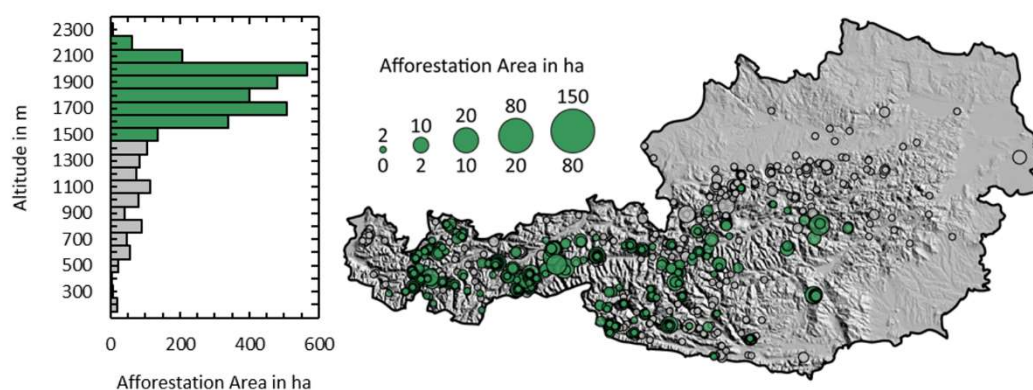


**Figure 1:** The map on the right shows Austrian afforestation sites at the timberline, respectively in high elevation, in order to establish protection forests. In total 3,200 afforestation sites on 9,000 ha have been established between 1906 and 2017. The left panel shows the distribution of the afforestation sites per altitude. More than 80%, in terms of area, are situated in the subalpine or alpine altitudinal zones (Source: Forest Technical Services for Torrent- and Avalanche Control, 2016).

High-elevation afforestation campaigns are nature-based solutions (NBS) for managing natural hazards and resulting risks with the advantages of low environmental impacts, relatively low investment costs and higher adaptability to changing conditions. Although NBS (like a protection forest) in general might exploit ecosystems with regard to their resilient adaptive ecosystem services and through their sustainable integrity (Albert et al., 2017), afforestation areas at high altitudes show low resilience, i.e. lower adaptability to change. This is because high elevation afforestation is mainly situated at the tree limit or even within the timberline ecotone - acting as absolute limits for the existence of upright trees so far (e.g.: Burga and Perret, 2001). In contrast to forest regeneration in the shelter of a stand, regeneration at the timberline is exposed to extreme conditions, as the timberline is

sensitive to climatic conditions, such as the length of the growing season, the effective temperature sum, the duration of the frost-free season, potential evapotranspiration, precipitation during the growing season, the amounts of light and nutrients, carbon dioxide deficiency, and relative humidity (Heikkinen et al., 2002; Tuhkanen, 1993; Wieser, 2012). This is also reflected by the fact that even small-scale topographic features can cause major deviations from the average climatic conditions in the respective timberline/treeline ecotone. This is, because exposure to wind and snow is strongly controlled by topographic conditions e.g.: the local relief, which may alter growth and survival conditions significantly.

## **High elevation afforestation from today's perspective**

The first challenge of reforestation within the ecotone timberline was to understand how to reforest unstocked areas. Research in Austria (Hampel et al., 1961, 1963) has led to groundbreaking results like the wind-snow-ecogram (“Wind-Schnee-Ökogramm”) introduced by Aulitzky (1963). It is based on the consideration that local relief of subalpine areas forms particularly sharp subdivision of favourable and unfavourable locations for afforestation sites, and these subdivisions are easily recognizable in the vegetation. For the later reason, many Austrian high elevation afforestation campaigns have been installed under consideration of the wind-snow-ecogram. Reports about experiences on the field of high-elevation afforestation in subalpine regions in Austria exists from Sauer Moser (1988) and have been summarised in Heumader (2000). As important condition for successful afforestation at the tree line both authors propose the use of suitable seed provenance (following the findings of e.g. Nather, 1972 and Stern, 1972), which should be ideally collected from stands in the same growth area and altitude as the afforestation site. However, more recent experiments show that genotypes from lower elevation may show comparable survival and even better development and thus recommend a broad mixture of genotypes to make full use the respective tree species diversity (Weißbacher et al., 2007) and the expected strong environmental selection (Kapeller et al., 2017). Within the subalpine environment, every irregularity in the slope surface causes extensive small-scale variation in the environmental conditions. Research results from Switzerland brought important supplementary knowledge, especially due to the experimental afforestation area at Stillberg, which has provided information on the long-term impact of various environmental factors on the Alpine treeline. Snow deposition, snow movement, radiation, temperature, wind, avalanche frequency, vegetation, and soil types have been found to change in a fine mosaic-like pattern according to the surface structure. This variation between microsites is reflected in the diverse performance patterns of afforestation sites (e.g. Schönenberger, 1986, 2001; Schönenberger et al., 1994; Senn, 1999). More recently, Barbeito et al. (2012) investigated the spatial and temporal dynamics of tree mortality and growth at the experimental afforestation area at Stillberg. They found that observed elevation thresholds (physiological upper limit of tree survival and growth), indicate a potential limit for the natural treeline to shift upward under current and expected future climatic conditions.

Figure 2 shows afforestation age distribution of subalpine forests of Austria based on cumulative area and number of high-elevation afforestation sites, conducted from 1945 to 2017. Regarding the reforested area (Fig. 2 - left panel), a period of high intensity is visible from 1965 to 1975. After an approximately 10-year long plateau of low activity an almost constant rate of 170 ha per year prevails from 1985 till 2011, which is followed by a second plateau till 2017. Similar patterns can be observed for the number of new afforestation sites per year (Fig. 2 – right panel).

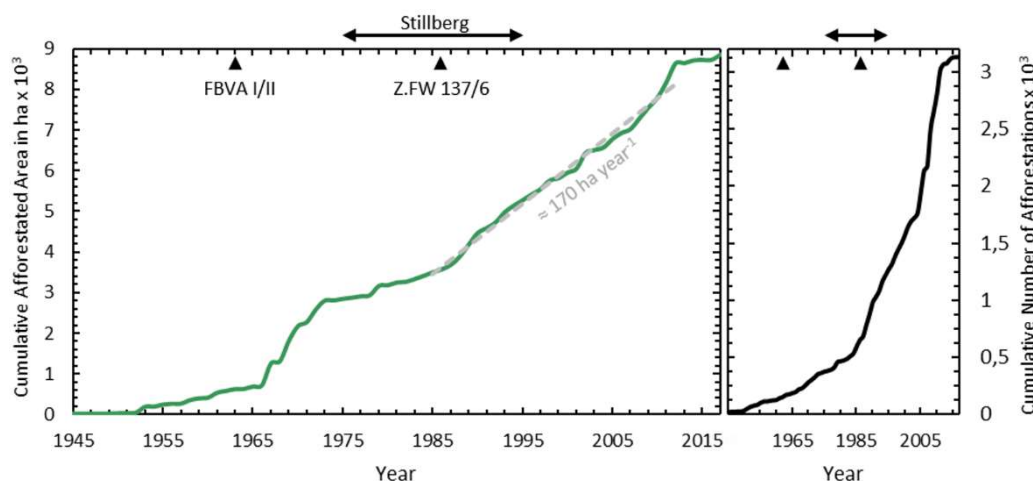


**Figure 2: Cumulative area and number of afforestation sites at the timberline, respectively at high elevation, conducted by the Forest technical Service for Torrent and Avalanche Control between 1945 and 2017 in Austria. The arrows refer to important research and test sites with respect to the establishment of forest in high elevations; with FBVA I/II (Hampel et al., 1961, 1963) laying the foundation for the wind-snow ecogram and Z.FW 137/6 (Schönenberger, 1986) introducing cluster afforestation and Stillberg referring to the test site in Davos, Switzerland from which important conclusion were drawn (e.g. Barbeito et al., 2012).**

While the study on tree mortality and growth of subalpine high-elevation afforestation raised a great number of publications or technical guidelines (e.g. Aulitzky, 1963; Schönenberger, 1990), only few systematic studies have investigated subsequent silvicultural management for forest evolved from high elevation afforestation as well as adaption strategies to climate change. This is important because as observed by Schönenberger (2001), many stands became homogeneous even after the afforestation had been established successfully and are considered to be susceptible to breakdowns through wind, snow or insect attacks (Ott et al., 1997) which ultimately decreases the forests intended protective functions.

These days, protective forests, evolved from the first high elevation afforestation in subalpine areas, reach average stand ages of about 40 to maximum 50 years. From more than 3,200 afforestation sites established between 1906 and 2017 (Figure 1), about 520 sites are older than 40 years, covering 3,800 ha (more than 1/3 of total area afforested until 2017). These forests which evolved from high elevation afforestation stands transferred from the initial stage to a so-called young stage which is, from a forest management perspective, also called stem exclusion stage. Different stages of stand development require

different silvicultural management strategies to keep the protective effect on an acceptable level. Common management strategies as proposed by Heumader (2000) and Schönenberger (2001) agree on tending and thinning of dense and closed afforestation at latest during thicket stage (preliminary young stage) to form cluster structures. However, there is a lack of strategies that combine traditional silvicultural management of subalpine protection forests with new concepts to increase the stability and resilience of forests in climate change (Ledermann and Kindermann, 2017) and that evaluate their future protective functions.

## What about the near future?

Former afforestation campaigns have not considered the present noticeable climate change and the rise of temperature as a risk for protection forests. As the Alpine regions were found to experience higher temperature increase than the global average (Kromp-Kolb et al., 2014), there is currently much interest in the rate at which the treeline may advance in response to environmental change, especially global warming. There are at least three aspects of environmental change to which plants are generally thought to respond: increasing temperature, rising concentration of carbon dioxide, and increasing deposition of nitrogen (Grace et al., 2002). Alpine treelines are assumed to be particularly sensitive to altered temperature regimes and climate warming (e.g. Dullinger et al., 2004; Wieser, 2012). However, also the occurrence of natural hazards undergoes changes in frequency and intensity. For example, thawing processes in the Alpine permafrost already increased the probability of rockfall events (Huggel et al. 2012). Also, although absolute snow cover is predicted to decrease in the future, the frequency of extreme snowfall events and ratios of wet snow is expected to increase and thus increases the risk of wet snow avalanches (Naaïm 2017) at higher elevations (Latenser and Schneebeili 2003).

Regarding the expected climate change impacts on forests, further major threats to desired forest structures are natural disturbances like wildfire, wind, and insects' outbreaks (Dale et al., 2001; Seidl et al., 2017) or pathologic damages (e.g. Porta et al., 2008).

Besides ongoing environmental changes also changing societal demands shape the perspectives of high elevation forests. For example, within the increasing climate crisis the role of forests as carbon sink is getting increasing awareness and possibly further regulations. For this reason, silvicultural adaptation strategies for "outgrown" high-elevation afforestation sites must consider expected climate change impacts and social demands on high elevation ecosystems.

## Conclusion

Without anthropogenic interactions, natural mountain forests evolve within repeated cycles of regeneration, optimal growth, ageing and forest breakdown and then starting again (Motta and Haudemand, 2000). This natural forest development results in continuously changing protective functions, from forest aging until the next transition phase, protective effects are relatively small. However, in coupled human-environmental systems like forest stands from high elevation afforestation, the complexity increases – particularly caused by the feedback loops between environmental dynamics and human decision-making

processes – making adaptation strategies a major challenge. A low risk awareness of forest managers for instance, is considered among the main causes of probable low preparedness, which in turn generates inadequate response to the threat (Fuchs et al., 2017).

Overall, stable and functional subalpine protection forests are expected to play an increasing role in climate change. Hence, the current establishment and management guidelines require assessment and adaptation based on experience and technical development since the implementation of the first afforestation campaigns. For this reason, we preliminary need to focus on (without claiming completeness):

- Evaluate the establishment, growth, vitality and stability of high elevation afforestation sites and study their relationship with afforestation techniques, selected species, past tending operations, climate change and additional site characteristics (c.f. Barbeito et al., 2012; Heumader et al., 2017). For instance, little is known about how many of the high-altitude afforestation shown in Figure 1 can be regarded as secured.
- Determine how protective effects of former high elevation afforestation campaigns evolved with ongoing forest development, climate change within the last decades and changing societal needs. Additionally, potential change of the original intended protective functions and additional societal demands (carbon sink) might also be investigated.
- Develop silvicultural management options to maintain and increase the protective effect of growing high-elevation afforestation in response to changing climate and/or local relief disturbance regimes.

We also need to consider assessments on risk perception and potential barriers to the implementation of nature-based solutions, such as high-elevation afforestation, that can benefit the protection against natural hazards. Investigating the perceptions of local and regional authorities, forest managers, and local decision makers and identifying limitations, boundaries, and motivations for the implementation of forest adaptation strategies in response to a changing climate must not be neglected. In the end the knowledge is to be attained if the theory matches the reality.

Indeed, the question is: "Do we have the answers to anticipate the consequences of climate change on the growth and development of forest ecosystems in high mountain regions?" In any case, we see the need for new research sites in the subalpine area, similar to the former sites Poschach (near Obergurgl, Tyrol-AUT) or Haggen im Sellraintal (Tyrol-AUT), which formed the basis of today's knowledge about high mountain afforestation in the Austrian Alps.

## References

- Albert, C., Spangenberg, J.H., and Schröter, B. (2017). Nature-based solutions: criteria. *Nature* 543, 315–315.
- Andréassian, V. (2004). Waters and forests: from historical controversy to scientific debate. *J. Hydrol.* 291, 1–27.

Aulitzky, H. (1963). Grundlagen und Anwendung des vorläufigen Wind-Schnee-Ökogrammes. In *Ökologische Untersuchungen in Der Subalpinen Stufe Zum Zwecke Der Hochlagenaufforstung Teil II*, pp. 763–834.

Barbeito, I., Dawes, M.A., Rixen, C., Senn, J., and Bebi, P. (2012). Factors driving mortality and growth at treeline: a 30-year experiment of 92 000 conifers. *Ecology* 93, 389–401.

Binder, F., Macher, C., and Müller, K. (2019). Dem Schutzwald auf der Spur. *LWF Aktuell* -120 11–13.

Brang, P., Schönenberger, W., Ott, E., and Gardner, B. (2008). Forests as Protection from Natural Hazards. In *The Forests Handbook, Volume 2: Applying Forest Science for Sustainable Management*, J. Evans, ed. (Blackwell Science Ltd), pp. 53–81.

Burga, C.A., and Perret, R. (2001). Monitoring of Eastern and Southern Swiss Alpine Timberline Ecotones. In *Biomonitoring: General and Applied Aspects on Regional and Global Scales*, C.A. Burga, and A. Kratochwil, eds. (Dordrecht: Springer Netherlands), pp. 179–194.

Duc, P., and Brändli, U.-B. (2010). Ergebnisse des dritten Landesforstinventars LFI3. Schutzwald hat sich verbessert. *Wald Holz* 91, 25–28.

Dullinger, S., Dirnböck, T., and Grabherr, G. (2004). Modelling climate change-driven treeline shifts: relative effects of temperature increase, dispersal and invasibility. *J. Ecol.* 92, 241–252.

Albert, C., Spangenberg, J.H., and Schröter, B. (2017). Nature-based solutions: criteria. *Nature* 543, 315–315.

Andréassian, V. (2004). Waters and forests: from historical controversy to scientific debate. *J. Hydrol.* 291, 1–27.

Aulitzky, H. (1963). Grundlagen und Anwendung des vorläufigen Wind-Schnee-Ökogrammes. In *Ökologische Untersuchungen in Der Subalpinen Stufe Zum Zwecke Der Hochlagenaufforstung Teil II*, pp. 763–834.

Barbeito, I., Dawes, M.A., Rixen, C., Senn, J., and Bebi, P. (2012). Factors driving mortality and growth at treeline: a 30-year experiment of 92 000 conifers. *Ecology* 93, 389–401.

Binder, F., Macher, C., and Müller, K. (2019). Dem Schutzwald auf der Spur. *LWF Aktuell* -120 11–13.

Brang, P., Schönenberger, W., Ott, E., and Gardner, B. (2008). Forests as Protection from Natural Hazards. In *The Forests Handbook, Volume 2: Applying Forest Science for Sustainable Management*, J. Evans, ed. (Blackwell Science Ltd), pp. 53–81.

Burga, C.A., and Perret, R. (2001). Monitoring of Eastern and Southern Swiss Alpine Timberline Ecotones. In *Biomonitoring: General and Applied Aspects on Regional and*

- Global Scales, C.A. Burga, and A. Kratochwil, eds. (Dordrecht: Springer Netherlands), pp. 179–194.
- Duc, P., and Brändli, U.-B. (2010). Ergebnisse des dritten Landesforstinventars LFI3. Schutzwald hat sich verbessert. *Wald Holz* 91, 25–28.
- Dullinger, S., Dirnböck, T., and Grabherr, G. (2004). Modelling climate change-driven treeline shifts: relative effects of temperature increase, dispersal and invasibility. *J. Ecol.* 92, 241–252.
- Fuchs, S., Karagiorgos, K., Kitikidou, K., Maris, F., Paparrizos, S., and Thaler, T. (2017). Flood risk perception and adaptation capacity: a contribution to the socio-hydrology debate. *Hydrol. Earth Syst. Sci.* 21, 3183–3198.
- Grace, J., Berninger, F., and Nagy, L. (2002). Impacts of climate change on the tree line. *Ann. Bot.* 90, 537–544.
- Hampel, R., Aulitzky, H., Bernard, S., Czell, A., Friedel, H., Fromme, G., Fuchs, A., Göbl, F., Hassenteufel, W., Holzer, K., et al. (1961). *Ökologische Untersuchungen in der subalpinen Stufe zum Zwecke der Hochlagenaufforstung Teil 1* (Österreichischer Agrarverlag, Wien).
- Hampel, R., Aulitzky, H., Bernard, S., Czell, A., Friedel, H., Fromme, G., Fuchs, A., Göbl, F., Hassenteufel, W., Holzer, K., et al. (1963). *Ökologische Untersuchungen in der subalpinen Stufe zum Zwecke der Hochlagenaufforstung Teil 2* (Österreichischer Agrarverlag, Wien).
- Heikkinen, O., Tuovinen, M., and Autio, J. (2002). What determines the timberline? *Fennia* 180, 67–74.
- Heumader, J. (2000). High elevation afforestation and regeneration of subalpine forest stands experiments in Austria. (Villach), pp. 29–40.
- Heumader, J., Neuner, J., and Markart, G. (2017). Evaluierung von Hochlagenaufforstungen in Österreich. *Wildbach Lawinenverbau* 180, 240–248.
- Hewlett, J.D. (1982). *Principles of Forest Hydrology* (University of Georgia Press).
- Kapeller, S., Dieckmann, U., and Schueler, S. (2017). Varying selection differential throughout the climatic range of Norway spruce in Central Europe. *Evol. Appl.* 10, 25–38.
- Kromp-Kolb, H., Nakicenovic, N., Seidl, R., and Steininger, K. (2014). Synthesis. In *Austrian Assessment Report Climate Change 2014 (AAR14)*, (Austrian Academy of Sciences Press, Vienna, Austria), p.
- Ledermann, T., and Kindermann, G. (2017). Wie geht man mit gefährdeten Fichtenbeständen? um. *BFW Praxisinformation* 44, 19–22.
- Motta, R., and Haudemand, J.-C. (2000). Protective Forests and Silvicultural Stability. *Mt. Res. Dev.* 20, 180–187.

- Nather, J. (1972). Die Bedeutung der Herkunftssicherung von Saatgut für Hochlagenaufforstungen. *Mitteilungen Forstl. Bundes-Vers. Wien* 96, 23–38.
- Ott, E., Frehner, M., Frey, H.U., and Lüscher, P. (1997). *Gebirgsnadelwälder. Ein praxisorientierter Leitfaden für eine standortsgerechte Waldbehandlung* (Bern, Stuttgart, Wien, Verlag Paul Haupt).
- Porta, N.L., Capretti, P., Thomsen, I.M., Kasanen, R., Hietala, A.M., and Weissenberg, K.V. (2008). Forest pathogens with higher damage potential due to climate change in Europe. *Can. J. Plant Pathol.* 30, 177–195.
- Sauermoser, S. (1988). Former experiences on the field of afforestations in subalpine regions gained by the forest-technical service of torrent and avalanche control for the last 35 years in Tyrol. In *International Congress Interpraevent, (Graz)*, pp. 253–266.
- Schönenberger, W. (1986). Rottenaufforstung im Gebirge. *Schweiz. Z. F Forstwes.* 137, 501–509.
- Schönenberger, W. (1990). *Oekologie und Technik der Aufforstung im Gebirge: Anregungen für die Praxis* (Flück-Wirth [in Komm.]).
- Schönenberger, W. (2001). Cluster afforestation for creating diverse mountain forest structures — a review. *For. Ecol. Manag.* 145, 121–128.
- Schönenberger, W., Senn, J., and Wasem, U. (1994). Factors affecting establishment of planted trees near timberline. In *Proceedings of the Symposium on Ecology and Management of Larix Forests: A Look Ahead*. Whitefish, Montana, October 1992, (USDA, Forest Service, Intermountain Research Station, General Technical Report), pp. 170–175.
- Senn, J. (1999). Tree mortality caused by *Gremmeniella abietina* in a subalpine afforestation in the central Alps and its relationship with duration of snow cover. *Eur. J. For. Pathol.* 29, 65–74.
- Sidle, R.C., and Ochiai, H. (2013). Summary. In *Landslides: Processes, Prediction, and Land Use*, (American Geophysical Union), pp. 239–242.
- Stern, R. (1972). Versuche mit Nadelholz - Saaten auf subalpinen Standorten. *Mitteilungen Forstl. Bundes-Vers. Wien* 96, 51–59.
- Tuhkanen, S. (1993). Treeline in Relation to Climate, with Special Reference to Oceanic Areas. In *Forest Development in Cold Climates*, (Springer, Boston, MA), pp. 115–134.
- Weißbacher, L., Schueler, S., and Zwerger, P. (2007). Fichtenstecklinge - eine Alternative für Hochlagenaufforstungen. *Österr. Forstztg.* 6, 36–38.
- Wieser, G. (2012). Lessons from the timberline ecotone in the Central Tyrolean Alps: a review. *Plant Ecol. Divers.* 5, 127–139.
- WIFO (1963). Mehr Holz durch Wiederbewaldung und Neuaufforstung. *Austrian Inst. Econ. Res. WIFO Heft* 1, 9–15.

---

# Evaluation of an awareness raising campaign in Styria, Austria

Sabrina Scheuer<sup>1</sup>, Markus Eder<sup>2</sup>, Helmut Habersack<sup>3</sup>

**Keywords:** flood risk; awareness raising; self-protection; good practice; risk communication

## Abstract

In order to cope with the future increase in hazard potential due to climate change, suitable and effective educational concepts for risk communication and information of the public are needed. Within the framework of this project, the analysis and evaluation of an existing awareness raising campaign of the federal state Styria in flood risk management was carried out. A telephone survey with the participants of this campaign was conducted and the results were evaluated. The evaluation of the campaign and the strategy concept showed that public awareness could be increased. There is still a need for optimization in terms of reaching the target group under the age of 35 and focusing on measures in the area of education. The results of the evaluation were discussed at a stakeholder workshop together with good practice examples. Further, the implementation of the derived recommendations was also decided.

## Introduction

In the last two decades (1997-2017) about 2 billion people were affected by more than 3.000 floods and about 142.000 people died, which makes it to the most frequent natural disaster that affects most people worldwide, but also the economic loss sums up to 656 billion US\$ (CRED&UNISDR 2018). Scientific research already shows the global increase of record-breaking rainfall events by 12% over 1981-2010 (Lehmann et al. 2015). Therefore, decision makers will face new problems and challenges to cope with events and to reduce damage and fatalities caused by floods. Technical measures are one way to reduce the effects of a flood, but high construction and maintenance costs hamper the implementation of such measures. Organisational measures are strongly needed to cope with extreme events and the citizens must take self-provision measures on their own. Therefore, awareness raising is a crucial part to increase the resilience of Europe and its citizens.

In the federal state of Styria in Austria, awareness raising is a fundamental part of the integrated flood risk management and one of the four strategies of the HORST (HOchwasserRisikOmanagement STEiermark - flood risk management Styria) based on

---

<sup>1</sup> MSc., Dipl.-Ing., Water, Atmosphere and Environment, Universität für Bodenkultur Wien, AUSTRIA, ([sabrina.scheuer@boku.ac.at](mailto:sabrina.scheuer@boku.ac.at))

<sup>2</sup> Dipl.-Ing., University of Natural Resources and Life Sciences, Vienna

<sup>3</sup> Univ.Prof. Dipl.-Ing. Dr., University of Natural Resources and Life Sciences, Vienna

the flood risk management plans of Austria. To inform citizens about flood risks, an information campaign was developed by the federal state of Styria together with other stakeholders. The campaign includes presentations by the Styrian civil defence organisation offered to all municipalities in Styria and a flood folder with check lists, emergency plans etc. A project was conducted to analyse and evaluate the Styrian awareness raising strategy as well as an information campaign and to develop mitigation measures based on the evaluation results and a literature review. The results of the project are presented and discussed in this paper.

## Methods

### Analysis of the awareness raising strategy in HORST

The awareness raising strategy as part of HORST was evaluated by collecting all measures which are part of this strategy and then divided them into three categories: already executed, currently in execution and planned. A list of measures was provided by the federal state of Styria including general information regarding each measure. The measures were then assigned to the four measure types which are also part of the HORST. Based on these results, measure types with only few measures could be identified and important measures that are not in the focus of the federal state of Styria could be suggested.

### Analysis and evaluation of the information campaign

The evaluation campaign of the Styrian civil defence organisation consisted of a lecture given by the members of the organisation and a folder with additional information material, checklists and guidelines. The lecture included personal flood examples of Styria, investments of the state and province for flood defence, types of floods and types of self-provision measures. To evaluate the current status of the information campaign named “Selbstschutz Hochwasser” (self-provision flood) a telephone survey of people who attended the presentation was carried out. In total 27 open questions were asked by the interviewer about three months after the presentation visit. The questions were categorised in 5 categories including the interest in the event, the efficiency and sustainability of the lecture, feedback to the information materials, general feedback to the event and demographic aspects to evaluate these aspects. All 27 questions were analysed, but here only the most interesting results will be presented, therefore focusing on the following questions: “Why did you attend the event?”, “Do you have structural (flood-proof windows etc.) and / or non-structural (higher storage in the basement, sandbags etc.) measures implemented or are planning to implement them due to the event?”, “Do you know if your property lies in a risk zone?” and “What was the key message of the event?”. The survey was carried out two times, once at the beginning of the evaluation and a second time, after some of the recommendations were implemented in the campaign. Additionally, the Styrian civil defence organisation provided information about the districts where an event already took place.

### Review of good practice examples

A systematic literature review was carried out (searching forwards and backwards) during the project to identify good practice examples in flood risk management by using Google Scholar and Scopus using the following key words: risk perception, awareness, preparedness, adaptation, response, human behaviour, natural hazards, floods, flood risk, flood management, disaster, resilience, communication, crisis. The publications were then sorted by their relevance and analysed, including a review of cited publications of these papers. A paper was identified as relevant, if it contained tested recommendations for awareness raising or information campaigns. The most relevant publications and results for the improvement of the campaign, focusing especially on recommendations mentioned in more than one paper, served as basis for the development of improvement measures.

### Development of strategy recommendations

In the last step of the paper, strategy recommendations for an effective education program in the field of disaster prevention were developed, based on the two evaluations of the information campaign, the analysis of the awareness raising strategy and the results of the literature review.

## Results and discussion

### Analysis of the awareness raising strategy in HORST

The analysis of the awareness raising strategy as one of the four strategies of the HORST (flood risk management Styria) showed that four measures of the type “Information”, one measure of the type “Education”, four measures of the type “Research” and one measure of the type “Documentation” were identified. Only two of the ten reported measures are finished, the other ones are not finished yet or are continually done (Table 1). A potential for additional measures in the section of education was identified, as only one measure was reported for this type.

nr.	measure	type	status
1	flood website	Information	ongoing
2	information campaign „self-protection floods“	Information	ongoing
3	folder „floods –I prepare“	Information	done
4	folder „flood risk management plans Styria“	Information	done
5	master thesis	Education	ongoing
6	research assignments (e.g. damage potential analysis Graz, HORST)	Research	ongoing
7	participation and cooperation with professional working groups	Research	ongoing
8	participation in international, relevant working groups	Research	ongoing
9	regional: permanent working group "flood risk management"	Research	ongoing
10	flood-documentations: e.g. 2017, 2013, 2016	Documentation	ongoing

**Table 1: list of measures of the awareness raising strategy in HORST (based on Fordinal et al. 2019)**

#### Analysis and evaluation of the information campaign

The information campaign aimed to raise awareness for possible dangers regarding floods, to improve the abilities and knowledge to cope with floods and implement self-provision measures.

In a first step, the penetration rate of the presentations in the 13 different districts as well as Styria in total was calculated. The rate for the different districts lies between 4% (Graz, the capital city as one of the districts has 0%) and 53%. For the federal state of Styria, the rate lies at 30% (85 municipalities out of 287) counted at the beginning of the campaign in October 2017 and July 2019.

Looking at the age structure of the attendees of the presentations, the picture is for both surveys quite the same. In total only 10% of the attendees were below 34 years and none below 25 years. This shows that additional measures should be taken to reach the younger generation, because they may decide in the next years where to live or build a house. 27% of the attendees were between 35 and 49 and 23% were between 50 and 60 years, but the biggest group were the people over 60 years, with a total percentage of 39%. (see graph 1)

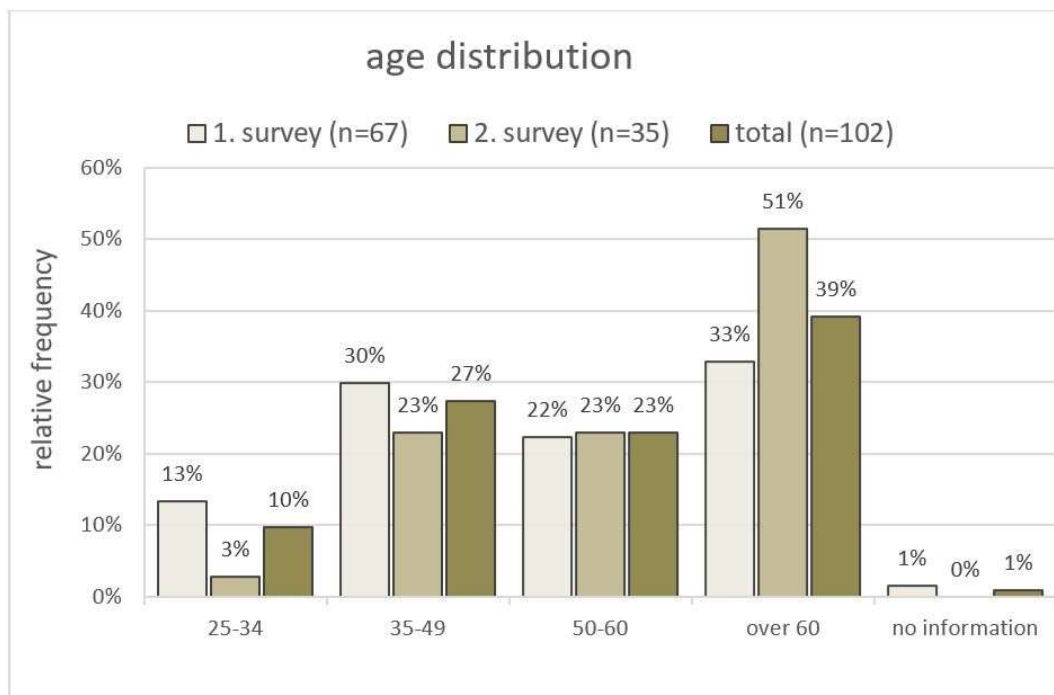


**Figure 1: age structure of both interviews separated into four age classes**

Most of the attendees came to the presentation because they were affected by a flood in the past (41% first survey, 49% second survey) and more than 1/3 of them because they were interested in the topic (29% first survey, 43% second survey). Only a minor part came because of other topics before or after the presentation (14% first survey, 9% second survey). The interviews also came to the result, that in total a quarter of the interviewees already implemented self-provision measures (including structural, like flood-proof windows, flood gates, and non-structural measures, like putting relevant documents in a ready to take folder, put important belongings in upper floors, as mentioned during the information event) and 14% planned to do it because of the presentation. Another 26% already had everything and 25% think that they don't need anything (see Graph 2).

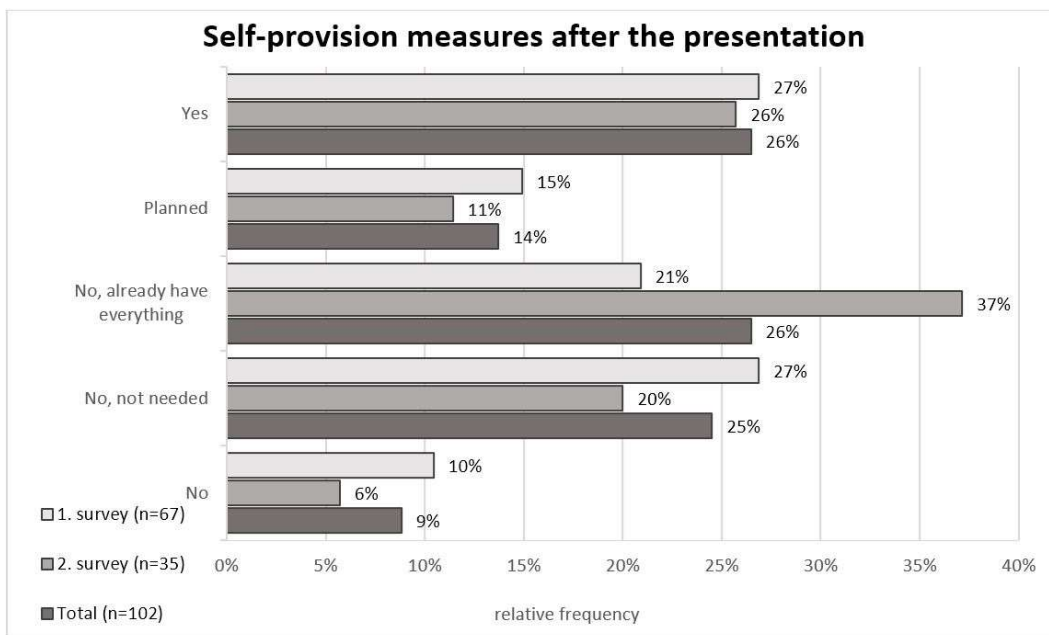


**Figure 2: willingness of interviewees for self-provision**

As the aim of the information campaign was to raise awareness regarding the danger of a flood, the survey should find out if people are aware of their risk. Therefore, it was asked if the interviewees know if they live in a flood risk zone or not. This answered in total 92% with a Yes. This is a much higher number than in another survey conducted by Zahnt et al. 2018 where ¼ of the interviewees were not aware of this. It was also asked for the key message of the presentations. 49 out of 102 interviewees think that the key message was “self-provision is possible and important” and 22 out of 102 people identified the message “sharpen awareness for floods”. Both is in line with the aims of the presentations.

#### Review of good practice examples

After reviewing the literature about flood risk communication and management five papers were identified which show important examples of good practice. Two of them will be summarized here to show what improvement measures were identified based on the paper.

A very interesting work is done by O’Sullivan et al. 2012 who developed a framework and recommendations for effective flood risk communication (see Graph 3): (O’Sullivan et al. 2012)

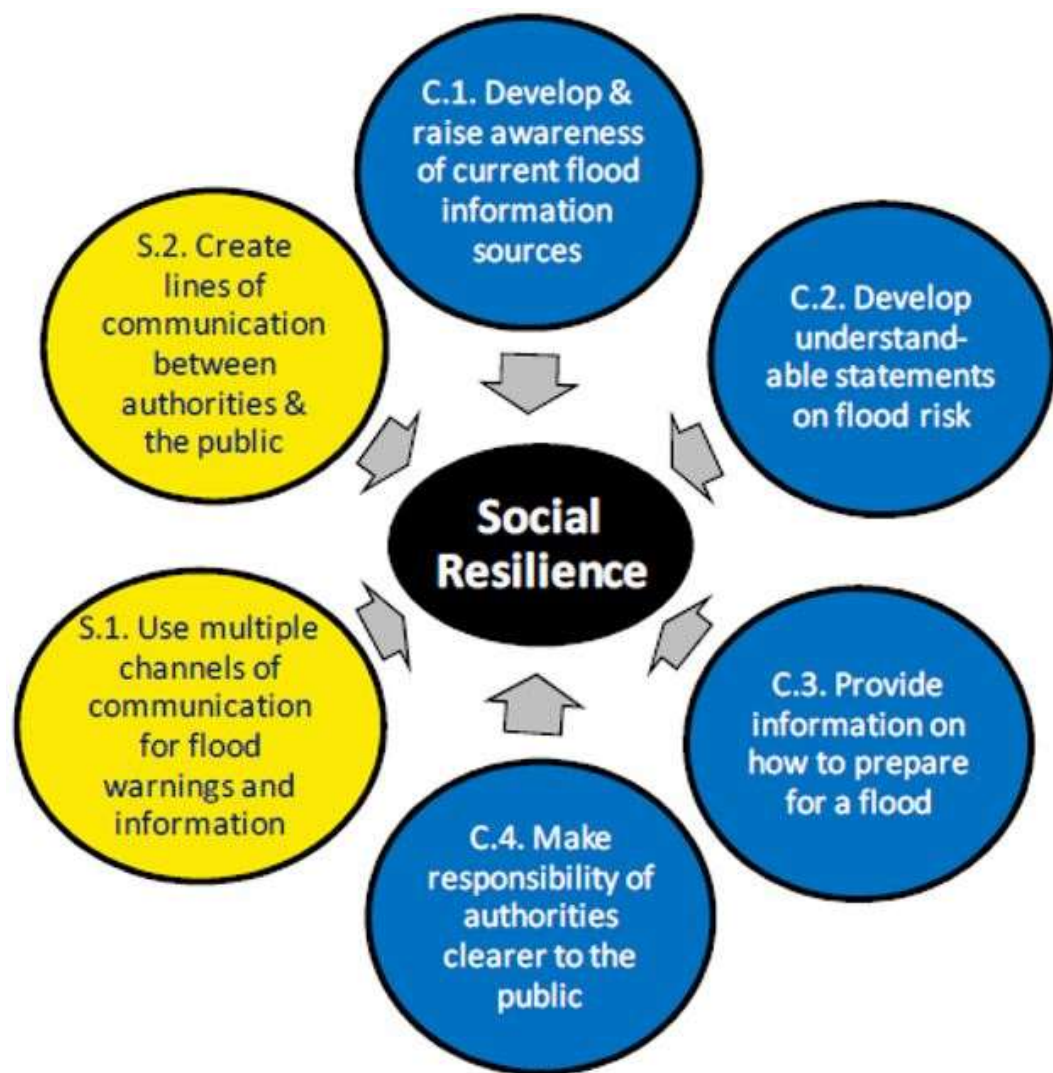


**Figure 3: Social resilience framework for improving flood risk communications (O’Sullivan et al. 2012)**

Moreover, 60 risk communication practices were analysed by Höppner et al. 2012 to identify criteria and aims for good risk communication. The following messages were identified as very important for the Styrian information campaign (see Graph 4): (Höppner et al. 2012)



**Figure 4: criteria for good risk communication (based on Höppner et al. 2012)**

#### Development of strategy recommendations

At the stakeholder workshop with the federal state of Styria, the Styrian civil defence organisation, the torrent and avalanche control Styria and the consulting firm which developed the information campaign the results of the evaluation, the literature research and the developed improvement measures were presented. As an output, the responsible stakeholders decided on the uptake of the suggested measures and agreed to use the window of opportunity after events and to combine the presentations with other events where possible. A feedback form was developed as an implementation to provide a feedback possibility for the citizens and FAQs were developed to offer standardised answers to the relevant questions which regularly appear during the presentations. The organizers are also going to use social media to get the attraction of younger people and the local fire fighters will hold a part of the presentation at the event. The conclusion was reached to extend the project duration to reach more municipalities. General strategy recommendations accepted by the stakeholders were regarding target-oriented measures, use of up to date media and channels, combination of different measure types and the accompanying analyses and evaluations of ongoing measures.

## Conclusion

By evaluating the awareness raising strategy and flood risk information campaign of Styria this paper contributes to a better understanding on how and if such information campaigns are really improving peoples understanding of their flood risk and the willingness to take self-provision and self-protection measures. We have analysed and evaluated the strategy itself to identify improvements as well as the information campaign to suggest modifications based on these results and the reviewed good practice examples. Together

with the relevant stakeholders we were able to decide on the implementation of the suggested mitigation measures and we were then able to do another telephone survey. Due to the project timeline it was not possible to do a statistically significant number of interviews and therefore we concentrated more on the overall results of the two surveys. The fact that we only interviewed people which are attended such an event has to be taken into account when comparing the results with general data on the uptake of self-provision measures, because these people are already more aware than the general public, but this was necessary as the aim of the project was to evaluate the campaign. For the strategy we identified a potential for the uptake of more measures in the area of education and some additional organisational suggestions. The results of the survey clearly show, that with this kind of information campaign it is not possible to reach the generation below 25 years. Therefore, we suggest implementing another measure for this target group, like a mobile application that is more broadly used in this age group. Other than that, we conclude that the information campaign is clearly reaching their aims, it is only necessary to do such presentations every couple of years and if possible in all municipalities to really reach a broad auditorium.

## References

- Dittrich, R., A. Wreford, A. Butler & D. Moran. 2016. The impact of flood action groups on the uptake of flood management measures. *Climatic Change* 138. Climatic Change. 471–489.
- CRED&UNISDR. 2018. Economic losses, poverty & disasters. Centre for Research on the Epidemiology of Disasters CRED, United Nations Office for Disaster Risk Reduction UNISDR.
- Fordinal, I., A. Schwingshandl, C. Jöbstl, H. Eitner, H. Uhl & G. Macher. 2019. Informationskampagne Selbstschutz Hochwasser - Endbericht. Vienna.
- Habersack, H., M. Eder, S. Scheuer & V. Pelzmann. (2019): Analyse eines Strategiekonzepts zur Bewusstseinsbildung im Hochwasserrisikomanagement. Endbericht von StartClim2018.E in StartClim2018: Weitere Beiträge zur Umsetzung der österreichischen Anpassungsstrategie, Auftraggeber: BMLFUW, BMWF, ÖBf, Land Oberösterreich
- Höppner, C., R. Whittle, M. Bründl & M. Buchecker. 2012. Linking social capacities and risk communication in Europe : a gap between theory and practice ? *Natural Hazards* 64. 1753–1778.
- Lehmann, J., D. Coumou & K. Frieler. 2015. Increased record-breaking precipitation events under global warming. *Climate Change* 132. 501–515.
- O’Sullivan, J. J., R. A. Bradford, M. Bonaiuto, S. De Dominicis, P. Rotko, J. Aaltonen, K. Waylen & S. J. Langan. 2012. Enhancing flood resilience through improved risk communications. *Natural Hazards and Earth System Sciences* 12. 2271–2282.

Zahnt, N., M. Eder & H. Habersack. 2018. Herausforderungen durch pluviale Überflutungen – Grundlagen , Schäden und Lösungsansätze. Österreichische Wasser- und Abfallwirtschaft. 64–77.

---

# Integrated operational avalanche risk management

Walter Steinkogler<sup>1</sup>, Stian Langeland<sup>2</sup>, Sophia Demmel<sup>2</sup>

**Keywords:** Integrated operational avalanche risk management; digitalization; hazard and risk-based decision making; platform

## Abstract

Avalanche professionals must continuously collect and interpret large amounts of data from a variety of sources on which they base their (hazard or risk-based) decisions. This operational phase needs to be considered already in the planning phase of avalanche safety projects. Frameworks to allow for a continuous workflow from the planning phase into the operational phase already (partly) exist. The challenge is now to create a digital platform that implements such a (hazard or risk-based) decision framework and in the end leads to a reduction and optimization of time and resources needed in the operational phase, allows for better documentation and also facilitates the integration of a variety of input data and sensors. The operational example from Davos (Switzerland) combines different avalanche control and detection systems and highlights the benefits of integrating the systems' data together with external information in a tool such as the “Cockpit” platform.

## Introduction

Avalanche professionals must continuously collect and interpret large amounts of data from a variety of sources. Often operational decisions and work tasks must be performed within short times. To perform their daily work in an efficient and professional way, optimized workflows, frameworks and tools are essential for the practitioners and need to be considered already in the planning phase of avalanche safety projects.

In the planning phase risk-oriented approaches have become a common practice for the evaluation of effectiveness and efficiency of mitigation projects. As an example, the Federal Office for the Environment (FOEN) of Switzerland introduced the software EconoMe as a mandatory tool for a comparable evaluation of the effectiveness and the economic efficiency of mitigation measures against gravitational natural hazards (Bründl et al., 2009).

In the operational phase, i.e. the daily local decision-making process of avalanche services in Switzerland, risk is not explicitly considered. The decisions on avalanche safety for public roads are based on the evaluation of a specific hazard situation (Bründl et al., 2019).

---

<sup>1</sup> Dr., Wyssen Avalanche Control, Feld 1, Reichenbach, Switzerland (walter@wyssen.com)

<sup>2</sup> Wyssen Avalanche Control

In other countries such as Canada, USA and Norway, and for operations with other specific needs, a risk-based decision approach was used (Kristensen, Breien & Lacasse, 2013; Statham & Gould, 2016; Langeland et. al., 2018). Local avalanche warning services which conduct the (daily) forecasting and operations have been put in place and have proven to work reliably – i.e. in Switzerland, Austria or Canada (Stoffel et. al., 2007). In other countries, such as Norway, the focus has historically been on permanent protections measures, but in recent years there has been a change towards more operational solutions as well.

Frameworks to allow for a continuous workflow from the planning phase into the operational phase combined with an ongoing review process (Figure 1) have been developed and implemented (Canadian Avalanche Association, 2016). These frameworks mainly follow the ISO 31000 standard (CSA, 2011). With the widespread use of smartphones and rising mobile network coverage, it has become fairly straightforward to create a web-based app for almost any task or problem in the world. The challenge is now to design a digital platform that implements such a (hazard or risk-based) framework, combines the relevant data and serves as a central tool to work with and allow for improved decision making of practitioners (Meier et. al., 2018).

This paper presents an integrated approach for avalanche risk management combined with operational examples. The overall aim is to achieve:

- A reduction and optimisation of time and resources needed in the operational phase
- A better framework for (hazard or risk-based) decision making
- An automatic documentation (for liability reasons but also for improved knowledge transfer)

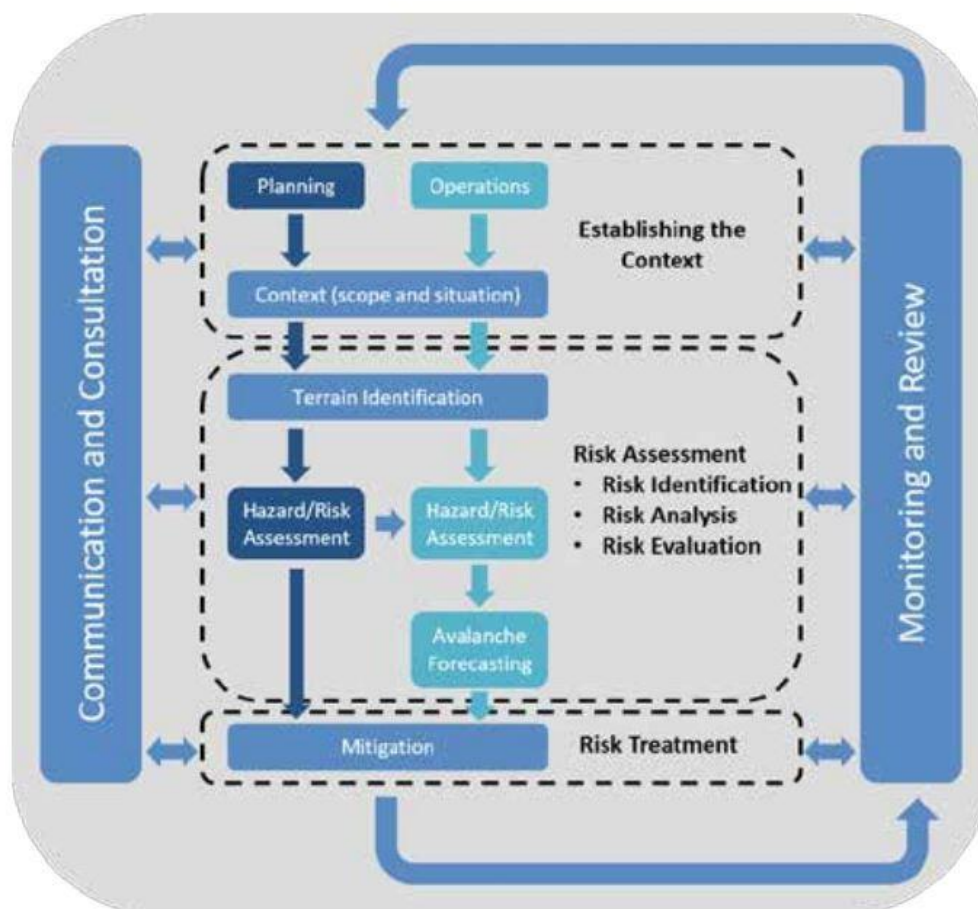


Figure 1. The avalanche risk management process. The center of the diagram illustrates the parallel paths that focus on either planning or operational activities and identifies how this structure aligns under the ISO 31000 umbrella (CSA, 2010) and (Canadian Avalanche Association, 2016).

## Methods

It is important to establish the context of the operation and its specific needs clearly when setting up the operational phase. A continuous review should be carried out in the planning phase. The same should be implemented as part of the operational concept. It has proven to be essential to involve the operational personnel, i.e. the local forecasters, involved engineering offices or decisionmakers in the clients' operation, early on to incorporate their input and describe the framework and workflow.

On the technical side the integration and visualisation of a variety of data sources is one of the main challenges. The platform, and its underlying framework, must also allow to cover needs that are specific to the operation as an avalanche control team in a ski resort might operate differently and have different needs than a forecaster for a public road.

Under the framework of the WAC.3 web-based control of avalanche control and detection systems, the information platform "Cockpit" has been developed. The platform is designed

for an individual setup of the main sources of information for operation by using tiles to visualize the different internal or external data sources. The chronology of comments, pictures and geographic input linking to these tiles and recapitulating their past status can help the operations team to keep themselves updated.

In a next step the gathered data can be fed into models to e.g. simulate the snowpack or compare to days with similar avalanche activity via a Nearest Neighbour Analysis. These “intelligent systems” can provide now- or even forecasting and propose suitable measures. It is important to stress that the aim of this tool is to support the practitioners, never to automatize the decision making process.

## Results

The integration and merging of all relevant data sources of an operation into a single platform (Figure 2) has proven to be accepted very well amongst practitioners. Especially during stressful forecasting situations, the time savings due to the possibility of accessing the key information for decision making are significant. The digitalisation of established workflows and processes allows to bring the local knowledge of individual people into the organisation. This is especially important when forecasting duties are handed over to a new person – either on a work shift basis or when a person retires. Such a framework also allows for much easier documentation and reporting which is a key element for liability reasons.

Moreover, data sharing between existing platforms of different organizations or into a public database, e.g. the Norwegian public crowdsourcing tool “Regobs”, can be automatized to a large extent.

The direct integration of different technologies opens up new possibilities for data processing and to reduce uncertainty. For example, the confirmation of a specific avalanche event by different detection systems and the processing and illustration of this information on a single platform can reduce uncertainty in the decision making. Also combining data from varying information sources, e.g. directly coupling new snow heights to avalanche activity, is facilitated by this integrated approach.

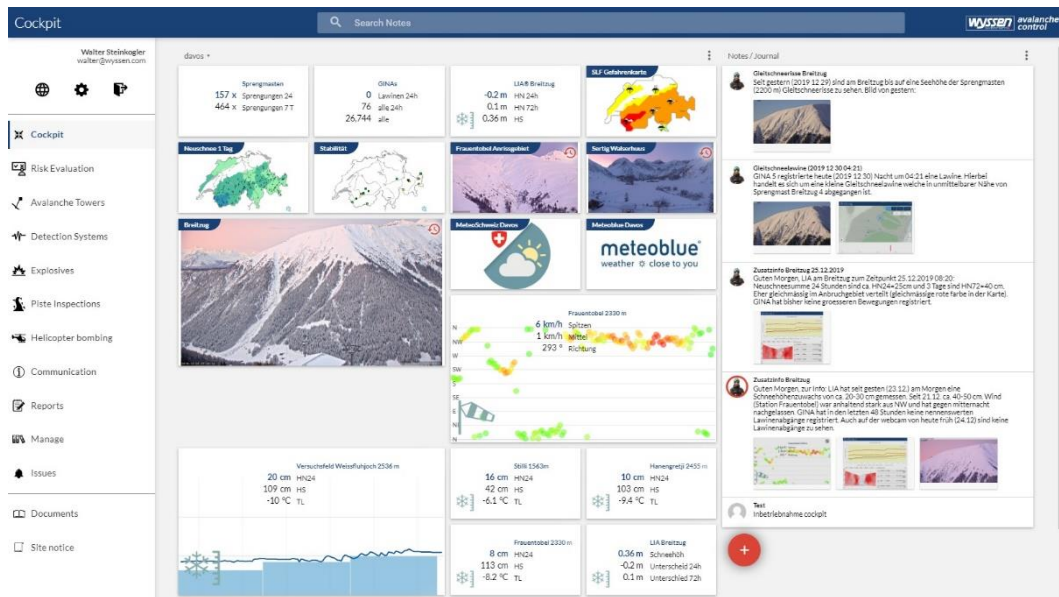


**Figure 2.** Example illustration of the Cockpit platform that combines a variety of data sources and offers different modules depending on the clients' needs.

## Operational example

Numerous examples in different countries and for different operations exist where this integrated operational approach has been implemented with success – both on the technological as well as on the operational level.

For the protection of a road and railway sector close to Davos (Switzerland) that is exposed to avalanche hazard a combination of different sensor types (Figure 3) and the integration into a single platform allows efficient decision making and avalanche control. Along the mountain ridge four remote avalanche control systems (Wyssen tower) were installed to be able to perform avalanche during day and nighttime as well as during a snowstorm. At one of these towers a 3D snow depth measuring device (LIA) was installed which performs detailed measurements of the snow height directly in the release area allowing the safety personnel to accurately assess the hazard. In the paths and the runout six seismic sensors (GINA) monitor the natural avalanche activity and allow to verify the success of controlled avalanche releases with the towers. A webcam on the counter slope allows to acquire valuable additional information when visibility is sufficient. All this information was integrated and merged into a single platform which makes it very user friendly and efficient. In a next step other existing data sources were integrated into the platform such as automatic weather stations, regional avalanche forecasts and external webcams.



**Figure 3.** Example of integration of different technology for an operation close to Davos, Switzerland. 3D snow depth measurement in the release area (LIA), remote avalanche control systems along the ridge (Wyssen tower) and avalanche detection systems (GINA) to monitor natural and controlled avalanche activity with geophones.

## Discussion

Whether a hazard or risk-based approach can be applied in the planning and/or the operational phase of avalanche mitigation is depending on local or country regulations and laws. Recent studies started re-evaluating which approach is best implemented for public roads or the more specific demands of e.g. construction sites (Bründl et. al., 2018). New concepts such as the Operational Specific Avalanche Risk Matrix (OSARM) seek to improve the integration of the risk analysis in the planning phase, with the decision making and applied mitigation measures as part of the operational phase. In the planning phase a qualitative risk assessment is conducted to determine the avalanche size to which the element at risk is exposed to and how vulnerable it is to each avalanche size. In the next step the accepted risk and possible mitigation strategies are elaborated together with the client. Based on this analysis, two or three risk ratings with associated mitigation strategies are defined (Langeland et. al., 2018).

Assessing and communicating uncertainty during the decision-making process has shown to be of essential importance. Both in planning and operational phase the framework needs

to ensure the communication of key information and decisions between all involved stake holders.

## Conclusion

- Comprehensive frameworks and the digital representation of such have significant potential to improve the daily decision-making process of avalanche safety operations.
- The integration of a variety of data sources into a central platform like the “Cockpit” reduces the needed time and resources and allows for simplified documentation.
- The planning phase needs to be conducted with a focus on the (hazard or risk-based) operational phase and a continuous review process in place.
- The ongoing digitalisation and integration of all individual steps will allow to improve the involved workflows even more.

## References

Bründl M., Stoffel L., Steinkogler W. (2018) Risk-oriented vs hazard-oriented decision making for opening and closing of traffic routes. Proceedings of International Snow Science Workshop 2018, Innsbruck, Austria.

Canadian Avalanche Association CAA. (2016). Technical Aspects of Snow Avalanche Risk Management—Resources and Guidelines for Avalanche Practitioners in Canada (C. Campbell, S. Conger, B. Gould, P. Haegeli, B. Jamieson, & G. Statham Eds.). Revelstoke, BC, Canada: Canadian Avalanche Association.

Canadian Standards Association CSA. (2011). Implementation guide to CAN/CSA-ISO 31000, Risk management – Principles and guidelines. Mississauga, ON, Canada: Canadian Standards Association.

Kristensen, K., Breien, H. and Lacasse, S, 2013: Avalanche Forecasting and risk mitigation for specific objects at risk. Proceedings of the International Snow Science Workshop, Grenoble – Chamonix Mont-Blanc

Langeland S., Velsand P., Solemsli L., Steinkogler W. (2018). An operational specific avalanche risk matrix (OSARM): Combining the conceptual model of avalanche hazard with risk analysis and operational mitigation strategies. Proceedings of International Snow Science Workshop 2018, Innsbruck, Austria.

Meier B., Wyssen C., Wyssen S., Steinkogler W. (2018). Using cloud-based solutions for avalanche operations – merging data collection, documentation, communication and avalanche control. Proceedings of International Snow Science Workshop 2018, Innsbruck, Austria.

Statham, G. and Gould, B., 2016: Risk-based avalanche program design, Proceedings of the International Snow Science Workshop, Breckenridge, Colorado

Stoffel, L.; Schweizer, J. (2007). Praxishilfe. Arbeit im Lawinendienst: Organisation, Beurteilung lokale Lawinengefährdung und Dokumentation. Schweizerische Interessengemeinschaft

Lawinenwarnsysteme (SILS), WSL, Eidg. Institut für Schneeund Lawinenforschung SLF; Bundesamt für Umwelt BAFU. Münster; Davos; Bern.

---

# “How-to” manage a torrential protection system in a holistic way: Integrated Torrent Development Concept (IWEK)

Quirin Stimm<sup>1</sup>, Franz Grüsser<sup>2</sup>, Karl Mayer<sup>3</sup>, Wolfgang Rieger<sup>4</sup>, Andreas Rimböck<sup>5</sup>

**Keywords:** integrated river management; structural protection; regional strategy

## Abstract

In Bavaria, we find many old and often broken control structures. The constructions rest upon different boundary conditions and motivations compared to nowadays (e.g. change of land-use, increasing vulnerability, torrent control for silvicultural reasons). The state of Bavaria is responsible for the rehabilitation of damaged control structures. A total reinstatement of the protection systems would generate high costs and even then, the protection goal for settlements and important infrastructure (HQ 100) might not be ensured. To limit reinstatement and maintenance costs and to achieve the protection goal with flexible and adaptable solutions, it is necessary to analyse the completely torrential catchment and its developments from the past to the future. Therefore, we want to implement a common procedure for the management of protection systems in torrential catchments, which contains the synergy of structural and organizational measures to encounter natural events in the future and the collaboration of different stakeholders. The outcomes of the above-mentioned analysis and the resultant planning of measures are summarized in “Integrated Torrent Development Concepts” (IWEK).

## Introduction

Humans have started to build structural measures in torrents hundreds of years ago in order to protect themselves against torrential hazards (Aulitzky et Stritzl 1984, Goettle 1996, Piton et al. 2016). In the Alps, there exist thousands of structural measures in mountain streams and many of them are in need of rehabilitation, which means high financial expense for reconstruction and maintenance (Rimboeck et al. 2014). The construction often based on (very) different boundary conditions and motivations compared to nowadays. For example, over time some of the former alpine pastures in torrent catchments have changed to forest stands or vice versa. In addition, the areas of settlement have changed too (fig. 1).

---

<sup>1</sup> Bavarian Environment Agency, GERMANY, corresponding author: Christiane Mögele, ([christiane.moegle@lfu.bayern.de](mailto:christiane.moegle@lfu.bayern.de))

<sup>2</sup> Wasserwirtschaftsamt Traunstein

<sup>3</sup> Bavarian Environment Agency

<sup>4</sup> Dr.-Ing. Bavarian Environment Agency

<sup>5</sup> Dr.-Ing. Wasserwirtschaftsamt Donauwörth

These shifts have led to changes in the runoff characteristics, erosion susceptibility and vulnerability. Thus, we should scrutinize whether old structural measures and especially their location and type of construction correspond to present conditions in the catchment and to the actual protection goal. Likewise, we should take future developments, such as climate change, technological progress and change of land use, into account. For this reason, we need flexible and adaptable solutions, which include a holistic consideration of torrent catchments (Rimboeck et al. 2015). In Bavaria, such processes and objectives are worked out in the so called "Integrated Torrent Development Concepts" (IWEK) for important torrents with a complex catchment, which needs a detailed study (e.g. high amount of damaged structural measures, different kind of natural processes and stakeholders).

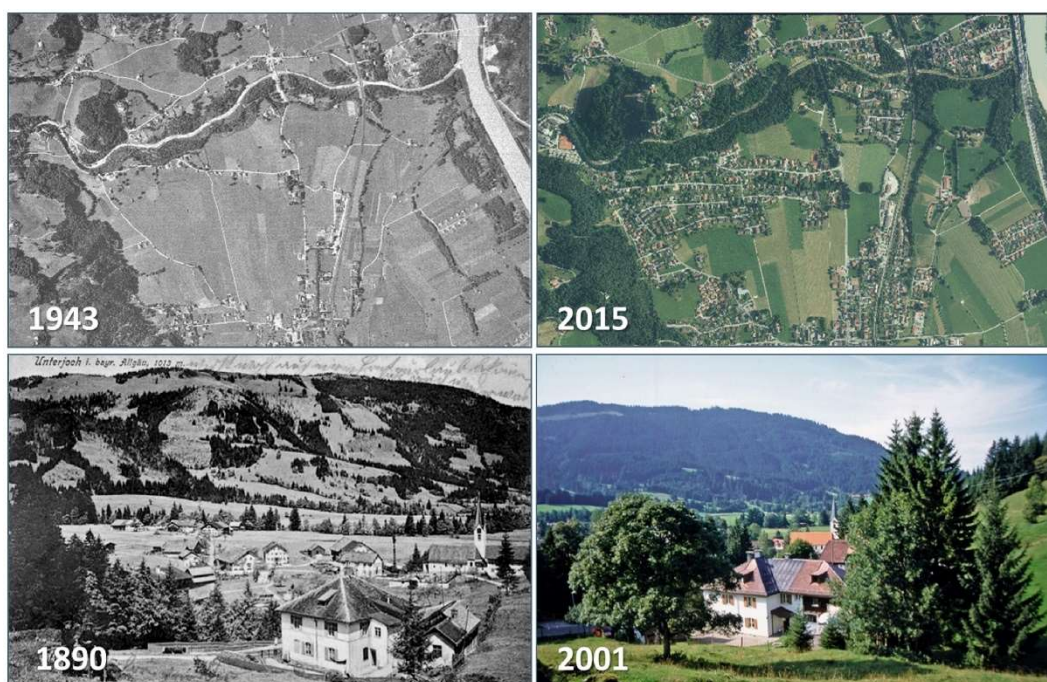


**Figure 1: Spatial development between 1945 and 2015 in Oberaudorf (Bavaria, Germany) (up) and land-use change in an alpine environment between 1890 and 2001 in Unterjoch (Bavaria, Germany) (down).**

An IWEK targets the long-term protection of settlements and important infrastructure and rests upon the integrated risk management, which includes the different stages in dealing with natural events and their resultant losses (Response, Recovery and Preparedness). The measures of an IWEK are the result of a holistic view of the entire catchment, which is a dynamic complex of natural (e.g. forest, geomorphology), protective (e.g. structural/organizational measures) and social systems (e.g. politics, community). The consideration as a dynamic complex respects the changes in the systems over time and enables a sustainable, target-orientated management of the catchment including the participation of local communities.

## IWEK Strategy

By law, the Bavarian state is responsible for the maintenance of structural measures in torrents. Due to the high number of damaged and unreliable structural measures the need of maintenance work is given. In addition, the implementation of an IWEK takes time and costs even before the maintenance work starts. Therefore, we identified some criteria in order to decide, whether the usual maintenance works are sufficient or if an IWEK is necessary. The local authorities (water agencies, district governments) will take the final decision. In case of an implementation, we have to determine the IWEK strategy. There are four different strategies depending on the existence of structural measures, a protection deficit and arguments for the consideration level (fig. 2):

- (1) Overhaul of the protection system: restoration of the protection level and optimization of maintenance work concerning the full catchment
- (2) Optimization of the protection system: no deterioration of the protection level and optimization of maintenance work concerning the full catchment
- (3) Optimization of the considered torrent section: optimization of maintenance work concerning the torrential section with structural measures
- (4) Set-up of a new protection system: new construction of structural measures to achieve the protection level by considering maintenance work in the future

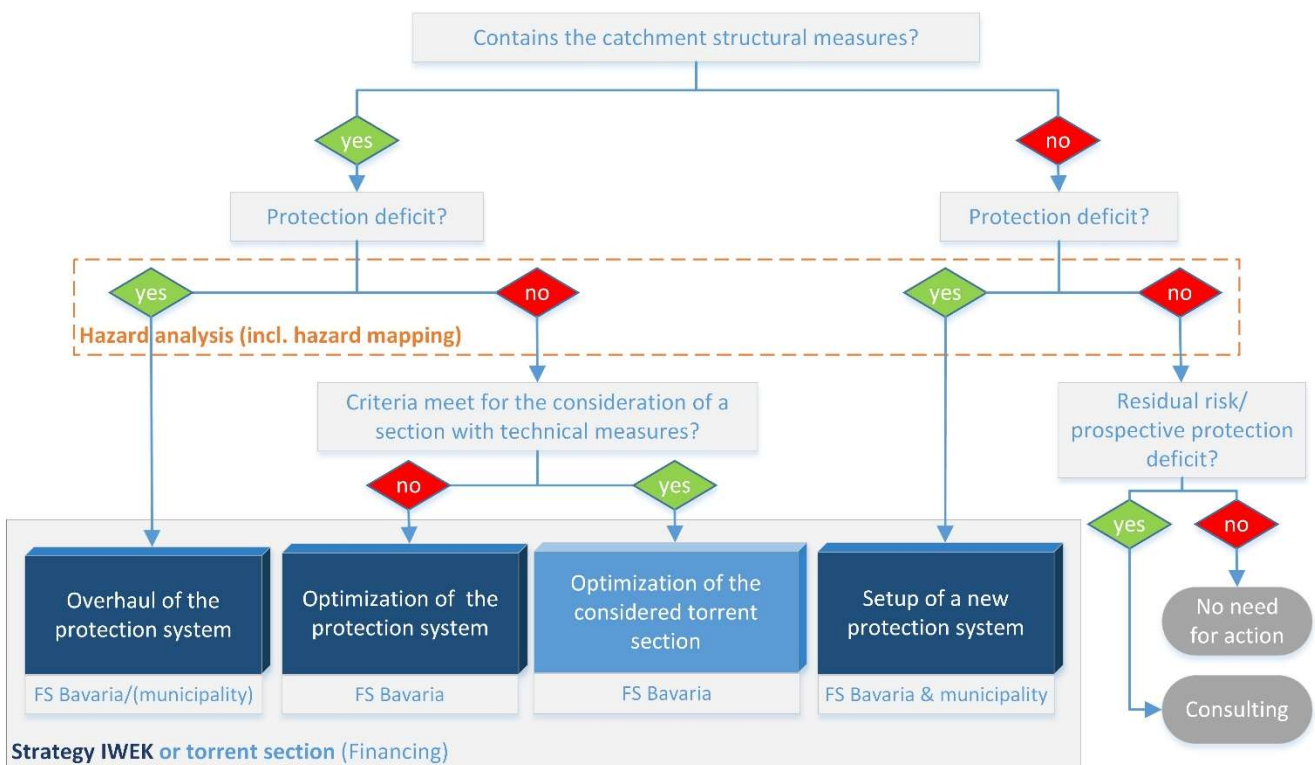


Figure 2: Decision making process to determine the strategy of an IWEK.

In any case, a hazard analysis (including hazard mapping) is required. If there is no actual protection deficit given and no future protection deficit foreseeable, there is no need for action. Nevertheless, in respect of the residual risk (HQextrem) or a prospective protection deficit, the local water management agency has to undertake an advisory function.

## IWEK Structure

The structure of an IWEK consists of an inventory analysis, the planning of the protection concept and an associated communication concept (fig. 3). The first two components form the main concept, which focuses on the protection system. The primary function of the communication concept is to give assistance for the local authorities through all planning stages. Communicative aspects are to be found in each working step (fig. 3, letter ‘C’).

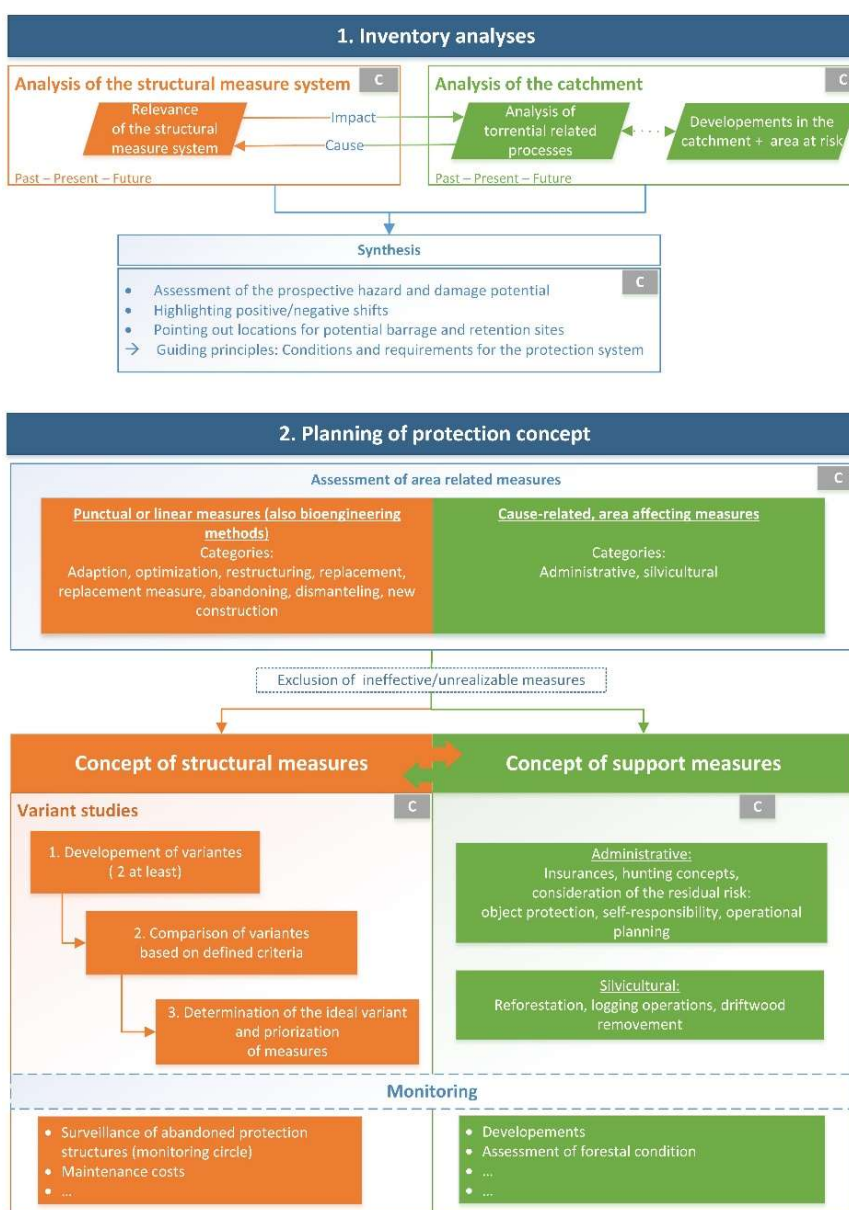


Figure 3: IWEK structure with the respective modules and working steps.

## Inventory analysis

The inventory analysis is the basis for further planning. It is subdivided into two components: the analysis of structural measure system and the analysis of catchment (fig. 3). Both components consider the changes over time and the results of the previous hazard analysis.

The key task of the structural measure system analysis is to identify the initial purpose and the current protective effect on the area at risk or on the protective objective. Therefore it is required to scrutinize old construction plans, to determine the dates of construction work and to draw conclusions from type, material, condition and site of the structural measure.

The analysis of catchments is divided again into the analysis of torrential relevant processes and the analysis of different developments in the catchment and in the area at risk. Old (aerial) images of the catchment and torrential events, reports and testimonies are a very good source to reconstruct former conditions and to understand the current existing protection system. Each catchment has its own characteristics with different important developments. The most important developments related to torrential hazards are the spatial development and the change of river course, forest stands and grazing areas. In some extent, these changes interact with torrential related processes. It is necessary to identify these interactions. Besides the key process (defined by the previous hazard analysis), we have to identify and dissect all the other torrential related processes (e.g. landslides, bank- and riverbed erosion, driftwood accumulation) in detail. Furthermore, we have to examine the effect of existing structural measures on these processes too.

In a next step, we combine the results of both analysis (structural measure system and catchment). This synthesis form the guiding principles of the prospective protection system. The prospective hazard and damage potential is assessed based on the previous analysis, positive and negative shifts are highlighted and potential sites for (non-) structural measures are pointed out (fig. 3). The characteristics of the catchment and of its components (subcatchments, sections) with the required functions are determined.

## Planning of the protection system

The protection system does not only include structural measures but also organisational, administrative and area-related measures. These measures are summarized under the term support measures. Some of the support measures (esp. silvicultural measures) have only an effect on cause-related processes (e.g. discharge, erosion, shallow landslides) for what reason they cannot substitute structural measures one-on-one. Therefore, the complete planning process of the protection concept is subdivided in the assessment, handling and concept of structural measures and the assessment, identification and concept of support measures (fig. 3).

Each structure (or series of structures) has to be assessed, in order to identify the most suitable structural measures for the concept. As a result of the inventory analysis, we already know what the initial function and (former) protection goal/objective of the structural measures were, which characteristics, torrential-related processes and required

functions of each torrent section have and what the actual and prospective protection goal/objective is. By combining these circumstances, we can decide, how to deal with the existing structural measure. Each measure or series of measures can be classified as seen in table 1.

category	description
adaption	the initial function of the structural measure is not (longer) required; the measure can be structurally modified to fulfill another required function
optimization	the initial function and type of the structural measure is still required; the structural measure has to be improved due to the shift of the protection goal/objective and the state of the art
maintenance	the structural measure is renovated one-on-one
replacement	the structural measure is destroyed and has to be reconstructed
replacement measure	a new structural measure can adopt the function of an old measure; the function is still required
abandoning	the structural measure is no longer required for different reasons; a degradation has no negative effect on the protection goal/objective
dismantling	the structural measure is no longer required for different reasons; a degradation has a negative effect on the protection goal/objective for what reason it has to be stripped down
new construction	a new structural measure has to be constructed to fulfill a required function

**Table 1: Different categories of dealing with existing structural measures.**

Some of the assessed structural measures can fall into different categories. In order to avoid a vast number of variants for the variant study, it is necessary to rate them applying various criteria. The exclusion criteria have to match with the local conditions. Therefore, we have different kinds of exclusion criteria for each catchment. For example, the prospective maintenance costs could be an exclusion criterion for the optimization of a series of check dams (cat. optimization) in a hardly accessible upper catchment. Instead, it is more efficient to retain the incidental bedload downstream (cat. replacement measure). Further exclusion criteria could be limited space conditions, no sufficient protective effect or too high construction work costs. The next step is to combine the preselection of structural measures to sensible variants. At least two variants are required for the variant study. The comparison of variants follows the principles of a multi-criteria-analysis (MCA). Like the definition of exclusion criteria, we have to modify the criteria for each catchment. Beside the ‘hard’ criteria (e.g. costs, benefit) there are several ‘soft’ criteria (e.g. acceptance, ecology and geomorphology). Both the ratio of hard and soft criteria and the criterion itself can be weighted differently. As a result, we will get the best combination of structural measures. The prioritisation of the different measures helps to plan various construction and maintenance works, which arise at the local water management authorities.

Each protection system requires monitoring. Bavaria already has a standard procedure to monitor structural measures with focus on their condition. Because of the integrated consideration, the standard monitoring alone is not sufficient. Dealing with structural

measures (e.g. abandoning) and the change of torrential processes with effect on structural measure require additional ways of monitoring. Due to the lack of personnel and financial resources, the monitoring measures have to be economical and less time-consuming. To simplify the monitoring, we have to merge standard and new monitoring measures together. For example, the monitoring frequency for abandoned structural measures is every two years like the one for structural measures with a key function. The inspections are temporally synchronized. Sometimes the analysis of aerial images or digital terrain models is enough for the observation of torrential-related processes depending on their effect on the hazard potential.

In some extent, planning a concept of support measures goes beyond the responsibility of the local water management authorities. It is necessary to involve other relevant stakeholders, administrations and agencies. Support measures are divided in administrative and silvicultural measures. Latter are very important for the most catchments in Bavaria due to the high amount of forest stands and well-organized forest authorities. Actually, every forest owner and the Bavarian State Forest Enterprise are legally bound to ensure the protective effect of protection forests. Silvicultural measures comprise reforestation (programs), felling operations (e.g. thinning) and removal of driftwood. By contrast, administrative measures include organisational measures (e.g. operational planning, hunting concepts and insurances), legal consequences (e.g. building ban or building with restrictions) and awareness raising (e.g. self-responsibility and consideration of the residual risk). Based on the catchment analysis, we identified the relevant developments, which effects the hazard and damage potential. Now we have to assign the above-mentioned support measures to the proper area of application. By general agreement, the implementation follows by the person in charge or responsible administration/authority. The effect of the particular measure has to be monitored and recorded.

## **Communication concept**

In Bavaria, communication played a minor part in the field of torrent control yet, it was restricted to in-house communication or the presentation of hazard maps and final project plannings. With an IWEK, we want to involve citizens, stakeholders and decision makers from the beginning. In addition, the communication process shall not steer only in one direction. The key-tasks are to inform the local people, to get information about past and future developments and to involve stakeholders in the planning process. Therefore, we added communicative aspects to almost every working step. These aspects contain hints who the communication partners are and what the subject and the suitable medium of communication is. In addition, we establish a general schedule of the whole communication process with more detailed information. Table 2 shows the working steps with communicative aspects in an exemplary way.

Phase	Communication		
	goals	partner	medium
Preparation	information about the project and the further proceeding	- authorities - local administrations - local people	- one-on-one conversation - internet - local newspaper
Hazard analysis	presentation of the hazardous situation and residual risk discussion	- authorities - local administrations - consulting engineers - local people	- in-house conversations - presentation
Inventory analysis	data acquisition and exchange of information and knowledge	- authorities - local administrations - local people	- interviews - surveys
Planning of the concept	contribution for the study of variants (e.g. weighting factors) and identification and realization of support measures	- authorities - local administrations - consulting engineers - local people	- workshops - conversations
Finalisation	presentation of the final outcomes and the next steps, awareness raising, sharing responsibility	- authorities - local administrations - consulting engineers - local people	- presentation - local newspaper - internet

**Table 2: Overview of the different communication goals, partner and medium for each phase of an IWEK.**

## Outlook

To implement the procedure, we have to transfer the presented approach into universal guidelines for the management of torrent catchments in Bavaria. To find appropriate and general methods, we conduct four various studies together with the four water management agencies of the alpine region and four different consultant engineers (cf. poster IWEK Auerbach, other contribution at INTERPRAEVENT 2020). The method description of the studies conforms more or less to the structure of an IWEK. We will review the outcomes and compare them with already existing approaches. The best methods will be transferred into the final guidelines.

## References

- Aulitzky H., Stritzl J. (1984). 100 Jahre Wildbachverbauung in Oesterreich: 1884 - 1984. Bundesministerium für Land- u. Forstwirtschaft. Wien.
- Goettle A. (1996). Hundert Jahre Wildbachverbauung in Bayern: Bilanz und Ausblick. Tagungspublikation Interpraevent 1996, Bd. 1: 1-26.
- Hoehne R., Rimboeck A. (2016): Self-monitoring of torrent control protection structures in Bavaria. 13th Congress Interpraevent 2016, Lucerne. Switzerland.

Piton G., Carladous S., Recking A., Tacnet J.-M., Liébault F., Kuss D., Quefféléan Y., Marco O. (2016). Why do we build check dams in Alpine streams? An historical perspective from the French experience. *Earth Surface Processes and Landforms* 42: 91–108.

Rimboeck A., Rudolf-Miklau F., Pichler A., Suda J., Hoehne R., Mazzorana B., Papez J. (2014). Persistence of Alpine natural hazard protection. Platform on Natural Hazards of the Alpine Convention. Vienna.

Rimboeck A., Hoehne R., Mayer K., Wolter-Krautblatter R. (2015). Wildbachbericht Bayern - Teil 1. Bayerisches Staatsministerium fuer Umwelt und Verbraucherschutz. Muenchen.

Rudolf-Miklau F., Rimboeck A., Mazzorana B., Pichler A. (2016): Applying systems engineering (SE) and life cycle management (LCM) principles to protection systems. 13th Congress Interpraevent 2016, Lucerne. Switzerland.



**Statens vegvesen**  
Norwegian Public Roads  
Administration



**NVE**

**NGI**